frontiers | Research Topics

Alzheimer's disease: new insights into biomechanisms and therapeutic target

Edited by
Wenjuan Yao, Yuping Tang, Maoli Duan and Wenchang Tan

Published in
Frontiers in Aging Neuroscience

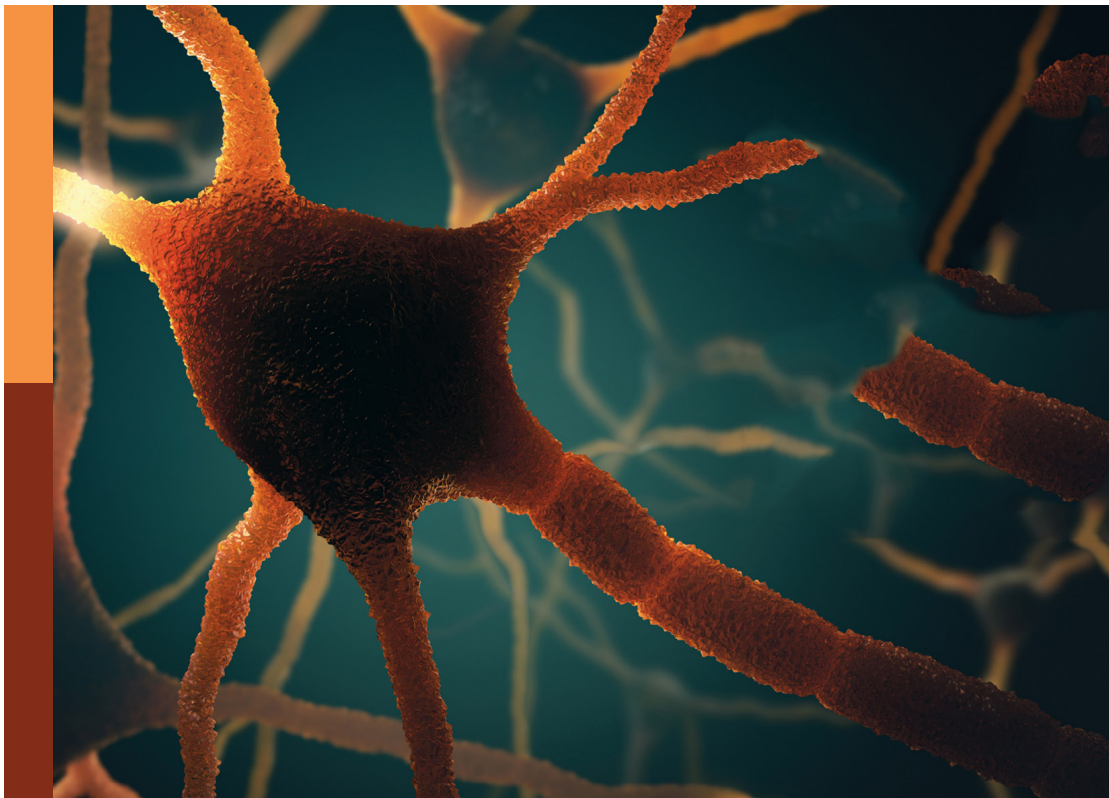

ISSN 1664-8714
ISBN 978-2-8325-6140-9
DOI 10.3389/978-2-8325-6140-9

About Frontiers

Frontiers is more than just an open access publisher of scholarly articles: it is a pioneering approach to the world of academia, radically improving the way scholarly research is managed. The grand vision of Frontiers is a world where all people have an equal opportunity to seek, share and generate knowledge. Frontiers provides immediate and permanent online open access to all its publications, but this alone is not enough to realize our grand goals.

Frontiers journal series

The Frontiers journal series is a multi-tier and interdisciplinary set of open-access, online journals, promising a paradigm shift from the current review, selection and dissemination processes in academic publishing. All Frontiers journals are driven by researchers for researchers; therefore, they constitute a service to the scholarly community. At the same time, the *Frontiers journal series* operates on a revolutionary invention, the tiered publishing system, initially addressing specific communities of scholars, and gradually climbing up to broader public understanding, thus serving the interests of the lay society, too.

Dedication to quality

Each Frontiers article is a landmark of the highest quality, thanks to genuinely collaborative interactions between authors and review editors, who include some of the world's best academicians. Research must be certified by peers before entering a stream of knowledge that may eventually reach the public - and shape society; therefore, Frontiers only applies the most rigorous and unbiased reviews. Frontiers revolutionizes research publishing by freely delivering the most outstanding research, evaluated with no bias from both the academic and social point of view. By applying the most advanced information technologies, Frontiers is catapulting scholarly publishing into a new generation.

What are Frontiers Research Topics?

Frontiers Research Topics are very popular trademarks of the *Frontiers journals series*: they are collections of at least ten articles, all centered on a particular subject. With their unique mix of varied contributions from Original Research to Review Articles, Frontiers Research Topics unify the most influential researchers, the latest key findings and historical advances in a hot research area.

Find out more on how to host your own Frontiers Research Topic or contribute to one as an author by contacting the Frontiers editorial office: frontiersin.org/about/contact

Alzheimer's disease: new insights into biomechanisms and therapeutic target

Topic editors

Wenjuan Yao — Shanghai University, China
Yuping Tang — Fudan University, China
Maoli Duan — Department of Clinical Science, Intervention and Technology, Karolinska Institutet (KI), Sweden
Wenchang Tan — Peking University, China

Citation

Yao, W., Tang, Y., Duan, M., Tan, W., eds. (2025). *Alzheimer's disease: new insights into biomechanisms and therapeutic target*. Lausanne: Frontiers Media SA.
doi: 10.3389/978-2-8325-6140-9

Table of contents

frontiers | Frontiers in Aging Neuroscience

TYPE Editorial
PUBLISHED 05 March 2025
DOI 10.3389/fnagi.2025.1569412

OPEN ACCESS

EDITED AND REVIEWED BY
Allison B. Reiss,
New York University, United States

*CORRESPONDENCE
Maoli Duan
maoli.duan@ki.se

RECEIVED 31 January 2025
ACCEPTED 11 February 2025
PUBLISHED 05 March 2025

CITATION
Zhang Y, Zhu J and Duan M (2025) Editorial: Alzheimer's disease: new insights into biomechanisms and therapeutic target. *Front. Aging Neurosci.* 17:1569412. doi: 10.3389/fnagi.2025.1569412

Editorial: Alzheimer's disease: new insights into biomechanisms and therapeutic target

Yang Zhang[1], Jie Zhu[2,3] and Maoli Duan[4,5]*

[1]Department of Neurology, Affiliated Drum Tower Hospital of Nanjing University Medical School, Nanjing, China, [2]Department of Neurology, Neuroscience Center, The First Hospital of Jilin University, Changchun, China, [3]Division of Neurogeriatrics, Department of Neurobiology, Care Sciences and Society, Karolinska University Hospital, Karolinska Institute, Stockholm, Sweden, [4]Department of Otolaryngology Head and Neck Surgery and Audiology and Neurotology, Karolinska University Hospital, Karolinska Institute, Stockholm, Sweden, [5]Division of ENT Section, Department of Clinical Science, Intervention and Technology, Karolinska Institute, Stockholm, Sweden

KEYWORDS

Alzheimer's disease, amyloid-beta, therapeutic targets, sphingolipid metabolism, clathrin-mediated endocytosis

Editorial on the Research Topic
Alzheimer's disease: new insights into biomechanisms and therapeutic target

Alzheimer's disease (AD) is the most common age-related dementia and primarily characterized by the extracellular deposition of amyloid-beta (Aβ) plaques and intracellular neurofibrillary tangles in the brain. Over the last decade, significant progress has been made in understanding etiology and therapeutic targets of AD. However, due to the complex pathogenesis of AD, we still face severe challenges in clinical treatment.

The Research Topic of this issue is "*Alzheimer's disease: new insights into biomechanisms and therapeutic targets*", which aims to explore the various molecular mechanisms of AD pathogenesis and discover new promising potential therapeutic targets. Here are 10 articles, including 6 original works and 4 reviews, which collectively address various facets of biomechanisms aspects of biological mechanisms and therapeutic targets in the context of AD, such as abnormal sphingolipid metabolism, clathrin-mediated endocytosis (CME) and the role of hypoxia in the pathogenesis of AD. The contents of these articles are briefly summarized as follows:

1. This study explored changes in the effective connectivity (EC) network of the basal forebrain in AD patients before and after donepezil intervention using rs-fMRI data and the Granger causality analysis (GCA) approach. The findings suggested that donepezil enhanced the strength of connections between the basal forebrain with the default mode network and middle occipital gyrus, thereby improving cognitive function in AD patients. These results are helpful for better understanding of the neural mechanism of donepezil in the treatment of AD and for finding clinical targets for intervention (Yang et al.).

2. The role of sphingolipids was investigated in AD brains, Cerad score B brains and induced pluripotent stem (iPS) cells. AD brains exhibited higher levels of sphingosine (Sph), total ceramide 1-phosphate (Cer1P) and total ceramide (Cer), while higher levels of sphingomyelin (SM) exclusively in Cerad-B brains, which suggested the importance of sphingolipid metabolism in AD pathology (Uranbileg et al.).

3. The neuroprotective effects and mechanism of 4,4′-methylenediphenol in AD model worms were examined in this study. The results showed that 4,4′-methylenediphenol improved motility and stress tolerance, while also delaying the onset of paralysis and senescence in the AD model. Along with upregulating the expression of SKN-1, SOD-3, and GST-4 in the corresponding GFP reporter lines and promoting the nuclear translocation of DAF-16, 4,4′-methylenediphenol also increased antioxidant activity and decreased Aβ toxicity, suggesting to further study the anti-AD effects of Gastrodia elata and its active ingredients (Yu et al.).

4. The study investigated the degree of GluN2A or GluN2B-containing NMDAR contribute to Aβ (1–42) mediated impairments of hippocampal function. The results showed that GluN2A subunit knockdown modified the membrane characteristics of hippocampal neurons and lowered the amount of long-term potentiation (LTP). LTP's early phase was diminished by GluN2B knockdown, while its later stages were unaffected. However, neither GluN2A nor GluN2B-containing NMDAR mediated the aged hippocampus's susceptibility to Aβ-mediated impairments of LTP. It suggested that the pathogenic effects of oligomeric Aβ (1–42) on hippocampal function were not propagated via NMDAR in the aged hippocampus (Südkamp et al.).

5. Abnormal dynamic functional connectivity (DFC) is a neuroimage feature of AD. Energy landscape analysis was applied to the resting-state fMRI data to characterize the aberrant brain network dynamics in AD patients and controls. Their results suggested that the co-activation state could be important to cognitive processing and AD group possibly raised cognitive ability by increasing the occurrence and transition between the impaired cognitive control and sensory integration states (Xing et al.).

6. The authors carried out a MR study to investigate causal links between a variety of immune cell phenotypes and AD using GWAS data from European cohorts. Findings showed that HLA DR expression on B cells and the absolute number of CD28–CD4–CD8—T cells were associated with a protective effect against AD, while 13 other immunological phenotypes were risk factors. This work offers novel insights into the immunopathogenesis of AD (Zhang et al.).

7. This review summarized the research progress on cognition-related neural network oscillations, and complex anatomical and projective relationships between nucleus basalis of Meynert (NBM) and other cognitive structures. The important functions of the NBM in neuromodulation were also reviewed. The authors believe that neuromodulation based on the NBM plays an important and complex role in treating neurodegenerative disorders (Jiao et al.).

8. The review explored the impact of clathrin-mediated endocytosis (CME) on AD etiology. Disrupted CME in neurons leads to synaptic dysfunction, Aβ processing, and Tau pathology in early AD pathogenesis. CME alterations also affect the ability of astrocytes and microglia to clear Aβ, and neuroinflammation. Dysregulated CME in these cells highlights its AD pathophysiological implications (Jaye et al.).

9. Hypoxia has long been identified as one of the potential causes of AD. This review elucidated the effect of hypoxia-inducible factors-1α and oxidative stress in AD process, including inflammation, Aβ deposition, and mitochondrial dysfunction. The authors speculated that antioxidants could be a potential therapeutic approach for AD (Tao et al.).

10. This systematic review seeked to explore the correlation between sTREM2 levels and AD progression through a meta-analysis of sTREM2 levels in both cerebrospinal fluid (CSF) and blood. The findings indicated a positive correlation between elevated CSF sTREM2 levels and a higher risk of AD and MCI. Besides, plasma sTREM2 levels were notably higher in the AD group, which may serve as a promising biomarker for AD (Wang et al.).

In short, all articles published in this Research Topic contribute to a better understanding of the biomechanisms underlying AD. The findings have the potential to affect clinical practice, inspire new therapeutic targets, and guide the development of novel intervention and approaches of AD. We look forward to additional revolutionary studies in this Research Topic that provides a new perspective.

Author contributions

YZ: Writing – original draft, Writing – review & editing. JZ: Writing – original draft, Writing – review & editing. MD: Writing – original draft, Writing – review & editing.

Conflict of interest

The authors declare that the research was conducted in the absence of any commercial or financial relationships that could be construed as a potential conflict of interest.

Publisher's note

frontiers | Frontiers in Aging Neuroscience

TYPE Review
PUBLISHED 08 April 2024
DOI 10.3389/fnagi.2024.1376764

OPEN ACCESS

EDITED BY
Allison B. Reiss,
Long Island School of Medicine,
New York University, United States

REVIEWED BY
Heling Chu,
Shanghai Sixth People's Hospital,
Shanghai Jiao Tong University, China
Costa Vakalopoulos,
Richmond Hill Medical Centre, Australia

*CORRESPONDENCE
Kai Shu
✉ kshu@tjh.tjmu.edu.cn

†These authors have contributed equally to this work and share first authorship

RECEIVED 26 January 2024
ACCEPTED 28 March 2024
PUBLISHED 08 April 2024

CITATION
Jiao L, Kang H, Geng Y, Liu X, Wang M and Shu K (2024) The role of the nucleus basalis of Meynert in neuromodulation therapy: a systematic review from the perspective of neural network oscillations.
Front. Aging Neurosci. 16:1376764.
doi: 10.3389/fnagi.2024.1376764

The role of the nucleus basalis of Meynert in neuromodulation therapy: a systematic review from the perspective of neural network oscillations

Liwu Jiao[1†], Huicong Kang[2†], Yumei Geng[2], Xuyang Liu[1], Mengying Wang[2] and Kai Shu[1*]

[1]Department of Neurosurgery, Tongji Hospital, Tongji Medical College, Huazhong University of Science and Technology, Wuhan, Hubei, China, [2]Department of Neurology, Tongji Hospital, Tongji Medical College, Huazhong University of Science and Technology, Wuhan, Hubei, China

As a crucial component of the cerebral cholinergic system and the Papez circuit in the basal forebrain, dysfunction of the nucleus basalis of Meynert (NBM) is associated with various neurodegenerative disorders. However, no drugs, including existing cholinesterase inhibitors, have been shown to reverse this dysfunction. Due to advancements in neuromodulation technology, researchers are exploring the use of deep brain stimulation (DBS) therapy targeting the NBM (NBM-DBS) to treat mental and neurological disorders as well as the related mechanisms. Herein, we provided an update on the research progress on cognition-related neural network oscillations and complex anatomical and projective relationships between the NBM and other cognitive structures and circuits. Furthermore, we reviewed previous animal studies of NBM lesions, NBM-DBS models, and clinical case studies to summarize the important functions of the NBM in neuromodulation. In addition to elucidating the mechanism of the NBM neural network, future research should focus on to other types of neurons in the NBM, despite the fact that cholinergic neurons are still the key target for cell type-specific activation by DBS.

KEYWORDS

nucleus basalis of Meynert, neurophysiology, Alzheimer's disease, deep brain stimulation, neural network, oscillations, cross-frequency coupling

1 Introduction

As the largest group of cholinergic neurons in the basal forebrain, the nucleus basalis of Meynert (NBM) is a crucial source of cholinergic efferents to the neocortex and plays an indispensable role in supporting vital brain functions, such as arousal, attention, multimodal encoding, visual processing, and experience-dependent cortical plasticity (Goard and Dan, 2009; Sanchez-Alavez et al., 2014; Liu et al., 2015; Ljubojevic et al., 2018; Martinez-Rubio et al., 2018; Meir et al., 2018; Wan et al., 2019). NBM dysfunction is implicated in multiple neuropsychiatric and neurological disorders, including Alzheimer's disease (AD), schizophrenia, Parkinson's disease (PD), Lewy body dementia (LBD), and Down syndrome (Williams et al., 2013; González et al., 2021; Mehraram et al., 2022; Schumacher et al., 2022). The involvement of the NBM may be a critical prodrome or an early molecular cascade event.

For instance, research has demonstrated that in AD, the earliest accumulation of neurofibrillary tangles (NFTs) occurs in the NBM, preceding the accumulation in the entorhinal cortex and locus coeruleus (Braak et al., 2011; Arendt et al., 2015; Chung et al., 2016; Hanna et al., 2020). Drugs that regulate the activity of cholinergic neurons in the NBM and its cortical efferent have been proposed as promising therapeutic approaches for various neurodegenerative diseases. However, current drugs targeting this pathway, including existing cholinesterase inhibitors, have limited efficacy and cannot halt or reverse neurodegenerative diseases (Yu et al., 2021). Based on advancements in neuromodulation technology, deep brain stimulation (DBS) has been proven to be the most effective strategy for treating neurodegenerative diseases due to its precise circuit-targeted neuromodulation (Krauss et al., 2021). Therefore, DBS has been approved by the Food and Drug Administration (FDA) for treating PD, essential tremor, dystonia and other movement disorders, and it has yielded satisfactory clinical outcomes and evidence (Krauss et al., 2021). In addition, DBS has been used to treat pain syndromes, such as neuropathic pain and cluster headache, as well as epilepsy (Pereira and Aziz, 2014; Lee et al., 2019). Based on the key role of the NBM in cognition, many published studies have focused on the effect of cognitive neuromodulation via DBS targeting the NBM (NBM-DBS) in various diseases (Kuhn et al., 2015; Gratwicke et al., 2018, 2020; Cappon et al., 2022; Sasikumar et al., 2022). A phase I clinical trial conducted by Kuhn et al. (2015) investigated the effects of NBM-DBS on the treatment of AD, revealing a mere 3-point deceleration in the rate of progression according to the Alzheimer's Disease Assessment Scale-Cognitive Subscale (ADAS-Cog) and an increase in cerebral cortical glucose metabolism revealed by [18F]-fluoro-desoxyglucose-PET at a 12-month follow-up. Davide Cappon et al. explored the effects of NBM-DBS in five Parkinson's disease dementia (PDD) patients, two of whom experienced slower cognitive decline; however, the Mini-Mental State Examination (MMSE) score still exhibited an annual mean decrease of 0.3 points at the 36-month follow-up (Cappon et al., 2022). However, studies from Sasikumar S and Gratwicke J found that NBM-DBS did not improve cognitive function in PDD patients (Gratwicke et al., 2018; Sasikumar et al., 2022). In addition, Gratwicke J found that although no consistent improvements were observed in exploratory clinical outcome measures for NBM-DBS, but the severity of neuropsychiatric symptoms reduced with NBM-DBS in 3 of 5 dementia with Lewy bodies (DLB) patients (Gratwicke et al., 2018).

The mechanisms of NBM-DBS have also been investigated recently in animal models of AD, and a variety of hypotheses have been proposed, such as regulating the cholinergic system (Hotta et al., 2009), modulating regional glucose metabolism (Wang et al., 2018), increasing regional cerebral blood flow (Adachi et al., 1990a,b), providing neuroprotective effects (Temel et al., 2006; Wallace et al., 2007) and regulating neural circuits (Singh et al., 2022). However, the significant treatment effects of NBM-DBS on cognitive dysfunction that have been observed in animal studies have not been replicated in clinical trials. Therefore, NBM-DBS is still in the preliminary stage of exploration.

The current review aims to provide a comprehensive update and summary of progress on cognition-related neural networks or circuits as well as the neuroanatomical and neurophysiological properties of the NBM. Additionally, this study aims to provide evidence from animal and clinical studies regarding the effect of NBM-DBS on cognitive dysfunction in various neurological diseases. The findings of this study will provide a basis for obtaining a precise understanding of the important and promising role of the NBM in neuromodulation.

2 Neural network oscillations related to cognition

Rhythmic neural electrical activity, also known as oscillations, has attracted research attention for nearly a century. Behavior-dependent oscillations are the result of dynamic interactions between intrinsic cellular and circuit properties within the brain and are ubiquitous in mammals (Berger, 1929; Berger, 1969; Llinas, 1988; Steriade, 2001; Laurent, 2002; Destexhe and Sejnowski, 2003). The neural network contains multiple frequency bands of oscillations, ranging from 0.05 Hz to 500 Hz, which are categorized as slow oscillations (<1.5 Hz), δ oscillations (1.5–4 Hz), θ oscillations (4–8 Hz), α oscillations (8–13 Hz), β oscillations (13–30 Hz), γ oscillations (30–80 Hz) and fast oscillations (>100 Hz) based on frequency (Jasper and Penfield, 1949; Nokia and Penttonen, 2022). Oscillations are currently thought to be shaped by the summations of thousands of neurons in a particular brain region (Engel et al., 2001; Varela et al., 2001). In normal cognitive processes, each oscillatory frequency band is associated with a specific behavioral or executive function. Studies have shown that the δ oscillation phase correlates with the reaction time of behavior and plays a role in neural group synchronization in multiple brain regions (Stefanics et al., 2010). In addition, these oscillations are often associated with resting states, and slow oscillations (<1 Hz) can trigger thalamically generated spindles (Amzica and Steriade, 1998). θ oscillations are believed to play a crucial role in almost all cognitive functions. Previous studies have revealed the key roles of these proteins in learning, memory and synaptic plasticity (Herweg et al., 2020; Senoussi et al., 2022). Additionally, it is common for pyramidal neurons to fire phase locking with θ oscillations, indicating their key roles in interconnecting various brain regions (Pare and Gaudreau, 1996; Buzsaki, 2002; Jacobs et al., 2007; Rutishauser et al., 2010). θ oscillations are also the fundamental bands for cross-frequency coupling (CFC), as they synchronizing with the gamma band in a phenomenon known as θ–γ cross-frequency coupling; the role of θ–γ cross-frequency coupling in working memory has been extensively studied (Lisman and Jensen, 2013). α oscillations are also the most widely understood frequency bands, mostly due to their well-defined roles in attention needs and visual perception (Başar et al., 1997; Klimesch, 2012). β oscillations are often associated with motor-induced events (Pittman-Polletta et al., 2018). Synchronization of β oscillations has always been an indicator of normal motor system function and has also been shown to play a role in working memory (Schmidt et al., 2019). Finally, γ oscillations also play a crucial role in memory, as observed in the θ-γ coupled oscillations throughout the hippocampus and cortex (Lisman and Buzsaki, 2008).

Although each frequency band appears to be separated into a variety of behavioral or cognitive functions, synchronization between different bands through CFC analysis has provided new insights into the complexity of neural networks (Palva and Palva, 2007). CFCs are thought to be integral to the spatiotemporal activation of specific cortical circuits (Canolty and Knight et al., 2010; Yakubov et al., 2022). For example, phenomena such as the θ-γ phase-amplitude (p-a) CFC – which refers to the γ amplitude modulated by the θ phase (Bragin

et al., 1995; Montgomery et al., 2008; Colgin et al., 2009; Sakalar et al., 2022) and is known for its crucial role in working memory and memory formation in the hippocampal CA1 region – are among the many modes of CFCs (Lisman and Jensen, 2013). By optogenetic selectively targeting fast-spiking GABAergic interneurons in the barrel cortex *in vivo*, Cardin JA et al. tested whether the synchronous activity of fast-spiking GABAergic interneurons generates γ oscillations, which produce rhythmic inhibitory postsynaptic potentials (IPSPs) to distal dendrites of local pyramidal neurons; their findings showed that the rhythmic inhibition produced excitatory neural ensemble synchrony to process information (Cardin et al., 2009). Sakalar E et al. found that neurogliaform cells (NGFCs), which form synaptic connections with excitatory neuronal ensembles, lead to delayed synchronous firing; moreover, this delay leads to GABAergic inhibition to excitatory neural ensembles when information processing is complete, thereby resulting in actively disengaged excitatory neural ensemble synchronization that enables the formation of new patterns of information processing (Sakalar et al., 2022). These findings represent compelling examples of the significance of cell type-specific activation in rhythmic neural electrical activity and provide a reference for research on the mechanism underlying neural networks. Based on these studies, we constructed a schematic diagram of how θ-γ p-a CFC regulates neuronal firing patterns and cognitive processes (Figure 1).

The cholinergic system plays a key role in controlling neural oscillations throughout the brain and cortical structures (Semba and Fibiger, 1989). Cholinergic neurons suppressed specific low-frequency oscillations, including δ, θ, and α oscillations, while high-frequency oscillations, such as β and γ oscillations, were accompanied by increased acetylcholine release in the thalamus and cortex (Steriade, 2004). Furthermore, cholinergic neurons appear to play a crucial role in influencing θ oscillations in the hippocampus. Acetylcholine (ACh) levels are directly related to θ oscillations in hippocampal neurons and have a direct effect on the amplitude of θ waves (Danışman et al., 2022). θ-γ p-a CFC also appears to rely heavily on ACh modulation, with detected cues evoking phasic ACh release as well as neuronal synchrony across several frequency bands and the emergence of θ-γ coupling (Howe et al., 2017). It is reasonable to assume that the NBM, as the largest group of cholinergic neurons in the basal forebrain, plays an independent role in the regulation of nerve concussion. Although the NBM acetylcholine system has an important influence on neural network oscillations, as shown by Rodriguez R et al., the cholinergic system may also regulate neural network oscillations through muscarinic receptors in addition to nicotinic receptors (Rodriguez et al., 2004), indicating that other types of NBM neurons or receptor components also play an important role in the generation and regulation of neural network oscillations. There are few relevant studies, which need to be explored in the future.

3 Anatomy and electrophysiology properties of the NBM

3.1 Anatomy of the NBM

The basal forebrain is one of the four regions containing cholinergic neurons in the mammalian brain (the others being the brainstem, striatum, and limbic system). This region is anatomically situated above the optic nerve, below the anterior commissure and medially adjacent to the lateral ventricular wall, and it includes the medial septal nucleus (MS), the diagonal band of the Broca nucleus (DBB) (with vertical and horizontal branches), the preoptic nucleus, the basal ganglia (NB) and the anonymous substance (SI) (Woolf, 1991). Mesulam et al. investigated acetyl cholinergic neurons in nonhuman primate brain tissue and introduced the Ch1-Ch4 nomenclature to classify four distinct cholinergic neuron groups located in the basal forebrain. Ch1 corresponds to the MS; many of its neurons are embedded among the fibers of the precommissural fornix, and approximately 10% of its neurons are cholinergic, thus providing a substantial projection to the hippocampus (Figure 2). Ch2 corresponds to the vertical limb of DBB; at least 70% of its neurons are cholinergic, and they merge with the Ch1 cell group dorsally and with Ch3 and Ch4 ventrally. Furthermore, Ch2 is the major source of innervation that the hippocampus and hypothalamus receive from the basal forebrain (Figure 3). The Ch3 group most closely corresponds to the horizontal limb of the DBB. It extends from the septal-preoptic region medially to the amygdaloid region laterally. Only 1% of its neurons can definitely be proven to be cholinergic; furthermore, this group is the major source of basal forebrain projections to the olfactory bulb (Figure 4) (Mesulam et al., 1983, 1984).

Ch4 encompasses a complex network of basal nuclear giant cells, including the substantia innominate (SI), NBM, preoptic nucleus, and ventral pallidum. Ch4 is further divided into five subregions: the anterior portion (Ch4a), which is subdivided into anteromedial (Ch4am) and anterolateral (Ch4al) regions; the middle portion (Ch4i), which is subdivided into dorsal middle (Ch4id) and ventral middle (Ch4iv) regions; and the posterior portion (Ch4p). (Mesulam et al., 1983) In humans, the Ch4 nucleus is situated in the posterior region of the basal forebrain and measures approximately 13–14 mm in length and 16–18 mm in width. However, a distinct subregion known as Ch4ai exists between Ch4a and Ch4i within the human brain; this subregion may have emerged due to an increased demand for cholinergic neurons and projection fibers to accommodate the expanded lateral surface area of the neocortex during the evolution of primates into *Homo sapiens* (Mesulam and Geula, 1988). Liu et al. (2015) proposed a conceptual definition for the anterior, intermediate and posterior subsectors of the human Ch4 to simplify its original classification. The anterior division of Ch4 (Ch4a) is situated laterally to the supraoptic nucleus and ventrally to the anterior commissure. The intermediate division (Ch4i) is located in the inferior part of the globus pallidus, medially adjacent to the lateral end of the anterior commissure. At this level, the intermedullary lamina divides the globus pallidus into internal and external components, with the lateral end of the anterior commissure located ventral to the putamen and sometimes the infundibulum visible. The posterior division (Ch4p) is anatomically connected to the globus pallidus medially and superiorly, the putamen laterally and superiorly, and the amygdala inferiorly; furthermore, Ch4p passes through the optic tract medially (Figure 5) (Liu et al., 2015).

Mesulam MM et al. utilized HRP retrograde tracer and acetylcholinesterase (AChE) colocalization technology to effectively demonstrate that cortical topographical innervations originate from distinct subregions of CH4 in the macaque brain. In summary, Ch4a cells innervate limbic regions. Specifically, Ch4am projects to medial cortical regions such as the cingulate cortex, while Ch4al targets fronto-parietal opercular regions and the amygdala. Additionally, Ch4p is responsible for superior temporal and temporal polar regions,

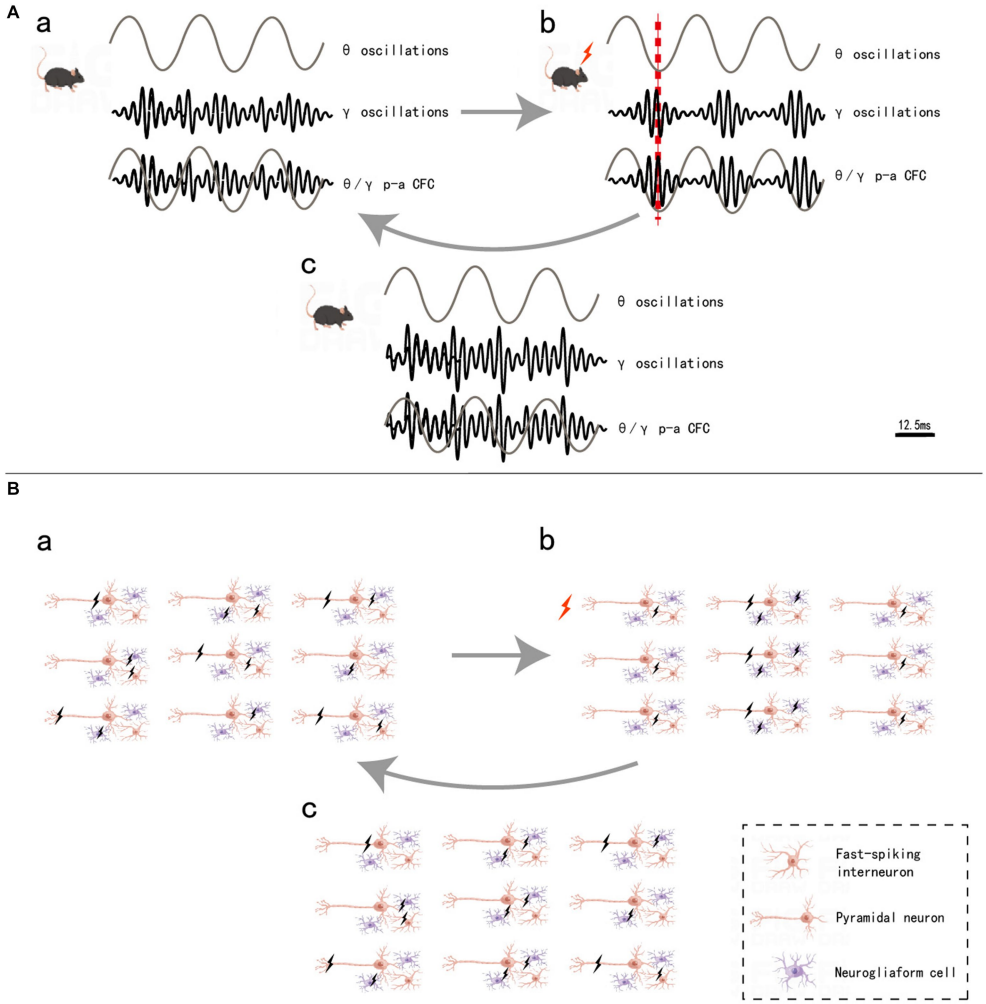

FIGURE 1
θ/γ p-a CFC regulation **(A)** and neuronal firing pattern **(B)**. a, in mice without stimulation, θ oscillations did not form coupling with γ oscillations **(A)**, and the firing of the three types of neurons was irregular **(B)**. b, when mice are stimulated, the fast-spiking interneurons synchronous firing (IPSP) causes γ oscillations, θ oscillations and γ oscillations, thus leading to θ-γ p-a CFC **(A)**. The pyramidal neurons, which are inhibited by GABA released by interneurons, do not fire, while the uninhibited pyramidal neurons form an ensemble and fire synchronously, completing the information encoding. Additionally, neurogliaform cells that form synaptic connections with this pyramidal neuronal ensemble also form delayed synchronous firing **(B)**. c, after a very short interval when the information processing is done, the delayed synchronous firing from neurogliaform cells cause the release of GABA from the synaptic, which inhibits the pyramidal neuronal ensemble and stops fire **(B)**, and decouples of the θ-γ p-a CFC and return to state awaiting to receive new information **(A)**. Black lightning bolt, neuronal firing, red lightning bolt and red dashed line, the moment when mice are stimulated.

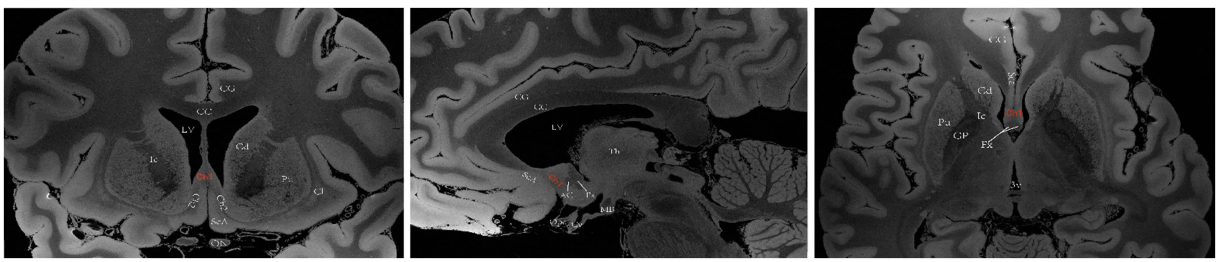

FIGURE 2
A diagram depicting the location of the human Ch1 on MRI. Images sourced from https://openneuro.org/datasets/ds002179/versions/1.1.0 (Marceglia et al., 2021). Ch1 represents the cholinergic component of MS. Coronal (left), sagittal (middle), axial (right). LV lateral ventricle, CG cingulate gyrus, 3 V third ventricle, Fx Fornix, Th thalamus, Cd caudatum, Cl claustrum, Gp globus pallidus, Pu putamen, Ic Internal capsule, ON optic nerve, Opc optic chiasma, CC corpus callosum, ScA subcallosal area, AC anterior commissure, MB mamillary body, Cy cyathus.

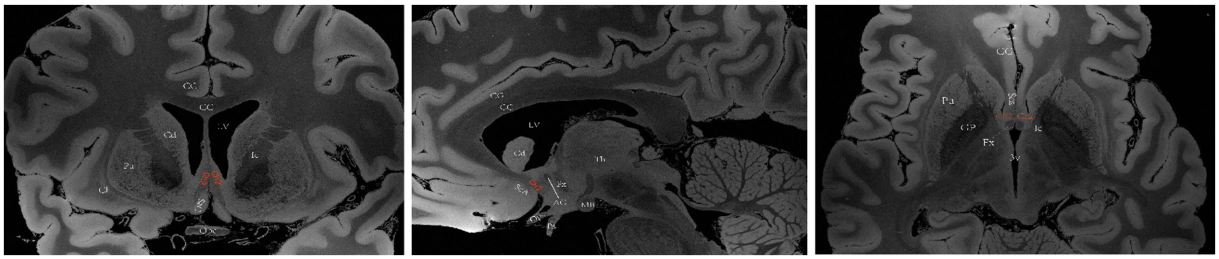

FIGURE 3
A diagram depicting the location of the human Ch2 on MRI. Images sourced from https://openneuro.org/datasets/ds002179/versions/1.1.0. (Marceglia et al., 2021) Ch2 corresponds to the cholinergic component of the vertical branch of DBB. Coronal (left), sagittal (middle), axial (right). LV lateral ventricle, CG cingulate gyrus, 3 V third ventricle, Fx Fornix, Th thalamus, Cd caudatum, Cl claustrum, Gp globus pallidus, Pu putamen, Ic Internal capsule, Opc optic chiasma, CC corpus callosum, ScA subcallosal area, AC anterior commissure, MB mamillary body, Ps pituitary stalk.

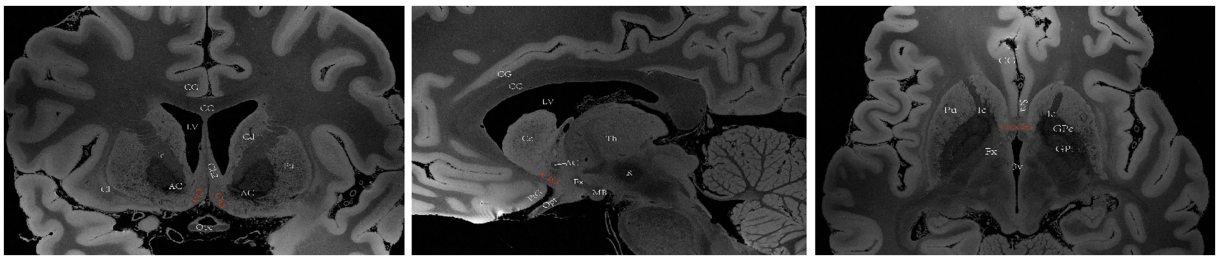

FIGURE 4
A diagram depicting the location of the human Ch3 on MRI. Images sourced from https://openneuro.org/datasets/ds002179/versions/1.1.0.33 (Marceglia et al., 2021). Ch3 refers to the cholinergic component of the horizontal branch of DBB. Coronal (left), sagittal (middle), axial (right). LV lateral ventricle, CG cingulate gyrus, 3 V third ventricle, Fx Fornix, Th thalamus, Cd caudatum, Cl claustrum, GPi internal globus pallidus, GPe external globus pallidus, Pu putamen, Ic Internal capsule, Opt optic tract, Opc optic chiasma, PtG paraterminal gyrus, CC corpus callosum, ScA subcallosal area, AC anterior commissure, MB mamillary body, R red nucleus.

while Ch4i covers all remaining cortical areas (Mesulam et al., 1983). By examining human cadaveric brain tissue sections and performing diffusion tensor imaging (DTI) studies, it was discovered that cholinergic efferent fibers originating from the NBM converged into medial and lateral bundles before diffusing throughout the target cortex. The medial bundle fibers converge toward the rostrum of the corpus callosum, penetrate into the cingulate gyrus, and extend posteriorly to reach the splenium and retrosplenial white matter. These axons emanate from the bundle to innervate various regions, including the medial orbitofrontal cortex, subcallosal cortex, cingulate cortex, pericingulate cortex and retrosplenial cortex. The lateral bundle comprises two additional divisions. The capsule division traverses the external capsule and projects fibers to the amygdala and temporal cortex, while the perisylvian division initially enters white matter surrounding the claustrum before radiating laterally to innervate the frontoparietal cortex, superior temporal gyrus, and insula (Selden et al., 1998; Hong and Jang, 2010).

Notably, not all magnocellular neurons in the basal forebrain are cholinergic, and basal forebrain cholinergic neurons are interspersed with noncholinergic neurons and distributed across these nuclei. Therefore, the terms NBM and Ch4 cannot be used interchangeably. Additionally, NBM afferent fibers are primarily derived from the central amygdala, with additional nonsensory and nonmotor cortical input originating from the orbitofrontal cortex, anterior insular lobe, temporal pole, entorhinal cortex, and medial temporal lobe. Subcortical input is received from the diencephalon (midthalamic nucleus and lateral hypothalamus) as well as brainstem structures such as the tegmental area of the midbrain, pontine reticular formation, and nucleus tractus solitarius. These synaptic inputs to the NBM include cholinergic, catecholaminergic, and γ-aminobutyric acid (GABA) axons (Jones et al., 1976; Woolf and Butcher, 1982; Russchen et al., 1985; Kasa, 1986; Mesulam and Geula, 1988; Jones and Cuello, 1989; Smiley and Mesulam, 1999; Zheng et al., 2018). From an anatomical perspective, in addition to emitting cholinergic projection fibers to the neocortex, the NBM also forms bidirectional projections with numerous structures within the limbic system and Papez loops.

3.2 Electrophysiology properties of the NBM

Cholinergic neurons in the NBM possess a resting membrane potential of approximately −45 mV and are equipped with voltage-gated ion channels, including fast-activated and rapidly inactivated Na + channels as well as fast-activated and delayed rectification K+ channels (Song et al., 2013; Morelli et al., 2017). Additionally, these neurons are equipped with various ligand-gated ion channels, such as ACh, nicotinic receptors (Morelli et al., 2017), muscarinic receptors (Khateb et al., 1993), epinephrine α1 and β receptors (Fort et al., 1995), histamine H1 and H2 receptors (Khateb et al., 1995; Knoche et al., 2003; Luo and Leung, 2009) and GABA receptors (Khateb et al., 1998; Manfridi et al., 2001). These properties enable the NBM to respond excitably or inhibitably to various neuromodulators, including ACh, nerve growth factor (NGF), estrogen, GABA and

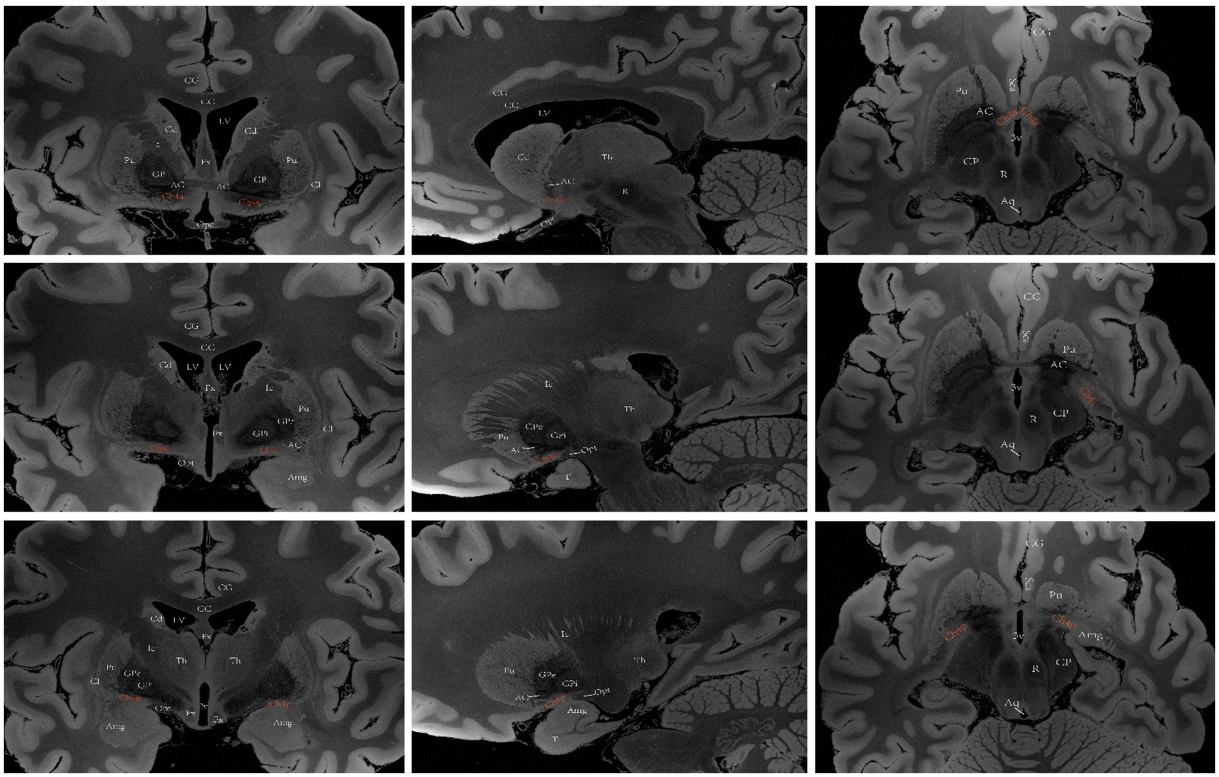

FIGURE 5
A diagram depicting the location of the human Ch4 on MRI. Images sourced from https://openneuro.org/datasets/ds002179/versions/1.1.0.33 (Marceglia et al., 2021). Coronal (left), sagittal (middle), axial (right). Ch4a (top), Ch4i (middle), Ch4p (bottom). LV lateral ventricle, CG cingulate gyrus, 3 V third ventricle, Fx Fornix, T temporal lobe, Th thalamus, Cd caudatum, Cl claustrum, Gp globus pallidus, GPi internal globus pallidus, GPe external globus pallidus, Pu putamen, Ic Internal capsule, Opt optic tract, Opc optic chiasma, CC corpus callosum, ScA subcallosal area, AC anterior commissure, Amg Amygdala, CP cerebral peduncle, Aq aqueduct of midbrain, R red nucleus.

dopamine. Cholinergic neurons in the NBM account for approximately 5% of all neurons in this region and exhibit high-frequency pulse bursts that have been shown to be correlated with cortical activation, including cortical γ and θ oscillations; these bursts occur during both awake (AW) and paradoxical sleep (PS) states but are almost completely absent during slow-wave sleep (SWS) (Lee et al., 2005). Spencer JP et al. examined the induction of γoscillations in rat hippocampal slices by AChE inhibitors *in vitro* (Spencer et al., 2010). Chernyshev BV et al. discovered a significant negative correlation between cortical δ oscillation power and the spontaneous firing rate of cholinergic neurons in the NBM by simultaneously recording basal forebrain cholinergic cell firing rates and frontal lobe EEG in spontaneous behavior rabbits; the results indicated that cortical δ oscillation power can serve as an indicator of the activity of cholinergic neurons in the NBM (Chernyshev et al., 2004). These studies demonstrated the indispensable role of ACh pathways in maintaining normal neural network function.

4 The role of the NBM in neural network activation and modulation

4.1 Evidence from NBM injury animal models

An increasing number of researchers have focused on alterations in neural network oscillations in numerous animal models of NBM injury (Table 1). These findings indicated that NBM lesions caused some consistent changes in neural network oscillations: (1) an increase in the total power of electroencephalography (EEG), particularly in low-frequency bands (δ and θ); (2) a significant decrease in high-frequency oscillations, especially in the γ band; and (3) a reduction in event-related oscillation (ERO) phase-locking index (PLI) (Berntson et al., 2002; Rispoli et al., 2004, 2008, 2013; Sanchez-Alavez et al., 2014; Sanchez-Alavez and Ehlers, 2016). Despite these consistent changes, Rispoli et al. (2013) performed a quantitative EEG (qEEG) analysis of θ oscillations in the hippocampus and the entire EEG spectrum in the cerebral cortexes of rats with bilateral NBM lesions induced by 2-amino-3-(3 hydroxy-5-methylisoxazol-4-yl)-propionic acid (AMPA); the results showed increased power of θ oscillations in the frontal parietal cortex but not in the hippocampus, indicating that the EEG effect of NBM lesions might depend on brain regions. Ljubojevic et al. (2018) reported that the accuracy of visual and olfactory target detection was lower in rats with NBM lesions induced by the selective cholinergic immunotoxin 192 IgG-saporin than in healthy controls; furthermore, the detection accuracy was correlated with decreased local field potential (LFP) coherence in the β range between the prefrontal and posterior parietal cortex and with decreased β power in the posterior parietal cortex before the target's appearance. Ciric et al. (2016) performed sleep EEG monitoring and found that δ-amplitude attenuation in the sensorimotor cortex during rapid eye movement sleep (REMS) was the earliest indication following bilateral NBM lesions induced by ibotenic acid (IBO) (Ciric et al., 2016). Similarly, Chernyshev et al. (2004)

TABLE 1 Effects of the NBM on the neural network –evidence from NBM injury animal models.

Study	Subjects (n), NBM lesion method	Recording method	Results
Knox and Berntson (2008)	Sprague–Dawley rats (24), the selective cholinergic immunotoxin 192 IgG-saporin	Prefrontal and retrosplenial cortex EEG	During anxiety-like states, increases in the γ power/δ power ratio and augmented θ power were observed on prefrontal and retrosplenial cortical EEGs. NBM lesions attenuated anxiety-like states and the γ power/δ power ratio but had no effect on increased θ power. The effect of NBM lesions on the γ power/δ power ratio was influenced by the effect of increased δ power after lesions.
Ljubojevic et al. (2018)	Long-Evans rats (20), the selective cholinergic immunotoxin 192 IgG-saporin	Prelimbic frontal cortex (PFC) and the posterior parietal cortex (PPC) LFP	Accurate detection of visual and olfactory targets was associated with increased LFP coherence in the β range, between the PFC and PPC, and with increased β power in the PPC before the target's appearance in sham-lesioned rats. Readiness-associated changes in brain activity and visual and olfactory target detection were attenuated in the NBM lesion group.
Berntson et al. (2002)	Sprague–Dawley rats (19), the selective cholinergic immunotoxin 192 IgG-saporin	Frontoparietal dural surface EEG	Relative to sham-lesioned control animals, the NBM lesion group displayed a significant reduction in high frequency activities on EEG, characterized especially by a reduction in γ power.
Ciric et al. (2016)	Wistar Rats (15), IBO	Sensorimotor cortex EEG	EEG δ amplitude attenuation within sensorimotor cortex during rapid eye movement sleep (REMS) was the earliest sign of aging in the NBM lesion.
Rispoli et al. (2013)	Rats (7), AMPA	Frontoparietal cortex and hippocampus CA1 region EEG	In the NBM lesion group, compared with the control group, an increased θ power in the cortex and a reduced θ rhythm oscillation in the hippocampus were found. In rats with NBM lesions, Hup-A, a selective AChE inhibitor isolated from *Huperzia serrata*, was able to restore EEG architecture, producing cortical desynchronization and reduction in θ power. However, in the hippocampus, this drug increased θ oscillation and reduced the impairment in attention/working memory as well as spatial navigation performance in the behavioral tasks.
Rispoli et al. (2008)	Rats (7), AMPA	Frontoparietal cortex EEG	Bilateral NBM lesions induced an increase of the total EEG power, particularly in δ and θ power, and high-voltage spindle activity the systemic administration of choline pivaloyl esters (CPE) for 3 weeks reversed the above EEG changes.
Rispoli et al. (2004)	Rats (7), AMPA	Frontoparietal cortex EEG	Choline pivaloyl esters (CPE) induced EEG desynchronization, leading to a significant decrease in the total EEG power, especially in the lower frequency δ and θ bands.
Sanchez-Alavez and Ehlers (2016)	Wistar rats (18), AMPA	Frontal cortex EEG and auditory stimuli-ERO	NBM lesions resulted in an increase in auditory stimuli-ERO power in the δ, θ, α and β bands as well as an increase in PLI in the θ band.

n, number of participants or samples; AChE, acetylcholinesterase; LFP, local field potential; IBO, Ibotenic acid; AMPA, 2-Amino-3-(3-hydroxy-5-methylisoxazol-4-yl) propionic acid; EROs, event-related oscillations; PLI, phase locking index; REMS, rapid eye movement sleep.

reported a significant negative correlation between cortical δ power and the spontaneous firing rate of cholinergic neurons in the NBM through simultaneous recordings of basal forebrain cholinergic cell firing rates and frontal lobe EEG signals in spontaneous behavior rabbits (Chernyshev et al., 2004). These two studies above indicating that cortical δ oscillation power can serve as an indicator of the activity of cholinergic neurons in the NBM, and future targeted studies are needed to verify this association and explain the underlying mechanisms. Rispoli et al. (2013) examined the use of Huperzine A, a natural selective AChE inhibitor; after this inhibitor was intraperitoneally injected into rats with NBM lesions, the EEG architecture was partially reversed, and desynchronization and reduced θ-power were observed in the frontal and parietal cortexes. Spencer et al. (2010) revealed that the use of AChE inhibitors induced γ oscillations in rat hippocampal slices *in vitro*. These two studies provide further evidence regarding the indispensable role of ACh pathways in the maintenance of normal neural network functioning within the hippocampus.

4.2 Neuromodulation effects of NBM-DBS in animal models

Due to the challenges of current drug therapy and the confirmed mechanism of neural network dysfunction in neurodegenerative diseases, there is an urgent need for research on neuromodulation strategies, especially NBM-DBS. Previous animal studies have provided evidence that NBM-DBS could improve cognitive function in AD models, for example, Liu et al. (2018) showed that NBM-DBS could improve performance in monkeys on a continuous performance task, Lee et al. (2016), Nagasaka et al. (2017), and Huang et al. (2019) demonstrated that NBM-DBS could improve spatial memory performance in AD mice, as assessed by Morris water maze. While these animal studies have focused on behavioral outcomes, cellular and molecular mechanisms, and neural network effects. Relatively consistent findings indicate that NBM-DBS leads to decreased power in θ and α oscillations but increased power in γ oscillations in the visual and auditory cortexes and prefrontal cortex (Table 2) (McLin et al., 2002,

TABLE 2 Neuromodulation effects of NBM-DBS in animal models.

Study	Subjects (n), DBS parameters	Recording method	Results
Goard and Dan (2009)	Long-Evans rats (49), NBM-DBS delivered for 500 ms/trial with 100 Hz and pulse width 100 μs	Primary sensory cortex (V1) LFP simultaneous with NBM-DBS	NBM-DBS caused a marked change in the power spectrum of LFP of V1 area, with an increase in power at 10 to 100 Hz (particularly in the γ band, 30 to 50 Hz) and a decrease at low frequencies (<10 Hz). As quantified by the power ratio (LFP power at 10 to 100 Hz divided by that at 1 to 10 Hz), this effect on spontaneous cortical activity lasted for 5 to 10 s.
Singh et al. (2022)	Rhesus monkeys (2), NBM-DBS delivered for 15 s/trial with 80 Hz pulse amplitude 0.2 mA, width 100 μs	Prefrontal cortex LFP after a trial of NBM-DBS	NBM-DBS decreased α power during the delay interval of working memory tasks. No modulation was observed in the γ power in the delay interval of working memory tasks, which has previously been implicated in the maintenance of working memory.
Dezawa et al. (2021)	NBM injury rats (5) with immunotoxin 192 IgG-saporin, NBM-DBS delivered for 500 ms/trial with 100 Hz and pulse amplitude 0.1 mA, width 100 μs	Primary somatosensory cortex (S1) sensory stimuli-ERO after a trial of NBM-DBS and forepaw stimulation	NBM-DBS facilitated ACh release in the S1 subregion and suppressed subsequent sensory stimuli-ERO to forepaw stimulation.
McLin 3rd et al. (2002, 2003)	Sprague–Dawley rats (7), NBM-DBS delivered for 300 ms/trial, 200 trials/day for 14 days, with 100 Hz and pulse amplitude 0.1 mA, width 200 μs	Auditory cortex EEG after 14 days of NBM-DBS	NBM-DBS decreased θ and α power and increases in γ power for several seconds during and after 6 kHz tone presentation.
Weinberger et al. (2006)	Sprague–Dawley rats (11), NBM-DBS delivered for 200 ms/trial, with 100 Hz and pulse width 200 μs, amplitude 47 or 66 μA	Auditory cortex EEG after a trial of NBM-DBS	NBM-DBS produced a reduction of low frequency power (δ, θ, and α) and an increase in high frequency power, β2 and especially γ waves; (2) the moderate level of stimulation (66 μA) produced a longer duration of α power reduction than did the weaker level of stimulation (47 μA).
Schumacher et al. (2021)	Adult cats (11), NBM-DBS delivered for 4 s/trial, with 50 Hz and pulse width 50 μs, amplitude 100 μA	S1 and visual cortex LFP after a trial of NBM-DBS	(1) NBM-DBS shifted LFP activity from high amplitude-low frequency (asleep-like pattern) to low amplitude-high frequency activity (awake-like pattern); (2) NBM-DBS increased cortical NO, which was blocked by systemic NOS inhibition, and the ability of NBM-DBS to induce cortical LFP activation was severely impaired after blocking NOS activity, suggesting that the NBM is involved in the arousal mechanism through the NO pathway.

n, number of participants or samples; NO, nitric oxide; NOS, nitric oxide synthase; V1, primary sensory cortex; S1, primary somatosensory cortex; ACh, acetylcholine; LFP, local field potential; EROs, event-related oscillations.

2003; Weinberger et al., 2006; Goard and Dan, 2009; Singh et al., 2022). In addition, Dezawa et al. (2021) reported that NBM-DBS facilitated the release of ACh in the primary somatosensory cortex (S1) of rats with NBM lesions and partially reversed the increase in the peak LFP amplitude in S1 after forepaw stimulation. Goard M et al. performed NBM-DBS on healthy rats and recorded the LFP and neuron spike rate in the primary sensory cortex (V1); the findings revealed that (1) NBM-DBS induces notable changes in the power spectrum of the V1 LFP, including increased γ band power and decreased power at low frequencies (<10 Hz), and (2) NBM-DBS leads to prominent decorrelation among neurons and marked improvement in the reliability of neuronal responses to natural scenes by analyzing each single-neuron response to 30 repeats of a natural movie (Goard and Dan, 2009).

4.3 Evidence of the role of the NBM in neuromodulation from clinical cases

In recent years, many studies have performed qEEG analysis on clinical patients with diseases related to NBM lesions (Table 3). Wan et al. (2019) examined the role of NBM-visual cortex functional connectivity in α reactivity by analyzing simultaneous EEG-multimodal MRI data from cohorts of young and older adults; the results showed that the decrease in α reactivity in older adults was associated with a reduced volume of the fiber bundles connecting the NBM to the visual cortex quantified by leukoaraiosis volume. Similarly, patients with AD (Schumacher et al., 2020) and DLB (Rea et al., 2021) also exhibited decreased α reactivity, which was correlated with a reduced volume of NBM. Furthermore, Schumacher et al. (2021) found that, compared to healthy controls and MCI-AD patients, MCI-DLB patients generally displayed a slower EEG background due to shifts in power from the β and α bands to the preα and θ bands, which was also linked to decreased NBM volume. The evidence above suggests that general sluggishness of EEG signals, an increase in energy at slow frequencies, and a decrease in α reactivity are common characteristics in the process of both natural aging and neurodegenerative diseases and may be associated with lesions of the NBM and its projected fibers. However, the observed decrease in γ oscillation power in animal models with NBM lesions has not been replicated in humans. This may be due to the poor spatial resolution

TABLE 3 Effects of the NBM on the neural network: evidence from clinical cases.

Study	Subjects (n)	Recording method	Results
Wan et al. (2019)	Healthy young adults (21) and older adults (40)	Simultaneous EEG-fMRI	Lesions of the fiber tracts linking NBM and the visual cortex quantified by leukoaraiosis volume were revealed in older adults and found to be associated with reduced α reactivity.
Oswal et al. (2021)	Patients with PDD (6) and patients with DLB (5)	MRI, MEG and NBM-LFP	NBM-cortical structural and functional connectivity were correlated within spectrally segregated networks, including the following: (1) a β band network to supplementary motor area, and activity in which was found to drive the β band activity in the NBM; (2) a δ/θ band network to medial temporal lobe structures encompassing the parahippocampal gyrus and visual areas including lingual gyrus, revealed that NBM networks are likely to subserve in motor control, memory and visual function, respectively.
Schumacher et al. (2020)	Patients with LBD (including 24 patients with DLB and 17 with PDD), AD (21), and healthy controls (40)	EEG and MRI	α reactivity was reduced in AD and LBD patients compared to healthy controls, and a significantly greater reduction was observed in LBD patients than in AD patients. Reduced α reactivity was associated with decreased volumes of the NBM across all groups, especially in the PDD group.
Schumacher et al. (2021)	Patients with MCI-DBL (37), patients with MCI-AD (34), and healthy controls (31)	EEG and MRI	There was a general slowing of the EEG in MCI-DBL patients compared to healthy controls and MCI-AD by a shift in power from β and α bands toward slower frequencies of the preα and θ bands, and a greater reduction in NBM volume was correlated with more severe EEG slowing.
Rea et al. (2021)	Patients with PDD (31), patients with MCI (21), and healthy controls (21)	EEG and MRI	(1) PDD patients showed increased power in the pre-α band (5.5–8 Hz) and reduced α reactivity compared to healthy controls; (2) the volumes of cholinergic cell clusters corresponding to the MS, vertical and horizontal branches of the diagonal band, and the posterior NBM, were positively correlated with α reactivity in patients with PD and pre-α power in patients with MCI.
Nazmuddin et al. (2018)	Patients with PDD (2) who underwent bilateral GPi-DBS with one or more electrodes close to or inside the NBM	EEG and NBM-LFP	PDD patients showed increased δ power in the NBM region and decreased temporal cortical connectivity compared to its proximal structures, including the GPi.
Lee et al. (2019)	Patients with MCI-PDD (5) who underwent bilateral NBM/GPi-DBS	Firing rates	In MCI-PDD patients off medication, the neuronal discharge rates were specific to each area, populated by GPi cells (92.6 ± 46.1 Hz), border cells (34 ± 21 Hz), and NBM cells (13 ± 10 Hz), and during the oddball task, firing rates of NBM cells were decreased (from 2.9 ± 0.9 Hz to 2.0 ± 1.1 Hz).
Cappon et al. (2022)	Patients with PDD (6) and DLB (5) who underwent NBM/GPi-DBS	NBM/GPi-LFP, MEG and EEG	(1) a θ band (2–8 Hz) network linking the NBM/GPi to temporal cortex, and a β band (13–22 Hz) network linking the NBM/GPi to sensorimotor cortex; (2) power of the low β (13–22 Hz) band was significantly higher in the GPi in PDD patients compared to DLB, and coherence in the high β (22–35 Hz) band between the GPi and lateral sensorimotor cortex was significantly higher in DLB patients compared to PDD.
Kuhn et al. (2015)	Patients with mild to moderate AD (6) who underwent NBM-DBS	EEG and PET	A decrease in α power and an increase in θ power after NBM-DBS was observed in only one patient; for all the other patients, no significant changes were observed in EEG frequency power after NBM-DBS.

n, number of patients; LFP, local field potential; PDD, Parkinson's disease dementia; DLB, dementia with Lewy bodies; LBD, Lewy body dementia (LBD), which includes DLB and PDD; MCI, mild cognitive impairment; GPi, globus pallidus.

of EEG analysis in humans, which reduces the accuracy of local cortical function represented by γ oscillations compared to LFPs generally applied in animal models.

With the development of advanced techniques such as fMRI and LFP recording by microelectrodes in NBM-DBS, the NBM neural network can now be explored in greater depth in patients with neurodegenerative diseases. Oswal et al. analyzed the LFP of NBMs with DBS electrodes recorded from PDD (6 patients) and DLB (5 patients) patients treated with NBM-DBS, along with MEG and MRI tractography, to explore the intersection between the NBM neural network and fiber junction (Oswal et al., 2021). First, a β band network strongly related to the projection fiber from the supplementary motor area to the NBM was identified, indicating that the supplementary motor region might be the driver of NBM activity. Then, a δ/θ band network was further identified to be strongly related to the projection fiber from the NBM to the

parahippocampal gyrus and lingual gyrus, which might play important roles in memory and visual function. Lee DJ et al. observed distinct neuronal discharge rates in internal globus pallidus (GPi) cells (92.6 ± 46.1 Hz), border cells (34 ± 21 Hz), and NBM cells (13 ± 10 Hz) by performing microelectrode recordings through the GPi and NBM in five PDD patients who received bilateral GPi/NBM-DBS. In addition, the oddball task significantly reduced the discharge rate of NBM cells (from 2.9 ± 0.9 to 2.0 ± 1.1 Hz, $p < 0.05$) (Lee et al., 2019). Nazmuddin M et al. recorded LFP in two PDD patients who underwent GPi-DBS with microelectrodes in the GPi and one or more distal contacts close to or inside the NBM and found that δ (1–4 Hz) oscillations were more prominently present in the NBM region than in its vicinity (Nazmuddin et al., 2018). Considering the negative correlation between δ oscillations and spontaneous discharge of cholinergic neurons in the NBM in an NBM lesion animal model (Chernyshev et al., 2004), the often-ignored δ oscillations can serve as a potential indicator of the specific effects and mechanisms of the NBM on neural network oscillations. In the phase I clinical trial of NBM-DBS for AD patients completed by Kuhn J et al., a positive effect was observed in slowing the decline in ADAS-Cog and increasing cortical glucose metabolism on FDG-PET. However, regarding neural network changes, only one patient exhibited significantly decreased power of α oscillations, and the expected increase in high-frequency oscillation power was not observed. (Kuhn et al., 2015) The possible reason is bias due to the small clinical sample size, while another possible reason that cannot be ignored is the complex relationship between neural network oscillations and different types of cholinergic receptors in the cortex. As shown in the study by Rodriguez R et al., cortical muscarinic receptors can also regulate neural networks (Rodriguez et al., 2004), so the effect of NBM-DBS must be affected simultaneously by the muscarinic and nicotine receptors, and the changes of cortical cholinergic receptor types are different in different neurodegenerative diseases (Graham et al., 2002).

4.4 Effects of the NBM in arousal, sleep, and epilepsy

Luo T et al. reversed the frontal EEG inhibition effect of isoflurane by stereotactically injecting histamine into the NBM of anesthetized rats under isoflurane, resulting in a shift from burst inhibition to δ activity, which can be blocked by NBM premicroinjection with an H1 receptor antagonist but not by an H2 receptor antagonist (Luo and Leung, 2009). Similarly, Marino J et al. discovered that cortical nitric oxide (NO) was elevated after basal forebrain electrical stimulation but could be inhibited by systemic nitric oxide synthase (NOS). Additionally, blocking the activity of NOS in the sensory cortex of anesthetized cats significantly weakened the ability of basal forebrain electrical stimulation to induce cortical activation, as evidenced by decreased low-frequency high-amplitude oscillatory activity and increased high-frequency low-amplitude activity (Marino and Cudeiro, 2003). Manfridi's study on sleep EEG in rats revealed that the activation of $GABA_A$ and $GABA_B$ receptors in NBM neurons led to increased SWS time and decreased wake time and that only the activation of $GABA_A$ receptors led to decreased REMS time (Manfridi et al., 2001). Berdiev et al. (2007) discovered that in the WAG/Rij rat (a model of absence epilepsy), NBM lesions (induced by the selective cholinergic immunotoxin 192 IgG-saporin) increased frontal cortical synchronous activity characterized by the number of spike–wave discharges (SWDs), which were successfully inhibited by the NBM/reticular nucleus of the thalamus (RT)-DBS. Combined with the findings of above studies, NBM neurons are involved in modulating arousal, sleep and epilepsy -related neural networks (Table 4).

TABLE 4 Effects of the NBM on the neural network in arousal, sleep and epilepsy.

Study	Subjects, (n)	Recording method	Results
Luo and Leung (2009)	Long Evans rats (8)	Frontal cortex EEG	Injection of histamine to the NBM shifted the EEG activity from burst suppression pattern by isoflurane toward delta activity, and histamine-evoked activation of EEG was blocked by NBM injection with a H1 receptor antagonist, triprolidine, rather than a H2 receptor antagonist.
Marino and Cudeiro (2003)	Adult cats (11)	Primary somatosensory (S1) and visual cortex LFP after a trial of NBM-DBS	NBM-DBS increased cortical NO, which was blocked by systemic NOS inhibition, and the ability of NBM-DBS to induce cortical LFP activation was severely impaired after blocking NOS activity. These findings suggested that the NBM is involved in the arousal mechanism through the NO pathway.
Manfridi et al. (2001)	Albino rats (13)	EEG and nuchal electromyographic (EMG) monitor states of sleep and wakefulness	Unilateral injection in the NBM with muscimol hydrobromide (a $GABA_A$ receptor subtype agonist) and baclofen (a $GABA_B$ receptor subtype agonist) induced an increase in slow-wave sleep (SWS) time and an inhibition of wakefulness, while muscimol hydrobromide, but not baclofen, caused a decrease in rapid eye movement sleep (REMS) time.
Berdiev et al. (2007); Berdiev and van Luijtelaar (2009)	WAG/Rij rats (28)	Frontal cortex EEG	NBM lesions induced by injections of 192 IgG-saporin increased spontaneous spike-and-wave discharges (SWDs, a charact of absence epilepsy), while the peaks of the SWDs were less sharp in the hemisphere with the NBM lesion. There was a broader SWD peak frequency in the lesioned hemisphere than in the intact hemisphere (17–18 Hz range vs. 8.3–8.8 Hz), and the injection of carbachol, a cholinergic agonist, in the NBM decreased the number and the mean duration of SWDs.

n, number of participants; S1, primary somatosensory cortex; LFP, local field potential; NO, nitric oxide; NOS, nitric oxide synthase; SWDs, spike-and-wave discharges; SWS, slow-wave sleep; REMS, rapid eye movement sleep.

5 Future research prospects of the NBM for neuromodulation

Neuromodulation, represented by DBS and brain-computer interfaces (BCIs), is undoubtedly a promising therapeutic method that meets the urgent need for more effective therapies for a range of debilitating diseases and conditions, including inflammatory and autoimmune disorders, obesity, diabetes, cardiovascular disease, cancer, neurodegenerative and neuromuscular disorders and paralysis (Fetz, 2007; Jackson and Fetz, 2011; Orsborn and Carmena, 2013). The aforementioned findings collectively underscore the pivotal role of the NBM in the neural network, thereby emphasizing the need to investigate its function within the neural network by using advanced techniques such as optogenetics, multielectrode recording, and computer modeling to unravel the underlying mechanisms. Such research will serve as a fundamental basis for precise modulation via DBS and BCIs in the future (Wang, 2010; Bensmaia and Miller, 2014; Shenoy and Carmena, 2014; Guidetti et al., 2021; Marceglia et al., 2021). Moreover, with regard to cholinergic neurons in the NBM that have diffuse projections and diverse functions, it is crucial to avoid treating them as a homogeneous population. Instead, distinguishing them based on histological differences is imperative. Furthermore, cholinergic neurons account for only 5% of the neurons in the NBM; the other cellular components of the NBM have received little attention (Buzsaki et al., 1988; King et al., 1998; Lee et al., 2005). The involvement of other cell types, including glial cells, interneurons, glutamatergic neurons, etc., in each anatomical subdivision unit of the NBM poses an inevitable challenge for investigating the underlying neural network mechanism.

Considering the complexity of neural networks and the multi-site damage of brain tissue in neurodegenerative diseases, it is necessary to break the boundary of single nucleus, and future neural network research needs to be integrated from the perspective of the whole brain. On the one hand, in addition to cholinergic neurons, other neurons or receptor components, such as serotonergic (Viana et al., 2021), GABAergic (Iaccarino et al., 2016), glutamatergic neurons (Xu et al., 2015) and even muscarinic receptor (Velazquez-Moctezuma et al., 1991) also play important roles in the generation and modulation of neural network oscillations. On the other hand, in addition to NBM, other sites, such as the dorsal raphe nucleus (Qamhawi et al., 2015), entorhinal cortex (Leng et al., 2021), and hippocampus (Moodley and Chan, 2014) also play an important role in the development of neurodegenerative diseases, this may explain why so far evidence for NBM-DBS of improving cognitive function in clinical AD patients is rather scant, so dual-target NBM-DBS in the treatment of neurodegenerative diseases is a promising strategy and worth exploring in the future.

6 Conclusion

The NBM plays an important and complex role in the neural network dysfunction of various neurodegenerative diseases. The above studies demonstrated that lesions in the NBM can induce alterations in neuronal firing patterns within the prefrontal cortex, auditory cortex, and visual cortex, leading to a reduction in γ oscillation power and an increase in θ and α oscillation power. The underlying mechanism for these changes primarily involves the degradation of cholinergic neurons within the NBM and their cortical projection fibers; however, the contribution of other cellular components within the NBM, such as interneurons, should not be disregarded. Animal experiments utilizing NBM-DBS have shown that NBM-DBS partially reverses neural network abnormalities following NBM lesions, as indicated by decreased cortical θ and α oscillation power, increased γ oscillation power, and improved animal memory function. Although clinical trials investigating the effectiveness of NBM-DBS may not demonstrate outcomes as significant as studies in animal models, delayed cognitive decline associated with AD has been observed. With further advancements in our understanding of neural networks and the development of neuromodulation technologies, neuromodulation based on the NBM will play a transformative role in treating neurodegenerative disorders.

Author contributions

LJ: Data curation, Software, Writing – original draft. HK: Conceptualization, Data curation, Writing – review & editing. YG: Investigation, Software, Writing – review & editing. XL: Data curation, Formal analysis, Writing – review & editing. MW: Software, Writing – review & editing. KS: Project administration, Resources, Supervision, Writing – review & editing.

Funding

The author(s) declare that financial support was received for the research, authorship, and/or publication of this article. All sources of fundings received for the research have been submitted. National Natural Science Foundation of China [81974279], which supported the information retrieval; National Key Project of Common and Frequently Occurring Diseases [2022YFC2503800], which supported the analysis and summary of related literatures; Natural Science Foundation of Hubei Province [2022CFB279], which supported language polishing and Health Commission of Hubei Province [WJ2021M131], which supported the publication fee.

Conflict of interest

The authors declare that the research was conducted in the absence of any commercial or financial relationships that could be construed as a potential conflict of interest.

Publisher's note

References

Adachi, T., Biesold, D., Inanami, O., and Sato, A. (1990a). Stimulation of the nucleus basalis of Meynert and substantia innominata produces widespread increases in cerebral blood flow in the frontal, parietal and occipital cortices. *Brain Res.* 514, 163–166. doi: 10.1016/0006-8993(90)90452-H

Adachi, T., Inanami, O., Ohno, K., and Sato, A. (1990b). Responses of regional cerebral blood flow following focal electrical stimulation of the nucleus basalis of Meynert and the medial septum using the [14C]iodoantipyrine method in rats. *Neurosci. Lett.* 112, 263–268. doi: 10.1016/0304-3940(90)90214-T

Amzica, F., and Steriade, M. (1998). Electrophysiological correlates of sleep delta waves. *Electroencephalogr. Clin. Neurophysiol.* 107, 69–83. doi: 10.1016/S0013-4694(98)00051-0

Arendt, T., Brückner, M. K., Morawski, M., Jäger, C., and Gertz, H. J. (2015). Early neurone loss in Alzheimer's disease: cortical or subcortical? *Acta Neuropathol. Commun.* 3:10. doi: 10.1186/s40478-015-0187-1

Başar, E., Schürmann, M., Başar-Eroglu, C., and Karakaş, S. (1997). Alpha oscillations in brain functioning: an integrative theory. *Int. J. Psychophysiol.* 26, 5–29. doi: 10.1016/S0167-8760(97)00753-8

Bensmaia, S. J., and Miller, L. E. (2014). Restoring sensorimotor function through intracortical interfaces: progress and looming challenges. *Nat. Rev. Neurosci.* 15, 313–325. doi: 10.1038/nrn3724

Berdiev, R. K., Chepurnov, S. A., Veening, J. G., Chepurnova, N. E., and van Luijtelaar, G. (2007). The role of the nucleus basalis of Meynert and reticular thalamic nucleus in pathogenesis of genetically determined absence epilepsy in rats: a lesion study. *Brain Res.* 1185, 266–274. doi: 10.1016/j.brainres.2007.09.010

Berdiev, R. K., and van Luijtelaar, G. (2009). Cholinergic stimulation of the nucleus basalis of Meynert and reticular thalamic nucleus affects spike-and-wave discharges in WAG/Rij rats. *Neurosci. Lett.* 463, 249–253. doi: 10.1016/j.neulet.2009.07.068

Berger, H. (1929). Über das Elektrenkephalogramm des Menschen. *Arch. Psychiatr. Nervenkr.* 87, 527–570. doi: 10.1007/BF01797193

Berger, H. (1969). On the electroencephalogram of man. *Electroencephalogr. Clin. Neurophysiol.*:37.

Berntson, G. G., Shafi, R., and Sarter, M. (2002). Specific contributions of the basal forebrain corticopetal cholinergic system to electroencephalographic activity and sleep/waking behaviour. *Eur. J. Neurosci.* 16, 2453–2461. doi: 10.1046/j.1460-9568.2002.02310.x

Braak, H., Thal, D. R., Ghebremedhin, E., and del Tredici, K. (2011). Stages of the pathologic process in Alzheimer disease: age categories from 1 to 100 years. *J. Neuropathol. Exp. Neurol.* 70, 960–969. doi: 10.1097/NEN.0b013e318232a379

Bragin, A., Jando, G., Nadasdy, Z., Hetke, J., Wise, K., and Buzsaki, G. (1995). Gamma (40-100 Hz) oscillation in the hippocampus of the behaving rat. *J. Neurosci.* 15, 47–60. doi: 10.1523/JNEUROSCI.15-01-00047.1995

Buzsaki, G. (2002). Theta oscillations in the hippocampus. *Neuron* 33, 325–340. doi: 10.1016/S0896-6273(02)00586-X

Buzsaki, G., Bickford, R. G., Ponomareff, G., Thal, L. J., Mandel, R., and Gage, F. H. (1988). Nucleus basalis and thalamic control of neocortical activity in the freely moving rat. *J. Neurosci.* 8, 4007–4026. doi: 10.1523/JNEUROSCI.08-11-04007.1988

Canolty, R. T., and Knight, R. T. (2010). The functional role of cross-frequency coupling. *Trends Cogn. Sci.* 14, 506–515. doi: 10.1016/j.tics.2010.09.001

Cappon, D., Gratwicke, J., Zrinzo, L., Akram, H., Hyam, J., Hariz, M., et al. (2022). Deep brain stimulation of the nucleus basalis of Meynert for Parkinson's disease dementia: a 36 months follow up study. *Movement Disord. Clin. Pract.* 9, 765–774. doi: 10.1002/mdc3.13510

Cardin, J. A., Carlén, M., Meletis, K., Knoblich, U., Zhang, F., Deisseroth, K., et al. (2009). Driving fast-spiking cells induces gamma rhythm and controls sensory responses. *Nature* 459, 663–667. doi: 10.1038/nature08002

Chernyshev, B. V., Panasyuk, Y. A., Semikopnaya, I. I., and Timofeeva, N. O. (2004). Activity of neurons in the basal magnocellular nucleus during performance of an operant task. *Neurosci. Behav. Physiol.* 34, 907–918. doi: 10.1023/B:NEAB.0000042575.79517.b6

Chung, J. K., et al. (2016). Alzheimer's disease neuroimaging initiative. Cortical amyloid beta deposition and current depressive symptoms in Alzheimer disease and mild cognitive impairment (vol 29, pg 149, 2015). *J. Geriatr. Psychiatry Neurol.* 29, 237–241. doi: 10.1177/0891988715606230

Ciric, J., Lazic, K., Petrovic, J., Kalauzi, A., and Saponjic, J. (2016). Age-related disorders of sleep and motor control in the rat models of functionally distinct cholinergic neuropathology. *Behav. Brain Res.* 301, 273–286. doi: 10.1016/j.bbr.2015.12.046

Colgin, L. L., Denninger, T., Fyhn, M., Hafting, T., Bonnevie, T., Jensen, O., et al. (2009). Frequency of gamma oscillations routes flow of information in the hippocampus. *Nature* 462, 353–357. doi: 10.1038/nature08573

Danışman, B., Akçay, G., Gökçek-Saraç, Ç., Kantar, D., Aslan, M., and Derin, N. (2022). The role of acetylcholine on the effects of different doses of sulfite in learning and memory. *Neurochem. Res.* 47, 3331–3343. doi: 10.1007/s11064-022-03684-z

Destexhe, A., and Sejnowski, T. J. (2003). Interactions between membrane conductances underlying thalamocortical slow-wave oscillations. *Physiol. Rev.* 83, 1401–1453. doi: 10.1152/physrev.00012.2003

Dezawa, S., Nagasaka, K., Watanabe, Y., and Takashima, I. (2021). Lesions of the nucleus basalis magnocellularis (Meynert) induce enhanced somatosensory responses and tactile hypersensitivity in rats. *Exp. Neurol.* 335:113493. doi: 10.1016/j.expneurol.2020.113493

Engel, A. K., Fries, P., and Singer, W. (2001). Dynamic predictions: oscillations and synchrony in top-down processing. *Nat. Rev. Neurosci.* 2, 704–716. doi: 10.1038/35094565

Fetz, E. E. (2007). Volitional control of neural activity: implications for brain-computer interfaces. *J. Physiol.* 579, 571–579. doi: 10.1113/jphysiol.2006.127142

Fort, P., Khateb, A., Pegna, A., Mühlethaler, M., and Jones, B. E. (1995). Noradrenergic modulation of cholinergic nucleus basalis neurons demonstrated by in vitro pharmacological and immunohistochemical evidence in the guinea-pig brain. *Eur. J. Neurosci.* 7, 1502–1511. doi: 10.1111/j.1460-9568.1995.tb01145.x

Goard, M., and Dan, Y. (2009). Basal forebrain activation enhances cortical coding of natural scenes. *Nat. Neurosci.* 12, 1444–1449. doi: 10.1038/nn.2402

González, H. F. J., Narasimhan, S., Johnson, G. W., Wills, K. E., Haas, K. F., Konrad, P. E., et al. (2021). Role of the nucleus basalis as a key network node in temporal lobe epilepsy. *Neurology* 96, E1334–E1346. doi: 10.1212/WNL.0000000000011523

Graham, A. J., Martin-Ruiz, C., Teaktong, T., Ray, M., and Court, J. (2002). Human brain nicotinic receptors, their distribution and participation in neuropsychiatric disorders. *Curr. Drug Targets CNS Neurol. Disord.* 1, 387–397. doi: 10.2174/1568007023339283

Gratwicke, J., Oswal, A., Akram, H., Jahanshahi, M., Hariz, M., Zrinzo, L., et al. (2020). Resting state activity and connectivity of the nucleus basalis of Meynert and globus pallidus in Lewy body dementia and Parkinson's disease dementia. *NeuroImage* 221:117184. doi: 10.1016/j.neuroimage.2020.117184

Gratwicke, J., Zrinzo, L., Kahan, J., Peters, A., Beigi, M., Akram, H., et al. (2018). Bilateral deep brain stimulation of the nucleus basalis of Meynert for Parkinson disease dementia: a randomized clinical trial. *JAMA Neurol.* 75, 169–178. doi: 10.1001/jamaneurol.2017.3762

Guidetti, M., Marceglia, S., Loh, A., Harmsen, I. E., Meoni, S., Foffani, G., et al. (2021). Clinical perspectives of adaptive deep brain stimulation. *Brain Stimul.* 14, 1238–1247. doi: 10.1016/j.brs.2021.07.063

Hanna, A. S. F. S., Duara, R., and Crook, J. E. (2020). Selective vulnerability of the nucleus basalis of Meynert among Neuropathologic subtypes of Alzheimer disease. *JAMA Neurol.* 77:265. doi: 10.1001/jamaneurol.2019.3606

Herweg, N. A., Solomon, E. A., and Kahana, M. J. (2020). Theta oscillations in human memory. *Trends Cogn. Sci.* 24, 208–227. doi: 10.1016/j.tics.2019.12.006

Hong, J. H., and Jang, S. H. (2010). Neural pathway from nucleus basalis of Meynert passing through the cingulum in the human brain. *Brain Res.* 1346, 190–194. doi: 10.1016/j.brainres.2010.05.088

Hotta, H., Kagitani, F., Kondo, M., and Uchida, S. (2009). Basal forebrain stimulation induces NGF secretion in ipsilateral parietal cortex via nicotinic receptor activation in adult, but not aged rats. *Neurosci. Res.* 63, 122–128. doi: 10.1016/j.neures.2008.11.004

Howe, W. M., Gritton, H. J., Lusk, N. A., Roberts, E. A., Hetrick, V. L., Berke, J. D., et al. (2017). Acetylcholine release in prefrontal cortex promotes gamma oscillations and Theta-gamma coupling during Cue detection. *J. Neurosci.* 37, 3215–3230. doi: 10.1523/JNEUROSCI.2737-16.2017

Huang, C., Chu, H., Ma, Y., Zhou, Z., Dai, C., Huang, X., et al. (2019). The neuroprotective effect of deep brain stimulation at nucleus basalis of Meynert in transgenic mice with Alzheimer's disease. *Brain Stimul.* 12, 161–174. doi: 10.1016/j.brs.2018.08.015

Iaccarino, H. F., Singer, A. C., Martorell, A. J., Rudenko, A., Gao, F., Gillingham, T. Z., et al. (2016). Gamma frequency entrainment attenuates amyloid load and modifies microglia. *Nature* 540, 230–235. doi: 10.1038/nature20587

Jackson, A., and Fetz, E. E. (2011). Interfacing with the computational brain. *IEEE Trans. Neural Syst. Rehabil. Eng.* 19, 534–541. doi: 10.1109/TNSRE.2011.2158586

Jacobs, J., Kahana, M. J., Ekstrom, A. D., and Fried, I. (2007). Brain oscillations control timing of single-neuron activity in humans. *J. Neurosci.* 27, 3839–3844. doi: 10.1523/JNEUROSCI.4636-06.2007

Jasper, H., and Penfield, W. (1949). Electrocorticograms in man: effect of voluntary movement upon the electrical activity of the precentral gyrus. *Eur. Arch. Psychiatry Clin. Neurosci.* 183, 163–174. doi: 10.1007/BF01062488

Jones, E. G., Burton, H., Saper, C. B., and Swanson, L. W. (1976). Midbrain, diencephalic and cortical relationships of the basal nucleus of Meynert and associated structures in primates. *J. Comp. Neurol.* 167, 385–419. doi: 10.1002/cne.901670402

Jones, B. E., and Cuello, A. C. (1989). Afferents to the basal forebrain cholinergic cell area from pontomesencephalic--catecholamine, serotonin, and acetylcholine--neurons. *Neuroscience* 31, 37–61. doi: 10.1016/0306-4522(89)90029-8

Kasa, P. (1986). The cholinergic systems in brain and spinal cord. *Prog. Neurobiol.* 26, 211–272. doi: 10.1016/0301-0082(86)90016-X

Khateb, A., Fort, P., Alonso, A., Jones, B. E., and Mülethaler, M. (1993). Pharmacological and immunohistochemical evidence for serotonergic modulation of

cholinergic nucleus basalis neurons. *Eur. J. Neurosci.* 5, 541–547. doi: 10.1111/j.1460-9568.1993.tb00519.x

Khateb, A., Fort, P., Pegna, A., Jones, B. E., and Mühlethaler, M. (1995). Cholinergic nucleus basalis neurons are excited by histamine in vitro. *Neuroscience* 69, 495–506. doi: 10.1016/0306-4522(95)00264-J

Khateb, A., Fort, P., Williams, S., Serafin, M., Mühlethaler, M., and Jones, B. E. (1998). GABAergic input to cholinergic nucleus basalis neurons. *Neuroscience* 86, 937–947. doi: 10.1016/S0306-4522(98)00094-3

King, C., Recce, M., and O'Keefe, J. (1998). The rhythmicity of cells of the medial septum/diagonal band of Broca in the awake freely moving rat: relationships with behaviour and hippocampal theta. *Eur. J. Neurosci.* 10, 464–477. doi: 10.1046/j.1460-9568.1998.00026.x

Klimesch, W. (2012). Alpha-band oscillations, attention, and controlled access to stored information. *Trends Cogn. Sci.* 16, 606–617. doi: 10.1016/j.tics.2012.10.007

Knoche, A., Yokoyama, H., Ponomarenko, A., Frisch, C., Huston, J., and Haas, H. L. (2003). High-frequency oscillation in the hippocampus of the behaving rat and its modulation by the histaminergic system. *Hippocampus* 13, 273–280. doi: 10.1002/hipo.10057

Knox, D., and Berntson, G. G. (2008). Cortical modulation by nucleus basalis magnocellularis corticopetal cholinergic neurons during anxiety-like states is reflected by decreases in delta. *Brain Res.* 1227, 142–152. doi: 10.1016/j.brainres.2008.06.060

Krauss, J. K., Lipsman, N., Aziz, T., Boutet, A., Brown, P., Chang, J. W., et al. (2021). Technology of deep brain stimulation: current status and future directions. *Nat. Rev. Neurol.* 17, 75–87. doi: 10.1038/s41582-020-00426-z

Kuhn, J., Hardenacke, K., Lenartz, D., Gruendler, T., Ullsperger, M., Bartsch, C., et al. (2015). Deep brain stimulation of the nucleus basalis of Meynert in Alzheimer's dementia. *Mol. Psychiatry* 20, 353–360. doi: 10.1038/mp.2014.32

Laurent, G. (2002). Olfactory network dynamics and the coding of multidimensional signals. *Nat. Rev. Neurosci.* 3, 884–895. doi: 10.1038/nrn964

Lee, M. G., Hassani, O. K., Alonso, A., and Jones, B. E. (2005). Cholinergic basal forebrain neurons burst with theta during waking and paradoxical sleep. *J. Neurosci.* 25, 4365–4369. doi: 10.1523/JNEUROSCI.0178-05.2005

Lee, J. E., Jeong, D. U., Lee, J., Chang, W. S., and Chang, J. W. (2016). The effect of nucleus basalis magnocellularis deep brain stimulation on memory function in a rat model of dementia. *BMC Neurol.* 16:6. doi: 10.1186/s12883-016-0529-z

Lee, D. J., Lozano, C. S., Dallapiazza, R. F., and Lozano, A. M. (2019). Current and future directions of deep brain stimulation for neurological and psychiatric disorders. *J. Neurosurg.* 131, 333–342. doi: 10.3171/2019.4.JNS181761

Lee, D. J., Milosevic, L., Gramer, R., Sasikumar, S., al-Ozzi, T. M., de Vloo, P., et al. (2019). Nucleus basalis of Meynert neuronal activity in Parkinson's disease. *J. Neurosurg.* 132, 574–582. doi: 10.3171/2018.11.JNS182386

Leng, K., Li, E., Eser, R., Piergies, A., Sit, R., Tan, M., et al. (2021). Molecular characterization of selectively vulnerable neurons in Alzheimer's disease. *Nat. Neurosci.* 24, 276–287. doi: 10.1038/s41593-020-00764-7

Lisman, J., and Buzsaki, G. (2008). A neural coding scheme formed by the combined function of gamma and theta oscillations. *Schizophr. Bull.* 34, 974–980. doi: 10.1093/schbul/sbn060

Lisman, J. E., and Jensen, O. (2013). The theta-gamma neural code. *Neuron* 77, 1002–1016. doi: 10.1016/j.neuron.2013.03.007

Liu, A. K., Chang, R. C. C., Pearce, R. K. B., and Gentleman, S. M. (2015). Nucleus basalis of Meynert revisited: anatomy, history and differential involvement in Alzheimer's and Parkinson's disease. *Acta Neuropathol.* 129, 527–540. doi: 10.1007/s00401-015-1392-5

Liu, R., Crawford, J., Callahan, P. M., Terry, A. V., Constantinidis, C., and Blake, D. T. (2018). Intermittent stimulation in the nucleus basalis of meynert improves sustained attention in rhesus monkeys. *Neuropharmacology* 137, 202–210. doi: 10.1016/j.neuropharm.2018.04.026

Ljubojevic, V., Luu, P., Gill, P. R., Beckett, L. A., Takehara-Nishiuchi, K., and de Rosa, E. (2018). Cholinergic modulation of Frontoparietal cortical network dynamics supporting Supramodal attention. *J. Neurosci.* 38, 3988–4005. doi: 10.1523/JNEUROSCI.2350-17.2018

Llinas, R. R. (1988). The intrinsic electrophysiological properties of mammalian neurons: insights into central nervous system function. *Science* 242, 1654–1664. doi: 10.1126/science.3059497

Luo, T., and Leung, L. S. (2009). Basal forebrain histaminergic transmission modulates electroencephalographic activity and emergence from isoflurane anesthesia. *Anesthesiology* 111, 725–733. doi: 10.1097/ALN.0b013e3181b061a0

Manfridi, A., Brambilla, D., and Mancia, M. (2001). Sleep is differently modulated by basal forebrain GABA(a) and GABA(B) receptors. *Am. J. Phys. Regul. Integr. Comp. Phys.* 281, R170–R175. doi: 10.1152/ajpregu.2001.281.1.R170

Marceglia, S., Guidetti, M., Harmsen, I. E., Loh, A., Meoni, S., Foffani, G., et al. (2021). Deep brain stimulation: is it time to change gears by closing the loop? *J. Neural Eng.* 18:061001. doi: 10.1088/1741-2552/ac3267

Marino, J., and Cudeiro, J. (2003). Nitric oxide-mediated cortical activation: a diffuse wake-up system. *J. Neurosci.* 23, 4299–4307. doi: 10.1523/JNEUROSCI.23-10-04299.2003

Martinez-Rubio, C., Paulk, A. C., McDonald, E. J., Widge, A. S., and Eskandar, E. N. (2018). Multimodal encoding of novelty, reward, and learning in the primate nucleus basalis of Meynert. *J. Neurosci.* 38, 1942–1958. doi: 10.1523/JNEUROSCI.2021-17.2017

McLin, D. E. 3rd, Miasnikov, A. A., and Weinberger, N. M. (2002). The effects of electrical stimulation of the nucleus basalis on the electroencephalogram, heart rate, and respiration. *Behav. Neurosci.* 116, 795–806. doi: 10.1037/0735-7044.116.5.795

McLin, D. E. 3rd, Miasnikov, A. A., and Weinberger, N. M. (2003). CS-specific gamma, theta, and alpha EEG activity detected in stimulus generalization following induction of behavioral memory by stimulation of the nucleus basalis. *Neurobiol. Learn. Mem.* 79, 152–176. doi: 10.1016/S1074-7427(02)00009-6

Mehraram, R., Peraza, L. R., Murphy, N. R. E., Cromarty, R. A., Graziadio, S., O'Brien, J. T., et al. (2022). Functional and structural brain network correlates of visual hallucinations in Lewy body dementia. *Brain* 145, 2190–2205. doi: 10.1093/brain/awac094

Meir, I., Katz, Y., and Lampl, I. (2018). Membrane potential correlates of network decorrelation and improved SNR by cholinergic activation in the somatosensory cortex. *J. Neurosci.* 38, 10692–10708. doi: 10.1523/JNEUROSCI.1159-18.2018

Mesulam, M. M., and Geula, C. (1988). Nucleus basalis (Ch4) and cortical cholinergic innervation in the human brain: observations based on the distribution of acetylcholinesterase and choline acetyltransferase. *J. Comp. Neurol.* 275, 216–240. doi: 10.1002/cne.902750205

Mesulam, M. M., Mufson, E. J., Levey, A. I., and Wainer, B. H. (1983). Cholinergic innervation of cortex by the basal forebrain: cytochemistry and cortical connections of the septal area, diagonal band nuclei, nucleus basalis (substantia innominata), and hypothalamus in the rhesus monkey. *J. Comp. Neurol.* 214, 170–197. doi: 10.1002/cne.902140206

Mesulam, M. M., Mufson, E. J., Levey, A. I., and Wainer, B. H. (1984). Atlas of cholinergic neurons in the forebrain and upper brainstem of the macaque based on monoclonal choline acetyltransferase immunohistochemistry and acetylcholinesterase histochemistry. *Neuroscience* 12, 669–686. doi: 10.1016/0306-4522(84)90163-5

Montgomery, S. M., Sirota, A., and Buzsaki, G. (2008). Theta and gamma coordination of hippocampal networks during waking and rapid eye movement sleep. *J. Neurosci.* 28, 6731–6741. doi: 10.1523/JNEUROSCI.1227-08.2008

Moodley, K. K., and Chan, D. (2014). The hippocampus in neurodegenerative disease. *Front. Neurol. Neurosci.* 34, 95–108. doi: 10.1159/000356430

Morelli, A., Sarchielli, E., Guarnieri, G., Coppi, E., Pantano, D., Comeglio, P., et al. (2017). Young human cholinergic neurons respond to physiological regulators and improve cognitive symptoms in an animal model of Alzheimer's disease. *Front. Cell. Neurosci.* 11:339. doi: 10.3389/fncel.2017.00339

Nagasaka, K., Watanabe, Y., and Takashima, I. (2017). Topographical projections from the nucleus basalis magnocellularis (Meynert) to the frontal cortex: a voltage-sensitive dye imaging study in rats. *Brain Stimul.* 10, 977–980. doi: 10.1016/j.brs.2017.06.008

Nazmuddin, M., Oterdoom, D. L. M., van Dijk, J. M. C., van Zijl, J. C., Kampman, A. K., Drost, G., et al. (2018). Oscillatory activity and cortical coherence of the nucleus basalis of Meynert in Parkinson's disease dementia. *Parkinsonism Relat. Disord.* 52, 102–106. doi: 10.1016/j.parkreldis.2018.03.024

Nokia, M. S., and Penttonen, M. (2022). Rhythmic memory consolidation in the hippocampus. *Front. Neurol. Circuits.* 16:885684. doi: 10.3389/fncir.2022.885684

Orsborn, A. L., and Carmena, J. M. (2013). Creating new functional circuits for action via brain-machine interfaces. *Front. Comput. Neurosci.* 7:157.

Oswal, A., Gratwicke, J., Akram, H., Jahanshahi, M., Zaborszky, L., Brown, P., et al. (2021). Cortical connectivity of the nucleus basalis of Meynert in Parkinson's disease and Lewy body dementias. *Brain* 144, 781–788. doi: 10.1093/brain/awaa411

Palva, S., and Palva, J. M. (2007). New vistas for alpha-frequency band oscillations. *Trends Neurosci.* 30, 150–158. doi: 10.1016/j.tins.2007.02.001

Pare, D., and Gaudreau, H. (1996). Projection cells and interneurons of the lateral and basolateral amygdala: distinct firing patterns and differential relation to theta and delta rhythms in conscious cats. *J. Neurosci.* 16, 3334–3350. doi: 10.1523/JNEUROSCI.16-10-03334.1996

Pereira, E. A., and Aziz, T. Z. (2014). Neuropathic pain and deep brain stimulation. *Neurotherapeutics* 11, 496–507. doi: 10.1007/s13311-014-0278-x

Pittman-Polletta, B. R., Quach, A., Mohammed, A. I., Romano, M., Kondabolu, K., Kopell, N. J., et al. (2018). Striatal cholinergic receptor activation causes a rapid, selective and state-dependent rise in cortico-striatal beta activity. *Eur. J. Neurosci.* 48, 2857–2868. doi: 10.1111/ejn.13906

Qamhawi, Z., Towey, D., Shah, B., Pagano, G., Seibyl, J., Marek, K., et al. (2015). Clinical correlates of raphe serotonergic dysfunction in early Parkinson's disease. *Brain* 138, 2964–2973. doi: 10.1093/brain/awv215

Rea, R. C., Berlot, R., Martin, S. L., Craig, C. E., Holmes, P. S., Wright, D. J., et al. (2021). Quantitative EEG and cholinergic basal forebrain atrophy in Parkinson's disease and mild cognitive impairment. *Neurobiol. Aging* 106, 37–44. doi: 10.1016/j.neurobiolaging.2021.05.023

Rispoli, V., Marra, R., Costa, N., Rotiroti, D., Tirassa, P., Scipione, L., et al. (2008). Choline pivaloyl ester enhances brain expression of both nerve growth factor and high-affinity receptor TrkA, and reverses memory and cognitive deficits, in rats with

excitotoxic lesion of nucleus basalis magnocellularis. *Behav. Brain Res.* 190, 22–32. doi: 10.1016/j.bbr.2008.02.002

Rispoli, V., Ragusa, S., Nisticò, R., Marra, R., Russo, E., Leo, A., et al. (2013). Huperzine a restores cortico-hippocampal functional connectivity after bilateral AMPA lesion of the nucleus basalis of meynert. *J. Alzheimers Dis.* 35, 833–846. doi: 10.3233/JAD-130278

Rispoli, V., Rotiroti, D., Carelli, V., Liberatore, F., Scipione, L., Marra, R., et al. (2004). Electroencephalographic effects induced by choline pivaloyl esters in scopolamine-treated or nucleus basalis magnocellularis lesioned rats. *Pharmacol. Biochem. Behav.* 78, 667–673. doi: 10.1016/j.pbb.2004.04.031

Rodriguez, R., Kallenbach, U., Singer, W., and Munk, M. H. J. (2004). Short- and long-term effects of cholinergic modulation on gamma oscillations and response synchronization in the visual cortex. *J. Neurosci.* 24, 10369–10378. doi: 10.1523/JNEUROSCI.1839-04.2004

Russchen, F. T., Amaral, D. G., and Price, J. L. (1985). The afferent connections of the substantia innominata in the monkey, *Macaca fascicularis*. *J. Comp. Neurol.* 242, 1–27. doi: 10.1002/cne.902420102

Rutishauser, U., Ross, I. B., Mamelak, A. N., and Schuman, E. M. (2010). Human memory strength is predicted by theta-frequency phase-locking of single neurons. *Nature* 464, 903–907. doi: 10.1038/nature08860

Sakalar, E., Klausberger, T., and Lasztoczi, B. (2022). Neurogliaform cells dynamically decouple neuronal synchrony between brain areas. *Science* 377:324. doi: 10.1126/science.abo3355

Sanchez-Alavez, M., and Ehlers, C. L. (2016). Event-related oscillations (ERO) during an active discrimination task: effects of lesions of the nucleus basalis magnocellularis. *Int. J. Psychophysiol.* 103, 53–61. doi: 10.1016/j.ijpsycho.2015.02.010

Sanchez-Alavez, M., Robledo, P., Wills, D. N., Havstad, J., and Ehlers, C. L. (2014). Cholinergic modulation of event-related oscillations (ERO). *Brain Res.* 1559, 11–25. doi: 10.1016/j.brainres.2014.02.043

Sasikumar, S., Cohn, M., Harmsen, I. E., Loh, A., Cho, S. S., Sáenz-Farret, M., et al. (2022). Single-trajectory multiple-target deep brain stimulation for parkinsonian mobility and cognition. *Mov. Disord.* 37, 635–640. doi: 10.1002/mds.28870

Schmidt, R., Herrojo Ruiz, M., Kilavik, B. E., Lundqvist, M., Starr, P. A., and Aron, A. R. (2019). Beta oscillations in working memory, executive control of movement and thought, and sensorimotor function. *J. Neurosci.* 39, 8231–8238. doi: 10.1523/JNEUROSCI.1163-19.2019

Schumacher, J., Ray, N. J., Hamilton, C. A., Donaghy, P. C., Firbank, M., Roberts, G., et al. (2022). Cholinergic white matter pathways in dementia with Lewy bodies and Alzheimer's disease. *Brain* 145, 1773–1784. doi: 10.1093/brain/awab372

Schumacher, J., Taylor, J. P., Hamilton, C. A., Firbank, M., Cromarty, R. A., Donaghy, P. C., et al. (2021). In vivo nucleus basalis of Meynert degeneration in mild cognitive impairment with Lewy bodies. *Neuroimage Clin* 30:102604. doi: 10.1016/j.nicl.2021.102604

Schumacher, J., Thomas, A. J., Peraza, L. R., Firbank, M., Cromarty, R., Hamilton, C. A., et al. (2020). EEG alpha reactivity and cholinergic system integrity in Lewy body dementia and Alzheimer's disease. *Alzheimers Res. Ther.* 12:46. doi: 10.1186/s13195-020-00613-6

Selden, N. R., Gitelman, D. R., Salamon-Murayama, N., Parrish, T. B., and Mesulam, M. M. (1998). Trajectories of cholinergic pathways within the cerebral hemispheres of the human brain. *Brain* 121, 2249–2257. doi: 10.1093/brain/121.12.2249

Semba, K., and Fibiger, H. C. (1989). Organization of central cholinergic systems. *Prog. Brain Res.* 79, 37–63. doi: 10.1016/S0079-6123(08)62464-4

Senoussi, M., Verbeke, P., Desender, K., de Loof, E., Talsma, D., and Verguts, T. (2022). Theta oscillations shift towards optimal frequency for cognitive control. *Nat. Hum. Behav.* 6, 1000–1013. doi: 10.1038/s41562-022-01335-5

Shenoy, K. V., and Carmena, J. M. (2014). Combining decoder design and neural adaptation in brain-machine interfaces. *Neuron* 84, 665–680. doi: 10.1016/j.neuron.2014.08.038

Singh, B., Qi, X. L., Blake, D. T., and Constantinidis, C. (2022). Rhythmicity of prefrontal local field potentials after nucleus basalis stimulation. *eNeuro* 9, ENEURO.0380–ENEU21.2022. doi: 10.1523/ENEURO.0380-21.2022

Smiley, J. F., and Mesulam, M. M. (1999). Cholinergic neurons of the nucleus basalis of meynert receive cholinergic, catecholaminergic and gabaergic synapses: an electron microscopic investigation in the monkey. *Neuroscience* 88, 241–255. doi: 10.1016/S0306-4522(98)00202-4

Song, M., Mohamad, O., Chen, D., and Yu, S. P. (2013). Coordinated development of voltage-gated Na+ and K+ currents regulates functional maturation of forebrain neurons derived from human induced pluripotent stem cells. *Stem Cells Dev.* 22, 1551–1563. doi: 10.1089/scd.2012.0556

Spencer, J. P., Middleton, L. J., and Davies, C. H. (2010). Investigation into the efficacy of the acetylcholinesterase inhibitor, donepezil, and novel procognitive agents to induce gamma oscillations in rat hippocampal slices. *Neuropharmacology* 59, 437–443. doi: 10.1016/j.neuropharm.2010.06.005

Stefanics, G., Hangya, B., Hernádi, I., Winkler, I., Lakatos, P., and Ulbert, I. (2010). Phase entrainment of human delta oscillations can mediate the effects of expectation on reaction speed. *J. Neurosci.* 30, 13578–13585. doi: 10.1523/JNEUROSCI.0703-10.2010

Steriade, M. (2001). Impact of network activities on neuronal properties in corticothalamic systems. *J. Neurophysiol.* 86, 1–39. doi: 10.1152/jn.2001.86.1.1

Steriade, M. (2004). Acetylcholine systems and rhythmic activities during the waking--sleep cycle. *Prog. Brain Res.* 145, 179–196. doi: 10.1016/S0079-6123(03)45013-9

Temel, Y., Visser-Vandewalle, V., Kaplan, S., Kozan, R., Daemen, M. A. R. C., Blokland, A., et al. (2006). Protection of nigral cell death by bilateral subthalamic nucleus stimulation. *Brain Res.* 1120, 100–105. doi: 10.1016/j.brainres.2006.08.082

Varela, F., Lachaux, J. P., Rodriguez, E., and Martinerie, J. (2001). The brainweb: phase synchronization and large-scale integration. *Nat. Rev. Neurosci.* 2, 229–239. doi: 10.1038/35067550

Velazquez-Moctezuma, J., Shalauta, M., Christian Gillin, J., and Shiromani, P. J. (1991). Cholinergic antagonists and REM sleep generation. *Brain Res.* 543, 175–179. doi: 10.1016/0006-8993(91)91064-8

Viana, M. B., Martins, R. S., Silva, M. S. C. F., Xapelli, S., Vaz, S. H., and Sebastião, A. M. (2021). Deep brain stimulation of the dorsal raphe abolishes serotonin 1A facilitation of AMPA receptor-mediated synaptic currents in the ventral hippocampus. *Behav. Brain Res.* 403:113134. doi: 10.1016/j.bbr.2021.113134

Wallace, B. A., Ashkan, K., Heise, C. E., Foote, K. D., Torres, N., Mitrofanis, J., et al. (2007). Survival of midbrain dopaminergic cells after lesion or deep brain stimulation of the subthalamic nucleus in MPTP-treated monkeys. *Brain* 130, 2129–2145. doi: 10.1093/brain/awm137

Wan, L., Huang, H., Schwab, N., Tanner, J., Rajan, A., Lam, N. B., et al. (2019). From eyes-closed to eyes-open: role of cholinergic projections in EC-to-EO alpha reactivity revealed by combining EEG and MRI. *Hum. Brain Mapp.* 40, 566–577. doi: 10.1002/hbm.24395

Wang, X. J. (2010). Neurophysiological and computational principles of cortical rhythms in cognition. *Physiol. Rev.* 90, 1195–1268. doi: 10.1152/physrev.00035.2008

Wang, X., Hu, W. H., Zhang, K., Zhou, J. J., Liu, D. F., Zhang, M. Y., et al. (2018). Acute fornix deep brain stimulation improves hippocampal glucose metabolism in aged mice. *Chin. Med. J.* 131, 594–599. doi: 10.4103/0366-6999.226067

Weinberger, N. M., Miasnikov, A. A., and Chen, J. C. (2006). The level of cholinergic nucleus basalis activation controls the specificity of auditory associative memory. *Neurobiol. Learn. Mem.* 86, 270–285. doi: 10.1016/j.nlm.2006.04.004

Williams, M. R., Marsh, R., Macdonald, C. D., Jain, J., Pearce, R. K. B., Hirsch, S. R., et al. (2013). Neuropathological changes in the nucleus basalis in schizophrenia. *Eur. Arch. Psychiatry Clin. Neurosci.* 263, 485–495. doi: 10.1007/s00406-012-0387-7

Woolf, N. J. (1991). Cholinergic systems in mammalian brain and spinal cord. *Prog. Neurobiol.* 37, 475–524. doi: 10.1016/0301-0082(91)90006-M

Woolf, N. J., and Butcher, L. L. (1982). Cholinergic projections to the basolateral amygdala: a combined Evans blue and acetylcholinesterase analysis. *Brain Res. Bull.* 8, 751–763. doi: 10.1016/0361-9230(82)90102-2

Xu, M., Chung, S., Zhang, S., Zhong, P., Ma, C., Chang, W. C., et al. (2015). Basal forebrain circuit for sleep-wake control. *Nat. Neurosci.* 18, 1641–1647. doi: 10.1038/nn.4143

Yakubov, B., das, S., Zomorrodi, R., Blumberger, D. M., Enticott, P. G., Kirkovski, M., et al. (2022). Cross-frequency coupling in psychiatric disorders: a systematic review. *Neurosci. Biobehav. Rev.* 138:104690. doi: 10.1016/j.neubiorev.2022.104690

Yu, T. W., Lane, H. Y., and Lin, C. E. H. (2021). Novel therapeutic approaches for Alzheimer's disease: an updated review. *Int. J. Mol. Sci.* 22:8208. doi: 10.3390/ijms22158208

Zheng, Y., Feng, S., Zhu, X., Jiang, W., Wen, P., Ye, F., et al. (2018). Different subgroups of cholinergic neurons in the basal forebrain are distinctly innervated by the olfactory regions and activated differentially in olfactory memory retrieval. *Front Neural Circuits* 12:99. doi: 10.3389/fncir.2018.00099

10.3389/fnagi.2024.1376764

Glossary

Event-related oscillations (EROs): EROs are a type of brainwave that occur in response to specific events or tasks. They are characterized by regular, rhythmic changes in the brain's electrical activity, with periods of high frequency (up to 30 Hz) and low amplitude, lasting from a few milliseconds to a few seconds. EROs are typically observed in the alpha, beta, and gamma frequency ranges, and they are thought to play a role in cognitive processing, attention, and working memory and can be measured using various types of EEG technology.
Phase lock index (PLI): The phase lock index is a measure of the synchronicity of the phase angle as a function of frequency and time relative to the stimulation initiation of each trial. The PLI ranges from 0 to 1.0, a higher PLI value of a certain time and frequency indicates that the phase angle of the time and frequency does not change much between tests (Sanchez-Alavez et al., 2014).
α reactivity: α reactivity is the decrease in power of α oscillations recorded in EEG by occipital electrodes after eye opening, and it has been considered to be a potential marker of cholinergic system integrity (Wan et al., 2019).
CFC: Cross-frequency coupling is one form of neural oscillatory coupling that refers to the statistical relationship between a combination of amplitude, phase, and frequency of two distinct frequency bands. There are four types of CFC: amplitude-amplitude coupling (AAC), phase-amplitude coupling (PAC). phase-frequency coupling (PFC) and phase-phase coupling (PPC) (Hanna et al., 2020).

frontiers | Frontiers in Aging Neuroscience

TYPE Original Research
PUBLISHED 10 April 2024
DOI 10.3389/fnagi.2024.1362790

OPEN ACCESS

EDITED BY
Allison B. Reiss,
New York University, United States

REVIEWED BY
Anthoula Charalampos Tsolaki,
Aristotle University of Thessaloniki, Greece
Peter Mukli,
University of Oklahoma Health Sciences Center, United States

*CORRESPONDENCE
Xiaozheng Liu
✉ lxz_2088@hotmail.com
Zhongwei Guo
✉ guozw1977@aliyun.com

RECEIVED 29 December 2023
ACCEPTED 27 March 2024
PUBLISHED 10 April 2024

CITATION
Yang T, Wei F, Guo Y, Zhu M, Hou H, Guo Z and Liu X (2024) The increased effective connectivity from left middle occipital gyrus to right medial septum/diagonal bands in AD patients after donepezil intervention. *Front. Aging Neurosci.* 16:1362790. doi: 10.3389/fnagi.2024.1362790

The increased effective connectivity from left middle occipital gyrus to right medial septum/diagonal bands in AD patients after donepezil intervention

Ting Yang[1], Fuquan Wei[2], Yufei Guo[3], Mengxiao Zhu[3], Hongtao Hou[2], Zhongwei Guo[2]* and Xiaozheng Liu[1,4]*

[1]The Second Affiliated Hospital and Yuying Children's Hospital, Wenzhou Medical University, Wenzhou, Zhejiang, China, [2]Tongde Hospital of Zhejiang Province, Hangzhou, Zhejiang, China, [3]The Second Clinical Medical College, Zhejiang Chinese Medical University, Hangzhou, Zhejiang, China, [4]Wenzhou Key Laboratory of Structural and Functional Imaging, Wenzhou, Zhejiang, China

Introduction: Donepezil enhances the function of cholinergic nerves by increasing the concentration of acetylcholine, thereby improving clinical symptoms in patients with Alzheimer's disease (AD). However, the neural mechanisms of how donepezil modulates the effective connectivity (EC) network of cholinergic system in AD patients remain unknown. We speculated that the effective network of the cholinergic system changes in AD patients after donepezil intervention.

Methods: We employed resting-state functional magnetic resonance imaging and Granger causality analysis approach to explore changes in the effective connectivity network of the basal forebrain in AD patients before and after donepezil intervention. This study included 32 participants, including 16 healthy controls (HCs) and 16 AD patients. In a 3T MRI scanner, the 16 AD patients were scanned before and after the donepezil intervention. To compare EC differences between the three groups of participants, ANOVA and *post-hoc t*-tests analysis were employed.

Results: Compared to baseline status, AD patients after donepezil intervention had an increased EC from left middle occipital gyrus to right medial septum/diagonal bands. Compared to HCs, AD patients after donepezil intervention had an increased EC from right inferior frontal gyrus/orbit part to right medial septum/diagonal bands, AD patients before donepezil intervention had a reduced EC from right precuneus to right medial septum/diagonal bands. A significant positive correlation was found between EC values in right precuneus and Mini-Mental State Examination in pre-intervention AD patients (r = 0.7338, p = 0.0012).

Discussion: Our study showed that effective connectivity of brain regions associated with the default mode network in the cholinergic pathway was enhanced after donepezil intervention. The results of this study will help us to better understand the neural mechanisms of donepezil intervention in AD and to find clinical targets for intervention.

KEYWORDS

Alzheimer's disease, cholinergic, functional magnetic resonance imaging, donepezil, effective connectivity

1 Introduction

Cholinesterase inhibitors are currently the first line of treatment for AD patients in clinical practice (Renn et al., 2018). Among them, donepezil is highly selective for acetylcholinesterase in the central nervous system (CNS). Cholinesterase inhibitors increases the concentration of acetylcholine in the CNS, particularly in cortical and basal forebrain (BF) synapses, little effect on peripheral acetylcholinesterase, thus effectively improving cognition. Donepezil hydrochloride is therefore widely used in clinical practice (Fan et al., 2022). AD is considered a "disconnection syndrome," suggesting that loss of neurons and their connections disrupts the structural and functional connections between neurons and macroscopic brain regions, leading to clinical symptoms (Stam, 2014). Therefore, understanding the brain mechanisms by which donepezil modulates the cholinergic network to intervene in the clinical symptoms of AD may help to improve the theoretical basis for clinical drug selection.

In recent years, magnetic resonance imaging (MRI) technology has been used to study the brain mechanisms of donepezil intervention in AD (Saykin et al., 2004; Dubois et al., 2015; Griffanti et al., 2016; Luo et al., 2019). Short-term treatment with cholinesterase inhibitors enhances neuronal activity of frontal circuits in mild cognitive impairment (MCI) patients, and this increase is associated with improved cognitive performance and baseline hippocampal integrity (Saykin et al., 2004). The rate of hippocampal atrophy in prodromal AD was reduced by 45% after 1 year of treatment with donepezil compared to the placebo group (Dubois et al., 2015). Studies of functional connectivity showed an increase in functional connectivity (FC) in the orbitofrontal neural network in AD patients after donepezil intervention and correlated with post-treatment cognitive improvement (Griffanti et al., 2016). However, it has been shown that there is not only strength of connection but also directionality in the correlation between brain regions (Luo et al., 2019). A cross-sectional study of the Granger causality analysis (GCA) showed reduced EC from the posterior cingulate to the middle temporal gyrus, anterior cingulate and precuneus in patients with AD carried by APOEε4 (Luo et al., 2019). However, there are no studies examining the neural mechanisms underlying the effective connectivity network of cholinergic pathways in AD patients before and after donepezil intervention.

The basal forebrain can be divided into the nucleus basalis of Meynert and the medial septum/diagonal bands (MS/DB), depending on the brain region to which the cholinergic nerves project remotely (Zaborszky et al., 1999). Castaneda et al. (2015) explored changes in cholinergic neurons in a rat model in which the medial septal nucleus was injected with Aβ1-40 and memantine. They found that the number of cholinergic neurons in the medial septum and diagonal band was significantly reduced in the Aβ1-40 group compared to the Aβ/memantine treated group (Castaneda et al., 2015). Reduced MS/DB gray matter volume in AD patients also correlates with spatial cognitive function (Parizkova et al., 2020). Selective activation of cholinergic circuits that branch vertically from the medial septal nucleus of the basal forebrain and the diagonal band nucleus to the hippocampus attenuates memory deficits in APPswe/PSEN1dE9 (APP/PS1) mice (Liu et al., 2022). However, studies investigating the mechanisms of MS/DB-related brain networks in AD patients are still scarce.

Thus, we aimed to examine EC network modifications in cholinergic pathways in Alzheimer's disease patients following donepezil administration using rsfMRI data and the GCA approach. For EC analysis, we used the MNI standard space's basal forebrain subregions template as the region of interest. We predicted that changes in the basal forebrain EC network are linked to cognitive function in Alzheimer's disease patients.

2 Materials and methods

2.1 Patients

Between January 2018 and July 2022, sixteen individuals with Alzheimer's disease participated in this longitudinal study at Tongde Hospital in Hangzhou, Zhejiang Province, China. According to the National Institute on Aging-Association Alzheimer's recommendations (Gmitrowicz and Kucharska, 1994), patients with AD matched the criteria for probable AD. They were right-handed, had a CDR of 0.5, a Mini-Mental State Examination (MMSE) score of less than 24, and had completed more than six years of education. Sixteen healthy people were enrolled to serve as healthy controls (HC). They were cognitively normal and had a CDR score of 0. Participants with a history of mental illness, who were using antidepressants, or who had MR imaging contraindications were eliminated.

To determine the level of depression, the neuropsychiatric inventory (NPI) (Gmitrowicz and Kucharska, 1994) and the Cornell scale for depression in dementia (CSDD) (Alexopoulos

et al., 1988) were employed. Depression symptoms were declared present when the CSDD score was larger than 6 and the NPI depression domain score was larger than 4 (Alexopoulos et al., 1988; Cummings et al., 1994; Schneider et al., 2001).

At baseline (T1) and after 24 weeks (T2) of donepezil treatment, patients had MRI scans, neurological and medical examinations, and neuropsychological assessments (5 mg daily for the first 4 weeks, then 10 mg daily) (Zhang and Gordon, 2018). Everyone who took part signed an informed consent form. The Ethics Committee approved the study.

2.2 MRI scanning

This study was performed using a Siemens Magnetom Verio (Siemens Medical Systems, Erlangen, Germany), a 3.0 Tesla MRI scanner with an 8-channel head coil. Fast gradient echo images of anatomical T1-weighted whole brain magnetization-prepared were obtained using the following parameters: TI/TR/TE = 900/1,900/2.48 ms, 128 slices, 1 mm thickness, 0 mm gap, 9° FA, 256 × 256 acquisition matrix, 256 mm × 256 mm FOV. Gradient echo planar imaging was used to provide axial functional images with the following parameters Images: repetition rate (TR) = 2,000 ms, echo time (TE) = 30 ms, slice = 33, thickness = 4.8 mm, gap = 0 mm, field of view (FOV) = 200 mm × 200 mm, acquisition matrix = 64 × 64, flip angle = 90°. It took 6 min 40 s to complete the fMRI scan.

2.3 Data processing

Data preprocessing was done using SPM12[1] and Resting-State fMRI Data Analysis Toolkit plus V1.25 (RESTplus V1.25).[2] The first ten volumes were eliminated. Slice-timing was carried out and motion correction was applied. In terms of framewise displacement, participant head motion was minimal (mean FD < 0.5). We first coregistered the fMRI images to each subject's high-resolution T1 anatomical scan before normalizing them to Montreal Neurological Institute (MNI) space. The images were then adjusted to match the MNI152 template. 6 mm full widths at half maximum Gaussian kernel were used to smooth the normalized images and linear detrending. To reduce low-frequency drift and physiological high-frequency respiration, temporal bandpass filtering (0.01–0.08 Hz) were applied. White matter, cerebrospinal fluid and head motion artifacts were regressed out to eliminate false signals.

2.4 Effective connectivity calculation

For each participant, four BF seeds (two per hemisphere) were created using a method based on Julich-Brain Atlas (Schneider et al., 2001), respectively. The four subregions are ch123 in the left and right medial septum/diagonal bands and Ch4 in the left and right basal nuclei of Meynert (**Figure 1**).

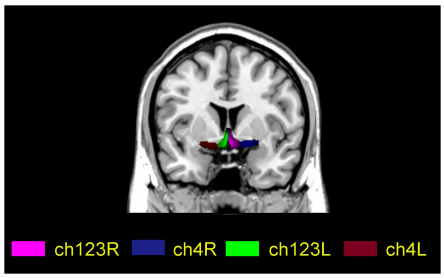

FIGURE 1
Localization map of basal forebrain subregions on a standard MNI spatial template. Ch123L and Ch123R indicate the left and right medial septum/diagonal bands, respectively; Ch4L and Ch4R indicate the left and right basal nuclei of Meynert, respectively.

Each subject underwent a voxel-wise GCA analysis using RESTplus V1.25. Four BF subregions were chosen for each participant in accordance with the available literature (Amunts et al., 2020). The seed time series X is the average time series of the seed regions, and the time series Y is the time series of the remaining voxels across the entire brain. In the entire brain, the linear direct effects of X on Y (information flow from X to Y) and Y on X (information flow from Y to X) are assessed voxel by voxel. In terms of directionality, a positive coefficient from X to Y denotes a causal relationship between activity in area X and Y. A negative coefficient from X to Y shows that activity in area X has a direct opposite influence on activity in area Y. A GCA map from the BF subregions to the whole brain (x2y) and a GCA map from the whole brain to the BF subregions (y2x) are represented as the results for each subject. For second-level group analyses, each individual-level EC map was then transformed using Fisher's r-to-z transformation into a z-map (Zang et al., 2012).

2.5 Statistical analysis

The demographics and clinical characteristics were analyzed using statistical software (Statistical Package for the Social Sciences v.15.0; SPSS, Inc., Chicago, IL, USA). A two sample *t*-test was used to analyze differences in age and education, and chi-squared tests were used to analyze differences in gender distribution.

Prior to statistical analyses, we tested the normality of the functional MRI data using the Lilliefors test. A one-way analysis of covariance (ANCOVA) was used to compare the BF EC maps voxel by voxel between the three groups. Then, from the ANCOVA analysis, we extracted brain masks that showed significant differences. Finally, we performed *post-hoc* *t*-tests between each pair of groups using the ANCOVA brain masks. The two sample *t*-test was used to compare the AD group to the HC group after the intervention, and the paired *t*-test was used to compare the AD group before and after the intervention. To ensure the accuracy of the results, we removed the mean relative displacements of head motion, age and gender as covariates in the ANCOVA and *t*-tests. The resulting statistical map was set to $p < 0.05$ for multiple comparisons (AlphaSim corrected for multiple comparisons, with a combined individual voxel *p*-value 0.005 with a cluster size > 25 voxels).

1 http://www.fil.ion.ucl.ac.uk/spm
2 http://www.restfmri.net

TABLE 1 Demographics and neuropsychological data.

	AD group	HC group	c2/*t*-value	*P*-value
Gender, *n* (M/F)	16 (8/8)	16 (7/9)	2	0.157
Age, years	65.2 ± 8.1	69.1 ± 4.5	1.659	0.107
Education, years	9.1 ± 2.0	8.3 ± 2.1	1.198	0.240
MMSE	19.7 ± 2.6	29.1 ± 0.90	−10.342	< 0.001
MMSE (24w)	20.1 ± 2.5			
NPI	4.56 ± 2.9	0.15 ± 0.36	12.632	< 0.001
NPI (24w)	1.38 ± 1.2			
CSDD	3.25 ± 2.40			
CSDD (24w)	0.75 ± 0.71			

Data are represented as the mean ± SD. The Chi-squared test was used to compare sex, and two-sample *t*-tests were used to compare age and neuropsychological data. HCs, healthy controls; AD, Alzheimer's disease; M, male; F, female; MMSE, Mini-Mental State Examination; NPI, the neuropsychiatric inventory; CSDD, Cornell scale for depression in dementia. CDR, clinical dementia rating.

TABLE 2 Brain regions with significantly different effective connectivity values with right medial septum/diagonal bands in the AD after intervention group compared with the AD group before intervention and HC group.

Brain regions	Voxels	BA	MNI coordinates			F/*t*-value	*P*-value
			x	y	z		
ANCOVA							
Frontal_Inf_Orb_R	53	47	48	36	−6	14.0965	< 0.005
Occipital_Mid_L	36	19	−39	−87	12	14.5534	< 0.005
Precuneus_R	26	7	6	−72	36	10.0772	< 0.005
t2 vs. t1							
Occipital_Mid_L	28	19	−39	−90	12	4.3210	< 0.005
t1 vs. HC							
Precuneus_R	40	7	6	−72	36	−4.3702	< 0.005
t2 vs. HC							
Frontal_Inf_Orb_R	74	47	48	33	−3	5.2935	< 0.005

AD, Alzheimer's disease; MNI, Montreal Neurological Institute; BA, Brodmann area. t1, pre-intervention AD patients; t2, post-intervention AD patients.

2.6 Relationship of EC with clinical variables

The mean BF EC values of the abnormal brain regions were extracted, and Pearson correlations were used to investigate the relationships between abnormal FC values and clinical variables in AD patients before and after intervention ($P < 0.05$).

3 Results

3.1 Neuropsychological results

Table 1 displays the demographics and clinical data. Age, gender distribution, and educational attainment differences between groups were not statistically significant ($p = 0.107$, 0.157, and 0.240, respectively). The AD group had significantly lower MMSE scores and higher NPI scores than the HC group ($p < 0.001$).

3.2 Abnormal BF EC values in the AD group

ANCOVA analysis revealed significant EC differences between the three groups in brain regions located in the left middle occipital gyrus, right inferior frontal gyrus/orbit part and right precuneus (Table 2 and Figure 2). Compared to baseline status, AD patients after donepezil intervention had an increased EC from left middle occipital gyrus to right MS/DB. Compared to HC, AD patients after donepezil intervention had an increased EC from right inferior frontal gyrus/orbit part to right MS/DB, AD patients before donepezil intervention had a reduced EC from right precuneus to right MS/DB (Table 2 and Figure 3).

3.3 Correlations of EC with clinical variables

A significant positive correlation was found between EC values in right precuneus and Mini-Mental State Examination in pre-intervention AD patients ($r = 0.7338$, $p = 0.0012$) (Figure 4).

4 Discussion

Using rsfMRI data and the GCA method, we investigated the alternation of the BF EC network in the AD groups before and after donepezil intervention in comparison to the HC group.

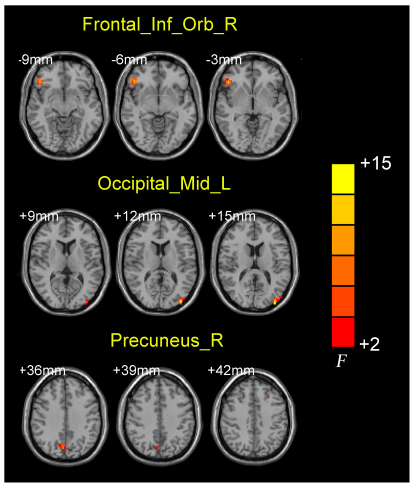

FIGURE 2
Brain regions showing the abnormal right medial septum/diagonal bands functional connectivity values among three groups.

Compared with their baseline status, AD patients after donepezil intervention had an increased EC from left middle occipital gyrus to right MS/DB. Compared to HCs, AD patients after donepezil intervention had an increased EC from right inferior frontal gyrus/orbit part to right MS/DB, AD patients before donepezil intervention had a reduced EC from right precuneus to right MS/DB. A significant positive correlation was found between EC values in right precuneus and Mini-Mental State Examination in pre-intervention AD patients.

Our research shows that AD patients after donepezil intervention exhibited an increased EC from right inferior frontal gyrus/orbit part and right precuneus to right MS/DB. The precuneus and orbitofrontal lobes belong to the default mode network (DMN). The DMN is a key brain network in the development of AD and is also the main brain network associated with cognitive function (Gomez-Ramirez and Wu, 2014). The donepezil-treated group showed increased volume of the precuneus and higher connectivity in the default mode network area compared to the untreated group (Solé-Padullés et al., 2013; Moon et al., 2016). High frequency stimulation of the precuneus in AD patients using repetitive transcranial magnetic stimulation (rTMS) was found to improve situational cognitive function in AD patients (Koch et al., 2018). Analysis of TMS-electroencephalogram (EEG) signals showed increased neural activity in the precuneus and altered functional connectivity with the medial frontal region of the DMN in AD patients (Koch et al., 2018, 2022). A Single-photon emission computed tomography (SPECT) imaging-based

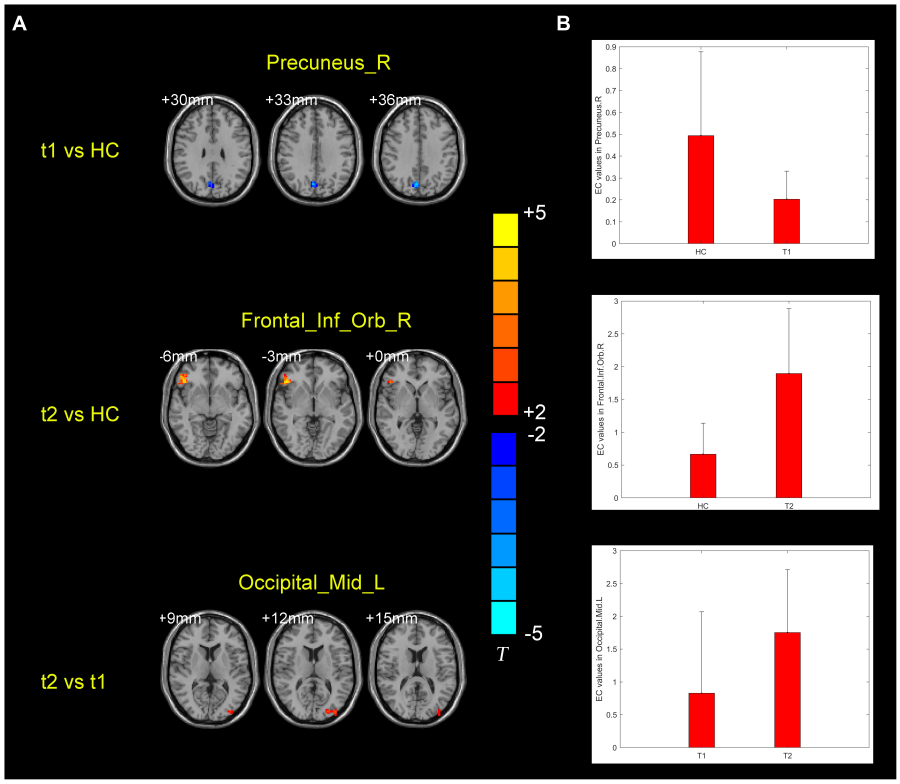

FIGURE 3
(A) Brain regions showing the alternation of right medial septum/diagonal bands effective connectivity values in the post-intervention AD group compared with pre-intervention AD and HC groups. **(B)** Means and standard deviations of the difference brain regions obtained from the comparison of the three groups of effective connectivity. t1, pre-intervention AD patients; t2, post-intervention AD patients.

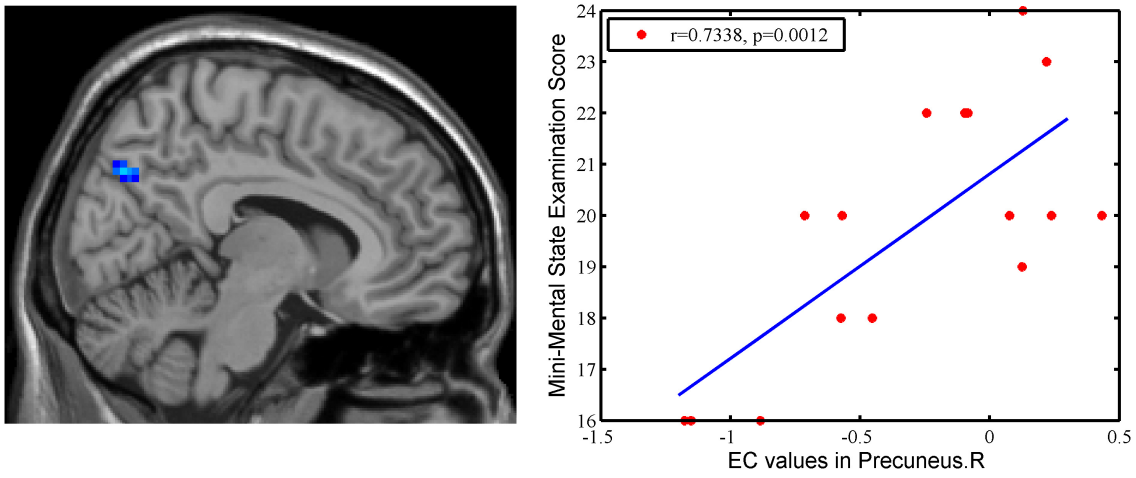

FIGURE 4
The correlation between EC values in the right precuneus and clinical variables in AD patients. There is a significant positive correlation was found between EC values in right precuneus and MMSE in pre-intervention AD patients (r = 0.7338, p = 0.0012).

study showed a significant increase in preconditioning stress, disinhibition and euphoria and a significant decrease in bilateral orbital frontal perfusion in responsive AD patients compared to non-responsive AD patients after donepezil intervention (Mega et al., 2000). Our findings are consistent with those of the previous study. Donepezil did not only enhance functional, but effective connections between the basal forebrain and the default mode network, thereby improving clinical symptoms in AD patients.

Our results show that, comparison to their baseline status, AD patients after donepezil intervention had an increased EC from left middle occipital gyrus to right MS/DB. Visual dysfunction is one of the main clinical symptoms of AD patients, symptoms including spatial disturbances and reduced visual field for cognitive range of vision (Kusne et al., 2017). Better orientation performance in AD patients is associated with enhanced cerebral metabolism in the bilateral middle and inferior temporal lobes, bilateral middle and posterior cingulate gyrus, left angular gyrus and left middle occipital gyrus. Orientation functions include list learning, recognition memory, visuospatial function, attention and language (Weissberger et al., 2017). Four hours after donepezil administration, there was a significant relative increase in perfusion in the left parietal, right superior frontal gyrus and right middle occipital gyrus in responders (Tepmongkol et al., 2019). Our findings suggest that donepezil enhances the strength of connections between the basal forebrain and middle occipital gyrus, thereby improving visual cognitive function in AD patients.

Our study adds to the neural mechanisms of donepezil intervention on clinical symptoms in AD patients. Previous findings have shown that donepezil modulates clinical symptoms in AD patients from different perspectives, such as hippocampal volume, frontal functional networks and MAPK/NLRP3 inflammasome/STAT3 signaling (Dubois et al., 2015; Griffanti et al., 2016; Kim et al., 2021). Moreover, the combination of machine learning methods and imaging data can provide guidance for clinical drug use. By increasing the amount of training data and the generalization ability of the machine learning model, it can better predict the efficacy of clinical drugs for AD patients and guide the use of clinical drugs (May, 2021).

We should be aware of some restrictions on our study. To further validate the accuracy of the results, larger samples and data from multiple sites are first required. Second, a growing body of evidence suggests that cognitive changes in preclinical AD may be more global (Salmon, 2012). Thus, more comprehensive scales, like the Montreal Cognitive Assessment and the Alzheimer's Disease Assessment Scale-cognitive subscale, could be used to assess the clinical status of AD patients since the scales used in this study to measure the cognitive function of AD patients are not sufficiently rich. Third, this study used rsfMRI to examine changes in the functional network of the cholinergic pathway in the gray matter of AD patients. Diffusion imaging may be used in the future to investigate abnormalities in the connections between white matter fibers in the cholinergic pathway in AD patients. Finally, T2-weighted MR images were not collected in this study to assess white matter hypersignal (WMH) in the patients. WMH loading indicates the severity of possible cerebral small-vessel disease or other cerebrovascular abnormalities, and may be an important influencing factor.

5 Conclusion

In the current study, we compared the BF EC in AD groups before and after donepezil intervention and HC groups. Our results showed that abnormal brain regions are located on the DMN and occipital lobe. These findings suggest that donepezil enhances the strength of connections between the basal forebrain with DMN and middle occipital gyrus, thereby improving cognitive function in AD patients.

Data availability statement

The original contributions presented in this study are included in the article/supplementary material, further inquiries can be directed to the corresponding authors.

Ethics statement

The studies involving humans were approved by the Ethics Committee of Tong De Hospital of Zhejiang Province (approval no. 2017-11-12). The studies were conducted in accordance with the local legislation and institutional requirements. The participants provided their written informed consent to participate in this study.

Author contributions

TY: Formal analysis, Investigation, Methodology, Visualization, Writing – original draft, Writing – review & editing. FW: Investigation, Methodology, Resources, Software, Writing – review & editing. YG: Formal analysis, Resources, Data curation, Validation, Writing – review & editing. MZ: Data curation, Formal analysis, Investigation, Validation, Writing – review & editing. HH: Investigation, Methodology, Software, Writing – review & editing. ZG: Formal analysis, Conceptualization, Funding acquisition, Project administration, Resources, Writing – review & editing. XL: Software, Conceptualization, Funding acquisition, Project administration, Writing – original draft, Writing – review & editing.

Funding

The authors declare that financial support was received for the research, authorship, and/or publication of this article. This research was supported by the General Project of the Department of Science and Technology of Zhejiang Province (2017KY109 and 2020KY182 to XL) and the General Project of the Department of Science and Technology of Zhejiang Province (2018KY031 and 2024KY873 to ZG).

Conflict of interest

The authors declare that the research was conducted in the absence of any commercial or financial relationships that could be construed as a potential conflict of interest.

Publisher's note

All claims expressed in this article are solely those of the authors and do not necessarily represent those of their affiliated organizations, or those of the publisher, the editors and the reviewers. Any product that may be evaluated in this article, or claim that may be made by its manufacturer, is not guaranteed or endorsed by the publisher.

References

Alexopoulos, G., Abrams, R., Young, R., and Shamoian, C. (1988). Cornell scale for depression in dementia. *Biol. Psychiatry* 23, 271–284.

Amunts, K., Mohlberg, H., Bludau, S., and Zilles, K. (2020). Julich-Brain: A 3D probabilistic atlas of the human brain's cytoarchitecture. *Science* 369, 988–992. doi: 10.1126/science.abb4588

Castaneda, M., Lopez, E., Touhami, A., Tovar, R., Ortega, M., and Rodriguez, J. (2015). Neuroprotection of medial septal cholinergic neurons by memantine after intralateral septal injection of Aβ1-40. *Neuroreport* 26, 450–454.

Cummings, J. L., Mega, M., Gray, K., Rosenberg-Thompson, S., Carusi, D. A., and Gornbein, J. (1994). The Neuropsychiatric Inventory: Comprehensive assessment of psychopathology in dementia. *Neurology* 44, 2308–2314.

Dubois, B., Chupin, M., Hampel, H., Lista, S., Cavedo, E., Croisile, B., et al. (2015). Hippocampus Study Group"; Hippocampus Study Group. Donepezil decreases annual rate of hippocampal atrophy in suspected prodromal Alzheimer's disease. *Alzheimers Dement.* 11, 1041–1049. doi: 10.1016/j.jalz.2014.10.003

Fan, F., Liu, H., Shi, X., Ai, Y., Liu, Q., and Cheng, Y. (2022). The efficacy and safety of Alzheimer's Disease therapies: An updated umbrella review. *J. Alzheimers Dis.* 85, 1195–1204. doi: 10.3233/JAD-215423

Gmitrowicz, A., and Kucharska, A. (1994). [Developmental disorders in the fourth edition of the American classification: Diagnostic and statistical manual of mental disorders (DSM IV – optional book)]. *Psychiatr. Pol.* 28, 509–521.

Gomez-Ramirez, J., and Wu, J. (2014). Network-based biomarkers in Alzheimer's disease: Review and future directions. *Front. Aging Neurosci.* 6:12. doi: 10.3389/fnagi.2014.00012

Griffanti, L., Wilcock, G., Voets, N., Bonifacio, G., Mackay, C., Jenkinson, M., et al. (2016). Donepezil enhances frontal functional connectivity in Alzheimer's Disease: A pilot study. *Dement. Geriatr. Cogn. Dis. Extra* 6, 518–528. doi: 10.1159/000450546

Kim, J., Lee, H.-J., Park, S. K., Park, J.-H., Jeong, H.-R., Lee, S., et al. (2021). Donepezil Regulates LPS and Aβ-stimulated neuroinflammation through MAPK/NLRP3 inflammasome/STAT3 signaling. *Int. J. Mol. Sci.* 22:10637.

Koch, G., Bonnì, S., Pellicciari, M., Casula, E., Mancini, M., Esposito, R., et al. (2018). Transcranial magnetic stimulation of the precuneus enhances memory and neural activity in prodromal Alzheimer's disease. *Neuroimage* 169, 302–311. doi: 10.1016/j.neuroimage.2017.12.048

Koch, G., Casula, E., Bonnì, S., Borghi, I., Assogna, M., Minei, M., et al. (2022). Precuneus magnetic stimulation for Alzheimer's disease: A randomized, sham-controlled trial. *Brain* 145, 3776–3786.

Kusne, Y., Wolf, A., Townley, K., Conway, M., and Peyman, G. (2017). Visual system manifestations of Alzheimer's disease. *Acta Ophthalmol.* 95, e668–e676.

Liu, W., Li, J., Yang, M., Ke, X., Dai, Y., Lin, H., et al. (2022). Chemical genetic activation of the cholinergic basal forebrain hippocampal circuit rescues memory loss in Alzheimer's disease. *Alzheimers Res. Ther.* 14:53. doi: 10.1186/s13195-022-00994-w

Luo, X., Li, K., Jia, Y., Zeng, Q., Jiaerken, Y., Qiu, T., et al. (2019). Altered effective connectivity anchored in the posterior cingulate cortex and the medial prefrontal cortex in cognitively intact elderly APOE ε4 carriers: A preliminary study. *Brain Imaging Behav.* 13, 270–282.

May, M. (2021). Eight ways machine learning is assisting medicine. *Nat. Med.* 27, 2–3.

Mega, M., Dinov, I., Lee, L., O'Connor, S., Masterman, D., Wilen, B., et al. (2000). Orbital and dorsolateral frontal perfusion defect associated with behavioral response to cholinesterase inhibitor therapy in Alzheimer's disease. *J. Neuropsychiatry Clin. Neurosci.* 12, 209–218. doi: 10.1176/jnp.12.2.209

Moon, C., Kim, B., and Jeong, G. (2016). Effects of donepezil on brain morphometric and metabolic changes in patients with Alzheimer's disease: A DARTEL-based VBM and (1)H-MRS. *Magn. Reson. Imaging* 34, 1008–1016. doi: 10.1016/j.mri.2016.04.025

Parizkova, M., Lerch, O., Andel, R., Kalinova, J., Markova, H., Vyhnalek, M., et al. (2020). Spatial pattern separation in early Alzheimer's Disease. *J. Alzheimers Dis.* 76, 121–138.

Renn, B., Asghar-Ali, A., Thielke, S., Catic, A., Martini, S., Mitchell, B., et al. (2018). Systematic review of practice guidelines and recommendations for discontinuation of cholinesterase inhibitors in dementia. *Am. J. Geriatr. Psychiatry* 26, 134–147.

Salmon, D. (2012). Neuropsychological features of mild cognitive impairment and preclinical Alzheimer's disease. *Curr. Top. Behav. Neurosci.* 10, 187–212.

Saykin, A., Wishart, H., Rabin, L., Flashman, L., McHugh, T., Mamourian, A., et al. (2004). Cholinergic enhancement of frontal lobe activity in mild cognitive impairment. *Brain* 127(Pt 7), 1574–1583.

Schneider, L. S., Tariot, P. N., Lyketsos, C. G., Dagerman, K. S., Davis, K. L., Davis, S., et al. (2001). National institute of mental health clinical antipsychotic trials of intervention effectiveness (CATIE): Alzheimer disease trial methodology. *Am. J. Geriatr. Psychiatry* 9, 346–360.

Solé-Padullés, C., Bartrés-Faz, D., Lladó, A., Bosch, B., Peña-Gómez, C., Castellví, M., et al. (2013). Donepezil treatment stabilizes functional connectivity during resting state and brain activity during memory encoding in Alzheimer's disease. *J. Clin. Psychopharmacol.* 33, 199–205. doi: 10.1097/JCP.0b013e3182825bfd

Stam, C. (2014). Modern network science of neurological disorders. *Nat. Rev. Neurosci.* 15, 683–695.

Tepmongkol, S., Hemrungrojn, S., Dupont, P., Tunvirachaisakul, C., Aniwattanapong, D., Likitjareon, Y., et al. (2019). Early prediction of donepezil cognitive response in Alzheimer's disease by brain perfusion single photon emission tomography. *Brain Imaging Behav.* 13, 1665–1673. doi: 10.1007/s11682-019-00182-9

Weissberger, G., Melrose, R., Fanale, C., Veliz, J., and Sultzer, D. (2017). Cortical metabolic and cognitive correlates of disorientation in Alzheimer's Disease. *J. Alzheimers Dis.* 60, 707–719.

Zaborszky, L., Pang, K., Somogyi, J., Nadasdy, Z., and Kallo, I. (1999). The basal forebrain corticopetal system revisited. *Ann. N. Y. Acad. Sci.* 877, 339–367. doi: 10.1111/j.1749-6632.1999.tb09276.x

Zang, Z., Yan, C., Dong, Z., Huang, J., and Zang, Y. (2012). Granger causality analysis implementation on MATLAB: A graphic user interface toolkit for fMRI data processing. *J. Neurosci. Methods* 203, 418–426. doi: 10.1016/j.jneumeth.2011.10.006

Zhang, N., and Gordon, M. (2018). Clinical efficacy and safety of donepezil in the treatment of Alzheimer's disease in Chinese patients. *Clin. Interv. Aging* 13, 1963–1970.

frontiers | Frontiers in Aging Neuroscience

TYPE Review
PUBLISHED 17 April 2024
DOI 10.3389/fnagi.2024.1378576

OPEN ACCESS

EDITED BY
Allison B. Reiss,
New York University, United States

REVIEWED BY
Vaishnavi Jadhav,
University of Washington, United States
Lotta Emilia Oikari,
The University of Queensland, Australia

*CORRESPONDENCE
Julie A. Saugstad
✉ saugstad@ohsu.edu

RECEIVED 29 January 2024
ACCEPTED 03 April 2024
PUBLISHED 17 April 2024

CITATION
Jaye S, Sandau US and Saugstad JA (2024) Clathrin mediated endocytosis in Alzheimer's disease: cell type specific involvement in amyloid beta pathology.
Front. Aging Neurosci. 16:1378576.
doi: 10.3389/fnagi.2024.1378576

Clathrin mediated endocytosis in Alzheimer's disease: cell type specific involvement in amyloid beta pathology

Sierra Jaye, Ursula S. Sandau and Julie A. Saugstad*

Department of Anesthesiology & Perioperative Medicine, Oregon Health & Science University, Portland, OR, United States

This review provides a comprehensive examination of the role of clathrin-mediated endocytosis (CME) in Alzheimer's disease (AD) pathogenesis, emphasizing its impact across various cellular contexts beyond neuronal dysfunction. In neurons, dysregulated CME contributes to synaptic dysfunction, amyloid beta (Aβ) processing, and Tau pathology, highlighting its involvement in early AD pathogenesis. Furthermore, CME alterations extend to non-neuronal cell types, including astrocytes and microglia, which play crucial roles in Aβ clearance and neuroinflammation. Dysregulated CME in these cells underscores its broader implications in AD pathophysiology. Despite significant progress, further research is needed to elucidate the precise mechanisms underlying CME dysregulation in AD and its therapeutic implications. Overall, understanding the complex interplay between CME and AD across diverse cell types holds promise for identifying novel therapeutic targets and interventions.

KEYWORDS

Alzheimer's disease, amyloid beta, clathrin mediated endocytosis, endolysosomal dysfunction, therapeutics

1 Introduction

Endocytosis is a ubiquitous and essential function of mammalian cells as it mediates many downstream pathways through the internalization of extracellular material from the cell surface. Many types of endocytosis have been described, including clathrin-mediated endocytosis (CME), dynamin-dependent endocytosis, caveolin dependent endocytosis, micropinocytosis, and phagocytosis (Doherty and McMahon, 2009). Of these, CME is one of the most well characterized and mechanistically understood. Processes that rely on CME include uptake of intracellular signals, transmembrane receptor recycling, regulation of membrane composition, synaptic vesicle recycling, and initiation/regulation of downstream intercellular signaling cascades such as the endolysosomal system. The distinct phases of CME are comprised of nucleation, cargo selection, coat assembly, scission, and uncoating. Each step is moved forward by an essential hub protein, which are supported by additional accessory proteins, described in detail through decades of studies (McMahon and Boucrot, 2011; Kaksonen and Roux, 2018). Hub and accessory proteins are indicated in Figure 1.

CME is initiated by proteins involved in nucleation (Figure 1, Step 1), including FCH and mu domain containing endocytic adaptor 1/2 (FCHO1,2), Intersectin1 (ITSN1), and Epidermal growth factor receptor substrate 15 (EPS15). These proteins cluster and bind to the plasma membrane to initiate membrane curvature and recruit other proteins, such as the

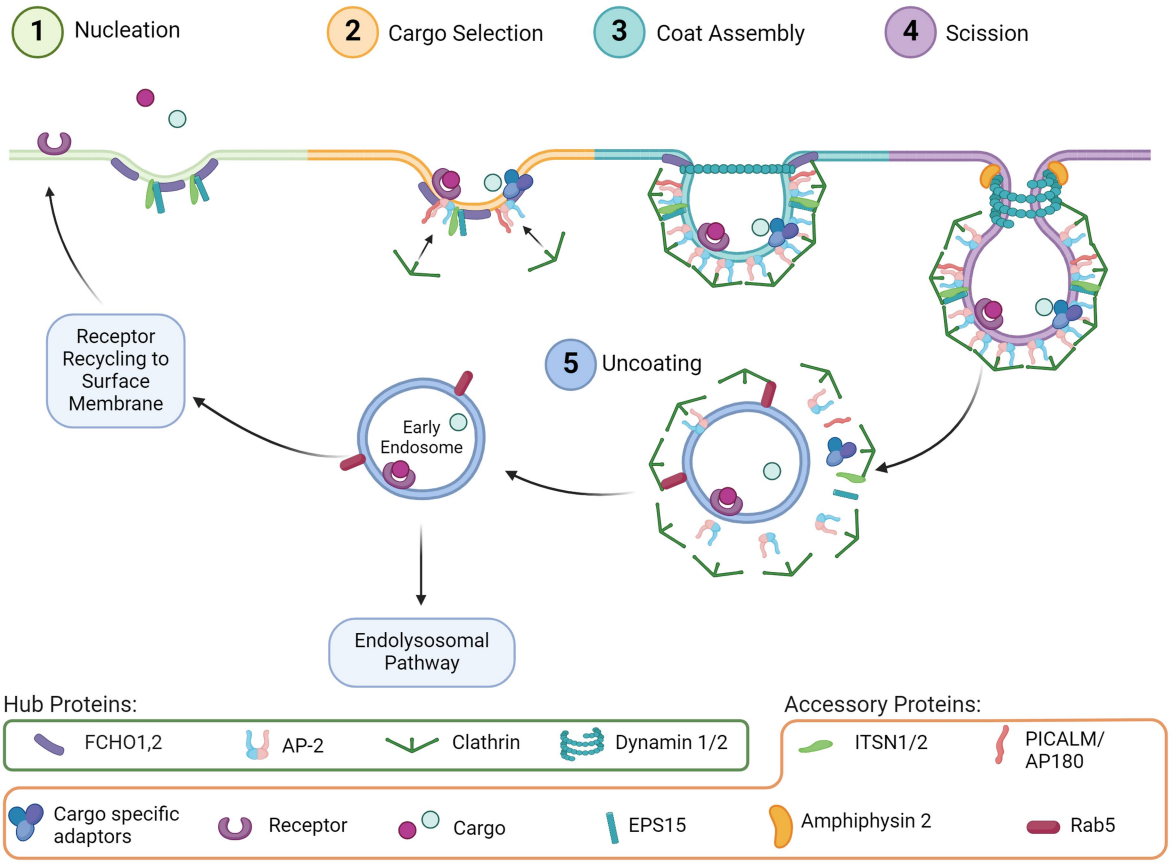

FIGURE 1
CME step-by-step. (1) Nucleation: Initial invagination of the membrane surface and recruitment of support proteins to the pit. (2) Cargo selection: Budding vesicle couples with the intended cargo via receptors and adaptor proteins, which concurrently begin recruiting clathrin. (3) Coat assembly: Clathrin begins forming a lattice around the budding vesicle. (4) Scission: Dynamin assembles around the vesicle neck, and with support from accessory proteins the vesicle is removed from the extracellular membrane. (5) Uncoating: The clathrin lattice disassembles and the early endosome can be trafficked through several pathways including back to the cell surface or through the endolysosomal pathway.

Adaptor protein 2 complex (AP-2), for cargo selection (Figure 1, Step 2). Clathrin is also recruited by AP-2, which then begins the clathrin coat assembly (Figure 1, Step 3) of the endosome and curves the membrane further, forming the vesicle around the clustered cargo. The vesicle then undergoes scission from the membrane (Figure 1, Step 4) by recruitment of Dynamin via the BAR-domain containing proteins. Uncoating of clathrin (Figure 1, Step 5) is subsequently initiated by Auxilin of G-associated kinase (GAK), which recruits ATPase HSC70 to disassemble the clathrin coat allowing the machinery to be available for the next endocytosis event. Cargo internalized through CME is typically sorted through the endolysosomal pathway for delivery to the appropriate cellular compartment (Boulant et al., 2011; McMahon and Boucrot, 2011; Mettlen and Danuser, 2014).

Given the fundamental need for cells to utilize this process, there are many diseases associated with disruption of CME. However, dysfunction is more common in accessory proteins, as genetic mutations of essential hub proteins, for example those that make up the AP-2 complex, can be embryonic lethal (Mitsunari et al., 2005; Azarnia et al., 2019). Changes in accessory proteins can still have profound effects on CME function and are associated with cancer, psychiatric diseases, and various neurodegenerative diseases (McMahon and Boucrot, 2011). For example, in Parkinson's disease, mutations in synaptojanin and auxilin have been shown to be causative for early onset Parkinson's (Schreij et al., 2016). In Alzheimer's disease (AD), genetic links have been made to endocytic protein genes such as *AP-2* (cargo selection), Clusterin (*CLU*, cargo selection), Bridging integrator 1 (*BIN1*, scission), CD2 associated protein (*CD2AP*, scission/uncoating), and Phosphatidylinositol binding clathrin assembly protein (*PICALM*, cargo selection) (Raj et al., 2018; Azarnia et al., 2019; Ando et al., 2022; Szabo et al., 2022). *BIN1* and *PICALM* are two of the most significant risk factors for late onset AD (Andrade-Guerrero et al., 2023). Importantly, while not directly involved in CME, many other significant AD risk factors like Apolipoprotein E (*APOE*), Ras and rab interactor 1 (*RIN1*), and Sortilin related receptor 1 (*SORL1*) have been related to endosomal and lysosomal dysfunction downstream from CME and are reviewed elsewhere (Szabo et al., 2022; Maninger et al., 2024).

AD is the most common form of dementia (Alzheimer's Association, 2023) and is characterized by the progressive development of amyloid beta (Aβ) plaques and neurofibrillary Tau protein tangles in the brain (Braak and Braak, 1991; Selkoe and Hardy, 2016). AD is often diagnosed 15–20 years after pathology begins to develop, so there is a need for reliable tools to detect early brain

changes that lead to it (Deture and Dickson, 2019) and the effort to identify early cellular changes before the onset of symptoms is of great importance. As AD progression is a highly complex process, many mechanisms have been associated with disease progression, such as neuroinflammation, impaired autophagy, oxidative stress, vascular dysfunction, and endolysosomal dysfunction (Nixon et al., 2000; Theerasri et al., 2022). Perhaps one of the most widely referenced mechanisms is the Aβ cascade hypothesis, a well-established model of disease progression, in which intercellular Aβ accumulates as plaques in the brain, induces Tau pathology, and ultimately neuronal death (Hardy and Allsop, 1991; Hardy and Higgins, 1992). Others have since suggested that the imbalance of extracellular Aβ clearance and intracellular accumulation of Aβ initiates neuronal dysfunction rather than merely the accumulation of extracellular plaques (Selkoe and Hardy, 2016; Volloch and Rits-Volloch, 2022, 2023). As such, the processes of Aβ production and clearance have been of particular interest in the field of AD.

The pathogenic form of Aβ ($Aβ_{1-42}$) is produced when Amyloid precursor protein (APP) is endocytosed and processed in the endolysosomal pathway of neurons (Koo and Squazzo, 1994; Selkoe and Hardy, 2016). CME has also been related to Tau pathology, primarily as a function of intercellular propagation in which aggregated pathologic Tau (Lamontagne-Kam et al., 2023) is internalized via many types of endocytosis including CME (Ando et al., 2020). While the potential cellular effects of Tau internalization by endocytosis are substantial (Thal and Tome, 2022), the ratio of Tau internalized via CME versus other endocytic pathways is unknown and thus studies are needed to determine if CME is as prominent a mechanism of Tau internalization, as it is for Aβ uptake.

As the primary process that feeds into the endolysosome, disruption of CME has the potential to affect this and many other downstream cellular pathways implicated with AD. The endolysosomal pathway in AD has been extensively studied downstream of CME (Nixon, 2017; Szabo et al., 2022), yet few investigators have evaluated the upstream changes and contribution of actual endocytosis, specifically CME, to AD pathogenesis. Additionally, in other brain cell types like microglia and astrocytes, CME is implicated in extracellular debris uptake and could be important to $Aβ_{1-42}$ clearance, illustrating the potential for CME to affect the balance of both intra- and extracellular $Aβ_{1-42}$ accumulation in multiple ways via multiple cell types. Here, we discuss how CME in different brain cell types has thus far been implicated in AD risk and progression. Aside from neurons, there is a gap in knowledge regarding a role for CME in Tau pathology. Thus, we will be focusing on CME and its relation to Aβ but will include Tau where information is available. We also focus the review on research that examines the importance of CME as a potential early disease modifier. For a detailed review of the role of downstream endosomal trafficking on AD pathogenesis see (Nixon, 2020; Behl et al., 2022; Szabo et al., 2022).

2 AD and endolysosomal function

The endolysosomal pathway systematically internalizes and sorts extracellular molecules that can either be used in the cell, recycled back to the cell membrane, or degraded internally through lysosomes and autophagosomes. Classically, molecular cargo is internalized through CME or other endocytic pathways and trafficked to early endosomes and then late endosomes, recycled to the surface membrane, or sent to the lysosome for degradation (Cullen and Steinberg, 2018). In AD, defects in the endolysosomal pathway cause cellular stress in multiple ways, including decreased endosomal transport, altered endosome signaling, reduction in vesicle recycling, decreased lysosomal acidification, and oxidative stress. These defects then result in various neuropathological outcomes such as $Aβ_{1-42}$ over production and clearance deficits, as well as dystrophic neurites (Nixon, 2017; Colacurcio et al., 2018; Szabo et al., 2022).

Interestingly, the earliest presenting cytopathology in sporadic AD, even before accumulation of extracellular Aβ plaques are observed, is enlargement of early endosomes in neurons containing soluble Aβ (Cataldo et al., 2000, 2004). Indeed, this intracellular Aβ frequently associated with the enlarged endosomes (Cataldo et al., 2004). This phenotype is specific to sporadic AD and has not been observed in familial AD or other neurodegenerative diseases like Parkinson's and Huntington's disease (Cataldo et al., 2000). Enlarged early endosomes are also observed in induced pluripotent stem cell (iPSC) derived neurons from sporadic AD patients (Israel et al., 2012) and iPSC lines with *APP* and presenilin 1 (*PSEN1*) mutations, both genetic risk factors for early-onset AD (Kwart et al., 2019; Lacour et al., 2019). Interestingly, endolysosomal dysregulation and enlarged early endosomes are also seen in Down syndrome, a genetic disorder caused by a triplication of chromosome HSA21 (Cataldo et al., 2000). People with Down syndrome have a significantly higher risk of developing AD, with nearly all patients developing neuropathology and symptoms by age 65 (McCarron et al., 2017; Fortea et al., 2021). This phenomenon is thought to be due to several AD related genes encoded on HSA21, such as *APP* and *PSEN1* (Colacurcio et al., 2018; Jiang et al., 2019; Botté and Potier, 2020; Filippone and Praticò, 2021). This connection between Down syndrome and AD could point toward endocytic processes as a potential driver of early endolysosomal dysfunction in AD.

Increased size and/or number of early endosomes is thought to correlate with an increase in general endocytosis, which results in the enlarged endosomal phenotype (Stenmark et al., 1994). This effect could indicate that changes in upstream endocytosis are important factors in downstream endolysosomal dysfunction in AD. The impact of cargo processed into this pathway has also been shown to alter endosomal function. For instance, in primary cortical rat neurons, internalization of $Aβ_{1-42}$ resulted in increased levels and altered distribution of endolysosomal markers, as well as triggered neuronal degeneration. Inhibiting general endocytosis via phenylarsine oxide, and CME specifically with sucrose, attenuated this effect and returned endolysosomal markers to normal, suggesting that endocytosis of pathogenic $Aβ_{1-42}$ contributes to downstream endosomal dysfunction (Song et al., 2011). Therefore, changes in CME may contribute to AD endolysosomal dysregulation in multiple ways.

Small et al. (2017) and Kimura and Yanagisawa (2018) summarize many of these endolysosomal disruptions into the "traffic jam" hypothesis. This hypothesis posits that disruptions in endocytosis and downstream endosome trafficking could be involved in altering the metabolism of AD related proteins and thus act as a pathogenic hub in AD. Similarly, Limone et al., proposed using the related genetic changes in endolysosomal trafficking as a "genetic hub" of AD which could contribute to many pathological events and illuminate potential drug targets (Limone et al., 2022). However, as these hypotheses focus primarily on trafficking of endosomes after endocytosis, how

endocytosis itself may be altered and affect cellular phenotypes in the context of AD remains to be considered.

3 Clathrin mediated endocytosis in AD

CME has been well studied under normal physiological conditions, but little is known about how it may be changed during AD progression. In addition to its downstream connection with the endolysosomal pathway, several studies have indirectly implicated CME in AD in humans and animal models through genomics, transcriptomics, and proteomics of CME-related genes and proteins. A current summary of CME proteins associated with AD, their function in CME, and which AD brain regions are affected is presented in Table 1.

In 2018, Ahmad et al., calculated weighted genetic risk scores by combining data from the longitudinal AD Rotterdam Study (Hofman et al., 2015) and 20 AD genetic risk variants. These risk scores were then clustered within cellular pathways and associated with AD, mild cognitive impairment (MCI), and brain MRI phenotypes. The risk score of endocytic pathways was significantly associated with MCI, and the clathrin/AP-2 adaptor complex pathway was modestly associated with white matter lesions (Ahmad et al., 2018). Interestingly, other studies assessing genetic risk factors of AD found that the endocytosis pathway was significantly associated with reliance against AD (Tesi et al., 2020) and that abnormal Aβ levels, but not Tau, are significantly associated with endocytosis (Schork and Elman, 2023). These associations suggest an early involvement of endocytosis, specifically CME, in AD risk/etiology and potential resilience. Indeed, proteins involved in CME such as AP180 (cargo selection), AP-2 (cargo selection/clathrin recruitment), and Dynamin 1 (scission) are shown to be decreased in AD in various regions of human post-mortem brains at both the RNA and protein level (Yao et al., 1999, 2000, 2003; Cao et al., 2010; Piras et al., 2019). Together, the changes of CME protein levels point toward involvement of the pathway in AD and its potential to be both disease contributing or neuroprotective, but each protein must be evaluated individually to understand how its changes may affect or contribute to potential CME dysfunction in AD.

Several of these protein changes also translate to a transgenic mouse model of AD with a mutation in humanized *APP* (APP_{SWE}) (Hsiao et al., 1996). Dynamin 1 and AP180 were decreased in APP_{SWE} brains versus controls, with varying degrees of specificity in subregions of the hippocampus, entorhinal cortex, and temporal cortex, similar to their changes in human AD brains (Cao et al., 2010). Interestingly, a separate study of the cortex in APP_{SWE} mice showed several CME proteins (APP, Clathrin, Dynamin 2, and PICALM) were upregulated, not downregulated as was observed in other brain areas. Importantly, proteins related to clathrin-independent endocytosis such as flotillin-1, and caveolin-1 and -3 were not changed (Thomas et al., 2011). These observations demonstrate that proteins specific to CME, and not to other common endocytic pathways, are changed and could point toward CME being specifically responsible for downstream endocytic abnormalities in APP_{SWE} mice. However, it is unknown whether more recently studied AD models with multiple transgenes, such as the 3xTg (Oddo et al., 2003) or 5xFAD lines (Oakley et al., 2006), recapitulate these changes or have CME disruptions. Several studies have shown that pharmacological modulation of downstream endolysosomal functions in 5xFAD mice (Cuddy et al., 2022) and in the 3xTg improved endolysosomal function and disease phenotypes (Kim et al., 2023), though how these manipulations may affect and be affected by upstream CME function is unclear.

Another consideration is whether normal aging affects levels of CME proteins and CME function. It is well known that the biggest risk factor of developing AD is aging, and a change in CME proteins over time could account for a possible connection between this risk factor and early cellular phenotypes. To date, only one study has attempted to address this possible connection. In 2018, Alsquati et al., examined how endocytosis-related proteins change in the frontal cortex of neurologically normal males from different age groups: 20–30 (young), 45–55 (middle aged), and 70–90 (old) (Alsaqati et al., 2018). Interestingly, both CME and clathrin-independent proteins were changed in an age-dependent manner. Four CME proteins, Dynamin I, isoform 4 of PICALM, AP180, and Rab5, were all significantly increased from the young to old age groups. Clathrin-independent proteins such as caveolin-2 and flotillin-2, increased with age, while caveolin-3 was decreased with age. Of note, some of these protein changes contrast with those seen in AD brains in the studies described above (Yao et al., 1999, 2000, 2003; Cao et al., 2010; Piras et al., 2019) and in Table 1, and may be related to general changes in endocytosis rather than specific changes to CME. It is unclear whether this effect may be due to evaluation of different brain regions, or to the exclusion of females from the aging study. Prior studies examining CME proteins in AD included both females and males in their cohorts, which is important, as females have a much higher incidence of AD (Rajan et al., 2021; Alzheimer's Association, 2023). Thus, examination of protein levels in males only does not allow any exploration of potential sex difference in endocytosis during aging, which could be a factor in the differential direction of expression changes between the aging study and others mentioned above. Additionally, the 15-year gap between each age group in these data should be considered. While the average age of AD diagnosis is about 75 years of age (Barnes et al., 2015), brain changes can occur for many years beforehand; thus, the 15 year gap between the middle aged (45–55) and old aged (70–90) groups could be enlightening and thus an important time point to evaluate. While the Alsquati study is a very promising initial study, more research is needed to elucidate the potential role of CME in early AD and if, or how, aging may be involved.

When thinking about how these observed differences in AD CME proteins may affect function, we must also consider the potential for specific CME functions in different brain regions and cell types. CME proteins show different changes depending on what brain region was analyzed (summarized in Table 1). Also, CME proteins may not change in the same way in all cells, since AD has varying effects on many brain cell types (e.g., neurons, astrocytes, and microglia) throughout disease progression (Maninger et al., 2024). Studies are still needed to examine how the effect on overall CME function might be different in each brain region depending on how a specific protein, or set of proteins, is changed. It is possible that an increase in one protein potentially reduces CME, while the same increase in a different protein could decrease CME in a different brain region. Additionally, depending on the cell type, dysregulation of CME proteins and resulting downstream dysfunction may have distinct cellular outcomes. However, studies using whole brain lysate are not able to distinguish protein expression in different cell types. Thus, studies focused on individual cell types are needed to establish whether CME is altered

TABLE 1 CME proteins in human post-mortem AD brains.

Gene: protein name	Role in CME	Change in AD	Method	Brain region	References
AP2A1: AP-2 complex subunit alpha-1	Nucleation	Decreased	IHC	Layer II superior frontal gyrus	Yao et al. (2000)
		No change	IB	Total superior frontal gyrus, total hippocampus	
		Localized to NFTs	IHC	Temporal neocortex	Srinivasan et al. (2022)
FCHO1: FCH and mu domain containing endocytic adaptor 1	Nucleation	Unknown	–	–	–
SNAP91: Synaptosome associated protein a1 (AP180)	Paralog of PICALM, cargo selection	Decreased	IHC	All layers superior frontal gyrus, hippocampus CA3/Hilus	Yao et al. (1999)
		Decreased	IHC, IB	Dentate gyrus, CA3, entorhinal cortex, temporal cortex	Cao et al. (2010)
ITSN1: Intersectin 1	Nucleation, cargo selection	Increased	RT-PCR	Frontal cortex	Wilmot et al. (2008)
		no change	IB	Frontal cortex, temporal cortex	Malakooti et al. (2019)
PICALM: Phosphatidylinositol-binding clathrin assembly protein	Cargo selection	Increased	RT-PCR	Frontal cortex	Baig et al. (2010)
		Localized to NFTs	IHC	Hippocampus CA4	Ando et al. (2013), Alsaqati et al. (2023)
		Decreased	IB	Neocortex	
CLTA: Clathrin, light chain	Coat assembly, scission, uncoating	Localized to Some NFTs	IHC	Hippocampus	Nakamura et al. (1994)
CLTC: Clathrin, heavy chain		Increased	IHC	Frontal cortex	Alsaqati et al. (2023)
DNM1: Dynamin 1	Scission	Decreased	IHC	Hippocampus, entorhinal cortex	Cao et al. (2010)
DMN2: Dynamin 2	Scission	Decreased	qRT-PCR	Hippocampus	Aidaralieva et al. (2008)
		Decreased	RT-PCR	Temporal cortex	Kamagata et al. (2009)
BIN1: Amphiphysin 2	Scission	Increased	PCR	Frontal cortex	Chapuis et al. (2013)
		Decreased	IB	Frontal cortex	De Rossi et al. (2016)
AMPH: Amphyphysin 1	Paralog of BIN1, scission	Decreased	IB	Frontal cortex	De Jesus-Cortes et al. (2012)
RAB5A: Ras-related protein Rab-5A	Uncoating, early endosome fusion	Increased	IB	Frontal cortex	Alsaqati et al. (2023)
		Increased	qPCR, IB	Hippocampus CA1, frontal cortex	Ginsberg et al. (2010)

The table includes the gene and protein name, role in CME, change in protein in AD, method of detection, brain region evaluated, and reference(s). NFT, neurofibrillary tangles; IHC, Immunohistochemistry; IB, Immunoblot; PCR, Polymerase Chain Reaction; RT-PCR, Real-time PCR; qRT-PCR, Quantitative RT-PCR.

in distinct ways. Though brain region-specific changes are more challenging to evaluate due to difficulty obtaining the appropriate samples, many studies have begun to tease apart the potential cell type differences of CME proteins in AD, and will be further described in the remainder of this review.

4 CME dysfunction and AD cellular disruptions across multiple cell types

4.1 Neurons

4.1.1 CME involvement in synaptic dysfunction

As AD is characterized by increasing loss of neurons throughout disease, many studies to date have focused on how altered neuronal functions may affect disease progression. It is well established that synaptic dysfunction, loss, and subsequent neuronal degeneration contributes to the progressive nature of AD. Reduced synapse numbers are observed throughout disease progression and are strongly correlated with cognitive decline (Terry et al., 1991), but synapses start to show dysfunction even before measurable cellular degeneration. Normally, functioning synapses rely on the quick release of pre-synaptic vesicles which are rapidly recycled via CME to maintain the pool of vesicles available for transmission (Soykan et al., 2016). Synaptic disruption in AD can be induced by both extracellular $A\beta_{1\text{-}42}$ oligomers and intracellular hyperphosphorylated Tau, and as such, may be connected to other aspects of AD neuropathology, such as altered APP processing, abnormal phosphorylation, and calcium imbalance (Yao, 2004; Pei et al., 2020; Hori et al., 2022; Ratan et al.,

2023). Of note, synaptic vesicle recycling is reduced in AD, and multiple CME proteins that are involved in maintenance of synaptic vesicle size, uniformity, and turnover, are clustered at pre-synaptic sites (Pechstein et al., 2010; Milosevic, 2018). While several other mechanisms work in parallel to CME to maintain the synaptic vesicle pool, studies have shown that blocking CME significantly reduces synaptic vesicle recycling (Soykan et al., 2016), indicating that CME is a major recycling mechanism, and supporting that disruption of this machinery could contribute to AD synapse dysfunction.

Synaptic dysfunction in AD can also result from disrupted regulation of AMPA receptors (AMPARs) in the post-synaptic cleft. Regulation of AMPARs at the membrane is involved in learning and memory, with receptor presentation leading to long-term potentiation (LTP) and internalization leading to long-term depression (LTD) (Chater and Goda, 2022). In AD, AMPAR trafficking is changed such that LTP is impaired and LTD is enhanced which contributes to cognitive deficits (Al-Hallaq et al., 2007; Pei et al., 2020; Babaei, 2021). In LTD, AMPARs are internalized via CME, and internalization can be induced by interaction with $A\beta_{1\text{-}42}$ (Man et al., 2000; Lacor et al., 2004; Snyder et al., 2005; Guntupalli et al., 2017) suggesting that CME could be involved in the LTP/LTD changes in AD. Additionally, the AD risk factor and CME protein PICALM is involved in surface regulation of AMPARs. Loss of PICALM in mice initiates LTP and reduces LTD which improves learning (Azarnia Tehran et al., 2022). This directly implicates CME in AMPAR trafficking alterations and potential effects on learning and memory in AD. If CME dysfunction is an initial piece of this early synaptic dysfunction in multiple contexts, it could very well be an upstream driver in disruption of many neuronal functions.

4.1.2 CME involvement in Aβ processing and uptake

As briefly mentioned above, in AD APP is preferentially processed into amyloidogenic $A\beta_{1\text{-}42}$ in the endolysosomal pathway of neurons after internalization via CME (Koo and Squazzo, 1994; Wu and Yao, 2009). This processing occurs in the early endosome, where the enzyme BACE1 and APP are individually delivered, and APP is cleaved by BACE1 and α-secretase into the pathogenic $A\beta_{1\text{-}42}$. Regulators of endosomal trafficking, which normally prevent BACE1 and APP from being delivered to the same compartment, have been identified as genetic risk factors for AD (*APOE4, PICALM, BIN1*) (Szabo et al., 2022; Maninger et al., 2024). Disrupted expression of these regulators could contribute to the increased production of $A\beta_{1\text{-}42}$ in the endosome (Thomas et al., 2016; Guimas Almeida et al., 2018). After amyloidogenic cleavage of APP, $A\beta_{1\text{-}42}$ peptides are secreted from the cell and aggregate to form toxic fibrils and plaques (Zhang et al., 2011). In aged mouse hippocampal neurons, APP endocytosis is reduced with CME inhibition, but it is unclear if this directly results in less $A\beta_{1\text{-}42}$ production (Burrinha et al., 2021). How CME alterations directly affect APP internalization and $A\beta_{1\text{-}42}$ production in an AD model has not yet been closely studied, but it is plausible that increased CME could cause a subsequent increase in APP internalization and processing, and conversely, that decreased CME may therefore decrease $A\beta_{1\text{-}42}$ production.

The production of $A\beta_{1\text{-}42}$ has also been connected to synaptic activity, which can stimulate CME and increase the internalization of APP. In fact, electrical stimulation in the hippocampus of the APP_{swe} mouse model increased $A\beta_{1\text{-}42}$ in brain interstitial fluid but was prevented up to 70% by CME inhibition using a Dynamin dominant-negative inhibitory peptide (Cirrito et al., 2005, 2008). This result suggests that endocytosis, both synaptic activity-mediated and clathrin-mediated, affects the levels of $A\beta_{1\text{-}42}$ produced and released from neurons, which could contribute to the development of extracellular $A\beta_{1\text{-}42}$ aggregation and spreading.

In addition to APP being endocytosed through CME, different forms of processed Aβ have also been shown to be internalized into neurons and accumulate in insoluble aggregates within endolysosomal compartments in AD brains (Gouras et al., 2000). This accumulation of $A\beta_{1\text{-}42}$ in late endosomes and lysosomes could contribute to endolysosomal dysfunction and associated cellular disruptions (Colacurcio et al., 2018; Lai et al., 2021). Furthermore, endocytosed $A\beta_{1\text{-}42}$ can also cause intraneuronal dysfunction outside of lysosomal accumulation; for example, cultured rat hippocampal neurons treated with $A\beta_{1\text{-}42}$ showed decreased synaptic vesicle endocytosis and Dynamin 1 expression after stimulation, indicating that the replenishing of vesicles to the readily available pool is impaired by $A\beta_{1\text{-}42}$ (Cao et al., 2010). Another of many observed intercellular effects of $A\beta_{1\text{-}42}$ fibrils is the induction of neuritic defects and growth cone collapse. In cultured cortical neurons, $A\beta_{1\text{-}42}$ internalization can result in failure of axonal repair and contribute to axonal degeneration (Kuboyama et al., 2005; Laferla et al., 2007). It has since been shown that endocytosis in growth cones is increased after $A\beta_{1\text{-}42}$, and that inhibition of CME prevents the cone collapse (Kuboyama et al., 2015) suggesting that CME is a primary mechanism driving downstream effects of $A\beta_{1\text{-}42}$.

However, there are conflicting reports as to which endocytic mechanism is responsible for taking up each form of processed Aβ (e.g., monomeric, oligomeric, or fibrillar $A\beta_{1\text{-}42}$). One study that evaluated the uptake of monomeric non-pathogenic $A\beta_{1\text{-}40}$ and pathogenic $A\beta_{1\text{-}42}$ in SH-Sy5Y neuroblastoma cells found that uptake of $A\beta_{1\text{-}42}$ is twice as efficient as that of $A\beta_{1\text{-}40}$ and is primarily independent of CME (Wesén et al., 2017). A subsequent study from the same group found that while the mechanism of Aβ uptake observed was similar to some established endocytic pathways, there are likely more undiscovered molecular components regulating $A\beta_{1\text{-}42}$ uptake (Wesén et al., 2020). Yet other studies report that several forms of Aβ are internalized through CME in different cell types. For example, in rat primary hippocampal neurons, prefibrillar oligomeric forms of $A\beta_{1\text{-}42}$ were rapidly taken into cells in a Dynamin-dependent manner, accumulated in lysosomes, and caused disruption to endolysosomal function. Importantly, a non-misfolded variant of $A\beta_{1\text{-}42}$ was not internalized and did not show any effects on endolysosomal function (Marshall et al., 2020). In addition, in mouse neuro-2a cells, both $A\beta_{1\text{-}42}$ monomers and oligomers showed minimal capacity for binding with the membrane itself but were not able to enter cells under CME inhibition (Shi et al., 2020), meaning that toxicity of $A\beta_{1\text{-}42}$ fragments could be due to their internalization through receptors.

These observed differences in uptake methods for each $A\beta_{1\text{-}42}$ form could be due to the use of multiple experimental models or structural changes in receptor binding to initiate endocytosis. They point to aggregation state of $A\beta_{1\text{-}42}$ as an important factor to consider when evaluating the mechanisms and further effects of $A\beta_{1\text{-}42}$ internalization. Indeed, several studies have shown that oligomeric and aggregated $A\beta_{1\text{-}42}$ are internalized more and are more toxic to

neurons than fibrillar or monomeric $A\beta_{1-42}$ (Chafekar et al., 2008; Jin et al., 2016). However, these studies do not clarify which mechanism of endocytosis is involved, clathrin mediated or otherwise. Additionally, when comparing uptake of pathogenic $A\beta_{1-42}$ vs. non-pathogenic $A\beta_{1-40}$, $A\beta_{1-42}$ and not $A\beta_{1-40}$ is internalized by Dynamin-dependent endocytosis (Omtri et al., 2012) which can include more endocytic processes than purely CME (Mayor et al., 2014; Rennick et al., 2021). Taken together, it is still unclear how each different form of Aβ is internalized into neurons and what downstream effects they may have inside the cell. Nevertheless, there are many indications that CME is clearly an important player in neuronal AD mechanisms and should be studied further to tease the emerging nuances apart.

4.1.3 CME involvement in Tau dysfunction

While we have thus far focused on how CME disruptions may relate to Aβ pathology, it may also play a role in Tau dysfunction. During its propagation, pathological Tau is excreted and then internalized by neighboring cells (Mohamed et al., 2013). Internalization of extracellular Tau aggregates, as opposed to monomers, has recently been suggested to initiate Tau propagation in recipient cells (Usenovic et al., 2015; Kolarova et al., 2017). Uptake of Tau has been observed to occur through many types of endocytosis, including phagocytosis, Dynamin-dependent endocytosis, bulk endocytosis, CME, and others (Calafate et al., 2016; Ando et al., 2020; De La-Rocque et al., 2021; Zhao et al., 2021). However, as with CME effects on Aβ, there are few direct experiments that examine how CME disruption in AD may affect Tau propagation and resulting neuronal dysfunction or vice versa.

In non-disease state, it has been shown that heathy human neurons uptake both aggregated and soluble Tau in similar ways (Evans et al., 2018) and so Tau internalization may not be solely a toxic disease process. On the other hand, cultured mouse neurons with overexpressed human Tau show pre-synaptic endocytosis deficits by decreasing Dynamin RNA and protein but not clathrin, indicating that dysregulation of Tau, such that occurs in AD, may interfere with synaptic transmission via endocytic disruption (Xie et al., 2019). Additionally, a fragment of BIN1, a CME protein and AD risk factor, accelerates Tau aggregate uptake in primary cultured neurons. This process is inhibited by Dynasore, a Dynamin-dependent endocytosis inhibitor which reduces CME and several other Dynamin-dependent endocytic processes (Mayor et al., 2014; Zhang et al., 2024). Of note, it has been reported that inhibition of clathrin specifically does not reduce Tau endocytosis (Holmes et al., 2013; Wu et al., 2013), so these effects could be mediated by non-CME specific processes that still rely on Dynamin.

It is also important to consider that it may be difficult to distinguish AD-specific Tau endocytic changes from changes in other tauopathies. One study applied brain derived Tau oligomers from human post-mortem tissue of tauopathies including AD, progressive supranuclear palsy, and dementia with Lewy bodies to mouse primary neurons and showed that Tau oligomers from each disease state were internalized via the same non-Dynamin dependent endocytic mechanisms (Puangmalai et al., 2020). Thus, as multiple endocytic pathways seem to be involved, more work needs to be done to tease apart the nuances of how CME specifically might affect or be affected by Tau pathology in healthy neurons and in AD versus other tauopathies.

4.2 Astrocytes

As CME is a ubiquitous process, changes in non-neuronal cell types during AD must be considered. Here, we will focus on astrocytes and microglia, which have myriad functions essential for maintaining a healthy nervous system and respond quickly to changes in environment (Vainchtein and Molofsky, 2020). Both have been implicated in reactivity to and protection from AD pathology, often in synchrony (Al-Ghraiybah et al., 2022).

Astrocytes perform many essential functions in a healthy central nervous system, including regulating synapse activity, interactions with blood vessels and endothelial cells to facilitate the blood brain barrier, neurogenesis, and maintenance of neuronal homeostasis. Astrocytes have diverse morphology and mechanisms of action for these functions (Eroglu and Barres, 2010; Sofroniew and Vinters, 2010; Sofroniew, 2020; Torres-Ceja and Olsen, 2022). In AD, many astrocytes become reactive, localize around $A\beta_{1-42}$ plaques, and excrete inflammatory cytokines that contribute to widespread neuroinflammation and subsequent neuronal dysfunction (Al-Ghraiybah et al., 2022). It has also been shown that activated microglia can induce astrocytes to lose neuronal support abilities, and these neurotoxic astrocytes are abundant in AD and other neurodegenerative diseases (Liddelow et al., 2017).

Astrocytes are closely tied to the clearance of dying neurons and take up large amounts of neuronal $A\beta_{1-42}$ and debris (Yuan et al., 2023; Mun et al., 2024). However, astrocytes can become overburdened with Aβ, resulting in impaired phagocytosis of diseased synapses and potentially contributing to the increased amount of dystrophic neurites seen in early stages of AD (Sanchez-Mico et al., 2021). Additionally, Aβ protofibrils engulfed by mouse primary astrocytes are not degraded in the cell and induce lysosomal dysfunction within them (Söllvander et al., 2016). Astrocytes of aged primate brains show enlarged early endosomes filled with Aβ, suggesting that aging may also play a role in astrocytic dysfunction (Kimura et al., 2014). And while it is largely thought that astrocytes internalize Aβ through phagocytosis, it has recently been shown that multiple forms of Aβ (1-40 and 1-42) are internalized via clathrin-coated vesicles in rat primary astrocytes, where they induce increased reactive oxygen species production and decreased cell viability. When treated with chlorpromazine, a pharmacological inhibitor of CME, astrocytes exhibit significantly decreased uptake of $A\beta_{1-42}$ and a partial rescue of $A\beta_{1-42}$ induced cell death (Domínguez-Prieto et al., 2018). Additionally, astrocytes can take up and accumulate monomeric and oligomeric Tau (Martini-Stoica et al., 2018; Brezovakova et al., 2022; Eltom et al., 2024; Giusti et al., 2024), though to the best of our knowledge the specific endocytic mechanisms involved have not been thoroughly examined and there is no strong link to CME specifically in astrocytes.

Another consideration of astrocytic involvement in AD is their connection to the genetic risk factor of apolipoprotein E4 (*APOE4*). *APOE* is mainly expressed in astrocytes as their primary cholesterol carrier, and expressing the *APOE4* allele is one of the biggest risk factors for developing AD (Martens et al., 2022). Many AD phenotypes are affected by *APOE* status including Aβ clearance and lipid metabolism (Koistinaho et al., 2004; Kim et al., 2009; Lin et al., 2018). Human iPSC derived astrocytes with *APOE4* exhibit both decreased CME and early endosomal markers, suggesting that *APOE4* disrupts CME. Interestingly, increased expression of *PICALM* rescues endocytic defects in the *APOE4* astrocytes (Narayan et al., 2020). The

connection of these two major genetic risk factors of AD through CME suggests that CME is instrumental in disease development.

Taken together, it is possible that the changes in CME protein levels observed in AD post-mortem brains contribute to the dysfunction of astrocytes and their role in driving subsequent AD pathology. Moreover, the involvement of CME in astrocytic responses to $A\beta_{1\text{-}42}$ illustrates the importance of evaluating CME in cell types other than neurons. It also opens questions regarding how aberrant CME early in AD contributes to non-neuronal disease phenotypes.

4.3 Microglia

Microglia, central nervous system resident phagocytes, are well recognized to have a dual role in AD, as reviewed recently (Cai et al., 2014; Al-Ghraiybah et al., 2022; Wendimu and Hooks, 2022; Zhao et al., 2022). Briefly, microglia can act in both a neurotoxic and neuroprotective role in AD, and which role they perform depends on many factors. Microglia activated from their resting state into neurotoxic phenotypes promote neuroinflammation through release of neurotoxic cytokines and other inflammatory factors. Contrasting this response, activated microglia in their neuroprotective phenotype can limit plaque formation by clearing extracellular $A\beta_{1\text{-}42}$. Paradoxically, both phenotypes can be initiated by $A\beta_{1\text{-}42}$. One prominent hypothesis in AD pathogenesis is that an initial problem that arises in disease progression is the loss of neuroprotective microglial function due to age-associated microglial senescence, which in turn leads to loss of $A\beta_{1\text{-}42}$ clearance and accumulation of $A\beta_{1\text{-}42}$. This accumulation of $A\beta_{1\text{-}42}$ then activates microglial neurotoxic states, which increase neuroinflammation and eventually leads to dementia (Streit et al., 2021). This idea implicates microglia, and specifically a disruption in $A\beta_{1\text{-}42}$ clearance, in early stages of AD.

Endocytic clearance of $A\beta_{1\text{-}42}$ by microglia can occur through several mechanisms, the most commonly studied being micropinocytosis and phagocytosis (Ni et al., 2024). However, recent studies have begun to implicate CME in this process. In HMO6 cells, a human microglial cell line, treated with an amyloid-degrading enzyme activator, $A\beta_{1\text{-}42}$ uptake was significantly increased, and both clathrin and caveolin expression were upregulated (Jang et al., 2015). However, no studies were done to examine the effect of inhibiting clathrin- or caveolae-dependent endocytosis independently, so it is unclear whether one process is more prominent that the other. Nevertheless, these findings suggest an involvement of CME in microglial $A\beta_{1\text{-}42}$ clearance, although it may not be the only mechanism at play.

More recently, a study using a mouse microglial cell line treated with fibrillar $A\beta_{1\text{-}42}$ found that clathrin colocalized with internalized $A\beta_{42}$ and that inhibition of CME resulted in 80% reduction of $A\beta_{1\text{-}42}$ uptake (Fujikura et al., 2019), further supporting the hypothesis that CME is involved in microglial Aβ uptake. Additionally, in another mouse microglia cell line, a novel form of endocytosis has been described, autophagy protein Light Chain 3 (LC3)-associated endocytosis (LANDO) (Heckmann et al., 2019). LANDO supports the clearance of Aβ and prevents activation of inflammatory microglia, yet inhibition of actin polymerization and phagocytosis had no effect on internalization of Aβ. This finding suggests that LANDO occurs though CME, as LC3 is colocalized with clathrin and Rab5 early endosomes (Heckmann et al., 2019). Also, it is important to note that these studies have not yet been replicated *in vivo* and should be validated further, as microglia function is strongly influenced by the surrounding environment. However, the recent evidence of CME in microglial clearance of $A\beta_{1\text{-}42}$ does point toward another potential effect of CME disruption in AD. When considering microglial involvement in Tau pathology, to our knowledge there has been no specific link between microglial uptake and propagation of Tau via CME mechanisms. How microglia contribute to Tau pathology is reviewed in depth elsewhere (Das et al., 2020; Ayyubova, 2023; Chen and Yu, 2023; Ou-Yang et al., 2023). CME in microglia needs to be further investigated to clarify what degree it and other endocytic mechanisms are disrupted in AD in relation to both Aβ and Tau pathology. Reduction in CME could contribute to neurotoxic microglial function through reduction of $A\beta_{1\text{-}42}$ clearance. Alternatively, if CME is not changed or is increased in AD microglia, it could be driving neuroprotection of microglia, whereby $A\beta_{1\text{-}42}$ clearance is actually contributing to a slowing of disease progression.

5 Targeting CME for AD treatment

Currently, most clinical treatments for AD are Aβ-targeting monoclonal antibodies and have varying success in reducing Aβ burden and slowing cognitive decline (Alshamrani, 2023; Rabinovici and La Joie, 2023). However, they are also most effective in early stages of disease, as characterized by Aβ and Tau levels (Alshamrani, 2023). Aβ burden can be decreased in some patients, but progression is not completely halted (Sevigny et al., 2016; Mintun et al., 2021; Swanson et al., 2021; Budd Haeberlein et al., 2022) suggesting that targeting Aβ is not sufficient to significantly alter other molecular pathways involved in later stage AD pathophysiology. Therapies targeting Tau have recently become more heavily studied with several immunotherapies in clinical trials (Ji and Sigurdsson, 2021; Alshamrani, 2023). However, early intervention is still sorely needed for patients and modulation of other AD pathophysiology outside of targeting Aβ and Tau directly are being considered for treatment (Zhang et al., 2021).

As discussed within this review, there is abundant evidence that CME is a potential early disease modifier of AD in neurons, astrocytes, and microglia upstream of endolysosomal involvement. There have been several clinical trials evaluating endocytosis inhibitors which specifically block CME to treat coronavirus infection (Szewczyk-Roszczenko et al., 2023). These inhibitors include Ruxolitinib and Simvastatin, Chlorpromazine, and most interestingly Hydroxychloroquine (HCQ) which reduces PICALM expression (Szewczyk-Roszczenko et al., 2023). HCQ is a common treatment for arthritis and in 2001 was found to have no significant benefit to early AD (Van Gool et al., 2001). More recently, HCQ was found to reduce dementia risk in humans and rescued AD phenotypes *in vitro* and *in vivo* (Varma et al., 2023). While HCQ treatment is promising, its mechanism of action in specific cell types should be evaluated as it can also affect other non-CME pathways (Schrezenmeier and Dörner, 2020). Thus far, to our knowledge no other endocytic inhibitors have been applied to a clinical context of AD.

So, while there is great therapeutic potential of modulating CME in AD due to the many ways its disruption can interface with aspects of disease pathophysiology, it is also clear that treatments must be targeted to specific cell types. This is an area of interest for

the delivery of anticancer drugs to specifically target diseased tissue and cells and reduce off target effects (Zhao et al., 2020; Mitchell et al., 2021) the application of which could be applied to AD treatment in the future. Additionally, since CME itself can be a mechanism of uptake for therapeutics (Congdon et al., 2013; Rennick et al., 2021), if its function is disrupted in AD already, drug delivery into cells may be compromised and should also be considered. There is still much to unravel before potential therapeutic developments using CME modulation for AD are possible, such as the directionality of CME functional changes and how it may vary between cell types.

6 Conclusion

In conclusion, CME is emerging as a critical player in the development and progression of AD in multiple brain cell types. CME is an important intersection between early neuronal dysfunction via $A\beta_{1\text{-}42}$ accumulation and downstream effects that contribute to neuronal viability, such as synaptic vesicle recycling deficits and disruption of AMPAR regulation. Not only is $A\beta_{1\text{-}42}$ produced following CME of APP, but internalization of multiple forms of extracellular $A\beta_{1\text{-}42}$ contribute to downstream neuronal pathology. In astrocytes and microglia, which are heavily involved in clearance of extracellular $A\beta_{1\text{-}42}$ in the brain, CME disruptions reduce internalization of $A\beta_{1\text{-}42}$. Importantly, other brain cell types, including endothelial cells, oligodendrocytes, and ependymal cells that are not reviewed herein, should also be considered in the context of CME and AD as they could also be affected by changes in CME. Further, other copathologies associated with AD that may also affect or be affected by CME disruption, such as TDP-43 (Root et al., 2021), should be considered. Ultimately, CME appears to be involved in dysfunction in multiple cell types across early and late stages of AD. Thus, elucidating the mechanisms of CME and how their disruption is related to AD pathogenesis or neuroprotection in each brain cell type would both lead to a better understanding of AD mechanisms and potentially point to novel targets for the treatment or prevention of AD.

Author contributions

SJ: Writing – review & editing, Conceptualization, Data curation, Investigation, Writing – original draft, Funding acquisition. US: Supervision, Writing – review & editing. JS: Supervision, Writing – review & editing.

Funding

The author(s) declare financial support was received for the research, authorship, and/or publication of this article. These studies were generously supported by NIH grants R36 AG073792 (SJ) and RF1 AG059392 (JS).

Acknowledgments

Figure 1 adapted from "Clathrin-Mediated Endocytosis," by BioRender.com (2023). Retrieved from https://app.biorender.com/biorender-templates. We also thank Randall Woltjer for his contributions in conversations regarding Alzheimer's pathophysiology.

Conflict of interest

The authors declare that the research was conducted in the absence of any commercial or financial relationships that could be construed as a potential conflict of interest.

Publisher's note

References

Ahmad, S., Bannister, C., Lee, S. J., Vojinovic, D., Adams, H. H. H., Ramirez, A., et al. (2018). Disentangling the biological pathways involved in early features of Alzheimer's disease in the Rotterdam study. *Alzheimers Dement.* 14, 848–857. doi: 10.1016/j.jalz.2018.01.005

Aidaralieva, N. J., Kamino, K., Kimura, R., Yamamoto, M., Morihara, T., Kazui, H., et al. (2008). Dynamin 2 gene is a novel susceptibility gene for late-onset Alzheimer disease in non-APOE-ε4 carriers. *J. Hum. Genet.* 53, 296–302. doi: 10.1007/s10038-008-0251-9

Al-Ghraiybah, N. F., Wang, J., Alkhalifa, A. E., Roberts, A. B., Raj, R., Yang, E., et al. (2022). Glial cell-mediated neuroinflammation in Alzheimer's disease. *Int. J. Mol. Sci.* 23:10572. doi: 10.3390/ijms231810572

Al-Hallaq, R. A., Conrads, T. P., Veenstra, T. D., and Wenthold, R. J. (2007). NMDA Di-Heteromeric receptor populations and associated proteins in rat hippocampus. *J. Neurosci.* 27, 8334–8343. doi: 10.1523/jneurosci.2155-07.2007

Alsaqati, M., Thomas, R. S., and Kidd, E. J. (2018). Proteins involved in endocytosis are upregulated by ageing in the Normal human brain: implications for the development of Alzheimer's disease. *J. Gerontol. A Biol. Sci. Med. Sci.* 73, 289–298. doi: 10.1093/gerona/glx135

Alsaqati, M., Thomas, R. S., and Kidd, E. J. (2023). Upregulation of endocytic protein expression in the Alzheimer's disease male human brain. *Aging Brain* 4:100084. doi: 10.1016/j.nbas.2023.100084

Alshamrani, M. (2023). Recent trends in active and passive immunotherapies of Alzheimer's disease. *Antibodies (Basel)* 12, 41. doi: 10.3390/antib12020041

Alzheimer's Association (2023). 2023 Alzheimer's disease facts and figures. *Alzheimers Dement.* 19, 1598–1695. doi: 10.1002/alz.13016

Ando, K., Brion, J. P., Stygelbout, V., Suain, V., Authelet, M., Dedecker, R., et al. (2013). Clathrin adaptor CALM/PICALM is associated with neurofibrillary tangles and is cleaved in Alzheimer's brains. *Acta Neuropathol.* 125, 861–878. doi: 10.1007/s00401-013-1111-z

Ando, K., Houben, S., Homa, M., de Fisenne, M. A., Potier, M. C., Erneux, C., et al. (2020). Alzheimer's disease: tau pathology and dysfunction of endocytosis. *Front. Mol. Neurosci.* 13:583755. doi: 10.3389/fnmol.2020.583755

Ando, K., Nagaraj, S., Küçükali, F., De Fisenne, M.-A., Kosa, A.-C., Doeraene, E., et al. (2022). PICALM and Alzheimer's disease: an update and perspectives. *Cells* 11:3994. doi: 10.3390/cells11243994

Andrade-Guerrero, J., Santiago-Balmaseda, A., Jeronimo-Aguilar, P., Vargas-Rodríguez, I., Cadena-Suárez, A. R., Sánchez-Garibay, C., et al. (2023). Alzheimer's disease: an updated overview of its genetics. *Int. J. Mol. Sci.* 24:3754. doi: 10.3390/ijms24043754

Ayyubova, G. (2023). Dysfunctional microglia and tau pathology in Alzheimer's disease. *Rev. Neurosci.* 34, 443–458. doi: 10.1515/revneuro-2022-0087

Azarnia, T., and López, H.Maritzen (2019). Endocytic adaptor proteins in health and disease: lessons from model organisms and human mutations. *Cells* 8:1345. doi: 10.3390/cells8111345

Azarnia Tehran, D., Kochlamazashvili, G., Pampaloni, N. P., Sposini, S., Shergill, J. K., Lehmann, M., et al. (2022). Selective endocytosis of ca(2+)-permeable AMPARs by the Alzheimer's disease risk factor CALM bidirectionally controls synaptic plasticity. *Sci. Adv.* 8:eabl5032. doi: 10.1126/sciadv.abl5032

Babaei, P. (2021). NMDA and AMPA receptors dysregulation in Alzheimer's disease. *Eur. J. Pharmacol.* 908:174310. doi: 10.1016/j.ejphar.2021.174310

Baig, S., Joseph, S. A., Tayler, H., Abraham, R., Owen, M. J., Williams, J., et al. (2010). Distribution and expression of Picalm in Alzheimer disease. *J. Neuropathol. Exp. Neurol.* 69, 1071–1077. doi: 10.1097/nen.0b013e3181f52e01

Barnes, J., Dickerson, B. C., Frost, C., Jiskoot, L. C., Wolk, D., and Flier, W. M. (2015). Alzheimer's disease first symptoms are age dependent: evidence from the NACC dataset. Alzheimer's & amp. *Dementia* 11, 1349–1357. doi: 10.1016/j.jalz.2014.12.007

Behl, T., Kaur, D., Sehgal, A., Singh, S., Makeen, H. A., Albratty, M., et al. (2022). Exploring the potential role of rab5 protein in endo-lysosomal impairment in Alzheimer's disease. *Biomed. Pharmacother.* 148:112773. doi: 10.1016/j.biopha.2022.112773

Botté, A., and Potier, M.-C. (2020, 2020). Focusing on cellular biomarkers: the endo-lysosomal pathway in Down syndrome. *Prog. Brain Res.* 251, 209–243. doi: 10.1016/bs.pbr.2019.10.002

Boulant, S., Kural, C., Zeeh, J.-C., Ubelmann, F., and Kirchhausen, T. (2011). Actin dynamics counteract membrane tension during clathrin-mediated endocytosis. *Nat. Cell Biol.* 13, 1124–1131. doi: 10.1038/ncb2307

Braak, H., and Braak, E. (1991). Neuropathological stageing of Alzheimer-related changes. *Acta Neuropathol.* 82, 239–259. doi: 10.1007/bf00308809

Brezovakova, V., Sykova, E., and Jadhav, S. (2022). Astrocytes derived from familial and sporadic Alzheimer's disease iPSCs show altered calcium signaling and respond differently to misfolded protein tau. *Cells* 11:1429. doi: 10.3390/cells11091429

Budd Haeberlein, S., Aisen, P. S., Barkhof, F., Chalkias, S., Chen, T., Cohen, S., et al. (2022). Two randomized phase 3 studies of Aducanumab in early Alzheimer's disease. *J. Prev Alzheimers Dis.* 9, 197–210. doi: 10.14283/jpad.2022.30

Burrinha, T., Martinsson, I., Gomes, R., Terrasso, A. P., Gouras, G. K., and Almeida, C. G. (2021). Upregulation of APP endocytosis by neuronal aging drives amyloid-dependent synapse loss. *J. Cell Sci.* 134. doi: 10.1242/jcs.255752

Cai, Z., Hussain, M. D., and Yan, L.-J. (2014). Microglia, neuroinflammation, and beta-amyloid protein in Alzheimer's disease. *Int. J. Neurosci.* 124, 307–321. doi: 10.3109/00207454.2013.833510

Calafate, S., Flavin, W., Verstreken, P., and Moechars, D. (2016). Loss of Bin1 promotes the propagation of tau pathology. *Cell Rep.* 17, 931–940. doi: 10.1016/j.celrep.2016.09.063

Cao, Y., Xiao, Y., Ravid, R., and Guan, Z. Z. (2010). Changed clathrin regulatory proteins in the brains of Alzheimer's disease patients and animal models. *J. Alzheimers Dis.* 22, 329–342. doi: 10.3233/JAD-2010-100162

Cataldo, A. M., Petanceska, S., Terio, N. B., Peterhoff, C. M., Durham, R., Mercken, M., et al. (2004). Aβ localization in abnormal endosomes: association with earliest Aβ elevations in AD and Down syndrome. *Neurobiol. Aging* 25, 1263–1272. doi: 10.1016/j.neurobiolaging.2004.02.027

Cataldo, A. M., Peterhoff, C. M., Troncoso, J. C., Gomez-Isla, T., Hyman, B. T., and Nixon, R. A. (2000). Endocytic pathway abnormalities precede amyloid β deposition in sporadic Alzheimer's disease and Down syndrome. *Am. J. Pathol.* 157, 277–286. doi: 10.1016/s0002-9440(10)64538-5

Chafekar, S. M., Baas, F., and Scheper, W. (2008). Oligomer-specific Abeta toxicity in cell models is mediated by selective uptake. *Biochim. Biophys. Acta* 1782, 523–531. doi: 10.1016/j.bbadis.2008.06.003

Chapuis, J., Hansmannel, F., Gistelinck, M., Mounier, A., Van Cauwenberghe, C., Kolen, K. V., et al. (2013). Increased expression of BIN1 mediates Alzheimer genetic risk by modulating tau pathology. *Mol. Psychiatry* 18, 1225–1234. doi: 10.1038/mp.2013.1

Chater, T. E., and Goda, Y. (2022). The shaping of AMPA receptor surface distribution by neuronal activity. *Front. Synaptic Neurosci.* 14:833782. doi: 10.3389/fnsyn.2022.833782

Chen, Y., and Yu, Y. (2023). Tau and neuroinflammation in Alzheimer's disease: interplay mechanisms and clinical translation. *J. Neuroinflammation* 20:165. doi: 10.1186/s12974-023-02853-3

Cirrito, J. R., Kang, J.-E., Lee, J., Stewart, F. R., Verges, D. K., Silverio, L. M., et al. (2008). Endocytosis is required for synaptic activity-dependent release of amyloid-β in vivo. *Neuron* 58, 42–51. doi: 10.1016/j.neuron.2008.02.003

Cirrito, J. R., Yamada, K. A., Finn, M. B., Sloviter, R. S., Bales, K. R., May, P. C., et al. (2005). Synaptic activity regulates interstitial fluid amyloid-β levels in vivo. *Neuron* 48, 913–922. doi: 10.1016/j.neuron.2005.10.028

Colacurcio, D. J., Pensalfini, A., Jiang, Y., and Nixon, R. A. (2018). Dysfunction of autophagy and endosomal-lysosomal pathways: roles in pathogenesis of Down syndrome and Alzheimer's disease. *Free Radic. Biol. Med.* 114, 40–51. doi: 10.1016/j.freeradbiomed.2017.10.001

Congdon, E. E., Gu, J., Sait, H. B. R., and Sigurdsson, E. M. (2013). Antibody uptake into neurons occurs primarily via clathrin-dependent Fcγ receptor endocytosis and is a prerequisite for acute tau protein clearance. *J. Biol. Chem.* 288, 35452–35465. doi: 10.1074/jbc.m113.491001

Cuddy, L. K., Alia, A. O., Salvo, M. A., Chandra, S., Grammatopoulos, T. N., Justman, C. J., et al. (2022). Farnesyltransferase inhibitor LNK-754 attenuates axonal dystrophy and reduces amyloid pathology in mice. *Mol. Neurodegener.* 17:54. doi: 10.1186/s13024-022-00561-9

Cullen, P. J., and Steinberg, F. (2018). To degrade or not to degrade: mechanisms and significance of endocytic recycling. *Nat. Rev. Mol. Cell Biol.* 19, 679–696. doi: 10.1038/s41580-018-0053-7

Das, R., Balmik, A. A., and Chinnathambi, S. (2020). Phagocytosis of full-length tau oligomers by actin-remodeling of activated microglia. *J. Neuroinflammation* 17:10. doi: 10.1186/s12974-019-1694-y

De Jesus-Cortes, H. J., Nogueras-Ortiz, C. J., Gearing, M., Arnold, S. E., and Vega, I. E. (2012). Amphiphysin-1 protein level changes associated with tau-mediated neurodegeneration. *Neuroreport* 23, 942–946. doi: 10.1097/WNR.0b013e32835982ce

De La-Rocque, S., Moretto, E., Butnaru, I., and Schiavo, G. (2021). Knockin' on heaven's door: molecular mechanisms of neuronal tau uptake. *J. Neurochem.* 156, 563–588. doi: 10.1111/jnc.15144

De Rossi, P., Buggia-Prévot, V., Clayton, B. L. L., Vasquez, J. B., Van Sanford, C., Andrew, R. J., et al. (2016). Predominant expression of Alzheimer's disease-associated BIN1 in mature oligodendrocytes and localization to white matter tracts. *Mol. Neurodegener.* 11, 59. doi: 10.1186/s13024-016-0124-1

Deture, M. A., and Dickson, D. W. (2019). The neuropathological diagnosis of Alzheimer's disease. *Mol. Neurodegener.* 14:32. doi: 10.1186/s13024-019-0333-5

Doherty, G. J., and McMahon, H. T. (2009). Mechanisms of endocytosis. *Annu. Rev. Biochem.* 78, 857–902. doi: 10.1146/annurev.biochem.78.081307.110540

Domínguez-Prieto, M., Velasco, A., Tabernero, A., and Medina, J. M. (2018). Endocytosis and transcytosis of amyloid-β peptides by astrocytes: a possible mechanism for amyloid-β clearance in Alzheimer's disease. *J. Alzheimers Dis.* 65, 1109–1124. doi: 10.3233/jad-180332

Eltom, K., Mothes, T., Libard, S., Ingelsson, M., and Erlandsson, A. (2024). Astrocytic accumulation of tau fibrils isolated from Alzheimer's disease brains induces inflammation, cell-to-cell propagation and neuronal impairment. *Acta Neuropathol. Commun.* 12:34. doi: 10.1186/s40478-024-01745-8

Eroglu, C., and Barres, B. A. (2010). Regulation of synaptic connectivity by glia. *Nature* 468, 223–231. doi: 10.1038/nature09612

Evans, L. D., Wassmer, T., Fraser, G., Smith, J., Perkinton, M., Billinton, A., et al. (2018). Extracellular monomeric and aggregated tau efficiently enter human neurons through overlapping but distinct pathways. *Cell Rep.* 22, 3612–3624. doi: 10.1016/j.celrep.2018.03.021

Filippone, A., and Praticò, D. (2021). Endosome dysregulation in Down syndrome: a potential contributor to Alzheimer disease pathology. *Ann. Neurol.* 90, 4–14. doi: 10.1002/ana.26042

Fortea, J., Zaman, S. H., Hartley, S., Rafii, M. S., Head, E., and Carmona-Iragui, M. (2021). Alzheimer's disease associated with Down syndrome: a genetic form of dementia. *Lancet Neurol.* 20, 930–942. doi: 10.1016/S1474-4422(21)00245-3

Fujikura, M., Iwahara, N., Hisahara, S., Kawamata, J., Matsumura, A., Yokokawa, K., et al. (2019). CD14 and toll-like receptor 4 promote Fibrillar Aβ42 uptake by microglia through a clathrin-mediated pathway. *J. Alzheimers Dis.* 68, 323–337. doi: 10.3233/jad-180904

Ginsberg, S. D., Alldred, M. J., Counts, S. E., Cataldo, A. M., Neve, R. L., Jiang, Y., et al. (2010). Microarray analysis of hippocampal CA1 neurons implicates early endosomal dysfunction during Alzheimer's disease progression. *Biol. Psychiatry* 68, 885–893. doi: 10.1016/j.biopsych.2010.05.030

Giusti, V., Kaur, G., Giusto, E., and Civiero, L. (2024). Brain clearance of protein aggregates: a close-up on astrocytes. *Mol. Neurodegener.* 19:5. doi: 10.1186/s13024-024-00703-1

Gouras, G. K., Tsai, J., Naslund, J., Vincent, B., Edgar, M., Checler, F., et al. (2000). Intraneuronal Aβ42 accumulation in human brain. *Am. J. Pathol.* 156, 15–20. doi: 10.1016/s0002-9440(10)64700-1

Guimas Almeida, C., Sadat Mirfakhar, F., Perdigão, C., and Burrinha, T. (2018). Impact of late-onset Alzheimer's genetic risk factors on beta-amyloid endocytic production. *Cell. Mol. Life Sci.* 75, 2577–2589. doi: 10.1007/s00018-018-2825-9

Guntupalli, S., Jang, S. E., Zhu, T., Huganir, R. L., Widagdo, J., and Anggono, V. (2017). GluA1 subunit ubiquitination mediates amyloid-β-induced loss of surface α-amino-3-hydroxy-5-methyl-4-isoxazolepropionic acid (AMPA) receptors. *J. Biol. Chem.* 292, 8186–8194. doi: 10.1074/jbc.m116.774554

Hardy, J., and Allsop, D. (1991). Amyloid deposition as the central event in the aetiology of Alzheimer's disease. *Trends Pharmacol. Sci.* 12, 383–388. doi: 10.1016/0165-6147(91)90609-v

Hardy, J. A., and Higgins, G. A. (1992). Alzheimer's disease: the amyloid cascade hypothesis. *Science* 256, 184–185. doi: 10.1126/science.1566067

Heckmann, B. L., Teubner, B. J. W., Tummers, B., Boada-Romero, E., Harris, L., Yang, M., et al. (2019). LC3-associated endocytosis facilitates β-amyloid clearance and

mitigates neurodegeneration in murine Alzheimer's disease. *Cell* 178, 536–551.e14. doi: 10.1016/j.cell.2019.05.056

Hofman, A., Brusselle, G. G. O., Murad, S. D., Van Duijn, C. M., Franco, O. H., Goedegebure, A., et al. (2015). The Rotterdam study: 2016 objectives and design update. *Eur. J. Epidemiol.* 30, 661–708. doi: 10.1007/s10654-015-0082-x

Holmes, B. B., Devos, S. L., Kfoury, N., Li, M., Jacks, R., Yanamandra, K., et al. (2013). Heparan sulfate proteoglycans mediate internalization and propagation of specific proteopathic seeds. *Proc. Natl. Acad. Sci.* 110, E3138–E3147. doi: 10.1073/pnas.1301440110

Hori, T., Eguchi, K., Wang, H.-Y., Miyasaka, T., Guillaud, L., Taoufiq, Z., et al. (2022). Microtubule assembly by tau impairs endocytosis and neurotransmission via dynamin sequestration in Alzheimer's disease synapse model. *eLife* 11. doi: 10.7554/elife.73542

Hsiao, K., Chapman, P., Nilsen, S., Eckman, C., Harigaya, Y., Younkin, S., et al. (1996). Correlative memory deficits, Abeta elevation, and amyloid plaques in transgenic mice. *Science* 274, 99–103. doi: 10.1126/science.274.5284.99

Israel, M. A., Yuan, S. H., Bardy, C., Reyna, S. M., Mu, Y., Herrera, C., et al. (2012). Probing sporadic and familial Alzheimer's disease using induced pluripotent stem cells. *Nature* 482, 216–220. doi: 10.1038/nature10821

Jang, S. K., Yu, J. M., Kim, S. T., Kim, G. H., Park, D. W., Lee, D. I., et al. (2015). An Aβ42 uptake and degradation via Rg3 requires an activation of caveolin, clathrin and Aβ-degrading enzymes in microglia. *Eur. J. Pharmacol.* 758, 1–10. doi: 10.1016/j.ejphar.2015.03.071

Ji, C., and Sigurdsson, E. M. (2021). Current status of clinical trials on tau immunotherapies. *Drugs* 81, 1135–1152. doi: 10.1007/s40265-021-01546-6

Jiang, Y., Sato, Y., Im, E., Berg, M., Bordi, M., Darji, S., et al. (2019). Lysosomal dysfunction in Down syndrome is APP-dependent and mediated by APP-βCTF (C99). *J. Neurosci.* 39, 5255–5268. doi: 10.1523/jneurosci.0578-19.2019

Jin, S., Kedia, N., Illes-Toth, E., Haralampiev, I., Prisner, S., Herrmann, A., et al. (2016). Amyloid-β(1–42) aggregation initiates its cellular uptake and cytotoxicity. *J. Biol. Chem.* 291, 19590–19606. doi: 10.1074/jbc.m115.691840

Kaksonen, M., and Roux, A. (2018). Mechanisms of clathrin-mediated endocytosis. *Nat. Rev. Mol. Cell Biol.* 19, 313–326. doi: 10.1038/nrm.2017.132

Kamagata, E., Kudo, T., Kimura, R., Tanimukai, H., Morihara, T., Sadik, M. G., et al. (2009). Decrease of dynamin 2 levels in late-onset Alzheimer's disease alters Abeta metabolism. *Biochem. Biophys. Res. Commun.* 379, 691–695. doi: 10.1016/j.bbrc.2008.12.147

Kim, J., Basak, J. M., and Holtzman, D. M. (2009). The role of apolipoprotein E in Alzheimer's disease. *Neuron* 63, 287–303. doi: 10.1016/j.neuron.2009.06.026

Kim, S.-H., Cho, Y.-S., Kim, Y., Park, J., Yoo, S.-M., Gwak, J., et al. (2023). Endolysosomal impairment by binding of amyloid beta or MAPT/tau to V-ATPase and rescue via the HYAL-CD44 axis in Alzheimer disease. *Autophagy* 19, 2318–2337. doi: 10.1080/15548627.2023.2181614

Kimura, N., Okabayashi, S., and Ono, F. (2014). Dynein dysfunction disrupts beta-amyloid clearance in astrocytes through endocytic disturbances. *Neuroreport* 25, 514–520. doi: 10.1097/WNR.0000000000000124

Kimura, N., and Yanagisawa, K. (2018). Traffic jam hypothesis: relationship between endocytic dysfunction and Alzheimer's disease. *Neurochem. Int.* 119, 35–41. doi: 10.1016/j.neuint.2017.07.002

Koistinaho, M., Lin, S., Wu, X., Esterman, M., Koger, D., Hanson, J., et al. (2004). Apolipoprotein E promotes astrocyte colocalization and degradation of deposited amyloid-β peptides. *Nat. Med.* 10, 719–726. doi: 10.1038/nm1058

Kolarova, M., Sengupta, U., Bartos, A., Ricny, J., and Kayed, R. (2017). Tau oligomers in sera of patients with Alzheimer's disease and aged controls. *J. Alzheimers Dis.* 58, 471–478. doi: 10.3233/JAD-170048

Koo, E., and Squazzo, S. (1994). Evidence that production and release of amyloid @ protein involves the endocytic pathway. *J. Biol. Chem.* 269, 17386–17389. doi: 10.1016/S0021-9258(17)32449-3

Kuboyama, T., Lee, Y.-A., Nishiko, H., and Tohda, C. (2015). Inhibition of clathrin-mediated endocytosis prevents amyloid β-induced axonal damage. *Neurobiol. Aging* 36, 1808–1819. doi: 10.1016/j.neurobiolaging.2015.02.005

Kuboyama, T., Tohda, C., and Komatsu, K. (2005). Neuritic regeneration and synaptic reconstruction induced by withanolide A. *Br. J. Pharmacol.* 144, 961–971. doi: 10.1038/sj.bjp.0706122

Kwart, D., Gregg, A., Scheckel, C., Murphy, E. A., Paquet, D., Duffield, M., et al. (2019). A large panel of isogenic APP and PSEN1 mutant human iPSC neurons reveals shared endosomal abnormalities mediated by APP β-CTFs, not Aβ. *Neuron* 104, 256–270.e255. doi: 10.1016/j.neuron.2019.07.010

Lacor, P. N., Buniel, M. C., Chang, L., Fernandez, S. J., Gong, Y., Viola, K. L., et al. (2004). Synaptic targeting by Alzheimer's-related amyloid beta oligomers. *J. Neurosci.* 24, 10191–10200. doi: 10.1523/JNEUROSCI.3432-04.2004

Lacour, M., Quenez, O., Rovelet-Lecrux, A., Salomon, B., Rousseau, S., Richard, A.-C., et al. (2019). Causative mutations and genetic risk factors in sporadic early onset Alzheimer's disease before 51 years. *J. Alzheimers Dis.* 71, 227–243. doi: 10.3233/jad-190193

Laferla, F. M., Green, K. N., and Oddo, S. (2007). Intracellular amyloid-β in Alzheimer's disease. *Nat. Rev. Neurosci.* 8, 499–509. doi: 10.1038/nrn2168

Lai, S. S. M., Ng, K. Y., Koh, R. Y., Chok, K. C., and Chye, S. M. (2021). Endosomal-lysosomal dysfunctions in Alzheimer's disease: pathogenesis and therapeutic interventions. *Metab. Brain Dis.* 36, 1087–1100. doi: 10.1007/s11011-021-00737-0

Lamontagne-Kam, D., Ulfat, A. K., Hervé, V., Vu, T.-M., and Brouillette, J. (2023). Implication of tau propagation on neurodegeneration in Alzheimer's disease. *Front. Neurosci.* 17. doi: 10.3389/fnins.2023.1219299

Liddelow, S. A., Guttenplan, K. A., Clarke, L. E., Bennett, F. C., Bohlen, C. J., Schirmer, L., et al. (2017). Neurotoxic reactive astrocytes are induced by activated microglia. *Nature* 541, 481–487. doi: 10.1038/nature21029

Limone, A., Veneruso, I., D'Argenio, V., and Sarnataro, D. (2022). Endosomal trafficking and related genetic underpinnings as a hub in Alzheimer's disease. *J. Cell. Physiol.* 237, 3803–3815. doi: 10.1002/jcp.30864

Lin, Y.-T., Seo, J., Gao, F., Feldman, H. M., Wen, H.-L., Penney, J., et al. (2018). APOE4 causes widespread molecular and cellular alterations associated with Alzheimer's disease phenotypes in human iPSC-derived brain cell types. *Neuron* 98, 1141–1154.e7. doi: 10.1016/j.neuron.2018.05.008

Malakooti, N., Fowler, C., Volitakis, I., McLean, C. A., Kim, R. C., Bush, A. I., et al. (2019, 2019). The down syndrome-associated protein, regulator of Calcineurin-1, is altered in Alzheimer's disease and dementia with lewy bodies. *J. Alzheimers Dis. Parkinsonism* 9:462. doi: 10.4172/2161-0460.1000462

Man, H.-Y., Lin, J. W., Ju, W. H., Ahmadian, G., Liu, L., Becker, L. E., et al. (2000). Regulation of AMPA receptor–mediated synaptic transmission by clathrin-dependent receptor internalization. *Neuron* 25, 649–662. doi: 10.1016/s0896-6273(00)81067-3

Maninger, J.-K., Nowak, K., Goberdhan, S., O'Donoghue, R., and Connor-Robson, N. (2024). Cell type-specific functions of Alzheimer's disease endocytic risk genes. *Philos. Trans. R Soc. Lond. B Biol. Sci.* 379. doi: 10.1098/rstb.2022.0378

Marshall, K. E., Vadukul, D. M., Staras, K., and Serpell, L. C. (2020). Misfolded amyloid-β-42 impairs the endosomal–lysosomal pathway. *Cell. Mol. Life Sci.* 77, 5031–5043. doi: 10.1007/s00018-020-03464-4

Martens, Y. A., Zhao, N., Liu, C. C., Kanekiyo, T., Yang, A. J., Goate, A. M., et al. (2022). ApoE Cascade hypothesis in the pathogenesis of Alzheimer's disease and related dementias. *Neuron* 110, 1304–1317. doi: 10.1016/j.neuron.2022.03.004

Martini-Stoica, H., Cole, A. L., Swartzlander, D. B., Chen, F., Wan, Y.-W., Bajaj, L., et al. (2018). TFEB enhances astroglial uptake of extracellular tau species and reduces tau spreading. *J. Exp. Med.* 215, 2355–2377. doi: 10.1084/jem.20172158

Mayor, S., Parton, R. G., and Donaldson, J. G. (2014). Clathrin-independent pathways of endocytosis. *Cold Spring Harb. Perspect. Biol.* 6:a016758. doi: 10.1101/cshperspect.a016758

McCarron, M., McCallion, P., Reilly, E., Dunne, P., Carroll, R., and Mulryan, N. (2017). A prospective 20-year longitudinal follow-up of dementia in persons with Down syndrome. *J. Intellect. Disabil. Res.* 61, 843–852. doi: 10.1111/jir.12390

McMahon, H. T., and Boucrot, E. (2011). Molecular mechanism and physiological functions of clathrin-mediated endocytosis. *Nat. Rev. Mol. Cell Biol.* 12, 517–533. doi: 10.1038/nrm3151

Mettlen, M., and Danuser, G. (2014). Imaging and modeling the dynamics of clathrin-mediated endocytosis. *Cold Spring Harb. Perspect. Biol.* 6:a017038. doi: 10.1101/cshperspect.a017038

Milosevic, I. (2018). Revisiting the role of clathrin-mediated endoytosis in synaptic vesicle recycling. *Front. Cell. Neurosci.* 12:27. doi: 10.3389/fncel.2018.00027

Mintun, M. A., Lo, A. C., Duggan Evans, C., Wessels, A. M., Ardayfio, P. A., Andersen, S. W., et al. (2021). Donanemab in early Alzheimer's disease. *N. Engl. J. Med.* 384, 1691–1704. doi: 10.1056/NEJMoa2100708

Mitchell, M. J., Billingsley, M. M., Haley, R. M., Wechsler, M. E., Peppas, N. A., and Langer, R. (2021). Engineering precision nanoparticles for drug delivery. *Nat. Rev. Drug Discov.* 20, 101–124. doi: 10.1038/s41573-020-0090-8

Mitsunari, T., Nakatsu, F., Shioda, N., Love, P. E., Grinberg, A., Bonifacino, J. S., et al. (2005). Clathrin adaptor AP-2 is essential for early embryonal development. *Mol. Cell. Biol.* 25, 9318–9323. doi: 10.1128/MCB.25.21.9318-9323.2005

Mohamed, N. V., Herrou, T., Plouffe, V., Piperno, N., and Leclerc, N. (2013). Spreading of tau pathology in Alzheimer's disease by cell-to-cell transmission. *Eur. J. Neurosci.* 37, 1939–1948. doi: 10.1111/ejn.12229

Mun, B.-R., Park, S.-B., and Choi, W.-S. (2024). The oligomeric form of amyloid Beta triggers astrocyte activation, independent of neurons. *Chonnam Med. J.* 60, 27–31. doi: 10.4068/cmj.2024.60.1.27

Nakamura, Y., Takeda, M., Yoshimi, K., Hattori, H., Hariguchi, S., Kitajima, S., et al. (1994). Involvement of clathrin light chains in the pathology of Alzheimer's disease. *Acta Neuropathol.* 87, 23–31. doi: 10.1007/bf00386251

Narayan, P., Sienski, G., Bonner, J. M., Lin, Y.-T., Seo, J., Baru, V., et al. (2020). PICALM rescues endocytic defects caused by the Alzheimer's disease risk factor APOE4. *Cell Rep.* 33:108224. doi: 10.1016/j.celrep.2020.108224

Ni, J., Xie, Z., Quan, Z., Meng, J., and Qing, H. (2024). How brain 'cleaners' fail: mechanisms and therapeutic value of microglial phagocytosis in Alzheimer's disease. *Glia* 72, 227–244. doi: 10.1002/glia.24465

Nixon, R. A. (2017). Amyloid precursor protein and endosomal-lysosomal dysfunction in Alzheimer's disease: inseparable partners in a multifactorial disease. *FASEB J.* 31, 2729–2743. doi: 10.1096/fj.201700359

Nixon, R. A. (2020). The aging lysosome: an essential catalyst for late-onset neurodegenerative diseases. *Biochim. Biophys. Acta Proteins Proteom.* 1868:140443. doi: 10.1016/j.bbapap.2020.140443

Nixon, R. A., Cataldo, A. M., and Mathews, P. M. (2000). The endosomal-lysosomal system of neurons in Alzheimer's disease pathogenesis: a review. *Neurochem. Res.* 25, 1161–1172. doi: 10.1023/a:1007675508413

Oakley, H., Cole, S. L., Logan, S., Maus, E., Shao, P., Craft, J., et al. (2006). Intraneuronal β-amyloid aggregates, neurodegeneration, and neuron loss in transgenic mice with five familial Alzheimer's disease mutations: potential factors in amyloid plaque formation. *J. Neurosci.* 26, 10129–10140. doi: 10.1523/jneurosci.1202-06.2006

Oddo, S., Caccamo, A., Shepherd, J. D., Murphy, M. P., Golde, T. E., Kayed, R., et al. (2003). Triple-transgenic model of Alzheimer's disease with plaques and tangles. *Neuron* 39, 409–421. doi: 10.1016/s0896-6273(03)00434-3

Omtri, R. S., Davidson, M. W., Arumugam, B., Poduslo, J. F., and Kandimalla, K. K. (2012). Differences in the cellular uptake and intracellular itineraries of amyloid beta proteins 40 and 42: ramifications for the Alzheimer's drug discovery. *Mol. Pharm.* 9, 1887–1897. doi: 10.1021/mp200530q

Ou-Yang, P., Cai, Z.-Y., and Zhang, Z.-H. (2023). Molecular regulation mechanism of microglial autophagy in the pathology of Alzheimer's disease. *Aging Dis.* 14, 1166–1177. doi: 10.14336/ad.2023.0106

Pechstein, A., Bacetic, J., Vahedi-Faridi, A., Gromova, K., Sundborger, A., Tomlin, N., et al. (2010). Regulation of synaptic vesicle recycling by complex formation between intersectin 1 and the clathrin adaptor complex AP2. *Proc. Natl. Acad. Sci.* 107, 4206–4211. doi: 10.1073/pnas.0911073107

Pei, Y. A., Davies, J., Zhang, M., and Zhang, H. T. (2020). The role of synaptic dysfunction in Alzheimer's disease. *J. Alzheimers Dis.* 76, 49–62. doi: 10.3233/JAD-191334

Piras, I. S., Krate, J., Delvaux, E., Nolz, J., De Both, M. D., Mastroeni, D. F., et al. (2019). Association of AEBP1 and NRN1 RNA expression with Alzheimer's disease and neurofibrillary tangle density in middle temporal gyrus. *Brain Res.* 1719, 217–224. doi: 10.1016/j.brainres.2019.06.004

Puangmalai, N., Bhatt, N., Montalbano, M., Sengupta, U., Gaikwad, S., Ventura, F., et al. (2020). Internalization mechanisms of brain-derived tau oligomers from patients with Alzheimer's disease, progressive supranuclear palsy and dementia with Lewy bodies. *Cell Death Dis.* 11, 314. doi: 10.1038/s41419-020-2503-3

Rabinovici, G. D., and La Joie, R. (2023). Amyloid-targeting monoclonal antibodies for Alzheimer disease. *JAMA* 330, 507–509. doi: 10.1001/jama.2023.11703

Raj, T., Li, Y. I., Wong, G., Humphrey, J., Wang, M., Ramdhani, S., et al. (2018). Integrative transcriptome analyses of the aging brain implicate altered splicing in Alzheimer's disease susceptibility. *Nat. Genet.* 50, 1584–1592. doi: 10.1038/s41588-018-0238-1

Rajan, K. B., Weuve, J., Barnes, L. L., McAninch, E. A., Wilson, R. S., and Evans, D. A. (2021). Population estimate of people with clinical Alzheimer's disease and mild cognitive impairment in the United States (2020–2060). *Alzheimers Dement.* 17, 1966–1975. doi: 10.1002/alz.12362

Ratan, Y., Rajput, A., Maleysm, S., Pareek, A., Jain, V., Pareek, A., et al. (2023). An insight into cellular and molecular mechanisms underlying the pathogenesis of neurodegeneration in Alzheimer's disease. *Biomedicines* 11:1398. doi: 10.3390/biomedicines11051398

Rennick, J. J., Johnston, A. P. R., and Parton, R. G. (2021). Key principles and methods for studying the endocytosis of biological and nanoparticle therapeutics. *Nat. Nanotechnol.* 16, 266–276. doi: 10.1038/s41565-021-00858-8

Root, J., Merino, P., Nuckols, A., Johnson, M., and Kukar, T. (2021). Lysosome dysfunction as a cause of neurodegenerative diseases: lessons from frontotemporal dementia and amyotrophic lateral sclerosis. *Neurobiol. Dis.* 154:105360. doi: 10.1016/j.nbd.2021.105360

Sanchez-Mico, M. V., Jimenez, S., Gomez-Arboledas, A., Muñoz-Castro, C., Romero-Molina, C., Navarro, V., et al. (2021). Amyloid-β impairs the phagocytosis of dystrophic synapses by astrocytes in Alzheimer's disease. *Glia* 69, 997–1011. doi: 10.1002/glia.23943

Schork, N. J., and Elman, J. A. (2023). Pathway-specific polygenic risk scores correlate with clinical status and Alzheimer's disease-related biomarkers. *J. Alzheimers Dis.* 95, 915–929. doi: 10.3233/jad-230548

Schreij, A. M. A., Fon, E. A., and McPherson, P. S. (2016). Endocytic membrane trafficking and neurodegenerative disease. *Cell. Mol. Life Sci.* 73, 1529–1545. doi: 10.1007/s00018-015-2105-x

Schrezenmeier, E., and Dörner, T. (2020). Mechanisms of action of hydroxychloroquine and chloroquine: implications for rheumatology. *Nat. Rev. Rheumatol.* 16, 155–166. doi: 10.1038/s41584-020-0372-x

Selkoe, D. J., and Hardy, J. (2016). The amyloid hypothesis of Alzheimer's disease at 25 years. *EMBO Mol. Med.* 8, 595–608. doi: 10.15252/emmm.201606210

Sevigny, J., Chiao, P., Bussiere, T., Weinreb, P. H., Williams, L., Maier, M., et al. (2016). The antibody aducanumab reduces Abeta plaques in Alzheimer's disease. *Nature* 537, 50–56. doi: 10.1038/nature19323

Shi, J.-M., Zhu, L., Lan, X., Zhao, D.-W., He, Y.-J., Sun, Z.-Q., et al. (2020). Endocytosis is a key mode of interaction between extracellular β-amyloid and the cell membrane. *Biophys. J.* 119, 1078–1090. doi: 10.1016/j.bpj.2020.07.035

Small, S. A., Simoes-Spassov, S., Mayeux, R., and Petsko, G. A. (2017). Endosomal traffic jams represent a pathogenic hub and therapeutic target in Alzheimer's disease. *Trends Neurosci.* 40, 592–602. doi: 10.1016/j.tins.2017.08.003

Snyder, E. M., Nong, Y., Almeida, C. G., Paul, S., Moran, T., Choi, E. Y., et al. (2005). Regulation of NMDA receptor trafficking by amyloid-β. *Nat. Neurosci.* 8, 1051–1058. doi: 10.1038/nn1503

Sofroniew, M. V. (2020). Astrocyte reactivity: subtypes, states, and functions in CNS innate immunity. *Trends Immunol.* 41, 758–770. doi: 10.1016/j.it.2020.07.004

Sofroniew, M. V., and Vinters, H. V. (2010). Astrocytes: biology and pathology. *Acta Neuropathol.* 119, 7–35. doi: 10.1007/s00401-009-0619-8

Söllvander, S., Nikitidou, E., Brolin, R., Söderberg, L., Sehlin, D., Lannfelt, L., et al. (2016). Accumulation of amyloid-β by astrocytes result in enlarged endosomes and microvesicle-induced apoptosis of neurons. *Mol. Neurodegener.* 11:38. doi: 10.1186/s13024-016-0098-z

Song, M. S., Baker, G. B., Todd, K. G., and Kar, S. (2011). Inhibition of beta-amyloid1-42 internalization attenuates neuronal death by stabilizing the endosomal-lysosomal system in rat cortical cultured neurons. *Neuroscience* 178, 181–188. doi: 10.1016/j.neuroscience.2010.12.055

Soykan, T., Maritzen, T., and Haucke, V. (2016). Modes and mechanisms of synaptic vesicle recycling. *Curr. Opin. Neurobiol.* 39, 17–23. doi: 10.1016/j.conb.2016.03.005

Srinivasan, S., Gal, J., Bachstetter, A., and Nelson, P. T. (2022). Alpha adaptins show isoform-specific association with neurofibrillary tangles in Alzheimer's disease. *Neuropathol. Appl. Neurobiol.* 48:e12776. doi: 10.1111/nan.12776

Stenmark, H., Parton, R. G., Steele-Mortimer, O., Lütcke, A., Gruenberg, J., and Zerial, M. (1994). Inhibition of rab5 GTPase activity stimulates membrane fusion in endocytosis. *EMBO J.* 13, 1287–1296. doi: 10.1002/j.1460-2075.1994.tb06381.x

Streit, W. J., Khoshbouei, H., and Bechmann, I. (2021). The role of microglia in sporadic Alzheimer's disease. *J. Alzheimers Dis.* 79, 961–968. doi: 10.3233/jad-201248

Swanson, C. J., Zhang, Y., Dhadda, S., Wang, J., Kaplow, J., Lai, R. Y. K., et al. (2021). A randomized, double-blind, phase 2b proof-of-concept clinical trial in early Alzheimer's disease with lecanemab, an anti-Abeta protofibril antibody. *Alzheimers Res. Ther.* 13:80. doi: 10.1186/s13195-021-00813-8

Szabo, M. P., Mishra, S., Knupp, A., and Young, J. E. (2022). The role of Alzheimer's disease risk genes in endolysosomal pathways. *Neurobiol. Dis.* 162:105576. doi: 10.1016/j.nbd.2021.105576

Szewczyk-Roszczenko, O. K., Roszczenko, P., Shmakova, A., Finiuk, N., Holota, S., Lesyk, R., et al. (2023). The chemical inhibitors of endocytosis: from mechanisms to potential clinical applications. *Cells* 12:2312. doi: 10.3390/cells12182312

Terry, R. D., Masliah, E., Salmon, D. P., Butters, N., Deteresa, R., Hill, R., et al. (1991). Physical basis of cognitive alterations in Alzheimer's disease: synapse loss is the major correlate of cognitive impairment. *Ann. Neurol.* 30, 572–580. doi: 10.1002/ana.410300410

Tesi, N., Van Der Lee, S. J., Hulsman, M., Jansen, I. E., Stringa, N., Van Schoor, N. M., et al. (2020). Immune response and endocytosis pathways are associated with the resilience against Alzheimer's disease. *Transl. Psychiatry* 10:332. doi: 10.1038/s41398-020-01018-7

Thal, D. R., and Tome, S. O. (2022). The central role of tau in Alzheimer's disease: from neurofibrillary tangle maturation to the induction of cell death. *Brain Res. Bull.* 190, 204–217. doi: 10.1016/j.brainresbull.2022.10.006

Theerasri, A., Janpaijit, S., Tencomnao, T., and Prasansuklab, A. (2022). Beyond the classical amyloid hypothesis in Alzheimer's disease: molecular insights into current concepts of pathogenesis, therapeutic targets, and study models. *WIREs Mech. Dis.* 15:e1591. doi: 10.1002/wsbm.1591

Thomas, R. S., Henson, A., Gerrish, A., Jones, L., Williams, J., and Kidd, E. J. (2016). Decreasing the expression of PICALM reduces endocytosis and the activity of β-secretase: implications for Alzheimer's disease. *BMC Neurosci.* 17:50. doi: 10.1186/s12868-016-0288-1

Thomas, R. S., Lelos, M. J., Good, M. A., and Kidd, E. J. (2011). Clathrin-mediated endocytic proteins are upregulated in the cortex of the Tg2576 mouse model of Alzheimer's disease-like amyloid pathology. *Biochem. Biophys. Res. Commun.* 415, 656–661. doi: 10.1016/j.bbrc.2011.10.131

Torres-Ceja, B., and Olsen, M. L. (2022). A closer look at astrocyte morphology: development, heterogeneity, and plasticity at astrocyte leaflets. *Curr. Opin. Neurobiol.* 74:102550. doi: 10.1016/j.conb.2022.102550

Usenovic, M., Niroomand, S., Drolet, R. E., Yao, L., Gaspar, R. C., Hatcher, N. G., et al. (2015). Internalized tau oligomers cause neurodegeneration by inducing accumulation of pathogenic tau in human neurons derived from induced pluripotent stem cells. *J. Neurosci.* 35, 14234–14250. doi: 10.1523/jneurosci.1523-15.2015

Vainchtein, I. D., and Molofsky, A. V. (2020). Astrocytes and microglia: in sickness and in health. *Trends Neurosci.* 43, 144–154. doi: 10.1016/j.tins.2020.01.003

Van Gool, W. A., Weinstein, H. C., Scheltens, P. K., and Walstra, G. J. M. (2001). Effect of hydroxychloroquine on progression of dementia in early Alzheimer's disease: an 18-month randomised, double-blind, placebo-controlled study. *Lancet* 358, 455–460. doi: 10.1016/S0140-6736(01)05623-9

Varma, V. R., Desai, R. J., Navakkode, S., Wong, L.-W., Anerillas, C., Loeffler, T., et al. (2023). Hydroxychloroquine lowers Alzheimer's disease and related dementias risk and rescues molecular phenotypes related to Alzheimer's disease. *Mol. Psychiatry* 28, 1312–1326. doi: 10.1038/s41380-022-01912-0

Volloch, V., and Rits-Volloch, S. (2022). The amyloid Cascade hypothesis 2.0: on the possibility of once-in-a-lifetime-only treatment for prevention of Alzheimer's disease and for its potential cure at symptomatic stages. *J. Alzheimers Dis. Rep.* 6, 369–399. doi: 10.3233/ADR-220031

Volloch, V., and Rits-Volloch, S. (2023). The amyloid cascade hypothesis 2.0: generalization of the concept. *J. Alzheimers Dis. Rep.* 7, 21–35. doi: 10.3233/ADR-220079

Wendimu, M. Y., and Hooks, S. B. (2022). Microglia phenotypes in aging and neurodegenerative diseases. *Cells* 11:2091. doi: 10.3390/cells11132091

Wesén, E., Jeffries, G. D. M., Matson Dzebo, M., and Esbjörner, E. K. (2017). Endocytic uptake of monomeric amyloid-β peptides is clathrin- and dynamin-independent and results in selective accumulation of Aβ(1–42) compared to Aβ(1–40). *Sci. Rep.* 7:2021. doi: 10.1038/s41598-017-02227-9

Wesén, E., Lundmark, R., and Esbjörner, E. K. (2020). Role of membrane tension sensitive endocytosis and rho GTPases in the uptake of the Alzheimer's disease peptide Aβ(1-42). *ACS Chem. Neurosci.* 11, 1925–1936. doi: 10.1021/acschemneuro.0c00053

Wilmot, B., McWeeney, S. K., Nixon, R. R., Montine, T. J., Laut, J., Harrington, C. A., et al. (2008). Translational gene mapping of cognitive decline. *Neurobiol. Aging* 29, 524–541. doi: 10.1016/j.neurobiolaging.2006.11.008

Wu, J. W., Herman, M., Liu, L., Simoes, S., Acker, C. M., Figueroa, H., et al. (2013). Small misfolded tau species are internalized via bulk endocytosis and anterogradely and retrogradely transported in neurons. *J. Biol. Chem.* 288, 1856–1870. doi: 10.1074/jbc.M112.394528

Wu, F., and Yao, P. J. (2009). Clathrin-mediated endocytosis and Alzheimer's disease: an update. *Ageing Res. Rev.* 8, 147–149. doi: 10.1016/j.arr.2009.03.002

Xie, A. J., Hou, T. Y., Xiong, W., Huang, H. Z., Zheng, J., Li, K., et al. (2019). Tau overexpression impairs neuronal endocytosis by decreasing the GTPase dynamin 1 through the miR-132/MeCP2 pathway. *Aging Cell* 18:e12929. doi: 10.1111/acel.12929

Yao, P. J. (2004). Synaptic frailty and clathrin-mediated synaptic vesicle trafficking in Alzheimer's disease. *Trends Neurosci.* 27, 24–29. doi: 10.1016/j.tins.2003.10.012

Yao, P. J., Morsch, R., Callahan, L. M., and Coleman, P. D. (1999). Changes in synaptic expression of clathrin assembly protein AP180 in Alzheimer's disease analysed by immunohistochemistry. *Neuroscience* 94, 389–394. doi: 10.1016/s0306-4522(99)00360-7

Yao, P. J., Weimer, J. M., O'Herron, T. M., and Coleman, P. D. (2000). Clathrin assembly protein AP-2 is detected in both neurons and glia, and its reduction is prominent in layer II of frontal cortex in Alzheimer's disease. *Neurobiol. Aging* 21, 921–929. doi: 10.1016/s0197-4580(00)00228-1

Yao, P. J., Zhu, M., Pyun, E. I., Brooks, A. I., Therianos, S., Meyers, V. E., et al. (2003). Defects in expression of genes related to synaptic vesicle trafficking in frontal cortex of Alzheimer's disease. *Neurobiol. Dis.* 12, 97–109. doi: 10.1016/s0969-9961(02)00009-8

Yuan, W. Q., Huang, W. P., Jiang, Y. C., Xu, H., Duan, C. S., Chen, N. H., et al. (2023). The function of astrocytes and their role in neurological diseases. *Eur. J. Neurosci.* 58, 3932–3961. doi: 10.1111/ejn.16160

Zhang, Y.-W., Thompson, R., Zhang, H., and Xu, H. (2011). APP processing in Alzheimer's disease. *Mol. Brain* 4:3. doi: 10.1186/1756-6606-4-3

Zhang, F., Zhong, R.-J., Cheng, C., Li, S., and Le, W.-D. (2021). New therapeutics beyond amyloid-β and tau for the treatment of Alzheimer's disease. *Acta Pharmacol. Sin.* 42, 1382–1389. doi: 10.1038/s41401-020-00565-5

Zhang, X., Zou, L., Tang, L., Xiong, M., Yan, X.-X., Meng, L., et al. (2024). Bridging integrator 1 fragment accelerates tau aggregation and propagation by enhancing clathrin-mediated endocytosis in mice. *PLoS Biol.* 22:e3002470. doi: 10.1371/journal.pbio.3002470

Zhao, Y., Liu, B., Wang, J., Xu, L., Yu, S., Fu, J., et al. (2022). Aβ and tau regulate microglia metabolism via exosomes in Alzheimer's disease. *Biomedicines* 10:1800. doi: 10.3390/biomedicines10081800

Zhao, Z., Ukidve, A., Kim, J., and Mitragotri, S. (2020). Targeting strategies for tissue-specific drug delivery. *Cell* 181, 151–167. doi: 10.1016/j.cell.2020.02.001

Zhao, J., Wu, H., and Tang, X. Q. (2021). Tau internalization: a complex step in tau propagation. *Ageing Res. Rev.* 67:101272. doi: 10.1016/j.arr.2021.101272

frontiers | Frontiers in Aging Neuroscience

TYPE Original Research
PUBLISHED 07 May 2024
DOI 10.3389/fnagi.2024.1368839

OPEN ACCESS

EDITED BY
Allison B. Reiss,
New York University, United States

REVIEWED BY
Suman Chowdhury,
The State University of New Jersey, United States
Wen Xiong,
Baylor College of Medicine, United States
Jie Zhu,
Karolinska University Hospital Solna, Sweden

*CORRESPONDENCE
Makoto Kurano
✉ kurano-tky@umin.ac.jp

RECEIVED 11 January 2024
ACCEPTED 10 April 2024
PUBLISHED 07 May 2024

CITATION
Uranbileg B, Isago H, Sakai E, Kubota M, Saito Y and Kurano M (2024) Alzheimer's disease manifests abnormal sphingolipid metabolism.
Front. Aging Neurosci. 16:1368839.
doi: 10.3389/fnagi.2024.1368839

Alzheimer's disease manifests abnormal sphingolipid metabolism

Baasanjav Uranbileg[1], Hideaki Isago[1], Eri Sakai[2], Masayuki Kubota[2], Yuko Saito[3] and Makoto Kurano[1]*

[1]Department of Clinical Laboratory Medicine, Graduate School of Medicine, The University of Tokyo, Tokyo, Japan, [2]Nihon Waters K.K., Tokyo, Japan, [3]Tokyo Metropolitan Geriatric Hospital and Institute of Gerontology, Tokyo, Japan

Introduction: Alzheimer's disease (AD) is associated with disturbed metabolism, prompting investigations into specific metabolic pathways that may contribute to its pathogenesis and pathology. Sphingolipids have garnered attention due to their known physiological impact on various diseases.

Methods: We conducted comprehensive profiling of sphingolipids to understand their possible role in AD. Sphingolipid levels were measured in AD brains, Cerad score B brains, and controls, as well as in induced pluripotent stem (iPS) cells (AD, PS, and control), using liquid chromatography mass spectrometry.

Results: AD brains exhibited higher levels of sphingosine (Sph), total ceramide 1-phosphate (Cer1P), and total ceramide (Cer) compared to control and Cerad-B brains. Deoxy-ceramide (Deoxy-Cer) was elevated in Cerad-B and AD brains compared to controls, with increased sphingomyelin (SM) levels exclusively in Cerad-B brains. Analysis of cell lysates revealed elevated dihydroceramide (dhSph), total Cer1P, and total SM in AD and PS cells versus controls. Multivariate analysis highlighted the relevance of Sph, Cer, Cer1P, and SM in AD pathology. Machine learning identified Sph, Cer, and Cer1P as key contributors to AD.

Discussion: Our findings suggest the potential importance of Sph, Cer1P, Cer, and SM in the context of AD pathology. This underscores the significance of sphingolipid metabolism in understanding and potentially targeting mechanisms underlying AD.

KEYWORDS

Alzheimer's disease (AD), sphingosine (Sph), ceramide 1-phosphate (Cer1P), ceramide (Cer), sphingomyelin (SM)

1 Introduction

Alzheimer's disease (AD) is a widespread neurodegenerative condition that affects millions of individuals worldwide, with a far-reaching impact on not only the patients themselves, but also their families, society, and healthcare systems (Winblad et al., 2016). AD is responsible for approximately two-thirds of all dementia cases (Livingston et al., 2017) and is characterized by the presence of aggregates of pathologically misfolded proteins, mainly of amyloid β (Aβ), which is a product of the proteolytic cleavage of the transmembrane Aβ precursor protein (Karran et al., 2011; Brunkhorst et al., 2014). The precise pathogenesis of AD remains incompletely understood, and the true significance of the numerous disruptions observed in these patients remains ambiguous. Several established mechanisms have been linked to neuronal and synaptic degeneration in the brains of patients with AD. These established mechanisms include oxidative damage,

perturbed redox signaling, and mitochondrial dysfunction (Chen and Zhong, 2014; Yuyama et al., 2014; Ashleigh et al., 2023), impaired glucose metabolism (Serviddio et al., 2011), and an inflammatory response (Hansen et al., 2018; Singh, 2022).

However, the changes in lipid components and their relationship with AD still remain inadequately understood. The central nervous system (CNS) is rich in lipoprotein components, particularly apolipoprotein-E (ApoE)-rich high-density lipoprotein (HDL) (Vance and Hayashi, 2010), and the ApoE polymorphism has been stablished as a major risk factor for AD (Corder et al., 1993). In addition to cholesterol, ApoE types can affect the metabolism of sphingolipids. Actually, emerging evidence suggests that sphingolipids play important roles in the pathogenesis of AD, starting from earlier stages of the disease (Kosicek et al., 2012). For example, sphingolipids play structural roles in cellular membranes, including lipid rafts, which imply their involvement in Aβ metabolism (Olsen and Faergeman, 2017).

The brain expresses various sphingolipids, and multiple studies have examined the changes in sphingolipid levels in patients with AD. Among them, sphingosine 1-phosphate (S1P) and ceramides (Cer) have been extensively studied in the field of neurology (Ceccom et al., 2014; Couttas et al., 2014; Ghasemi et al., 2016). Sphingolipids can interconvert among themselves, forming a dynamic and intricate metabolic map. For instance, S1P is produced from sphingosine, and ceramides are derived from sphingomyelins, which can also be converted into sphingosine. Moreover, dihydrosphingosine 1-phosphate (dhS1P) is another ligand for S1P receptors that is produced from dihydrosphingosine (dhSph). The levels of sphingomyelins (SMs) have been reported to be elevated in AD brains (Kosicek et al., 2012; Barbash et al., 2017), whereas S1P levels are decreased (He et al., 2010; Couttas et al., 2014). However, the findings pertaining to ceramides are conflicting, with some studies reporting increased levels (Satoi et al., 2005) and one study reporting decreased levels in AD brains (Barbash et al., 2017). Because sphingolipids form an intricate metabolic map; and not only S1P and Cer, but also other sphingolipids [such as ceramide 1-phosphate (Cer1P) and deoxy-ceramide (Deoxy-Cer)] can be involved in the pathogenesis of AD, considering their potential biological properties (Bertea et al., 2010; Othman et al., 2012; Presa et al., 2020), a comprehensive analysis of sphingolipids is necessary to understand their modulation and estimate the potential roles of the disturbed metabolism of sphingolipids in AD.

Therefore, in the current study, we aimed to obtain a deeper understanding of the role of sphingolipids in AD by employing an advanced analytical method. We recently developed a novel LC-MS/MS method (Uranbileg et al., 2024) that allowed us to analyze a broader range of sphingolipid species using consistent solvent, column, and measurement conditions. This innovation expanded our capacity to explore the dynamic changes in sphingolipid metabolism in pathological conditions.

In this study, we utilized this advanced method to comprehensively analyze sphingolipids in both human postmortem brain tissue samples and AD induced pluripotent stem (iPS) cells. Our aim was to obtain insights into how these sphingolipids are modulated and involved in AD. To understand our findings better, we integrated our sphingolipid data with statistical methods based on machine learning techniques, which enabled us to pinpoint the factors that are most closely associated with AD.

TABLE 1 Patients characteristics.

	Control	Cerad-B	AD
N	6	7	6
Age (mean, SD)	83.17 (3.34)	85.43 (3.33)	86.17 (1.07)
Gender (M/F)	4/2	2/5	3/3
SP (SD)	0.67 (0.47)	1.57 (0.49)	3.00 (0.00)
Braak (SD)	1.33 (0.47)	1.57 (0.49)	5.00 (0.00)
Aβ (pmol/L, SD)	0.636 (0.171)	1.579 (0.380)	1.591 (0.242)
PMI (min, SD)	377 (306)	825 (278)	702 (346)
RIN (SD)	7.9 (0.74)	8.3 (0.40)	8.1 (0.31)

SP, senile plaque; Aβ, amyloid beta; PMI, postmortem interval; RIN, RNA integrity number.

2 Materials and methods

2.1 Tissue samples

Sphingolipids and ceramides were measured in the following samples: human postmortem brain tissues (cerebral cortex) obtained from subjects who had no medical history of AD or showed no evidence of other CNS disorders at the Tokyo Metropolitan Geriatric Medical Center (Braak stage 1–2; $n = 6$); human postmortem brain tissues obtained from subjects with Cerad-B (classified as an intermediate probability of AD, Braak stage 1–2; $n = 7$) (Murayama and Saito, 2004); and human postmortem brain tissues obtained from subjects with AD (Braak stage 5; $n = 6$), representing an advanced pathology related to end-stage disease. All specimens collected from autopsies were obtained from the Brain Bank for Aging Research.[1] The Aβ contents were measured using a Human β Amyloid (1–40) and (1–42) ELISA kits (298-64601 and 298–62401, WAKO Pure Chemical Industries, Osaka, Japan), and adjusted to the brain protein levels. The characteristics of these patients are listed in **Table 1**.

This study was conducted in accordance with the ethical guidelines outlined in the Declaration of Helsinki. Written informed consent was obtained in advance from the brain donors and/or the next of kin. The study design was approved by the Tokyo Metropolitan Geriatric Medical Center and The University of Tokyo Medical Research Center Ethics Committee (2018088NI).

2.2 Cell culture

Human AD-patient-derived iPS cells (iPS cell derived neuronal progenitor cells; ReproNeuro AD-patient 1, RCDN003P); PS [a genetically modified variant (P117L) of Presenilin 1, which is one of the causative molecules in AD], introduced into induced pluripotent stem (iPS) cells derived from healthy

1 https://www.tmig.or.jp/eresearch/a23.html

individuals; and ReproNeuro AD-mutation (RCDN002N) and Control (normal model neurons, RCDN001N) cells were purchased from ReproCELL, Inc. (Tokyo, Japan) and cultured according to the manufacturer's protocol.

2.3 Sample preparation

For the measurement of all sphingolipids, a total of 10 μl of homogenized tissue samples and cell lysates samples were mixed with 10 μl of internal standards [SPLASH LipidoMix^{TM}, Cer1P-d7, hexosyl ceramide (HexCer), C_{17}S1P, C_{17}dhS1P, C1 7:1 Sphingosine (Sph), C17:1 dihydrosphingosine (dhSph), d18:1/17:0 Ceramide (Avanti Polar Lipids)] at 1 ng/ml (final concentration), and the sphingolipid content was extracted with 100 μl of 0.1% formic acid in methanol (Wako Pure Chemical Industries) and 80 μl of acetonitrile (Wako Pure Chemical Industries). The mixtures were sonicated for 5 min and then centrifuged at 16,400 × *g* for 10 min at 4°C. The supernatants were then analyzed using the LC-MS/MS method.

2.4 LC-MS/MS analysis

Sphingolipids were measured using the LC-MS/MS system (WATERS Corporation). Briefly, 5.0-μl samples were injected and LC separation was performed using a normal-phase column [InertSustain Amide 3-μm column: 2.1 × 100 mm (UP)] with a gradient elution of solvent A (10 mM ammonium acetate, 95% acetonitrile, and 5% water) and solvent B (10 mM ammonium acetate, 50% acetonitrile) at 0.6 ml/min. The conditions used in this experiment were as follows: a gradient run was performed at 99% solvent A and 1% solvent B for 1 min, followed by a run at 90% solvent A and 10% solvent B for 1 min, a run at 60% solvent A and 40% solvent B for 3 min, and a run at 20% solvent A and 80% solvent B for 2 min. The total run time was 11 min, the target column temperature was 50°C, and the target sample temperature was 10°C.

The mass spectrometer was operated in electrospray ionization-positive ion mode using the following analytical conditions: the cone gas flow was set at 50 L/h, the desolvation gas flow was set at 1,000 L/h, the source temperature was set at 150°C, and the desolvation temperature was set at 600°C.

The analyses were performed in the multiple reaction monitoring mode in the positive ion mode for sphingolipids. The data were analyzed by MassLynx, TargetLynx XS (WATERS Corporation). The monitored lipids are described in **Supplementary Table 1**. Both the intra-day and inter-day coefficients of variation for this assay were below 20%.

Using this newly established LC-MS/MS method, we conducted an analysis of sphingolipids and their species, including S1P, Sph, dhS1P, dhSph, Cer (24 species), Cer1P (12 species), HexCer (23 species), lactosyl-ceramide (LacCer, 5 species), dh-ceramide (9 species), deoxy-ceramide (9 species), deoxy-dh-ceramide (9 species), and SM (9 species).

After LC-MS/MS measurement, the areas of each sphingolipid are utilized in the subsequent analysis to determine their respective levels. The protein levels of each sample, which were determined by a colorimetric assay for protein concentration (DC protein assay, 500-0116, Bio-Rad Laboratories, Inc. Hercules, CA, USA), and the areas of the corresponding internal standards were then employed to calculate the final concentrations of the measured sphingolipids.

2.5 Statistical analysis

Data processing and analysis were performed using the SPSS (Chicago, IL, USA), MetaboAnalyst 5.0[2] and GraphPad Prism 8.0 software (GraphPad Software, San Diego, CA, USA). To examine the statistical significance of the differences detected in the sphingolipid levels and among the control brains, Cerad-B brains, and AD brains or cells, we used a one-way analysis of variance test or multiple comparisons with Tukey correction using SPSS. The results pertaining to the lipid levels are expressed as the mean and SD. To assess correlations, Spearman's rank analysis was employed to examine the association between sphingolipids and other components using SPSS. A sparse Partial Least Square-Discriminant Analysis (PLS-DA) or machine learning study was performed using MetaboAnalyst or by SPSS Modeler, respectively, to explore the characteristics of the three diagnostic groups.

Variable Importance in the Projection (VIP) is a metric that was used to quantify the weighted contribution of sphingolipids to the differences between the groups. VIP was calculated as the sum of squares of the PLS loadings, considering the amount of variation explained in each dimension (for additional details, see text footnote 2). The Kendall rank correlation was employed to investigate the association of sphingolipids or clinical (pathological) data [Aβ levels, Braak stage, and senile plaque (SP) grade] with different groups, considering age and gender as covariates of interest.

Significance was set at $p < 0.05$.

3 Results

3.1 Overall modulation of sphingolipids in AD brains

Figures 1A, B reports the total levels of all measured sphingolipids in the three groups. The levels of Sph, total Cer1P, and total Cer were significantly higher in the AD brains compared with the control or Cerad-B brains. The total level of Deoxy-Cer was higher in both the Cerad-B and AD brains compared with the control brains. The levels of dhSph and SM were increased exclusively in the Cerad-B brains, and the levels of S1P were not significantly different among the groups (**Figure 1A**). The differences in the levels of sphingolipid species with significant changes among the three groups are shown in **Supplementary Figures 1A–D**.

2 https://www.metaboanalyst.ca/

10.3389/fnagi.2024.1368839

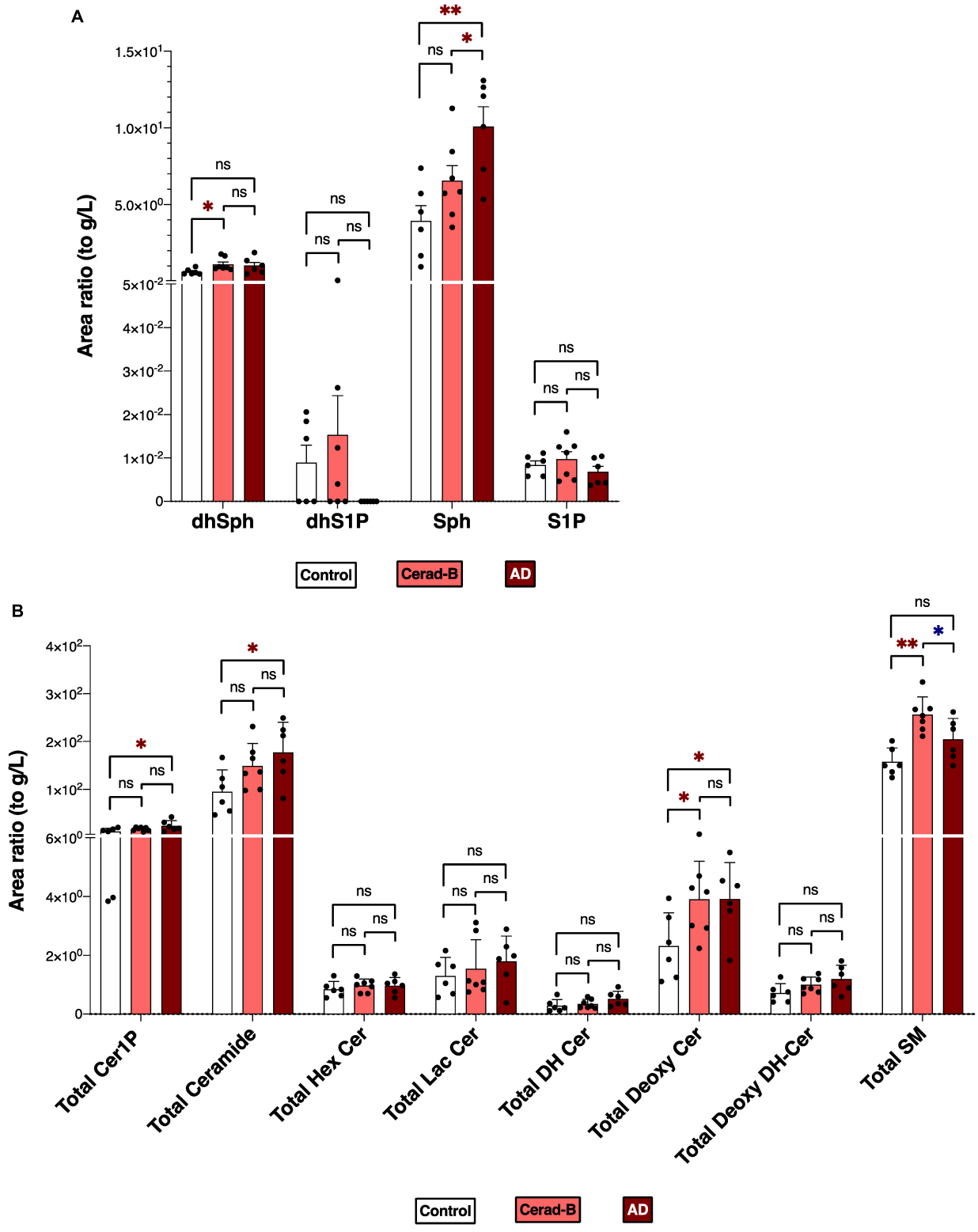

FIGURE 1
Sphingolipid modulation in AD brain tissues. Sphingolipid levels were assessed in the brains of control subjects (n = 6), the patients with Cerad-b (n = 7), and those with AD (n = 6). Statistical evaluation of differences was conducted using one-way analysis of variance (ANOVA) and multiple comparisons with Tukey correction. **(A)** Dihydrosphingosine (dhSph), dihydrosphingosine 1-phosphate (dhS1P), sphingosine (Sph), and sphingosine 1-phosphate (S1P) levels. **(B)** Total levels of the ceramide 1-phosphate (Cer1P), ceramide (Cer), hexosyl ceramide (HexCer), lactosyl-ceramide (LacCer), dihydroceramide (DH Cer), deoxy-ceramide (Deoxy-Cer), deoxy dihydroceramide (Deoxy-dhCer), and sphingomyelin (SM). Statistical significance was denoted as follows: * for $p < 0.05$, ** for $p < 0.01$, *** for $p < 0.001$. Red * indicates a significant increase, while blue * indicates a significant decrease.

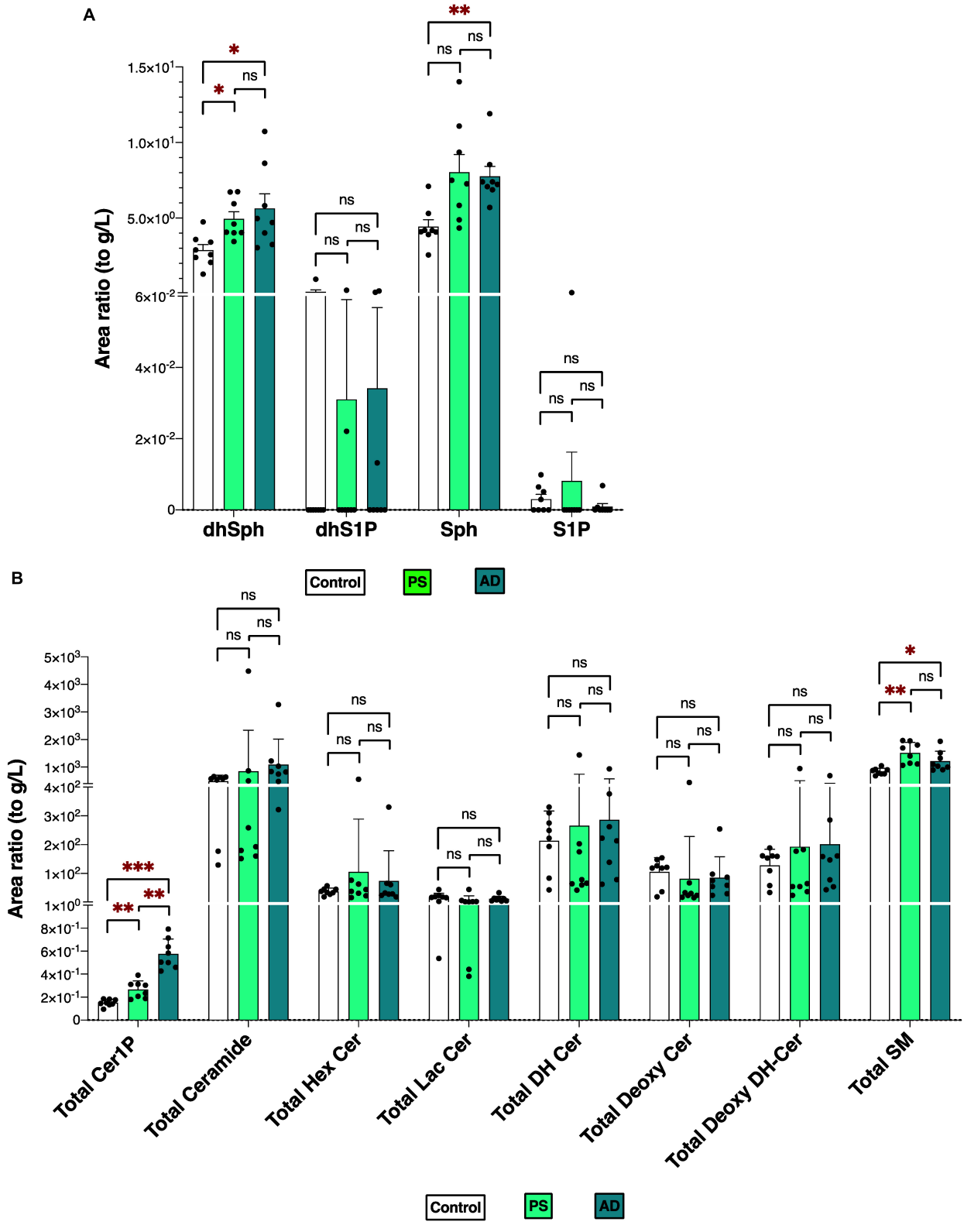

FIGURE 2
Sphingolipid modulation in iPS cells. Sphingolipid levels were measured in normal model neurons (C), mutated Presenilin 1-inserted iPS cell (PS), and AD patient derived iPS cell (AD), each group $N = 8$. Statistical evaluation of differences was conducted using one-way analysis of variance (ANOVA) and multiple comparisons with Tukey correction. **(A)** DhSph, dhS1P, Sph, and S1P levels. **(B)** Total levels of the Cer1P, Cer, Hex Cer, LacCer, dhCer, Deoxy-Cer, Deoxy-dhCer, and SM. Statistical significance was denoted as follows: * for $p < 0.05$, ** for $p < 0.01$, *** for $p < 0.001$. Red * indicates a significant increase.

3.2 Modulation of sphingolipid level changes in AD cells

Taking into account that Presenilin is one of the causative genes for familial AD, showing altered Aβ processing and impaired synaptic function, which are characteristics of AD, and considering potential postmortem effects on tissue sphingolipid levels, a similar measurement was conducted on cell lysates from the following three groups (each comprising n = 8): iPS cells derived from AD patients (AD), iPS cells with inserted mutations in Presenilin 1 (PS), and control neurons.

Figures 2A, B depicts the total levels of all measured sphingolipid species among the three groups. The dhSph, total Cer1P, and total SM levels were higher in both the PS and AD cells compared with the control cell. The Sph level was enhanced in both the PS and AD cell lines, although statistical significance observed in AD cells exclusively. The levels of S1P were not different among the groups (Figure 2A). Significant differences in the levels of sphingolipid species among the three groups are shown in Supplementary Figures 2A, B.

The comparable modulations observed in Sph and Cer1P levels between the two experiments (Figures 1, 2) offer significant

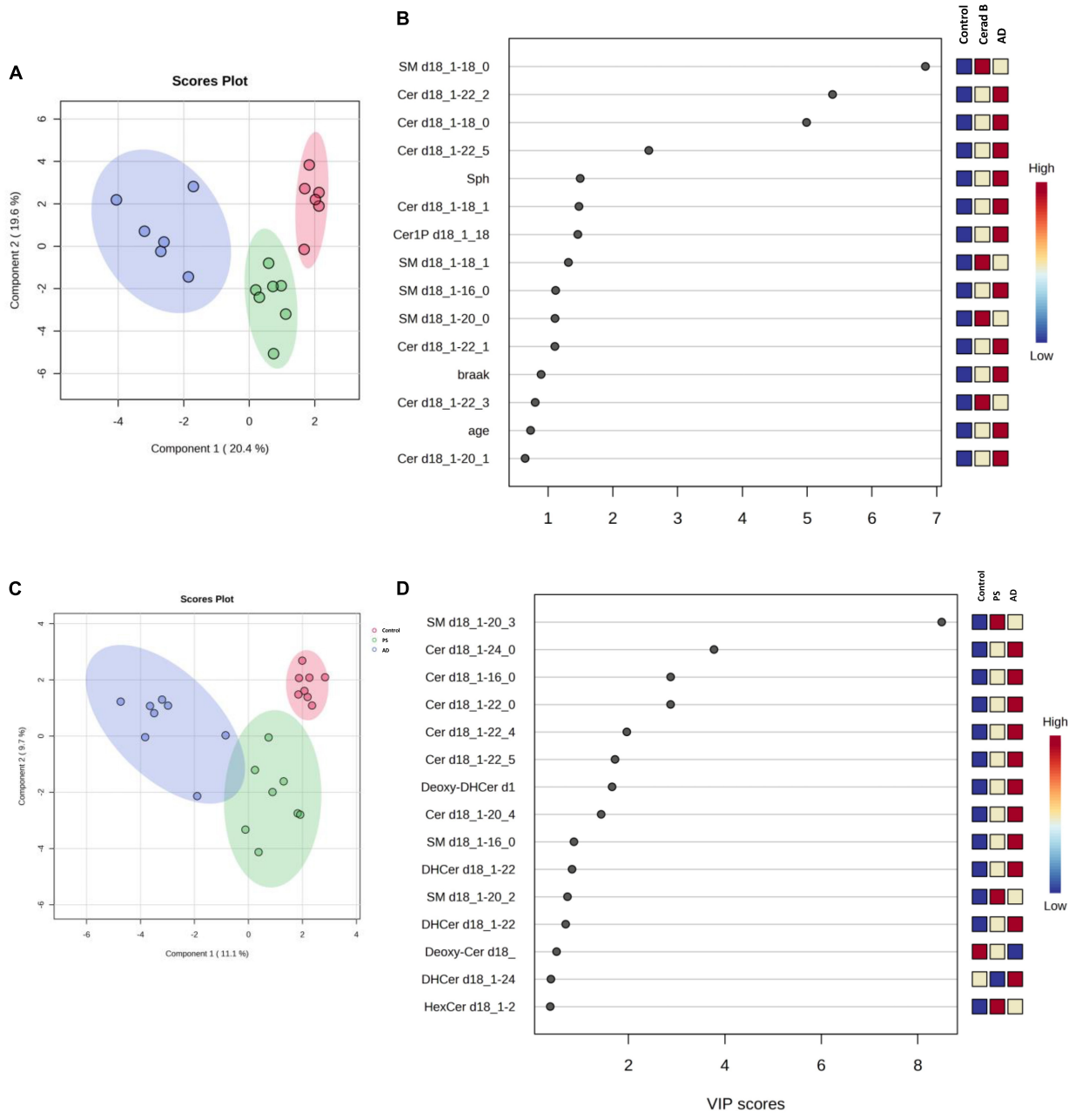

FIGURE 3
Multivariate analysis of sphingolipids in AD brain tissues and cells. Score plots illustrate distinct profiles of sphingolipids among AD brains **(A)**, Cerad-B brains, and control brains, as well as among AD, PS, and control cells **(C)**. Variable Importance in the Projection (VIP) plots, derived from the PLS-DA models, ranked sphingolipids according to their discriminative ability in brain tissue **(B)** and cell samples **(D)**.

insights into the possible contributions of these sphingolipids to the pathogenesis of AD.

3.3 Multivariate data analysis of the sphingolipids

The differential profiles of sphingolipids between AD, Cerad-B, and control brains were investigated using a PLS-DA. The score plots, as depicted in **Figure 3A**, revealed a significant difference among these three groups. A similar notable difference was observed in the cell samples, as illustrated in **Figure 3C**.

VIP plots for component 1, which separated the three groups well, were generated from the PLS-DA models, and sphingolipids were ranked based on their discriminatory power for distinguishing the three groups in both brain tissue (**Figure 3B**) and cell (**Figure 3D**) samples. Notably, several Cer species exhibited high VIP scores in both the brain tissue and cell samples. Subsequently, the SM species were ranked as significant, although they showed elevated levels in the Cerad-B group (SM 18:0) in the tissue samples and in the PS group (SM 20:3) in the cell samples. Interestingly, the sphingolipid profiles obtained in postmortem brain tissues exhibited a stronger discriminatory power than did the Braak score, which is a measure used to describe the progression of AD, as shown in **Figure 3B**.

In **Table 2**, we present an overview of the correlations between patient characteristics and the measured sphingolipids. Notably, Spearman's Rho analysis revealed strong correlations between Sph and the Braak score or SP (**Figures 4A, B**). Additionally, we observed significant correlations between Aβ levels as follows: Aβ40 with total dhCer or total Deoxy-dhCer (**Figures 4C, D**), and Aβ42 with total Deoxy-Cer or total Cer (**Figures 4E, F**). The levels of measured Aβ40, Aβ42, and their ratio are provided in **Supplementary Table 2**. Aβ40 exhibited strong correlations with parameters such as SP and Braak scores, compared to Aβ42. Furthermore, it showed strong correlations with dhCer or total Deoxy-dhCer, in addition to correlations similar to Aβ42.

3.4 Prediction model identified ceramides and sphingomyelins as key sphingolipids in AD

Lastly, we constructed machine learning models for discriminating the groups using IBM SPSS Modeler, which recommended three different models to identify the most relevant sphingolipids associated with AD. The diagnostic performance of these selected machine learning models, together with the most important sphingolipids, exhibited an excellent predictive performance, with nearly 100% accuracy (**Supplementary Table 3**). As illustrated in **Figure 5A**, the predictor importance analysis identified specific sphingolipids, including Cer 22:2, SM 20:0, Cer 18:0, and SM 18:0, as having a higher value than the Braak score in postmortem brain tissue samples. Furthermore, we conducted additional correlation analyses, incorporating patients' age, gender, Aβ levels, Braak stage, and SP grade as covariates of interest with groups (**Figure 5B**). Notably, SP showed a robust positive association with AD among clinical and pathological data. In relation to sphingolipids, Sph, several species as well as total Cer1P, and certain species of Cer and SM, demonstrated positive associations with AD.

For cell samples, the most important predictors included Cer 24:0, Cer 18:0, Cer 16:0, Cer 22:0, and SM 16:0 (**Figure 5C**). The assessment of predictor importance was conducted using the Support Vector Machine model, which is an effective and flexible classification method. Across all recommended models, Deoxy-Cer and its species emerged as the most crucial sphingolipids, ranking just below Aβ in importance (**Supplementary Table 4**) in both brain tissue samples and cell samples.

This application of machine learning models highlighted sphingolipids, including Deoxy-Cer, Sph, several species of Cer, and SM, as key contributors to AD, and suggested their potential for application in AD diagnosis and research.

4 Discussion

In the current study, we used our newly established method (Uranbileg et al., 2024) in combination with multivariate analysis and machine learning models to identify Sph, Cer1P, Cer, and SM as possible candidates for involvement in the pathogenesis of AD. Considering Presenilin as one of the causative genes for familial AD, and acknowledging the potential influence of postmortem effects and background pathological conditions of the patients, such as type 2 diabetes mellitus, on sphingolipid modulation, we also investigated the modulation of sphingolipids using iPS cells as one of models of AD. We obtained similar results in the latter analysis, which helped us conclude on the significant modulation of sphingolipids, especially Sph and Cer1P, in the pathogenesis of AD (summarized in **Figure 6A**-tissue, **Figure 6B**-cell).

Sphingolipids are among the well-studied bioactive lipid mediators, playing crucial roles in the physiology and pathology of human diseases (Kluk and Hla, 2002; Hla, 2003; Nakamura et al., 2021; Kurano et al., 2022a,b,d; Uranbileg et al., 2022). In the field of neurology, their structural role in cellular membranes, particularly in lipid rafts, is a crucial aspect of their interaction with the amyloid beta (Aβ) metabolism (Olsen and Faergeman, 2017), suggesting the potential to investigate their role in AD. Recently, we developed a method that enabled us to measure not only an extended range of sphingolipids, but also numerous species of these sphingolipids simultaneously (Uranbileg et al., 2024; **Supplementary Table 1**). Sphingolipids can interconvert among themselves, thus forming a dynamic and intricate metabolic network; this method allows us to observe comprehensive dynamic changes in sphingolipid levels.

The total ceramide levels were elevated in the brain tissue of patients with AD and its species were identified as either those with the highest VIP score or one of the top 10 important sphingolipid predictors (**Figures 1**, **3B**) in the AD group. This finding was supported by evidence that indicates the presence of increased Cer (Satoi et al., 2005; Akyol et al., 2021) in the cerebrospinal fluid (CSF) or tissues of patients with AD. Furthermore, the exogenous addition of Cer and an increase in endogenous Cer levels lead to higher levels of Aβ and the progression of AD (Puglielli et al., 2003). The total Cer level was also positively correlated with SP grade and Aβ40, 42 (**Figure 4** and **Table 2**), which suggests its importance in AD. Over the past two decades, Cer has been

TABLE 2 Correlation between sphingolipids and patient characteristics.

		Sph	SP	Braak	Age	Abeta 40	Abeta 42	dhSph	Total HexCer	Total LacCer	Total dhCer	Total Deoxy-Cer	Total Cer	Total Deoxy-dhCer	Gender	dhS1P	S1P
Total Cer1P	Rho coefficient	0.4884	0.3950	0.4719	0.2783	0.5228	0.2754	0.0885	0.1043	0.3957	0.3331	0.3194	0.4755	0.4382	−0.0072	−0.3394	−0.1978
	p-Value	0.0339	0.0941	0.0414	0.2486	0.0216	0.2538	0.7186	0.6708	0.0935	0.1635	0.1825	0.0396	0.0606	0.9767	0.1551	0.4170
Sph	Rho coefficient		0.5966	0.6302	−0.0954	0.5947	0.3749	0.4545	0.2847	0.0884	0.0932	0.3172	0.3588	0.2941	−0.0669	0.1520	−0.1758
	p-Value		0.0070	0.0038	0.6976	0.0072	0.1138	0.0506	0.2374	0.7189	0.7044	0.1857	0.1314	0.2217	0.7855	0.5345	0.4717
SP	Rho coefficient			0.8670	0.2838	0.7998	0.5723	0.2023	0.0100	0.2343	0.4544	0.3573	0.4572	0.4669	0.0666	−0.1351	−0.0928
	p-Value			0.0000	0.2391	0.0000	0.0104	0.4063	0.9677	0.3344	0.0506	0.1332	0.0491	0.0439	0.7865	0.5814	0.7056
Braak	Rho coefficient				0.3076	0.6892	0.4425	0.0873	0.0254	0.0865	0.3934	0.2113	0.3728	0.3582	0.0753	−0.3142	−0.2523
	p-Value				0.2002	0.0010	0.0578	0.7223	0.9177	0.7247	0.0956	0.3852	0.1160	0.1321	0.7595	0.1903	0.2973
Age	Rho coefficient					0.3958	0.5096	0.1492	0.1968	−0.0184	0.3959	0.3576	0.3769	0.3541	0.1888	−0.3858	−0.0960
	p-Value					0.0935	0.0258	0.5420	0.4195	0.9404	0.0934	0.1328	0.1117	0.1369	0.4390	0.1028	0.6957
Abeta 40	Rho coefficient						0.6719	0.4509	0.3246	0.4123	0.6930	0.6649	0.7544	0.7211	−0.0193	−0.4692	−0.2737
	p-Value						0.0016	0.0527	0.1752	0.0794	0.0010	0.0019	0.0002	0.0005	0.9377	0.0427	0.2357
Abeta 42	Rho coefficient							0.4776	0.3443	0.2767	0.3679	0.5887	0.5274	0.4204	0.1915	−0.2497	−0.1001
	p-Value							0.0386	0.1489	0.2515	0.1212	0.0080	0.0203	0.0731	0.4323	0.3026	0.6834
dhSph	Rho coefficient								0.5045	0.2407	0.2016	0.5729	0.4937	0.4150	−0.2045	0.0862	−0.1697
	p-Value								0.0276	0.3210	0.4079	0.0103	0.0317	0.0772	0.4011	0.7258	0.4875
Total HexCer	Rho coefficient									0.3281	0.3214	0.6073	0.5525	0.4186	−0.2941	−0.0067	−0.0421
	p-Value									0.1702	0.1797	0.0058	0.0142	0.0745	0.2217	0.9783	0.8642
Total LacCer	Rho coefficient										0.6086	0.6233	0.6738	0.6618	−0.3416	−0.2241	0.0793
	p-Value										0.0057	0.0044	0.0016	0.0020	0.1524	0.3564	0.7469

(Continued)

10.3389/fnagi.2024.1368839

TABLE 2 (Continued)

		Sph	SP	Braak	Age	Abeta 40	Abeta 42	dhSph	Total HexCer	Total LacCer	Total dhCer	Total Deoxy-Cer	Total Cer	Total Deoxy-dhCer	Gender	dhS1P	S1P
Total dhCer	Rho coefficient											0.7615	0.8446	0.8468	−0.4141	−0.0751	−0.1302
	p-Value											0.0002	0.0000	0.0000	0.0780	0.7600	0.5953
Total Deoxy-Cer	Rho coefficient												0.9395	0.9029	−0.1635	0.0534	−0.1773
	p-Value												0.0000	0.0000	0.5037	0.8280	0.4678
Total Cer	Rho coefficient													0.9748	−0.2670	−0.0952	−0.1526
	p-Value													0.0000	0.2691	0.6982	0.5328
Total Deoxy-dhCer	Rho coefficient														−0.2171	−0.0811	−0.1516
	p-Value														0.3720	0.7415	0.5357
Gender	Rho coefficient															−0.1911	−0.0442
	p-Value															0.4332	0.8573
dhS1P	Rho coefficient																0.2447
	p-Value																0.3126

Cer1P, ceramide 1-phosphate; Sph, sphingosine; SP, senile plaque; Abeta, amyloid beta; dhSph, dihydrosphingosine; HexCer, hexosyl ceramide; LacCer, lactosyl-ceramide; dhCer, dihydroceramide; Deoxy-Cer, deoxy-ceramide; Cer, ceramide; Deoxy-dhCer, deoxy dihydroceramide; dhS1P, dihydrosphingosine 1-phosphate; S1P, sphingosine 1-phosphate. The background color dimension indicates the correlation rate, with a stronger correlation represented by the darkest color.

10.3389/fnagi.2024.1368839

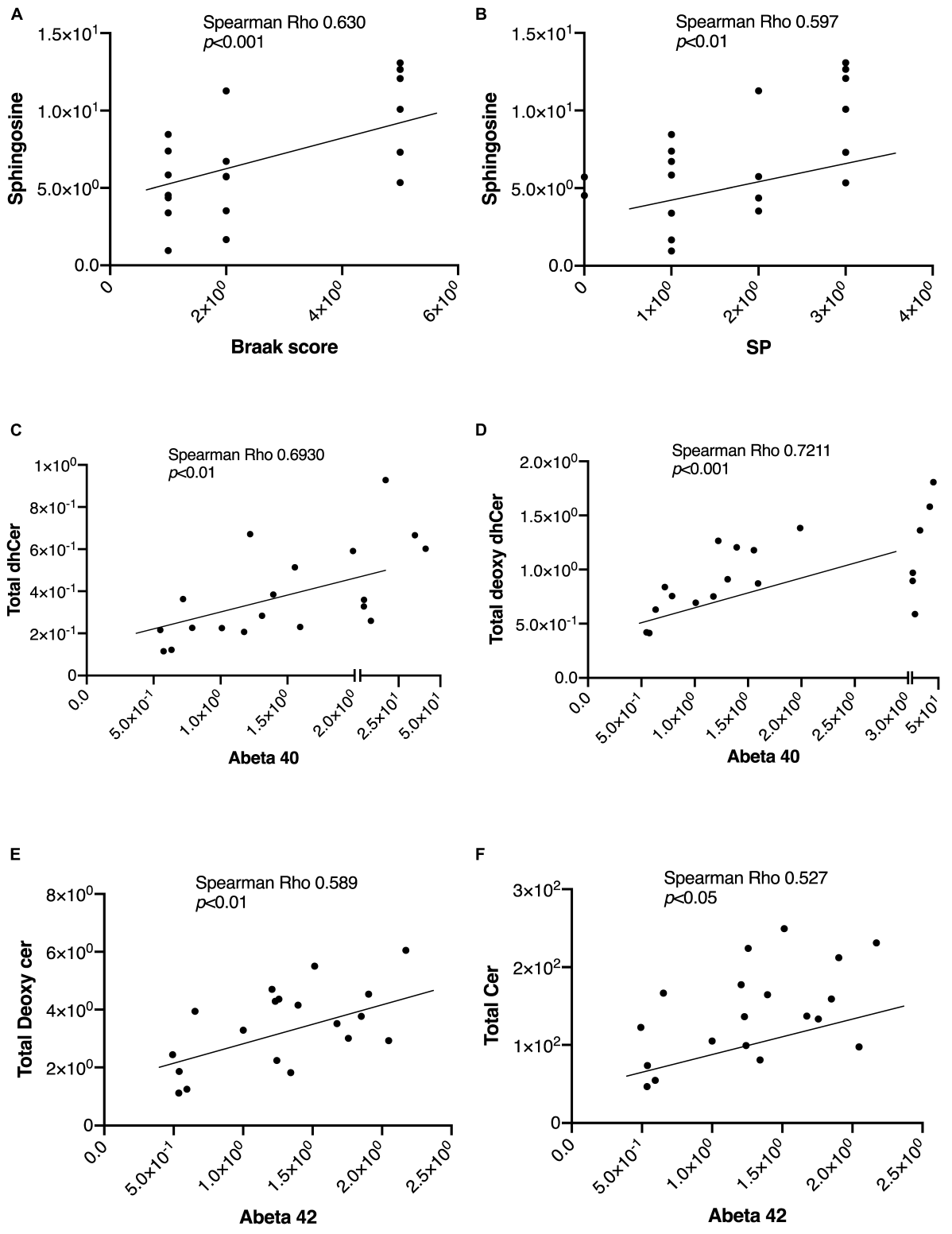

FIGURE 4
Representative correlations between sphingolipids and the AD-associated markers. The correlations between sphingolipids and AD-associated markers were assessed using Spearman rank correlation. **(A,B)** Sph correlation with the Braak score and SP. **(C,D)** Correlations of Aβ40 levels with total Deoxy-dhCer and total dhCer. **(E,F)** Correlations of Aβ42 levels with total Deoxy-Cer and total Cer.

intensively studied regarding its function in inflammation and apoptosis. Many stimuli, such as inflammatory mediators, UV radiation, and oxidative stress, activate cellular sphingomyelinase (SMase) to produce Cer (Kolesnick and Fuks, 2003; Ogretmen and Hannun, 2004). In turn, Aβ activates SMase to produce Cer from SM, and promotes the intracellular accumulation of Cer, which

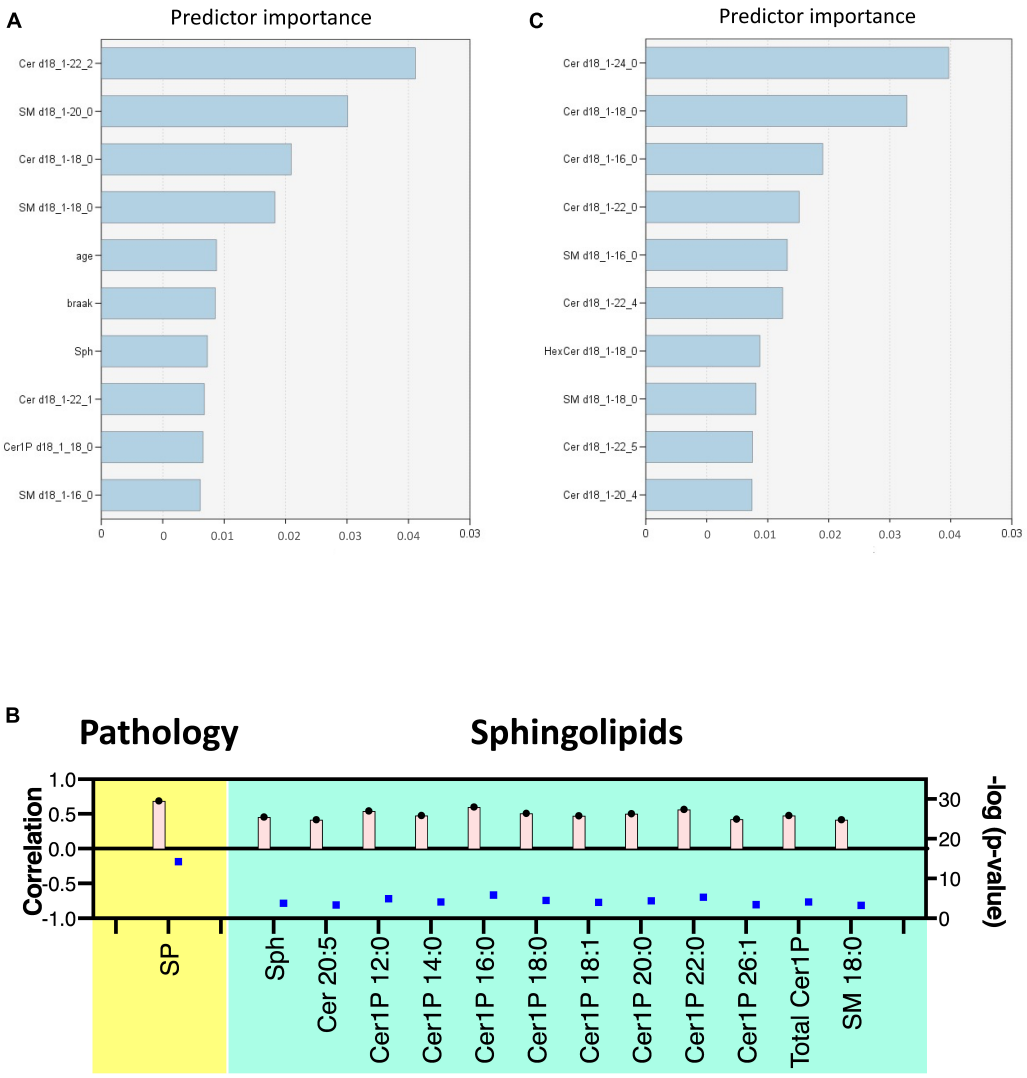

FIGURE 5
Discriminant analysis using the machine learning model. Illustration of predictor importance in brain tissue **(A)** and cell samples **(C)** using SPSS Modeler's Predictor Importance Chart in the SVM model. This chart delineates the relative importance of each predictor, highlighting the top 10 sphingolipids ranked by their importance. **(B)** Association of measured sphingolipids with study groups was examined using the Kendall rank correlation. The analysis considered age, gender, and clinical (pathological) data [Aβ levels, Braak stage, and senile plaque (SP) grade] as covariates of interest.

induces oligodendrocyte death (Lee et al., 2004). Cer accumulation is observable at the very early stages of AD, and even in subjects with mild cognitive impairment, which is a disorder that has been associated with risk of AD (Han et al., 2002), and it levels increase before the clinical recognition stages and are elevated in various brain regions (Katsel et al., 2007). Considering the proapoptotic properties of Cer, it seems reasonable that its levels are higher in AD brains and AD cells, thus promoting the pathogenesis of AD.

In both brain tissues and cell lines from individuals with AD, the Sph levels were significantly increased compared with the remaining two groups (**Figures 1**, **2**). Sph was identified as an important factor in AD based on multivariate analysis and machine learning models, suggesting its potential role in AD (**Figures 3B**, **5A**). In addition, Sph was positively and strongly correlated with the SP grade and Braak score of patients with AD (**Figures 4A, B** and **Table 2**), which suggests its importance in the diagnosis and underlying mechanism of AD. In similar studies that employed lipid profiling (Cutler et al., 2004; Akyol et al., 2021), sphingolipids such as Cer, SM, and S1P were predominantly mentioned, with less emphasis placed on Sph. Sph and S1P are interconverted by the actions of sphingosine kinase (SK) and S1P phosphatase (S1PP) (Cuvillier, 2002; Maceyka et al., 2002). Aβ disturbs S1P signaling by promoting the accumulation of the proapoptotic Cer, and downregulates SKs, leading to decreased S1P levels (Gassowska et al., 2014). In our case, the S1P levels remained unchanged in tissue or cell samples, which is consistent with previous studies (He et al., 2010; Ceccom et al., 2014; Couttas et al., 2014; Kurano et al., 2022c), which reported either unchanged or decreased S1P levels and SK activity, suggesting a difficulty to employ S1P receptor agonists. These discrepancies might be attributed to postmortem effects, because S1P can be intracellularly degraded (Uranbileg et al., 2022) or because of the lower accuracy

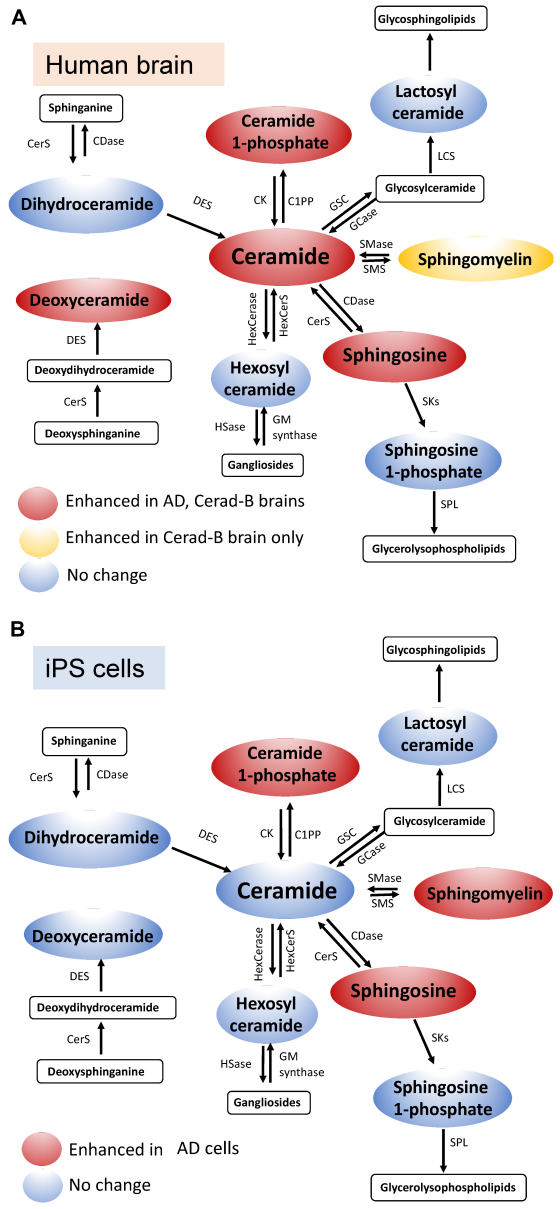

FIGURE 6
Schematic illustration of sphingolipid modulation in AD. Graphs depicting the modulation of sphingolipids in brain tissue **(A)** and cell samples **(B)** relevant to AD.

of the comprehensive measuring method in the measurement of S1P versus the specific measuring methods of S1P. In fact, in our previous paper using a specific measuring method of S1P, the brain S1P levels were lower in the AD brains (Kurano et al., 2022c).

Regarding Cer1P, our research was the first to suggest that the total levels of Cer1P were higher in the brains of patient with AD and in PS or AD cells. Similar to Sph, Cer1P exhibited a positive correlation with the Braak score of patients with AD, indicating its potential involvement in AD pathology. Cer1P, which is derived from Cer via the action of ceramide kinase (CerK), is recognized for its role in stimulating cell growth and migration, as well as its association with inflammation and apoptosis (Presa et al., 2020). Notably, previous studies have indicated that Cer1P stimulates cell proliferation and adipogenesis, rather than inflammation and apoptosis. Nevertheless, although its precise involvement in AD remains unclear, our study demonstrated its elevation in AD cases. As a downstream product of Cer, further research is crucial to provide conclusive evidence of the role of Cer1P in AD in the near future.

Compared with significantly altered sphingolipids, the newly measured sphingolipid, Deoxy-Cer, exhibited an increase in brain tissues from individuals with Cerad-B scores and patients with AD compared with the control group (**Figure 1B**). This suggests its importance, as indicated by machine learning models that ranked it just after Aβ, whether considering its total levels or those of its species (**Supplementary Table 4**) or its strong correlations with Aβ40 and Aβ42 (**Table 2**) both in brain tissues and cell lines. The involvement of Deoxy-Cer in hereditary sensory autonomic neuropathy and type 2 diabetes mellitus (DM) has been acknowledged, emphasizing its significance in specific medical conditions (Bertea et al., 2010; Othman et al., 2012). Because of the association between Deoxy-Cer and the neuropathy caused by type 2 DM, its potential involvement in AD might be explained by the close relationship between metabolic syndrome or insulin resistance and the progression of AD (Farooqui et al., 2012). Although the physiological properties of Deoxy-Cer remain largely unknown at present, our study suggested the necessity for investigating its roles in CNS diseases.

Although the patterns of the levels of other sphingolipids, such as dhSph and especially SM, were somewhat distinct, some of those species were selected as important factors for AD in the multivariate analysis and machine learning models. Elevated SM levels have been reported in the CSF of patients with prodromal AD (Kosicek et al., 2012), supporting our findings of notably high SM levels in the Cerad-B group among patients or PS cells. Compared with our previous study, in which we conducted lipid profiling for all bioactive lipids and their related factors (Kurano et al., 2022c), we noticed some discrepancies in the levels of Sph, SM, and dhSph, which could be attributed to the improved methodology.

Because of the progressive nature of AD and the gradual worsening of dementia-related symptoms and pathology over time, the significance of early-stage dementia biomarkers becomes increasingly important. Therefore, here, we employed three groups for each type of sample (control, mild stage; Cerad-B for brain tissue; and AD for advanced stage) to explore the differences in sphingolipid metabolism at various stages of AD. With the exception of Cer1P in cell lines, which exhibited a significant gradual increase, no significant variations in lipid profiles were observed across the different AD stages, excluding a gradually increasing tendency in the levels of the Sph and total Cer.

The ApoE gene, particularly its ε4 allele, is widely recognized as the most influential genetic risk factor for AD, affecting over half of all cases (Raulin et al., 2022). ApoE proteins, encoded by various alleles, primarily facilitate lipid transport while also participating in diverse biological functions. Therefore, we conducted additional analysis based on ApoE gene alleles. Although we observed a tendency toward increased levels of certain sphingolipids in Group 1 (ApoE 3/4), the findings were not statistically significant (**Supplementary Figure 3**). It is worth noting that there were no patients with the ApoE 4/4 allele in our study group. Although the present study did not show the impact of ApoE allele

on sphingolipid metabolism, further research is warranted to thoroughly elucidate the modulation of sphingolipids in response to the ApoE ε4 allele.

The primary limitations of this study included the sample size of each group and the absence of clinical information beyond what is presented here, as well as the possible postmortem effects on metabolites. Although the postmortem interval (PMI) tended to be shorter in the control subjects, no significant difference was observed among the three groups. The conditions of the brain samples seemed not to be significantly different, considering that the RNA integrity number was not so different among the samples (**Table 1**). The RIN values are higher than 7, indicating the good quality of the brain tissues. It should also be noted that, considering the variability of the tissue sample origin, in this instance, we utilized postmortem cerebral cortex tissues. Therefore, further sphingolipid profiling should encompass analyses of the white matter and hippocampal sections from brain tissues, as well as glial cells in cell line studies, considering that we utilized neurons in the present analysis. Another limitation concerns the iPS cells used in this study, as it is important to note that the iPS cell lines utilized here are characterized by Presenilin mutations. While these mutated lines exhibit certain AD-associated traits (Kim and Tanzi, 1997; Chen et al., 2002; Bagaria et al., 2022), including altered Aβ processing (Chen et al., 2002) and compromised synaptic function (Naruse et al., 1998; Yoo et al., 2000), they do not fully replicate all AD hallmark features. Therefore, future investigations should involve additional AD-specific iPS lines, such as those with MAPT mutations (Strang et al., 2019), and explore the use of more physiologically relevant models like organoids or animal models. These approaches aim to better encompass the diverse spectrum of lipid profiles observed within the brain, providing the possibility to elucidate the main mechanisms of the modulated sphingolipids, whether they are related to certain mutations or to outcomes observed in AD brain tissue.

5 Conclusion

In summary, a novel method combined with an advanced data analysis identified key sphingolipids for diagnosing AD, including Sph, Cer, Cer1P, and SMs. These sphingolipids were highlighted as a critical AD marker, as they exhibited strong correlations with AD-related factors and ranked above the Braak score as an important factor. We believe that this study could serve as a foundational pillar for further AD research, particularly for understanding the involvement of bioactive lipids.

Data availability statement

The original contributions presented in this study are included in this article/**Supplementary material**, further inquiries can be directed to the corresponding author.

Ethics statement

The studies involving humans were approved by the Tokyo Metropolitan Geriatric Medical Center and The University of Tokyo Medical Research Center Ethics Committee (2018088NI). The studies were conducted in accordance with the local legislation and institutional requirements. The participants provided their written informed consent to participate in this study.

Author contributions

BU: Data curation, Formal analysis, Investigation, Visualization, Writing – original draft. HI: Formal analysis, Validation, Writing – review and editing. ES: Methodology, Writing – review and editing. MKb: Methodology, Writing – review and editing. YS: Project administration, Resources, Writing – review and editing. MKr: Conceptualization, Formal analysis, Funding acquisition, Project administration, Validation, Writing – review and editing.

Funding

The author(s) declare financial support was received for the research, authorship, and/or publication of this article. This work was supported by JSPS KAKENHI Grant Number 20H03573 (MKr), the Takeda Science Foundation (MKr), AMED the Research Project on Elucidation of Chronic Pain (22ek0610028h0001 and JP21wm0425019) (YS), and JSPS KAKENHI JP22H04923 (CoBiA) (YS).

Conflict of interest

The present study was a collaborative research project undertaken by The University of Tokyo and Nihon Waters Masayuki Kubota. ES is now an employee of Japan Waters Corporation. ES and MKb were employed by Nihon Waters K.K.

The remaining authors declare that the research was conducted in the absence of any commercial or financial relationships that could be construed as a potential conflict of interest.

Publisher's note

Supplementary material

The Supplementary Material for this article can be found online at: https://www.frontiersin.org/articles/10.3389/fnagi.2024.1368839/full#supplementary-material

References

Akyol, S., Ugur, Z., Yilmaz, A., Ustun, I., Gorti, S. K. K., Oh, K., et al. (2021). Lipid profiling of Alzheimer's disease brain highlights enrichment in glycerol(phospho)lipid, and sphingolipid metabolism. *Cells* 10:2591. doi: 10.3390/cells10102591

Ashleigh, T., Swerdlow, R. H., and Beal, M. F. (2023). The role of mitochondrial dysfunction in Alzheimer's disease pathogenesis. *Alzheimers Dement.* 19, 333–342. doi: 10.1002/alz.12683

Bagaria, J., Bagyinszky, E., and AN, S. S. A. (2022). Genetics, functions, and clinical impact of presenilin-1 (PSEN1) Gene. *Int. J. Mol. Sci.* 23.

Barbash, S., Garfinkel, B. P., Maoz, R., Simchovitz, A., Nadorp, B., Guffanti, A., et al. (2017). Alzheimer's brains show inter-related changes in RNA and lipid metabolism. *Neurobiol. Dis.* 106, 1–13. doi: 10.1016/j.nbd.2017.06.008

Bertea, M., Rutti, M. F., Othman, A., Marti-Jaun, J., Hersberger, M., Von Eckardstein, A., et al. (2010). Deoxysphingoid bases as plasma markers in diabetes mellitus. *Lipids Health Dis.* 9:84. doi: 10.1186/1476-511X-9-84

Brunkhorst, R., Vutukuri, R., and Pfeilschifter, W. (2014). Fingolimod for the treatment of neurological diseases-state of play and future perspectives. *Front. Cell Neurosci.* 8:283. doi: 10.3389/fncel.2014.00283

Ceccom, J., Loukh, N., Lauwers-Cances, V., Touriol, C., Nicaise, Y., Gentil, C., et al. (2014). Reduced sphingosine kinase-1 and enhanced sphingosine 1-phosphate lyase expression demonstrate deregulated sphingosine 1-phosphate signaling in Alzheimer's disease. *Acta Neuropathol. Commun.* 2:12. doi: 10.1186/2051-5960-2-12

Chen, F., Gu, Y., Hasegawa, H., Ruan, X., Arawaka, S., Fraser, P., et al. (2002). Presenilin 1 mutations activate gamma 42-secretase but reciprocally inhibit epsilon-secretase cleavage of amyloid precursor protein (APP) and S3-cleavage of notch. *J. Biol. Chem.* 277, 36521–36526.

Chen, Z., and Zhong, C. (2014). Oxidative stress in Alzheimer's disease. *Neurosci. Bull.* 30, 271–281. doi: 10.1007/s12264-013-1423-y

Corder, E. H., Saunders, A. M., Strittmatter, W. J., Schmechel, D. E., Gaskell, P. C., Small, G. W., et al. (1993). Gene dose of apolipoprotein E type 4 allele and the risk of Alzheimer's disease in late onset families. *Science* 261, 921–923. doi: 10.1126/science.8346443

Couttas, T. A., Kain, N., Daniels, B., Lim, X. Y., Shepherd, C., Kril, J., et al. (2014). Loss of the neuroprotective factor sphingosine 1-phosphate early in Alzheimer's disease pathogenesis. *Acta Neuropathol. Commun.* 2:9. doi: 10.1186/2051-5960-2-9

Cutler, R. G., Kelly, J., Storie, K., Pedersen, W. A., Tammara, A., Hatanpaa, K., et al. (2004). Involvement of oxidative stress-induced abnormalities in ceramide and cholesterol metabolism in brain aging and Alzheimer's disease. *Proc. Natl. Acad. Sci. U.S.A.* 101, 2070–2075. doi: 10.1073/pnas.0305799101

Cuvillier, O. (2002). Sphingosine in apoptosis signaling. *Biochim. Biophys. Acta* 1585, 153–162. doi: 10.1016/S1388-1981(02)00336-0

Farooqui, A. A., Farooqui, T., Panza, F., and Frisardi, V. (2012). Metabolic syndrome as a risk factor for neurological disorders. *Cell. Mol. Life Sci.* 69, 741–762. doi: 10.1007/s00018-011-0840-1

Gassowska, M., Cieslik, M., Wilkaniec, A., and Strosznajder, J. B. (2014). Sphingosine kinases/sphingosine-1-phosphate and death signalling in App-transfected cells. *Neurochem. Res.* 39, 645–652. doi: 10.1007/s11064-014-1240-3

Ghasemi, R., Dargahi, L., and Ahmadiani, A. (2016). Integrated sphingosine-1 phosphate signaling in the central nervous system: From physiological equilibrium to pathological damage. *Pharmacol. Res.* 104, 156–164. doi: 10.1016/j.phrs.2015.11.006

Han, X., Holtzman, D. M., Mckeel, D. W. Jr., Kelley, J., and Morris, J. C. (2002). Substantial sulfatide deficiency and ceramide elevation in very early Alzheimer's disease: Potential role in disease pathogenesis. *J. Neurochem.* 82, 809–818. doi: 10.1046/j.1471-4159.2002.00997.x

Hansen, D. V., Hanson, J. E., and Sheng, M. (2018). Microglia in Alzheimer's disease. *J. Cell Biol.* 217, 459–472. doi: 10.1083/jcb.201709069

He, X., Huang, Y., Li, B., Gong, C. X., and Schuchman, E. H. (2010). Deregulation of sphingolipid metabolism in Alzheimer's disease. *Neurobiol. Aging* 31, 398–408. doi: 10.1016/j.neurobiolaging.2008.05.010

Hla, T. (2003). Signaling and biological actions of sphingosine 1-phosphate. *Pharmacol. Res.* 47, 401–407. doi: 10.1016/S1043-6618(03)00046-X

Karran, E., Mercken, M., and De Strooper, B. (2011). The amyloid cascade hypothesis for Alzheimer's disease: An appraisal for the development of therapeutics. *Nat. Rev. Drug Discov.* 10, 698–712. doi: 10.1038/nrd3505

Katsel, P., Li, C., and Haroutunian, V. (2007). Gene expression alterations in the sphingolipid metabolism pathways during progression of dementia and Alzheimer's disease: A shift toward ceramide accumulation at the earliest recognizable stages of Alzheimer's disease? *Neurochem. Res.* 32, 845–856. doi: 10.1007/s11064-007-9297-x

Kim, T. W., and Tanzi, R. E. (1997). Presenilins and Alzheimer's disease. *Curr. Opin.* Neurobiol. 7, 683–688.

Kluk, M. J., and Hla, T. (2002). Signaling of sphingosine-1-phosphate via the S1P/Edg-family of G-protein-coupled receptors. *Biochim. Biophys. Acta* 1582, 72–80. doi: 10.1016/S1388-1981(02)00139-7

Kolesnick, R., and Fuks, Z. (2003). Radiation and ceramide-induced apoptosis. *Oncogene* 22, 5897–5906. doi: 10.1038/sj.onc.1206702

Kosicek, M., Zetterberg, H., Andreasen, N., Peter-Katalinic, J., and Hecimovic, S. (2012). Elevated cerebrospinal fluid sphingomyelin levels in prodromal Alzheimer's disease. *Neurosci. Lett.* 516, 302–305. doi: 10.1016/j.neulet.2012.04.019

Kurano, M., Jubishi, D., Okamoto, K., Hashimoto, H., Sakai, E., Morita, Y., et al. (2022a). Dynamic modulations of urinary sphingolipid and glycerophospholipid levels in COVID-19 and correlations with Covid-19-associated kidney injuries. *J. Biomed. Sci.* 29:94. doi: 10.1186/s12929-022-00880-5

Kurano, M., Okamoto, K., Jubishi, D., Hashimoto, H., Sakai, E., Saigusa, D., et al. (2022b). Dynamic modulations of sphingolipids and glycerophospholipids in Covid-19. *Clin. Transl. Med.* 12:e1069. doi: 10.1002/ctm2.1069

Kurano, M., Saito, Y., Uranbileg, B., Saigusa, D., Kano, K., Aoki, J., et al. (2022c). Modulations of bioactive lipids and their receptors in postmortem Alzheimer's disease brains. *Front. Aging Neurosci.* 14:1066578. doi: 10.3389/fnagi.2022.1066578

Kurano, M., Tsukamoto, K., Sakai, E., and Yatomi, Y. (2022d). Differences in the distribution of ceramides and sphingosine among lipoprotein and lipoprotein-depleted fractions in patients with type 2 diabetes mellitus. *J. Atheroscler. Thromb.* 29, 1727–1758. doi: 10.5551/jat.63249

Lee, J. T., Xu, J., Lee, J. M., Ku, G., Han, X., Yang, D. I., et al. (2004). Amyloid-beta peptide induces oligodendrocyte death by activating the neutral sphingomyelinase-ceramide pathway. *J. Cell Biol.* 164, 123–131. doi: 10.1083/jcb.200307017

Livingston, G., Sommerlad, A., Orgeta, V., Costafreda, S. G., Huntley, J., Ames, D., et al. (2017). Dementia prevention, intervention, and care. *Lancet* 390, 2673–2734. doi: 10.1016/S0140-6736(17)31363-6

Maceyka, M., Payne, S. G., Milstien, S., and Spiegel, S. (2002). Sphingosine kinase, sphingosine-1-phosphate, and apoptosis. *Biochim. Biophys. Acta* 1585, 193–201. doi: 10.1016/S1388-1981(02)00341-4

Murayama, S., and Saito, Y. (2004). Neuropathological diagnostic criteria for Alzheimer's disease. *Neuropathology* 24, 254–260. doi: 10.1111/j.1440-1789.2004.00571.x

Nakamura, N., Honjo, M., Yamagishi, R., Kurano, M., Yatomi, Y., Watanabe, S., et al. (2021). Neuroprotective role of sphingolipid rheostat in excitotoxic retinal ganglion cell death. *Exp. Eye Res.* 208:108623. doi: 10.1016/j.exer.2021.108623

Naruse, S., Thinakaran, G., Luo, J. J., Kusiak, J. W., Tomita, T., Iwatsubo, T., et al. (1998). Effects of PS1 deficiency on membrane protein trafficking in neurons. *Neuron* 21, 1213–1221.

Ogretmen, B., and Hannun, Y. A. (2004). Biologically active sphingolipids in cancer pathogenesis and treatment. *Nat. Rev. Cancer* 4, 604–616. doi: 10.1038/nrc1411

Olsen, A. S. B., and Faergeman, N. J. (2017). Sphingolipids: Membrane microdomains in brain development, function and neurological diseases. *Open Biol.* 7:170069. doi: 10.1098/rsob.170069

Othman, A., Rutti, M. F., Ernst, D., Saely, C. H., Rein, P., Drexel, H., et al. (2012). Plasma deoxysphingolipids: A novel class of biomarkers for the metabolic syndrome? *Diabetologia* 55, 421–431. doi: 10.1007/s00125-011-2384-1

Presa, N., Gomez-Larrauri, A., Dominguez-Herrera, A., Trueba, M., and Gomez-Munoz, A. (2020). Novel signaling aspects of ceramide 1-phosphate. *Biochim. Biophys. Acta Mol. Cell Biol. Lipids* 1865:158630. doi: 10.1016/j.bbalip.2020.158630

Puglielli, L., Ellis, B. C., Saunders, A. J., and Kovacs, D. M. (2003). Ceramide stabilizes beta-site amyloid precursor protein-cleaving enzyme 1 and promotes amyloid beta-peptide biogenesis. *J. Biol. Chem.* 278, 19777–19783. doi: 10.1074/jbc.M300466200

Raulin, A. C., Doss, S. V., Trottier, Z. A., Ikezu, T. C., Bu, G., and Liu, C. C. (2022). ApoE in Alzheimer's disease: Pathophysiology and therapeutic strategies. *Mol. Neurodegener.* 17:72. doi: 10.1186/s13024-022-00574-4

Satoi, H., Tomimoto, H., Ohtani, R., Kitano, T., Kondo, T., Watanabe, M., et al. (2005). Astroglial expression of ceramide in Alzheimer's disease brains: A role during neuronal apoptosis. *Neuroscience* 130, 657–666. doi: 10.1016/j.neuroscience.2004.08.056

Serviddio, G., Romano, A. D., Cassano, T., Bellanti, F., Altomare, E., and Vendemiale, G. (2011). Principles and therapeutic relevance for targeting mitochondria in aging and neurodegenerative diseases. *Curr. Pharm. Des.* 17, 2036–2055. doi: 10.2174/138161211796904740

Singh, D. (2022). Astrocytic and microglial cells as the modulators of neuroinflammation in Alzheimer's disease. *J. Neuroinflamm.* 19:206. doi: 10.1186/s12974-022-02565-0

Strang, K. H., Golde, T. E., and Giasson, B. I. (2019). Mapt mutations, tauopathy, and mechanisms of neurodegeneration. *Lab. Invest.* 99, 912–928. doi: 10.1038/s41374-019-0197-x

Uranbileg, B., Kurano, M., Kano, K., Sakai, E., Arita, J., Hasegawa, K., et al. (2022). Sphingosine 1-phosphate lyase facilitates cancer progression through converting sphingolipids to glycerophospholipids. *Clin. Transl. Med.* 12:e1056. doi: 10.1002/ctm2.1056

Uranbileg, B., Sakai, E., Kubota, M., Isago, H., Sumitani, M., Yatomi, Y., et al. (2024). Development of an advanced liquid chromatography-tandem mass spectrometry measurement system for simultaneous sphingolipid analysis. *Sci. Rep.* 14:5699. doi: 10.1038/s41598-024-56321-w

Vance, J. E., and Hayashi, H. (2010). Formation and function of apolipoprotein E-containing lipoproteins in the nervous system. *Biochim. Biophys. Acta* 1801, 806–818. doi: 10.1016/j.bbalip.2010.02.007

Winblad, B., Amouyel, P., Andrieu, S., Ballard, C., Brayne, C., Brodaty, H., et al. (2016). Defeating Alzheimer's disease and other dementias: A priority for European science and society. *Lancet Neurol.* 15, 455–532. doi: 10.1016/S1474-4422(16)00062-4

Yoo, A. S., Cheng, I., Chung, S., Grenfell, T. Z., Lee, H., Pack-Chung, E., et al. (2000). Presenilin-mediated modulation of capacitative calcium entry. *Neuron* 27, 561–572.

Yuyama, K., Mitsutake, S., and Igarashi, Y. (2014). Pathological roles of ceramide and its metabolites in metabolic syndrome and Alzheimer's disease. *Biochim. Biophys. Acta* 1841, 793–798. doi: 10.1016/j.bbalip.2013.08.002

frontiers | Frontiers in Aging Neuroscience

TYPE Original Research
PUBLISHED 15 May 2024
DOI 10.3389/fnagi.2024.1375091

OPEN ACCESS

EDITED BY
Teresa Wu,
Arizona State University, United States

REVIEWED BY
Mario Hernandes Alejandro,
National Polytechnic Institute (IPN), Mexico
Takahiro Ezaki,
The University of Tokyo, Japan

*CORRESPONDENCE
Zhiying Long
✉ friskying@163.com

RECEIVED 23 January 2024
ACCEPTED 30 April 2024
PUBLISHED 15 May 2024

CITATION
Xing L, Guo Z and Long Z (2024) Energy landscape analysis of brain network dynamics in Alzheimer's disease.
Front. Aging Neurosci. 16:1375091.
doi: 10.3389/fnagi.2024.1375091

Energy landscape analysis of brain network dynamics in Alzheimer's disease

Le Xing[1], Zhitao Guo[2] and Zhiying Long[2]*

[1]The State Key Laboratory of Cognitive Neuroscience and Learning & IDG/McGovern Institute for Brain Research, Beijing Normal University, Beijing, China, [2]School of Artificial Intelligence, Beijing Normal University, Beijing, China

Background: Alzheimer's disease (AD) is a common neurodegenerative dementia, characterized by abnormal dynamic functional connectivity (DFC). Traditional DFC analysis, assuming linear brain dynamics, may neglect the complexity of the brain's nonlinear interactions. Energy landscape analysis offers a holistic, nonlinear perspective to investigate brain network attractor dynamics, which was applied to resting-state fMRI data for AD in this study.

Methods: This study utilized resting-state fMRI data from 60 individuals, comparing 30 Alzheimer's patients with 30 controls, from the Alzheimer's Disease Neuroimaging Initiative. Energy landscape analysis was applied to the data to characterize the aberrant brain network dynamics of AD patients.

Results: The AD group stayed in the co-activation state for less time than the healthy control (HC) group, and a positive correlation was identified between the transition frequency of the co-activation state and behavior performance. Furthermore, the AD group showed a higher occurrence frequency and transition frequency of the cognitive control state and sensory integration state than the HC group. The transition between the two states was positively correlated with behavior performance.

Conclusion: The results suggest that the co-activation state could be important to cognitive processing and that the AD group possibly raised cognitive ability by increasing the occurrence and transition between the impaired cognitive control and sensory integration states.

KEYWORDS

resting-state fMRI, energy landscape analysis, Alzheimer's disease, brain dynamics, brain state

1 Introduction

Alzheimer's disease (AD) is a neurodegenerative disease characterized by a progressive decline in memory and other cognitive abilities. At present, there is no curative treatment for AD, but medication can aid in controlling the symptoms and slowing the advancement of cognitive impairment. The functional magnetic resonance imaging (fMRI) technique has been widely applied to investigate the neural mechanism of Alzheimer's disease (AD) and identify brain abnormalities specific to clinical behavior (Greicius et al., 2004; Buckner et al., 2009; Jagust, 2018).

Resting-state fMRI is a noninvasive imaging technique that indirectly measures synchronized blood oxygen level-dependent (BOLD) fluctuations in the brain, providing insights into the functional connectivity patterns of the brain (Biswal et al., 1995; Jagust, 2018). Among various resting brain networks, the default mode network (DMN) has been considered the core network reflecting AD pathological features. For AD patients, there was a significant decrease in the functional connectivity of the DMN (Greicius et al., 2004). In addition to the DMN, other brain networks, such as the executive control network (ECN) and salience network (SN), also showed changes induced by AD (Hahn et al., 2013; Badhwar et al., 2017). The alterations in functional connectivity may reflect cognitive dysfunction and compensatory responses to neurodegeneration damage in AD.

It should be noted that static functional connectivity analysis cannot capture the dynamic nature of the brain and fully reveal intricate temporal characteristics. Many previous studies have demonstrated that functional connectivity fluctuates dynamically with time (Chang and Glover, 2010). Dynamic functional connectivity (DFC) analysis has been used to distinguish functional states that vary between healthy controls and AD patients (Badhwar et al., 2017; Preti et al., 2017). Some studies have examined the dynamics of functional connectivity across diverse subnetworks, revealing aberrant dwell times specifically within memory-associated networks in AD brains (Jones et al., 2012; Filippi et al., 2019). Other studies demonstrated a gradual decline in whole-brain FC strengths that correlated with the increasing severity of cognitive impairment throughout the course of AD (Demirtaş et al., 2017; Pathak et al., 2022). The DFC analysis method used in previous studies assumes linearity of the brain dynamic system, while the dynamics of the brain are usually nonlinear (Hutchison et al., 2013; Preti et al., 2017). Thus, the dysfunction of the brain dynamic network in a complex and nonlinear brain system of AD remains to be elucidated.

Recently, energy landscape analysis based on statistical physics has been extensively applied in the analysis of brain dynamics during rest (Watanabe et al., 2014a; Ezaki et al., 2017, 2018; Kang et al., 2021; Klepl et al., 2022) and bi-stable visual perception tasks (Watanabe et al., 2014b). In contrast with the previous DFC method, energy landscape analysis has several advantages in exploring brain dynamics. First, energy landscape analysis can provide insights into the stability and robustness of brain dynamics because it reveals information about the attractor dynamics of a system. Second, energy landscape analysis is particularly useful in nonlinear systems and can provide a deeper understanding of brain dynamics. Third, energy landscape analysis provides a visual representation of the system, which can help to clarify and simplify complex brain systems.

Energy landscape analysis has been utilized to analyze abnormalities in brain dynamic dysfunction, including autism spectrum disorder (Watanabe and Rees, 2017), poststroke aphasia (Fan et al., 2022) and AD (Klepl et al., 2022; Li et al., 2023). For the AD patient, it was found that the dynamics of AD patients' EEG were shown to be more constrained - with more local minima, less variation in basin size, and smaller basins (Klepl et al., 2022). Due to poor spatial resolution of EEG, the EEG study cannot reveal the dynamic changes of brain networks in AD patients. Li et al. (2023) applied the energy landscape analysis to the resting fMRI data of AD and investigate the dynamic changes of the DMN, the SN, and the ECN. The study revealed that the dynamics of patients with AD tend to be unstable, with an unusually high flexibility in switching between states (Li et al., 2023). However, Li's study analyzes the DMN, SN and ECN separately by using the energy landscape method and ignored the interaction between the three networks. It has been demonstrated that several resting-state networks existed and interacted with each other in the resting fMRI data (Filippi et al., 2019; Puttaert et al., 2020; Cruzat et al., 2023). Therefore, it is essential to investigate the dynamic changes of the interactions between the resting networks by using the energy landscape analysis method to provide a more comprehensive understanding of the pathogenic mechanisms of Alzheimer's disease.

This study aimed at revealing the abnormal dynamics of AD patient by treating all the resting-state networks as a whole activity pattern and examining the dynamic changes of the interactions between the resting networks collectively. In this study, we applied independent component analysis (ICA) to extract 9 resting fMRI networks and utilized the pairwise maximum entropy model to construct the energy landscape by using time series driving the 9 resting networks from 30 Alzheimer's patients and 30 normal individuals. The maximum entropy model (MEM), as part of our energy landscape analysis, is used to estimate state energy distributions. We chose MEM due to its established effectiveness in deriving reliable and unbiased statistical inferences from limited datasets, with minimal prior assumptions (Jaynes, 1957; Schneidman et al., 2006). In the energy landscape analysis, the probability distribution of the brain states follows the Boltzmann distribution (the more frequently the state occurs, the lower its energy is). Our analysis methodology is illustrated schematically in Figure 1. The brain's energy landscape comprises several valleys with local minima (referred to as "stable states" or "attractors"). The local minima have energy lower than their neighbours in the valley. The major brain activity patterns are defined as those that are frequently visited and situated in the lowest points of the energy landscape. We then assessed the ease of dynamic transitions by measuring the frequency of visits to these major activity patterns. The fMRI results revealed that AD symptoms could lead to an increased transition frequency between the cognitive control state and the sensory integration state as well as the occurrence frequency of the two states, which suggests that AD patients possibly used the compensatory mechanism to improve cognitive ability by increasing the transition frequency between the cognitive control and sensory integration states.

2 Materials and methods

2.1 Subjects

The dataset was from the Alzheimer's Disease Neuroimaging Initiative (ADNI) database.[1] The ADNI was established in 2003 as a public–private partnership led by Principal Investigator Michael W. Weiner, MD. The ADNI is a longitudinal database that aims to develop biomarkers for the early detection and tracking of AD progression. It collects clinical, imaging, genetic, and bio-specimen data related to AD and cognitive impairments. A total of 60 subjects, including 30 patients diagnosed with Alzheimer's disease and 30 controls, were used in this study. Ethical approval was granted by the local ethical committees of all involved sites.

According to the protocols, AD was diagnosed based on a combination of clinical and cognitive assessments, along with

1 http://adni.loni.usc.edu/

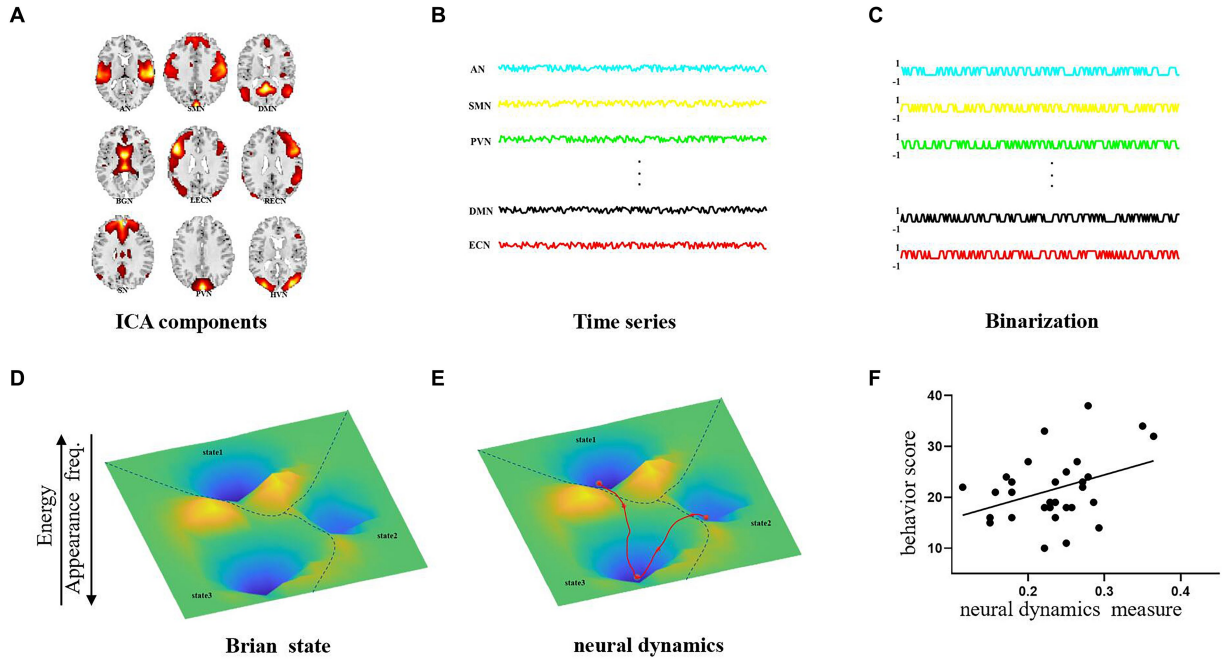

FIGURE 1
Pipeline of energy landscape analysis. **(A)** Functional brain network extraction by ICA. **(B)** The time series driving each network. **(C)** Binarized time series in **(B)**. **(D)** Identification of brain states in energy landscapes. **(E)** Extraction of the brain dynamic measures. **(F)** Relationship between brain dynamic measures and behavior scores.

TABLE 1 Demographic data.

	HC	AD	*t* value	*p*-value
Age	74.69 ± 6.3	72.88 ± 6.3	1.08	0.284
Male/female	14/16	14/16		
MMSE	28.7 ± 1.3	22.5 ± 2.5	12.01	<0.001
MoCA	25.3 ± 1.9	16.1 ± 5.1	9.20	<0.001
RAVLT	43.03 ± 10.3	21.53 ± 6.6	9.58	<0.001
FAQ	0.06 ± 0.25	15.4 ± 7.64	−11.23	<0.001

biomarker data. The criteria used for AD diagnosis were primarily based on the National Institute on Aging-Alzheimer's Association (NIA-AA) guidelines for the diagnosis of Alzheimer's disease. Participants underwent a comprehensive battery of neuropsychological tests evaluating various cognitive domains, including memory, language, attention, executive function, and visuospatial skills. Key tests included the Mini-Mental State Examination (MMSE), Rey Auditory Verbal Learning Test (RAVLT), Montreal Cognitive Assessment (MoCA), Functional Activities Questionnaire (FAQ) and others. The sample descriptions are presented in Table 1. Details on Alzheimer's Disease Stages can be found in Supplementary Table S1.

2.2 Image acquisition

All participants underwent MRI scanning using a 3 T Philips MRI scanner to acquire resting-state functional images. The scanning protocol employed an echo-planar imaging (EPI) sequence with the following acquisition parameters: 140 volumes, repetition time (TR) = 3,000 ms, echo time (TE) = 30 ms, flip angle = 80°, number of slices = 48, slice thickness = 3.3 mm, spatial resolution = 3 × 3 × 3 mm^3, and matrix size = 64 × 64. The original image files from this study are accessible to the broader scientific community for further analysis and research purposes. Additional information regarding the fMRI images can be found on the ADNI homepage.[2]

2.3 Data preprocessing

The present study utilized the Data Processing Assistant for Resting-State fMRI (DPARSF) software (Yan et al., 2016)[3] to perform preprocessing steps on the rs-fMRI data. Specifically, each subject's functional images underwent slice-timing correction, motion correction, and spatial normalization to the Montreal Neurological Institute (MNI) space. The resulting images were resliced into a voxel size of 3 × 3 × 3 mm and underwent spatial smoothing (Gaussian kernel with a full width at half maximum of 6 mm). Subsequently, linear detrending was applied, and the images were bandpass filtered (0.01–0.1 Hz).

2.4 Resting brain network extraction by ICA

Group independent component analysis (group-ICA) was performed to identify functional networks of the resting state. All preprocessed fMRI data were subjected to analysis using the GIFT

2 http://adni.loni.usc.edu/methods/mri-tool/mri-analysis/
3 http://rfmri.org/dpabi

toolbox.[4] The optimal number of independent components (ICs) was estimated by the MDL criteria and was set to 30. The Component Labelling toolbox in GIFT was used to label the resulting independent components. Each component was identified according to its correlation with the resting-state network mask (Shirer et al., 2012). We finally selected 9 components (i.e., brain networks) relevant to AD according to a previous study (Badhwar et al., 2017): auditory network (AN), basal ganglia network (BGN), left executive control network (LECN), right executive control network (RECN), DMN, sensorimotor network (SMN), primary visual network (PVN), higher visual network (HVN), and SN.

2.5 Fitting of the pairwise MEM

To conduct energy landscape analysis, we applied the pairwise maximum entropy model (MEM) to the time series of the 9 brain networks in the same manner as in previous studies (Watanabe et al., 2014a; Watanabe and Rees, 2017; Ezaki et al., 2018; Fan et al., 2022). The pairwise MEM and the model fitting procedures are briefly described as follows.

For each group, the time series corresponding to N brain networks of S subjects were concatenated, and the data matrix $Z_{N\times ST}=[Z^1_{N\times T}Z^2_{N\times T}\ldots Z^S_{N\times T}]$ was obtained. T is the number of time points in the time series. In this study, N was equal to 9, T was equal to 140 and S was equal to 30. The matrix $Z^i_{N\times T}$ represents the time series of N networks for the *i*th subject. The nine mean values $m=[m_1,m_2,\ldots,m_N]^T$ that represent the average network activity of the nine brain networks were calculated by averaging Z across the columns. The data matrix Z was binarized based on the threshold of the mean values m. If $Z(i,j)>m_i$, $Z(i,j)=1$; otherwise, $Z(i,j)=-1$. A value of 1 represented the active state, while −1 represented the inactive state. Each column of Z represented the activity pattern of N networks at each time point. The total number of possible activity patterns amounted to 2^N. $V_k=[\sigma_1,\sigma_2,\ldots,\sigma_N]$ represents the *k*th activity pattern of all 2^N possible activity patterns, where σ_i represents a binary activity of network *i*.

According to the principle of maximum entropy, the probability distribution $P(V_k)$ of the network activity pattern V_k should follow the Boltzmann distribution when the mean network activity and the mean pairwise interaction are constrained by the empirical data (see Eqs 1, 2).

$$P(V_k)=e^{-E(V_k)}/\sum_{i-1}^{2^N}e^{-E(V_k)} \quad (1)$$

$$E(V_k)=-\sum_{i-1}^{N}h_i\sigma_i(V_k)-\frac{1}{2}\sum_{i-1}^{N}\sum_{j-1,j\neq i}^{N}J_{ij}\sigma_i(V_k)\sigma_j(V_k) \quad (2)$$

Here, $E(V_k)$ is the energy of activity pattern V_k, $\sigma_i(V_k)$ represents the binarized activity of network *i* in activity pattern V_k, h_i represents the activation tendency (baseline activity) of network *i* and J_{ij}indicates a pairwise interaction between networks *i* and *j*. No interaction exists between networks i and j for $J_{ij}=0$ while interaction exists for $J_{ij}\neq 0$. It is important to note that the energy *E* does not represent biological energy. Rather, it serves as a statistical indicator of the likelihood of occurrence of each brain activity pattern. Brain activity patterns with lower energy values tend to occur more frequently.

The model-based mean network activity $\langle\sigma_i\rangle_m=\Sigma_{k=1}^{2^N}\sigma_i(V_k)P(V_k)$ and model-based mean pairwise interaction $\langle\sigma_i\sigma_j\rangle_m=\Sigma_{k=1}^{2^N}\sigma_i(V_\ell)\sigma_j(V_k)P(V_k)$ were calculated using $P(V_k)$ in Eq. 1. The empirical mean network activity $\langle\sigma_i\rangle=\frac{1}{T}\sum_{t=1}^{T}\sigma_i^t$ and empirical mean pairwise interaction $\langle\sigma_i\sigma_j\rangle=\frac{1}{T}\sum_{t=1}^{T}\sigma_i^t\sigma_j^t$ were estimated from the empirical data, where σ_i^t represented a binary activity of network i at time t. The parameters h_i and J_{ij} were iteratively adjusted by using a gradient ascent algorithm until $\langle\sigma_i\rangle_m$ and $\langle\sigma_i\sigma_j\rangle_m$ were approximately equal to the empirically obtained $\langle\sigma_i\rangle$ and $\langle\sigma_i\sigma_j\rangle$ for each group.

2.6 Accuracy of fit

According to previous studies (Watanabe et al., 2014a; Watanabe and Rees, 2017), the accuracy measure R was calculated by Eq. 3 to evaluate the goodness of fit of the pairwise MEM to the fMRI data of each group.

$$R=\frac{D_1-D_2}{D_1} \quad (3)$$

$$D_1=\sum_{k=1}^{2^N}p_{empirical}(V_k)\log_2\frac{p_{empirical}(V_k)}{p_{independent}(V_k)} \quad (4)$$

$$D_2=\sum_{k=1}^{2^N}p_{empirical}(V_k)\log_2\frac{p_{empirical}(V_k)}{p(V_k)} \quad (5)$$

where D_1 represents the Kullback–Leibler divergence between the MEM with $J_{ij}=0$ and the empirical data, as calculated using Eq. 4. D_2 represents the Kullback–Leibler divergence between the MEM with $J_{ij}\neq 0$ and the empirical data, was calculated using by Eq. 5. The accuracy measure R ranges from 0 to 1. MEM perfectly reproduces the empirical distribution of activity patterns for R = 1 and the pairwise interactions have no contribution to the MEM model fit for R = 0.

Additionally, the Pearson correlation coefficient between the appearance probability derived from the pairwise MEM and the empirical appearance probability was calculated. The greater the Pearson correlation coefficient was, the more accurately the maximum entropy model could explain the empirical data.

2.7 Construction of energy landscapes

To characterize the resting dynamics of the brain system, an energy landscape analysis was conducted for each group according to the procedure described in previous works (Watanabe et al., 2014a; Watanabe and Rees, 2017).

4 mialab.mrn.org/software/gift/

A network of activity patterns was constructed by setting each activity pattern as a network node. Two nodes were defined as adjacent if the two activity patterns were the same across all brain networks except one. Therefore, an activity pattern V_k was adjacent to N activity patterns. The network of activity patterns with their node energy E (V_k) was defined as the energy landscape. In the energy landscape, the local energy minima (attractors) were the nodes with energy values smaller than those of their N adjacent nodes.

A dysconnectivity graph (Becker and Karplus, 1997) was constructed according to the following six steps, as depicted in the flowchart in Figure 2. First, all the local energy minima were achieved by thoroughly searching the energy landscape. Second, the energy threshold E_{th}, was set to the highest energy value present among all 2^N nodes. Third, the nodes with energy values equal to or larger than E_{th} were removed. Fourth, a connectivity check was performed to ensure that each pair of local minima was connected via a path within the reduced network. Fifth, E_{th} was adjusted by the subsequent largest energy value. The third, fourth and fifth steps were repeated until each local minimum was isolated in a reduced network. Finally, a hierarchical tree was generated. The terminal leaves represented the local minima, and the internal nodes indicated the branching points of different local minima. The leaves' vertical positions reflected their energy values.

2.8 Estimation of the sizes of dominant brain states

The basin sizes of the detected local minima were used to measure the dominance of each local minimum. A starting node i was selected from the 2^N nodes. If there was any neighbouring node that had lower energy than node i, node i was moved to its neighbouring node with the lowest energy value. If no such neighbouring node existed, node i was a local minimum, and no movement occurred. This procedure was repeated until a local minimum was obtained. The starting node i was defined as an element of the basin of the local minimum that was reached by the starting node i. This process was applied to all 2^N nodes repeatedly. All the brain activity patterns that belonged to the basin constituted the basin of a local minimum. Consequently, the basin size was defined as the fraction of the number of brain activity patterns belonging to the basin.

In this study, six local minima were grouped into three brain states according to the hierarchical structures of these minima (local minima 1, 2 and 4 for State 1; local minima 3 and 5 for State 2 and local minimum 3 for State 3; Figure 1C). The size of each brain state was defined as the summation of the basin sizes of all the local minima that belonged to the brain state.

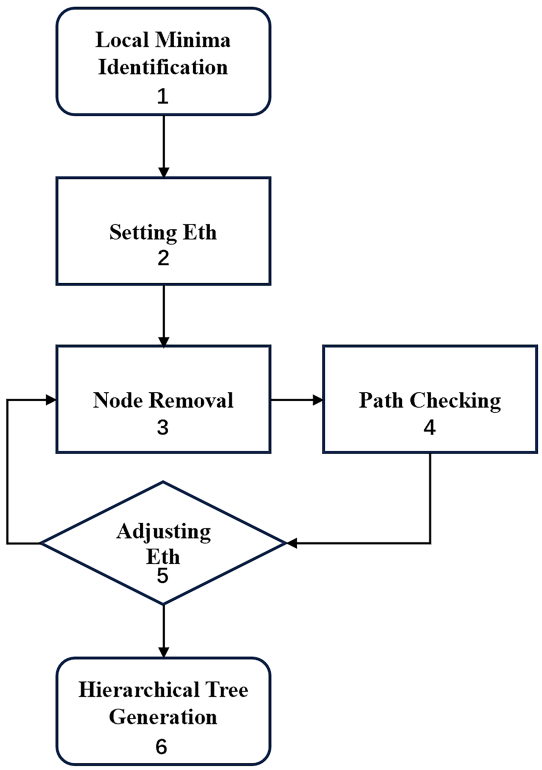

FIGURE 2
Work flow of dysconnectivity graph.

2.9 Dynamic measures of brain states

According to the definition of the three brain states, the activity pattern at each time point was classified as one of the three brain states for each participant. Seven dynamic measures, including the appearance frequency, mean duration, mean energy, transition frequency, direct transition frequency, indirect transition frequency and transition in/out frequency, were calculated from the empirical data of each subject. For each participant, the appearance frequency of a state was calculated as the ratio of the occurrence number of the state to the total number of all states observed. The mean dwell time of a state was measured as the average number of consecutive occurrences of the state. The mean energy was calculated by averaging the energy levels of states across all time points. The state transition frequency from state A to B was measured as the ratio of the transition number from state A to B to the total transition number between states. Specifically, the state transition was further classified into direct transition and indirect transition. Indirect transitions involved intermediate states between the initial and target states. The transition in/out frequency was defined as the transition frequency at which a particular state transitioned to or from other states. Two-sample t tests with a Bernoulli correction were applied to all dynamic measures to evaluate the differences between the HC and AD groups.

2.10 Numerical simulations

According to the energy landscape estimated for each group (HC/AD), the movement of the brain activity patterns was numerically simulated using a Markov chain Monte Carlo method with Metropolis-Hasting's algorithm (Metropolis et al., 1953; Hastings, 1970). In this method, any brain activity pattern $V_i$was only allowed to move to its neighbour pattern V_j that was selected from all N neighbours with a uniform probability of $1/N$. The probability of transition from V_i to V_j was $P_{ij} = \min\left[1, e^{E(V_i)-E(V_j)}\right]$. For each group, we repeated the random walk of 10^5 steps with a randomly selected initial pattern $V_k$so that the simulated data could fully describe the transition of the brain activity pattern. Using this numerical simulation, the mean duration, mean energy and transition probability

of the brain states were calculated to characterize the brain dynamics. The differences in brain dynamics between the AD and HC groups were assessed through the utilization of chi-square ($\chi 2$) tests and *post hoc* residual tests.

2.11 Associations between brain dynamics and behaviors

We further explored the relationships between brain dynamics and behavior performance. The analysis focused on the DFC measures that showed significant intergroup differences. The Pearson correlations between behavior performances and the brain dynamic measures were calculated for the two groups separately.

3 Results

3.1 Accuracy of model fitting

Figure 3 displays the fitting results of the pairwise MEM for the empirical data of the AD and HC groups. The results indicated that the MEM could accurately predict the empirical data for both the AD and HC groups (accuracy: $R_{AD}=0.822$, $R_{HC}=0.836$). Moreover, the appearance probability derived from the pairwise MEM was highly correlated with the empirical appearance probability for both groups ($r_{AD=}0.930$, $p<0.001$; $r_{HC=}0.945$, $p<0.001$).

3.2 Energy landscapes and basin size

The hierarchal structures of the two groups' energy landscapes are shown in Figures 4A,B. The energy landscapes of the AD and HC groups showed a similar hierarchal structure with the same six local minima (Figure 4C). The six local minima were grouped into three brain states (local minima 1, 2 and 4 for State 1; local minima 3 and 5 for State 2; local minimum 3 for State 3). Figure 4D shows the sizes of the three brain states of the two groups. The distributions of the brain states were significantly different between the two groups ($\chi^2=7.95$, $p<0.05$ in a χ^2-test). For State 3, the state size of the AD group was significantly smaller than that of the HC group ($p<0.05$ in a *post hoc* residual test).

3.3 Characterization of brain dynamics

Figure 5 shows a comparison of the appearance frequency, mean duration and mean energy of the three states in the empirical data. In contrast to the HC group, the AD group displayed a significantly higher appearance frequency in State 1 ($t=3.33$, $p<10^{-2}$, $P_{Bonferroni}<0.05$) and State 2 ($t=3.14$, $p<10^{-2}$, $P_{Bonferroni}<0.05$) and a significantly lower appearance frequency in State 3 ($t=7.46$, $p<10^{-3}$, $P_{Bonferroni}<0.05$). Moreover, the HC group exhibited a significantly longer mean duration of State 3 than the AD group ($t=3.88$, $p<10^{-3}$, $P_{Bonferroni}<0.05$). State 2 showed significantly higher mean energy ($t=2.77$, $p<10^{-2}$, $P_{Bonferroni}<0.05$), and State 3 showed significantly lower mean energy in the HC group versus the AD group ($t=10.06$, $p<10^{-3}$, $P_{Bonferroni}<0.05$).

The transition frequencies of the three states in the empirical data of the two groups are presented in Figure 6. The transition frequency, including direct transition and indirect transition, between States 1 and 2 was significantly reduced in the HC group compared to the AD group ($t=2.83$, $p<10^{-2}$, $P_{Bonferroni}<0.05$). Compared with the AD group, the HC group showed a significantly higher transition frequency between States 1 and 3 ($t=4.03$, $p<10^{-3}$, $P_{Bonferroni}<0.05$) and between States 2 and 3 ($t=4.85$, $p<10^{-3}$, $P_{Bonferroni}<0.05$). For the direct transition frequency, the HC group showed a significantly lower frequency between States 1 and 2 ($t=4.35$, $p<10^{-3}$, $P_{Bonferroni}<0.05$) and a significantly higher frequency between States 1 and 3 ($t=2.73$, $p<10^{-2}$, $P_{Bonferroni}<0.05$) and between States 2 and 3 ($t=4.55$, $p<10^{-2}$,

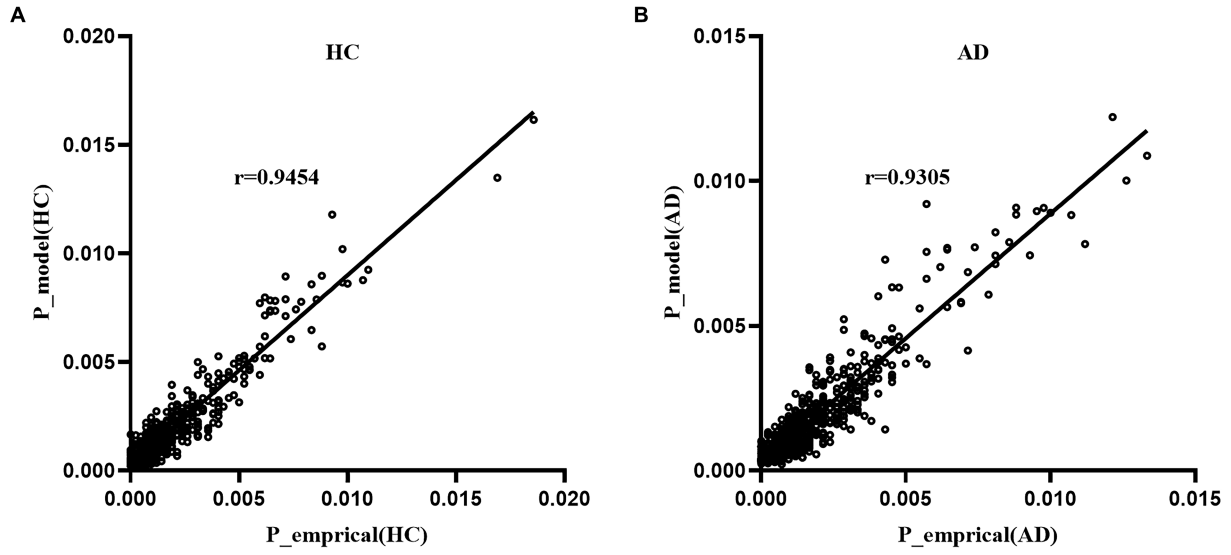

FIGURE 3
Fitting of the pairwise MEM for the AD group **(A)** and HC group **(B)**.

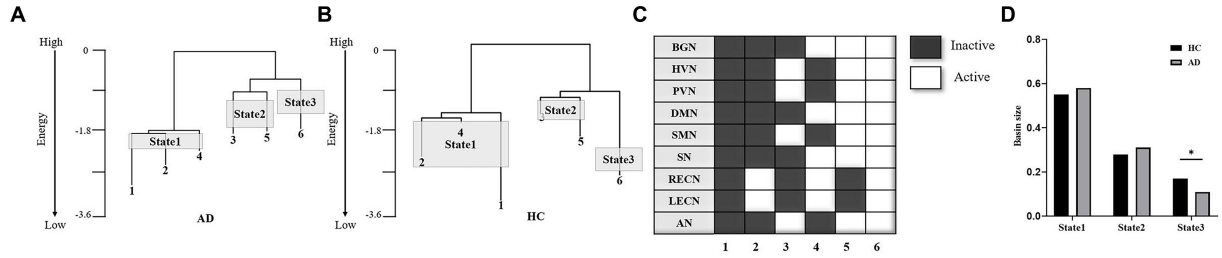

FIGURE 4
Comparison of energy landscape structures. **(A,B)** Hierarchal structure of the energy landscape for the AD **(A)** and HC **(B)** groups. **(C)** The six local minima of the landscapes of the two groups. **(D)** Basin sizes of the three brain states for the two groups. *$p < 0.05$.

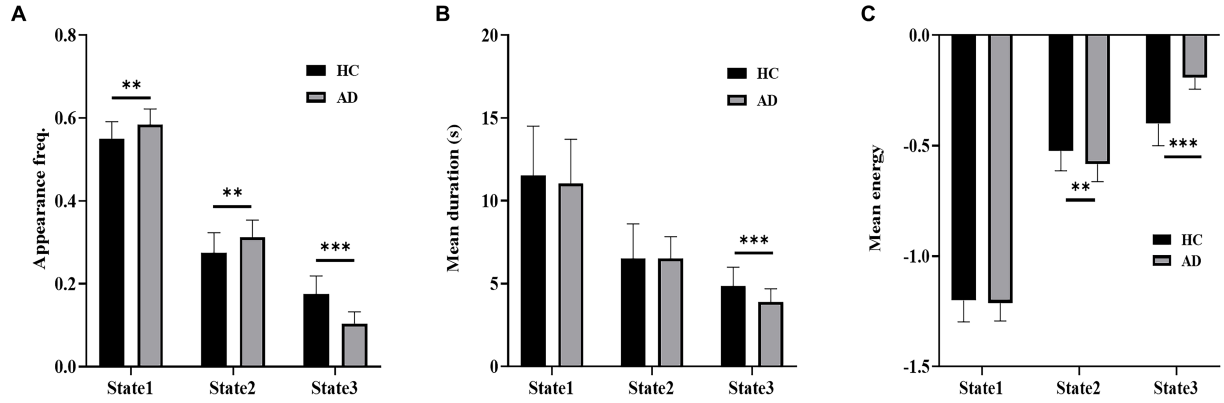

FIGURE 5
Dynamic properties of brain states. **(A)** Appearance frequency of the three brain states for the HC and AD groups. **(B)** Mean duration of the three brain states for the HC and AD groups. **(C)** Mean energy of the three brain states for the HC and AD groups. *$p < 0.05$, **$p < 10^{-2}$, ***$p < 10^{-3}$.

$P_{Bonferroni} < 0.05$) compared with the AD group. For the indirect transition frequency, the HC group showed a significantly higher frequency between States 1 and 2 ($t = 4.73$, $p < 10^{-3}$, $P_{Bonferroni} < 0.05$), between States 1 and 3 ($t = 3.53$, $p < 10^{-3}$, $P_{Bonferroni} < 0.05$), and between States 2 and 3 ($t = 2.11$, $p < 10^{-2}$, $P_{Bonferroni} < 0.05$) than the AD group. Moreover, the transition in/out frequency of State 3 was significantly higher for the HC group than for the AD group ($t = 4.91$, $p < 10^{-3}$, $P_{Bonferroni} < 0.05$).

3.4 Association between brain dynamics and cognitive ability

Figure 7 illustrates the relationships that had a significant correlation between neuropsychological assessments and the measurements of brain dynamics. For the RAVLT, the average score of AD patients was significantly lower than that of HCs ($t = 9.58$, $p < 10^{-3}$, $P_{Bonferroni} < 0.05$). For the AD group, the RAVLT score showed a significant positive correlation with the transition frequency between States 1 and 2 ($r = 0.55$, $p < 0.05$), the transition frequency between States 1 and 3 ($r = 0.45$, $p < 0.05$), the direct transition frequency between States 1 and 2 ($r = 0.43$, $p < 0.05$), the direct transition frequency between States 1 and 3 ($r = 0.45$, $p < 0.05$), and the transition in/out frequency of State 3 ($r = 0.45$, $p < 0.05$).

3.5 Numerical simulation results

The dynamic measurements of the three states in the simulated data of the AD and HC groups are displayed in Figure 8. The distributions of the mean duration of each state exhibited significant differences between the two groups ($\chi^2 = 106.9$, $p < 10^{-3}$ in a χ^2-test). In contrast to the AD group, the HC group showed a significantly longer mean duration for State 1 ($p < 10^{-3}$ in a *post hoc* residual test) and State 3 ($p < 10^{-4}$ in a *post hoc* residual test) and a significantly shorter duration for State 2 ($p < 0.05$ in a *post hoc* residual test). The distribution of the mean energy of states displayed a significant difference between the HC and AD groups ($\chi^2 = 1272.17$, $p < 10^{-3}$ in a χ^2-test). The mean energy of the AD group was significantly larger for State 1 ($p < 10^{-4}$ in a *post hoc* residual test) and State 2 ($p < 10^{-4}$ in a *post hoc* residual test; Figure 8B) and significantly lower for State 3 compared to that of the HC group ($p < 10^{-4}$ in a *post hoc* residual test).

Moreover, significant intergroup differences were observed in the distributions of state transition probabilities, including transition probability ($\chi^2 = 208.9$, $p < 10^{-3}$ in a χ^2-test), direct transition probability ($\chi^2 = 404.4$, $p < 10^{-3}$ in a χ^2-test), indirect transition probability ($\chi^2 = 61.7$, $p < 10^{-3}$ in a χ^2-test), and transition in/out probability ($\chi^2 = 116.3$, $p < 10^{-3}$ in a χ^2-test) in the simulated data. For both the transition frequency and direct transition frequency, the HC group exhibited a significantly higher frequency between States 1 and 3 ($p < 10^{-4}$ in a *post hoc* residual test) and between States 2 and 3

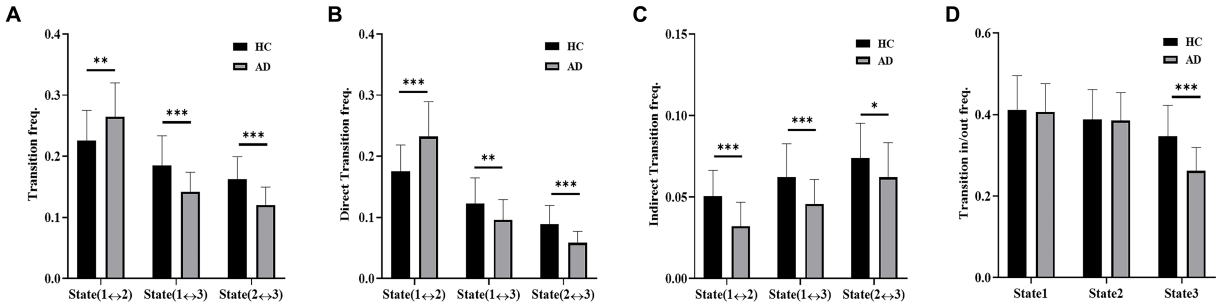

FIGURE 6
Dynamic transition of states. **(A)** Transition frequency of the AD and HC groups. **(B)** Direct transition frequency of the AD and HC groups. **(C)** Indirect transition frequency of the AD and HC groups. **(D)** Transition in/out frequency of the AD and HC groups.

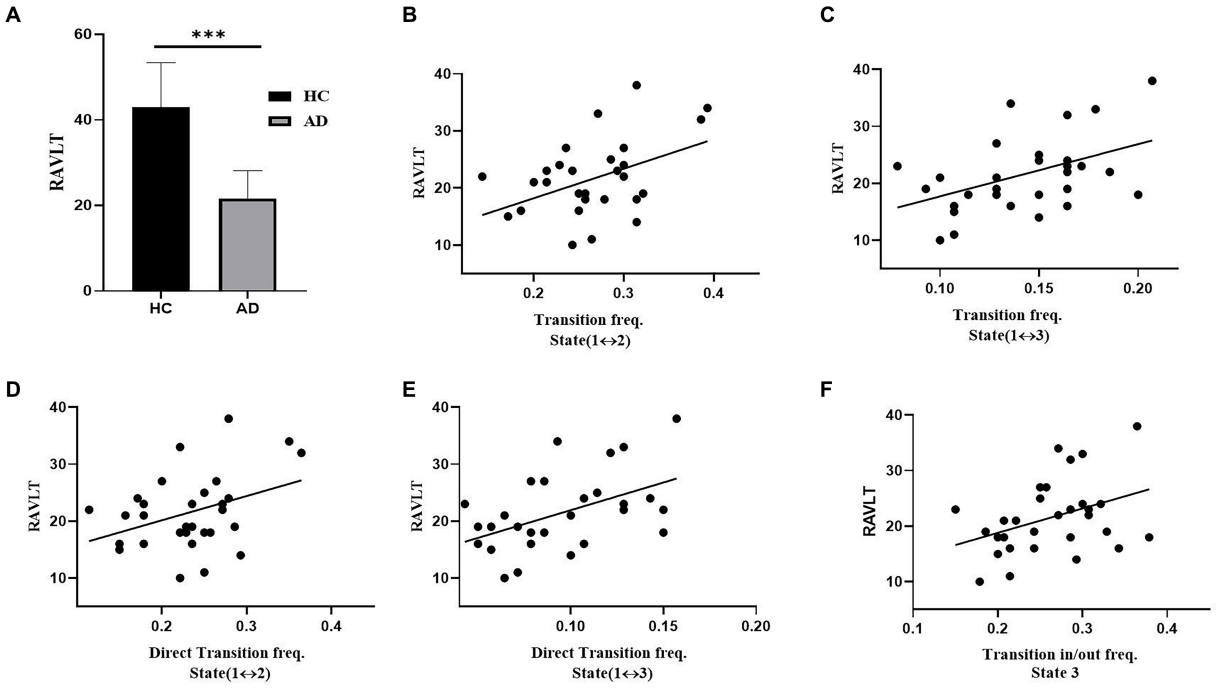

FIGURE 7
Association between transition rates and cognitive ability (RAVLT) in the AD group. **(A)** RAVLT scores of the HC and AD groups. **(B)** The relation between RAVLT and the transition frequency of States 1 and 2. **(C)** The relation between RAVLT and the transition frequency of States 1 and 3. **(D)** The relation between RAVLT and the direct transition frequency of States 1 and 2. **(E)** The relation between RAVLT and the direct transition frequency between States 1 and 3. **(F)** The relation between RAVLT and the transition in/out frequency of State 3.

($p < 10^{-4}$ in a *post hoc* residual test; Figure 8A) than the AD group, while the AD group had a significantly higher frequency between States 1 and 2 ($p < 10^{-4}$ in a *post hoc* residual test) than the HC group. For indirection transitions, the frequency of the HC group was significantly higher between States 1 and 2 ($p < 10^{-4}$ in a *post hoc* residual test) and between States 1 and 3 ($p < 0.05$ in a *post hoc* residual test) and significantly lower between States 2 and 3 ($p < 10^{-4}$ in a *post hoc* residual test) compared to that of the AD group. For the transition in/out frequency, the HC group displayed a significantly lower frequency for State 1 ($p < 10^{-4}$ in a *post hoc* residual test) and State 2 ($p < 10^{-3}$ in a *post hoc* residual test) and a significantly higher frequency for State 3 in contrast to the AD group ($p < 10^{-4}$ in a *post hoc* residual test).

4 Discussion

In the present study, we investigated the impact of AD on resting-state dynamics by using an energy landscape analysis. Both the AD and HC groups showed dynamic direct and indirect transitions among the cognitive control state (State 1), the sensory integration state (State 2) and the co-activation state (State 3). In contrast to the HC group, the AD group spent significantly less time in State 3, and State 1 and State 2 occurred significantly more frequently. Moreover, the AD group tended to switch directly between State 1 and State 2, while the HC group tended to transit in/out of State 3. In the AD group, the RAVLT score showed a positive correlation with the transition in/out frequency of State 3 and the transition frequency between State 1 and State 2. The

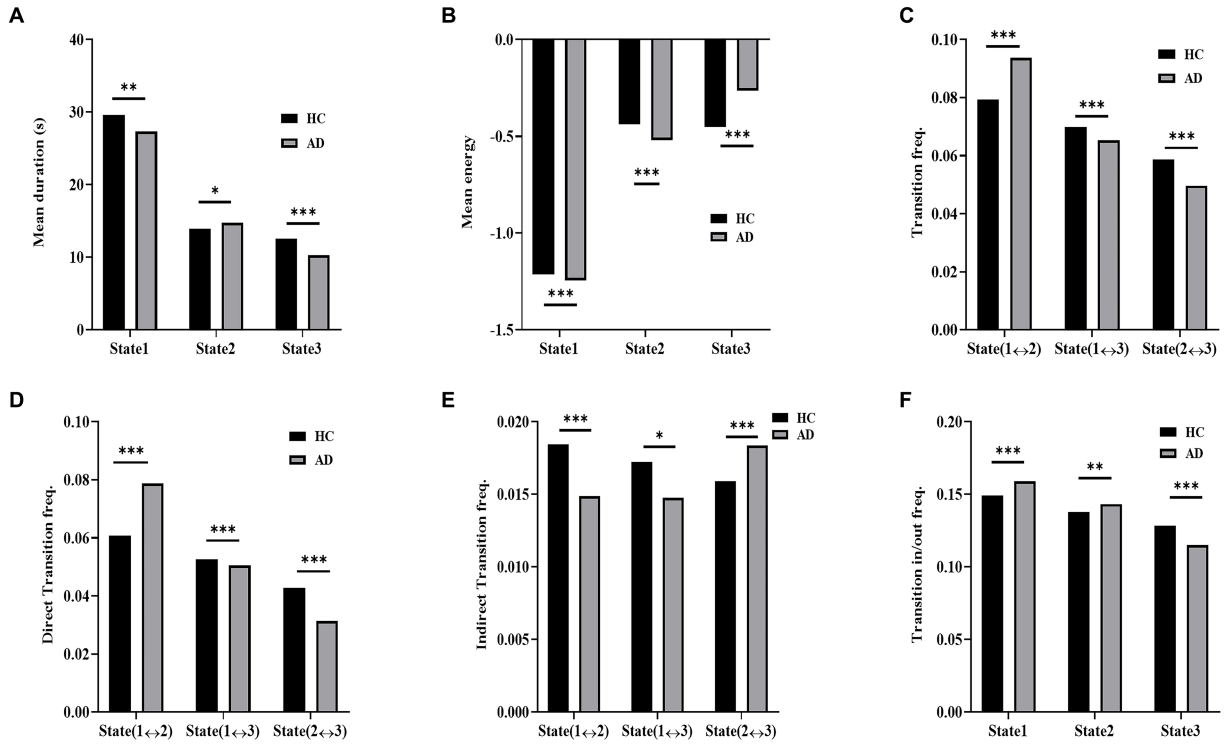

FIGURE 8
Dynamic measurement comparison of simulated data. **(A)** Mean duration of HC and AD. **(B)** Mean energy of HC and AD. **(C)** Transition frequency of AD and HC. **(D)** Direct transition frequency of AD and HC. **(E)** Indirect transition frequency of AD and HC. **(F)** Transition in/out frequency of AD and HC.

results suggest that State 3 could play an important role in cognitive processing and that AD patients possibly use the compensatory mechanism to improve cognitive ability by increasing the transition frequency between State 1 and State 2.

4.1 Brain state

A similar hierarchal structure with the same six local minima was detected in the energy landscapes of the AD and HC groups. The first local minima with all 9 networks inactivated may represent an inactive state. The second local minimum with RECN and LECN activation possibly represents the cognitive control state (Joo et al., 2016). The third local minimum with HVN, PVN, SMN and AN activation possibly represents a sensory processing state that includes visual, auditory and motor perception (Hutchison et al., 2013). The fourth local minimum exhibits activation of the BGN, DMN, SN, RECN and LECN. The SN has been implicated in modulating the switch between the internally directed cognition of the DMN and the externally directed cognition of the RECN and LECN (Sridharan et al., 2008). Thus, the fourth local minimum may represent a switching state between internal and external cognition. The fifth local minimum exhibits activation of the BGN, HVN, PVN, DMN, SMN, SN and AN. Because the SN plays a role in the detection and integration of salient sensory stimuli (Downar et al., 2000), it may work with the HVN, PVN and AN to detect and integrate visual and auditory stimuli. The BGN was reported to be involved in motor control (Turner and Desmurget, 2010) and may work with the SMN to perform motor processing. Thus, the fifth local minimum may be relevant to the integration of various sensory stimuli and motor function. The sixth local minimum with all networks activated represents an activated state.

In the hierarchal structure of the energy landscape, local minima 1, 2 and 4 were on the left branch, and local minima 3 and 5 were on the same branch for the AD and HC groups. Local minima 1, 2 and 4 were grouped into State 1, which may be related to cognitive control. Local minima 3 and 5 were grouped into State 2, which may be related to the integration of sensory stimuli and motor processing. Local minimum 6 was assigned to State 3, which may be related to the co-activation state.

4.2 Dynamic property of brain states

In contrast to the HC group, the AD group showed a significantly lower mean energy in State 2 and a higher mean energy in State 3. Because subjects prefer to stay in a stable state with low energy, State 3 occurred less frequently and State 2 more frequently in the AD group than in the HC group (Figure 5A). In State 3, all 9 networks cooperated and showed co-activation. Many previous studies observed altered functional connectivity between brain regions in AD patients (Filippi et al., 2019). Because the altered functional connectivity pattern may impact the co-activation of the 9 networks, State 3 occurred less frequently in the AD group than in the HC group. This result may suggest that the 9 networks of the HC group tended to interact more closely with each other than those of the AD group. State 2 was relevant to sensory and motor processing. Previous evidence indicated that sensory and motor changes may precede the

cognitive symptoms of AD by several years and may signify an increased risk of developing AD (Albers et al., 2015). Moreover, visual, auditory and motor dysfunctions are selectively observed in subgroups of AD patients (Albers et al., 2015; Weintraub et al., 2018). Therefore, the higher appearance frequency of State 2 in AD patients possibly provides a compensatory mechanism for sensory and motor impairment in AD (Brier et al., 2012). State 1 showed a significantly higher appearance frequency in the AD group than in the HC group. In State 1, the SN, CEN and DMN interacted closely to control cognitive processes. It has been reported that functional organizations of CEN and DMN were impaired in AD (Joo et al., 2016), and functional connectivity between the SN and the other two networks (CEN and DMN) was also altered in AD patients (He et al., 2014). Furthermore, a triple-network (SN, CEN and DMN) analysis of Alzheimer's disease, focusing on the energy landscape of these networks, revealed that the dynamics of patients with AD tend to be unstable, suggesting fluctuations in network interactions (Li et al., 2023). An increased occupancy rate in State 1 of AD patients possibly suggests a potential brain compensatory mechanism for enhancing cognitive control and coordination.

In terms of the transition between states, AD patients switched directly between State 1 and State 2 more frequently and between State 3 and the other two states less frequently than HCs. The results indicated that the AD group liked to stay in States 1 and 2, whereas the HC group liked to stay in State 3, which was consistent with the results of appearance frequency. It was reported that transitions to co-activated states within brain networks became more challenging in the aging population (Ezaki et al., 2017), which is consistent with the finding that the transition to State 3 is suppressed in AD patients in this study. For the AD group, the increased transition frequency between State 1 and State 2 and the higher appearance frequency of State 1 and State 2 may serve as a compensatory strategy to offset cognitive impairment in sensory processing and cognitive control (Brier et al., 2012; Hillary et al., 2015).

4.3 Association between brain dynamics and cognitive ability

Associations between atypical brain dynamics and cognitive ability were observed in AD patients. These associations were also observed in other cognitive impairment patients (McKeith et al., 2017; Premi et al., 2019). For the AD group, the transition frequency between State 1 and State 2 showed a significantly positive correlation with the RAVLT score (Figure 7B). The RAVLT score is often used to evaluate verbal memory performance (Moradi et al., 2017). High RAVLT score represents high verbal memory performance. In contrast to HCs, AD patients had a significantly lower RAVLT score due to their memory impairment (Figure 7A). However, the AD group showed a significantly higher transition frequency between State 1 and State 2 than the HC group. Thus, the positive correlation between the transition frequency and RAVLT score further supported the compensatory mechanism in the AD group of enhancing the RAVLT score by increasing the transition frequency between State 1 and State 2. Moreover, the RAVLT score of the AD group was highly correlated with the transition in/out frequency of State 3 and the transition frequency between State 1 and State 3 (Figure 7F). In contrast to the HC group, the AD group showed a significantly lower transition in/out frequency of State 3 and transition frequency between State 1 and State 3. For the AD group, subjects with a higher transition of State 3 had less impairment of coactivation of all 9 networks, and subjects with a high RAVLT score had less cognitive impairment. Therefore, the AD group displayed a positive correlation between the transition frequency of State 3 and the RAVLT score, which may suggest that the high transition frequency of State 3 improves the RAVLT score.

5 Conclusion

In summary, this study explored the brain dynamics of AD patients by applying energy landscape analysis to resting-state fMRI data. Three stable brain states were identified from both the AD group and the HC group. The results revealed that cognitive impairments in AD primarily reduced the average dwell time in State 3 and the transition frequencies associated with State 3. The positive correlation between the transition in/out frequency of State 3 and RAVLT score of the AD group suggested that State 3 was important for cognitive processing. Furthermore, the increased transition frequency of State 1 and State 2 that was positively correlated with the RAVLT score suggests a compensatory mechanism of the AD group to raise cognitive ability by increasing the occurrence and transition between the two states with impaired cognitive function.

Data availability statement

The original contributions presented in the study are included in the article/Supplementary material, further inquiries can be directed to the corresponding author.

Ethics statement

The studies involving humans were approved by Alzheimer's Disease Neuroimaging Initiative. The studies were conducted in accordance with the local legislation and institutional requirements. The participants provided their written informed consent to participate in this study. Written informed consent was obtained from the individual(s) for the publication of any potentially identifiable images or data included in this article.

Author contributions

LX: Conceptualization, Data curation, Formal analysis, Methodology, Software, Writing – original draft, Writing – review & editing. ZG: Data curation, Methodology, Software, Conceptualization, Writing – review & editing, Writing – original draft. ZL: Conceptualization, Funding acquisition, Investigation, Methodology, Writing – original draft, Writing – review & editing.

Funding

The author(s) declare financial support was received for the research, authorship, and/or publication of this article. This research was funded by National Natural Science Foundation of China (grant number 62071050).

Conflict of interest

The authors declare that the research was conducted in the absence of any commercial or financial relationships that could be construed as a potential conflict of interest.

Publisher's note

All claims expressed in this article are solely those of the authors and do not necessarily represent those of their affiliated organizations, or those of the publisher, the editors and the reviewers. Any product that may be evaluated in this article, or claim that may be made by its manufacturer, is not guaranteed or endorsed by the publisher.

Supplementary material

The Supplementary material for this article can be found online at: https://www.frontiersin.org/articles/10.3389/fnagi.2024.1375091/full#supplementary-material

References

Albers, M. W., Gilmore, G. C., Kaye, J., Murphy, C., Wingfield, A., Bennett, D. A., et al. (2015). At the interface of sensory and motor dysfunctions and Alzheimer's disease. *Alzheimers Dement.* 11, 70–98. doi: 10.1016/j.jalz.2014.04.514

Badhwar, A., Tam, A., Dansereau, C., Orban, P., Hoffstaedter, F., and Bellec, P. (2017). Resting-state network dysfunction in Alzheimer's disease: a systematic review and meta-analysis. *Alzheimer's Dement.* 8, 73–85. doi: 10.1016/j.dadm.2017.03.007

Becker, O. M., and Karplus, M. (1997). The topology of multidimensional potential energy surfaces: theory and application to peptide structure and kinetics. *J. Chem. Phys.* 106, 1495–1517. doi: 10.1063/1.473299

Biswal, B., Zerrin Yetkin, F., Haughton, V. M., and Hyde, J. S. (1995). Functional connectivity in the motor cortex of resting human brain using echo-planar mri. *Magn. Reson. Med.* 34, 537–541. doi: 10.1002/mrm.1910340409

Brier, M. R., Thomas, J. B., Snyder, A. Z., Benzinger, T. L., Zhang, D., Raichle, M. E., et al. (2012). Loss of intranetwork and internetwork resting state functional connections with Alzheimer's disease progression. *J. Neurosci.* 32, 8890–8899. doi: 10.1523/JNEUROSCI.5698-11.2012

Buckner, R. L., Sepulcre, J., Talukdar, T., Krienen, F. M., Liu, H., Hedden, T., et al. (2009). Cortical hubs revealed by intrinsic functional connectivity: mapping, assessment of stability, and relation to Alzheimer's disease. *J. Neurosci.* 29, 1860–1873. doi: 10.1523/JNEUROSCI.5062-08.2009

Chang, C., and Glover, G. H. (2010). Time–frequency dynamics of resting-state brain connectivity measured with fMRI. *NeuroImage* 50, 81–98. doi: 10.1016/j.neuroimage.2009.12.011

Cruzat, J., Herzog, R., Prado, P., Sanz-Perl, Y., Gonzalez-Gomez, R., Moguilner, S., et al. (2023). Temporal irreversibility of large-scale brain dynamics in Alzheimer's disease. *J. Neurosci.* 43, 1643–1656. doi: 10.1523/JNEUROSCI.1312-22.2022

Demirtaş, M., Falcon, C., Tucholka, A., Gispert, J. D., Molinuevo, J. L., and Deco, G. (2017). A whole-brain computational modeling approach to explain the alterations in resting-state functional connectivity during progression of Alzheimer's disease. *NeuroImage Clin.* 16, 343–354. doi: 10.1016/j.nicl.2017.08.006

Downar, J., Crawley, A. P., Mikulis, D. J., and Davis, K. D. (2000). A multimodal cortical network for the detection of changes in the sensory environment. *Nat. Neurosci.* 3, 277–283. doi: 10.1038/72991

Ezaki, T., Sakaki, M., Watanabe, T., and Masuda, N. (2018). Age-related changes in the ease of dynamical transitions in human brain activity. *Hum. Brain Mapp.* 39, 2673–2688. doi: 10.1002/hbm.24033

Ezaki, T., Watanabe, T., Ohzeki, M., and Masuda, N. (2017). Energy landscape analysis of neuroimaging data. *Phil. Trans. R. Soc. A* 375:20160287. doi: 10.1098/rsta.2016.0287

Fan, L., Li, C., Huang, Z., Zhao, J., Wu, X., Liu, T., et al. (2022). The longitudinal neural dynamics changes of whole brain connectome during natural recovery from poststroke aphasia. *NeuroImage Clin.* 36:103190. doi: 10.1016/j.nicl.2022.103190

Filippi, M., Spinelli, E. G., Cividini, C., and Agosta, F. (2019). Resting state dynamic functional connectivity in neurodegenerative conditions: a review of magnetic resonance imaging findings. *Front. Neurosci.* 13:657. doi: 10.3389/fnins.2019.00657

Greicius, M. D., Srivastava, G., Reiss, A. L., and Menon, V. (2004). Default-mode network activity distinguishes Alzheimer's disease from healthy aging: evidence from functional MRI. *Proc. Natl. Acad. Sci. USA* 101, 4637–4642. doi: 10.1073/pnas.0308627101

Hahn, K., Myers, N., Prigarin, S., Rodenacker, K., Kurz, A., Förstl, H., et al. (2013). Selectively and progressively disrupted structural connectivity of functional brain networks in Alzheimer's disease — revealed by a novel framework to analyze edge distributions of networks detecting disruptions with strong statistical evidence. *NeuroImage* 81, 96–109. doi: 10.1016/j.neuroimage.2013.05.011

Hastings, W. K. (1970). Monte Carlo sampling methods using Markov chains and their applications. *Biometrika* 57, 97–109. doi: 10.1093/biomet/57.1.97

He, X., Qin, W., Liu, Y., Zhang, X., Duan, Y., Song, J., et al. (2014). Abnormal salience network in normal aging and in amnestic mild cognitive impairment and Alzheimer's disease. *Hum. Brain Mapp.* 35, 3446–3464. doi: 10.1002/hbm.22414

Hillary, F. G., Roman, C. A., Venkatesan, U., Rajtmajer, S. M., Bajo, R., and Castellanos, N. D. (2015). Hyperconnectivity is a fundamental response to neurological disruption. *Neuropsychology* 29, 59–75. doi: 10.1037/neu0000110

Hutchison, R. M., Womelsdorf, T., Allen, E. A., Bandettini, P. A., Calhoun, V. D., Corbetta, M., et al. (2013). Dynamic functional connectivity: promise, issues, and interpretations. *NeuroImage* 80, 360–378. doi: 10.1016/j.neuroimage.2013.05.079

Jagust, W. (2018). Imaging the evolution and pathophysiology of Alzheimer disease. *Nat. Rev. Neurosci.* 19, 687–700. doi: 10.1038/s41583-018-0067-3

Jaynes, E. T. (1957). Information theory and statistical mechanics. *Phys. Rev.* 106, 620–630. doi: 10.1103/PhysRev.106.620

Jones, D. T., Vemuri, P., Murphy, M. C., Gunter, J. L., Senjem, M. L., Machulda, M. M., et al. (2012). Non-stationarity in the "resting Brain's" modular architecture. *PLoS One* 7:e39731. doi: 10.1371/journal.pone.0039731

Joo, S. H., Lim, H. K., and Lee, C. U. (2016). Three large-scale functional brain networks from resting-state functional MRI in subjects with different levels of cognitive impairment. *Psychiatry Investig.* 13, 1–7. doi: 10.4306/pi.2016.13.1.1

Kang, J., Jeong, S. O., Pae, C., and Park, H. J. (2021). Bayesian estimation of maximum entropy model for individualized energy landscape analysis of brain state dynamics. *Hum. Brain Mapp.* 42, 3411–3428. doi: 10.1002/hbm.25442

Klepl, D., He, F., Wu, M., Marco, M. D., Blackburn, D. J., and Sarrigiannis, P. G. (2022). Characterising Alzheimer's disease with EEG-based energy landscape analysis. *IEEE J. Biomed. Health Inform.* 26, 992–1000. doi: 10.1109/JBHI.2021.3105397

Li, Y., An, S., Zhou, T., Su, C., Zhang, S., Li, C., et al. (2023). Triple-network analysis of Alzheimer's disease based on the energy landscape. *Front. Neurosci.* 17:1171549. doi: 10.3389/fnins.2023.1171549

McKeith, I. G., Boeve, B. F., Dickson, D. W., Halliday, G., Taylor, J.-P., Weintraub, D., et al. (2017). Diagnosis and management of dementia with Lewy bodies: fourth consensus report of the DLB consortium. *Neurology* 89, 88–100. doi: 10.1212/WNL.0000000000004058

Metropolis, N., Rosenbluth, A. W., Rosenbluth, M. N., Teller, A. H., and Teller, E. (1953). Equation of state calculations by fast computing machines. *J. Chem. Phys.* 21, 1087–1092. doi: 10.1063/1.1699114

Moradi, E., Hallikainen, I., Hänninen, T., and Tohka, J. (2017). Rey's auditory verbal learning test scores can be predicted from whole brain MRI in Alzheimer's disease. *NeuroImage Clin.* 13, 415–427. doi: 10.1016/j.nicl.2016.12.011

Pathak, A., Roy, D., and Banerjee, A. (2022). Whole-brain network models: from physics to bedside. *Front. Comput. Neurosci.* 16:866517. doi: 10.3389/fncom.2022.866517

Premi, E., Calhoun, V. D., Diano, M., Gazzina, S., Cosseddu, M., Alberici, A., et al. (2019). The inner fluctuations of the brain in presymptomatic frontotemporal dementia: the chronnectome fingerprint. *NeuroImage* 189, 645–654. doi: 10.1016/j.neuroimage.2019.01.080

Preti, M. G., Bolton, T. A., and Van De Ville, D. (2017). The dynamic functional connectome: state-of-the-art and perspectives. *NeuroImage* 160, 41–54. doi: 10.1016/j.neuroimage.2016.12.061

Puttaert, D., Coquelet, N., Wens, V., Peigneux, P., Fery, P., Rovai, A., et al. (2020). Alterations in resting-state network dynamics along the Alzheimer's disease continuum. *Sci. Rep.* 10:21990. doi: 10.1038/s41598-020-76201-3

Schneidman, E., Berry, M. J., Segev, R., and Bialek, W. (2006). Weak pairwise correlations imply strongly correlated network states in a neural population. *Nature* 440, 1007–1012. doi: 10.1038/nature04701

Shirer, W. R., Ryali, S., Rykhlevskaia, E., Menon, V., and Greicius, M. D. (2012). Decoding subject-driven cognitive states with whole-brain connectivity patterns. *Cereb. Cortex* 22, 158–165. doi: 10.1093/cercor/bhr099

Sridharan, D., Levitin, D. J., and Menon, V. (2008). A critical role for the right fronto-insular cortex in switching between central-executive and default-mode networks. *Proc. Natl. Acad. Sci. USA* 105, 12569–12574. doi: 10.1073/pnas.0800005105

Turner, R. S., and Desmurget, M. (2010). Basal ganglia contributions to motor control: a vigorous tutor. *Curr. Opin. Neurobiol.* 20, 704–716. doi: 10.1016/j.conb.2010.08.022

Watanabe, T., Hirose, S., Wada, H., Imai, Y., Machida, T., Shirouzu, I., et al. (2014a). Energy landscapes of resting-state brain networks. *Front. Neuroinform.* 8:12. doi: 10.3389/fninf.2014.00012

Watanabe, T., Masuda, N., Megumi, F., Kanai, R., and Rees, G. (2014b). Energy landscape and dynamics of brain activity during human bistable perception. *Nat. Commun.* 5:4765. doi: 10.1038/ncomms5765

Watanabe, T., and Rees, G. (2017). Brain network dynamics in high-functioning individuals with autism. *Nat. Commun.* 8:16048. doi: 10.1038/ncomms16048

Weintraub, S., Carrillo, M. C., Farias, S. T., Goldberg, T. E., Hendrix, J. A., Jaeger, J., et al. (2018). Measuring cognition and function in the preclinical stage of Alzheimer's disease. *Alzheimers Dement.* 4, 64–75. doi: 10.1016/j.trci.2018.01.003

Yan, C.-G., Wang, X.-D., Zuo, X.-N., and Zang, Y.-F. (2016). DPABI: data processing & analysis for (resting-state) brain imaging. *Neuroinformatics* 14, 339–351. doi: 10.1007/s12021-016-9299-4

frontiers | Frontiers in Aging Neuroscience

TYPE Original Research
PUBLISHED 20 May 2024
DOI 10.3389/fnagi.2024.1377085

OPEN ACCESS

EDITED BY
Ana Lloret,
University of Valencia, Spain

REVIEWED BY
Alejandro O. Sodero,
CONICET Institute for Biomedical Research (BIOMED), Argentina
Kathy R. Magnusson,
Oregon State University, United States
Mikel Pérez-Rodríguez,
MRC Laboratory of Molecular Biology (LMB), United Kingdom

*CORRESPONDENCE
Denise Manahan-Vaughan
✉ denise.manahan-vaughan@rub.de

RECEIVED 26 January 2024
ACCEPTED 26 April 2024
PUBLISHED 20 May 2024

CITATION
Südkamp N, Shchyglo O and Manahan-Vaughan D (2024) GluN2A or GluN2B subunits of the NMDA receptor contribute to changes in neuronal excitability and impairments in LTP in the hippocampus of aging mice but do not mediate detrimental effects of oligomeric Aβ (1–42). *Front. Aging Neurosci.* 16:1377085. doi: 10.3389/fnagi.2024.1377085

GluN2A or GluN2B subunits of the NMDA receptor contribute to changes in neuronal excitability and impairments in LTP in the hippocampus of aging mice but do not mediate detrimental effects of oligomeric Aβ (1–42)

Nicolina Südkamp, Olena Shchyglo and Denise Manahan-Vaughan*

Department of Neurophysiology, Medical Faculty, Ruhr University Bochum, Bochum, Germany

Studies in rodent models have revealed that oligomeric beta-amyloid protein [Aβ (1–42)] plays an important role in the pathogenesis of Alzheimer's disease. Early elevations in hippocampal neuronal excitability caused by Aβ (1–42) have been proposed to be mediated via enhanced activation of GluN2B-containing N-methyl-D-aspartate receptors (NMDAR). To what extent GluN2A or GluN2B-containing NMDAR contribute to Aβ (1–42)-mediated impairments of hippocampal function in advanced rodent age is unclear. Here, we assessed hippocampal long-term potentiation (LTP) and neuronal responses 4–5 weeks after bilateral intracerebral inoculation of 8–15month old GluN2A$^{+/-}$ or GluN2B$^{+/-}$ transgenic mice with oligomeric Aβ (1–42), or control peptide. Whole-cell patch-clamp recordings in CA1 pyramidal neurons revealed a more positive resting membrane potential and increased total spike time in GluN2A$^{+/-}$, but not GluN2B$^{+/-}$-hippocampi following treatment with Aβ (1–42) compared to controls. Action potential 20%-width was increased, and the descending slope was reduced, in Aβ–treated GluN2A$^{+/-}$, but not GluN2B$^{+/-}$ hippocampi. Sag ratio was increased in Aβ–treated GluN2B$^{+/-}$-mice. Firing frequency was unchanged in wt, GluN2A$^{+/-}$, and GluN2B$^{+/-}$hippocampi after Aβ–treatment. Effects were not significantly different from responses detected under the same conditions in wt littermates, however. LTP that lasted for over 2h in wt hippocampal slices was significantly reduced in GluN2A$^{+/-}$ and was impaired for 15min in GluN2B$^{+/-}$-hippocampi compared to wt littermates. Furthermore, LTP (>2h) was significantly impaired in Aβ–treated hippocampi of wt littermates compared to wt treated with control peptide. LTP induced in Aβ–treated GluN2A$^{+/-}$ and GluN2B$^{+/-}$-hippocampi was equivalent to LTP in control peptide-treated transgenic and Aβ–treated wt animals. Taken together, our data indicate that knockdown of GluN2A subunits subtly alters membrane properties of hippocampal neurons and reduces the magnitude of LTP. GluN2B knockdown reduces the early phase of LTP but leaves later phases intact. Aβ (1–42)-treatment slightly exacerbates changes in action potential properties in GluN2A$^{+/-}$-mice. However, the vulnerability of the aging hippocampus to Aβ–mediated impairments of LTP is not mediated by GluN2A or GluN2B-containing NMDAR.

KEYWORDS

NMDA, GluN2, CA1, amyloid-beta, amyloidosis, Alzheimer, rodent

1 Introduction

Early changes in the brain during Alzheimer's disease (AD) arise in part due to the pathophysiological effects of oligomeric Aβ (1–42) (Mucke et al., 2000; Fukumoto et al., 2010; Edwards, 2019). A characteristic feature of oligomeric Aβ (1–42) is the impairment of hippocampal long-term potentiation (LTP), whereby acute effects occur (Wang et al., 2004; Klyubin et al., 2005; Kalweit et al., 2015). Furthermore, deficits in both LTP and learning days after intracerebral treatment with Aβ (1–42) have been reported (Zhang et al., 2017; Khodadadi et al., 2018). Examination of the effects of oligomeric Aβ have indicated that topical application of Aβ to the slice chamber causes a suppression of $GABA_A$ receptor function in the hippocampus of young (P25-P40) rats *in vitro* (Orr et al., 2014). It has been proposed that this can lead to elevated levels of extrasynaptic glutamate that, in turn, enable enhanced activation of GluN2B-containing N-methyl-D-aspartate receptors (NMDAR), which then mediate hyperexcitability (Lei et al., 2016). Others have reported that antagonism of GluN2B-containing NMDAR prevents Aβ (1–42)-mediated deficits in LTP in the hippocampal CA1 region of young adult rats (Hu et al., 2009).

LTP in the CA1 region is predominantly NMDAR-dependent and postsynaptically mediated (Malenka et al., 1988, but see also Falcón-Moya et al., 2020 and Grover and Teyler, 1990 for examples of exceptions). NMDAR are typically composed of two GluN1 subunits and two GluN2 subunits (Dingledine et al., 1999). GluN2A and GluN2B-containing NMDAR play a key role in the enablement of hippocampal LTP (Bartlett et al., 2007; Berberich et al., 2007; Ballesteros et al., 2016) Although GluN2C and GluN2D subunits also occur in NMDAR, these do not appear to play a critical role in LTP (Banerjee et al., 2009). Whereas co-agonist binding of glycine or D-serine occurs at the GluN1 subunit (Hirai et al., 1996; Mothet et al., 2001; Henneberger et al., 2010), glutamate binds to the GluN2 subunit (McBain and Mayer, 1994; Laube et al., 1997). GluN2A-containing NMDAR exhibit faster kinetics compared to GluN2B-containing NMDAR (Punnakkal et al., 2012), lose their Mg^{2+} block at lower membrane potentials compared to GluN2B-containing NMDAR (Clarke and Johnson, 2006; Clarke et al., 2013), but allow half as much charge transfer, deactivate faster, and enable less Ca^{2+}-influx per unit of current than GluN2B-containing NMDAR (Vicini et al., 1998; Erreger et al., 2005; Sobczyk et al., 2005; Clarke et al., 2013). Furthermore, GluN2A-containing NMDAR respond to weaker stimuli (Köhr et al., 2003; Berberich et al., 2005, 2007) and enable weaker and less persistent forms of LTP compared to GluN2B-containing NMDAR (Ballesteros et al., 2016).

Excessive activation of NMDAR leads to excitotoxity (Rothman and Olney, 1987) and NMDAR antagonists have proven effective in the treatment of cognitive deficits in early AD (Paoletti et al., 2013; Zhou and Sheng, 2013). It is widely believed that the excitotoxic effects of NMDAR in AD are mediated by excessive extracellular glutamate that leads to overactivation of GluN2B-containing NMDAR (Texidó et al., 2011; Danysz and Parsons, 2012; Paoletti et al., 2013; Talantova et al., 2013; Zhou and Sheng, 2013). In addition, NMDAR have been reported to mediate specific cellular and biochemical actions of Aβ in processes that involve both GluN2A and GluN2B subunits (Roselli et al., 2005; Snyder et al., 2005; Domingues et al., 2007; Abbott et al., 2008; Deshpande et al., 2009; Li et al., 2009) in a process that may involve Aβ–binding to NMDAR (Cowburn et al., 1997; De Felice et al., 2007; Lacor et al., 2007).

The contribution of different GluN subunits to NMDAR toxicity, or Aβ–mediated pathophysiology, may change along the lifespan of an individual. Developmental changes in the expression of GluN2A and GluN2B have been reported, whereby a systematic increase of GluN2A subunits and a decline of GluN2B subunits occurs in the period encompassing early postnatal stages (12 days postnatally) through early adulthood (35 days postnatally) (Carmignoto and Vicini, 1992). More recent findings suggest that GluN2A and GluN2B levels remain abundant and largely equivalent in later adulthood (2–4 months postnatally), at least in C57BL/6 mice, although relative differences in murine strains occur (Beckmann et al., 2020). Furthermore, differences in GluN2A:GluN2B ratios occur along the dorsoventral axis of the hippocampus (Dubovyk and Manahan-Vaughan, 2018). GluN2A:GluN2B ratios are also modulated by synaptic activity, whereby lower levels lead to an increase in GluN2B and a decrease in GluN2A subunits (Chen and Bear, 2007; Yashiro and Philpot, 2008). The consequence is a prolongation of NMDAR currents and a reduction in LTP thresholds (Chen and Bear, 2007; Yashiro and Philpot, 2008). Thus, reductions in synaptic activity triggered by Aβ (Balleza-Tapia et al., 2010) may lead to a preferential recruitment of GluN2B-containing NMDAR into synaptic plasticity processes.

In the present study, we explored to what extent GluN2A and GluN2B-containing NMDAR contribute to changes in hippocampal excitability and LTP triggered by intracerebral inoculation with oligomeric Aβ (1–42) in aging mice. We treated 8–15 month old $GluN2A^{+/-}$ and $GluN2B^{+/-}$ animals, and their wt littermates, with oligomeric Aβ (1–42), or control peptide, 4–5 weeks before assessing neuronal excitability and LTP in the hippocampal slice preparation. Effects of Aβ (1–42) on neuronal excitability were minimal. LTP was reduced in $GluN2A^{+/-}$ and $GluN2B^{+/-}$ mice compared to their wt littermates. In wt hippocampi, intracerebral pretreatment with Aβ (1–42) potently reduced the magnitude of LTP. Strikingly, however, pretreatment with Aβ (1–42) had no impact on the profile of LTP expressed in the hippocampi of $GluN2A^{+/-}$ and $GluN2B^{+/-}$ mice. These findings suggest that in old age, the detrimental effects of Aβ (1–42) on LTP are not mediated by GluN2A and GluN2B containing NMDAR.

2 Materials and methods

2.1 Animals

Eight-to-fifteen month old heterozygote GluN2A (Sakimura et al., 1995) and GluN2B heterozygote (von Engelhardt et al., 2008) transgenic mice and their wildtype littermates (Zentrale Versuchstierhaltung Medizin, Ruhr University Bochum) were used in this study. Homozygotes of GluN2B knockout mice do not survive postnatally (von Engelhardt et al., 2008).

Mice were housed in a custom-made ventilated and acclimatized vivarium in a rodent-housing room (12-h light/dark cycle) with unlimited access to food and water. Experiments were carried out in accordance with the European Communities Council Directive of September 22nd, 2010 (2010/63/EU) for care of laboratory animals, and were conducted according to the guidelines of the German Animal Protection Law. Experiments were authorized in advance by the North Rhine-Westphalia (NRW) State Authority

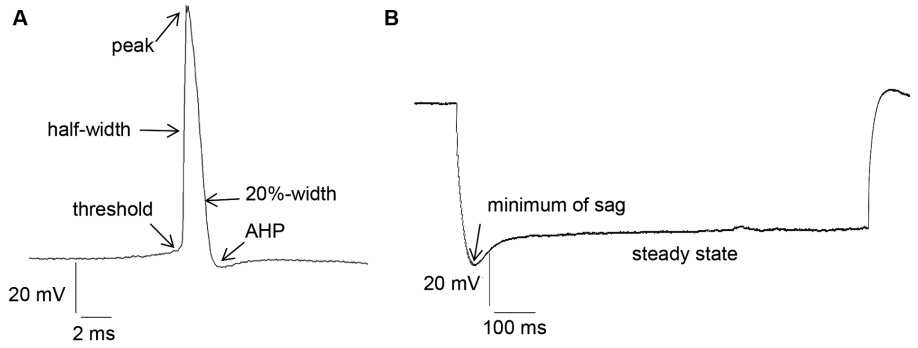

FIGURE 1
(A) Examples of action potential (AP) measurement: threshold, half-width, peak, 20%-width and afterhyperpolarization (AHP). **(B)** Measurement of Sag and Sag ratio: Sag ratio was determined from the ratio between the steady-state decrease in voltage and the greatest decrease in voltage after a hyperpolarizing current step.

(Landesamt für Arbeitsschutz, Naturschutz, Umweltschutz und Verbraucherschutz, NRW).

2.2 Treatment with Aβ (1–42)

Oligomeric Aβ (1–42) was prepared and aggregated as described previously (Kalweit et al., 2015). The soluble Aβ (1–42) peptide was prepared in phosphate-buffered saline at pH 7.4, diluted to a dose of 50 µM, shock-frozen with liquid nitrogen and stored at −80°C. On the day of treatment, the peptide solution was incubated for 3 h to allow for oligomerization (Kalweit et al., 2015). It was applied at room temperature in a dose of 10 µM (1 µL volume) to both lateral cerebral ventricles of anesthetized mice by means of a Hamilton syringe (Kalweit et al., 2015). Control animals received 10 µM scrambled Aβ-peptide (Yamin et al., 2016) in a volume of 1 µL in a procedure that followed identical steps as described above. Treatment was implemented 4–5 weeks prior to conducting the *in vitro* experiments.

2.3 Slice preparation

Mice were deeply anaesthetized with isoflurane before decapitation and sagittal hippocampal slices (350 µm) were prepared in cold (1–4°C), oxygenated saccharose solution (in mM: 87 NaCl, 2.6 $MgSO_4$, 75 Saccharose, 2.5 KCl, 1.25 NaH_2PO_4, 26 $NaHCO_3$, 0.5 $CaCl_2$, 2 D-Glucose) (95% O_2, 5% CO_2). Slices were subsequently incubated, for at least 30 min before recordings were commenced, in a holding chamber in artificial cerebrospinal fluid (aCSF, in mM: 125 mM NaCl, 3 mM KCl, 2.5 mM $CaCl_2$, 1.3 mM $MgSO_4$, 1.25 mM NaH_2PO_4, 26 mM $NaHCO_3$ and 13 mM D-Glucose) using a constant flow rate of 2 mL/min at 30°C.

2.4 Patch clamp recordings

Whole cell patch clamp recordings were conducted according to established procedures (Novkovic et al., 2015). The recording chamber was located under an upright microscope. Slices were continuously perfused with oxygenated aCSF (constant flow rate of 1–2 mL/min). Recording pipettes were prepared from borosilicate glass tubes (1.5 mm external diameter) with a resistance of 6–10 MΩ and were filled with intracellular solution (in mM: 97.5 potassium gluconate, 32.5 KCl, 5 EGTA, 10 Hepes, 1 $MgCl_2$, 4 Na_2 ATP, adjusted to pH 7.3 with KOH). Patch clamp recordings were conducted on visually identified soma of pyramidal neurons in the CA1 region. Corrections related to the liquid junction potential (Neher, 1992) were not conducted.

Intrinsic membrane properties were assessed using an HEKA EPC10 amplifier and the PATCHMASTER acquisition software (HEKA Elektronik Dr. Schulze GmbH, Lambrecht/Pfalz, Germany). We scrutinized resting membrane potential, input resistance, membrane time constant, excitatory threshold, Sag, sag ratio, firing frequency, action potential (AP) threshold, spike amplitude, AP peak, half-width, 20%-width, time-to-peak, afterhyperpolarization (AHP), time peak to AHP (Figure 1A). Sag ratio was determined as the ratio between the steady-state decrease in voltage and the greatest decrease in voltage after a hyperpolarizing current step, i.e., steady state voltage/peak voltage (Figure 1B).

Data underwent low-pass filtering at 2.9 kHz and were digitized at 10 kHz. FITMASTER software (HEKA Elektronik Dr. Schulze GmbH, Lambrecht/Pfalz, Germany) was used for offline data analysis. Input resistance was calculated from the slope of the linear fit of the relationship between the change in membrane potential (ΔV) and the intensity of the injected current (between −120 pA and + 90 pA). The time constant was determined from an exponential fit of the averaged voltage decay. The resting membrane potential was determined from the mean of 30 s basal recording time. The minimum current needed to induce an action potential was defined as the threshold current. The action potential amplitude was measured as the voltage difference between the threshold and the peak. Firing properties were investigated by applying current steps of Δ50 pA in hyperpolarizing and depolarizing square pulses (1-s duration) through the patch-clamp electrode (in the range of −300 pA to 400 pA). Here, we calculated both the absolute number of spikes

during the current application, the firing frequency (in Hz), and the spike frequency adaptation. The latter was determined by counting the number of spikes separately during each 100 ms of the 1 s depolarizing square pulse of 300 pA and converting the number into a frequency in Hz.

2.5 fEPSP recordings and induction of LTP

To record field potentials, we placed a bipolar stimulation electrode (Fredrick Haer, Bowdowinham, ME, United States) in the stratum radiatum of the CA1 region of the hippocampus and a glass field recording electrode (impedance: 1–2 MΩ, filled with aCSF) was placed in the CA1 dendritic area.

Field excitatory post-synaptic potentials (fEPSPs) were evoked by means of test-pulse stimuli (0.025 Hz, 0.2 ms duration, sample rate of 10,000 Hz). For each time-point, five fEPSPs were averaged. Before recordings were started, a stimulus–response relationship was determined using a stimulation intensity range of 60–660 μA (50 μA steps). The stimulation strength used for test-pulses was the intensity that evoked *ca.* 50% of the maximal fEPSP. Basal synaptic transmission was recorded for 40 min, after which period LTP was induced by theta burst stimulation (TBS, three trains 10 s apart, each consisting of 10 bursts of 4 pulses at 100 Hz, delivered 100 ms apart; Novkovic et al., 2015).

2.6 Statistical analysis

Analysis of variance (ANOVA) with repeated measures, or a Student's t-test was used for statistical analysis. Where appropriate, a *post-hoc* Fischer's test was used to determine if statistical significances occurred between two individual test conditions. Data are expressed as the mean ± standard error of the mean. 'N' signifies the number of animals and 'n' signifies the number of hippocampal slices (LTP experiments), or cells (for patch clamp data).

3 Results

3.1 Aging wildtype mice exhibited a higher input resistance after Aβ-treatment. Other membrane properties were largely unchanged

Given that little is known about the response of aging hippocampi to intracerebral treatment with oligomeric Aβ (1–42), we first compared the effect of Aβ-treatment with control peptide-treatment in the wildtype (wt) littermates of GluN2A$^{+/-}$ (control-treated $N=5$, $n=24$; Aβ-treated $N=5$, $n=24$) and GluN2B$^{+/-}$ mice (control-treated $N=6$, $n=29$; Aβ-treated $N=6$, $n=31$). Following Aβ-treatment of these two different wt littermate cohorts (Figures 2A,B), no changes in resting potential were evident (Tables 1A, 2A).

With the exception of input resistance, which was increased in GluN2A wt littermates (Figure 2C), but unchanged in GluN2B wt littermates after Aβ-treatment (Figure 2D), no other neuronal property was affected by Aβ-treatment in the wt littermates of either transgenic strain (Figures 2D–F; Tables 1A, B, 2A, B).

3.2 GluN2 subunit deletion and Aβ-treatment differentially affected the resting membrane potential in GluN2A$^{+/-}$ but not GluN2B$^{+/-}$ mice. Other membrane properties were unaffected by Aβ

Four to five weeks after intracerebral treatment, we observed that control peptide-treated GluN2A$^{+/-}$ mice ($N=5$, $n=25$) exhibited an equivalent resting membrane potential ($p=0.195$) compared to that seen in wt controls (Figure 2A; Table 1B). After treatment with Aβ (1–42) ($N=5$, $n=26$), resting membrane potential became more positive ($p=0.002$) in GluN2A$^{+/-}$ mice, compared to control peptide-treated GluN2A$^{+/-}$ hippocampi (Figure 2A; Table 1A), although the membrane voltage was very similar to responses evoked in Aβ-treated wt hippocampi (Figure 2A). This suggests that the effect of Aβ in GluN2A$^{+/-}$ hippocampi may have derived from the change in membrane potential in the transgenic mice, rather than due to a direct effect of Aβ.

In GluN2B$^{+/-}$ hippocampi, we detected no changes in resting membrane potential following control peptide treatment compared to effects detected in their wt littermates ($p=0.15$, $N=5$, $n=28$) (Figure 2B; Table 2B). Levels achieved were also similar to the resting membrane potential detected in Aβ-treated wt mice (Figure 2B; Table 2B). In addition, treatment with Aβ had no significant effect on resting membrane potential in GluN2B$^{+/-}$ hippocampi ($N=6$, $n=31$) compared to control peptide-treated GluN2B$^{+/-}$ hippocampi (Figure 2B; Table 2A).

Input resistance (Figures 2C,D) and excitatory threshold (Figures 2C,D) were unaffected by Aβ-treatment of GluN2A$^{+/-}$ or GluN2B$^{+/-}$ mice compared to control peptide treatment of each transgenic group (Tables 1A, B, 2A, B).

3.3 Sag was unaltered after Aβ-treatment of transgenic mice. Sag ratio was increased by Aβ-treatment of GluN2B transgenics, but not of GluN2B wild type littermates

Sag reflects a rebound depolarization that is enabled by hyperpolarization-activated cation currents (I_h) that are mediated by the opening of hyperpolarization-activated cation non-selective (HCN) channels (Robinson and Siegelbaum, 2003). This process serves to limit the negativity of the resting membrane potential and to regulate synaptic transmission. Given that we detected changes in the resting membrane potential in the abovementioned experiments, we wondered if deletion of a GluN2 subunit or Aβ-treatment affects sag.

We detected an increased negativity of sag, but an unchanged sag ratio was observed in GluN2A wt littermates that were treated with Aβ compared to control peptide–treatment (Figures 3A,C; Table 1A). Sag and sag ratio were equivalent in control peptide–treated wt and control peptide–treated GluN2A$^{+/-}$ (Figures 3A,C) and in Aβ-treated GluN2A$^{+/-}$ compared to control peptide–treated transgenics (Figures 3A,C; Tables 1A, B). Thus, the only notable sag change we detected was in Aβ-treated wt littermates compared to control wt. In other words, GluN2A transgenics had altered sag but this was not further affected by Aβ.

In the GluN2B$^{+/-}$ mice, sag was unchanged in Aβ-treated GluN2B$^{+/-}$ hippocampi compared to hippocampi from control

10.3389/fnagi.2024.1377085

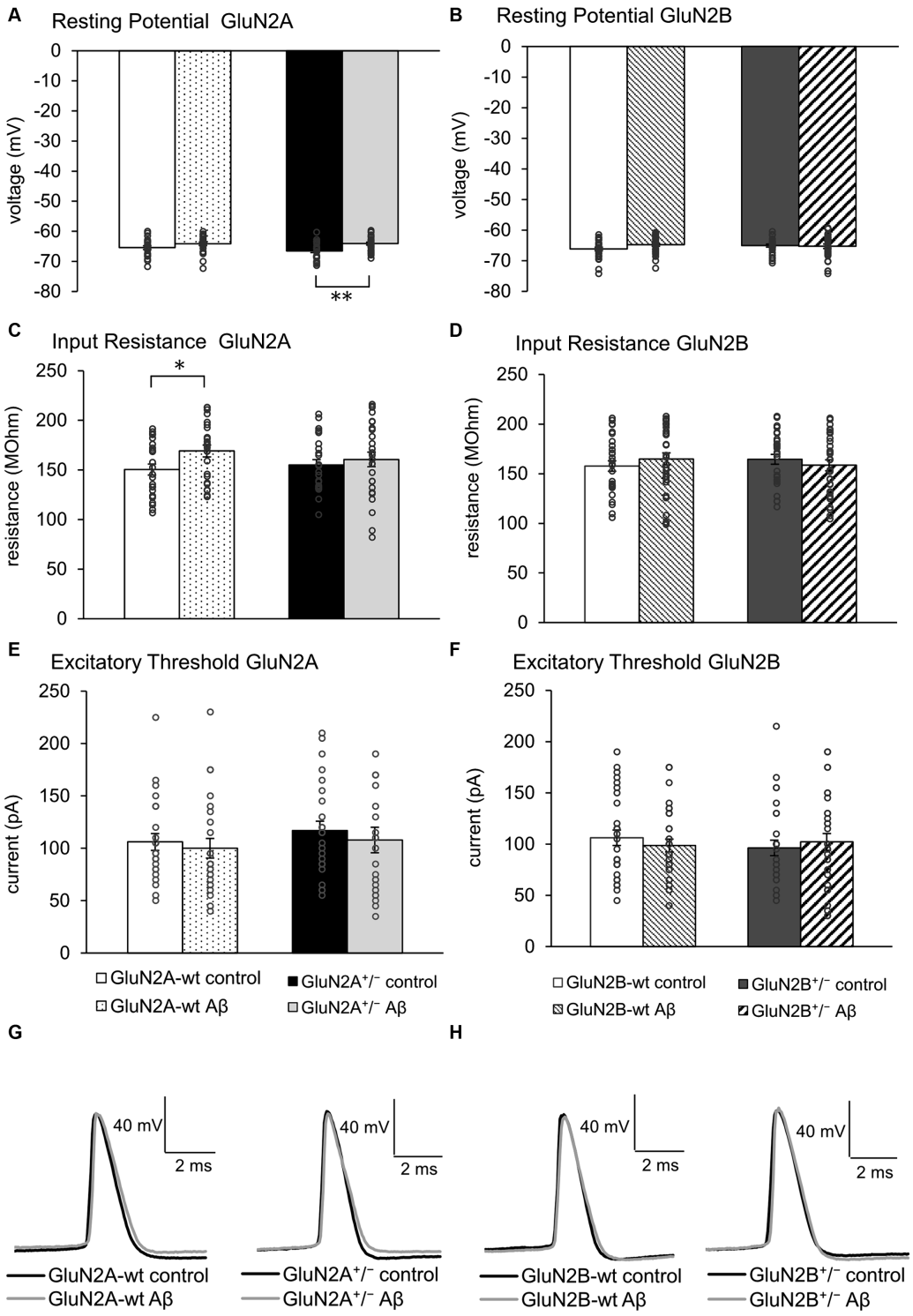

FIGURE 2
Effects of Aβ-treatment on membrane properties of hippocampal neurons. **(A)** Resting (membrane) potential was not different in GluN2A$^{+/-}$ mice ($N = 5$, $n = 25$) compared to their wt littermates ($N = 5$, $n = 24$) under control conditions. Aβ-treated GluN2A$^{+/-}$ mice ($N = 5$, $n = 26$) exhibited a significant difference in responses compared to control GluN2A$^{+/-}$. This effect derived moreso from the more negative resting potential in control transgenic mice, than a direct effect of oligomeric Aβ (1–42) on the potential. See Tables 1, 2 for statistics. **(B)** Resting (membrane) potential was not different in wt littermates of GluN2B$^{+/-}$ mice following Aβ-treatment ($N = 6$, $n = 31$) compared to control peptide-treated wt ($N = 6$, $n = 29$). GluN2B$^{+/-}$ mice exhibited a similar resting membrane potential following control peptide-treatment ($N = 5$, $n = 28$) compared to control wt. Following Aβ-treatment, no difference in membrane potential was evident when effects in GluN2B$^{+/-}$ transgenics ($N = 6$, $n = 31$) were compared with control peptide-treated GluN2B$^{+/-}$transgenics. See Tables 1, 2 for statistics. **(C,D)** Input resistance was higher in Aβ-treated wt littermates of GluN2A$^{+/-}$ compared to control wt **(C)**. This effect was absent in Aβ-treated GluN2A$^{+/-}$ transgenics compared to control GluN2A$^{+/-}$ mice **(C)**. No effect of Aβ-treatment was detected in GluN2B$^{+/-}$transgenics or their wt littermates **(D)**. See Tables 1, 2 for statistics. **(E,F)** Excitatory threshold was unaffected by Aβ-treatment of GluN2A$^{+/-}$

(Continued)

FIGURE 2 (Continued)
transgenics **(E)** or GluN2B$^{+/-}$ transgenics **(F)** or their wildtype littermates **(E,F)**. See Tables 1, 2 for statistics. **(G,H)** Representative examples of action potentials in control peptide and Aβ-treated GluN2A$^{+/-}$ transgenics and their wt littermates **(G)** and in control peptide and Aβ-treated GluN2B$^{+/-}$ transgenics and their wt littermates **(H)**. The circles on the error bars show the distribution of individual responses in each condition that contributed the mean effect represented by the bar.

peptide–treatment GluN2B$^{+/-}$ transgenics (Figure 3B; Table 2A). Sag ratio was significantly increased by Aβ-treatment, however (Figure 3D; Table 2A), suggesting that in Aβ-treated GluN2B$^{+/-}$ transgenics, HCN channels may require a more negative membrane potential in order for them to become activated (see Figures 3E,F for representative examples).

3.4 Action potential properties were changed by Aβ-treatment in GluN2A$^{+/-}$, but not GluN2B$^{+/-}$ mice

Action potential properties (see Figures 2G,H for representative examples) such as time to peak (Figures 4A,B), time from peak to afterhyperpolarization (AHP) (Figures 4C,D), and total spike time (Figures 4E,F), were unaltered in wt littermates of GluN2A$^{+/-}$ and GluN2B$^{+/-}$ mice after Aβ-treatment, compared to responses evoked after treatment of wt with control peptide (Tables 3A, B). Time to peak was also unaffected by Aβ-treatment of either GluN2A$^{+/-}$ (Figure 4A) or GluN2B$^{+/-}$ transgenic mice (Figure 4B; Tables 3A, B) compared to control transgenic responses. The time of the peak to AHP was unchanged in Aβ-treated GluN2A$^{+/-}$ compared to control peptide-treated GluN2A$^{+/-}$ hippocampi (Figure 4C; Table 3A), and no Aβ-mediated effect was evident in Aβ-treated GluN2B$^{+/-}$, compared to control peptide-treated GluN2B$^{+/-}$ hippocampi (Figure 4D; Table 3B). Total spike time was significantly increased in Aβ-treated GluN2A$^{+/-}$ compared to control peptide-treated GluN2A$^{+/-}$ hippocampi (Figure 4E; Table 3A), but effects were absent in GluN2B$^{+/-}$ compared to control peptide-treated GluN2B$^{+/-}$ hippocampi (Figure 4F; Table 3B). Thus, only GluN2A$^{+/-}$ hippocampi showed a sensitivity of the peak to AHP and the total spike time to oligomeric Aβ (1–42)-treatment.

When we assessed the ascending and descending slope of the action potential, we found no changes following Aβ-treatment of wt littermates compared to control peptide treatment of wt (Figures 5A–D; Tables 3A, B). No significant changes in the ascending slope were detected following Aβ-treatment of GluN2A$^{+/-}$ mice, compared to control peptide-treatment of GluN2A$^{+/-}$ mice (Figure 5A; Table 3A). The descending slope was significantly slower, however (Figure 5A). No differences in ascending (Figure 5B), or descending, slope (Figure 5D) were detected in GluN2B$^{+/-}$ hippocampi following Aβ–treatment (Table 3B).

The half width (Figure 5E) and 20%-width (Figure 5G) of the action potential was unchanged following Aβ-treatment of wt littermates of the GluN2A$^{+/-}$ mice (Table 3A). Effects were significant (20%-width) following Aβ-treatment of GluN2A$^{+/-}$ mice compared to control peptide effects (Figures 5E,G; Table 3A). Thus, Aβ-treatment altered the width of the action potential in GluN2A$^{+/-}$ mice.

In GluN2B$^{+/-}$ mice or their wt littermates, Aβ-treatment had no effect on the width of the action potential (Figures 5F,H; Table 3B). No differences in Aβ-treatment effects were evident when the two wt cohorts were compared.

Taken together, the slowing of the action potential may serve to explain why the time to AHP and the total spike time was increased in Aβ-treated GluN2A$^{+/-}$ mice (Figures 4C,E). Aβ-treatment had no effect whatsoever on action potential properties in GluN2B$^{+/-}$ and their wt littermates.

3.5 Action potential firing frequency was not altered in GluN2A$^{+/-}$ and GluN2B$^{+/-}$ mice compared to wildtype littermates. Aβ-treatment had no effect

When we compared action potential firing frequency and spike frequency adaptation in control peptide-treated GluN2A$^{+/-}$ mice and their wt littermates, we detected no significant differences (Figures 6A,E; Table 1B). Treatment with Aβ failed to alter firing frequency, or spike frequency adaptation in either wt or GluN2A$^{+/-}$ hippocampi (Figures 6A,E; Tables 1A, 4).

No differences in firing frequency (ANOVA $F(3,115) = 1.2631$, $p = 0.29$), or spike frequency adaptation were detected between GluN2B$^{+/-}$ mice and their wt littermates after control peptide-treatment (Figures 6B,F; Table 2B). Although a tendency towards increased firing frequency and higher currents was evident after Aβ-treatment of GluN2B$^{+/-}$ mice, this was not significant compared to control peptide-treated transgenics (Figure 6B; Tables 2A, 4).

Thus, Aβ-treatment had no effect on firing frequency in GluN2A$^{+/-}$ or GluN2B$^{+/-}$ mice and their wildtype littermates (see Figures 6C,D for representative examples).

3.6 LTP duration was differentially curtailed in GluN2A$^{+/-}$ or GluN2B$^{+/-}$ hippocampi. LTP was impaired by Aβ-treatment of wt littermates. LTP was not further altered by Aβ-treatment of GluN2A$^{+/-}$ or GluN2B$^{+/-}$ mice

LTP, induced by theta-burst stimulation (TBS), was significantly impaired in the hippocampi of control-peptide treated GluN2A$^{+/-}$transgenic mice ($N = 7$, $n = 9$) compared to their wt littermates (control-peptide treated) ($N = 6$, $n = 9$) (Figure 7A). Impairments were evident throughout the entire monitoring period and were still evident 30 min (ANOVA F (1, 15) $= 6.67$, $p = 0.02$), 60 min (ANOVA F (1, 15) $= 5.88$, $p = 0.03$) and 120 min post-TBS (ANOVA F (1, 15) $= 5.09$, $p = 0.04$) (Figure 7A).

Treatment of GluN2A$^{+/-}$ transgenic mice with Aβ (1–42) ($N = 6$, $n = 7$) resulted in LTP that was not statistically different from LTP elicited in control peptide-treated transgenics ($N = 7$, $n = 9$) (Figure 7A) (ANOVA 30 min post-TBS: F (1, 14) $= 0.80$, $p = 0.39$). Thus, the impairment of LTP that was evident in wt littermates, was not present in GluN2A$^{+/-}$hippocampi. Rather the reduced LTP that occurred in control peptide-treated GluN2A$^{+/-}$ transgenics was not further exacerbated by Aβ (1–42)-treatment.

In GluN2B$^{+/-}$ transgenics ($N = 6$, $n = 6$), the early phase of LTP, induced by TBS, was significantly impaired in the hippocampi of

TABLE 1 Passive and active neuronal properties in GluN2A$^{+/-}$ mice and their wildtype littermates after Aβ or control peptide treatment.

A						
	GluN2A-wt control	GluN2A-wt Aβ	*T*-test$^{\$}$/ ANOVA	GluN2A$^{+/-}$ control	GluN2A$^{+/-}$ Aβ	*T*-test$^{\$}$/ ANOVA
Resting potential (mV)	−65.42 ± 0.59	−64.14 ± 0.58	$p = 0.14^{\$}$	−66.52 ± 0.56	−64.07 ± 0.49	**p = 0.002**$^{\$}$
Input resistance (MΩ)	150.37 ± 5.55	169.11 ± 5.94	**p = 0.029**$^{\$}$	154.96 ± 5.45	160.59 ± 7.39	$p = 0.55^{\$}$
Tau (ms)	14.73 ± 0.61	15.24 ± 0.73	$p = 0.604^{\$}$	14.01 ± 0.67	14.86 ± 0.61	$p = 0.36^{\$}$
Excitatory threshold (pA)	106.04 ± 8.07	100 ± 9.38	$p = 0.63^{\$}$	117 ± 8.85	107.88 ± 12.18	$p = 0.56^{\$}$
Firing frequency 50pA	0.04 ± 0.04	0.21 ± 0.17	$F(3,95) = 1.74$, $p = 0.16$	0 ± 0	0.12 ± 0.06	$F(3,95) = 1.74$, $p = 0.16$
Firing frequency 100pA	1.04 ± 0.57	1.92 ± 0.57	$F(3,95) = 1.74$, $p = 0.16$	0.44 ± 0.16	1.46 ± 0.47	$F(3,95) = 1.74$, $p = 0.163$
Firing frequency 150pA	3.21 ± 0.90	4.21 ± 0.80	$F(3,95) = 1.74$, $p = 0.16$	1.76 ± 0.32	2.73 ± 0.59	$F(3,95) = 1.74$, $p = 0.16$
Firing frequency 200pA	5.38 ± 1.09	4.88 ± 0.86	$F(3,95) = 1.74$, $p = 0.16$	3.2 ± 0.45	3.73 ± 0.63	$F(3,95) = 1.74$, $p = 0.16$
Firing frequency 250pA	6.13 ± 1.14	5.58 ± 0.82	$F(3,95) = 1.74$, $p = 0.16$	3.76 ± 0.46	4.35 ± 0.70	$F(3,95) = 1.74$, $p = 0.16$
Firing frequency 300pA	6.67 ± 1.21	5.46 ± 0.71	$F(3,95) = 1.74$, $p = 0.16$	4.2 ± 0.37	4.65 ± 0.64	$F(3,95) = 1.74$, $p = 0.16$
Firing frequency 350pA	6.86 ± 1.12	5.29 ± 0.74	$F(3,95) = 1.74$, $p = 0.16$	4.2 ± 0.42	4.92 ± 0.58	$F(3,95) = 1.74$, $p = 0.16$
Firing frequency 400pA	6.84 ± 1.00	5.38 ± 0.69	$F(3,95) = 1.74$, $p = 0.16$	4.52 ± 0.40	4.81 ± 0.49	$F(3,95) = 1.74$, $p = 0.16$
Sag (mV)	−10.29 ± 0.68	−12.55 ± 0.77	**p = 0.037**$^{\$}$	−10.96 ± 0.63	−11.46 ± 0.76	$p = 0.63^{\$}$
Sag ratio	0.910 ± 0.005	0.895 ± 0.005	$p = 0.05^{\$}$	0.907 ± 0.005	0.902 ± 0.005	$p = 0.47^{\$}$

B						
	GluN2A-wt control	GluN2A$^{+/-}$ control	*T*-test$^{\$}$/ ANOVA	GluN2A-wt Aβ	GluN2A$^{+/-}$ Aβ	*T*-test/ANOVA
Resting potential (mV)	−65.42 ± 0.59	−66.52 ± 0.56	p = 0.195$^{\$}$	−64.14 ± 0.58	−64.07 ± 0.49	$p = 0.93^{\$}$
Input resistance (MΩ)	150.37 ± 5.55	154.96 ± 5.45	$p = 0.57^{\$}$	169.11 ± 5.94	160.59 ± 7.39	p = 0.39$^{\$}$
Tau (ms)	14.73 ± 0.61	14.01 ± 0.67	$p = 0.44^{\$}$	15.24 ± 0.73	14.86 ± 0.61	$p = 0.698^{\$}$
Excitatory threshold (pA)	106.04 ± 8.07	117 ± 8.85	$p = 0.38^{\$}$	100 ± 9.38	107.88 ± 12.18	$p = 0.62^{\$}$
Firing frequency 50pA	0.04 ± 0.04	0 ± 0	$F(3,95) = 1.74$, $p = 0.16$	0.21 ± 0.17	0.12 ± 0.06	$F(3,95) = 1.74$, $p = 0.16$
Firing frequency 100pA	1.04 ± 0.57	0.44 ± 0.16	$F(3,95) = 1.74$, $p = 0.16$	1.92 ± 0.57	1.46 ± 0.47	$F(3,95) = 1.74$, $p = 0.16$ 3
Firing frequency 150pA	3.21 ± 0.90	1.76 ± 0.32	$F(3,95) = 1.74$, $p = 0.16$	4.21 ± 0.80	2.73 ± 0.59	$F(3,95) = 1.74$, $p = 0.16$
Firing frequency 200pA	5.38 ± 1.09	3.2 ± 0.45	$F(3,95) = 1.74$, $p = 0.16$	4.88 ± 0.86	3.73 ± 0.63	$F(3,95) = 1.74$, $p = 0.16$
Firing frequency 250pA	6.13 ± 1.14	3.76 ± 0.46	$F(3,95) = 1.74$, $p = 0.16$	5.58 ± 0.82	4.35 ± 0.70	$F(3,95) = 1.74$, $p = 0.16$

(Continued)

TABLE 1 (Continued)

B						
	GluN2A-wt control	GluN2A$^{+/-}$ control	*T*-test$^{\$}$/ ANOVA	GluN2A-wt Aβ	GluN2A$^{+/-}$ Aβ	*T*-test/ANOVA
Firing frequency 300pA	6.67 ± 1.21	4.2 ± 0.37	$F(3,95) = 1.74$, $p = 0.16$	5.46 ± 0.71	4.65 ± 0.64	$F(3,95) = 1.74$, $p = 0.16$
Firing frequency 350pA	6.86 ± 1.12	4.2 ± 0.42	$F(3,95) = 1.74$, $p = 0.16$	5.29 ± 0.74	4.92 ± 0.58	$F(3,95) = 1.74$, $p = 0.16$
Firing frequency 400pA	6.84 ± 1.00	4.52 ± 0.40	$F(3,95) = 1.74$, $p = 0.16$	5.38 ± 0.69	4.81 ± 0.49	$F(3,95) = 1.74$, $p = 0.16$
Sag (mV)	−10.29 ± 0.68	−10.96 ± 0.63	$p = 0.48^{\$}$	−12.55 ± 0.77	−11.46 ± 0.76	$p = 0.33^{\$}$
Sag ratio	0.910 ± 0.005	0.907 ± 0.005	$p = 0.64^{\$}$	0.895 ± 0.005	0.902 ± 0.005	$p = 0.37^{\$}$

(A) The table compares passive and active neuronal properties of Aβ (1–42) treatment versus control peptide in either GluN2A$^{+/-}$ mice or their wt littermates. Firing frequencies evoked with currents in the range of 50 through 400pA are shown. Responses obtained in GluN2A$^{+/-}$ mice and their wildtype littermates following treatment with Aβ or control peptide are compared. Significant effects are highlighted in bold. (B) The table compares passive and active neuronal properties in GluN2A$^{+/-}$ mice versus their wt littermates following treatment with either control peptide or Aβ (1–42). Firing frequencies evoked with currents in the range of 50 though 400pA are shown. Responses in GluN2A$^{+/-}$ mice and their wildtype littermates after injections of either Aβ or control injections are compared.

GluN2B$^{+/-}$ transgenic mice that had been treated with control peptide ($N = 7$, $n = 9$), compared to their wt littermates ($N = 7$, $n = 8$) (Figure 7B). Impairments were sustained until 15 min post-TBS ($p = 0.04$). Thereafter, responses exhibited increased variability. The entire monitoring period of LTP was significantly impaired in wt littermates following Aβ (1–42)-treatment ($N = 7$, $n = 8$) compared to wt that had been treated with control peptide ($N = 7$, $n = 8$), with effects being immediately apparent after TBS, and sustained at 30 min (ANOVA $F(1, 13) = 8.199$, $p = 0.013$), 60 min (ANOVA $F(1, 13) = 9.11$, $p = 0.0098$) and 120 min post-TBS (ANOVA $F(1, 13) = 8.65$, $p = 0.011$) (Figure 7B). By contrast, treatment of GluN2B$^{+/-}$ with Aβ ($N = 7$, $n = 8$) resulted in LTP that was not significantly different from LTP evoked in control peptide-treated GluN2B$^{+/-}$hippocampi ($N = 6$, $n = 6$) (ANOVA 30 min post-TBS: $F(1, 12) = 0.24$, $p = 0.63$).

No significant changes were detected in the stimulus–response relationship when treatment conditions were compared in GluN2A$^{+/-}$mice ($N = 6$, $n = 8$) and their wt littermates) ($N = 6$, $n = 9$) (Figure 7C), or in GluN2B$^{+/-}$ transgenics ($N = 6$, $n = 6$) and their wt littermates ($N = 7$, $n = 8$) (Figure 7D). Thus, treatment with Aβ did not alter the synaptic response to afferent stimulation.

Taken together, these results indicate that whereas GluN2A is required for prolonged LTP induced by TBS, under these afferent stimulation conditions GluN2B supported only the early phase of LTP. Treatment with oligomeric Aβ (1–42) significantly impaired LTP in wt mice. However, transgenic knockdown of GluN2A, or GluN2B, did not exacerbate the debilitating effects of Aβ on LTP in aging mice.

4 Discussion

In this study, we report that in 8–15 month old animals, neuronal properties were largely equivalent in the hippocampi of GluN2A$^{+/-}$ and GluN2B$^{+/-}$ transgenic mice compared to their wt littermates (Table 4). A limited range of changes in properties of CA1 pyramidal cells were detected 4–5 weeks following intracerebral oligomeric Aβ (1–42)-treatment of wildtype animals, comprising, for example, a higher input resistance and a more negative sag, in wt littermates of GluN2A$^{+/-}$ mice (Table 4). Aβ-treatment elicited a limited amount of changes in neuronal properties of the transgenic animals, whereby GluN2A$^{+/-}$ mice were more affected than GluN2B$^{+/-}$ mice (Table 4). LTP was impaired in both GluN2A$^{+/-}$ and GluN2B$^{+/-}$ hippocampi compared to their wt littermates. Furthermore, intracerebral treatment with oligomeric Aβ (1–42) resulted in an impairment of LTP in wt mice. Strikingly, the profile of LTP was unchanged in Aβ-treated GluN2A$^{+/-}$ or GluN2B$^{+/-}$ hippocampi compared to control peptide-treated transgenic hippocampi, meaning that the already deficient LTP (compared to wt) was not impaired further by Aβ-treatment. Taken together, these data indicate that in the aging brain, GluN2A-containing NMDAR played an important role in the homeostasis of neuronal excitability. Furthermore, neuronal function was only mildly affected by Aβ-treatment of aging wt or GluN2 deficient mice, and knockdown of GluN2A or GluN2B did not worsen the debilitating effects of oligomeric Aβ (1–42) on hippocampal LTP. This suggests that in the aging hippocampus, NMDAR were not instrumental in propagating the pathophysiological effects of oligomeric Aβ (1–42) on hippocampal function.

By and large, we detected no marked effects of Aβ-treatment on neuronal properties. We saw for example, a greater positivity of the resting membrane potential in GluN2A$^{+/-}$ hippocampi compared to control GluN2A$^{+/-}$ hippocampi, but no significant difference in the membrane potential in GluN2B$^{+/-}$ compared to control GluN2B$^{+/-}$ hippocampi. The former difference derived more from differences in control peptide effects in wt and transgenics than from direct effects of Aβ, however. Sag (I_h) ratio was increased in GluN2B$^{+/-}$ following Aβ-treatment but unaffected in GluN2A$^{+/-}$ hippocampi following treatment. The I_h stabilises the resting membrane potential, regulates the afterhyperpolarization and influences firing frequency (McCormick and Pape, 1990). Neuronal oscillations are supported by the I_h (McCormick and Pape, 1990; Wahl-Schott and Biel, 2009) and we have reported in the past that hippocampal neuronal oscillations are undermined by oligomeric Aβ (1–42) (Kalweit et al., 2015). Sag is enabled by HCN channels (Robinson and Siegelbaum, 2003). HCN channels modulate glutamate release in the hippocampus and thus, influence NMDAR currents (Neitz et al., 2014). It has been proposed that these channels support hippocampal plasticity processes (Honnuraiah and Narayanan, 2013). NMDAR-dependent spontaneous slow excitatory dendritic potentials are regulated by HCN channels and are mediated by GluN2B-containing NMDARS

TABLE 2 Passive and active neuronal properties in GluN2B$^{+/-}$ mice and their wildtype littermates following Aβ or control peptide treatment.

A						
	GluN2B-wt control	GluN2B-wt Aβ	*T*-test$^{\$}$/ ANOVA	GluN2B$^{+/-}$ control	GluN2B$^{+/-}$ Aβ	*T*-test$^{\$}$/ ANOVA
Resting potential (mV)	−66.14 ± 0.55	−64.75 ± 0.51	$p = 0.07^{\$}$	−65.02 ± 0.50	−65.23 ± 0.73	$p = 0.82^{\$}$
Input resistance (MΩ)	157.72 ± 5.27	164.77 ± 6.14	$p = 0.398^{\$}$	164.50 ± 4.96	158.48 ± 5.52	$p = 0.43^{\$}$
Tau (ms)	12.71 ± 0.56	13.13 ± 0.46	$p = 0.57^{\$}$	13.34 ± 0.75	14.28 ± 0.72	$p = 0.38^{\$}$
Excitatory threshold (pA)	106.21 ± 7.51	98.55 ± 6.26	$p = 0.44^{\$}$	96.25 ± 7.55	102.10 ± 8.24	$p = 0.61^{\$}$
Firing frequency 50pA	0.38 ± 0.21	0.03 ± 0.03	$F(3,115) = 1.26$, $p = 0.29$	0.36 ± 0.25	0.68 ± 0.35	$F(3,115) = 1.26$, $p = 0.29$
Firing frequency 100pA	3.24 ± 0.92	2 ± 0.48	$F(3,115) = 1.26$, $p = 0.29$	3.71 ± 0.97	3.65 ± 1.02	$F(3,115) = 1.26$, $p = 0.29$
Firing frequency 150pA	5.79 ± 1.14	4.23 ± 0.67	$F(3,115) = 1.26$, $p = 0.29$	6 ± 1.24	6.13 ± 1.26	$F(3,115) = 1.26$, $p = 0.29$
Firing frequency 200pA	7.59 ± 1.29	5.58 ± 0.76	$F(3,115) = 1.26$, $p = 0.29$	7.29 ± 1.24	8.06 ± 1.32	$F(3,115) = 1.26$, $p = 0.29$
Firing frequency 250pA	7.83 ± 1.29	6.13 ± 0.75	$F(3,115) = 1.26$, $p = 0.29$	7.68 ± 1.28	9.03 ± 1.32	$F(3,115) = 1.26$, $p = 0.29$
Firing frequency 300pA	8.10 ± 1.28	6.03 ± 0.63	$F(3,115) = 1.26$, p = 0.29	7.39 ± 1.14	9.35 ± 1.30	$F(3,115) = 1.26$, $p = 0.29$
Firing frequency 350pA	7.69 ± 1.25	5.87 ± 0.59	$F(3,115) = 1.26$, $p = 0.29$	7 ± 1.01	9.16 ± 1.19	$F(3,115) = 1.26$, $p = 0.29$
Firing frequency 400pA	7.31 ± 1.16	5.68 ± 0.50	$F(3,115) = 1.26$, $p = 0.29$	7 ± 0.85	8.97 ± 1.09	$F(3,115) = 1.26$, $p = 0.29$
Sag (mV)	−11.06 ± 0.54	−11.02 ± 0.46	$p = 0.96^{\$}$	−12.25 ± 0.64	−10.24 ± 0.77	$p = 0.056^{\$}$
Sag ratio	0.908 ± 0.004	0.907 ± 0.003	$p = 0.91^{\$}$	0.897 ± 0.005	0.913 ± 0.006	**$p = 0.0496^{\$}$**

B						
	GluN2B-wt control	GluN2B$^{+/-}$ control	*T*-test$^{\$}$/ ANOVA	GluN2B-wt Aβ	GluN2B$^{+/-}$ Aβ	*T*-test$^{\$}$/ ANOVA
Resting potential (mV)	−66.14 ± 0.55	−65.02 ± 0.50	$p = 0.15^{\$}$	−64.75 ± 0.51	−65.23 ± 0.73	$p = 0.60^{\$}$
Input resistance (MΩ)	157.72 ± 5.27	164.50 ± 4.96	$p = 0.36^{\$}$	164.77 ± 6.14	158.48 ± 5.52	$p = 0.46^{\$}$
Tau (ms)	12.71 ± 0.56	13.34 ± 0.75	$p = 0.51^{\$}$	13.13 ± 0.46	14.28 ± 0.72	$p = 0.19^{\$}$
Excitatory threshold (pA)	106.21 ± 7.51	96.25 ± 7.55	$p = 0.36^{\$}$	98.55 ± 6.26	102.10 ± 8.24	$p = 0.74^{\$}$
Firing frequency 50pA	0.38 ± 0.21	0.36 ± 0.25	$F(3,115) = 1.26$, $p = 0.29$	0.03 ± 0.03	0.68 ± 0.35	$F(3,115) = 1.26$, $p = 0.29$
Firing frequency 100pA	3.24 ± 0.92	3.71 ± 0.97	$F(3,115) = 1.26$, $p = 0.29$	2 ± 0.48	3.65 ± 1.02	$F(3,115) = 1.26$, $p = 0.29$
Firing frequency 150pA	5.79 ± 1.14	6 ± 1.24	$F(3,115) = 1.26$, $p = 0.29$	4.23 ± 0.67	6.13 ± 1.26	$F(3,115) = 1.26$, $p = 0.29$
Firing frequency 200pA	7.59 ± 1.29	7.29 ± 1.24	$F(3,115) = 1.26$, $p = 0.29$	5.58 ± 0.76	8.06 ± 1.32	$F(3,115) = 1.26$, $p = 0.29$
Firing frequency 250pA	7.83 ± 1.29	7.68 ± 1.28	$F(3,115) = 1.26$, $p = 0.29$	6.13 ± 0.75	9.03 ± 1.32	$F(3,115) = 1.26$, $p = 0.29$

(Continued)

TABLE 2 (Continued)

B						
	GluN2B-wt control	GluN2B$^{+/-}$ control	*T*-test$^{\$}$/ ANOVA	GluN2B-wt Aβ	GluN2B$^{+/-}$ Aβ	*T*-test$^{\$}$/ ANOVA
Firing frequency 300pA	8.10 ± 1.28	7.39 ± 1.14	$F(3,115) = 1.26$, $p = 0.29$	6.03 ± 0.63	9.35 ± 1.30	$F(3,115) = 1.26$, $p = 0.29$
Firing frequency 350pA	7.69 ± 1.25	7 ± 1.01	$F(3,115) = 1.26$, $p = 0.29$	5.87 ± 0.59	9.16 ± 1.19	$F(3,115) = 1.26$, $p = 0.29$
Firing frequency 400pA	7.31 ± 1.16	7 ± 0.85	$F(3,115) = 1.26$, $p = 0.29$	5.68 ± 0.50	8.97 ± 1.09	$F(3,115) = 1.26$, $p = 0.29$
Sag (mV)	−11.06 ± 0.54	−12.25 ± 0.64	$p = 0.17^{\$}$	−11.02 ± 0.46	−10.24 ± 0.77	$p = 0.39^{\$}$
Sag Ratio	0.908 ± 0.004	0.897 ± 0.005	$p = 0.105^{\$}$	0.907 ± 0.003	0.913 ± 0.006	$p = 0.40^{\$}$

(A) The table compares passive and active neuronal properties of Aβ (1–42) treatment versus control peptide in either GluN2B$^{+/-}$ mice or their wt littermates. Firing frequencies evoked with currents in the range of 50 though 400pA are shown. Responses in GluN2B$^{+/-}$ mice and their wildtype littermates following treatment with Aβ or control peptide are compared. Significant effects are highlighted in bold. (B) The table compares passive and active neuronal properties in GluN2B$^{+/-}$ mice versus their wt littermates following treatment with either control peptide or Aβ (1–42). Firing frequencies evoked with currents in the range of 50 though 400pA are shown. Responses in GluNB$^{+/-}$ mice and their wildtype littermates treatment with either Aβ or control peptide are compared.

(Ashhad and Narayanan, 2016). Others have reported a more positive resting membrane potential and enhanced I_h current in the hippocampus after intracerebral Aβ-treatment (Eslamizade et al., 2015). Our finding that sag ratio was more positive after Aβ-treatment of GluN2B$^{+/-}$ mice, suggesting that GluN2B contributed to these effects.

A role for GluN2B has been described in Aβ-mediated effects in the hippocampus: The reduction in network activity and LTP that occurs following topical application of Aβ to hippocampal slices or neuronal cultures, or intracerebral treatment of rats is prevented by antagonists of GluN2B (Hu et al., 2009; Rönicke et al., 2011). It has also been reported that the enhancement of NMDAR currents and intracellular calcium levels that occur following application of Aβ are mediated by GluN2B-containing NMDAR (Li et al., 2011; Ferreira et al., 2012). Furthermore, Aβ (1–40) triggers an increase in the expression of GluN2B in hippocampal neuronal cultures (Chang et al., 2016) and the GluN2A:GluN2B ratio decreases after Aβ (1–42) application (Huang et al., 2017). Interestingly, inhibition of GluN2B-containing NMDAR prevents Aβ-mediated impairments of LTP (Rönicke et al., 2011; Huang et al., 2017). The frequency-dependency of LTP was not assessed in these studies, but our findings suggest that less potent forms of LTP that do not critically require activation of GluN2B are not affected by Aβ (1–42). This is all the more interesting given the advanced age of the mice in our study: all of the studies mentioned above used young adult animals and treatment regimes of maximally 15 days before hippocampal scrutiny.

We previously reported that the frequency of the afferent input, and impulse number it delivers, determines the recruitment of GluN2A or GluN2B subunit-containing NMDAR to LTP in the CA1 region (Ballesteros et al., 2016). Weak afferent stimulation recruits a GluN2A-dependent form of LTP that is small in magnitude and short (>4 h) in duration. By contrast, strong afferent stimulation recruited LTP that required GluN2B-containing NMDAR that was much larger in magnitude and lasted over 24 h (Ballesteros et al., 2016). The form of LTP examined in the present study had both a GluN2A and a GluN2B-dependent component, as indicated by the reduction in LTP magnitude in GluN2A and GluN2B transgenic hippocampi compared to wt littermates. Effects were more potent in GluN2A transgenics, although the increased variability in responses in the later phase of LTP in GluN2B transgenics may have masked deficits in LTP compared to controls. Although we cannot entirely rule out the possibility that LTP was successfully induced, albeit less potently, in the GluN2A$^{+/-}$ or the GluN2B$^{+/-}$ mice by non-ionotropic mechanisms, this seems unlikely. Theta-burst stimulation induces a decremental form of LTP in the mouse hippocampal slice preparation that is distinct from more robust forms of LTP induced by high frequency afferent stimulation (Novkovic et al., 2015). The recruitment of, for example, voltage-dependent calcium channels into hippocampal LTP requires very fast high frequency stimulation (Grover and Teyler, 1990; Manahan-Vaughan et al., 1998) and forms of synaptic potentiation that can be induced by activation of metabotropic glutamate (mGlu), or catecholaminergic, receptors are temporally slow to become manifest (Manahan-Vaughan and Reymann, 1995; Tse et al., 2023) and do not fit the temporal dynamics of the LTP profiles induced in our study. We did not see a complete abolishment of LTP in the GluN2A$^{+/-}$, or the GluN2B$^{+/-}$ hippocampi presumably because the remaining subunits permitted a weaker form of LTP to occur. Evidence for this has been offered by pharmacological studies that showed that LTP, short-term potentiation and forms of synaptic depression can be induced with the same afferent stimulation frequency combined with a graded degree of activation of NMDAR (Cummings et al., 1996).

Forms of LTP that are intrinsically linked to learning are enabled by weak afferent activity in the hippocampus (Kemp and Manahan-Vaughan, 2004, 2008; Hagena and Manahan-Vaughan, 2012; Hoang et al., 2021). By contrast, very strong afferent stimulation induces robust LTP that is associated with reduced learning flexibility, reduced reversal learning and an absence of differentiated neuronal encoding in the hippocampus of rats (Barnes, 1979; Barnes et al., 1994; Hoang et al., 2021). This raises the question as to the functional requirement of GluN2B-dependent LTP in adulthood. It has been reported that the expression of GluN2-subunits declines after early postnatal development (Carmignoto and Vicini, 1992), but in adult C57Bl/6 mice, we did not observe an appreciable decline in receptor expression (Beckmann et al., 2020). This would suggest that both GluN2A and GluN2B-containing NMDAR contribute to LTP in adulthood. The

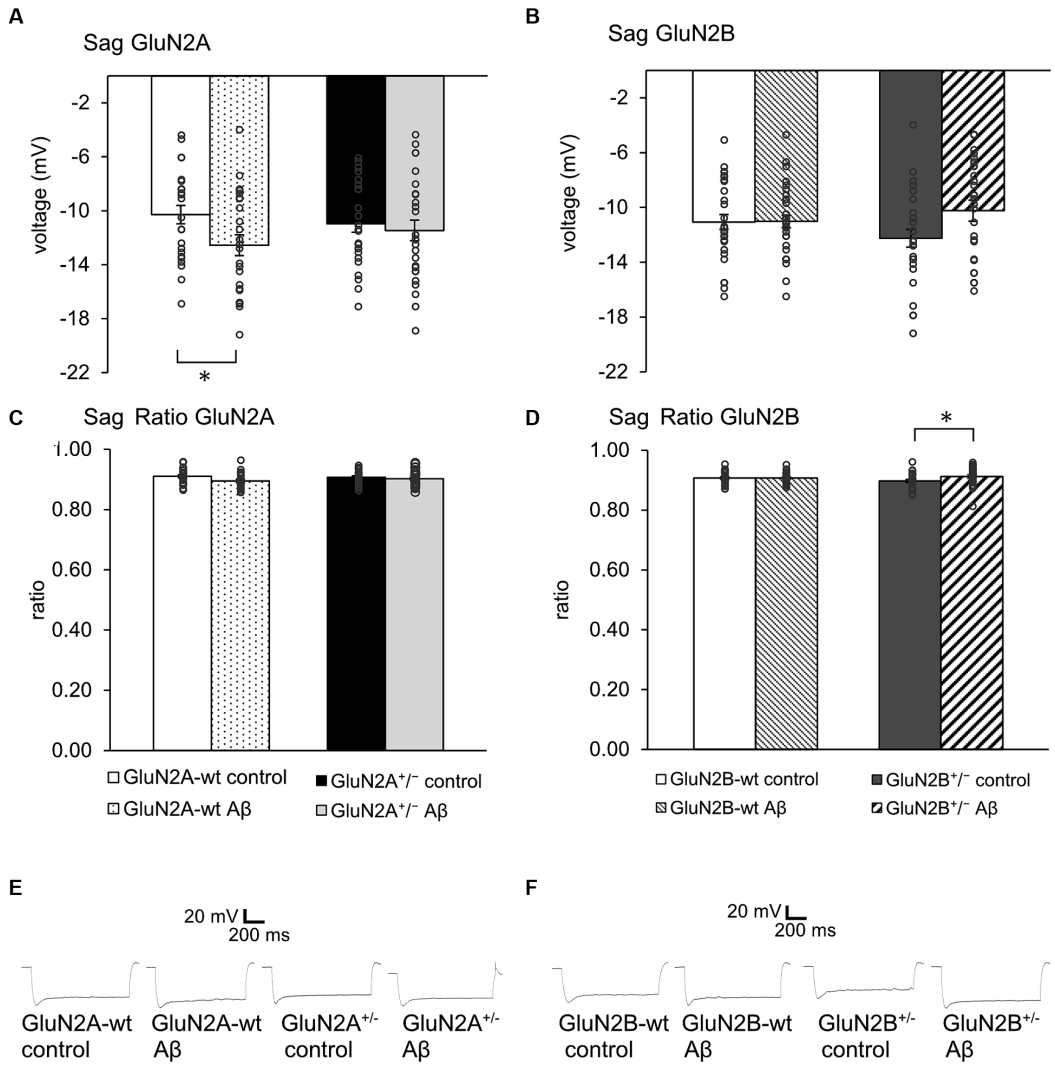

FIGURE 3
Aβ-treatment selectively altered sag in GluN2A wt littermates and GluN2B$^{+/-}$ **(A,C)**. Sag **(A)**, but not Sag ratio **(C)** was more negative in Aβ-treated wt littermates of GluN2A$^{+/-}$ mice ($N = 5$, $n = 24$) compared to control wt ($N = 5$, $n = 24$), but was unaffected in control peptide -treated GluN2A$^{+/-}$ ($N = 5$, $n = 25$) compared to oligomeric Aβ (1–42)-treated GluN2A$^{+/-}$ ($N = 5$, $n = 26$). See Tables 1, 2 for statistics. **(B,D)** No effect of Aβ-on sag **(B)** or sag ratio **(D)** was detected in wt littermates of GluN2B$^{+/-}$ mice ($N = 6$, $n = 29$; $N = 6$, $n = 31$), although Aβ-caused an increase in sag ratio **(D)**, but not in sag **(B)** in GluN2B$^{+/-}$ hippocampi ($N = 6$, $n = 31$) compared to GluN2B$^{+/-}$ controls ($N = 5$, $n = 28$). See Tables 1, 2 for statistics. **(E,F)** Representative examples of sag in control peptide and Aβ-treated GluN2A$^{+/-}$ transgenics and their wt littermates **(E)** and in control peptide and Aβ-treated GluN2B$^{+/-}$ transgenics and their wt littermates **(F)**. The circles on the error bars show the distribution of individual responses in each condition that contributed the mean effect represented by the bar.

kind of LTP (magnitude, persistency) may be determined by the kind of information that is encoded, however.

We previously reported that intracerebral treatment with oligomeric Aβ (1–42) 1 week prior to assessing LTP in 4–10 month old wildtype mice impairs the early phase of LTP (Südkamp et al., 2021). Animals in the present study were 8–15 months old at the time of treatment. Here, wildtypes showed a significant LTP impairment that extended to the later phases of plasticity. One possibility is that the increased age of the wildtypes may have caused a greater vulnerability to the debilitating effects of intracerebral Aβ-treatment. Age-dependent changes in hippocampal function have been reported (Barnes et al., 1994; Wilson et al., 2004; Twarkowski et al., 2016) that could underlie these effects. Another reason for the greater vulnerability of wildtype hippocampi in this study might be the enhanced time-period of exposure to Aβ-treatment. One cannot exclude, however, that although the background strain was identical for the wt mice in this and the abovementioned study (C57BL/6) (Sakimura et al., 1995; von Engelhardt et al., 2008; Dvoriantchikova et al., 2012), substrain-dependent differences influenced the outcome of Aβ-sensitivity. Genetic drift related to separation of breeding pools is likely to have an impact on the precise genomic identity of wildtype littermates derived from the C57BL/6 strain (Manahan-Vaughan, 2018), that could have influenced the sensitivity of the wildtypes to Aβ. For this reason, we included separate wt cohorts for both transgenic lines, whereby only wildtype littermates of either the GluN2A$^{+/-}$ or the GluN2B$^{+/-}$ were used.

The relatively mild effects of oligomeric Aβ (1–42) on neuronal responses, as detected by patch clamp in our study, corresponds to

10.3389/fnagi.2024.1377085

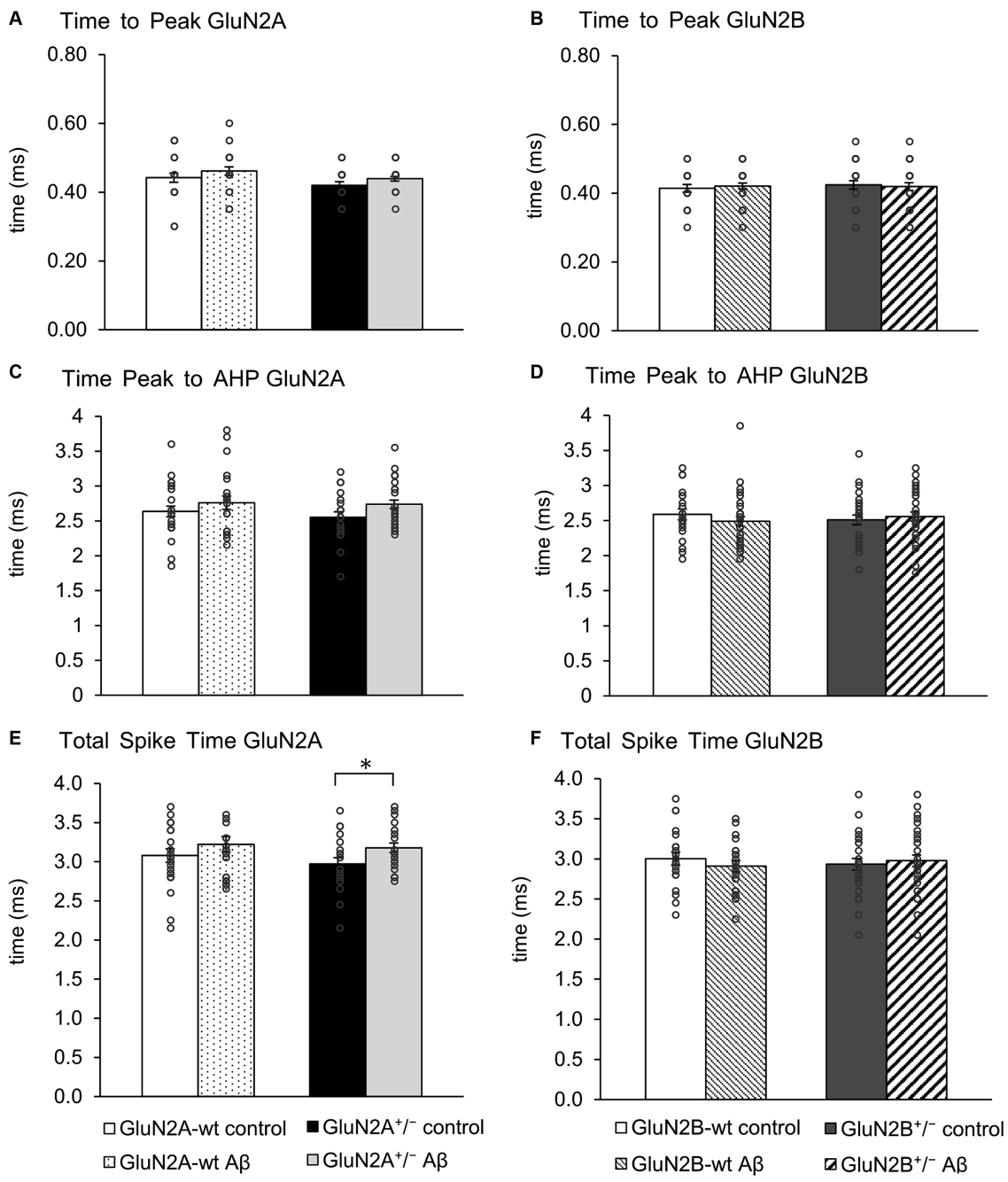

FIGURE 4
GluN2A$^{+/-}$ but not GluN2B$^{+/-}$ hippocampi showed sensitivity of spike time but not time to peak and AHP time, following Aβ-treatment. **(A,B)** Time to peak was unaffected by oligomeric Aβ (1–42)-treatment of GluN2A$^{+/-}$ **(A)** and GluN2B$^{+/-}$ mice **(B)** or their wt littermates **(A,B)** compared to control peptide-treated mice. See Table 3 for statistics. **(C,D)** The time from the peak of the action potential to the afterhyperpolarization (AHP) was not significantly increased by Aβ-treatment of GluN2A$^{+/-}$ mice ($N = 5$, $n = 25$) **(C)** compared to control peptide-treated transgenic mice ($N = 5$, $n = 20$). Wildtype littermates were unaffected ($N = 5$, $n = 25$; $N = 5$, $n = 22$) **(C)**. No significant changes in the time from the peak of the action potential to the AHP were detected in GluN2B$^{+/-}$ mice or their wt littermates after Aβ-treatment **(D)**. See Table 3 for statistics. **(E,F)** The total spike time was increased by Aβ-treatment of GluN2A$^{+/-}$ mice **(E)** compared to control peptide-treated ko mice. Wildtype littermates were unaffected **(E)**. No significant changes in total spike time occurred in GluN2B$^{+/-}$ mice or their wt littermates after Aβ-treatment **(F)**. See Table 3 for statistics. The circles on the error bars show the distribution of individual responses in each condition that contributed the mean effect represented by the bar.

reports that the peptide predominantly affects synaptic transmission and thus, dendritic responses (Shankar et al., 2008). It has been reported that application of oligomeric Aβ (1–42) onto hippocampal slices from young (P26-32) rats results in an acute increase in surface expression of the GluA1 subunit of α-amino-3-hydroxy-5-methyl-4-isoxazolepropionic acid receptors (AMPAR) (Whitcomb et al., 2015). By contrast, topical application of oligomeric Aβ to hippocampal cultures from P18 rats inhibits AMPAR trafficking (Rui et al., 2010) and reduces surface expression of AMPAR (Guntupalli et al., 2017). Reductions in GluA1 density in the

TABLE 3 Action potential properties in GluN2A$^{+/-}$ and GluN2B$^{+/-}$ mice and their wt littermates following treatment with Aβ or control peptide.

A						
	GluN2A-wt control	GluN2A-wt Aβ	*T*-Test	GluN2A$^{+/-}$ control	GluN2A$^{+/-}$ Aβ	*T*-test
AP threshold (mV)	−36.20 ± 0.88	−34.90 ± 1.11	$p = 0.37$	−35.92 ± 0.96	−36.33 ± 0.86	$p = 0.76$
Spike amplitude (mV)	92.52 ± 1.26	90.52 ± 1.88	$p = 0.38$	93.12 ± 1.10	91.61 ± 1.16	$p = 0.37$
Time to peak (ms)	0.44 ± 0.01	0.46 ± 0.01	$p = 0.298$	0.42 ± 0.01	0.44 ± 0.01	$p = 0.12$
Time peak to AHP (ms)	2.64 ± 0.08	2.76 ± 0.10	$p = 0.32$	2.55 ± 0.08	2.74 ± 0.06	$p = 0.07$
Total spike time (ms)	3.08 ± 0.09	3.22 ± 0.10	$p = 0.28$	2.97 ± 0.08	3.18 ± 0.06	**p = 0.046**
Ascending slope (mV/ms)	215.89 ± 9.4	200.5 ± 8.17	$p = 0.24$	224.87 ± 6.87	210.37 ± 4.74	$p = 0.08$
Descending slope (mV/ms)	39.27 ± 1.62	36.94 ± 1.56	$p = 0.32$	40.30 ± 1.34	36.57 ± 0.75	**p = 0.015**
Half-width (ms)	0.93 ± 0.02	0.99 ± 0.02	$p = 0.06$	0.92 ± 0.02	0.98 ± 0.02	$p = 0.052$
20%-width (ms)	1.40 ± 0.04	1.49 ± 0.03	$p = 0.054$	1.38 ± 0.03	1.48 ± 0.03	**p = 0.026**
AP peak (mV)	56.32 ± 0.71	55.63 ± 0.99	$p = 0.57$	57.20 ± 0.69	55.29 ± 0.53	**p = 0.035**

B						
	GluN2B-wt control	GluN2B-wt Aβ	*T*-test	GluN2B$^{+/-}$ control	GluN2B$^{+/-}$ Aβ	*T*-test
AP threshold (mV)	−36.73 ± 1.28	−37.74 ± 0.87	$p = 0.51$	−36.66 ± 0.84	−38.18 ± 0.87	$p = 0.23$
Spike amplitude (mV)	95.87 ± 1.82	94.52 ± 1.24	$p = 0.53$	94.28 ± 1.46	96.88 ± 1.26	$p = 0.19$
Time to peak (ms)	0.41 ± 0.01	0.42 ± 0.01	$p = 0.64$	0.42 ± 0.01	0.42 ± 0.01	$p = 0.78$
Time peak to AHP (ms)	2.59 ± 0.07	2.49 ± 0.07	$p = 0.35$	2.51 ± 0.07	2.56 ± 0.07	$p = 0.63$
Total spike time (ms)	3.00 ± 0.08	2.91 ± 0.07	$p = 0.399$	2.93 ± 0.07	2.98 ± 0.07	$p = 0.68$
Ascending slope (mV/ms)	236.92 ± 10.84	229.35 ± 7.83	$p = 0.57$	229.24 ± 9.55	236.99 ± 8.03	$p = 0.54$
Descending slope (mV/ms)	41.42 ± 1.50	42.06 ± 1.26	$p = 0.75$	41.66 ± 1.38	41.75 ± 1.21	$p = 0.96$
Half-width (ms)	0.91 ± 0.03	0.88 ± 0.01	$p = 0.42$	0.92 ± 0.02	0.93 ± 0.03	$p = 0.69$
20%-width (ms)	1.35 ± 0.04	1.32 ± 0.02	$p = 0.48$	1.37 ± 0.03	1.39 ± 0.04	$p = 0.68$
AP peak (mV)	59.14 ± 0.92	56.78 ± 0.70	**p = 0.048**	57.62 ± 0.83	58.70 ± 0.70	$p = 0.33$

(A) The table shows action potential properties of GluN2A$^{+/-}$ mice and their wt littermates, after control peptide treatment or treatment with Aβ. AP, Action potential. Significant effects are highlighted in bold. (B) The table shows action potential properties of GluN2B$^{+/-}$ mice and their wt littermates, after control peptide treatment or treatment with Aβ. AP, Action potential. Significant effects are highlighted in bold.

hippocampus have also been reported 30 days after intracerebral inoculation of 18 month old mice with Aβ (1–42) in a dose of 20 μM (Yeung et al., 2020). Scrutiny of the stimulus–response relationship of wildtype 8–15 month old mice that had been treated intracerebrally 4–5 weeks previously with 10 μM oligomeric Aβ (1–42) did not reveal any significant effects. The absence of deficits in the stimulus–response relationship that would indicate that AMPAR density had declined in Aβ (1–42)-treated wildtypes, may reflect differences in the oligomer doses used these two studies, or may indicate that although AMPAR density might have declined in the Aβ (1–42)-treated mice, this did not have a functional impact on synaptic transmission.

The maintenance of later phases of LTP beginning at around 90 min post-induction, are supported by phospholipase -C coupled (group 1) receptors (Hagena and Manahan-Vaughan, 2022; Mukherjee and Manahan-Vaughan, 2023). Group 1 mGlu receptors can functionally interact with NMDAR and alter NMDAR currents (Rosenbrock et al., 2010). Correspondingly pharmacological antagonists of group 1 mGlu receptors can alter the induction profile of hippocampal LTP (Neyman and Manahan-Vaughan, 2008). Aberrant mGlu5 receptor signaling is triggered by interactions of the receptor with Aβ (1–42) (Haas and Strittmatter, 2016) and mGlu5 receptors contribute to impairments of hippocampal LTP in 8–11 week old rats that are caused by acute cerebral treatment with Aβ (1–42) (Wang et al., 2004; Hu et al., 2014). Others have reported that Aβ (1–42) can form a complex with GluN2B and mGlu1 receptors (Taniguchi et al., 2022) and that mGlu5 receptors can bind with prion protein that serves as a target for Aβ (1–42) (Hu et al., 2014). We did not see any exacerbation of LTP deficits in GluN2A$^{+/-}$ or the

10.3389/fnagi.2024.1377085

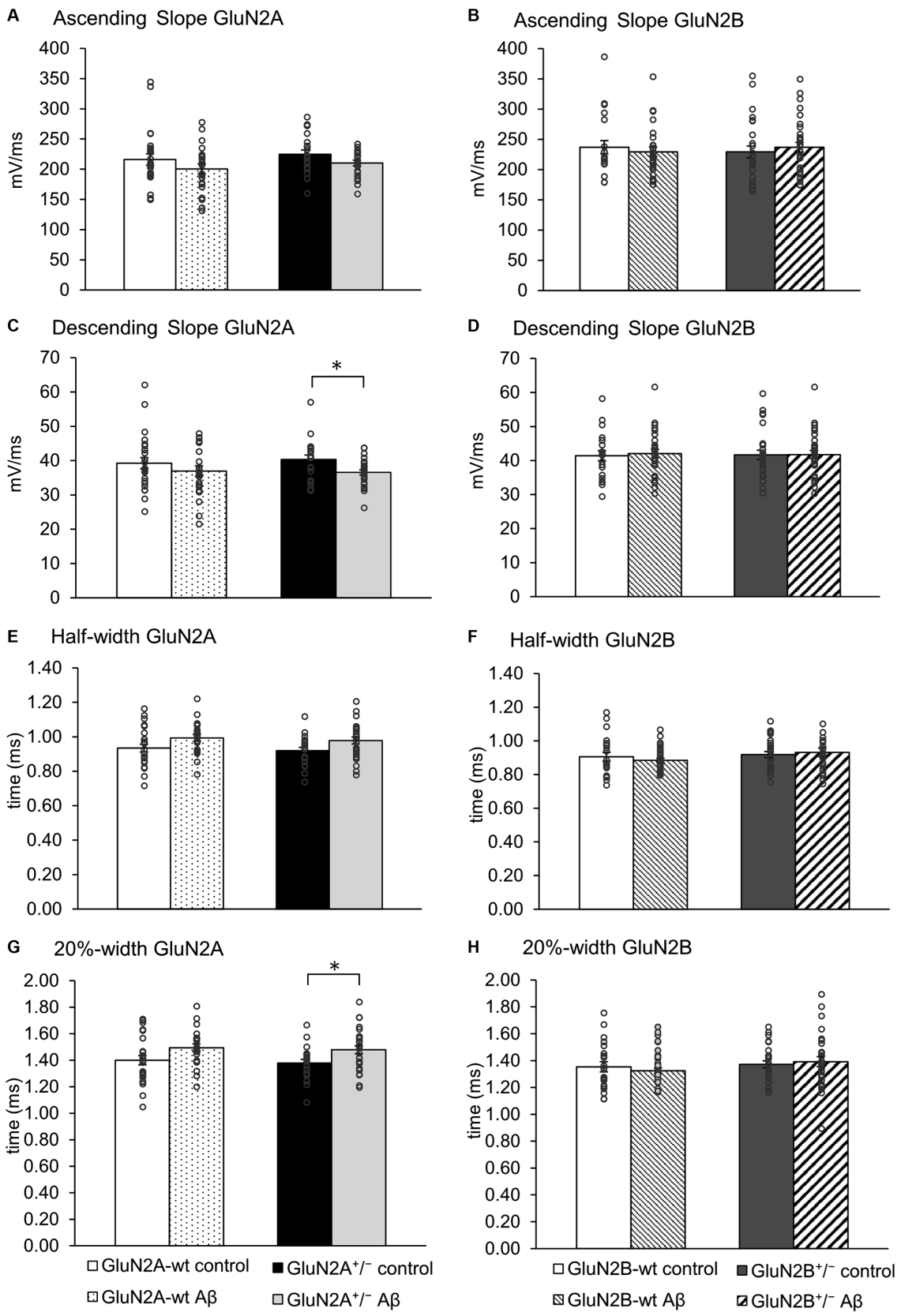

FIGURE 5
The action potential profile was altered in GluN2A$^{+/-}$, but not GluN2B$^{+/-}$ hippocampi following Aβ-treatment. **(A,B)** The ascending slope of the action potential (AP) was unaffected by Aβ-treatment in any of the groups. See Table 3 for statistics. **(C,D)** Aβ-treatment decreased the descending AP slope of GluN2A$^{+/-}$ transgenics (N=5, n=25), compared to control GluN2A$^{+/-}$ hippocampi (N=5, n=20) **(C)**. The descending slope **(D)** of the AP was not altered following Aβ-treatment of GluN2B$^{+/-}$ transgenics, or their wt littermates compared to treatment with control peptide. **(E,F)** Aβ-treatment had no effect

(Continued)

FIGURE 5 (Continued)

on the half-width of the AP in GluN2A$^{+/-}$ **(E)** and GluN2B$^{+/-}$ transgenics **(F)**, or their wt littermates compared to treatment with control peptide. See Table 3 for statistics. **(G,H)** Following Aβ-treatment, the 20% width **(G)** of the AP was increased in GluN2A$^{+/-}$ mice compared to control peptide-treated transgenics. GluN2A wt littermates exhibited an unchanged 20%-width **(G)** after Aβ-treatment compared to control wt. Aβ-treatment had no effect on the 20% width of the AP in GluN2B$^{+/-}$ transgenics, or their wt littermates compared to treatment with control peptide **(H)**. See Table 3 for statistics. The circles on the error bars show the distribution of individual responses in each condition that contributed the mean effect represented by the bar.

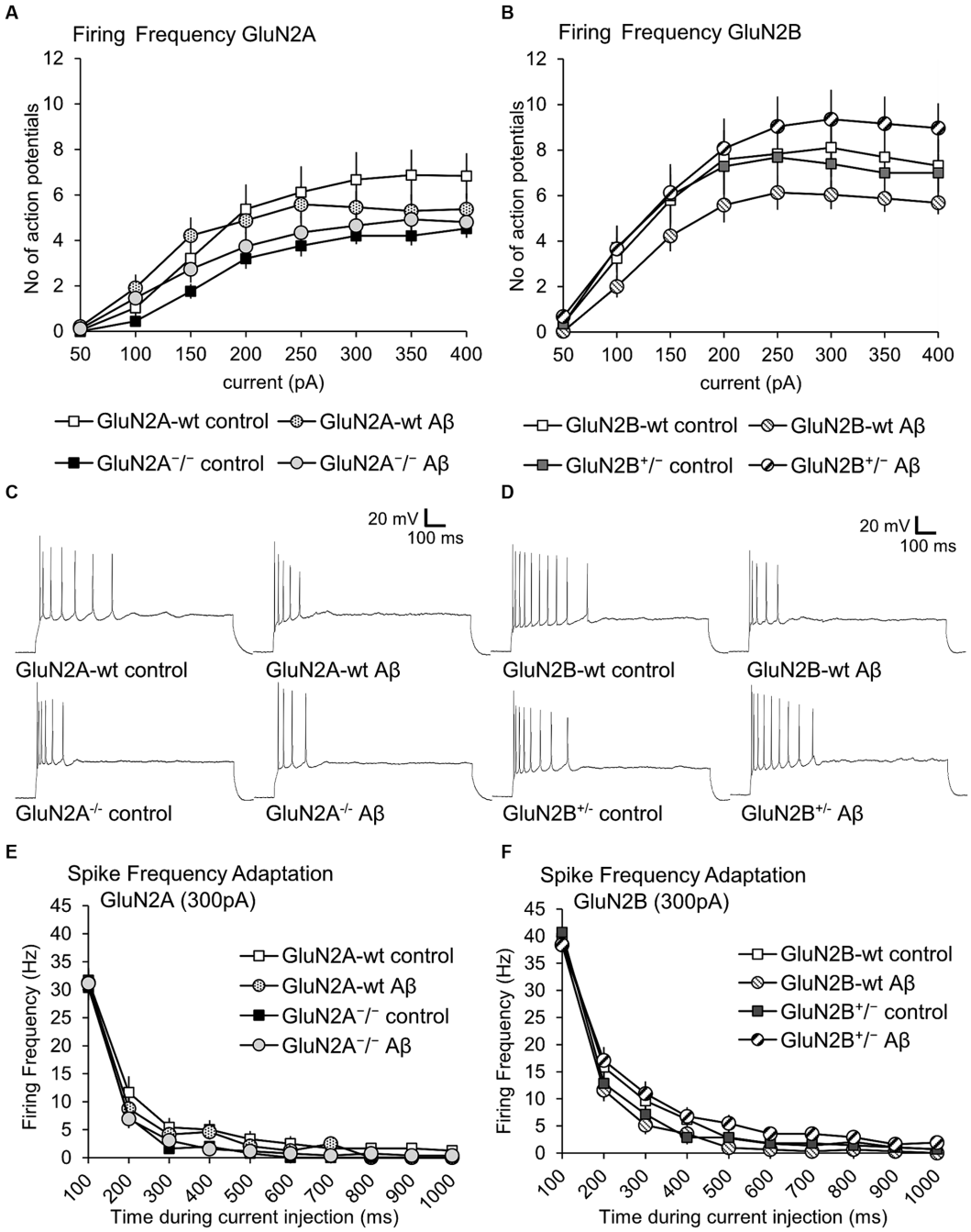

FIGURE 6

Firing frequency was not altered by Aβ-treatment of GluN2A$^{+/-}$ mice, GluN2B$^{+/-}$ mice and their wt littermates. **(A,B)** Firing frequency (FF) was not altered in control peptide-treated GluN2A$^{+/-}$ ($N = 5$, $n = 25$) or GluN2B$^{+/-}$ ($N = 5$, $n = 28$) transgenics compared to their wildtype (wt) littermates ($N = 5$, $n = 24$; $N = 6$, $n = 29$). See Tables 1, 2 for statistics. **(C)** Analog examples of action potential trains by a current intensity of 300pA in control peptide–treated wildtype (wt) littermates of GluN2A$^{+/-}$ mice (top left) and Aβ-treated wt littermates (top right), as well as control peptide–treated GluN2A$^{+/-}$ mice (bottom left), and Aβ-treated GluN2A$^{+/-}$mice (bottom right). **(D)** Analog examples of action potential trains by a current intensity of 300pA in control peptide–treated wildtype (wt) littermates of GluN2B$^{+/-}$ mice (top left) and Aβ-treated wt littermates (top right), as well as control peptide–treated GluN2B$^{+/-}$ mice (bottom left), and Aβ-treated GluN2B$^{+/-}$ mice (bottom right). **(E,F)** Spike frequency adaptation at 300 pA was not altered in control peptide-treated GluN2A$^{+/-}$ ($N = 5$, $n = 25$) or GluN2B$^{+/-}$ ($N = 5$, $n = 28$) transgenics compared to their wildtype (wt) littermates ($N = 5$, $n = 24$; $N = 6$, $n = 29$).

TABLE 4 Summary of effects of oligomeric Aβ (1–42) or control peptide-treatment on passive and active neuronal membrane properties of hippocampal pyramidal cells.

	Aβ versus control peptide				Control versus control		Aβ versus Aβ	
	GluN2A wt × wt	GluN2A ko × ko	GluN2B wt × wt	GluN2B ko × ko	GluN2A wt × ko	GluN2B wt × ko	GluN2A wt × ko	GluN2B wt × ko
Resting potential	–	↑	–	–	–	–	–	–
Input resistance	↑	–	–	–	–	–	–	–
Excitatory threshold	–	–	–	–	–	–	–	–
Sag	↑	–	–	–	–	–	–	–
Sag ratio	–	–	–	↑	–	–	–	–
Time to peak	–	–	–	–	–	–	–	–
Peak to AHP	–	–	–	–	–	–	–	–
Total spike time	–	↑	–	–	–	–	–	–
Ascending slope	–	–	–	–	–	–	–	–
Descending slope	–	↓	–	–	–	–	–	–
Half-width	–	–	–	–	–	–	–	–
20%-width	–	↑	–	–	–	–	–	–
Firing frequency	–	–	–	–	–	–	–	–

In all cases, the upward-pointing arrows indicate an increase, and the downward-pointing arrows indicate a decrease in values in the control condition. A dash signifies no effect. AHP, afterhyperpolarization.

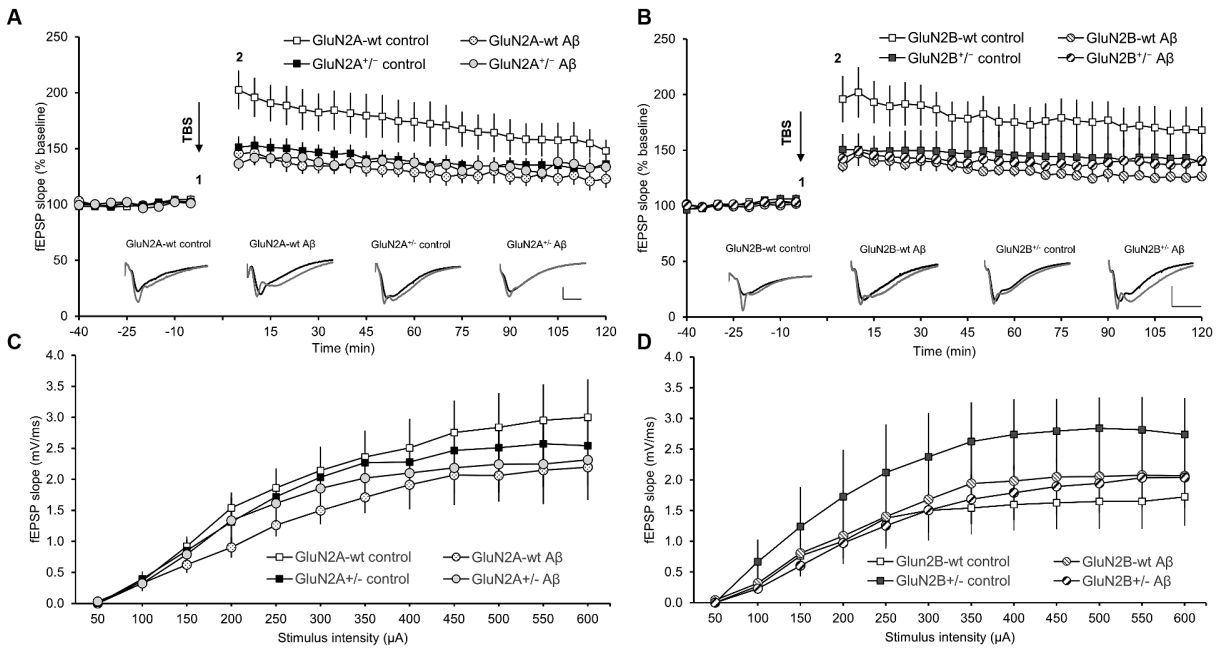

FIGURE 7
Deficits in LTP that were elicited in wild-type hippocampi by oligomeric Aβ (1–42) were absent in GluN2A$^{-/+}$ and GluN2B$^{-/+}$ hippocampi. The stimulus–response relationship is unaffected transgenic alteration or Aβ (1–42)-treatment. **(A,B)** Four to 5 weeks after Aβ–treatment, the early phase of hippocampal LTP was significantly impaired compared to control peptide-treated wt littermates of GluN2A$^{+/-}$ **(A)** or GluN2B$^{+/-}$-transgenic mice **(B)**. By contrast, LTP in GluN2A$^{+/-}$ **(A)** or GluN2B$^{+/-}$ transgenic hippocampi **(B)** was unaffected by Aβ–treatment, with responses being equivalent in Aβ–treated tg compared to control peptide-treated tg or Aβ–treated wt slices. Insets in A and B show analog examples of potentials evoked 5 min prior to (1) and 5 min after (2) theta burst stimulation (TBS). Scale bars represent 1 mV in the vertical, and 5 ms in the horizontal, axis. The stimulus–response relationship (obtained in steps ranging from 50 through 600 μA) was not significantly different in GluN2A$^{+/-}$ **(C)** or GluN2B$^{+/-}$ transgenic hippocampi **(D)**, compared to their wildtype littermates, after treatment with oligomeric Aβ (1–42) or control peptide.

GluN2B$^{+/-}$ mice that were treated with Aβ (1–42). This raises the interesting question as to whether the knockdown of NMDAR subunits left fewer interaction partners for the putative creation of an Aβ-prion protein-mGlu5 complex (Hu et al., 2014), or an Aβ-GluN2B-mGlu1 complex (Taniguchi et al., 2022), that would otherwise serve to further disrupt LTP in the transgenics.

5 Conclusion

In conclusion, this study shows that knockdown of GluN2A or GluN2B did not elicit substantial changes in neuronal properties within the hippocampus of aging (8–15 month old) mice. Nonetheless, loss of GluN2A appeared to result in a greater degree of change in neuronal properties suggesting that this subunit is more relevant than GluN2B for neuronal homeostasis in the aging hippocampus. Intracerebral treatment with oligomeric Aβ (1–42) 4–5 weeks before testing resulted in some changes in neuronal properties, but these were mostly apparent in GluN2A transgenics and a comparison of Aβ-mediated effects in the GluN2 transgenics and their wt littermates showed that responses were equivalent, suggesting that the knockdown of the subunits only slightly increased the vulnerability of the hippocampus to oligomeric Aβ (1–42). A similar profile was apparent with regard to hippocampal LTP: knockdown of GluN2A or GluN2B significantly impaired LTP in wt littermates. Treatment with oligomeric Aβ (1–42) resulted in an impaired LTP in wt littermates that was equivalent in magnitude to LTP in GluN2 transgenics. This impaired LTP was not debilitated further by Aβ (1–42)-treatment. The findings of this study show that although the aging hippocampus was affected by the intracerebral presence of oligomeric Aβ (1–42), and although knockdown of GluN2A or GluN2B impaired LTP, changes in the composition of the NMDAR did not contribute appreciably to the effects on neuronal properties or LTP caused by oligomeric Aβ (1–42). In sum, a loss of GluN2 subunit content in the hippocampus did not increase the vulnerability of this structure to the debilitating effects of oligomeric Aβ (1–42).

Data availability statement

The raw data supporting the conclusions of this article will be made available by the authors, without undue reservation.

Ethics statement

The animal study was approved by Landesamt für Arbeitsschutz, Naturschutz, Umweltschutz und Verbraucherschutz, NRW, Germany. The study was conducted in accordance with the local legislation and institutional requirements.

Author contributions

NS: Formal analysis, Investigation, Methodology, Writing – review & editing, Data curation. OS: Formal analysis, Investigation, Methodology, Writing – review & editing, Data curation. DM-V: Conceptualization, Formal analysis, Funding acquisition, Methodology, Resources, Supervision, Writing – original draft, Writing – review & editing.

Funding

The author(s) declare financial support was received for the research, authorship, and/or publication of this article. This work was supported by a grant from the German Research Foundation (Deutsche Forschungsgemeinschaft, DFG) to DM-V (SFB 874/B1, project ID: 122679504).

Acknowledgments

We gratefully thank Stephan Jansen, Jens Colitti-Klausnitzer, and Beate Krenzek and Dr. Hanna von Preetzmann for technical assistance, and Nadine Kollosch and Petra Küsener for animal care. The breeding line for the GluN2A-ko was a kind gift from Professor Masayoshi Mishina, Brain Science Laboratory, Research Organization of Science and Technology, Ritsumeikan University, Japan to DM-V. The breeding line for the GluN2B-ko was a kind gift from Professor Hannah Monyer, University of Heidelberg, Germany to DM-V.

Conflict of interest

The authors declare that the research was conducted in the absence of any commercial or financial relationships that could be construed as a potential conflict of interest.

The author(s) declared that they were an editorial board member of Frontiers, at the time of submission. This had no impact on the peer review process and the final decision.

Publisher's note

References

Abbott, J. J., Howlett, D. R., Francis, P. T., and Williams, R. J. (2008). Abeta(1–42) modulation of Akt phosphorylation via alpha7 nAChR and NMDA receptors. *Neurobiol. Aging* 29, 992–1001. doi: 10.1016/j.neurobiolaging.2007.01.003

Ashhad, S., and Narayanan, R. (2016). Active dendrites regulate the impact of gliotransmission on rat hippocampal pyramidal neurons. *Proc. Natl. Acad. Sci. USA* 113, E3280–E3289. doi: 10.1073/pnas.1522180113

Ballesteros, J. J., Buschler, A., Köhr, G., and Manahan-Vaughan, D. (2016). Afferent input selects NMDA receptor subtype to determine the persistency of hippocampal LTP in freely behaving mice. *Front. Behav. Neurosci.* 8:33. doi: 10.3389/fnsyn.2016.00033

Balleza-Tapia, H., Huanosta-Gutiérrez, A., Márquez-Ramos, A., Arias, N., and Peña, F. (2010). Amyloid β oligomers decrease hippocampal spontaneous network activity in an age-dependent manner. *Curr. Alzheimer Res.* 7, 453–462. doi: 10.2174/156720510791383859

Banerjee, A., Meredith, R. M., Rodríguez-Moreno, A., Mierau, S. B., Auberson, Y. P., and Paulsen, O. (2009). Double dissociation of spike timing-dependent potentiation and depression by subunit-preferring NMDA receptor antagonists in mouse barrel cortex. *Cereb. Cortex* 19, 2959–2969. doi: 10.1093/cercor/bhp067

Barnes, C. A. (1979). Memory deficits associated with senescence: a neurophysiological and behavioral study in the rat. *J. Comp. Physiol. Psychol.* 93, 74–104. doi: 10.1037/h0077579

Barnes, C. A., Jung, M. W., McNaughton, B. L., Korol, D. L., Andreasson, K., and Worley, P. F. (1994). LTP saturation and spatial learning disruption: effects of task variables and saturation levels. *J. Neurosci.* 14, 5793–5806. doi: 10.1523/JNEUROSCI.14-10-05793.1994

Bartlett, T. E., Bannister, N. J., Collett, V. J., Dargan, S. L., Massey, P. V., Bortolotto, Z. A., et al. (2007). Differential roles of NR2A and NR2B-containing NMDA receptors in LTP and LTD in the CA1 region of two-week old rat hippocampus. *Neuropharmacology* 52, 60–70. doi: 10.1016/j.neuropharm.2006.07.013

Beckmann, D., Feldmann, M., and Manahan-Vaughan, D. (2020). Hippocampal synaptic plasticity and plasticity-related neurotransmitter receptor expression are profoundly altered by gradual loss of hearing ability. *Cereb. Cortex* 30, 4581–4596. doi: 10.1093/cercor/bhaa061

Berberich, S., Jensen, V., Hvalby, O., Seeburg, P. H., and Kohr, G. (2007). The role of NMDAR subtypes and charge transfer during hippocampal LTP induction. *Neuropharmacology* 52, 77–86. doi: 10.1016/j.neuropharm.2006.07.016

Berberich, S., Punnakkal, P., Jensen, V., Pawlak, V., Seeburg, P. H., Hvalby, O., et al. (2005). Lack of NMDA receptor subtype selectivity for hippocampal long-term potentiation. *J. Neurosci.* 25, 6907–6910. doi: 10.1523/JNEUROSCI.1905-05.2005

Carmignoto, G., and Vicini, S. (1992). Activity-dependent decrease in NMDA receptor responses during development of the visual cortex. *Science* 258, 1007–1011. doi: 10.1126/science.1279803

Chang, L., Zhang, Y., Liu, J., Song, Y., Lv, A., Li, Y., et al. (2016). Differential regulation of N-methyl-D-aspartate receptor subunits is an early event in the actions of soluble amyloid-β (1-40) oligomers on hippocampal neurons. *J. Alzheimers Dis.* 51, 197–212. doi: 10.3233/JAD-150942

Chen, W. S., and Bear, M. F. (2007). Activity-dependent regulation of NR2B translation contributes to metaplasticity in mouse visual cortex. *Neuropharmacology* 52, 200–214. doi: 10.1016/j.neuropharm.2006.07.003

Clarke, R. J., Glasgow, N. G., and Johnson, J. W. (2013). Mechanistic and structural determinants of NMDA receptor voltage-dependent gating and slow Mg2+ unblock. *J. Neurosci.* 33, 4140–4150. doi: 10.1523/JNEUROSCI.3712-12.2013

Clarke, R. J., and Johnson, J. W. (2006). NMDA receptor NR2 subunit dependence of the slow component of magnesium unblock. *J. Neurosci.* 26, 5825–5834. doi: 10.1523/JNEUROSCI.0577-06.2006

Cowburn, R. F., Wiehager, B., Trief, E., Li-Li, M., and Sundstrom, E. (1997). Effects of beta-amyloid-(25–35) peptides on radioligand binding to excitatory amino acid receptors and voltage-dependent calcium channels: evidence for a selective affinity for the glutamate and glycine recognition sites of the NMDA receptor. *Neurochem. Res.* 22, 1437–1442. doi: 10.1023/A:1021942109490

Cummings, J. A., Mulkey, R. M., Nicoll, R. A., and Malenka, R. C. (1996). Ca2+ signaling requirements for long-term depression in the hippocampus. *Neuron* 16, 825–833. doi: 10.1016/s0896-6273(00)80102-6

Danysz, W., and Parsons, C. G. (2012). Alzheimer's disease, β-amyloid, glutamate, NMDA receptors and memantine – searching for the connections. *Br. J. Pharmacol.* 167, 324–352. doi: 10.1111/j.1476-5381.2012.02057.x

De Felice, F. G., Velasco, P. T., Lambert, M. P., Viola, K., Fernandez, S. J., Ferreira, S. T., et al. (2007). Abeta oligomers induce neuronal oxidative stress through an N-methyl-D-aspartate receptor-dependent mechanism that is blocked by the Alzheimer drug memantine. *J. Biol. Chem.* 282, 11590–11601. doi: 10.1074/jbc.M607483200

Deshpande, A., Kawai, H., Metherate, R., Glabe, C. G., and Busciglio, J. (2009). A role for synaptic zinc in activity-dependent Abeta oligomer formation and accumulation at excitatory synapses. *J. Neurosci.* 29, 4004–4015. doi: 10.1523/JNEUROSCI.5980-08.2009

Dingledine, R., Borges, K., Bowie, D., and Traynelis, S. F. (1999). The glutamate receptor ion channels. *Pharmacol. Rev.* 51, 7–61

Domingues, A., Almeida, S., da Cruz e Silva, E. F., Oliveira, C. R., and Rego, A. C. (2007). Toxicity of beta-amyloid in HEK293 cells expressing NR1/NR2A or NR1/NR2B N-methyl-D-aspartate receptor subunits. *Neurochem. Int.* 50, 872–880. doi: 10.1016/j.neuint.2007.03.001

Dubovyk, V., and Manahan-Vaughan, D. (2018). Less means more: the magnitude of synaptic plasticity along the hippocampal dorso-ventral axis is inversely related to the expression levels of plasticity-related neurotransmitter receptors. *Hippocampus* 28, 136–150. doi: 10.1002/hipo.22816

Dvoriantchikova, G., Ivanov, D., Barakat, D., Grinberg, A., Wen, R., Slepak, V. Z., et al. (2012). Genetic ablation of Pannexin1 protects retinal neurons from ischemic injury. *PLoS One* 7:e31991. doi: 10.1371/journal.pone.0031991

Edwards, F. A. (2019). A unifying hypothesis for Alzheimer's disease: from plaques to neurodegeneration. *Trends Neurosci.* 42, 310–322. doi: 10.1016/j.tins.2019.03.003

Erreger, K., Dravid, S. M., Banke, T. G., Wyllie, D. J. A., and Traynelis, S. F. (2005). Subunit-specific gating controls rat NR1/NR2A and NR1/NR2B NMDA channel kinetics and synaptic signalling profiles. *J. Physiol.* 563, 345–358. doi: 10.1113/jphysiol.2004.080028

Eslamizade, M. J., Saffarzadeh, F., Mousavi, S. M., Meftahi, G. H., Hosseinmardi, N., Mehdizadeh, M., et al. (2015). Alterations in CA1 pyramidal neuronal intrinsic excitability mediated by Ih channel currents in a rat model of amyloid beta pathology. *Neuroscience* 305, 279–292. doi: 10.1016/j.neuroscience.2015.07.087

Falcón-Moya, R., Pérez-Rodríguez, M., Prius-Mengual, J., Andrade-Talavera, Y., Arroyo-García, L. E., Pérez-Artés, R., et al. (2020). Astrocyte-mediated switch in spike timing-dependent plasticity during hippocampal development. *Nat. Commun.* 11:4388. doi: 10.1038/s41467-020-18024-4

Ferreira, I. L., Bajouco, L. M., Mota, S. I., Auberson, Y. P., Oliveira, C. R., and Rego, A. C. (2012). Amyloid beta peptide 1-42 disturbs intracellular calcium homeostasis through activation of GluN2B-containing N-methyl-d-aspartate receptors in cortical cultures. *Cell Calcium* 51, 95–106. doi: 10.1016/j.ceca.2011.11.008

Fukumoto, H., Tokuda, T., Kasai, T., Ishigami, N., Hidaka, H., Kondo, M., et al. (2010). High-molecular-weight beta-amyloid oligomers are elevated in cerebrospinal fluid of Alzheimer patients. *FASEB J.* 24, 2716–2726. doi: 10.1096/fj.09-150359

Grover, L. M., and Teyler, T. J. (1990). Two components of long-term potentiation induced by different patterns of afferent activation. *Nature* 347, 477–479. doi: 10.1038/347477a0

Guntupalli, S., Jang, S. E., Zhu, T., Huganir, R. L., Widagdo, J., and Anggono, V. (2017). GluA1 subunit ubiquitination mediates amyloid-β-induced loss of surface α-amino-3-hydroxy-5-methyl-4-isoxazolepropionic acid (AMPA) receptors. *J. Biol. Chem.* 292, 8186–8194. doi: 10.1074/jbc.M116.774554

Haas, L. T., and Strittmatter, S. M. (2016). Oligomers of amyloid β prevent physiological activation of the cellular prion protein-metabotropic glutamate receptor 5 complex by glutamate in Alzheimer disease. *J. Biol. Chem.* 291, 17112–17121. doi: 10.1074/jbc.M116.720664

Hagena, H., and Manahan-Vaughan, D. (2012). Learning-facilitated long-term depression and long-term potentiation at mossy fiber-CA3 synapses requires activation of β-adrenergic receptors. *Front. Integr. Neurosci.* 6:23. doi: 10.3389/fnint.2012.00023

Hagena, H., and Manahan-Vaughan, D. (2022). Role of mGlu5 in persistent forms of hippocampal synaptic plasticity and the encoding of spatial experience. *Cells* 11:3352. doi: 10.3390/cells11213352

Henneberger, C., Papouin, T., Oliet, S. H., and Rusakov, D. A. (2010). Long-term potentiation depends on release of D-serine from astrocytes. *Nature* 463, 232–236. doi: 10.1038/nature08673

Hirai, H., Kirsch, J., Laube, B., Betz, H., and Kuhse, J. (1996). The glycine binding site of the N-methyl-D-aspartate receptor subunit NR1: identification of novel determinants of co-agonist potentiation in the extracellular M3-M4 loop region. *Proc. Natl. Acad. Sci. USA* 93, 6031–6036. doi: 10.1073/pnas.93.12.6031

Hoang, T. H., Böge, J., and Manahan-Vaughan, D. (2021). Hippocampal subfield-specific Homer1a expression is triggered by learning-facilitated long-term potentiation and long-term depression at medial perforant path synapses. *Hippocampus.* 31, 897–915. doi: 10.1002/hipo.23333

Honnuraiah, S., and Narayanan, R. (2013). A calcium-dependent plasticity rule for HCN channels maintains activity homeostasis and stable synaptic learning. *PLoS One* 8:e55590. doi: 10.1371/journal.pone.0055590

Hu, N. W., Klyubin, I., Anwyl, R., and Rowan, M. J. (2009). GluN2B subunit-containing NMDA receptor antagonists prevent Abeta-mediated synaptic plasticity disruption in vivo. *Proc. Natl. Acad. Sci. USA* 106, 20504–20509. doi: 10.1073/pnas.0908083106

Hu, N. W., Nicoll, A. J., Zhang, D., Mably, A. J., O'Malley, T., Purro, S. A., et al. (2014). mGlu5 receptors and cellular prion protein mediate amyloid-β-facilitated synaptic long-term depression in vivo. *Nat. Commun.* 5:3374. doi: 10.1038/ncomms4374

Huang, Y., Shen, W., Su, J., Cheng, B., Li, D., Liu, G., et al. (2017). Modulating the balance of synaptic and Extrasynaptic NMDA receptors shows positive effects against amyloid-β-induced neurotoxicity. *J. Alzheimers Dis.* 57, 885–897. doi: 10.3233/JAD-161186

Kalweit, A. N., Yang, H., Colitti-Klausnitzer, J., Fülöp, L., Bozsó, Z., Penke, B., et al. (2015). Acute intracerebral treatment with amyloid-beta (1-42) alters the profile of neuronal oscillations that accompany LTP induction and results in impaired LTP in freely behaving rats. *Front. Behav. Neurosci.* 9:103. doi: 10.3389/fnbeh.2015.00103

Kemp, A., and Manahan-Vaughan, D. (2004). Hippocampal long-term depression and long-term potentiation encode different aspects of novelty acquisition. *Proc. Natl. Acad. Sci. USA* 101, 8192–8197. doi: 10.1073/pnas.0402650101

Kemp, A., and Manahan-Vaughan, D. (2008). The hippocampal CA1 region and dentate gyrus differentiate between environmental and spatial feature encoding through long-term depression. *Cereb. Cortex* 18, 968–977. doi: 10.1093/cercor/bhm136

Khodadadi, D., Gharakhanlou, R., Naghdi, N., Salimi, M., Azimi, M., Shahed, A., et al. (2018). Treadmill Exercise Ameliorates Spatial Learning and Memory Deficits Through Improving the Clearance of Peripheral and Central Amyloid-Beta Levels. *Neurochem. Res.* 43, 1561–1574. doi: 10.1007/s11064-018-2571-2

Klyubin, I., Walsh, D. M., Lemere, C. A., Cullen, W. K., Shankar, G. M., Betts, V., et al. (2005). Amyloid beta protein immunotherapy neutralizes Abeta oligomers that disrupt synaptic plasticity in vivo. *Nat. Med.* 11, 556–561. doi: 10.1038/nm1234

Köhr, G., Jensen, V., Koester, H. J., Mihaljevic, A. L., Utvik, J. K., Kvello, A., et al. (2003). Intracellular domains of NMDA receptor subtypes are determinants for long-term potentiation induction. *J. Neurosci.* 23, 10791–10799. doi: 10.1523/JNEUROSCI.23-34-10791.2003

Lacor, P. N., Buniel, M. C., Furlow, P. W., Clemente, A. S., Velasco, P. T., Wood, M., et al. (2007). Abeta oligomer-induced aberrations in synapse composition, shape, and density provide a molecular basis for loss of connectivity in Alzheimer's disease. *J. Neurosci.* 27, 796–807. doi: 10.1523/JNEUROSCI.3501-06.2007

Laube, B., Hirai, H., Sturgess, M., Betz, H., and Kuhse, J. (1997). Molecular determinants of agonist discrimination by NMDA receptor subunits: analysis of the glutamate binding site on the NR2B subunit. *Neuron* 18, 493–503. doi: 10.1016/S0896-6273(00)81249-0

Lei, M., Xu, H., Li, Z., Wang, Z., O'Malley, T. T., Zhang, D., et al. (2016). Soluble Aβ oligomers impair hippocampal LTP by disrupting glutamatergic/GABAergic balance. *Neurobiol. Dis.* 85, 111–121. doi: 10.1016/j.nbd.2015.10.019

Li, S., Hong, S., Shepardson, N. E., Walsh, D. M., Shankar, G. M., and Selkoe, D. (2009). Soluble oligomers of amyloid Beta protein facilitate hippocampal long-term depression by disrupting neuronal glutamate uptake. *Neuron* 62, 788–801. doi: 10.1016/j.neuron.2009.05.012

Li, S., Jin, M., Koeglsperger, T., Shepardson, N. E., Shankar, G. M., and Selkoe, D. J. (2011). Soluble Aβ oligomers inhibit long-term potentiation through a mechanism involving excessive activation of extrasynaptic NR2B-containing NMDA receptors. *J. Neurosci.* 31, 6627–6638. doi: 10.1523/JNEUROSCI.0203-11.2011

Malenka, R. C., Kauer, J. A., Zucker, R. S., and Nicoll, R. A. (1988). Postsynaptic calcium is sufficient for potentiation of hippocampal synaptic transmission. *Science* 242, 81–84. doi: 10.1126/science.2845577

Manahan-Vaughan, D. (ed.). (2018). "Special considerations when using mice for electrophysiology and long-term studies of hippocampal synaptic plasticity during behaviour" in *Handbook of in vivo Neural Plasticity Techniques, A Systems Neuroscience Approach to the Neural Basis of Memory and Cognition* (London, U.K: Academic Press).

Manahan-Vaughan, D., Braunewell, K. H., and Reymann, K. G. (1998). Subtype-specific involvement of metabotropic glutamate receptors in two forms of long-term potentiation in the dentate gyrus of freely moving rats. *Neuroscience* 86, 709–721. doi: 10.1016/s0306-4522(98)00111-0

Manahan-Vaughan, D., and Reymann, K. G. (1995). 1S,3R-ACPD dose-dependently induces a slow-onset potentiation in the rat hippocampal CA1 region in vivo. *Neuropharmacology* 34, 1103–1105. doi: 10.1016/0028-3908(95)00108-I

McBain, C. J., and Mayer, M. L. (1994). N-methyl-D-aspartic acid receptor structure and function. *Physiol. Rev.* 74, 723–760. doi: 10.1152/physrev.1994.74.3.723

McCormick, D. A., and Pape, H. C. (1990). Properties of a hyperpolarization-activated cation current and its role in rhythmic oscillation in thalamic relay neurones. *J. Physiol. Lond.* 431, 291–318. doi: 10.1113/jphysiol.1990.sp018331

Mothet, J. P., Parent, A. T., Wolosker, H., Brady, R. O. Jr., Linden, D. J., Ferris, C. D., et al. (2001). D-serine is an endogenous ligand for the glycine site of the N-methyl-D-aspartate receptor. *Proc. Natl. Acad. Sci. USA* 97, 4926–4931. doi: 10.1073/pnas.97.9.4926

Mucke, L., Masliah, E., Yu, G. Q., Mallory, M., Rockenstein, E. M., Tatsuno, G., et al. (2000). High-level neuronal expression of abeta 1-42 in wild-type human amyloid protein precursor transgenic mice. Synaptotoxicity without plaque formation. *J Neurosci* 20, 4050–4058. doi: 10.1523/JNEUROSCI.20-11-04050.2000

Mukherjee, S., and Manahan-Vaughan, D. (2023). Role of metabotropic glutamate receptors in persistent forms of hippocampal plasticity and learning. *Neuropharmacology* 66, 65–81. doi: 10.1016/j.neuropharm.2012.06.005

Neher, E. (1992). Correction for liquid junction potentials in patch clamp experiments. *Methods Enzymol* 207, 123–131. doi: 10.1016/0076-6879(92)07008-c(92)07008-C

Neitz, A., Mergia, E., Imbrosci, B., Petrasch-Parwez, E., Eysel, U. T., Koesling, D., et al. (2014). Postsynaptic NO/cGMP increases NMDA receptor currents via hyperpolarization-activated cyclic nucleotide-gated channels in the hippocampus. *Cereb. Cortex* 24, 1923–1936. doi: 10.1093/cercor/bht048

Neyman, S., and Manahan-Vaughan, D. (2008). Metabotropic glutamate receptor 1 (mGluR1) and 5 (mGluR5) regulate late phases of LTP and LTD in the hippocampal CA1 region in vitro. *Eur. J. Neurosci.* 27, 1345–1352. doi: 10.1111/j.1460-9568.2008.06109.x

Novkovic, T., Mittmann, T., and Manahan-Vaughan, D. (2015). BDNF contributes to the facilitation of hippocampal synaptic plasticity and learning enabled by environmental enrichment. *Hippocampus* 25, 1–15. doi: 10.1002/hipo.22342

Orr, A. L., Hanson, J. E., Li, D., Klotz, A., Wright, S., Schenk, D., et al. (2014). β-Amyloid inhibits E-S potentiation through suppression of cannabinoid receptor 1-dependent synaptic disinhibition. *Neuron* 82, 1334–1345. doi: 10.1016/j.neuron.2014.04.039

Paoletti, P., Bellone, C., and Zhou, Q. (2013). NMDA receptor subunit diversity. Impact on receptor properties, synaptic plasticity and disease. *Nat. Rev. Neurosci.* 14, 383–400. doi: 10.1038/nrn3504

Punnakkal, P., Jendritza, P., and Köhr, G. (2012). Influence of the intracellular GluN2 C-terminal domain on NMDA receptor function. *Neuropharmacology* 62, 1985–1992. doi: 10.1016/j.neuropharm.2011.12.018

Robinson, R. B., and Siegelbaum, S. A. (2003). Hyperpolarization-activated cation currents: from molecules to physiological function. *Annu. Rev. Physiol.* 65, 453–480. doi: 10.1146/annurev.physiol.65.092101.142734

Rönicke, R., Mikhaylova, M., Rönicke, S., Meinhardt, J., Schröder, U. H., Fändrich, M., et al. (2011). Early neuronal dysfunction by amyloid β oligomers depends on activation of NR2B-containing NMDA receptors. *Neurobiol. Aging* 32, 2219–2228. doi: 10.1016/j.neurobiolaging.2010.01.011

Roselli, F., Tirard, M., Lu, J., Hutzler, P., Lamberti, P., Livrea, P., et al. (2005). Soluble beta-amyloid1–40 induces NMDA-dependent degradation of postsynaptic density-95 at glutamatergic synapses. *J. Neurosci.* 25, 11061–11070. doi: 10.1523/JNEUROSCI.3034-05.2005

Rosenbrock, H., Kramer, G., Hobson, S., Koros, E., Grundl, M., Grauert, M., et al. (2010). Functional interaction of metabotropic glutamate receptor 5 and NMDA-receptor by a metabotropic glutamate receptor 5 positive allosteric modulator. *Eur. J. Pharmacol.* 639, 40–46. doi: 10.1016/j.ejphar.2010.02.057

Rothman, S. M., and Olney, J. W. (1987). Excitotoxity and the NMDA receptor. *Trends Neurosci.* 10, 299–302. doi: 10.1016/0166-2236(87)90177-9

Rui, Y., Gu, J., Yu, K., Hartzell, H. C., and Zheng, J. Q. (2010). Inhibition of AMPA receptor trafficking at hippocampal synapses by β-amyloid oligomers: the mitochondrial contribution. *Mol. Brain* 3:10. doi: 10.1186/1756-6606-3-10

Sakimura, K., Kutsuwada, T., Ito, I., Manabe, T., Takayama, C., Kushiya, E., et al. (1995). Reduced hippocampal LTP and spatial learning in mice lacking NMDA receptor epsilon 1 subunit. *Nature* 373, 151–155. doi: 10.1038/373151a0

Shankar, G. M., Li, S., Mehta, T. H., Garcia-Munoz, A., Shepardson, N. E., Smith, I., et al. (2008). Amyloid-beta protein dimers isolated directly from Alzheimer's brains impair synaptic plasticity and memory. *Nat. Med.* 14, 837–842. doi: 10.1038/nm1782

Snyder, E. M., Nong, Y., Almeida, C. G., Paul, S., Moran, T., Choi, E. Y., et al. (2005). Regulation of NMDA receptor trafficking by amyloid-beta. *Nat. Neurosci.* 8, 1051–1058. doi: 10.1038/nn1503

Sobczyk, A., Scheuss, V., and Svoboda, K. (2005). NMDA receptor subunit-dependent [Ca2+] signaling in individual hippocampal dendritic spines. *J. Neurosci.* 25, 6037–6046. doi: 10.1523/JNEUROSCI.1221-05.2005

Südkamp, N., Shchyglo, O., and Manahan-Vaughan, D. (2021). Absence of Pannexin 1 stabilizes hippocampal excitability after intracerebral treatment with Aβ (1-42) and prevents LTP deficits in middle-aged mice. *Front. Aging Neurosci.* 13:591735. doi: 10.3389/fnagi.2021.591735

Talantova, M., Sanz-Blasco, S., Zhang, X., Xia, P., Akhtar, M. W., Okamoto, S., et al. (2013). Aβ induces astrocytic glutamate release, extrasynaptic NMDA receptor activation, and synaptic loss. *Proc. Natl. Acad. Sci. USA* 110, E2518–E2527. doi: 10.1073/pnas.1306832110

Taniguchi, K., Yamamoto, F., Amano, A., Tamaoka, A., Sanjo, N., Yokota, T., et al. (2022). Amyloid-β oligomers interact with NMDA receptors containing GluN2B subunits and metabotropic glutamate receptor 1 in primary cortical neurons: relevance to the synapse pathology of Alzheimer's disease. *Neurosci. Res.* 180, 90–98. doi: 10.1016/j.neures.2022.03.001

Texidó, L., Martín-Satué, M., Alberdi, E., Solsona, C., and Matute, C. (2011). Amyloid β peptide oligomers directly activate NMDA receptors. *Cell Calcium* 49, 184–190. doi: 10.1016/j.ceca.2011.02.001

Tse, D., Privitera, L., Norton, A. C., Gobbo, F., Spooner, P., Takeuchi, T., et al. (2023). Cell-type-specific optogenetic stimulation of the locus coeruleus induces slow-onset potentiation and enhances everyday memory in rats. *Proc. Natl. Acad. Sci. USA* 120:e2307275120. doi: 10.1073/pnas.2307275120

Twarkowski, H., Hagena, H., and Manahan-Vaughan, D. (2016). The 5-Hydroxytryptamine$_4$ (5-HT$_4$) receptor enables differentiation of informational content and encoding in the hippocampus. *Hippocampus* 26, 875–891. doi: 10.1002/hipo.22569

Vicini, S., Wang, J. F., Li, J. H., Zhu, W. J., Wang, Y. H., Luo, J. H., et al. (1998). Functional and pharmacological differences between recombinant N-methyl-D-aspartate receptors. *J. Neurophysiol.* 79, 555–566. doi: 10.1152/jn.1998.79.2.555

von Engelhardt, J., Doganci, B., Jensen, V., Hvalby, Ø., Göngrich, C., Taylor, A., et al. (2008). Contribution of hippocampal and extra-hippocampal NR2B-containing NMDA receptors to performance on spatial learning tasks. *Neuron* 60, 846–860. doi: 10.1016/j.neuron.2008.09.039

Wahl-Schott, C., and Biel, M. (2009). HCN channels: structure, cellular regulation and physiological function. *Cell. Mol. Life Sci.* 66, 470–494. doi: 10.1007/s00018-008-8525-0

Wang, Q., Walsh, D. M., Rowan, M. J., Selkoe, D. J., and Anwyl, R. (2004). Block of long-term potentiation by naturally secreted and synthetic amyloid beta-peptide in hippocampal slices is mediated via activation of the kinases c-Jun N-terminal kinase, cyclin-dependent kinase 5, and p38 mitogen-activated protein kinase as well as metabotropic glutamate receptor type 5. *J. Neurosci.* 24, 3370–3378. doi: 10.1523/JNEUROSCI.1633-03.2004

Whitcomb, D. J., Hogg, E. L., Regan, P., Piers, T., Narayan, P., Whitehead, G., et al. (2015). Intracellular oligomeric amyloid-beta rapidly regulates GluA1 subunit of AMPA receptor in the hippocampus. *Sci. Rep.* 5:10934. doi: 10.1038/srep10934

Wilson, I. A., Ikonen, S., Gureviciene, I., McMahan, R. W., Gallagher, M., Eichenbaum, H., et al. (2004). Cognitive aging and the hippocampus: how old rats represent new environments. *J Neurosci.* 24, 3870–3878. doi: 10.1523/JNEUROSCI.5205-03.2004

Yamin, G., Coppola, G., and Teplow, D. B. (2016). Design, Characterization, and Use of a Novel Amyloid β-Protein Control for Assembly, Neurotoxicity, and Gene Expression Studies. *Biochemistry.* 55, 5049–5060. doi: 10.1021/acs.biochem.6b00579

Yashiro, K., and Philpot, B. D. (2008). Regulation of NMDA receptor subunit expression and its implications for LTD, LTP, and metaplasticity. *Neuropharmacology* 55, 1081–1094. doi: 10.1016/j.neuropharm.2008.07.046

Yeung, J. H. Y., Calvo-Flores Guzmán, B., Palpagama, T. H., Ethiraj, J., Zhai, Y., Tate, W. P., et al. (2020). Amyloid-beta1-42 induced glutamatergic receptor and transporter expression changes in the mouse hippocampus. *J. Neurochem.* 155, 62–80. doi: 10.1111/jnc.15099

Zhang, D., Qi, Y., Klyubin, I., Ondrejcak, T., Sarell, C. J., Cuello, A. C., et al. (2017). Targeting glutamatergic and cellular prion protein mechanisms of amyloid β-mediated persistent synaptic plasticity disruption: Longitudinal studies. *Neuropharmacology* 121, 231–246. doi: 10.1016/j.neuropharm.2017.03.036

Zhou, Q., and Sheng, M. (2013). NMDA receptors in nervous system diseases. *Neuropharmacology* 74, 69–75. doi: 10.1016/j.neuropharm.2013.03.030

frontiers | Frontiers in Aging Neuroscience

TYPE Systematic Review
PUBLISHED 22 May 2024
DOI 10.3389/fnagi.2024.1407980

OPEN ACCESS

EDITED BY
Rodrigo Morales,
University of Texas Health Science Center at Houston, United States

REVIEWED BY
Yingyue Zhou,
Stanford University, United States
Anthoula Charalampos Tsolaki,
Aristotle University of Thessaloniki, Greece

*CORRESPONDENCE
Jian Pei
✉ longhuaacup@aliyun.com

†These authors have contributed equally to this work and share first authorship

RECEIVED 27 March 2024
ACCEPTED 03 May 2024
PUBLISHED 22 May 2024

CITATION
Wang R, Zhan Y, Zhu W, Yang Q and Pei J (2024) Association of soluble TREM2 with Alzheimer's disease and mild cognitive impairment: a systematic review and meta-analysis.
Front. Aging Neurosci. 16:1407980.
doi: 10.3389/fnagi.2024.1407980

Association of soluble TREM2 with Alzheimer's disease and mild cognitive impairment: a systematic review and meta-analysis

Ruiqi Wang†, Yijun Zhan†, Wenyan Zhu, Qianwen Yang and Jian Pei*

Department of Acupuncture, Longhua Hospital, Shanghai University of Traditional Chinese Medicine, Shanghai, China

Objective: Soluble triggering receptor expressed on myeloid cells 2 (sTREM2) is a potential neuroinflammatory biomarker linked to the pathogenesis of Alzheimer's disease (AD) and mild cognitive impairment (MCI). Previous studies have produced inconsistent results regarding sTREM2 levels in various clinical stages of AD. This study aims to establish the correlation between sTREM2 levels and AD progression through a meta-analysis of sTREM2 levels in cerebrospinal fluid (CSF) and blood.

Methods: Comprehensive searches were conducted in PubMed, Embase, Web of Science, and the Cochrane Library to identify observational studies reporting CSF and blood sTREM2 levels in AD patients, MCI patients, and healthy controls. A random effects meta-analysis was used to calculate the standardized mean difference (SMD) and 95% confidence intervals (CIs).

Results: Thirty-six observational studies involving 3,016 AD patients, 3,533 MCI patients, and 4,510 healthy controls were included. CSF sTREM2 levels were significantly higher in both the AD [SMD = 0.28, 95% CI (0.15, 0.41)] and MCI groups [SMD = 0.30, 95% CI (0.13, 0.47)] compared to the healthy control group. However, no significant differences in expression were detected between the AD and MCI groups [SMD = 0.09, 95% CI (−0.09, 0.26)]. Furthermore, increased plasma sTREM2 levels were associated with a higher risk of AD [SMD = 0.42, 95% CI (0.01, 0.83)].

Conclusion: CSF sTREM2 levels are positively associated with an increased risk of AD and MCI. Plasma sTREM2 levels were notably higher in the AD group than in the control group and may serve as a promising biomarker for diagnosing AD. However, sTREM2 levels are not effective for distinguishing between different disease stages of AD. Further investigations are needed to explore the longitudinal changes in sTREM2 levels, particularly plasma sTREM2 levels, during AD progression.

Systematic review registration: https://www.crd.york.ac.uk/prospero/display_record.php?ID=CRD42024514593

KEYWORDS

soluble TREM2, Alzheimer's disease, mild cognitive impairment, neuroinflammation, meta-analysis

1 Introduction

Triggering receptor expressed on myeloid cells 2 (TREM2), a receptor on microglial membranes, has emerged as a research focus in Alzheimer's disease (AD), supported by the positive results of genome-wide association studies (GWAS) over the past decade (Bertram and Tanzi, 2019). Microglia dysfunction in the brain due to TREM2 risk variants, along with neuroinflammation can increase the risk of AD (Wang et al., 2024). Specifically, the rs75932628 (p.R47H) dysfunction variant of TREM2 has been identified as a major genetic risk factor, showing a significant association with AD in a meta-analysis of over 168,000 Greek populations (Korvatska et al., 2015; Rikos et al., 2022). Soluble TREM2 (sTREM2), the cleaved extracellular portion of TREM2 by metalloproteinases, is detectable in both cerebrospinal fluid (CSF) and blood (Deming et al., 2019). The incidence of all-cause dementia is notably increased with higher sTREM2 levels, including AD, vascular dementia (VaD) (Ohara et al., 2019), frontotemporal dementia (FTD) (Schulz et al., 2021) and dementia with Lewy bodies (DLB) (Morenas-Rodríguez et al., 2019). Its levels, particularly in CSF, possess significant diagnostic potential for differentiating patients with cognitive impairment from healthy individuals and serve as reliable indicators of cognitive decline and neuroinflammation in neurodegenerative diseases (Španić et al., 2023).

Neuroinflammation is recognized as a pathological hallmark of mild cognitive impairment (MCI) and AD. However, it alone is not a specific pathological marker, and its biomarkers, including TREM2, face limitations due to a lack of conclusive evidence (Kandiah et al., 2022). Previous research has underscored the value of CSF and blood sTREM2 levels as biomarkers for predicting disease progression in AD, although results have been inconsistent. A meta-analysis revealed elevated CSF sTREM2 levels in both AD and MCI patients, while no association was found between plasma sTREM2 levels and the risk of AD development (Gu et al., 2023). Recent studies focusing on sTREM2 in the progression of AD have advanced rapidly. Considering the better clinical operability of blood biomarkers, recent research has increasingly focused on the expression of sTREM2 in plasma and has identified significantly elevated levels in AD patients (Schulz et al., 2021; Zhao et al., 2022; La Rosa et al., 2023).

This meta-analysis aims to reassess the CSF and blood levels of sTREM2 in patients with MCI and AD and to explore the impact of sTREM2 on AD progression. It combines up-to-date data from relevant observational studies to test the hypothesis that elevated sTREM2 levels are associated with cognitive decline. These findings could provide insights into the underlying biomechanisms of AD and provide new diagnostic and therapeutic approaches.

2 Methods

The protocol is registered at the International Prospective Register of Systematic Reviews (PROSPERO) (registration number: CRD42024514593).

2.1 Search strategy

Two investigators (RW and WZ) conducted independent searches in the PubMed, Embase, Web of Science, and Cochrane Library databases for articles published up to 15 February 2024. The main keywords included (soluble TREM2 OR sTREM2) AND (Alzheimer's Disease OR Senile Dementia OR AD OR Mild Cognitive Impairment OR MCI), plus additional relevant keywords as outlined in Supplementary Table S1. Additionally, the reference lists of prior studies were extensively examined.

2.2 Selection criteria

The inclusion criteria were: (1) studies assessing CSF or blood (plasma or serum) sTREM2 in AD patients, MCI patients, or healthy controls. (2) Utilization of international diagnostic criteria for AD and MCI were reported. (3) Availability of sTREM2 data for both disease and control groups. The exclusion criteria included (1) studies lacking precise sTREM2 levels, even after contact with the corresponding author; and (2) reviews, abstracts, case reports, letters, and commentaries.

2.3 Data extraction

Following predefined criteria, two reviewers (QY and WZ) independently extracted data from the selected studies, including the first author's name, publication year, country, sample size, diagnostic criteria, mean age, and gender distribution, CSF and blood sTREM2 levels, and the assay method. For studies providing range data, means and standard deviation (SD) were calculated (Hozo et al., 2005). The data from each eligible study were compiled into a spreadsheet.

2.4 Quality assessment

The quality of the observational studies was assessed using the Newcastle-Ottawa scale (NOS), which comprises 3 sections totaling 8 entries with a maximum score of 9; a score of $\geq$7 was deemed high quality (Stang, 2010). Two reviewers (YZ and QY) performed the quality assessments independently; in cases of disagreement, a third reviewer (JP) was consulted to resolve the issue.

2.5 Statistical analysis

All the statistical analysis were performed using STATA version 14.0 (StataCorp LLC, College Station, TX, United States). The sTREM2 levels in the cognitively impaired patients and controls were assessed by calculating the combined standardized mean difference (SMD) and 95% confidence interval (CI). Interstudy heterogeneity was calculated using Higgins's I-squared test based on Cochrane's Q. A random-effects model was employed if $I^2 \geq 50\%$, indicating statistical heterogeneity; otherwise, a fixed-effects model was used. Additionally, subgroup analysis and meta-regression of the mean age, assay method, diagnostic criteria, and proportion of women were conducted to explore sources of heterogeneity. Sensitivity analysis was performed by systematically excluding each study to ensure the reliability of the combined estimates. Moreover, publication bias was assessed using Egger's test with the trim and fill method. A $p < 0.05$ was considered to statistically significant.

3 Results

3.1 Literature selection

Initially, 762 potentially relevant studies were retrieved. After removing 280 duplicates, 299 articles were extracted by screening titles and abstracts, and 147 studies were excluded after full-text review. Ultimately, thirty-six articles were included. The overall screening process and results are presented in Figure 1.

3.2 Study characteristics

The thirty-six articles (Hu et al., 2014, 2021a; Kleinberger et al., 2014; Gispert et al., 2016, 2017; Henjum et al., 2016; Heslegrave et al., 2016; Piccio et al., 2016; Suárez-Calvet et al., 2016; Bekris et al., 2018; Brosseron et al., 2018; Deming et al., 2019; Ewers et al., 2019; Morenas-Rodríguez et al., 2019; Nordengen et al., 2019; Banerjee et al., 2020; Edwin et al., 2020; Ferri et al., 2020; Franzmeier et al., 2020; Knapskog et al., 2020; Diaz-Lucena et al., 2021; Ma et al., 2021; Schulz et al., 2021; Van Hulle et al., 2021; Chen et al., 2022; Li et al., 2022; Shi et al., 2022; Winfree et al., 2022; Zhao et al., 2022; Finze et al., 2023; Giannisis et al., 2023; Hok-A-Hin et al., 2023; La Rosa et al., 2023; Paolini et al., 2023; Španić et al., 2023; Wang et al., 2023) were all published between 2014 and 2023, showed an increase in publications from 2017 to 2023. These studies involved 3,016 AD patients, 3,533 MCI patients, and 4,510 healthy controls, primarily conducted in Europe and the United States. Thirty studies (encompassing 32 comparisons) examined the relationship between CSF sTREM2 and AD, while 20 focused on the association with MCI. Additionally, eight studies explored plasma sTREM2 expression in AD patients. Five studies detected both CSF and plasma sTREM2 levels. Seventeen studies measured CSF sTREM2 levels in both AD and MCI patients, but only two assessed plasma sTREM2 levels. Twenty-four studies employed enzyme-linked immunosorbent assay (ELISA) as the primary assay method. The NOS score ranged from 6 to 8, with most studies classified as high quality and three as moderate quality (Supplementary Table S2).

3.3 Association between sTREM2 and AD progression

Pooled analysis showed significantly higher CSF sTREM2 concentrations in patients in both the AD [SMD = 0.28, 95% CI (0.15, 0.41)] and MCI [SMD = 0.30, 95% CI (0.13, 0.47)] groups compared to the HC group (Figures 2, 3). However, no significant difference in sTREM2 levels was observed between the AD and MCI groups [SMD = 0.09, 95% CI (−0.09, 0.26)] (Figure 4). For plasma sTREM2, elevated levels were found only in the AD group [SMD = 0.42, 95% CI (0.01, 0.83)] compared to the HC group (Figure 5). Due to high heterogeneity, random effects models were applied for the analysis.

3.4 Subgroup analysis and meta-regression analysis

As Figure 6 illustrates, the results of the subgroup analysis show elevated sTREM2 levels in the cognitive impairment group across different ages compared to the control group. ELISA tests confirmed that sTREM2 was elevated in the AD group regardless of the assay used, and also in the MCI group [SMD = 0.45, 95% CI (0.12, 0.78)]. Moreover, sTREM2 levels were higher in AD patients diagnosed using the NIA-AA criteria [SMD = 0.77, 95% CI (0.55, 0.99)] and in

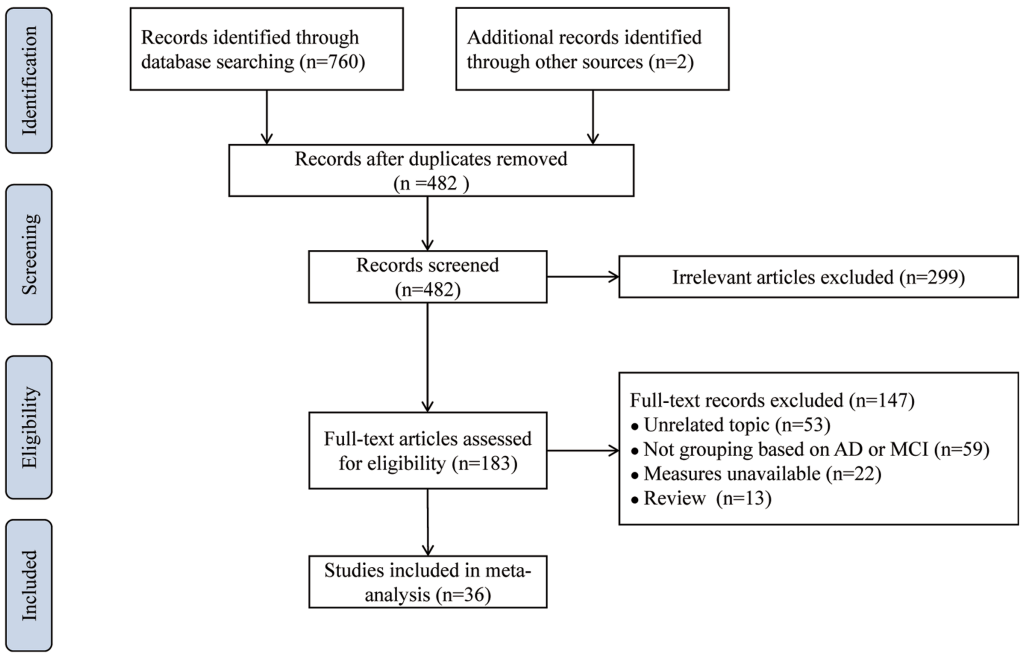

FIGURE 1
Flow chart of the study selection process and results.

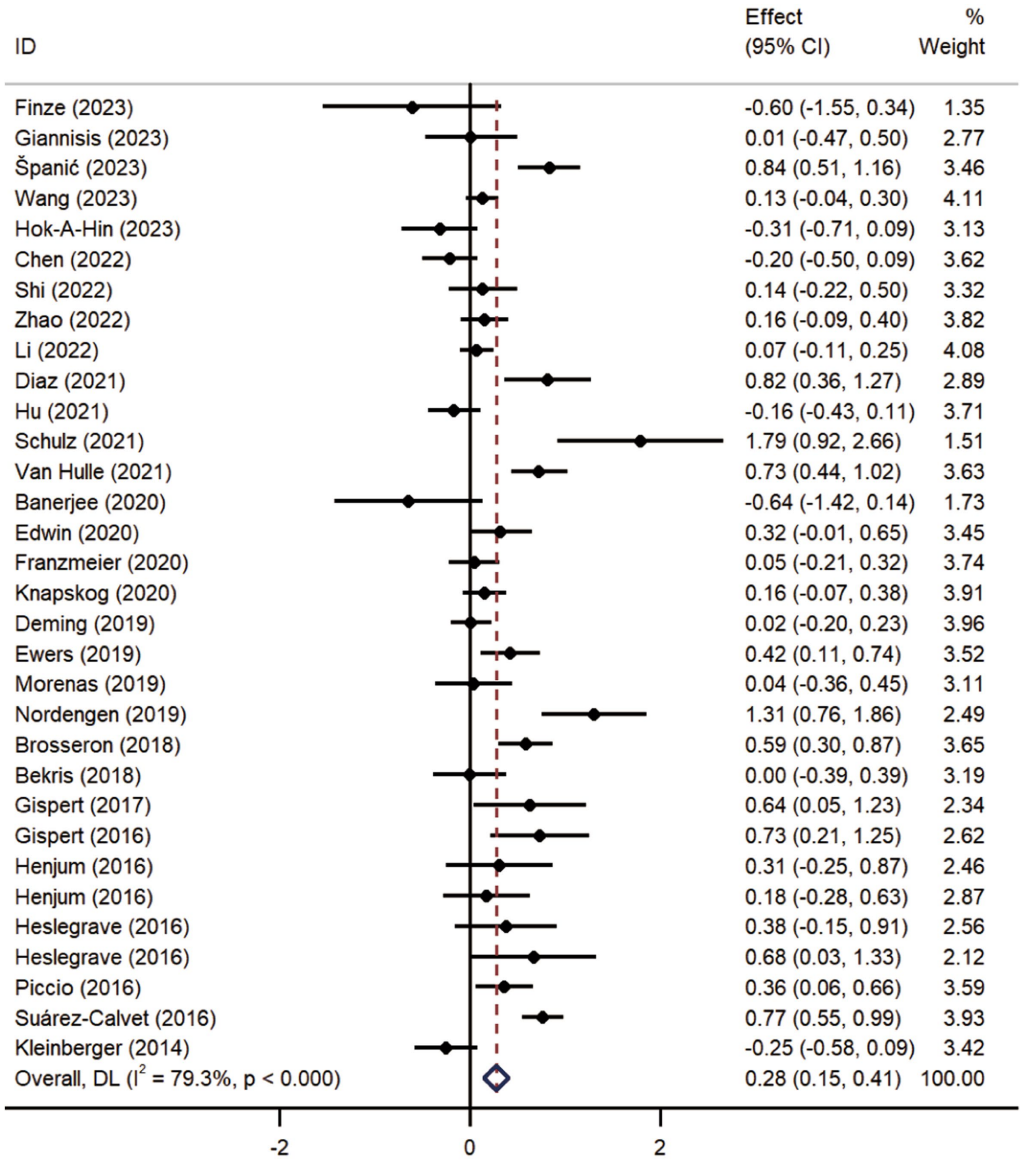

FIGURE 2
Forest plot of CSF sTREM2 levels in patients with AD compared to controls. Weights are from random-effects model.

studies with a higher proportion of female participants [SMD = 0.39, 95% CI (0.19, 0.59)]. MCI patients also showed increased sTREM2 levels in studies using NIA-AA criteria [SMD = 0.40, 95% CI (0.17, 0.62)], with no significant differences in sTREM2 levels related to gender variation. According to the subgroup analysis of plasma sTREM2, higher sTREM2 levels were detected in AD patients aged over 70 years [SMD = 0.55, 95% CI (0.11, 0.99)], as assessed by ELISA [SMD = 0.55, 95% CI (0.11, 0.99)], diagnosed using the NIA-AA criteria [SMD = 0.60, 95% CI (0.07, 1.14)], and in studies with a lower proportion of female participants [SMD = 1.05, 95% CI (0.07, 2.02)]. None of the factors significantly reduced heterogeneity. Meta-regression results indicated that these factors did not fully explain the source of heterogeneity in other component comparisons (Supplementary Table S3).

3.5 Sensitivity analysis and publication bias

After excluding any of the referenced studies, sensitivity analysis showed no statistically significant change in the meta-analysis results, underscoring the findings' relative reliability (Supplementary Figure S1). Publication bias was evaluated in each group's meta-analyses. Egger's test identified notable publication bias in the MCI vs. HC groups ($p = 0.042$), while no significant publication bias risk was found in the other groups (Supplementary Table S4). The trim and fill method indicated that no additional studies needed to be included, and the results remained unchanged [SMD = 1.35, 95% CI (1.14, 1.60)], demonstrating both stability and minimal impact from publication bias (Supplementary Figure S2).

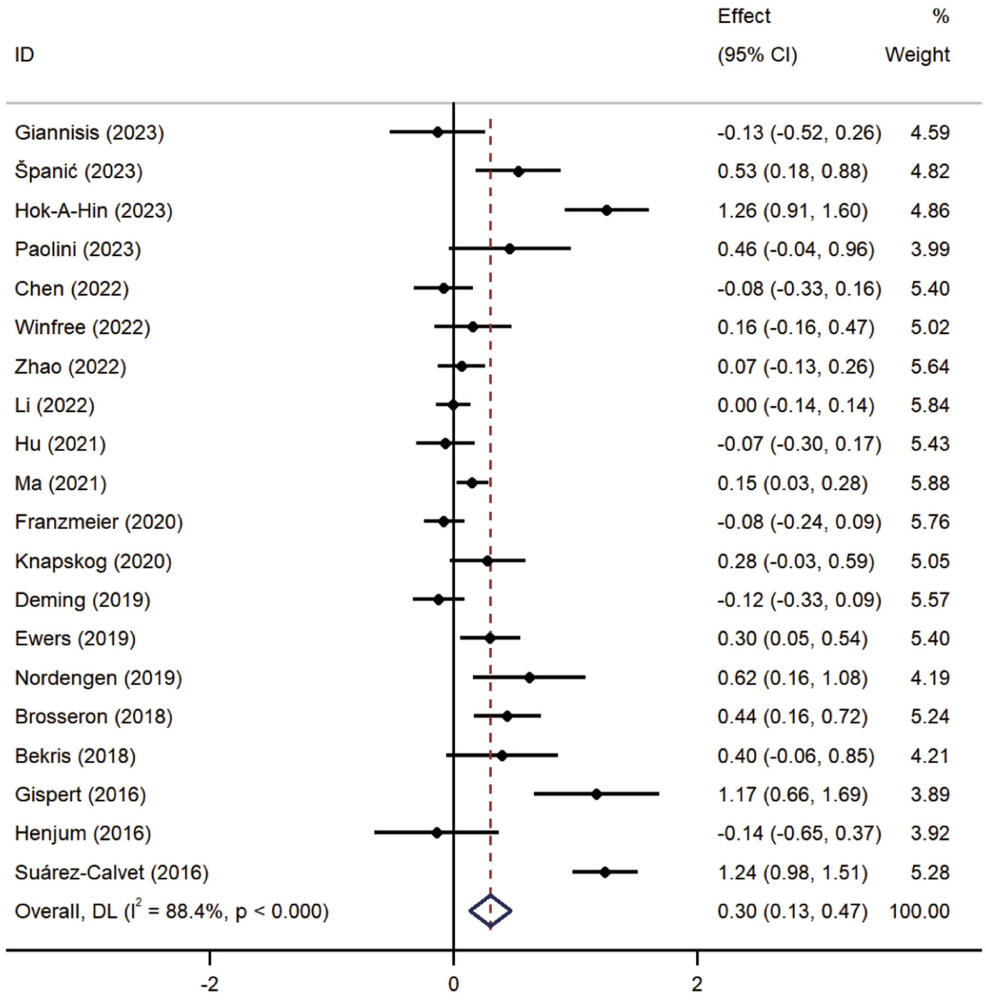

FIGURE 3
Forest plot of CSF sTREM2 levels in patients with MCI compared to controls. Weights are from random-effects model.

4 Discussion

4.1 Summary of findings

A sustained and excessive inflammatory response is a common pathological basis for AD progression. Identifying relevant sensitive biomarkers is crucial for early AD diagnosis and intervention. Changes in sTREM2 concentrations in the CSF and blood may indicate neuroinflammation and microglial activation during AD development. This study found higher CSF sTREM2 levels in both MCI and AD groups but no differences between them. However, contrary to a previous meta-analysis (Gu et al., 2023), elevated plasma sTREM2 levels were also observed in AD patients. While no link was found between plasma sTREM2 levels and MCI risk, a recent study indicated that elevated plasma sTREM2 levels in MCI patients could increase the likelihood of developing AD (Zhao et al., 2022). These varying results may reflect different microglial responses to the pathological features at various AD stages.

Subgroup analysis revealed that AD patients over 70 years exhibited increased plasma sTREM2 levels, whereas CSF sTREM2 levels showed no age-related differences. This inconsistency may stem from variations in study inclusion criteria and small sample sizes, contradicting previous research that found a direct correlation between CSF sTREM2 levels and age in AD patients (Knapskog et al., 2020). A positive correlation exists between age and CSF sTREM2 level disparities in AD patients and HCs (Hu et al., 2021b). In most studies, there was a notable age discrepancy between the cognitively impaired group and the healthy controls, with half of the healthy control group having an average age of less than 65 years. In two other studies (Heslegrave et al., 2016; Banerjee et al., 2020), the average age of AD patients was less than 65 years. Previous studies have confirmed that patients with late-onset AD (LOAD) have higher peripheral blood TREM2 mRNA levels than those with early-onset AD (EOAD), suggesting that this differential expression is linked to age rather than AD disease status (Guven et al., 2020). Additionally, higher CSF sTREM2 levels were observed in studies with a high proportion of females. Gender-specific responses to TREM2 in inducing disease-associated microglial states were demonstrated in earlier research (Krasemann et al., 2017). A research team found that TREM2 expression levels were higher in female aged mice compared to male mice during pathway enrichment analysis of gender-specific gene expression (Ocañas et al., 2023). Genetic polymorphisms, such as the R47H mutation, may also influence gender differences, increasing AD risks predominantly in female mice (Sayed et al., 2021). However, the impact of gender on

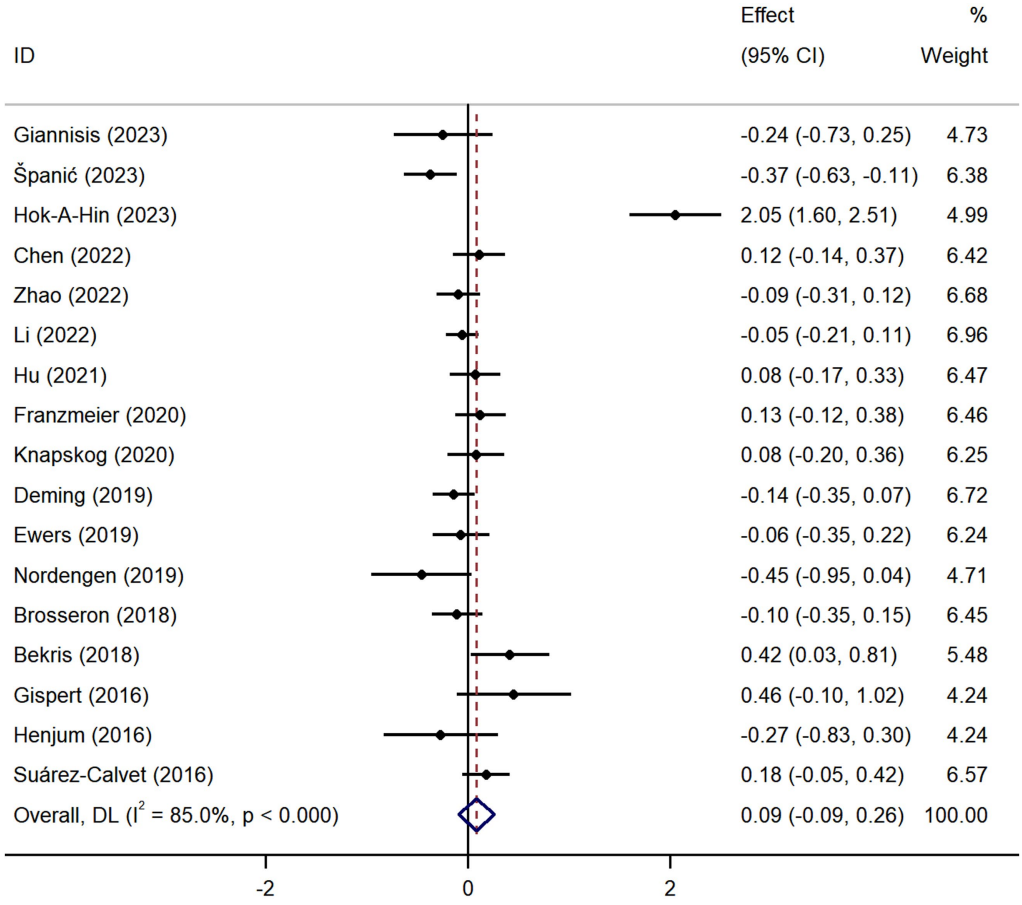

FIGURE 4
Forest plot of CSF sTREM2 levels in patients with AD compared to MCI patients. Weights are from random-effects model.

sTREM2 in clinical studies remains unclear (Piccio et al., 2016; Knapskog et al., 2020). ELISA is commonly used for sTREM2 detection, and the use of different kits may lead to heterogeneity. Moreover, sTREM2 values varied considerably across studies due to differences in analytical parameters and sample processing methods. The differences in findings among various studies may stem from differences in participant characteristics, including disease stage, all of which may introduce selection bias in the overall analysis.

4.2 Potential mechanism of sTREM2 in AD

TREM2 is an immunoglobulin superfamily transmembrane receptor mainly expressed by microglial cells in the brain (Piccio et al., 2016). Although it is generally thought that TREM2 acts protectively in AD, recent findings suggest that microglia with high TREM2 expression may be harmful (Rachmian et al., 2024). TREM2 activation may worsen Aβ-induced tau pathology, possibly accelerating its progression (Jain et al., 2023). Genetic variations significantly affect TREM2's structure and function, and a GWAS has identified 46 TREM2 variants linked with AD that increase the risk of late-onset AD (Carmona et al., 2018). Without TREM2 mutations, TREM2 levels correlate with disease pathology accumulation (Perez et al., 2017). TREM2 levels are markedly increased in the brains of AD patients and transgenic mouse models (Jiang et al., 2014; Lue et al., 2015). It has been confirmed that TREM2 expression also rises with age in neuropathologically normal human brains (Forabosco et al., 2013). The extracellular domain of TREM2 is cleaved by disintegrin and metalloproteinase 10 (ADAM10) and ADAM17, releasing a soluble N-terminal extracellular domain known as sTREM2 (Schlepckow et al., 2017). The shedding of TREM2 is influenced by various factors. The TREM2 H157Y variant (Schlepckow et al., 2017; Qiao et al., 2023), oligomeric Aβ and the membrane-spanning 4-domain subfamily A (MS4A) gene (Deming et al., 2019) can all increase TREM2 shedding.

A sharp rise in sTREM2 levels disrupts the blood–brain barrier, leading to leakage into the CSF and blood (Raha-Chowdhury et al., 2019), explaining the increased sTREM2 levels in AD and MCI patients. Furthermore, highly sTREM2 expression negatively affects the anti-inflammatory activity of the TREM2 receptor and contributes to disease progression (Dong et al., 2022). Additionally, sTREM2 expression is tightly linked with AD pathology. Significantly elevated sTREM2 levels were observed during Aβ accumulation in the AD mouse model, where it interacts with neurons and plaques (Song et al., 2018). It is reported that sTREM2 levels in CSF are directly correlated with microglial markers (Gispert et al., 2016) and proinflammatory protein levels in the early stages of AD (Rauchmann et al., 2020). Thus, sTREM2 presence is seen as a result of microglial activation and is intimately linked with early-stage neuroinflammation in AD (Nordengen et al., 2019). sTREM2 expression also reflects disease status. As the disease

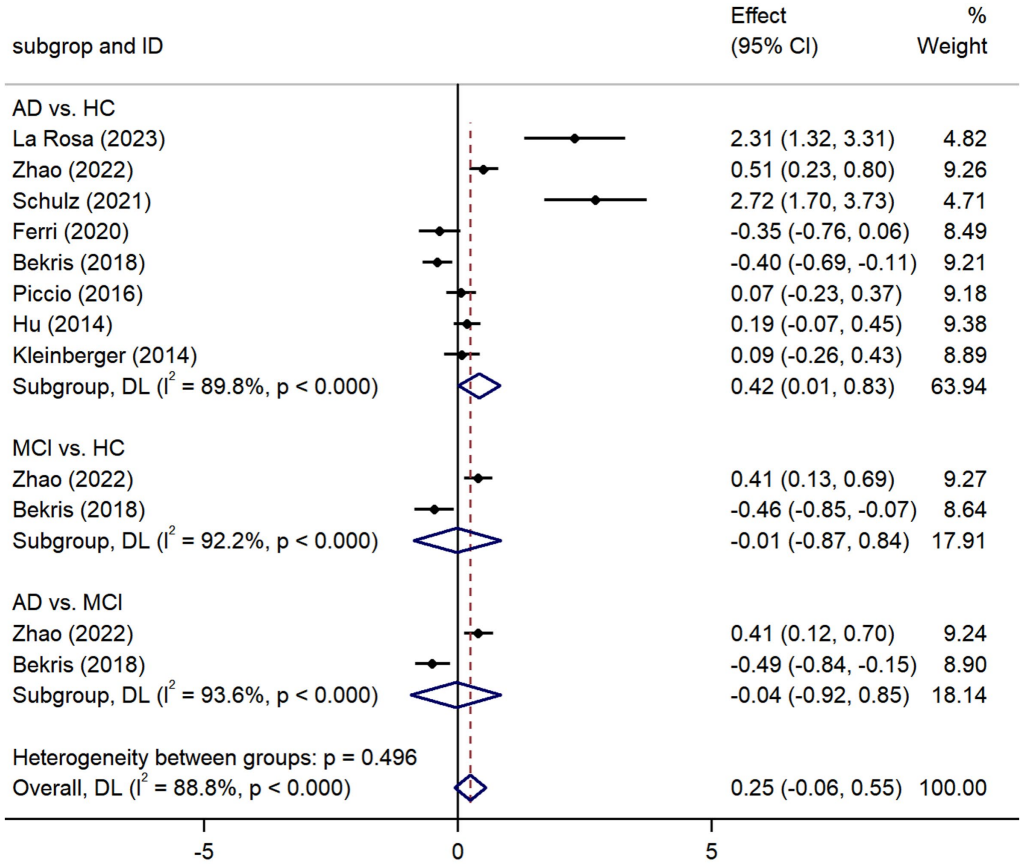

FIGURE 5
Forest plot of plasma sTREM2 expression levels in patients with AD and MCI. Weights and between-subgroup heterogeneity text are from random-effects model.

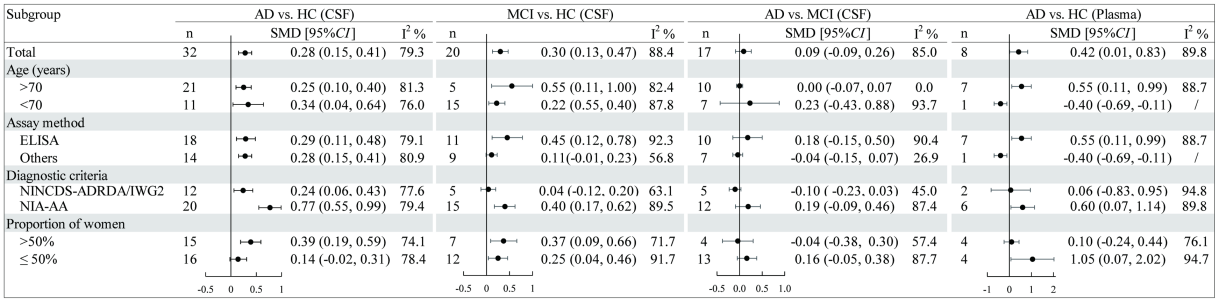

FIGURE 6
Subgroup analysis of CSF and plasma sTREM2 levels stratified by study characteristics.

progresses, TREM2 expression in microglial cells varies according to the degree of cell activation, inflammation, and tissue loss.

4.3 Association of sTREM2 with recognized AD biomarkers

Numerous studies have established that sTREM2 correlates with key neurodegenerative biomarkers, predominantly Aβ and tau. CSF sTREM2 levels are significantly elevated in AD patients and are strongly correlated with phosphorylated tau (p-tau). Additionally, the correlation between CSF sTREM2 levels and p-tau is a reliable indicator of cognitive decline in older individuals (Ewers et al., 2019). Research indicates that microglial activation accelerates tau protein deposition (Pascoal et al., 2021), and an increase of p-tau181 level is associated with a more rapid increase in CSF sTREM2 (Lan et al., 2024). Moreover, CSF sTREM2 levels fluctuate as AD progresses; Aβ pathology leads to decreased sTREM2 levels, while increases in sTREM2 are associated with Tau deposition (Ma et al., 2020). A recent study also confirmed that plasma Aβ concentrations positively

correlate with plasma sTREM2 levels in patients with cognitive impairment (Zhao et al., 2022).

4.4 Clinical implications

This is the first meta-analysis confirming that plasma sTREM2 levels are significantly higher in AD patients. The widespread use of CSF biomarkers in clinical practice faces challenges due to lumbar puncture limitations. Recently, clinicians and scientists have increasingly focused on easily accessible and minimally invasive blood biomarkers. It has great potential in the differential diagnosis and tracking of the progression of AD. The development and application of blood biomarkers could transform AD diagnosis and prognosis assessment (Hansson et al., 2022). Published studies on plasma sTREM2 have produced mixed results, but a recent study (Zhao et al., 2022) showed that plasma sTREM2 could serve as a peripheral biomarker to identify cognitive decline in the early stages of neurodegenerative diseases. According to Ohara et al. (2019), a 10-year follow-up indicated a higher risk of dementia in elderly individuals with elevated baseline blood sTREM2 levels. Another study (Min et al., 2021) reported a sensitivity of 81.8% in using plasma sTREM2 to distinguish AD patients from healthy controls. Therefore, more prospective studies are needed to assess the predictive value of plasma sTREM2 for AD progression.

4.5 Future perspectives

This study suggests a potential relationship between sTREM2 levels and AD, indicating that sTREM2 could be a biomarker for monitoring disease progression. However, several questions remain unanswered. First, sTREM2 levels are affected by factors such as Braak staging, neuropsychological test scores, and genetic polymorphisms. Future research should stratify AD samples to further explore this association. Second, the study offers insights into the role of gender as a sTREM2 biomarker, but detailed research on the gender-sTREM2-cognitive impairment link is lacking. Future studies should adopt more systematic and comprehensive approaches to examine gender's influence on this relationship. Finally, continued research on plasma sTREM2 will clarify cutoff values and standards, aiding its use in diagnosing and monitoring cognitive impairment. For consistent and comparable results, standardized experimental methods and uniform laboratory kit and measurement requirements are essential.

4.6 Limitations

This study has several limitations. The included studies in the analysis were cross-sectional and case–control, preventing a causal link between sTREM2 levels and AD or MCI. Only two studies focused on plasma sTREM2 levels in MCI patients. The studies showed high heterogeneity, besides the factors listed in our subgroup analysis, other variables like chronic diseases and genetic factors might have affected our findings. Additionally, the existing studies were primarily conducted in European countries and the United States. Therefore, geographic and ethnic influences on our results cannot be dismissed. More research on diverse populations is essential to confirm our findings.

5 Conclusion

This study found increased CSF and plasma sTREM2 levels in AD patients, while only CSF sTREM2 levels increased in those with MCI. Currently, no blood test is validated for monitoring brain immune cell activation AD. However, using plasma sTREM2 levels to stratify patient pathology shows tremendous potential. Despite these limitations, our results provide valuable insights into the role of sTREM2 levels in AD progression. Crucially, further validation and detailed functional studies are needed to determine the effects of sTREM2 on AD progression.

Data availability statement

The original contributions presented in the study are included in the article/Supplementary material, further inquiries can be directed to the corresponding author.

Author contributions

RW: Data curation, Investigation, Writing – original draft. YZ: Data curation, Investigation, Writing – review & editing. WZ: Methodology, Software, Visualization, Writing – original draft. QY: Methodology, Software, Visualization, Writing – original draft. JP: Conceptualization, Writing – review & editing.

Funding

The author(s) declare financial support was received for the research, authorship, and/or publication of this article. This study was supported by the Key Scientific Research Program of Shanghai Municipal Science and Technology Committee in China (23Y11921000 and 22Y11922900) and the TCM genre program of Shanghai Health Bureau [ZY (2021-2023)-0209-10].

Conflict of interest

The authors declare that the research was conducted in the absence of any commercial or financial relationships that could be construed as a potential conflict of interest.

Publisher's note

Supplementary material

The Supplementary material for this article can be found online at: https://www.frontiersin.org/articles/10.3389/fnagi.2024.1407980/full#supplementary-material

References

Banerjee, G., Ambler, G., Keshavan, A., Paterson, R. W., Foiani, M. S., Toombs, J., et al. (2020). Cerebrospinal fluid biomarkers in cerebral amyloid angiopathy. *J. Alzheimers Dis.* 74, 1189–1201. doi: 10.3233/JAD-191254

Bekris, L. M., Khrestian, M., Dyne, E., Shao, Y., Pillai, J. A., Rao, S. M., et al. (2018). Soluble TREM2 and biomarkers of central and peripheral inflammation in neurodegenerative disease. *J. Neuroimmunol.* 319, 19–27. doi: 10.1016/j.jneuroim.2018.03.003

Bertram, L., and Tanzi, R. E. (2019). Alzheimer disease risk genes: 29 and counting. *Nat. Rev. Neurol.* 15, 191–192. doi: 10.1038/s41582-019-0158-4

Brosseron, F., Traschütz, A., Widmann, C. N., Kummer, M. P., Tacik, P., Santarelli, F., et al. (2018). Characterization and clinical use of inflammatory cerebrospinal fluid protein markers in Alzheimer's disease. *Alzheimers Res. Ther.* 10:25. doi: 10.1186/s13195-018-0353-3

Carmona, S., Zahs, K., Wu, E., Dakin, K., Bras, J., and Guerreiro, R. (2018). The role of TREM2 in Alzheimer's disease and other neurodegenerative disorders. *Lancet Neurol.* 17, 721–730. doi: 10.1016/S1474-4422(18)30232-1

Chen, Y. H., Lin, R. R., Huang, H. F., Xue, Y. Y., and Tao, Q. Q. (2022). Microglial activation, tau pathology, and neurodegeneration biomarkers predict longitudinal cognitive decline in Alzheimer's disease continuum. *Front. Aging Neurosci.* 14:848180. doi: 10.3389/fnagi.2022.848180

Deming, Y., Filipello, F., Cignarella, F., Cantoni, C., Hsu, S., Mikesell, R., et al. (2019). The ms4a gene cluster is a key modulator of soluble TREM2 and Alzheimer's disease risk. *Sci. Transl. Med.* 11:2291. doi: 10.1126/scitranslmed.aau2291

Diaz-Lucena, D., Kruse, N., Thüne, K., Schmitz, M., Villar-Piqué, A., Da, C. J., et al. (2021). TREM2 expression in the brain and biological fluids in prion diseases. *Acta Neuropathol.* 141, 841–859. doi: 10.1007/s00401-021-02296-1

Dong, M. H., Zhou, L. Q., Tang, Y., Chen, M., Xiao, J., Shang, K., et al. (2022). CSF sTREM2 in neurological diseases: a two-sample Mendelian randomization study. *J. Neuroinflamm.* 19:79. doi: 10.1186/s12974-022-02443-9

Edwin, T. H., Henjum, K., Nilsson, L., Watne, L. O., Persson, K., Eldholm, R. S., et al. (2020). A high cerebrospinal fluid soluble TREM2 level is associated with slow clinical progression of Alzheimer's disease. *Alzheimers Dement-Diagn. Assess. Dis. Monit.* 12:e12128. doi: 10.1002/dad2.12128

Ewers, M., Franzmeier, N., Suárez-Calvet, M., Morenas-Rodriguez, E., Caballero, M., Kleinberger, G., et al. (2019). Increased soluble TREM2 in cerebrospinal fluid is associated with reduced cognitive and clinical decline in Alzheimer's disease. *Sci. Transl. Med.* 11:6221. doi: 10.1126/scitranslmed.aav6221

Ferri, E., Rossi, P. D., Geraci, A., Ciccone, S., Cesari, M., and Arosio, B. (2020). The sTREM2 concentrations in the blood: a marker of neurodegeneration? *Front. Mol. Biosci.* 7:627931. doi: 10.3389/fmolb.2020.627931

Finze, A., Biechele, G., Rauchmann, B. S., Franzmeier, N., Palleis, C., Katzdobler, S., et al. (2023). Individual regional associations between aβ-, tau- and neurodegeneration (atn) with microglial activation in patients with primary and secondary tauopathies. *Mol. Psychiatry* 28, 4438–4450. doi: 10.1038/s41380-023-02188-8

Forabosco, P., Ramasamy, A., Trabzuni, D., Walker, R., Smith, C., Bras, J., et al. (2013). Insights into TREM2 biology by network analysis of human brain gene expression data. *Neurobiol. Aging* 34, 2699–2714. doi: 10.1016/j.neurobiolaging.2013.05.001

Franzmeier, N., Suárez-Calvet, M., Frontzkowski, L., Moore, A., Hohman, T. J., Morenas-Rodriguez, E., et al. (2020). Higher CSF sTREM2 attenuates apoe4-related risk for cognitive decline and neurodegeneration. *Mol. Neurodegener.* 15:57. doi: 10.1186/s13024-020-00407-2

Giannisis, A., Al-Grety, A., Carlsson, H., Howell, J. C., Hu, W. T., Kultima, K., et al. (2023). Plasma apolipoprotein E levels, isoform composition, and dimer profile in relation to plasma lipids in racially diverse patients with Alzheimer's disease and mild cognitive impairment. *Alzheimers Res. Ther.* 15:119. doi: 10.1186/s13195-023-01262-1

Gispert, J. D., Monté, G. C., Suárez-Calvet, M., Falcon, C., Tucholka, A., Rojas, S., et al. (2017). The APOE ε4 genotype modulates CSF YKL-40 levels and their structural brain correlates in the continuum of Alzheimer's disease but not those of sTREM2. *Alzheimers Dement-Diagn. Assess. Dis. Monit.* 6, 50–59. doi: 10.1016/j.dadm.2016.12.002

Gispert, J. D., Suárez-Calvet, M., Monté, G. C., Tucholka, A., Falcon, C., Rojas, S., et al. (2016). Cerebrospinal fluid sTREM2 levels are associated with gray matter volume increases and reduced diffusivity in early Alzheimer's disease. *Alzheimers Dement.* 12, 1259–1272. doi: 10.1016/j.jalz.2016.06.005

Gu, L., Shu, H., and Wang, Y. (2023). Soluble TREM2 in body fluid in Alzheimer's disease and Parkinson's disease. *Neurol. Sci.* 44, 2743–2751. doi: 10.1007/s10072-023-06729-5

Guven, G., Bilgic, B., Samanci, B., Gurvit, H., Hanagasi, H., Donmez, C., et al. (2020). Peripheral TREM2 mRNA levels in early and late-onset Alzheimer disease's patients. *Mol. Biol. Rep.* 47, 5903–5909. doi: 10.1007/s11033-020-05661-7

Hansson, O., Edelmayer, R. M., Boxer, A. L., Carrillo, M. C., Mielke, M. M., Rabinovici, G. D., et al. (2022). The Alzheimer's association appropriate use recommendations for blood biomarkers in Alzheimer's disease. *Alzheimers Dement.* 18, 2669–2686. doi: 10.1002/alz.12756

Henjum, K., Almdahl, I. S., Rskog, V., Minthon, L., Hansson, O., Fladby, T., et al. (2016). Cerebrospinal fluid soluble TREM2 in aging and Alzheimer's disease. *Alzheimers Res. Ther.* 8:17. doi: 10.1186/s13195-016-0182-1

Heslegrave, A., Heywood, W., Paterson, R., Magdalinou, N., Svensson, J., Johansson, P., et al. (2016). Increased cerebrospinal fluid soluble TREM2 concentration in Alzheimer's disease. *Mol. Neurodegener.* 11:3. doi: 10.1186/s13024-016-0071-x

Hok-A-Hin, Y. S., Del, C. M., Boiten, W. A., Stoops, E., Vanhooren, M., Lemstra, A. W., et al. (2023). Neuroinflammatory CSF biomarkers MIF, sTREM1, and sTREM2 show dynamic expression profiles in Alzheimer's disease. *J. Neuroinflamm.* 20:107. doi: 10.1186/s12974-023-02796-9

Hozo, S. P., Djulbegovic, B., and Hozo, I. (2005). Estimating the mean and variance from the median, range, and the size of a sample. *BMC Med. Res. Methodol.* 5:13. doi: 10.1186/1471-2288-5-13

Hu, W. T., Ozturk, T., Kollhoff, A., Wharton, W., and Christina, H. J. (2021a). Higher CSF sTNFR1-related proteins associate with better prognosis in very early Alzheimer's disease. *Nat. Commun.* 12:4001. doi: 10.1038/s41467-021-24220-7

Hu, S., Pan, N., Liu, C., Wang, Y., and Zhang, T. (2021b). Age matching is essential for the study of cerebrospinal fluid sTREM2 levels and Alzheimer's disease risk: a meta-analysis. *Front. Aging Neurosci.* 13:775432. doi: 10.3389/fnagi.2021.775432

Hu, N., Tan, M. S., Yu, J. T., Sun, L., Tan, L., Wang, Y. L., et al. (2014). Increased expression of TREM2 in peripheral blood of Alzheimer's disease patients. *J. Alzheimers Dis.* 38, 497–501. doi: 10.3233/JAD-130854

Jain, N., Lewis, C. A., Ulrich, J. D., and Holtzman, D. M. (2023). Chronic TREM2 activation exacerbates aβ-associated tau seeding and spreading. *J. Exp. Med.* 220:e20220654. doi: 10.1084/jem.20220654

Jiang, T., Tan, L., Zhu, X. C., Zhang, Q. Q., Cao, L., Tan, M. S., et al. (2014). Upregulation of TREM2 ameliorates neuropathology and rescues spatial cognitive impairment in a transgenic mouse model of Alzheimer's disease. *Neuropsychopharmacology* 39, 2949–2962. doi: 10.1038/npp.2014.164

Kandiah, N., Choi, S. H., Hu, C. J., Ishii, K., Kasuga, K., and Mok, V. (2022). Current and future trends in biomarkers for the early detection of Alzheimer's disease in Asia: expert opinion. *J. Alzheimers Dis. Rep.* 6, 699–710. doi: 10.3233/ADR-220059

Kleinberger, G., Yamanishi, Y., Suárez-Calvet, M., Czirr, E., Lohmann, E., Cuyvers, E., et al. (2014). TREM2 mutations implicated in neurodegeneration impair cell surface transport and phagocytosis. *Sci. Transl. Med.* 6:243ra86. doi: 10.1126/scitranslmed.3009093

Knapskog, A. B., Henjum, K., Idland, A. V., Eldholm, R. S., Persson, K., Saltvedt, I., et al. (2020). Cerebrospinal fluid sTREM2 in Alzheimer's disease: comparisons between clinical presentation and at classification. *Sci. Rep.* 10:15886. doi: 10.1038/s41598-020-72878-8

Korvatska, O., Leverenz, J. B., Jayadev, S., Mcmillan, P., Kurtz, I., Guo, X., et al. (2015). R47h variant of TREM2 associated with Alzheimer disease in a large late-onset family: clinical, genetic, and neuropathological study. *JAMA Neurol.* 72, 920–927. doi: 10.1001/jamaneurol.2015.0979

Krasemann, S., Madore, C., Cialic, R., Baufeld, C., Calcagno, N., El, F. R., et al. (2017). The TREM2-APOE pathway drives the transcriptional phenotype of dysfunctional microglia in neurodegenerative diseases. *Immunity* 47, 566–581.e9. doi: 10.1016/j.immuni.2017.08.008

La Rosa, F., Agostini, S., Piancone, F., Marventano, I., Hernis, A., Fenoglio, C., et al. (2023). TREM2 expression and amyloid-beta phagocytosis in Alzheimer's disease. *Int. J. Mol. Sci.* 24:8626. doi: 10.3390/ijms24108626

Lan, G., Chen, X., Yang, J., Sun, P., Cai, Y., Li, A., et al. (2024). Microglial reactivity correlates with presynaptic loss independent of β-amyloid and tau. *Ann. Neurol.* 95, 917–928. doi: 10.1002/ana.26885

Li, T. R., Lyu, D. Y., and Liu, F. Q. (2022). Cerebrospinal fluid sTREM2 in Alzheimer's disease is associated with both amyloid and tau pathologies but not with cognitive status. *J. Alzheimers Dis.* 90, 1123–1138. doi: 10.3233/JAD-220598

Lue, L. F., Schmitz, C. T., Serrano, G., Sue, L. I., Beach, T. G., and Walker, D. G. (2015). TREM2 protein expression changes correlate with Alzheimer's disease neurodegenerative pathologies in post-mortem temporal cortices. *Brain Pathol.* 25, 469–480. doi: 10.1111/bpa.12190

Ma, L. Z., Tan, L., Bi, Y. L., Shen, X. N., Xu, W., Ma, Y. H., et al. (2020). Dynamic changes of csf strem2 in preclinical alzheimer's disease: the cable study. *Mol. Neurodegener.* 15, 25. doi: 10.1186/s13024-020-00374-8

Ma, L. Z., Hu, H., Wang, Z. T., Ou, Y. N., Dong, Q., Tan, L., et al. (2021). P-tau and neurodegeneration mediate the effect of β-amyloid on cognition in non-demented elders. *Alzheimers Res. Ther.* 13:200. doi: 10.1186/s13195-021-00943-z

Min, Z. X., Jing, L., Min, C., Ting, Y. T., Qi, W. Y., Li, H. Y., et al. (2021). TREM2: a novel potential biomarker of Alzheimer's disease. *Biomed. Environ. Sci.* 34, 719–724. doi: 10.3967/bes2021.099

Morenas-Rodríguez, E., Alcolea, D., Suárez-Calvet, M., Mu Oz-Llahuna, L., Vilaplana, E., Sala, I., et al. (2019). Different pattern of CSF glial markers between dementia with Lewy bodies and Alzheimer's disease. *Sci. Rep.* 9:7803. doi: 10.1038/s41598-019-44173-8

Nordengen, K., Kirsebom, B. E., Henjum, K., Selnes, P., Gísladóttir, B., Wettergreen, M., et al. (2019). Glial activation and inflammation along the Alzheimer's disease continuum. *J. Neuroinflamm.* 16:46. doi: 10.1186/s12974-019-1399-2

Ocañas, S. R., Pham, K. D., Cox, J., Keck, A. W., Ko, S., Ampadu, F. A., et al. (2023). Microglial senescence contributes to female-biased neuroinflammation in the aging mouse hippocampus: implications for Alzheimer's disease. *J. Neuroinflamm.* 20:188. doi: 10.1186/s12974-023-02870-2

Ohara, T., Hata, J., Tanaka, M., Honda, T., Yamakage, H., Yoshida, D., et al. (2019). Serum soluble triggering receptor expressed on myeloid cells 2 as a biomarker for incident dementia: the Hisayama study. *Ann. Neurol.* 85, 47–58. doi: 10.1002/ana.25385

Paolini, P. F., Gaetani, L., Bellomo, G., Chipi, E., Salvadori, N., Montanucci, C., et al. (2023). CSF neurochemical profile and cognitive changes in Parkinson's disease with mild cognitive impairment. *NPJ Parkinsons Dis.* 9:68. doi: 10.1038/s41531-023-00509-w

Pascoal, T. A., Benedet, A. L., Ashton, N. J., Kang, M. S., Therriault, J., Chamoun, M., et al. (2021). Microglial activation and tau propagate jointly across Braak stages. *Nat. Med.* 27, 1592–1599. doi: 10.1038/s41591-021-01456-w

Perez, S. E., Nadeem, M., He, B., Miguel, J. C., Malek-Ahmadi, M. H., Chen, K., et al. (2017). Neocortical and hippocampal TREM2 protein levels during the progression of Alzheimer's disease. *Neurobiol. Aging* 54, 133–143. doi: 10.1016/j.neurobiolaging.2017.02.012

Piccio, L., Deming, Y., Del-águila, J. L., Ghezzi, L., Holtzman, D. M., Fagan, A. M., et al. (2016). Cerebrospinal fluid soluble TREM2 is higher in Alzheimer disease and associated with mutation status. *Acta Neuropathol.* 131, 925–933. doi: 10.1007/s00401-016-1533-5

Qiao, W., Chen, Y., Zhong, J., Madden, B. J., Charlesworth, C. M., Martens, Y. A., et al. (2023). TREM2 H157Y increases soluble TREM2 production and reduces amyloid pathology. *Mol. Neurodegener.* 18:8. doi: 10.1186/s13024-023-00599-3

Raha-Chowdhury, R., Henderson, J. W., Raha, A. A., Vuono, R., Bickerton, A., Jones, E., et al. (2019). Choroid plexus acts as gatekeeper for TREM2, abnormal accumulation of APOE, and fibrillary tau in Alzheimer's disease and in Down syndrome dementia. *J. Alzheimers Dis.* 69, 91–109. doi: 10.3233/JAD-181179

Rauchmann, B. S., Sadlon, A., and Perneczky, R. (2020). Soluble TREM2 and inflammatory proteins in Alzheimer's disease cerebrospinal fluid. *J. Alzheimers Dis.* 73, 1615–1626. doi: 10.3233/JAD-191120

Rachmian, N., Medina, S., Cherqui, U., Akiva, H., Deitch, D., Edilbi, D., et al. (2024). Identification of senescent, TREM2-expressing microglia in aging and Alzheimer's disease model mouse brain. *Nat. Neurosci.* doi: 10.1038/s41593-024-01620-8

Rikos, D., Siokas, V., Mentis, A. A., Aloizou, A. M., Liampas, I., Tsouris, Z., et al. (2022). TREM2 R47H variant and risk for Alzheimer's disease: assessment in a Greek population and updated meta-analysis. *Int. J. Neurosci.* 1-9, 1–9. doi: 10.1080/00207454.2022.2150844

Sayed, F. A., Kodama, L., Fan, L., Carling, G. K., Udeochu, J. C., Le, D., et al. (2021). AD-linked R47H-TREM2 mutation induces disease-enhancing microglial states via AKT hyperactivation. *Sci. Transl. Med.* 13:eabe3947. doi: 10.1126/scitranslmed.abe3947

Schlepckow, K., Kleinberger, G., Fukumori, A., Feederle, R., Lichtenthaler, S. F., Steiner, H., et al. (2017). An Alzheimer-associated TREM2 variant occurs at the Adam cleavage site and affects shedding and phagocytic function. *EMBO Mol. Med.* 9, 1356–1365. doi: 10.15252/emmm.201707672

Schulz, I., Kruse, N., Gera, R. G., Kremer, T., Cedarbaum, J., Barbour, R., et al. (2021). Systematic assessment of 10 biomarker candidates focusing on α-synuclein-related disorders. *Mov. Disord.* 36, 2874–2887. doi: 10.1002/mds.28738

Shi, X., Zhong, X., Zhou, H., Zhou, N., Hu, Y., and Ning, Y. (2022). The association between cerebrospinal ferritin and soluble triggering receptor expressed on myeloid cells 2 along Alzheimer's continuum. *Front. Neurol.* 13:961842. doi: 10.3389/fneur.2022.961842

Song, W. M., Joshita, S., Zhou, Y., Ulland, T. K., Gilfillan, S., and Colonna, M. (2018). Humanized TREM2 mice reveal microglia-intrinsic and -extrinsic effects of R47H polymorphism. *J. Exp. Med.* 215, 745–760. doi: 10.1084/jem.20171529

Španić, P. E., Babić, L. M., Langer, H. L., Brgić, K., Vogrinc, Ž., Boban, M., et al. (2023). Soluble TREM2 concentrations in the cerebrospinal fluid correlate with the severity of neurofibrillary degeneration, cognitive impairment, and inflammasome activation in Alzheimer's disease. *Neurol. Int.* 15, 842–856. doi: 10.3390/neurolint15030053

Stang, A. (2010). Critical evaluation of the Newcastle-Ottawa scale for the assessment of the quality of nonrandomized studies in meta-analyses. *Eur. J. Epidemiol.* 25, 603–605. doi: 10.1007/s10654-010-9491-z

Suárez-Calvet, M., Kleinberger, G., Araque, C. M., Brendel, M., Rominger, A., Alcolea, D., et al. (2016). STREM2 cerebrospinal fluid levels are a potential biomarker for microglia activity in early-stage Alzheimer's disease and associate with neuronal injury markers. *EMBO Mol. Med.* 8, 466–476. doi: 10.15252/emmm.201506123

Van Hulle, C., Jonaitis, E. M., Betthauser, T. J., Batrla, R., Wild, N., Kollmorgen, G., et al. (2021). An examination of a novel multipanel of CSF biomarkers in the Alzheimer's disease clinical and pathological continuum. *Alzheimers Dement.* 17, 431–445. doi: 10.1002/alz.12204

Wang, Z. T., Fu, Y., Chen, S. D., Huang, Y. Y., Ma, Y. H., Wang, Y. J., et al. (2023). Association of rs2062323 in the TREM1 gene with Alzheimer's disease and cerebrospinal fluid-soluble TREM2. *CNS Neurosci. Ther.* 29, 1657–1666. doi: 10.1111/cns.14129

Wang, L., Nykänen, N. P., Western, D., Gorijala, P., Timsina, J., Li, F., et al. (2024). Proteo-genomics of soluble TREM2 in cerebrospinal fluid provides novel insights and identifies novel modulators for Alzheimer's disease. *Mol. Neurodegener.* 19:1. doi: 10.1186/s13024-023-00687-4

Winfree, R. L., Dumitrescu, L., Blennow, K., Zetterberg, H., Gifford, K. A., Pechman, K. R., et al. (2022). Biological correlates of elevated soluble TREM2 in cerebrospinal fluid. *Neurobiol. Aging* 118, 88–98. doi: 10.1016/j.neurobiolaging.2022.06.013

Zhao, A., Jiao, Y., Ye, G., Kang, W., Tan, L., Li, Y., et al. (2022). Soluble TREM2 levels associate with conversion from mild cognitive impairment to Alzheimer's disease. *J. Clin. Invest.* 132:158708. doi: 10.1172/JCI158708

frontiers | Frontiers in Aging Neuroscience

TYPE Original Research
PUBLISHED 30 May 2024
DOI 10.3389/fnagi.2024.1393721

OPEN ACCESS

EDITED BY
Philippe Léon Louis Poindron,
NeuroSys, France

REVIEWED BY
Naibedya Dutta,
University of Southern California, Los Angeles, United States
Anubhuti Dixit,
Amity University, India

*CORRESPONDENCE
Xiaohua Duan
✉ 1047896527@qq.com

RECEIVED 29 February 2024
ACCEPTED 22 April 2024
PUBLISHED 30 May 2024

CITATION
Yu X, Tao J, Xiao T and Duan X (2024) 4,4′-methylenediphenol reduces Aβ-induced toxicity in a *Caenorhabditis elegans* model of Alzheimer's disease.
Front. Aging Neurosci. 16:1393721.
doi: 10.3389/fnagi.2024.1393721

4,4′-methylenediphenol reduces Aβ-induced toxicity in a *Caenorhabditis elegans* model of Alzheimer's disease

Xingzhi Yu, Jie Tao, Tian Xiao and Xiaohua Duan*

Yunnan Key Laboratory of Dai and Yi Medicines, Yunnan University of Chinese Medicine, Kunming, Yunnan, China

Introduction: *Gastrodia elata Blume* is a widely used medicinal and edible herb with a rich chemical composition. Moreover, prescriptions containing *Gastrodia elata* are commonly used for the prevention and treatment of cardiovascular, cerebrovascular, and aging-related diseases. Recent pharmacological studies have confirmed the antioxidant and neuroprotective effects of *Gastrodia elata*, and, in recent years, this herb has also been used in the treatment of Alzheimer's disease (AD) and other neurodegenerative disorders. We have previously shown that 4,4′-methylenediphenol, a key active ingredient of *Gastrodia elata*, can mitigate amyloid-β (Aβ)-induced paralysis in AD model worms as well as prolong the lifespan of the animals, thus displaying potential as a treatment of AD.

Methods: We investigated the effects of 4,4′-methylenediphenol on AD and aging through paralysis, lifespan, and behavioral assays. In addition, we determined the anti-AD effects of 4,4′-methylenediphenol by reactive oxygen species (ROS) assay, lipofuscin analysis, thioflavin S staining, metabolomics analysis, GFP reporter gene worm assay, and RNA interference assay and conducted in-depth studies on its mechanism of action.

Results: 4,4′-Methylenediphenol not only delayed paralysis onset and senescence in the AD model worms but also enhanced their motility and stress tolerance. Meanwhile, 4,4′-methylenediphenol treatment also reduced the contents of reactive oxygen species (ROS) and lipofuscin, and decreased Aβ protein deposition in the worms. Broad-spectrum targeted metabolomic analysis showed that 4,4′-methylenediphenol administration had a positive effect on the metabolite profile of the worms. In addition, 4,4′-methylenediphenol promoted the nuclear translocation of DAF-16 and upregulated the expression of SKN-1, SOD-3, and GST-4 in the respective GFP reporter lines, accompanied by an enhancement of antioxidant activity and a reduction in Aβ toxicity; importantly, our results suggested that these effects of 4,4′-methylenediphenol were mediated, at least partly, via the activation of DAF-16.

Conclusion: We have demonstrated that 4,4′-methylenediphenol can reduce Aβ-induced toxicity in AD model worms, suggesting that it has potential for development as an anti-AD drug. Our findings provide ideas and references for further research into the anti-AD effects of *Gastrodia elata* and its active ingredients.

KEYWORDS

4,4′-methylenediphenol, Alzheimer's disease, *Caenorhabditis elegans*, antioxidant activity, Aβ protein, metabolomics

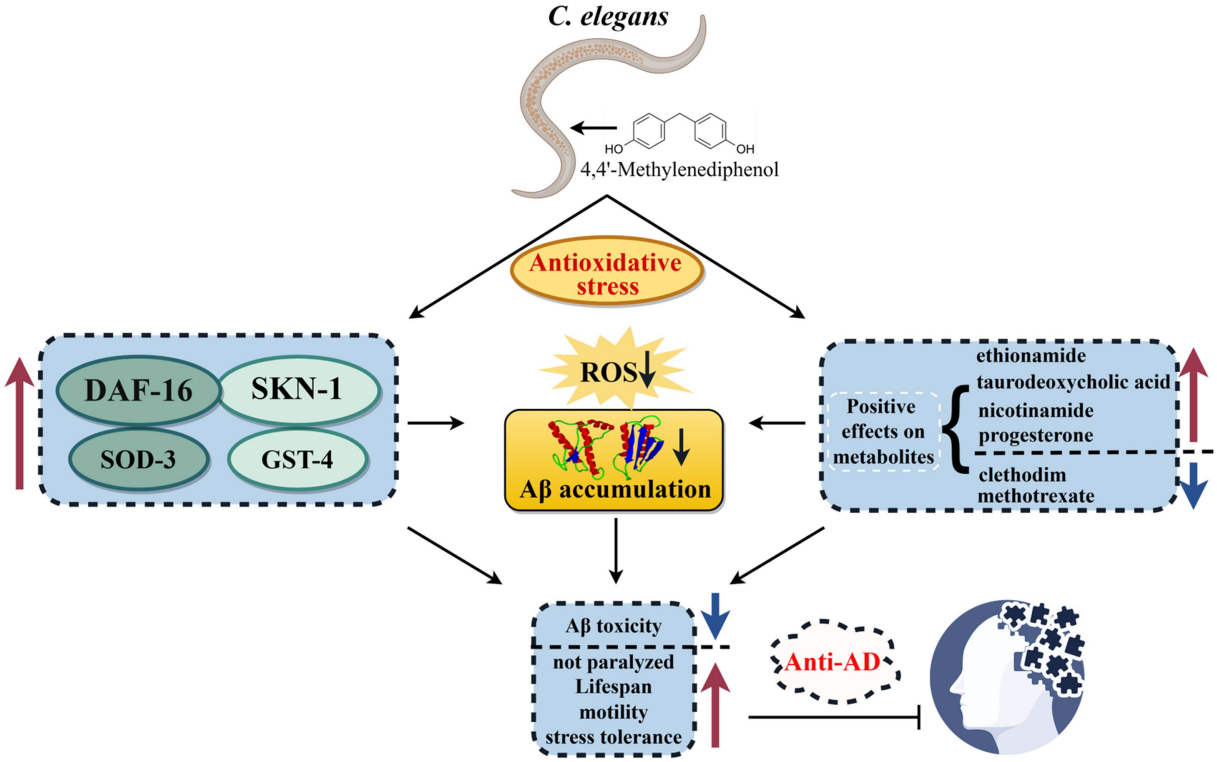

GRAPHICAL ABSTRACT
In this study, we investigated the anti-AD efficacy and mechanism of 4,4′-methylenediphenol, an active ingredient of *Gastrodia elata*, using the *C. elegans* model. Our study showed that 4,4′-methylenediphenol enhances the expression of DAF-16, SOD-3, SKN-1, and GST-4 by activating the DAF-16/FOXO and SKN-1/NRF2 signaling pathways and positively affects metabolites. These combined effects enhance antioxidant stress capacity, which in turn reduces ROS and Aβ aggregation, decreases Aβ toxicity and thus delays neuroparalysis, improves mobility and stress resistance, and ultimately achieves anti-AD effects. (The figure was drawn By Figdraw: www.figdraw.com).

1 Introduction

Alzheimer's disease (AD) is an irreversible age-related neurodegenerative disorder with an insidious onset and a long-term course. Affecting mostly older adults, the main clinical manifestations include cognitive deficits, mental and behavioral abnormalities, and impaired sociability. AD accounts for the highest proportion of dementia-related diseases (Knopman et al., 2021; Stocker et al., 2023). With the aging of the world's population, AD and other age-related disorders are increasingly becoming a global health concern (Jensen et al., 2020). Over 50 million people are thought to be living with AD worldwide, and this number is expected to triple to 152 million by 2050 (Weuve et al., 2014). The pathogenesis of AD is complex. The β-amyloid degradation toxicity hypothesis is currently the main theory explaining the pathophysiology of this condition. This hypothesis suggests that abnormal amyloid-β (Aβ) aggregation in the brain is the main triggering factor for AD and that this aggregation can exert direct toxic effects on neuronal cells, triggering a cascade of tau protein phosphorylation, inflammation, excitotoxicity, and oxidative stress, ultimately inducing neuronal death (Alafuzoff et al., 2008; Mohsenzadegan and Mirshafiey, 2012). Accordingly, it is expected that inhibiting Aβ aggregation and improving the body's antioxidative capacity represent promising therapeutic strategies for the prevention and management of AD. However, there is currently no treatment for this debilitating condition, and the available drugs are mainly used to improve disease symptoms. Accordingly, there is an urgent need for identifying and developing novel drugs aimed at the prevention and treatment of AD (Tan W. et al., 2022).

The effective natural compounds used in traditional Chinese medicine (TCM) and ethnomedicine have advantages such as abundant resource availability, high development potential, and wide-ranging pharmacological activities. *Gastrodia elata* Blume is a perennial herb within the family Orchidaceous and is one of the most valuable TCMs (Huang, 1985). In the "Compendium of Materia Medica," *Gastrodia elata* is listed as having the effects of calming the liver and suppressing liver Yang, dispelling wind and clearing channels, and stopping convulsions, and it is mainly used for the treatment of paralysis, trance, and aphasia in the state of shock (Tao et al., 2023). Indeed, *Gastrodia elata* has long been used in Chinese folk medicine for the prevention and treatment of neurological diseases that display symptoms similar to those of AD, such as amnesia, intellectual disability, hemiplegia, and speech disorders. Moreover, a group of well-known prescriptions containing *Gastrodia elata*, such as *Gastrodia (Tianma)* and *Uncaria* (*Gouteng*) decoction, have documented antioxidant, free radical scavenging, and neuroprotective effects, and have been used for the prevention and treatment of cardiovascular, cerebrovascular, and aging-related diseases (Liu and Mori, 1992; Deng et al., 2020). Recent pharmacological studies have also found that *Gastrodia elata* has the effects of promoting brain health, protecting nerves, and delaying aging. Additionally, *Gastrodia elata* has greater efficacy and is more

widely used than other TCMs with similar effects (e.g., *Ginseng*, *Astragalus membranaceus*), and has recently been applied for the treatment of AD and other related diseases in the clinic (Lu et al., 2023). Meanwhile, studies have shown that the ethyl acetate extract of *Gastrodia elata* (EEGE) has both neuroprotective and cerebral protective effect, and can improve the symptoms of AD in a nematode model of the condition by mitigating Aβ toxicity and oxidative stress (Shi et al., 2023b). In our preliminary study, we isolated a major component of EEGE, 4,4′-methylenediphenol, which is a bisphenol derivative with antioxidant activity (Yi-Ming et al., 1993; Tang et al., 2016). We found that 4,4′-methylenediphenol not only delayed Aβ protein-induced paralysis in AD model worms but also prolonged their lifespan, suggesting that it has the potential for use in the prevention and treatment of AD.

Caenorhabditis elegans is a widely used model animal for the study of age-related neurodegenerative diseases. It has the advantages of a short life cycle, small size (~1 mm), ease of cultivation and observation, low costs, freezing and resuscitation ability, and greater availability of transgenic lines compared with other AD model animals (Ewald and Li, 2012; Rani et al., 2023). In addition, *C. elegans* and human genes are highly homologous, and their key cellular metabolic and signaling pathways are highly conserved, making *C. elegans* amenable to *in vivo* studies of AD and other neurodegenerative diseases (Tissenbaum, 2015). Studies have demonstrated the suitability of employing the *C. elegans* model for the screening and development of natural drugs targeting AD. For example, one study found that the extract of *Radix Stellariae* can effectively reduce Aβ and tau protein expression and attenuate the damage they cause, which has therapeutic relevance for neurodegenerative disorders such as AD (Long et al., 2023). In addition, grape juice (Canedo-Reis et al., 2023), carnosic acid (Chen et al., 2022), and wolfberry (Meng et al., 2022) have all been shown to exert anti-AD effects in studies that have used *C. elegans* as a model. In conclusion, *C. elegans* has become an essential model for the screening of AD-targeting drugs.

In the present study, we leveraged the unique advantages of *C. elegans* to investigate the therapeutic efficacy of 4,4′-methylenediphenol against AD as well as the putative underlying mechanisms. First, the potential of this active ingredient as a treatment of AD was investigated in terms of its ability to mitigate Aβ-induced toxicity and oxidative stress, ameliorate AD-associated behavior, and delay aging and senescence. Meanwhile, the ability of 4,4′-methylenediphenol to improve AD symptoms was determined through the determination of ROS and lipofuscin contents and the levels of Aβ deposition. Finally, the mechanism underlying how 4,4′-methylenediphenol exerts its anti-AD effects was investigated in depth using broad-spectrum targeted metabolomics (TM) analysis, GFP reporter lines, and RNAi. Our findings provide a reference for further basic research into the therapeutic potential of the active ingredients of *Gastrodia elata* in AD prevention and treatment.

2 Materials and methods

2.1 Materials

4,4′-methylenediphenol was purchased from Chengdu Alfa Biotechnology Co. Ltd. (purity: 98%; 620–92-8). The worms were grown in nematode growth medium (NGM) containing sodium chloride, peptone, agar powder, cholesterol, anhydrous calcium chloride, anhydrous magnesium sulfate, and phosphate buffer. RNAi plates were prepared by adding ampicillin (96%; 7,177-48-2) and isopropyl-beta-D-thiogalactopyranoside (GC >8%; 367–93-1; Shanghai Macklin Biochemical Co., Ltd., China) to final concentrations of 100 μg/mL and 1 mM, respectively. To inhibit worm egg-laying, 5-fluoro-2′-deoxyuracil nucleoside (floxuridine, FUDR; 50–91–9; Shanghai Macklin Biochemical Co., Ltd., China) was added to the medium to a final concentration of 12 μM. The anesthetic levamisole hydrochloride (HPLC ≥98%; 16,595–80-5) was purchased from Sichuan Weikeqi-biotech Co. Ltd.; SuperKine Enhanced Antifluorescence Quencher (BMU104-CN) was supplied by Abbkine Scientific Co., Ltd.

2.2 *Caenorhabditis elegans* strains and maintenance

The *C. elegans* lines used in this study were CL4176 {dvIs27 [myo-3p::A-Beta (1–42)::let-851 3′UTR) + rol-6(su1006)] X.}, CL2006 {dvIs2 [pCL12(unc-54/human Abeta peptide 1–42 minigene) + rol-6(su1006)]}, TJ356 {zIs356 [daf-16p::daf-16a/b::GFP + rol-6 (su1006)]}, LD1 (ldIs7 [skn-1b/c::GFP + rol-6(su1006)]}, CF1553 {mu1s84[(pAD76) sod-3p::GFP) + rol-6(su1006)]}, CL2166 {dvIs19 [(pAF15) gst-4p::GFP::NLS] III}, and *C. elegans* N2 (wild-type strain). All worm strains were purchased from the *C. elegans* Genetics Center (CGC, University of Minnesota, Minneapolis, MN, United States). An uracil synthesis-deficient strain of *Escherichia coli* (OP50) was used as food. *C. elegans* CL4176 was grown and reproduced at 16°C; all other strains were grown and reproduced at 20°C.

2.3 Paralysis assay

4,4′-Methylenediphenol was weighed on an electronic precision balance, dissolved in deionized water [with DMSO (0.2%) as co-solvent] to a final concentration of 10 mM, filtered to remove bacteria, and stored at 4°C until needed. Different concentrations of the drug (0.125, 0.25, 0.5, 1, 2, and 4 mM) were generated by diluting the drug master mix with a solution containing inactivated OP50 bacteria (OD600 = 0.6, 30 min at 65°C). After mixing well, the mixture was added to the surface of the NGM, and allowed to air-dry before use. Worms in the Control group were given an equal volume of the bacterial solution. Subsequently, L1 stage-synchronized CL4176 worms were transferred to NGM plates with or without the drug (30–50 worms per plate). After incubation to the L3 stage at 16°C, the temperature was raised to 25°C, and incubation was continued for approximately another 24 h. The number of paralyzed worms was recorded every 2 h until all the worms were paralyzed. Paralysis was defined as rigid movement or only head movement following mechanical stimulation. The optimal effective concentration of the drug as determined by the paralysis assay was used the drug concentration in subsequent experiments.

2.4 Lifespan assay

L4 stage-synchronized CL4176 worms were transferred to plates with or without the drug (1 mM), which was recorded as day 0. FUDR

(12 μM) was added to each plate to prevent egg-laying and larval hatching affecting the experimental counts. Three plates were run in parallel for each group (30–50 worms per plate). Thereafter, the number of surviving worms was recorded every 2 days, following which the surviving worms were transferred to fresh medium containing the same drug concentration, and culture was continued until all of the worms had died. Worms that did not respond to stimulation with a picker were considered dead. Worms that developed a bag-like phenotype and did not die within the area coated with the drug were excluded from the statistical analysis. The lifespan assay was repeated three times with no less than 60 worms each time.

2.5 Lipofuscin assay

L1 stage-synchronized N2 worms were cultured to the L4 stage at 20°C and then transferred to NGM plates with or without the drug (1 mM). After 10 days of incubation, worms from each group (≥10 worms per group) were transferred to PBS containing anesthetic and analyzed for lipofuscin autofluorescence under a fluorescence microscope (LSM900, Carl Zeiss, Germany). Fluorescence intensity values were determined using ImageJ software. The experiment was repeated independently three times.

2.6 Reproductive and behavioral assays

2.6.1 Reproductive capacity assay

CL4176 worms that had not yet performed egg laying when synchronized at the L4 stage were transferred to NGM culture plates with or without the drug (1 mM) (two worms per plate, three plates in parallel per group) and incubated at 16°C; this was recorded as day 1 of reproduction. Every day thereafter, the worms were transferred to new culture plates containing the same drug concentrations, and the number of worms hatched in the old dishes on day 1 was counted on day 3 until the worms no longer produced new eggs. The effect of the drug on the reproductive ability of the worms was determined by recording and totaling the number of larvae hatched per plate in each group.

2.6.2 Behavioral assays, including pharyngeal pump beating and motility

L3 stage-synchronized CL4176 worms were transferred to NGM culture plates with or without the drug (1 mM) (three plates per group in parallel) and incubated at 16°C; this was recorded as day 0. Every second day, the worms were transferred to fresh culture plates containing the same drug concentrations. Pharyngeal pump beating and motility were observed under a stereoscopic microscope on days 4, 6, and 8 after drug treatment. Before observing the swallowing rate, the worms were transferred to new plates and observed again, and the number of times the worms swallowed in 30 s was used as the index of pharyngeal pump beating. The pharyngeal pump beating upward and downward once was considered a complete pharyngeal movement; 10 worms were randomly evaluated in each plate. Before observing motility, the worms were transferred to a new plate with 100 μL of M9 solution, and the number of sinusoidal movements in 30 s was recorded as an indicator of motility; 10 worms were randomly assessed in each plate. The behavioral experiments were repeated three times, and 30 worms were counted in each group each time.

2.7 Body length assays

N2 worms synchronized to the L4 stage were transferred to NGM plates (12 μM FUDR) with or without drug (1 mM), and the size of the worms was determined after continued incubation at 20°C for 2 days. Worms were collected with PBS buffer and anesthetized, and at least 20 worms in each group were imaged under an inverted biomicroscope (DMI1, Leica Microsystems (Shanghai) Co., Ltd.), and the pictures were saved. Worm body length (μm) was measured using Image J software. The experiments were repeated three times independently.

2.8 Stress tolerance assays

2.8.1 Heat stress assay

N2 worms synchronized at the L1 stage were transferred to NGM culture plates with or without the drug (1 mM) (three plates in parallel, ≥90 worms per group) and incubated at 20°C for 2 days, following which the incubation temperature was increased to 37°C. Thereafter, survival was observed every hour until all the worms had died.

2.8.2 Oxidative stress assay

L1 stage-synchronized N2 worms were transferred to NGM plates with or without the drug (1 mM) and, after incubation to the L4 stage at 20°C, the worms were transferred to NGM plates containing juglone (300 μM; 481–39-0; Shanghai Yuanye Bio-Technology Co., Ltd., China) (three plates per group, ~30 worms per plate). Worm survival was then observed every hour until all the worms had died. Worms that were stiff and motionless and did not respond to light sources or slight vibrations were considered dead. All the experiments were repeated independently three times.

2.9 Reactive oxygen species assay

N2 worms synchronized at the L1 stage were transferred to NGM culture plates with or without the drug (1 mM) (~50 worms per plate) and incubated at 20°C to the L4 stage. Then, 5 mM paraquat solution (methyl viologen dichloride hydrate; 1910-42-5; Shanghai Aladdin Biochemical Technology Co., Ltd) was added to the NGM plates for 4 h, after which the worms were collected and washed three times with PBS. Subsequently, 50 μL of 10 μM DCFH-DA solution (Reactive Oxygen Species Detection Kit; S0033S; Beyotime Biotech. Inc.) was added, and the worms were incubated at 37°C for 30 min. After washing three times with PBS, 30 μL of worm-containing fluid was placed on a slide, coverslipped, and observed under a fluorescence microscope (LSM900, Carl Zeiss), and adjust the parameters, save the picture, and measure the fluorescence intensity value using Image J software. At least 10 worms in each group.

2.10 Sedimentation assay for Aβ aggregation

L1 stage-synchronized CL2006 worms were transferred to NGM plates with OP50 bacterial solution only, incubated to the L4 stage at 20°C, and then transferred to NGM plates with or without the drug (1 mM). After 2 days of incubation, the worms were collected in M9

buffer, washed three times, and fixed in 1 mL of 4% paraformaldehyde (pH 7.4; BL539A; Labgic Technology Co., Ltd) at 4°C for 24 h. After discarding the fixative, the worms were incubated in 1 mL of permeabilizing solution [5% β-hydrophobic ethanol [60–24-2; Shanghai Macklin Biochemical Co., Ltd], 1% Triton X-100 [9002-93-1; Meilunbio Biotechnology Co., Ltd], and 125 mM Tris [pH 7.4; 77–86-1; Beijing Solarbio Science & Technology Co., Ltd]] at 37°C for 24 h and rinsed three times with TBST solution. Then, 100 μL of the fluorescent dye thioflavin S (0.125%) (1326-12-1; Shanghai Yuanye Bio-Technology Co., Ltd) was added, followed by incubation at room temperature for 2 min. After discarding the staining solution, the worms were cleared twice with 50% ethanol, and Aβ protein deposition in the head of worms (i.e., the part before the pharyngeal pump) was observed under a fluorescence microscope (LSM900, Carl Zeiss). For imaging, 30 μL of worm-containing fluid was aspirated and placed on a slide, coverslipped, and the parameters adjusted. At least 10 worms were assessed in each group.

2.11 Broad-spectrum TM analysis

2.11.1 Sample preparation

CL4176 worms synchronized to the L1 stage were transferred to NGM plates with or without the drug (1 mM) (≥1,000 per plate, 6 plates in parallel per group), cultured first at 16°C for 48 h, and then at 25°C for approximately 30 h. The worms were collected in EP tubes with M9 buffer, washed 2–3 times with sterile water, quick-frozen in liquid nitrogen, and stored at −80°C for sequencing.

2.11.2 Broad-spectrum TM analysis

Samples were thawed on ice, added to stainless steel balls, and homogenized with a ball mill (30 Hz) for 20 s. The samples were then extracted with a 70% methanol aqueous solution at 4°C and used for analysis. All operations were performed on ice. Sample analysis, including differential metabolite screening and metabolic pathway resolution, was performed at Wuhan Metware Biotechnology Co., Ltd. First, pooled samples were subjected to non-targeted metabolomics analysis to identify the metabolites in the samples. Subsequently, these metabolites were combined with those of Metware's in-house metabolite database (MWDB) for broad-spectrum TM analysis. Metabolomic differences between samples were assessed based on a combination of ultra-high performance liquid chromatography–tandem mass spectrometry (UPLC–MS/MS), the in-house database, and multivariate statistical analysis. Chromatographic separation was performed using a Waters ACQUITY UPLC HSS T3 C18 column (1.8 μm, 2.1 × 100 mm); mobile phase A was 0.1% formic acid in ultrapure water and mobile phase B was 0.1% formic acid in acetonitrile; the flow rate was 0.4 mL/min; the column temperature was 40°C; the injection volumes were 2 μL for extensive targeted detection and 5 μL for non-targeted detection. For hydrophilic interaction liquid chromatographic (HILIC) separation, a waters ACQUITY UPLC BEH HILIC column (1.7 μm, 1 × 100 mm) was used; mobile phase A consisted of 20 mM ammonium formate, 30% water, 10% methanol, and 60% acetonitrile, adjusted to pH 10.6 with ammonia; mobile phase B comprised 20 mM ammonium formate, 60% water, and 40% acetonitrile, adjusted to pH 10.6 with ammonia; the column temperature was 40°C; the flow rate was 0.4 mL/min; the injection volumes were 2 μL for broad-spectrum targeted detection and 5 μL for non-targeted detection. For non-targeted metabolomics profiling, data were acquired on a UPLC system[1] connected to a TripleTOF 6,600 quadrupole time-of-flight (QTOF) mass analyzer (AB SCIEX). For targeted metabolomics profiling, data were acquired on a UPLC system (see text footnote 1, respectively) and a Q-Trap mass spectrometer.[2] QC samples were formed by mixing equal amounts of all the samples. The QC samples were then analyzed on the LC–QTOF–MS/MS platform and accurately characterized based on MWDB (with secondary spectra and retention time), the AI-predicted library of the MWDB and all public databases (Metlin, HMDB, KEGG, and others), and MetDNA. Multi-ion pair and retention time information for the identified metabolites was also extracted, and this information was combined with the information in Metware's target database to form a new library exclusive to the project. Finally, for all the samples, the metabolites in the new library were quantified on the Q-Trap instrument in multiple-reaction monitoring mode. The differential metabolite screening criteria were VIP >1 and p-value <0.05.

2.12 Transgenic *daf-16*, *skn-1*, *sod-3*, and *gst-4* GFP reporter strains

For all gene expression experiments involving *C. elegans* GFP reporter strains, L1-stage worms were incubated on NGM plates with or without the drug (1 mM) for 72 h, transferred to slides, anesthetized, and fixed in 2% levamisole. Images were captured under a fluorescence microscope (LSM900, Carl Zeiss) at 10/40× magnification and analyzed using ImageJ software. As the positive controls for the TJ356 strain, worms were cultured on plates containing blank medium for 72 h, and the temperature was then increased to 37°C for 30 min for induction. SKN-1::GFP fluorescence intensity was measured in the intestinal region of LD1 worms under the pharynx. The nuclear localization of DAF-16 was expressed as the number of fluorescence puncta per TJ356 worm (Kang et al., 2022). Finally, the whole-body fluorescence intensity associated with SOD-3::GFP and GST-4::GFP expression was evaluated in CF1553 and CL2166 worms, respectively. The experiments were independently replicated three times, with a minimum of 10 worms per group per strain.

2.13 *Caenorhabditis elegans* RNA interference assay

After synchronization, the resulting eggs of CL4176 worms were transferred to culture plates coated with R13H8.1 *E. coli* containing *daf-16* dsRNA to knock down *daf-16* and incubated at 16°C. Eggs incubated on culture plates coated with the HT115 *E. coli* strain expressing the L4440 empty vector served as controls. After passing to the third generation, the worms were synchronized, and the resulting eggs were placed in M9 buffer and incubated at 16°C. RNAi efficiency was subsequently assessed by qPCR. Worms successfully subjected to RNAi were then transferred to NGM plates coated with a solution of either RNAi-expressing bacteria or the empty vector-expressing strain and with or without the drug (1 mM), and were cultured to the L3 stage

1 ExionLC AD, https://sciex.com.cn/

2 QTRAP, https://sciex.com/

at 16°C. Subsequently, the plates were transferred to 25°C for heat shock, which led to the expression of high levels of Aβ protein in the muscle cells of the body wall of the worms. This resulted in continuous Aβ peptide aggregation, leading to muscle paralysis in the worms. After 24 h, the number of paralyzed worms in each group was counted every 2 h until the proportion of paralyzed worms in the blank control group accounted for more than 80% of the total number of worms. Three plates were run in parallel, with a least 90 worms per group. The experiment was independently repeated three times.

2.14 Statistical analysis

The data were statistically analyzed and plotted using GraphPad Prism 8.0 and the results are expressed as means ± standard deviation. Differences between and among groups were analyzed by the *t*-test or one-way ANOVA, respectively. Survival was analyzed using the log-rank test. *p*-values <0.05 were considered significant (*$p < 0.05$, **$p < 0.01$, ***$p < 0.001$). The experiments were independently repeated 3 times.

3 Results

3.1 4,4′-methylenediphenol delayed beta amyloid-induced paralysis

Under normal conditions, the body of CL4176 transgenic worms is curved (i.e., C-shaped), and the worms can move normally in culture medium. However, when the culture temperature is increased, CL4176 worms express large quantities of the $A\beta_{1-42}$ peptide, which exerts toxic effects on the muscle cells of the animals through aggregation (Sola et al., 2015; Fu et al., 2023). To investigate the potential effect of 4,4′-methylenediphenol on the progression of Aβ toxicity-induced paralysis, we administered different concentrations (0.125, 0.25, 0.5, 1, 2, and 4 mM) of the drug to CL4176 worms and undertook a paralysis assay. The data showed that the time to paralysis was longer in all the 4,4′-methylenediphenol treatment groups than in the Control group (Figure 1A). Except for the group administered the lowest dose (0.125 mM), the time to paralysis for 50% (PT50) of the nematodes was greater in all dosing groups than in the Control group (Table 1). Although the PT50s of the 2 and 4 mM administration groups were longer than that of the 1 mM group, the difference was minimal, and the 1 mM concentration exerted a more significant effect in prolonging the overall paralysis rate of worms (Figure 1B). Based on the principle of selecting the lowest concentration among those with comparable efficacy, 1 mM was deemed to be the optimal effective concentration for this drug and was used for subsequent experiments. In conclusion, the above results indicated that 4,4′-methylenediphenol delayed the onset of paralysis in worms and had a protective effect against β-amyloid-induced toxicity.

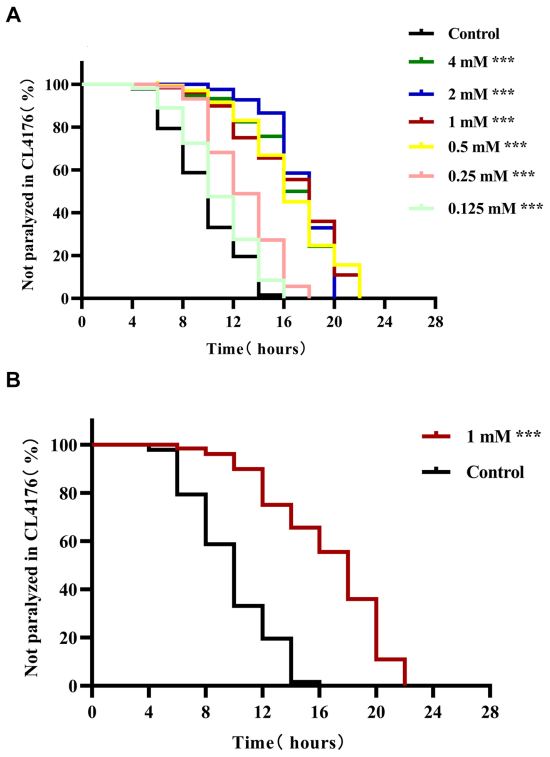

FIGURE 1
4,4′-methylenediphenol delays paralysis in AD worms. After synchronization to the L1 stage, AD transgenic worms CL4176 were treated with different concentrations of 4,4′-methylenediphenol, respectively, and incubated at 16°C for 48 h with equal volume of OP50 bacterial solution without the drug as a blank control (Control group) and then transferred to 25°C to induce the paralyzed phenotype. **(A)** 4,4′-methylenediphenol treatment delayed β-amyloid-induced paralysis, and although half of the worms were paralyzed for a longer period of time at concentrations of 2 and 4 mM, the drug concentration of 1 mM prolonged the overall paralysis of worms for a longer period of time, and so its optimal concentration was 1 mM ($p < 0.001$). **(B)** Paralysis curves of CL4176 worms under administered or non-administered (1 mM) treatments, with 1 mM administration having the most significant effect in delaying the paralysis of worms ($p < 0.001$).

TABLE 1 Time to half paralysis for each concentration of drug ($n = 3$).

Drug concentration(mM)	Half of the paralyzed time(PT50; h)
0.125	8.980
0	10.327
0.25	11.152
0.5	14.323
1	14.477
4	14.783
2	15.846

3.2 4,4′-methylenediphenol prolonged the lifespan and enhanced the motility of worms

The lifespan of worms is closely related to senescence, which plays an important role in the development of AD (Santoro et al., 2020). Here, we investigated the effect of 4,4′-methylenediphenol (1 mM) on the lifespan of AD model worms. The maximum lifespan of worms in the Control and 4,4′-methylenediphenol administration group was 22 and 26 days, respectively. Compared with the Control group, the median and mean lifespan of worms in the drug treatment group were

significantly prolonged ($p < 0.05$ and $p < 0.01$, respectively), with an average lifespan extension of 20.053%. Survival curves showed a rightward shift after 4,4′-methylenediphenol treatment, indicative of a significantly prolonged lifespan in AD model worms (Table 2; Figure 2A). In addition, lipofuscin accumulates in the intestinal tract of worms as their lifespan increases, so lipofuscin levels are strongly associated with worm aging (Höhn et al., 2010). Lipofuscin fluorescence intensity was stronger in the Control group than in the 4,4′-methylenediphenol administration group, and worms in the former group accumulated significantly higher levels ($p < 0.001$) of lipofuscin in their bodies (Figures 2B–D). The above findings indicated that 4,4′-methylenediphenol can reduce lipofuscin levels in worms, and further suggested that the drug can delay aging in the animals.

The effect of a drug on helminth senescence can be indirectly reflected by the determination of the effect of the drug on the reproductive function of the animals (Hyun et al., 2021). The results showed that the difference in the number of offspring between the Control group and the 1 mM 4,4′-methylenediphenol administration group was not significant ($p > 0.05$), indicating that the drug did not affect the reproductive capacity of the worms (Figure 2E). In addition, measurements of worm body length showed no statistically significant ($p > 0.05$) differences in worm body length between groups on day 2 after drug administration, indicating that the drug had no effect on worm development (Figures 2F,G). Under physiological conditions, the ability of worms to pump their pharynx is indicative of their ability to feed, which, in turn, reflects the extent of senescence (Gao et al., 2015). We found that there was no effect on the twitching ability of the worms on day 4 post-drug administration ($p > 0.05$); in contrast, on days 6 and 8 after treatment, the number of twitching events in the worms of the 4,4′-methylenediphenol administration group was significantly higher ($p < 0.001$) than that of the Control group. The motility of worms also has a large correlation with lifespan (Cogliati et al., 2020). Importantly, locomotor ability is the most basic index reflecting the function of the nervous system and is widely used in the toxicological assessment of drugs and poisons (Wang et al., 2021). Our data showed that, compared with the Control group, the motility of the worms in the treatment group was enhanced on days 4, 6, and 8 post-administration ($p < 0.001$). In conclusion, our findings implied that 4,4′-methylenediphenol enhanced motility in AD model worms, including pharyngeal pump beating and locomotion, and also delayed the aging of the animals (Figures 2H,I).

3.3 4,4′-methylenediphenol enhanced stress resistance and reduced ROS levels in N2 worms

Stress resistance refers to the ability of an organism to resist a stressful environment and there is a strong positive correlation between increased longevity and enhanced stress resistance (Tan L. et al., 2022). To investigate the effect of 4,4′-methylenediphenol on stress resistance in the nematodes, we first explored the changes in the ability of N2 worms to resist heat stress (37°C) following 4,4′-methylenediphenol administration. The results showed that the overall survival time of worms in the 4,4′-methylenediphenol (1 mM) administration group was prolonged compared with that in the Control group ($p < 0.001$), even after 7 h of administration ($p < 0.01$), indicating that treatment with 1 mM 4,4′-methylenediphenol augmented resistance to heat stress in the animals (Figures 3A,B). Next, to test the ability of the drug to protect against oxidative damage, we exposed N2 worms to juglone (300 μM), a strong oxidant that led to their deaths, and measured the survival rate of the worms. The results showed that compared with the Control group, the survival curve of worms in the 4,4′-methylenediphenol administration group was shifted to the right, and the survival rate was significantly increased ($p < 0.001$). After 7 h of treatment, the survival rates of worms in the Control and drug administration groups were 0 and 14.634%, respectively ($p < 0.001$), showing that 4,4′-methylenediphenol can improve the ability of worms to resist externally induced oxidative stress (Figures 3C,D).

When animals are subjected to a variety of harmful stimuli *in vivo*, ROS production is accelerated, leading to an imbalance between the oxidative and antioxidant systems, which then triggers a series of molecular-mechanical reactions. In AD model animals, it has been shown that these events contribute to Aβ accumulation, which, in turn, enhances ROS production and promotes neuronal damage and death, leading to the occurrence of AD. Accordingly, the determination of ROS levels is crucial in the assessment of the effects of AD-targeting drugs (Song et al., 2022). Here, we used paraquat (5 mM) to induce an increase in ROS contents in AD model worms and found that the average ROS fluorescence intensity in the drug administration group was significantly reduced compared with that in the Control group ($p < 0.01$), indicating that 4,4′-methylenediphenol inhibits the production of free radicals in worms to a certain extent, thereby reducing Aβ-induced toxicity (Figures 3E–G).

3.4 4,4′-methylenediphenol reduced Aβ protein deposition in worms

Transgenic *C. elegans* of the CL2006 strain become progressively paralyzed. As the worms age, Aβ gradually accumulates and forms plaques that become toxic, leading to paralysis. Here, we explored the effect of 4,4′-methylenediphenol on the formation of Aβ protein deposits using an *in vivo* Aβ aggregation assay (Fay et al., 1998). Thioflavin S is a homogeneous chemical mixture that can be used for the staining and observation of β-amyloid plaques in AD (DanQing et al., 2021). The results showed that there was no Aβ protein deposition in wild-type N2 worms. In CL2006 worms, however,

TABLE 2 Experimental statistics of CL4176 worm lifespan ($x \pm s$, $n = 3$).

Groups	Maximum lifespan/days	Median lifespan/days	Life expectancy/days	Average life extension rate/%
Control	22	11.940 ± 0.576	14.167 ± 0.629	–
1 mM	26	15.817 ± 0.585**	17.008 ± 0.905*	20.053

10.3389/fnagi.2024.1393721

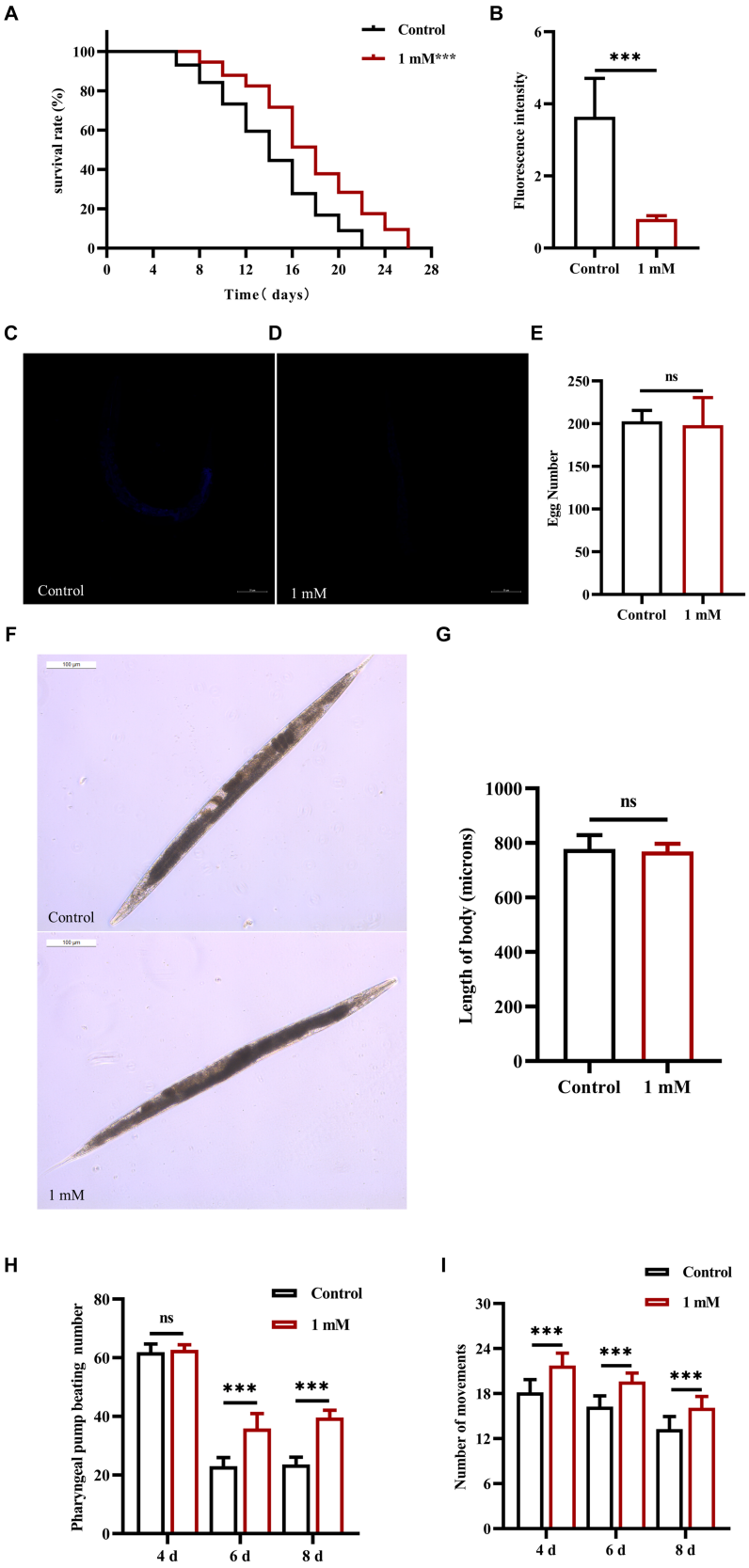

FIGURE 2
Effect of 4,4′-methylenediphenol on senescence-related indices in worms. **(A)** CL4176 worms were cultured in NGM plates with or without drug (1 mM). The survival curve of the drug-administered group was shifted to the right compared to the Control group, and 4,4′-methylenediphenol prolonged the lifespan of AD worms ($p < 0.001$). **(B)** To investigate whether 4,4′-methylenediphenol inhibits lipofuscin aggregation in worms to delay

(Continued)

FIGURE 2 (Continued)
aging, we observed the autofluorescence of lipofuscin in worms on the 10th day after administration of the treatment. The results showed that the lipofuscin level in worms was reduced after administration of the drug ($p < 0.001$). **(C)** Representative pictures of lipofuscin fluorescence in N2 worms not treated with 4,4′-methylenediphenol. **(D)** Representative pictures of lipofuscin fluorescence of N2 worms in the 1 mM administration group. **(E)** The number of eggs laid by worms in the Control group was 202.800 ± 12.795, whereas the number of eggs laid by worms in the 1 mM administration group was 198.300 ± 32.180, and there was no effect of 4,4′-methylenediphenol administration on the reproductive function of worms ($p > 0.05$). **(F)** Representative pictures of worm body lengths. **(G)** Differences in worm body lengths were not statistically significant ($p > 0.05$). Next, we observed the pharyngeal pump beating frequency and locomotor ability of worms on days 4, 6, and 8 within 30 s. 4,4′-methylenediphenol was able to improve the pharyngeal pump beating and locomotor ability of N2 worms ($p < 0.001$). **(H)** 4,4′-methylenediphenol was able to increase the number of pharyngeal pump beats of worms on days 6 and 8. **(I)** The motility of N2 worms was enhanced on days 4, 6, and 8 after the administration of the treatment.

4,4′-methylenediphenol (1 mM) administration significantly reduced Aβ protein aggregation in the head of the worms compared with that seen with the Control treatment ($p < 0.001$). These findings revealed that 4,4′-methylenediphenol can reduce Aβ protein deposition in worms, thus minimizing Aβ-induced toxic effects (Figures 4A–D).

3.5 4,4′-methylenediphenol affected metabolite abundance in CL4176 AD model worms

We performed a broad-spectrum TM analysis to investigate the effect of 4,4′-methylenediphenol treatment on the metabolite profile of the AD-like *C. elegans* CL4176 strain. First, Pearson's correlation analysis was performed on the QC samples, and it was found that the correlation coefficient (r) of the QC samples was close to 1, which indicated that the assay process was stable and the data quality was high (Figure 5A). Secondly, the coefficient of variation (CV) distribution plots of all the samples also showed that the percentage of substances with CVs lower than 0.3 in the QC samples was higher than 75%, indicating that the experimental data were stable (Figure 5B). Orthogonal Partial Least Squares Discriminant Analysis (OPLS-DA), which combines orthogonal signal correction and PLS-DA and decomposes X-matrix information into two categories, namely, Y-related and irrelevant, and filters the discrepant variables by removing irrelevant differences (Wang et al., 2022). As shown in Figure 5C, OPLS-DA demonstrated that there was significant separation between the two groups. Next, we screened for differential metabolites using VIP >1 and p-value <0.05 as the screening criteria. As shown in the volcano plot in Figures 5D, a total of 669 differentially abundant metabolites were identified, 627 of which were downregulated and 42 upregulated. To facilitate the observation of the relative changes in metabolite content, we generated a heatmap of differential metabolite hierarchical clustering. The first-level classification of the differential metabolites in the clustering heatmap indicated that they were related to amino acids and their metabolites, organic acids and their derivatives, nucleotides and their metabolites, coenzymes and vitamins, alkaloids, flavonoids, and terpenoids (Figure 5E). Finally, we performed KEGG pathway enrichment analysis on the metabolites identified as showing differential abundance (Figure 5F). We found that the top 20 p-value-ranked pathways included ABC transporter protein; ubiquinone and other terpene quinone biosynthesis; fatty acid metabolism; unsaturated fatty acid biosynthesis; glycine, serine, and threonine metabolism; and phenylalanine, tyrosine, and tryptophan biosynthesis, among other pathways.

3.6 The effects of 4,4′-methylenediphenol on the expression of DAF-16/FOXO, SKN-1/NRF2, GST-4, and SOD-3 in worms

The insulin signaling pathway plays a key role in the regulation of lifespan. DAF-16 (FOXO transcription factor homolog) is a major regulator of the insulin signaling pathway and its overexpression can delay aging and extend lifespan in worms (Wang et al., 2016). *skn-1*, *gst-4*, and *sod-3* are target genes of DAF-16, and all are associated with longevity and protection against oxidative stress (Liu et al., 2023; Wang et al., 2023). In this study, we first determined the nuclear localization of DAF-16 and the expression of SKN-1. The results showed that treatment with 4,4′-methylenediphenol accelerated the nuclear translocation of DAF-16 in strain TJ356 ($p < 0.001$) (Figures 6A–D), and upregulated SKN-1 expression in LD1 worms (Figures 6E–G). This suggested that the 4,4′-methylenediphenol-mediated mitigation of Aβ toxicity and enhancement of antioxidant properties was, at least partly, due to the activation of DAF-16. Next, we examined the expression of SOD-3 and GST-4. The results showed that 4,4′-methylenediphenol treatment enhanced the fluorescence intensity of SOD-3::GFP in the CF1553 strain (Figures 6H–J), and the fluorescence of the CL2166 strain expressing GST-4::GFP was also significantly increased after 4,4′-methylenediphenol treatment (Figures 6K–M). These results showed that 4,4′-methylenediphenol enhanced the expression of *sod-3* and *gst-4* in the worms ($p < 0.001$), thereby delaying paralysis onset and prolonging the lifespan of the worms.

3.7 DAF-16 plays a key role in the neuroprotective effects of 4,4′-methylenediphenol

DAF-16 acts as a major regulator of the insulin/insulin-like growth factor 1 signaling (IIS) pathway and plays an important role in mediating stress resistance, development, reproduction, metabolism, and longevity (Yang et al., 2016; Zullo et al., 2019). Because we found that 4,4′-methylenediphenol activates the nuclear translocation of DAF-16 in TJ356 worms, we next investigated whether the effect of 4,4′-methylenediphenol on paralysis onset in AD model worms was mediated through DAF-16 by knocking down DAF-16 using RNAi. To this end, we performed RNA interference by feeding to knock down DAF-16 in AD worms to verify whether 4,4′-methylenediphenol could continue to delay the paralytic process of the worms. The results showed that when DAF-16 was knocked down in the worms, there was no significant difference in the ability of the 1 mM administration

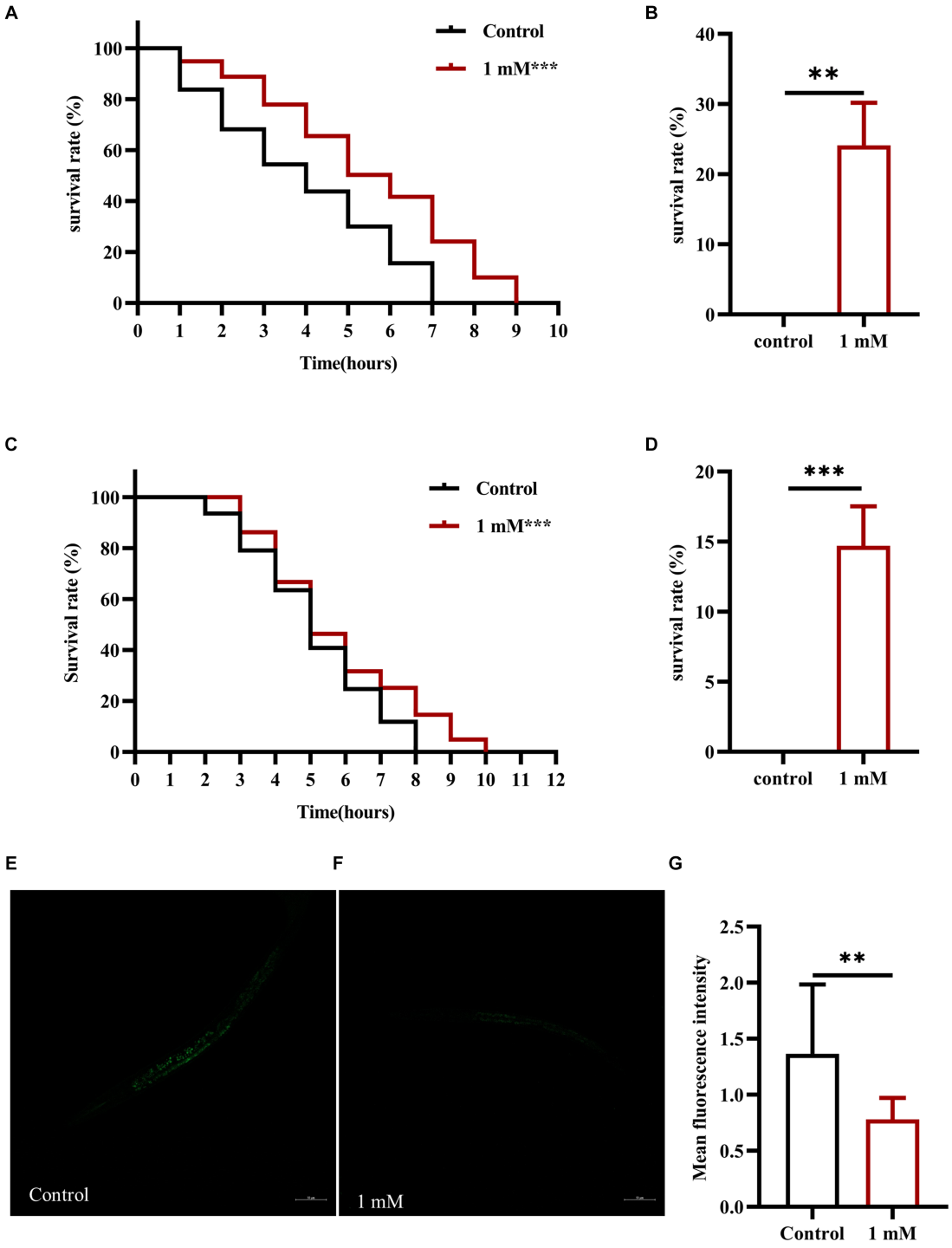

FIGURE 3
4,4′-methylenediphenol enhances stress resistance and reduces ROS levels in N2 worms. **(A)** Under the high temperature stress at 37°C, the overall lifespan of worms increased after 4,4′-methylenediphenol administration, and the drug enhanced their ability to resist heat stress. **(B)** At the 7th h of heat stress treatment, all worms in the Control group died, and the survival rate of worms in the drug-administered group was 24.138% at this time ($p < 0.01$). **(C)** Juglone (300 μM) was used to construct an oxidative stress damage environment. 4,4′-methylenediphenol administration treatment reduced the oxidative stress damage induced by juglone, and improved the oxidative stress resistance of worms. **(D)** At the 7th h of oxidative stress injury, the survival rate of worms was higher in the drug-administered group compared with the Control group. $p < 0.01$, $p < 0.001$, and the experiment was independently repeated three times. In addition, paraquat (5 mM) was used to induce ROS production in worms, and pictures were taken under a fluorescence microscope after staining with DCFH - DA solution. 4,4′-methylenediphenol reduced ROS levels in N2 worms. **(E)** Fluorescent representative pictures of ROS in N2 worms not treated with 4,4′-methylenediphenol. **(F)** ROS fluorescence pictures of N2 worms treated with 4,4′-methylenediphenol administration. **(G)** ROS fluorescence intensity was measured and analyzed using Image J software.

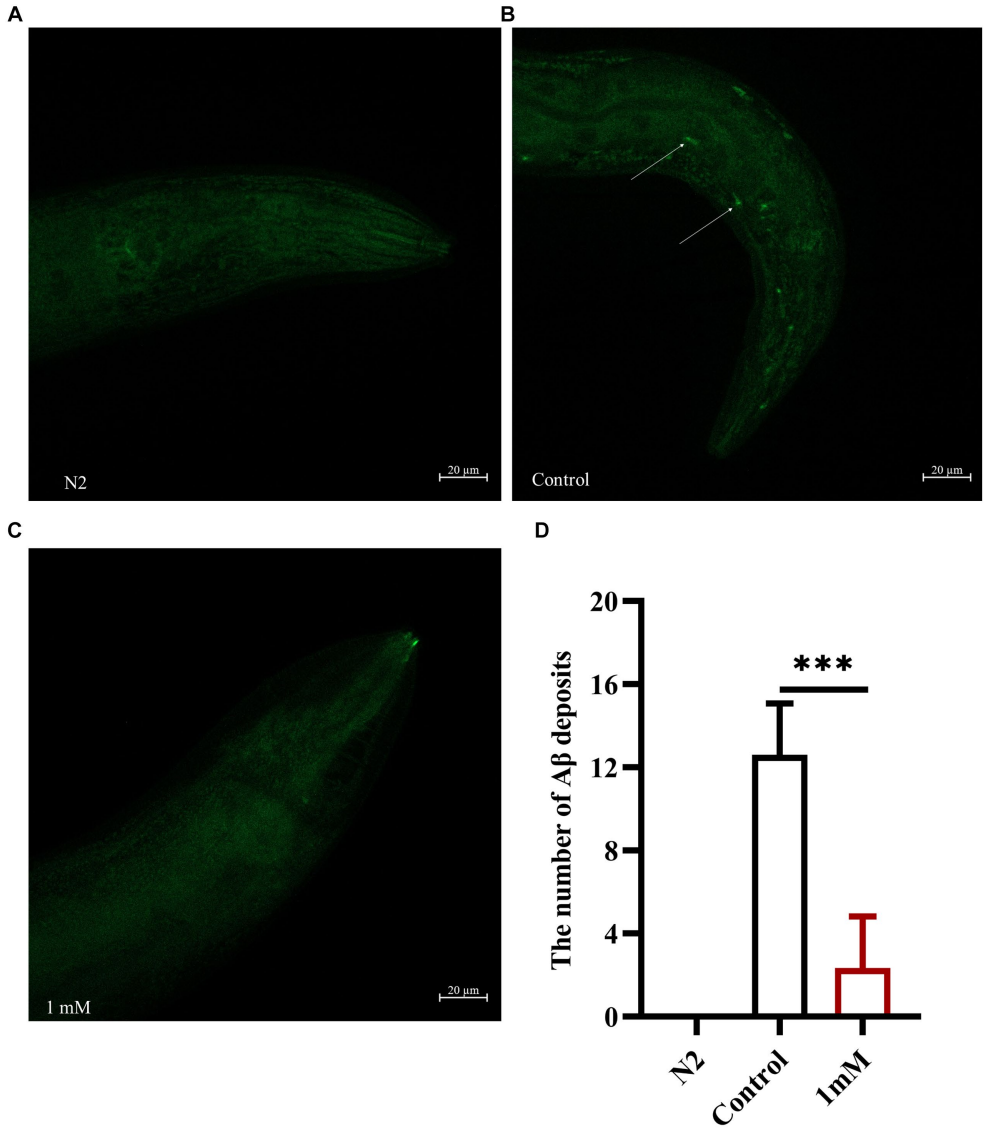

FIGURE 4
4,4′-methylenediphenol reduces the amount of Aβ protein deposited in transgenic worms CL2006. We measured the amount of Aβ protein deposition by thioflavin S staining. In CL2006 worms, staining with thioflavin S for Aβ protein produces distinct fluorescent patches near the pharynx with white arrows indicating Aβ deposition sites. **(A)** Wild-type N2 worms served as negative controls with no Aβ protein deposition. **(B)** Representative images of CL2006 worms not treated with 4,4′-methylenediphenol, with more deposits. **(C)** Representative images of 4,4′-methylenediphenol-treated worms with significantly less deposits. **(D)** Number of Aβ protein deposits in each group. ($p < 0.001$).

group to delay the paralysis of the worms compared with the Control group ($p > 0.05$). In contrast, the ability to delay Aβ-induced paralysis was significantly enhanced in the 1 mM-administered group in the control group of worms in which DAF-16 was not knocked down (Figures 7A,B). This indicated that DAF-16 plays a crucial role in mediating the neuroprotective effect of 4,4′-methylenediphenol in AD model nematodes.

4 Discussion

AD accounts for the highest proportion of dementia cases worldwide and occurs most frequently in older adults. The clinical manifestations of AD include memory loss, cognitive impairment, and impaired self-care ability (Jack et al., 2013). The prevalence and mortality rates of AD and other dementias in China are slightly higher than the global average (Xu et al., 2023), which not only seriously impacts the lives of patients and their families, but also represents a significant economic burden for society (Montgomery et al., 2018; Tahami Monfared et al., 2022). Despite this, currently available therapeutic drugs do not meet the clinical needs of patients or societal demands (Pilonieta et al., 2023).

Natural compounds have shown promise as therapeutic agents for neurodegenerative diseases such as AD (Chen et al., 2021; Li Y. et al., 2024; Ni et al., 2024). Accordingly, several animal models of AD, including mice, dogs, and non-human primates, have been developed aimed at investigating the efficacy and mechanisms of action of natural compounds. However, the high-throughput screening of drugs

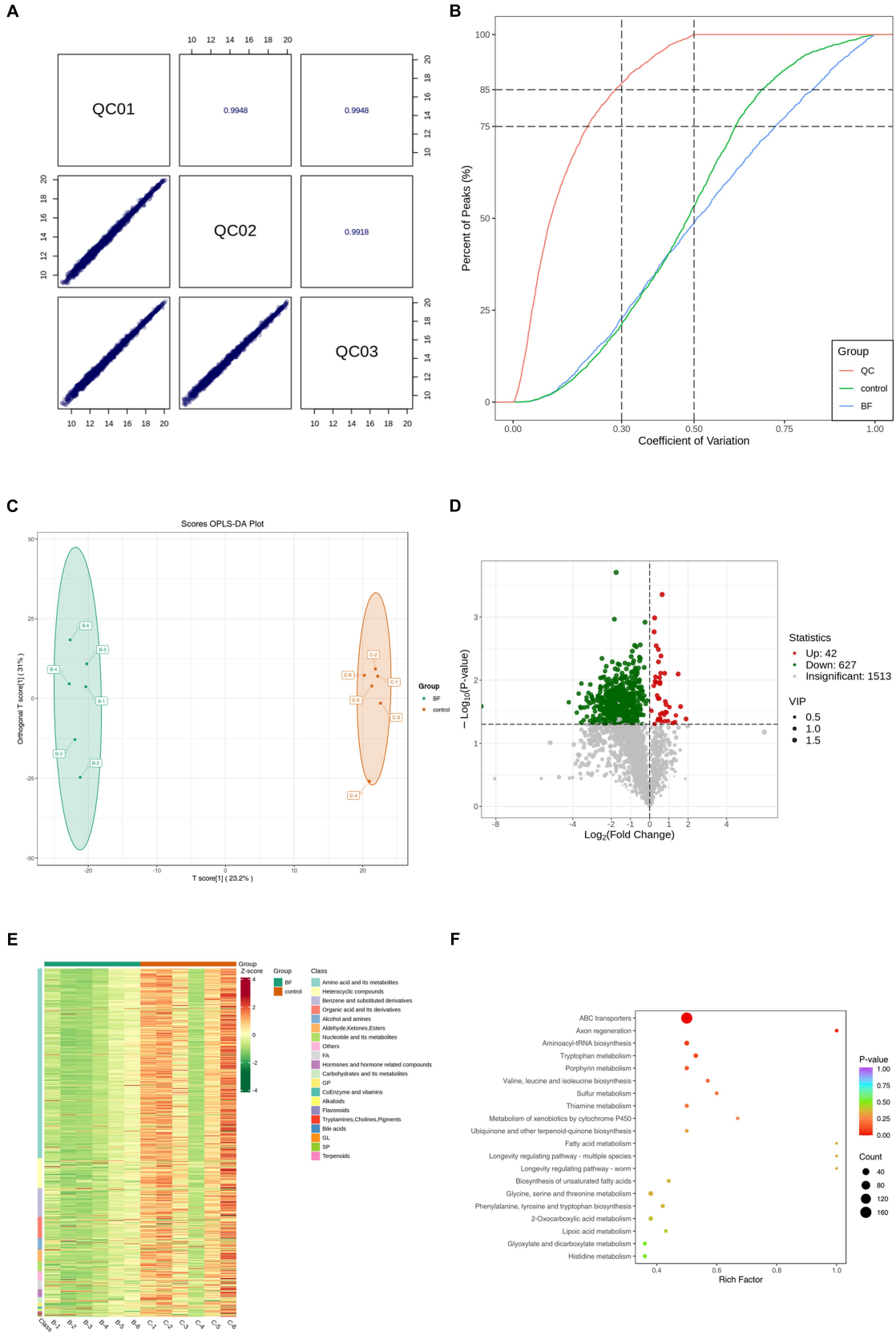

FIGURE 5
We performed TM wide target metabolome sequencing analysis of AD worms. After synchronization of transgenic AD worms CL4176 to the L1 stage, the worms were cultured on NGM plates with or without drug (1 mM), with no less than 1,000 worms per plate and six parallels per group. After incubation at 16°C for 48 h, the plates were warmed up to 25°C and continued to be incubated for about 30 h. Thereafter, the worms were collected in

(Continued)

FIGURE 5 (Continued)
EP tubes with M9 buffer and washed 2–3 times with sterile water. Sequencing analysis was performed after snap-freezing with liquid nitrogen. **(A)** Pearson correlation analysis was performed on the QC samples, and the higher the correlation of QC samples (| r | is closer to 1) indicates the better stability of the whole detection process and the higher quality of data. **(B)** CV distribution of samples in each group. The proportion of substances with CV value less than 0.5 in QC samples is higher than 85%, indicating that the experimental data are more stable; the proportion of substances with CV value less than 0.3 in QC samples is higher than 75%, indicating that the experimental data are very stable. **(C)** OPLS-DA score plot. Orthogonal Partial Least Squares Discriminant Analysis (OPLS-DA) combines Orthogonal Signal Correction (OSC) and PLS-DA methods, which is able to decompose the X matrix information into two types of information related to Y and irrelevant information, and filter the difference variables by removing the irrelevant differences. **(D)** Differential metabolite volcano plots. Volcano Plot (VP) is mainly used to demonstrate the difference in relative content of metabolites in two groups of samples and the statistical significance of the difference. **(E)** In order to facilitate the observation of the change rule of the relative content of metabolites, we used UV (Unit Variance Scaling) processing on the original relative content of differential metabolites obtained by applying the screening criteria for identification by rows, and plotted the differential metabolite clustering heatmap through the R software package. **(F)** Based on the differential metabolite results, KEGG pathway enrichment analysis was performed to obtain the differential metabolite pathway enrichment map. The closer the *p*-value is to 0, the more significant the enrichment is. The size of the dots in the graph represents the number of differentially significant metabolites enriched into the corresponding pathway. The Rich Factor is the ratio of the number of differential metabolites in the corresponding pathway to the total number of metabolites annotated to that pathway, with larger values indicating greater enrichment. The BF group in all plots is the 4,4′-methylenediphenol (1 mM) treatment group, and all results are for the 1 mM treatment group vs. Control group.

in these models is complicated due to limitations such as long experimental periods, high costs, and ethical concerns (Jiang and MacNeil, 2023). To overcome these drawbacks, we selected a smaller model organism, *C. elegans*, to investigate the anti-AD therapeutic potential of 4,4′-methylenediphenol. Compared with other model organisms, *C. elegans* has the advantages of small size, low cost, and short experimental period. Furthermore, many AD transgenic worm strains, such as CL2006, CL4176, and CL2166, have been widely used for relevant research applications. These strains can both better mimic Aβ deposition and other pathologic features of AD and more directly simulate the preventive and therapeutic effects of anti-AD drugs (Margie et al., 2013). In addition, *C. elegans* is transparent, allowing neuronal structure and morphology to be tracked through the expression of GFP in specific neurons, and cellular localization can be visualized using GFP-tagged proteins (Chalfie et al., 1994). Moreover, RNAi knockdown strains are available for approximately 86% of *C. elegans* genes, and, combined with the complete genome sequence information, each gene can be targeted in this model. The RNAi-mediated inhibition of target gene expression enables the assessment of the regulatory effect of a drug on both the gene of interest and the associated signaling pathway (Ketting and Plasterk, 2000). The unique advantages of *C. elegans* have allowed its wide use in screening for natural compounds with potential anti-AD effects. For instance, studies based on this model have demonstrated the antioxidant and anti-aging properties of *Lippia origanoides* essential oil, and highlighted its potential for the prevention and treatment of AD (Henrique Moniz et al., 2023).

Gastrodia elata is a well-known and valuable medicinal herb with a distinctive odor that is suitable for growing in moist and well-ventilated shady environments, such as Yunnan and Guizhou in China. Studies have shown that *Gastrodia elata* and its extracts have potential for use in the prevention and treatment of AD (Shi et al., 2023a). Indeed, one of the active ingredients of *Gastrodia elata*, p-hydroxybenzyl alcohol, was reported to ameliorate Aβ-induced toxic effects (Liu et al., 2022). However, whether another of its other active ingredients, 4,4′-methylenediphenol, also exerts anti-AD effects has not been investigated. In our preliminary study, we found that 4,4′-methylenediphenol, at an optimal effective concentration of 1 mM, had an ameliorative effect on the paralyzed phenotype of AD model worms, and also prolonged their lifespan. This suggested that this active ingredient may mediate, at least in part, the anti-AD action of *Gastrodia elata*. In a follow-up pharmacodynamic study, we further found that 4,4′-methylenediphenol enhanced the motility of, and was not reproductively toxic toward CL4176 worms. Moreover, it is well known that oxidative stress can exacerbate damage to neuronal cells and thus promote AD pathology (Kam et al., 2013; Mohamed et al., 2021). However, we found that 4,4′-methylenediphenol enhanced the resilience of N2 (wild-type) worms to high-temperature environments, as well as to oxidative stress induced by juglone, and improved resistance to oxidative stress damage, thus increasing their survival rate. In addition, ROS and lipofuscin fluorescence analyses showed that 4,4′-methylenediphenol can reduce ROS contents and lipofuscin levels in N2 worms, resulting in antioxidative stress and anti-aging effects. Aβ is considered a crucial marker of AD pathology in AD-related studies (Paul et al., 2020). Our results showed that 1 mM 4,4′-methylenediphenol treatment led to a significant reduction in Aβ protein deposition in the head of CL2006 worms, which, in turn, reduced Aβ-induced toxicity. Combined, these results suggested that 4,4′-methylenediphenol has considerable antioxidative and anti-Aβ toxicity properties.

The metabolite profile can serve as an indicator of an organism's phenotype (Favilli et al., 2023) and help to more effectively understand biological processes and their mechanisms. Critically, neurodegenerative disorders, including AD, are mediated by multiple metabolic pathways (Liu et al., 2022). Metabolomics is a high-throughput screening technology that simultaneously detects and quantifies hundreds of thousands of disturbed metabolites (small molecules in the mass range of 50–1,500 Da) in tissues or biofluids, depicting fluctuations in multiple networks affected by a given disease(Huo et al., 2020). Therefore, the qualitative and quantitative analysis of AD worm metabolites after drug administration treatment is essential for elucidating the pathogenesis of AD (Lista et al., 2023). Thus, we subsequently performed a broad-spectrum TM analysis of CL4176 AD model worms to assess the effect of 4,4′-methylenediphenol administration on its metabolites. Using VIP >1 and *p*-value <0.05 as the differential metabolite screening criteria, we identified a total of 669 metabolites that displayed differential abundance between the Control and drug treatment groups, including 42 that were upregulated and 627 that were downregulated. Among them, a pteridine and its derivative, ethionamide, were found to be upregulated after 4,4′-methylenediphenol administration. Treatment with ethionamide, an antibiotic commonly used for the treatment of tuberculosis, enhances the proliferation and migration of

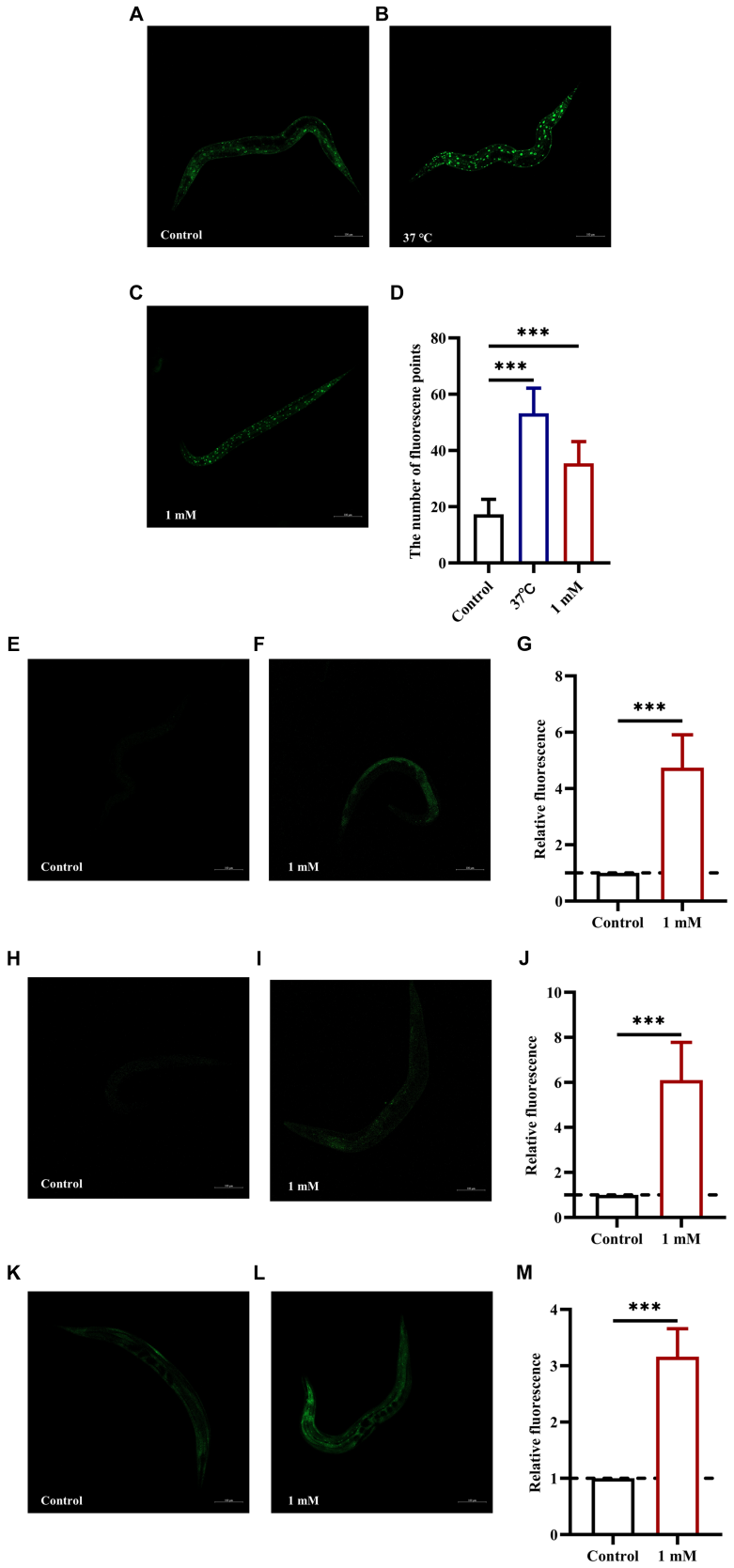

FIGURE 6
4,4′-Methylenediphenol enhances the expression of DAF-16, SKN-1, SOD-3 and GST-4 in GFP reporter gene worms. Fluorescence images were obtained under a laser confocal microscope, and the green fluorescent spots indicated the nucleus localization of DAF-16 in TJ356 worms treated at 37°C for 30 min as a positive control. Representative images of TJ356 worms: **(A)** Control group. **(B)** Positive control group. **(C)** 1 mM

(Continued)

FIGURE 6 (Continued)

4,4′-Methylenediphenol group. **(D)** Number of fluorescence points in each group ($p < 0.001$). Representative images of LD1 worms: **(E)** Control group. **(F)** 1 mM 4,4′-Methylenediphenol group. **(G)** Relative fluorescence intensity measurements of SKN-1::GFP in LD1 worms ($p < 0.001$). Representative images of CF1553 worms: **(H)** Control group. **(I)** 1 mM 4,4′-Methylenediphenol group. **(J)** Fluorescence intensity expression measurement of SOD-3::GFP *in vivo* in CF1553 strain in each group. 1 mM 4,4′-Methylenediphenol increased the expression of SOD-3 in worms ($p < 0.001$). Representative images of CL2166 worms: **(K)** Control group. **(L)** 1 mM 4,4′-Methylenediphenol group. **(M)** Relative fluorescence intensity of GST-4::GFP expression in CL2166 worms ($p < 0.001$). Experiments were repeated independently three times.

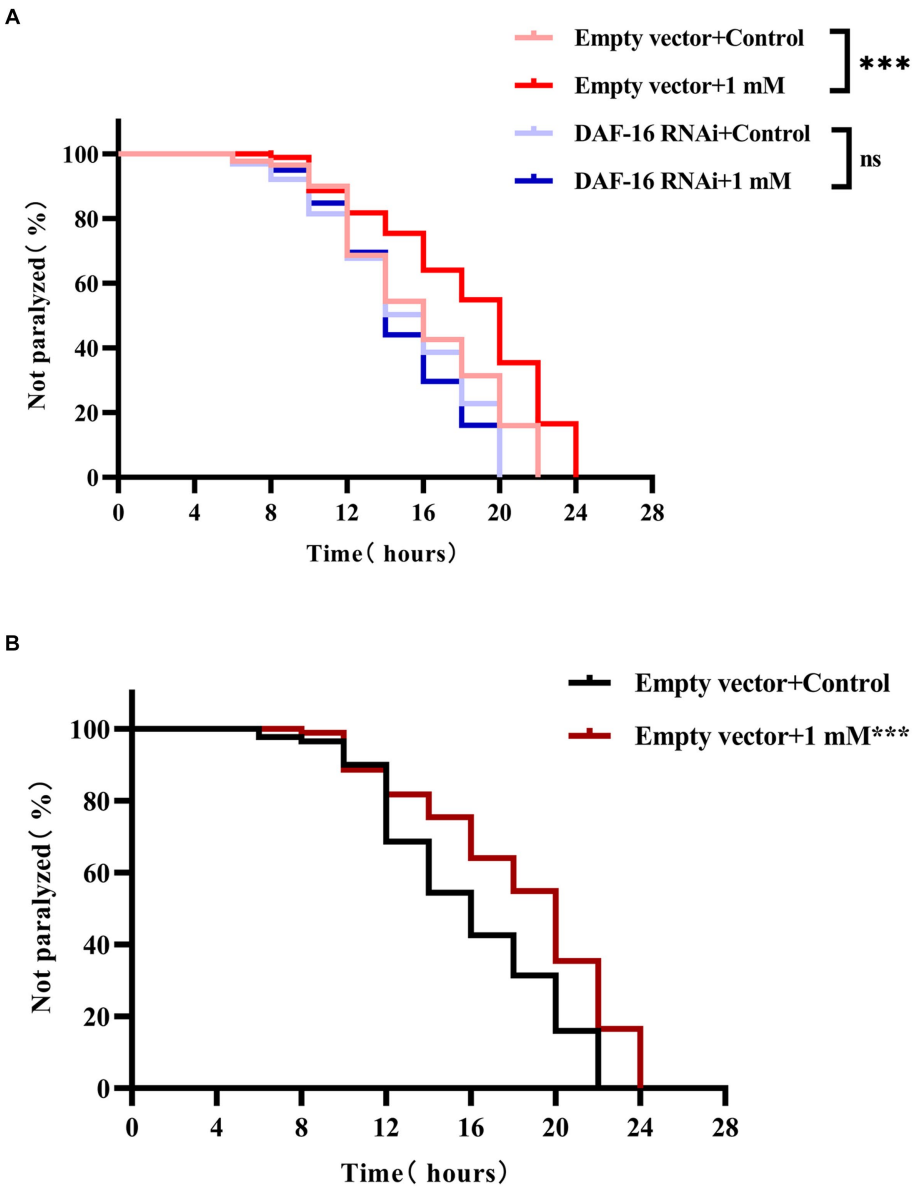

FIGURE 7
4,4′-methylenediphenol delays worm paralysis by activating DAF-16. **(A)** When the DAF-16 gene was knocked out in the transgenic Hidradenitis elegans cryptic nematode strain CL4176, 4,4′-methylenediphenol lost its ability to alleviate β-amyloid-induced paralysis. DAF-16 expression was knocked down by feeding AD worm CL4176 with *E. coli* strain R13H8.1 bacteria carrying DAF-16 dsRNA. Paralysis curves show that the inhibitory effect of 4,4′-methylenediphenol (1 mM) on worm paralysis disappears after DAF-16 knockdown. **(B)** Whereas control worms without DAF-16 knockdown were significantly delayed from paralysis by 1 mM 4,4′-methylenediphenol treatment. At least 50 worms were tested in each group and the experiment was repeated three times independently.

mesenchymal stem cells (MSCs), which are a useful source of cells for the treatment of a variety of immune-mediated diseases, including neurodegenerative disorders; however, the poor migratory and survival capacity of MSCs after brain transplantation limit their therapeutic efficacy in the disease microenvironment, and ethionamide pretreatment led to higher survival and enhanced the

migratory ability of MSCs in models of a variety of diseases, especially neurodegenerative disorders (Lee et al., 2020). The expression of the metabolite taurodeoxycholic acid (TUDCA) was also significantly upregulated by 4,4′-methylenediphenol. Studies have shown that TUDCA has significant antiapoptotic and neuroprotective activities, effects that are exerted both through the regulation and inhibition of the apoptotic cascade as well as the mitigation of oxidative stress, the protection of mitochondria, and the generation of antineuroinflammatory effects. Moreover, abundant experimental and clinical evidence supports that it may be useful as a disease modifier in the treatment of neurodegenerative diseases (Ochiai et al., 2021; Zangerolamo et al., 2021; Khalaf et al., 2022). Our results showed that 4,4′-methylenediphenol treatment upregulated nicotinamide levels. Nicotinamide, an endogenous PARP-1 inhibitor, has been shown to reduce the levels of oxidative stress, apoptosis, and PARP-1 activity in an Aβ protein-induced rat model of AD, and has therapeutic potential in neurodegenerative processes (Turunc Bayrakdar et al., 2014). TM analysis showed that 4,4′-methylenediphenol also upregulated progesterone contents. Progesterone was reported to significantly inhibit the Aβ-induced activation of the NLRP3 inflammasome in astrocytes by mitigating endoplasmic reticulum stress (Yang et al., 2020). In contrast, the expression of clethodim, an herbicide commonly used in agriculture, was downregulated following 4,4′-methylenediphenol treatment. Studies have shown that clethodim is reproductively toxic to zebrafish and induces neurological dysfunction in this model organism (Wang et al., 2019; Xiong et al., 2019). Methotrexate, which exerts cytotoxic effects through the induction of inflammation and oxidative stress and causes lung damage and hepatotoxicity, was similarly found to be downregulated following treatment with 4,4′-methylenediphenol (Fikry et al., 2023; Rajizadeh et al., 2024). The above observations indicated that the 4,4′-methylenediphenol-induced changes in metabolite abundance have an overall positive effect on neurodegenerative diseases. Our KEGG enrichment analysis also showed that the ABC transporter protein pathway was the most significantly enriched, implying that it may play an important role in mediating the neuroprotective effects of 4,4′-methylenediphenol. ABC transporters comprise a family of integral membrane proteins found in most organisms, and their functions include detoxification and nutrient uptake (Qu et al., 2020). Moreover, relevant studies have shown that ABC transporter proteins are highly expressed in the brain and are involved in the pathology of neurodegenerative diseases; they can also perform tissue-protective physiological functions by reducing or limiting the accumulation of neurotoxins in the brain (Gil-Martins et al., 2020; Katzeff and Kim, 2021). Indeed, the blood–brain barrier serves as one of the major pathways mediating the clearance of Aβ proteins from the brain parenchyma, and ABC transporter proteins play a key role in Aβ cytocytosis at the blood–brain barrier (Zhang et al., 2022). This can attenuate AD pathology by exerting an anti-oxidative stress effect and promoting blood–brain barrier integrity (Abuznait and Kaddoumi, 2012; Menet et al., 2020).

Finally, we used strains TJ356 (DAF-16::GFP), LD1 (SKN-1::GFP), CF1553 (SOD-3::GFP), and CL2166 (GST-4::GFP) to further decipher the mechanism of action of 4,4′-methylenediphenol. The results showed that 4,4′-methylenediphenol not only promoted the nuclear localization of DAF-16, but also enhanced the expression of SKN-1, SOD-3, and GST-4 in worms of the respective strains. Further RNAi analysis revealed that the administration of the drug to worms significantly reduced their paralysis rate, an effect that was not observed when DAF-16 was knocked down. DAF-16, a known nuclear transcription factor that induces transcriptional regulation of many genes involved in aging, development, and stress, is the most widely studied of the factors influencing the lifespan extension in *C. elegans* (Li L. et al., 2024). Meanwhile, SOD-3 is regulated by DAF-16 as a downstream target gene that can reduce ROS levels (Yang et al., 2016). The SKN-1 transcription factor, a direct homolog of mammalian nuclear factor red lineage 2-related factor 2 (Nrf-2), has also been associated with longevity and oxidative stress responses (Tullet et al., 2017). Gst-4, a downstream target gene of DAF-16 and SKN-1/Nrf2, improves the body's ability to resist oxidative stress-induced injury (Kahn et al., 2008). In summary, 4,4′-methylenediphenol exerts neuroprotective effects by activating the DAF-16/FOXO and SKN-1/NRF2 pathways, thereby reducing Aβ-induced toxicity in AD worms.

In conclusion, our results indicated that 4,4′-methylenediphenol enhances stress resistance in *C. elegans* by activating multiple cytoprotective pathways, possesses antioxidant and anti-aging activities, and has ameliorative effects on Aβ protein-induced toxicity, which, in turn, delays the onset of AD-like symptoms. In addition, 4,4′-methylenediphenol positively influences the metabolite profile of AD model worms and is expected to be a potential anti-AD drug candidate. However, the pathogenesis of AD is complex and regulated by multiple factors, and the anti-AD effects of 4,4′-methylenediphenol have not been investigated at the level of genes and transcription factors. In future studies, we will explore the targets and mechanisms of action of this active ingredient using a combination of transcriptomics and qPCR. We also aim to screen for genes and signaling pathways related to Aβ toxicity and oxidative stress in worms to further elucidate in-depth the mechanisms of anti-AD action of 4,4′-methylenediphenol.

Data availability statement

The original contributions presented in the study are included in the article/Supplementary material, further inquiries can be directed to the corresponding author.

Ethics statement

The manuscript presents research on animals that do not require ethical approval for their study.

Author contributions

XY: Conceptualization, Data curation, Formal analysis, Project administration, Software, Writing – original draft, Writing – review & editing, Investigation, Methodology, Validation, Visualization. JT: Conceptualization, Formal analysis, Investigation, Methodology, Writing – original draft. TX: Conceptualization, Formal analysis, Methodology, Writing – original draft, Validation. XD: Conceptualization, Formal analysis, Writing – original draft, Data

curation, Funding acquisition, Project administration, Resources, Software, Supervision, Writing – review & editing.

Funding

The author(s) declare that financial support was received for the research, authorship, and/or publication of this article. The present study was supported by the Xingdian Talent Support Program-Special for Young Talent (grant no. XDYC-QNRC-2022-0284), the Highlevel Talents Projects of Yunnan University of Chinese Medicine-Fifth Level Talents, the National Administration of Traditional Chinese Medicine High-level Key Discipline Construction Project "Minority medicine (Dai Medicine)" (No. Zyyzdxk-2023193), the Open Project of Yunnan Key Laboratory of Dai and Yi Medicines (No. 202210SS2209).

Acknowledgments

We thank the Caenorhabditis Genetic Center (CGC) for providing the worm strains.

Conflict of interest

The authors declare that the research was conducted in the absence of any commercial or financial relationships that could be construed as a potential conflict of interest.

Publisher's note

Supplementary material

The Supplementary material for this article can be found online at: https://www.frontiersin.org/articles/10.3389/fnagi.2024.1393721/full#supplementary-material

References

Abuznait, A. H., and Kaddoumi, A. (2012). Role of ABC transporters in the pathogenesis of Alzheimer's disease. *ACS Chem. Neurosci.* 3, 820–831. doi: 10.1021/cn300077c

Alafuzoff, I., Pikkarainen, M., Arzberger, T., Thal, D. R., Al-Sarraj, S., Bell, J., et al. (2008). Inter-laboratory comparison of neuropathological assessments of beta-amyloid protein: a study of the BrainNet Europe consortium. *Acta Neuropathol.* 115, 533–546. doi: 10.1007/s00401-008-0358-2

Canedo-Reis, N. A. P., De Oliveira Pereira, F. S., Ávila, D. S., Guerra, C. C., Flores da Silva, L., Junges, C. H., et al. (2023). Grape juice reduces the effects of amyloid β aggregation phenotype and extends the longevity in *Caenorhabditis elegans*. *Nutr. Neurosci.* 26, 1147–1158. doi: 10.1080/1028415x.2022.2140394

Chalfie, M., Tu, Y., Euskirchen, G., Ward, W. W., and Prasher, D. C. (1994). Green fluorescent protein as a marker for gene expression. *Science* 263, 802–805. doi: 10.1126/science.8303295

Chen, Y., Wang, Y., Qin, Q., Zhang, Y., Xie, L., Xiao, J., et al. (2022). Carnosic acid ameliorated Aβ-mediated (amyloid-β peptide) toxicity, cholinergic dysfunction and mitochondrial defect in *Caenorhabditis elegans* of Alzheimer's model. *Food Funct.* 13, 4624–4640. doi: 10.1039/d1fo02965g

Chen, X., Zhang, M., Ahmed, M., Surapaneni, K. M., Veeraraghavan, V. P., and Arulselvan, P. (2021). Neuroprotective effects of ononin against the aluminium chloride-induced Alzheimer's disease in rats. *Saudi J. Biol. Sci.* 28, 4232–4239. doi: 10.1016/j.sjbs.2021.06.031

Cogliati, S., Clementi, V., Francisco, M., Crespo, C., Argañaraz, F., and Grau, R. (2020). *Bacillus subtilis* delays neurodegeneration and behavioral impairment in the Alzheimer's disease model *Caenorhabditis elegans*. *J. Alzheimers Dis.* 73, 1035–1052. doi: 10.3233/jad-190837

DanQing, L., YuJie, G., ChengPeng, Z., HongZhi, D., Yi, H., BiSheng, H., et al. (2021). N-butanol extract of *Hedyotis diffusa* protects transgenic *Caenorhabditis elegans* from Aβ-induced toxicity. *Phytother. Res.* 35, 1048–1061. doi: 10.1002/ptr.6871

Deng, L. H., Li, L., Zhai, Y., Michael, S., Yang, C. Y., Guo, R., et al. (2020). Tianma Gouteng decoction exerts cardiovascular protection by upregulating OPG and TRAIL in spontaneously hypertensive rats. *Evid. Based Complement. Alternat. Med.* 2020, 3439191–3439111. doi: 10.1155/2020/3439191

Ewald, C. Y., and Li, C. (2012). *Caenorhabditis elegans* as a model organism to study APP function. *Exp. Brain Res.* 217, 397–411. doi: 10.1007/s00221-011-2905-7

Favilli, L., Griffith, C. M., Schymanski, E. L., and Linster, C. L. (2023). High-throughput *Saccharomyces cerevisiae* cultivation method for credentialing-based untargeted metabolomics. *Anal. Bioanal. Chem.* 415, 3415–3434. doi: 10.1007/s00216-023-04724-5

Fay, D. S., Fluet, A., Johnson, C. J., and Link, C. D. (1998). In vivo aggregation of beta-amyloid peptide variants. *J. Neurochem.* 71, 1616–1625. doi: 10.1046/j.1471-4159.1998.71041616.x

Fikry, E., Orfali, R., el-Sayed, S. S., Perveen, S., Ghafar, S., el-Shafae, A. M., et al. (2023). Potential Hepatoprotective effects of *Chamaecyparis lawsoniana* against methotrexate-induced liver injury: integrated phytochemical profiling, target network analysis, and experimental validation. *Antioxidants* 12:118. doi: 10.3390/antiox12122118

Fu, H. J., Zhou, X. Y., Li, Y. P., Chen, X., He, Y. N., Qin, D. L., et al. (2023). The protective effects of *Reineckia carnea* ether fraction against Alzheimer's disease pathology: an exploration in *Caenorhabditis elegans* models. *Int. J. Mol. Sci.* 24:536. doi: 10.3390/ijms242216536

Gao, C., Gao, Z., Greenway, F. L., Burton, J. H., Johnson, W. D., Keenan, M. J., et al. (2015). Oat consumption reduced intestinal fat deposition and improved health span in *Caenorhabditis elegans* model. *Nutr. Res.* 35, 834–843. doi: 10.1016/j.nutres.2015.06.007

Gil-Martins, E., Barbosa, D. J., Silva, V., Remião, F., and Silva, R. (2020). Dysfunction of ABC transporters at the blood-brain barrier: role in neurological disorders. *Pharmacol. Ther.* 213:107554. doi: 10.1016/j.pharmthera.2020.107554

Henrique Moniz, A. M., Xavier Junior, F. H., Melo Martins Silva, G., Reis de Melo, A. C. G., Silva, M., Paiva, W. S., et al. (2023). *Lippia origanoides* essential oil increases longevity and ameliorates β-amyloid peptide-induced toxicity in *Caenorhabditis elegans*. *Nat. Prod. Res.* 1-9, 1–9. doi: 10.1080/14786419.2023.2287183

Höhn, A., Jung, T., Grimm, S., and Grune, T. (2010). Lipofuscin-bound iron is a major intracellular source of oxidants: role in senescent cells. *Free Radic. Biol. Med.* 48, 1100–1108. doi: 10.1016/j.freeradbiomed.2010.01.030

Huang, Z. L. (1985). Recent developments in pharmacological study and clinical application of *Gastrodia elata* in China. *Zhong Xi Yi Jie He Za Zhi* 5, 251–254

Huo, Z., Yu, L., Yang, J., Zhu, Y., Bennett, D. A., and Zhao, J. (2020). Brain and blood metabolome for Alzheimer's dementia: findings from a targeted metabolomics analysis. *Neurobiol. Aging* 86, 123–133. doi: 10.1016/j.neurobiolaging.2019.10.014

Hyun, M., Rathor, L., Kim, H. J., McElroy, T., Hwang, K. H., Wohlgemuth, S., et al. (2021). Comparative toxicities of BPA, BPS, BPF, and TMBPF in the nematode Caenorhabditis elegans and mammalian fibroblast cells. *Toxicology* 461:152924. doi: 10.1016/j.tox.2021.152924

Jack, C. R., Knopman, D. S., Jagust, W. J., Petersen, R. C., Weiner, M. W., Aisen, P. S., et al. (2013). Tracking pathophysiological processes in Alzheimer's disease: an updated hypothetical model of dynamic biomarkers. *Lancet Neurol.* 12, 207–216. doi: 10.1016/s1474-4422(12)70291-0

Jensen, L., Monnat, S. M., Green, J. J., Hunter, L. M., and Sliwinski, M. J. (2020). Rural population health and aging: toward a multilevel and multidimensional research agenda for the 2020s. *Am. J. Public Health* 110, 1328–1331. doi: 10.2105/ajph.2020.305782

Jiang, Y., and MacNeil, L. T. (2023). Simple model systems reveal conserved mechanisms of Alzheimer's disease and related tauopathies. *Mol. Neurodegener.* 18:82. doi: 10.1186/s13024-023-00664-x

Kahn, N. W., Rea, S. L., Moyle, S., Kell, A., and Johnson, T. E. (2008). Proteasomal dysfunction activates the transcription factor SKN-1 and produces a selective oxidative-

stress response in *Caenorhabditis elegans*. *Biochem. J.* 409, 205–213. doi: 10.1042/bj20070521

Kam, T. I., Song, S., Gwon, Y., Park, H., Yan, J. J., Im, I., et al. (2013). FcγRIIb mediates amyloid-β neurotoxicity and memory impairment in Alzheimer's disease. *J. Clin. Invest.* 123, 2791–2802. doi: 10.1172/jci66827

Kang, N., Luan, Y., Jiang, Y., Cheng, W., Liu, Y., Su, Z., et al. (2022). Neuroprotective effects of oligosaccharides in *Rehmanniae* Radix on transgenic *Caenorhabditis elegans* models for Alzheimer's disease. *Front. Pharmacol.* 13:878631. doi: 10.3389/fphar.2022.878631

Katzeff, J. S., and Kim, W. S. (2021). ATP-binding cassette transporters and neurodegenerative diseases. *Essays Biochem.* 65, 1013–1024. doi: 10.1042/ebc20210012

Ketting, R. F., and Plasterk, R. H. (2000). A genetic link between co-suppression and RNA interference in *C. elegans*. *Nature* 404, 296–298. doi: 10.1038/35005113

Khalaf, K., Tornese, P., Cocco, A., and Albanese, A. (2022). Tauroursodeoxycholic acid: a potential therapeutic tool in neurodegenerative diseases. *Transl. Neurodegener.* 11:33. doi: 10.1186/s40035-022-00307-z

Knopman, D. S., Amieva, H., Petersen, R. C., Chételat, G., Holtzman, D. M., Hyman, B. T., et al. (2021). Alzheimer disease. *Nat. Rev. Dis. Primers* 7:33. doi: 10.1038/s41572-021-00269-y

Lee, N. H., Myeong, S. H., Son, H. J., Hwang, J. W., Lee, N. K., Chang, J. W., et al. (2020). Ethionamide preconditioning enhances the proliferation and migration of human Wharton's jelly-derived mesenchymal stem cells. *Int. J. Mol. Sci.* 21:7013. doi: 10.3390/ijms21197013

Li, L., Liu, Z., Hu, H., Cai, R., Bi, J., Wang, Q., et al. (2024). Dendrobium Nobile alcohol extract extends the lifespan of *Caenorhabditis elegans* via hsf-1 and daf-16. *Molecules* 29:908. doi: 10.3390/molecules29040908

Li, Y., Wu, H., Liu, M., Zhang, Z., Ji, Y., Xu, L., et al. (2024). Polysaccharide from Polygala tenuifolia alleviates cognitive decline in Alzheimer's disease mice by alleviating Aβ damage and targeting the ERK pathway. *J. Ethnopharmacol.* 321:117564. doi: 10.1016/j.jep.2023.117564

Lista, S., González-Domínguez, R., López-Ortiz, S., González-Domínguez, Á., Menéndez, H., Martín-Hernández, J., et al. (2023). Integrative metabolomics science in Alzheimer's disease: relevance and future perspectives. *Ageing Res. Rev.* 89:101987. doi: 10.1016/j.arr.2023.101987

Liu, H., Liu, B., Zhang, S., Fan, M., Ji, X., Zhang, S., et al. (2023). Lentinan protects *Caenorhabditis elegans* against fluopyram-induced toxicity through DAF-16 and SKN-1 pathways. *Ecotoxicol. Environ. Saf.* 265:115510. doi: 10.1016/j.ecoenv.2023.115510

Liu, Y., Lu, Y. Y., Huang, L., Shi, L., Zheng, Z. Y., Chen, J. N., et al. (2022). Para-Hydroxybenzyl alcohol delays the progression of neurodegenerative diseases in models of *Caenorhabditis elegans* through activating multiple cellular protective pathways. *Oxidative Med. Cell. Longev.* 2022, 8986287–8986218. doi: 10.1155/2022/8986287

Liu, J., and Mori, A. (1992). Antioxidant and free radical scavenging activities of *Gastrodia elata* Bl. and *Uncaria rhynchophylla* (Miq.) jacks. *Neuropharmacology* 31, 1287–1298. doi: 10.1016/0028-3908(92)90058-w

Long, T., Chen, X., Zhang, Y., Zhou, Y. J., He, Y. N., Zhu, Y. F., et al. (2023). Protective effects of Radix *Stellariae* extract against Alzheimer's disease via autophagy activation in Caenorhabditis elegans and cellular models. *Biomed. Pharmacother.* 165:115261. doi: 10.1016/j.biopha.2023.115261

Lu, Z., Fu, J., Wu, G., Yang, Z., Wu, X., Wang, D., et al. (2023). Neuroprotection and mechanism of gas-miR36-5p from *Gastrodia elata* in an Alzheimer's disease model by regulating glycogen synthase kinase-3β. *Int. J. Mol. Sci.* 24:295. doi: 10.3390/ijms242417295

Margie, O., Palmer, C., and Chin-Sang, I. (2013). *C. elegans* chemotaxis assay. *J. Vis. Exp.* 74:e50069. doi: 10.3791/50069

Menet, R., Bourassa, P., Calon, F., and ElAli, A. (2020). Dickkopf-related protein-1 inhibition attenuates amyloid-beta pathology associated to Alzheimer's disease. *Neurochem. Int.* 141:104881. doi: 10.1016/j.neuint.2020.104881

Meng, J., Lv, Z., Guo, M., Sun, C., Li, X., Jiang, Z., et al. (2022). A *Lycium barbarum* extract inhibits β-amyloid toxicity by activating the antioxidant system and mtUPR in a *Caenorhabditis elegans* model of Alzheimer's disease. *FASEB J.* 36:e22156. doi: 10.1096/fj.202101116RR

Mohamed, E. A., Ahmed, H. I., Zaky, H. S., and Badr, A. M. (2021). Sesame oil mitigates memory impairment, oxidative stress, and neurodegeneration in a rat model of Alzheimer's disease. A pivotal role of NF-κB/p38MAPK/BDNF/PPAR-γ pathways. *J. Ethnopharmacol.* 267:113468. doi: 10.1016/j.jep.2020.113468

Mohsenzadegan, M., and Mirshafiey, A. (2012). The immunopathogenic role of reactive oxygen species in Alzheimer disease. *Iran. J. Allergy Asthma Immunol.* 11, 203–216

Montgomery, W., Ueda, K., Jorgensen, M., Stathis, S., Cheng, Y., and Nakamura, T. (2018). Epidemiology, associated burden, and current clinical practice for the diagnosis and management of Alzheimer's disease in Japan. *Clinicoecon. Outcomes Res.* 10, 13–28. doi: 10.2147/ceor.S146788

Ni, H., Liu, M., Cao, M., Zhang, L., Zhao, Y., Yi, L., et al. (2024). Sinomenine regulates the cholinergic anti-inflammatory pathway to inhibit TLR4/NF-κB pathway and protect the homeostasis in brain and gut in scopolamine-induced Alzheimer's disease mice. *Biomed. Pharmacother.* 171:116190. doi: 10.1016/j.biopha.2024.116190

Ochiai, T., Nagayama, T., Matsui, K., Amano, K., Sano, T., Wakabayashi, T., et al. (2021). Tauroursodeoxycholic acid attenuates diet-induced and age-related peripheral endoplasmic reticulum stress and cerebral amyloid pathology in a mouse model of Alzheimer's disease. *J. Prev Alzheimers Dis.* 8, 483–494. doi: 10.14283/jpad.2021.33

Paul, D., Chipurupalli, S., Justin, A., Raja, K., and Mohankumar, S. K. (2020). *Caenorhabditis elegans* as a possible model to screen anti-Alzheimer's therapeutics. *J. Pharmacol. Toxicol. Methods* 106:106932. doi: 10.1016/j.vascn.2020.106932

Pilonieta, G., Pisu, M., Martin, R. C., Shan, L., Kennedy, R. E., Oates, G., et al. (2023). Specialist availability and drug adherence in older adults with dementia across regions of the United States. *J. Alzheimers Dis.* 93, 927–937. doi: 10.3233/jad-220620

Qu, J., Chen, T., Yao, M., Wang, Y., Xiao, W., and Li, B. (2020). ABC transporter and its application in synthetic biology. *Chin. J. Biotechnol.* 36, 1754–1766. doi: 10.13345/j.cjb.200005

Rajizadeh, M. A., Hosseini, M. H., Bahrami, M., Bahri, F., Rostamabadi, F., Bagheri, F., et al. (2024). High-intensity intermittent training ameliorates methotrexate-induced acute lung injury. *BMC Pulm. Med.* 24:45. doi: 10.1186/s12890-024-02853-w

Rani, N., Alam, M. M., Jamal, A., Bin Ghaffar, U., and Parvez, S. (2023). *Caenorhabditis elegans*: a transgenic model for studying age-associated neurodegenerative diseases. *Ageing Res. Rev.* 91:102036. doi: 10.1016/j.arr.2023.102036

Santoro, A., Martucci, M., Conte, M., Capri, M., Franceschi, C., and Salvioli, S. (2020). Inflammaging, hormesis and the rationale for anti-aging strategies. *Ageing Res. Rev.* 64:101142. doi: 10.1016/j.arr.2020.101142

Shi, X., Luo, Y., Yang, L., and Duan, X. (2023a). Protective effect of *Gastrodia elata* Blume in a *Caenorhabditis elegans* model of Alzheimer's disease based on network pharmacology. *Biomed Rep* 18:37. doi: 10.3892/br.2023.1620

Shi, X., Yu, X., Yang, L., and Duan, X. (2023b). Ethyl acetate extract of *Gastrodia elata* protects *Caenorhabditis elegans* from oxidative stress and amyloid β peptide toxicity. *Exp. Ther. Med.* 26:405. doi: 10.3892/etm.2023.12104

Sola, I., Viayna, E., Gómez, T., Galdeano, C., Cassina, M., Camps, P., et al. (2015). Multigram synthesis and in vivo efficacy studies of a novel multitarget anti-Alzheimer's compound. *Molecules* 20, 4492–4515. doi: 10.3390/molecules20034492

Song, X., Sun, Y., Wang, Z., Su, Y., Wang, Y., and Wang, X. (2022). Exendin-4 alleviates β-amyloid peptide toxicity via DAF-16 in a *Caenorhabditis elegans* model of Alzheimer's disease. *Front. Aging Neurosci.* 14:955113. doi: 10.3389/fnagi.2022.955113

Stocker, H., Trares, K., Beyer, L., Perna, L., Rujescu, D., Holleczek, B., et al. (2023). Alzheimer's polygenic risk scores, APOE, Alzheimer's disease risk, and dementia-related blood biomarker levels in a population-based cohort study followed over 17 years. *Alzheimers Res. Ther.* 15:129. doi: 10.1186/s13195-023-01277-8

Tahami Monfared, A. A., Byrnes, M. J., White, L. A., and Zhang, Q. (2022). Alzheimer's disease: epidemiology and clinical progression. *Neurol. Ther.* 11, 553–569. doi: 10.1007/s40120-022-00338-8

Tan, W., Qi, L., Hu, X., and Tan, Z. (2022). Research progress in traditional Chinese medicine in the treatment of Alzheimer's disease and related dementias. *Front. Pharmacol.* 13:921794. doi: 10.3389/fphar.2022.921794

Tan, L., Zheng, Z. Y., Huang, L., Jin, Z., Li, S. L., Wu, G. S., et al. (2022). Flavonol glycoside complanatoside a requires FOXO/DAF-16, NRF2/SKN-1, and HSF-1 to improve stress resistances and extend the life span of *Caenorhabditis elegans*. *Front. Pharmacol.* 13:931886. doi: 10.3389/fphar.2022.931886

Tang, C., Wang, L., Liu, X., Cheng, M., and Xiao, H. (2016). Chemical fingerprint and metabolic profile analysis of ethyl acetate fraction of *Gastrodia elata* by ultra-performance liquid chromatography/quadrupole-time of flight mass spectrometry. *J. Chromatogr. B Analyt. Technol. Biomed. Life Sci.* 1011, 233–239. doi: 10.1016/j.jchromb.2015.09.043

Tao, S., Hong-gao, L., and Yuan-zhong, W. (2023). Herbal textual and key problems discussion in modern resource utilization of *Gastrodiae rhizoma*. *Chin. Tradit. Herb. Drug* 54, 6106–6117.

Tissenbaum, H. A. (2015). Using *C. elegans* for aging research. *Invertebr. Reprod. Dev.* 59, 59–63. doi: 10.1080/07924259.2014.940470

Tullet, J. M. A., Green, J. W., Au, C., Benedetto, A., Thompson, M. A., Clark, E., et al. (2017). The SKN-1/Nrf2 transcription factor can protect against oxidative stress and increase lifespan in *C. elegans* by distinct mechanisms. *Aging Cell* 16, 1191–1194. doi: 10.1111/acel.12627

Turunc Bayrakdar, E., Uyanikgil, Y., Kanit, L., Koylu, E., and Yalcin, A. (2014). Nicotinamide treatment reduces the levels of oxidative stress, apoptosis, and PARP-1 activity in Aβ(1-42)-induced rat model of Alzheimer's disease. *Free Radic. Res.* 48, 146–158. doi: 10.3109/10715762.2013.857018

Wang, X., Cao, M., and Dong, Y. (2016). Royal jelly promotes DAF-16-mediated proteostasis to tolerate β-amyloid toxicity in *C. elegans* model of Alzheimer's disease. *Oncotarget* 7, 54183–54193. doi: 10.18632/oncotarget.10857

Wang, L. N., Gu, X. R., Si, N., Wang, H. J., Zhou, Y. Y., Bian, B. L., et al. (2022). Biomarkers related to cognitive dysfunction in APP/PS1 mice based on non-targeted metabonomics and intervention mechanism of *Huanglian jiedu* decoction. *Zhongguo Zhong Yao Za Zhi* 47, 6117–6126. doi: 10.19540/j.cnki.cjcmm.20220705.401

Wang, S., Lin, D., Cao, J., and Wang, L. (2023). APPA increases lifespan and stress resistance via lipid metabolism and insulin/IGF-1 signal pathway in *Caenorhabditis elegans*. *Int. J. Mol. Sci.* 24:682. doi: 10.3390/ijms241813682

Wang, Y., Liu, S. S., Huang, P., Wang, Z. J., and Xu, Y. Q. (2021). Assessing the combined toxicity of carbamate mixtures as well as organophosphorus mixtures to *Caenorhabditis elegans* using the locomotion behaviors as endpoints. *Sci. Total Environ.* 760:143378. doi: 10.1016/j.scitotenv.2020.143378

Wang, H., Zhou, L., Meng, Z., Su, M., Zhang, S., Huang, P., et al. (2019). Clethodim exposure induced development toxicity and behaviour alteration in early stages of zebrafish life. *Environ. Pollut.* 255:113218. doi: 10.1016/j.envpol.2019.113218

Weuve, J., Hebert, L. E., Scherr, P. A., and Evans, D. A. (2014). Deaths in the United States among persons with Alzheimer's disease (2010-2050). *Alzheimers Dement.* 10, e40–e46. doi: 10.1016/j.jalz.2014.01.004

Xiong, G., Zou, L., Deng, Y., Meng, Y., Liao, X., and Lu, H. (2019). Clethodim exposure induces developmental immunotoxicity and neurobehavioral dysfunction in zebrafish embryos. *Fish Shellfish Immunol.* 86, 549–558. doi: 10.1016/j.fsi.2018.12.002

Xu, Y., Wang, J., Wang, H., Wang, Y., Liu, Z., Yu, J., et al. (2023). 2023 data and strategies of prevention and control for Alzheimer's disease in China. *Chin. J. Alzheimers Dis. Relat. Dis.* 6, 175–192+173. doi: 10.3969/j.issn.2096-5516.2023.03.001

Yang, Y., Ma, D., Xu, W., Chen, F., Du, T., Yue, W., et al. (2016). Exendin-4 reduces tau hyperphosphorylation in type 2 diabetic rats via increasing brain insulin level. *Mol. Cell. Neurosci.* 70, 68–75. doi: 10.1016/j.mcn.2015.10.005

Yang, H., Ming-xia, W., Long-fei, X., and Yun-jiang, L. (2020). The protective mechanism of progesterone on Aβ-induced inflammasomes activation in astrocytes. *Chin. Pharmacol. Bull.* 36, 420–423.

Yi-Ming, L., Zhuo-Lun, Z., and Yong-Fu, H. (1993). New phenolic derivatives from *Galeola faberi*. *Planta Med.* 59, 363–365. doi: 10.1055/s-2006-959702

Zangerolamo, L., Vettorazzi, J. F., Rosa, L. R. O., Carneiro, E. M., and Barbosa, H. C. L. (2021). The bile acid TUDCA and neurodegenerative disorders: an overview. *Life Sci.* 272:119252. doi: 10.1016/j.lfs.2021.119252

Zhang, Y. L., Wang, J., Zhang, Z. N., Su, Q., and Guo, J. H. (2022). The relationship between amyloid-beta and brain capillary endothelial cells in Alzheimer's disease. *Neural Regen. Res.* 17, 2355–2363. doi: 10.4103/1673-5374.335829

Zullo, J. M., Drake, D., Aron, L., O'Hern, P., Dhamne, S. C., Davidsohn, N., et al. (2019). Regulation of lifespan by neural excitation and REST. *Nature* 574, 359–364. doi: 10.1038/s41586-019-1647-8

frontiers | Frontiers in Aging Neuroscience

TYPE Original Research
PUBLISHED 15 July 2024
DOI 10.3389/fnagi.2024.1433691

OPEN ACCESS

EDITED BY
Yuping Tang,
Fudan University, China

REVIEWED BY
Chandramouli Natarajan,
University of Texas Medical Branch at Galveston, United States
Heling Chu,
Shanghai Jiao Tong University, China

*CORRESPONDENCE
Fengqiu Dai
✉ daifq17@lzu.edu.cn
Xiangchun Shen
✉ shenxiangchun@126.com

RECEIVED 16 May 2024
ACCEPTED 25 June 2024
PUBLISHED 15 July 2024

CITATION
Zhang E, Chen T, Chen Y, Long C, Tao L, Shen X and Dai F (2024) The role of Immune cells in Alzheimer's disease: a bidirectional Mendelian randomization study. *Front. Aging Neurosci.* 16:1433691. doi: 10.3389/fnagi.2024.1433691

The role of Immune cells in Alzheimer's disease: a bidirectional Mendelian randomization study

Erdong Zhang[1,2,3], Tingting Chen[4], Yanqin Chen[1], Chenxiang Long[5], Ling Tao[1], Xiangchun Shen[1,2,3]* and Fengqiu Dai[5]*

[1]The Key Laboratory of Optimal Utilization of Natural Medicine Resources, School of Pharmaceutical Sciences, Guizhou Medical University, Guiyang, Guizhou, China, [2]The State Key Laboratory of Functions and Applications of Medicinal Plants, Guizhou Medical University, Guiyang, Guizhou, China, [3]The High Efficacy Application of Natural Medicinal Resources Engineering Center of Guizhou Province, School of Pharmaceutical Sciences, Guizhou Medical University, Guiyang, Guizhou, China, [4]The Pharmacy Department, Guiyang Maternal and Child Health-Care Hospital, Guiyang, Guizhou, China, [5]Department of Anatomy, School of Basic Medical Sciences, Guizhou Medical University, Guiyang, China

Background: Alzheimer's disease (AD) is a leading cause of dementia, characterized by the accumulation of amyloid-beta (Aβ) and hyperphosphorylated tau proteins, leading to neuroinflammation and neuronal damage. The role of the immune system in AD pathogenesis is increasingly recognized, prompting an exploration of the causal relationship between immune cells and AD by using Mendelian randomization (MR) approaches.

Methods: Utilizing genome-wide association study (GWAS) data from European cohorts, we conducted an MR study to investigate the causal links between immune cell phenotypes and AD. We selected single nucleotide polymorphisms (SNPs) associated with immune cell traits at a genome-wide significance threshold and applied various MR methods, including MR Egger, Weighted median, and inverse variance weighted analysis, to assess the causality between 731 immune phenotypes and AD.

Results: Our MR analysis identified 15 immune cell types with significant causal relationships to AD pathogenesis. Notably, the absolute count of $CD28^{-}CD4^{-}CD8^{-}$ T cells and the expression of HLA DR on B cells were linked to a protective effect against AD, while 13 other immune phenotypes were identified as contributing to the risk factors for the disease. The causal effects of AD on immunophenotypic traits are predominantly negative, implying that AD may impair the functionality of immune cells. Validation through independent datasets, such as FinnGen and GCST90027158, confirmed the causal association between six specific immune cells and AD.

Conclusion: This comprehensive MR study elucidates the intricate network of causal relationships between diverse immunophenotypic traits and AD, providing novel insights into the immunopathogenesis of AD. The findings suggest potential immunological targets that could be leveraged for early diagnosis, disease monitoring, and therapeutic intervention.

KEYWORDS

Alzheimer's disease, immune cells, Mendelian randomization study, HLA DR on B cells, $CD4^{+}CD8$ dim T cells, $CD14^{+}CD16^{-}$ monocyte

1 Introduction

Alzheimer's Disease (AD) is a major cause of dementia and is swiftly emerging as one of the most financially draining, lethal, and burdensome health issues of our time (Livingston et al., 2020). With the escalating trend of an aging global population, the incidence and prevalence of AD are on a continuous upswing, presenting unprecedented challenges for individuals, families, and society at large (Alzheimer's disease facts and figures, 2024). Data from the Alzheimer's Association and the World Health Organization (WHO) indicate that around 55 million individuals worldwide are affected by dementia, with projections estimating a doubling of this number by 2050 (Alzheimer's disease facts and figures, 2024). Within this demographic, AD, the most prevalent neurodegenerative condition, is responsible for approximately 50% to 70% of all neurodegenerative dementia cases (2024). The pathophysiology of AD is marked by the abnormal accumulation of two key proteins: amyloid-beta (Aβ) and tau. These aberrant protein deposits manifest as amyloid plaques and neurofibrillary tangles (NFTs) within the brain, culminating in impaired neuronal function and cell death (Villemagne et al., 2013). The presence of Aβ plaques and NFTs prompts the activation of brain immune cells, notably microglia, initiating a cascade of chronic neuroinflammation that further aggravates neuronal damage (Rajmohan and Reddy, 2017). Consequently, therapeutic strategies for AD are centered on reducing Aβ plaque accumulation, preventing the abnormal phosphorylation of tau protein, mitigating neuroinflammation, and enhancing neuronal function. The ultimate goal of these interventions is to halt or reverse the disease's pathological trajectory, thereby aiming to enhance cognitive abilities and the overall quality of life for patients.

The etiology of AD is exceptionally intricate, encompassing a spectrum of factors such as genetics, environmental exposures, and lifestyle choices. The role of the immune system in this context has introduced novel dimensions to our understanding of the condition (Frost et al., 2019). The activation patterns of the immune system within AD potentially provide pivotal insights for the early detection of the disease (Liddelow et al., 2017). Research has indicated the presence of a chronic inflammatory process within the brains of individuals with AD, a process that may initiate prior to the observable decline in cognitive abilities (Xiong et al., 2021). Specifically, microglia—the principal immune cells of the central nervous system—are intimately involved in the genesis and removal of Aβ (Sun et al., 2023b). The sustained activation of microglia in the brain tissue of AD patients can lead to the release of inflammatory mediators that intensify neuroinflammation and may inflict damage upon neurons (Xiong et al., 2021). Consequently, the surveillance of microglial activation levels could be instrumental in the preemptive identification of individuals at elevated risk for AD, prior to the onset of clinical symptoms. Furthermore, the heterogeneity and complexity inherent to immune cells present unique challenges for the therapeutic management of AD (Keren-Shaul et al., 2017). Diverse immune cell types may exert distinct effects within the context of AD, and even within a single cell type, varying activation states can lead to markedly different outcomes (Feng et al., 2021; Chen and Holtzman, 2022; Jorfi et al., 2023b). Therefore, the monitoring and regulation of immune cell activation could serve as a critical instrument in disease surveillance, facilitating the evaluation of disease activity and the rate of progression.

Traditional research has encountered significant challenges in delineating a causal link between immune cells and AD, largely attributable to constraints in study design and the confounding effects of factors such as age, gender, genetic lineage, lifestyle elements, and the presence of comorbidities, all of which can influence immune cell function and the risk profile for AD (Nebel et al., 2018; Xia et al., 2018; Zhang et al., 2021). While observational study methodologies, including cross-sectional and cohort studies, have furnished critical epidemiological understanding of AD, the alteration of immune cells could be both an effect and a precipitant of the disease, obfuscating the identification of a definitive causal sequence (Yu et al., 2020; Xu and Jia, 2021; Rajesh and Kanneganti, 2022). Mendelian Randomization (MR) studies, which utilize genetic variants as instrumental variables to investigate causality, present a methodological solution (Chen et al., 2022). This MR approach uses genetic variants, which are stochastically allocated during gametogenesis, mirroring the random assignment characteristic of randomized controlled trials, thereby diminishing the confounding effects (Emdin et al., 2017; Larsson et al., 2023). The inherent fixity of genetic variants, coupled with their extraneousness to disease status, positions MR as a robust tool for minimizing the risk of reverse causal inference (Chen et al., 2022). MR studies can capitalize on data from extensive Genome-Wide Association Studies (GWAS), offering genetic variants intimately linked to discrete traits and amplifying the statistical vigor of the research (Emdin et al., 2017; Larsson et al., 2023). Utilizing MR analysis, we have probed into the causal nexus between immune cells and the genesis and trajectory of AD, establishing a causal relationship between six distinct immune cell types and the evolution of AD. These findings not only illuminate potential therapeutic targets for AD but also herald the potential for personalized medical approaches. By scrutinizing patients' immunological profiles, including the phenotype and functionality of immune cells, it becomes feasible to anticipate individual responses to targeted treatments, enabling a bespoke therapeutic strategy.

2 Materials and methods

2.1 Data approval

This study leverages GWAS data sourced from public databases to explore the potential causal relationships between immune cells and AD, as outlined in Figure 1. Before the study's commencement, all pertinent datasets underwent stringent ethical review and were granted approval by the respective institutional review boards, thereby guaranteeing the research's adherence to ethical standards.

2.2 Data sources for AD

The underpinning data for this study are derived from European population samples pertaining to AD. We sourced single nucleotide polymorphisms (SNPs) linked to AD from the most extensive GWAS meta-analysis to date, as executed by the

National Institute on Aging Genetics of Alzheimer's Disease Data Storage Site (NIAGADS), under the accession code NG00075. This dataset encompasses a total of 35,274 individuals with AD and 59,163 control subjects (Kunkle et al., 2019). Furthermore, SNPs data from the FinnGen database (https://www.finngen.fi/en) were employed for the validation of our research findings, with a total of 10,520 cases and 401,661 controls (Kurki et al., 2023). In addition, we drew upon the summary statistics for AD as cataloged in the GWAS Catalog, identified by the accession number GCST90027158, which includes a total of 39,106 cases and 46,828 controls (Bellenguez et al., 2022). All AD patient samples were collected in strict accordance with established clinical diagnostic standards.

2.3 Sources of immunity-spanning GWAS data

The aggregated statistical data for all immunological traits analyzed in this study originate from the GWAS Catalog, with accession numbers spanning from GCST0001391 to GCST0002121. This GWAS investigation included a cohort of 3,757 genetically non-overlapping European individuals, with reference samples derived from the Sardinian population sequence. The study scrutinized approximately 22 million SNPs, conducting correlation tests that were adjusted for covariates such as age, age squared, and gender. Utilizing flow cytometry, a comprehensive analysis of 539 distinct immune cell characteristics was undertaken, encompassing 118 absolute cell counts, 389 median fluorescence intensity values for surface antigens, and 32 morphological parameters. Furthermore, the research integrated 192 relative cell counts, which are the ratios between different cell levels, culminating in the assessment of 731 cellular traits across a population of 3,757 Sardinian residents.

2.4 Genetic instrument selection

In our MR analyses, we screened SNPs associated with our exposure of interest at a significance threshold of $p < 5 \times 10^{-5}$, using these as instrumental variables. To ensure near-independence among these SNPs, we meticulously pruned our selection using a linkage disequilibrium (LD) threshold of $r^2 < 0.1$, with a physical distance criterion of 500 kilobase pairs, as implemented in PLINK (Vierstra et al., 2020). In our analysis, we leveraged the Linkage Disequilibrium (LD) reference panel from the 1000 Genomes Project, specifically curated for the European super-population. This panel was meticulously filtered to include only bi-allelic SNPs with a minor allele frequency exceeding 0.01, ensuring a robust genetic representation for our study. The F statistic, a measure widely utilized in the context of instrumental variable regression models to assess the strength of the instrumental variable, was calculated for each SNP. Subsequently, SNPs with an F statistic value below 10 were excluded from the analysis to mitigate the risk of weak instruments bias, as recommended in the literature (Burgess et al., 2011).

2.5 Statistical analyses

For this study, we employed R software (version 4.3.3) to perform comprehensive statistical analyses aimed at discerning the causal relationship between 731 distinct immune phenotypes and AD. Our analytical approach encompassed a suite of robust statistical techniques, including MR-Egger regression, the weighted median method, weighted mode analysis, the sample mode approach, and inverse variance weighted analysis. All these analyses were executed using the "TwoSampleMR" R package, which facilitated a streamlined workflow. To assess instrumental heterogeneity across variables, we applied Cochran's Q statistic in tandem with the horizontal multidimensional MR-Egger method. A significant intercept term in this method indicates the presence of heterogeneity. Upon identifying and excluding SNPs that contributed to this heterogeneity, we re-conducted the inverse variance weighted analysis to refine our results. Additionally, we conducted a targeted search for SNPs with suggestive associations ($p < 1 \times 10^{-5}$) relative to these risk factors, utilizing the Phenoscanner V2 platform. This allowed us to further explore potential genetic markers linked to AD. Finally, our visual assessment through a scatter plot indicated that outliers exert minimal influence on the dataset. Meanwhile, the funnel plot revealed a strong correlation among the results, with no significant heterogeneity observed.

3 Results

3.1 The causal relationship between immunophenotypic traits and AD

In a meticulous examination of the possible causal dynamics interconnecting immune cells and the initiation as well as the escalation of AD, we engaged a diverse array of statistical techniques to fortify the integrity and precision of our investigation. To elaborate, we harnessed five discrete yet methodologically robust approaches: the Inverse Variance Weighted, the MR Egger, the Weighted Median, the Weighted Mode, and the Simple Mode. Within this analytical arsenal, the Inverse Variance Weighted method emerged as the cornerstone of our methodology, selected for its exceptional statistical robustness and its demonstrated efficacy in providing stable and reliable estimates across a wide range of research contexts.

Our research findings suggest that 15 distinct immune cell types are involved in the pathogenesis of AD. Notably, two immunophenotypes appear to exert a protective effect against AD: the absolute count of $CD28^-CD4^-CD8^-$ T cells and the expression of HLA DR on B cells, as depicted in Figure 2. Using the Inverse Variance Weighted method, we evaluated the association between these immunophenotypes and AD risk. For $CD28^-CD4^-CD8^-$ T cells, we found an odds ratio (OR) of 0.960 (95% Confidence Interval [CI] 0.931-0.989, $p = 0.008$). Similarly, HLA DR on B cells was associated with a reduced risk, with an OR of 0.973 (95% CI 0.959-0.988, $p < 0.001$). In contrast, the remaining 13 immunophenotypes were identified as risk factors for AD, with varying OR and 95% CI, as detailed in Supplementary Table S1. The MR-Egger regression intercept provided evidence against

the potential for horizontal pleiotropy, reinforcing the reliability of our causal inference, as shown in Supplementary Table S2. Furthermore, visual assessments such as the funnel plot, scatter plot, forest plot, and a leave-one-out analysis consistently demonstrated the stability and reliability of our findings from multiple analytical perspectives (Supplementary Figures S1, S2). These rigorous diagnostic checks enhance the credibility of our study's conclusions and strengthen the confidence in the observed immunological relationships with AD.

3.2 The causal relationship between AD and immunophenotypic traits

The Inverse Variance Weighted analysis revealed a negative association between AD and several immunophenotypic traits. For instance, the OR and 95% CI for the association with AD were as follows: CD20 on switched memory B cell (OR = 1.007, 95% CI = 0.942–1.078, $p = 0.837$), CD27 on IgD$^-$ CD38$^+$ B cell (OR = 1.004, 95% CI = 0.946–1.067, $p = 0.885$), and so on for the remaining traits. Notably, all associations had $p > 0.05$, indicating no statistically significant effect. The MR analysis further explored the causal effects of AD on these immunophenotypic traits, with results depicted in Figure 3 and detailed in Supplementary Tables S3, S4. Additional visual assessments, including scatter plots and forest plots, are provided in Supplementary Figures S3, S4.

3.3 Validation of between immunophenotypic traits and AD

To further validate the causal relationship between immunophenotypic traits and the onset and progression of AD, we selected two distinct sets of AD data for verification: the FinnGen cohort and the dataset identified as GCST90027158.

Within the FinnGen dataset, we identified a causal relationship between AD and six specific immune cell types. These include CD4$^+$CD8^{dim} T cell leukocyte (OR = 1.021, 95%CI = 1.003–1.039, $p = 0.020$), CD4$^+$CD8^{dim} T cell lymphocyte (OR = 1.032, 95% CI = 1.012–1.053, $p = 0.001$), HLA DR on B cell (OR = 0.978, 95% CI = 0.964–0.992, $p = 0.002$), HLA DR on CD14$^+$CD16$^-$ monocyte (OR = 1.023, 95% CI = 1.009–1.037, $p < 0.001$), HLA DR on CD14$^+$ monocyte (OR = 1.027, 95% CI = 1.012–1.042, $p < 0.001$), and HLA DR on monocyte (OR = 1.023, 95% CI = 1.007–1.039, $p = 0.004$). These findings are illustrated in Figure 4A, with additional details provided in Supplementary Figures S5, S6, Supplementary Tables S5, S6. However, the analysis of the same FinnGen dataset did not reveal a causal relationship for the remaining immunophenotypic traits (Figure 4B, Supplementary Figures S7, S8, Supplementary Table S7).

In the GCST90027158 dataset, a causal relationship was found between two specific immune cell types and the development of AD: the CD4$^+$ CD8^{dim} T cell leukocyte (OR = 1.020, 95% CI = 1.007–1.033, $p = 0.002$) and the CD4$^+$ CD8^{dim} T cell lymphocyte (OR = 1.018, 95% CI = 1.005–1.031, $p = 0.007$). These results are presented in Figure 4C, with further details in Supplementary Figures S9, S10, Supplementary Tables S8, S9. However, no causal link was established between AD and other immunophenotypic traits (Figure 4D, Supplementary Figures S11, S12, Supplementary Table S10).

4 Discussion

Within the pathogenesis of AD, the roles of the immune system are becoming increasingly recognized. Utilizing publicly accessible GWAS data, this study conducted an exhaustive analysis to elucidate potential causal links between a spectrum of immune cell phenotypes and AD. This study examined a range of immune cell phenotypes, including CD4$^+$CD8^{dim} T cell leukocytes, CD4$^+$CD8^{dim} T cell lymphocytes, B cells expressing HLA DR, CD14$^+$CD16$^-$ monocytes, CD14$^+$ monocytes, and monocytes in general. Our research has not only confirmed the connection between AD and the immune system but also identified specific immune cell characteristics that may be key to early detection, disease monitoring, and the development of targeted treatments. Furthermore, these findings guide the direction of future research and clinical approaches.

During the maturation of T cells within the human immune system, CD4 and CD8 molecules are typically not found together on the surface of a single cell. These molecules distinguish the two primary subpopulations of T cells: CD4$^+$ T cells and CD8$^+$ T cells. Notably, the Th1 and Th17 subsets of CD4$^+$ T cells are capable of secreting various pro-inflammatory cytokines, such as interferon-gamma (IFN-γ) and tumor necrosis factor-alpha (TNF-α). These cytokines have the ability to activate microglia and intensify neuroinflammation, which significantly influences the pathogenesis of AD (Anderson et al., 2014; Machhi et al., 2021; Chen et al., 2023). Microglia are the primary immune cells of the central nervous system, and their activation in AD can promote inflammatory responses, which are associated with the formation of Aβ plaques and neurodegeneration (DeMaio et al., 2022). IFNγ, as an important cytokine, can enhance the activation state of microglia, leading to the release of inflammatory mediators such as TNF-α, interleukin-1 beta (IL-1β), and nitric oxide, all of which may cause neuronal damage and cognitive decline (Glass et al., 2010). IFNγ may also promote the entry of peripheral immune cells into the brain by altering the permeability of the blood-brain barrier, further exacerbating neuroinflammation. This inflammatory environment not only affects the clearance of Aβ but may also interfere with the normal function of tau protein, leading to its abnormal phosphorylation and aggregation, forming neurofibrillary tangles, and further intensifying the onset and progression of AD (Glass et al., 2010). Furthermore, the observation of clonal expansion of CD8$^+$ T cells in the cerebrospinal fluid of AD patients implies that they may have a pivotal role in the immune response within the central nervous system (Gate et al., 2020). Neuroinflammation is a critical pathological process in the brains of AD patients (Leng and Edison, 2021). Both CD4$^+$ and CD8$^+$ T cells have the capacity to traverse the blood-brain barrier, thereby gaining entry to the brain and engaging in the modulation of central neuroinflammation, which in turn affects the progression of AD (Jorfi et al., 2023b). In the context of AD pathology, there is a marked increase in the infiltration of CD4$^+$ T cells, CD8$^+$ T

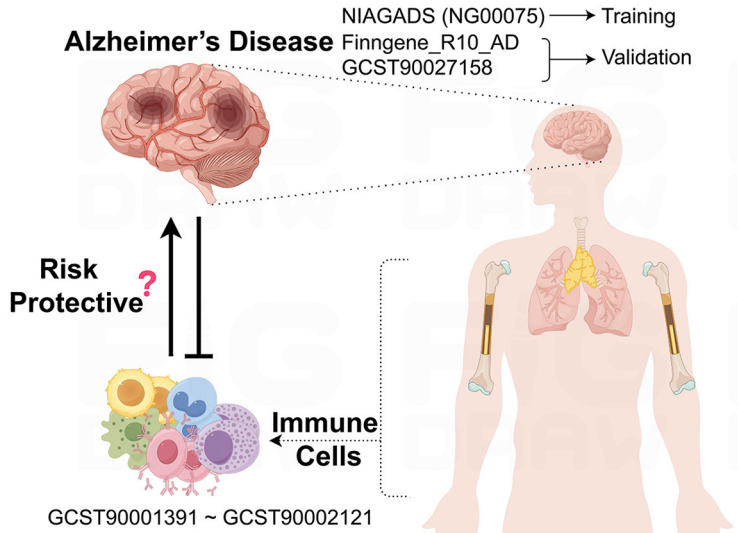

FIGURE 1
Schematic representation of the study design and data flow. This figure illustrates the process of leveraging publicly available GWAS data to investigate the causal links between immune cell phenotypes and AD.

exposure	nsnp	pval	OR(95% CI)
CD20 on switched memory B cell	85	0.003	1.036 (1.013 to 1.061)
CD27 on IgD– CD38+ B cell	38	0.003	1.063 (1.021 to 1.108)
CD28– CD4–CD8– T cell Absolute Count	61	0.008	0.960 (0.931 to 0.989)
CD38 on CD3– CD19–	39	0.003	1.040 (1.014 to 1.067)
CD4+ CD8dim T cell %leukocyte	96	0.005	1.035 (1.010 to 1.060)
CD4+ CD8dim T cell %lymphocyte	97	0.002	1.040 (1.015 to 1.065)
HLA DR on B cell	119	< 0.001	0.973 (0.959 to 0.988)
HLA DR on CD14– CD16+ monocyte	135	0.009	1.023 (1.005 to 1.040)
HLA DR on CD14+ CD16– monocyte	145	< 0.001	1.040 (1.024 to 1.055)
HLA DR on CD14+ CD16+ monocyte	155	0.002	1.023 (1.008 to 1.037)
HLA DR on CD14+ monocyte	140	< 0.001	1.042 (1.026 to 1.058)
HLA DR on CD33+ HLA DR+ CD14–	146	< 0.001	1.029 (1.016 to 1.042)
HLA DR on CD33+ HLA DR+ CD14dim	107	0.004	1.028 (1.009 to 1.048)
HLA DR on CD33dim HLA DR+ CD11b–	113	0.004	1.024 (1.008 to 1.041)
HLA DR on monocyte	138	< 0.001	1.030 (1.013 to 1.047)

FIGURE 2
Association between immunophenotypes and AD risk. The figure displays the results from the Inverse Variance Weighted analysis, highlighting the protective effect of two immunophenotypes: the absolute count of $CD28^{-}CD4^{-}CD8^{-}$ T cells and the expression of HLA DR on B cells. OR, 95% CI, and *p*-values are provided for each association.

cells, and monocytes within brain models, which is likely closely associated with neurologic damage related to AD (Jorfi et al., 2023b). Beyond these two predominant T cell types, researchers have identified a minor subset of T cells exhibiting a double-positive $CD4^{+}CD8^{dim}$ phenotype, which constitutes a small fraction of the $CD3^{+}$ T cell pool (Suni et al., 2001). Studies have shown that $CD4^{+}CD8^{dim}$ T cells possess a more potent specific cytotoxic capability against cytomegalovirus (CMV) compared to conventional $CD4^{+}$ T cells (Suni et al., 2001). Additionally, $CD4^{+}CD8^{dim}$ T cells, which originate from double-positive T cells, express CD13, a molecule that conveys signals for antigen stimulation and may thus participate in the regulation of immune responses (Sala et al., 1993; Sun et al., 2023a). As a result, $CD4^{+}CD8^{dim}$ T cells could potentially serve dual roles by both assisting and directly killing in the immune response. While there are no current reports on the role of $CD4^{+}CD8^{dim}$ T cells in the etiology of AD, our research suggests that these cells may have a significant risk association with the development of

outcome	nsnp	pval	OR(95% CI)
CD20 on switched memory B cell	139	0.837	1.007 (0.942 to 1.077)
CD27 on IgD– CD38+ B cell	139	0.885	1.004 (0.946 to 1.067)
CD28– CD4–CD8– T cell Absolute Count	139	0.093	0.949 (0.892 to 1.009)
CD38 on CD3– CD19–	139	0.325	1.042 (0.960 to 1.131)
CD4+ CD8dim T cell %leukocyte	139	0.453	0.977 (0.921 to 1.037)
CD4+ CD8dim T cell %lymphocyte	139	0.681	0.988 (0.930 to 1.048)
HLA DR on B cell	138	0.592	1.019 (0.952 to 1.091)
HLA DR on CD14+ CD16+ monocyte	137	0.611	0.983 (0.920 to 1.050)
HLA DR on CD14+ CD16– monocyte	137	0.335	0.968 (0.905 to 1.035)
HLA DR on CD14+ monocyte	137	0.402	0.972 (0.910 to 1.039)
HLA DR on CD14– CD16+ monocyte	138	0.704	1.013 (0.949 to 1.080)
HLA DR on CD33+ HLA DR+ CD14–	137	0.610	0.977 (0.894 to 1.068)
HLA DR on CD33+ HLA DR+ CD14dim	136	0.979	1.001 (0.912 to 1.100)
HLA DR on CD33dim HLA DR+ CD11b–	137	0.138	1.078 (0.976 to 1.191)
HLA DR on monocyte	136	0.306	0.967 (0.908 to 1.031)

1

FIGURE 3
Causal effects of AD on immunophenotypic traits. This figure presents the Inverse Variance Weighted analysis outcomes, indicating a predominantly association between AD and various immunophenotypic traits. The graphical representation includes OR, 95% CI, and *p*-values for each trait, demonstrating the lack of statistically significant effects.

A Finngene Database

exposure	nsnp	method	pval	OR(95% CI)
CD4+ CD8dim T cell %leukocyte	145	MR Egger	0.679	1.005 (0.981 to 1.030)
	145	Weighted median	0.855	1.003 (0.974 to 1.032)
	145	Inverse variance weighted	0.020	1.021 (1.003 to 1.039)
	145	Simple mode	0.346	1.028 (0.971 to 1.089)
	145	Weighted mode	0.247	1.014 (0.991 to 1.038)
CD4+ CD8dim T cell %lymphocyte	148	MR Egger	0.487	1.011 (0.980 to 1.043)
	148	Weighted median	0.033	1.029 (1.002 to 1.056)
	148	Inverse variance weighted	0.001	1.032 (1.012 to 1.053)
	148	Simple mode	0.514	1.019 (0.963 to 1.079)
	148	Weighted mode	0.078	1.024 (0.998 to 1.051)
HLA DR on B cell	173	MR Egger	0.200	0.986 (0.965 to 1.007)
	173	Weighted median	0.146	0.982 (0.957 to 1.007)
	173	Inverse variance weighted	0.002	0.978 (0.964 to 0.992)
	173	Simple mode	0.706	0.991 (0.947 to 1.038)
	173	Weighted mode	0.243	0.986 (0.963 to 1.010)
HLA DR on CD14+ CD16– monocyte	192	MR Egger	0.291	1.011 (0.991 to 1.032)
	192	Weighted median	0.174	1.013 (0.994 to 1.033)
	192	Inverse variance weighted	< 0.001	1.023 (1.009 to 1.037)
	192	Simple mode	0.140	1.035 (0.989 to 1.083)
	192	Weighted mode	0.225	1.012 (0.993 to 1.032)
HLA DR on CD14+ monocyte	185	MR Egger	0.303	1.013 (0.989 to 1.037)
	185	Weighted median	0.094	1.020 (0.997 to 1.044)
	185	Inverse variance weighted	< 0.001	1.027 (1.012 to 1.042)
	185	Simple mode	0.368	1.023 (0.974 to 1.073)
	185	Weighted mode	0.234	1.015 (0.990 to 1.040)
HLA DR on monocyte	175	MR Egger	0.964	1.001 (0.974 to 1.028)
	175	Weighted median	0.273	1.013 (0.990 to 1.038)
	175	Inverse variance weighted	0.004	1.023 (1.007 to 1.039)
	175	Simple mode	0.775	0.992 (0.937 to 1.050)
	175	Weighted mode	0.588	0.988 (0.947 to 1.031)

1

B Finngene Database

outcome	nsnp	method	pval	OR(95% CI)
CD4+ CD8dim T cell %leukocyte	386	MR Egger	0.403	1.011 (0.985 to 1.038)
	386	Weighted median	0.095	1.037 (0.994 to 1.081)
	386	Inverse variance weighted	0.191	1.014 (0.993 to 1.035)
	386	Simple mode	0.226	0.942 (0.856 to 1.037)
	386	Weighted mode	0.321	1.019 (0.982 to 1.056)
CD4+ CD8dim T cell %lymphocyte	386	MR Egger	0.395	1.011 (0.985 to 1.038)
	386	Weighted median	0.072	1.040 (0.996 to 1.085)
	386	Inverse variance weighted	0.174	1.014 (0.994 to 1.035)
	386	Simple mode	0.407	0.961 (0.876 to 1.055)
	386	Weighted mode	0.535	1.011 (0.976 to 1.048)
HLA DR on B cell	384	MR Egger	0.740	1.005 (0.977 to 1.033)
	384	Weighted median	0.647	0.992 (0.957 to 1.027)
	384	Inverse variance weighted	0.641	1.005 (0.984 to 1.027)
	384	Simple mode	0.690	0.978 (0.878 to 1.090)
	384	Weighted mode	0.746	1.006 (0.972 to 1.041)
HLA DR on CD14+ CD16– monocyte	383	MR Egger	0.711	1.005 (0.980 to 1.030)
	383	Weighted median	0.529	1.012 (0.976 to 1.049)
	383	Inverse variance weighted	0.913	1.001 (0.982 to 1.021)
	383	Simple mode	0.509	0.969 (0.881 to 1.065)
	383	Weighted mode	0.610	1.008 (0.979 to 1.038)
HLA DR on CD14+ monocyte	383	MR Egger	0.791	1.003 (0.979 to 1.029)
	383	Weighted median	0.513	1.011 (0.979 to 1.043)
	383	Inverse variance weighted	0.974	1.000 (0.981 to 1.020)
	383	Simple mode	0.630	0.977 (0.887 to 1.076)
	383	Weighted mode	0.353	1.014 (0.984 to 1.045)
HLA DR on monocyte	383	MR Egger	0.887	1.002 (0.977 to 1.027)
	383	Weighted median	0.596	1.009 (0.976 to 1.043)
	383	Inverse variance weighted	0.831	0.998 (0.979 to 1.018)
	383	Simple mode	0.966	0.998 (0.904 to 1.101)
	383	Weighted mode	0.885	0.998 (0.969 to 1.028)

1

C GCST90027158

exposure	nsnp	method	pval	OR(95% CI)
CD4+ CD8dim T cell %lymphocyte	145	MR Egger	0.004	1.033 (1.011 to 1.056)
	145	Weighted median	0.060	1.017 (0.999 to 1.036)
	145	Inverse variance weighted	0.002	1.020 (1.007 to 1.033)
	145	Simple mode	0.304	1.023 (0.979 to 1.069)
	145	Weighted mode	0.103	1.021 (0.996 to 1.046)
CD4+ CD8dim T cell %leukocyte	142	MR Egger	0.064	1.020 (0.999 to 1.042)
	142	Weighted median	0.103	1.016 (0.997 to 1.035)
	142	Inverse variance weighted	0.007	1.018 (1.005 to 1.031)
	142	Simple mode	0.197	1.036 (0.982 to 1.094)
	142	Weighted mode	0.496	1.009 (0.983 to 1.037)

1

D GCST90027158

outcome	nsnp	method	pval	OR(95% CI)
CD4+ CD8dim T cell %leukocyte	548	MR Egger	0.827	0.991 (0.911 to 1.078)
	548	Weighted median	0.365	0.966 (0.896 to 1.041)
	548	Inverse variance weighted	0.556	0.987 (0.944 to 1.031)
	548	Simple mode	0.916	0.990 (0.828 to 1.184)
	548	Weighted mode	0.668	0.976 (0.872 to 1.092)
CD4+ CD8dim T cell %lymphocyte	548	MR Egger	0.817	0.990 (0.910 to 1.077)
	548	Weighted median	0.373	0.969 (0.903 to 1.039)
	548	Inverse variance weighted	0.846	0.996 (0.953 to 1.040)
	548	Simple mode	0.992	0.999 (0.832 to 1.200)
	548	Weighted mode	0.733	0.981 (0.879 to 1.095)

1

FIGURE 4
Validation of the causal relationship between immunophenotypic traits and AD in the FinnGen and GCST90027158 datasets. **(A, B)** depict the confirmed causal associations with specific immune cell types, including $CD4^{+}CD8^{dim}$ T cell leukocyte and lymphocyte, and HLA DR expression on B cells and monocytes within the FinnGen dataset. **(C, D)** show the causal relationships for the immunophenotypic traits analyzed in the GCST90027158.

AD. Consequently, reducing the population of $CD4^{+}CD8^{dim}$ T cells could be crucial in mitigating neuroinflammation within the brains of AD patients and potentially slowing the onset of the disease.

The HLA DR molecules, an essential element of the major histocompatibility complex class II (MHC-II), are proficiently displayed on the B lymphocyte cell surface, where they act as a pivotal nexus facilitating the activation of these cells. Moreover,

HLA DR molecules on B cells play an instrumental role in presenting antigenic peptides to $CD4^+$ T cells, also known as helper T cells. This interaction activates T cells, which then stimulate the proliferation and differentiation of B cells, ultimately resulting in antibody production (Celis-Giraldo et al., 2024; Paterson et al., 2024). Notably, B cells may intensify neuroinflammation in AD by promoting T cell infiltration (Griffith et al., 2022; Abualrous et al., 2023; Chen et al., 2023). Once T cells cross the blood-brain barrier and enter the central nervous system (CNS), they can release a range of inflammatory mediators, including cytokines and chemokines (Cao and Zheng, 2018; Wu et al., 2021). These mediators not only recruit more immune cells but may also exacerbate local inflammatory responses. As inflammation persists, neurons may suffer damage or even die, thereby accelerating the onset and progression of AD (Cao and Zheng, 2018; Wu et al., 2021). In contrast, the interaction between T cells activated by B cells and microglia, the primary immune cells in the CNS, may lead to the activation of microglia. Microglia play a key role in clearing Aβ plaques and regulating neuroinflammation (Jorfi et al., 2023a; Zhang et al., 2023). This activation may help maintain the stability of the brain's internal environment, but during the pathological process of AD, it may also cause damage to neurons due to excessive or dysregulated immune responses (Jorfi et al., 2023a; Zhang et al., 2023). Therefore, the interaction between T cells and microglia plays a complex role in AD, as they can both promote neuroprotection and exacerbate neurodegeneration. Understanding the delicate balance between these cells is crucial for developing immune-modulating therapeutic strategies for AD. B cells are pivotal in humoral immunity, with the ability to differentiate into plasma cells that generate antibodies tailored to specific antigens. In the context of AD, these antibodies can bind to Aβ, thereby aiding in its removal (Kim et al., 2021). Additionally, the interaction between B cell-derived antibodies and the transmembrane protein TREM2 on microglia significantly influences microglial functionality and the clearance of Aβ plaques (Zhao et al., 2022). Studies have shown a correlation between a reduction in B cell count in the peripheral blood of AD patients and the severity of their condition (Kim et al., 2021; Xiong et al., 2021). Mouse model experiments have demonstrated that B cell depletion can exacerbate cognitive impairment in AD models and lead to a substantial buildup of Aβ in the brain (Kim et al., 2021; Xiong et al., 2021). Our research indicates that HLA DR on B cells may offer significant protection against the onset and progression of AD. Consequently, modulating B cell activity or the antibodies they produce could emerge as a promising therapeutic approach for AD. This insight paves the way for novel avenues in therapeutic research, potentially leading to the development of new treatments that target B cells or their antibodies, with the goal of mitigating or arresting the progression of AD.

Monocytes, the most sizable leukocytes in the circulatory system, possess the capacity to differentiate into macrophages and dendritic cells of monocyte origin. These cells, along with their progeny, play pivotal roles in modulating inflammatory responses and facilitating tissue repair, which are likely critical to the pathogenesis of AD (Sun et al., 2023b). Monocytes are categorized into three discrete subpopulations, delineated by their differential expression of CD14 and CD16 surface markers: classical monocytes ($CD14^+CD16^-$), intermediate monocytes ($CD14^+CD16^+$), and non-classical monocytes ($CD14^-CD16^+$) (Ziegler-Heitbrock et al., 2010). The $CD14^+$ subset of monocytes is notably involved in the recognition of bacteria and the subsequent immune response, facilitated by their interaction with lipopolysaccharide through CD14 molecules (Draude et al., 1999; Wu et al., 2019). CD16, also known as FcγRIII, serves as a receptor for the Fc fragment of immunoglobulin G and is primarily associated with the function of natural killer cells (Feng et al., 2021). Classical monocytes are especially significant in orchestrating inflammatory responses and in the presentation of antigens (Serbina et al., 2008). Upon infiltrating the brain, these cells mature into microglia, playing an essential part in neuroinflammatory processes and the clearance of Aβ associated with AD (Habib et al., 2020). Furthermore, classical monocytes have the ability to express MHC-II molecules, allowing them to present antigens to $CD4^+$ T cells. This potential to drive T cell infiltration and activation may contribute to the exacerbation of neuroinflammation in AD (Keren-Shaul et al., 2017; Simren et al., 2021). Our research has established a correlation between the expression of HLA DR on monocytes, specifically HLA DR on $CD14^+$ monocytes and HLA DR on the $CD14^+CD16^-$ subset, and an increased risk of developing AD. Given the manifold functions of monocytes within the AD pathology, they could present promising targets for therapeutic approaches. Interventions aimed at modulating the activity or differentiation pathways of monocytes may yield considerable therapeutic advantages in the clinical management of AD.

Utilizing a bidirectional MR strategy, this study conducted an exhaustive analysis of genomic data from 94,437 individuals with AD. The primary goal was to elucidate the causal relationship between AD and immune cells, with a focus on ensuring the precision and wide-ranging applicability of the statistical results. The research findings are grounded in genetic instrumental variables and feature a suite of robust MR analytical methods, meticulously designed to mitigate the influence of horizontal pleiotropy and other confounding factors. Moreover, the findings have been substantiated through cross-validation with multiple independent datasets, thereby reinforcing the reliability and validity of the study's conclusions. However, this analytical method still has its limitations. MR analysis primarily relies on common genetic variations and may underestimate the potential impact of rare genetic variations on disease risk. MR analysis may be affected by confounding factors, although we have employed various methods to mitigate this risk. The data for this study were all derived from European population samples, lacking statistical results from non-European populations, which makes the findings less generalizable. Therefore, this is also a main direction for our future research.

While providing substantial insights, this study faces certain limitations. First and foremost, its foundation on a database that is heavily skewed toward European populations may limit the broad applicability of its conclusions across different ethnic groups. Additionally, the lack of detailed individual-level data poses a challenge in thoroughly assessing the intricate interplay between genetic and environmental factors, which could, in turn, affect the precision of establishing causal relationships. Furthermore, the Mendelian Randomization (MR) analysis, which primarily

focuses on common genetic variants, risks underestimating the significant impact that rare genetic variations might have on disease risk, possibly indicating a gap in the current analytical approach. Lastly, although MR analysis presents an observational data-driven method to investigate the causal link between immune cells and Alzheimer's disease, the robustness of its conclusions would benefit from further substantiation through rigorous experimental research.

5 Conclusion

In conclusion, our thorough a bidirectional MR analysis has exposed the causal ties linking a spectrum of immunophenotypes to AD, and has shed light on the sophisticated interplay between the immune system and AD. Importantly, our research has effectively minimized the confounding effects of reverse causality, extraneous variables, and other uncontrollable confounding factors. This has equipped researchers with a novel vantage point from which to delve into the intricate biological foundations of AD. Our findings not only hold the potential to inform the creation of early intervention and therapeutic strategies but also contribute to the expansion of the field of psychoneuroimmunology. They provide significant insights that are instrumental for the prevention and management of AD.

Data availability statement

The original contributions presented in the study are included in the article/Supplementary material, further inquiries can be directed to the corresponding authors.

Ethics statement

The data for this study were obtained solely from publicly available datasets, and have been diligently reviewed the database usage guidelines. Given the nature of the data and the scope of the analysis, no ethical approval was required for this research.

Author contributions

EZ: Conceptualization, Investigation, Project administration, Writing – original draft, Writing – review & editing. TC: Conceptualization, Visualization, Writing – review & editing. YC: Data curation, Writing – review & editing. CL: Conceptualization, Writing – review & editing. LT: Conceptualization, Data curation, Writing – review & editing. XS: Writing – review & editing. FD: Project administration, Writing – review & editing.

Funding

The author(s) declare that financial support was received for the research, authorship, and/or publication of this article. This study was supported by the Doctoral Scientific Research Foundation of Guizhou Medical University (No. YJ20066), the National Natural Science Foundation of China Cultivation Project of Guizhou Medical University (No. 20NSP051), the Scientific and Technological Project of Guizhou Province [No. ZK (2022)398, ZK (2023)336], and the Fund of Science and Technology Project of Guizhou provincial health commission (No. Gzwkj2023-564).

Acknowledgments

We gratefully acknowledge the support and contributions from the National Institute on Aging Genetics of Alzheimer's Disease Data Storage Site (NIAGADS). Special thanks are due to the FinnGen project for granting access to the pivotal dataset, as well as the data provided by GCST90027158, which has played a significant role in the advancement of our research.

Conflict of interest

The authors declare that the research was conducted in the absence of any commercial or financial relationships that could be construed as a potential conflict of interest.

Publisher's note

Supplementary material

The Supplementary Material for this article can be found online at: https://www.frontiersin.org/articles/10.3389/fnagi.2024.1433691/full#supplementary-material

SUPPLEMENTARY FIGURE S1
Funnel plot assessing publication bias in the MR analysis of immunophenotypic traits as exposures and AD as the outcome. The plot visualizes the estimated effect size (β_{IV}) against the inverse of the standard error ($1/SE_{IV}$), with asymmetry potentially indicating publication bias.

SUPPLEMENTARY FIGURE S2
Scatter plots depict the results of MR tests for various immunophenotypic traits as exposures against AD as the outcome. The scatter plots illustrate the relationship between the effect of SNPs on the exposure and their corresponding effect on the outcome, allowing for the assessment of potential causal relationships.

SUPPLEMENTARY FIGURE S3
Funnel plot designed to assess publication bias in MR analysis where AD is the exposure and various immunophenotypic traits are the outcomes.

SUPPLEMENTARY FIGURE S4
Scatter plots depict the results of MR tests for AD as exposures against various immunophenotypic traits as the outcome.

SUPPLEMENTARY FIGURE S5
Funnel plot for assessing publication bias in MR analysis specific to the FinnGen dataset, with immunophenotypic traits as exposures and AD as the outcome.

SUPPLEMENTARY FIGURE S6
Scatter plot for FinnGen dataset, illustrating MR effect sizes for immunological exposures on AD outcome.

SUPPLEMENTARY FIGURE S7
Funnel plot for assessing publication bias in MR analysis of the FinnGen dataset, with AD as the exposure and immunophenotypic traits as outcomes.

SUPPLEMENTARY FIGURE S8
Scatter plot for FinnGen dataset, presenting MR effect sizes for AD exposure on immunological outcomes.

SUPPLEMENTARY FIGURE S9
Funnel plot for assessing publication bias in MR analysis specific to the GCST90027158 dataset, with immunophenotypic traits as exposures and AD as the outcome.

SUPPLEMENTARY FIGURE S10
Scatter plot for GCST90027158 dataset, displaying MR effect sizes for immunological exposures on AD outcome.

SUPPLEMENTARY FIGURE S11
Funnel plot for assessing publication bias in MR analysis of the GCST90027158 dataset, with AD as the exposure and immunophenotypic traits as outcomes.

SUPPLEMENTARY FIGURE S12
Scatter plot for GCST90027158 dataset, presenting MR effect sizes for AD exposure on immunological outcomes.

SUPPLEMENTARY TABLE S1
The Causal of immunophenotypic traits to Alzheimer's disease (NG00075).

SUPPLEMENTARY TABLE S2
MR result of pleiotropy test for immune cells to AD (NG00075).

SUPPLEMENTARY TABLE S3
The causal of Alzheimer's disease (NG00075) to immunophenotypic traits.

SUPPLEMENTARY TABLE S4
MR result of pleiotropy test for AD (NG00075) to immune cells.

SUPPLEMENTARY TABLE S5
The causal of immunophenotypic traits to Alzheimer's disease (FinnGen database).

SUPPLEMENTARY TABLE S6
MR result of pleiotropy test from immune cell t0 AD (FinnGen database).

SUPPLEMENTARY TABLE S7
MR result of pleiotropy test from AD (FinnGen database) to immune cells.

SUPPLEMENTARY TABLE S8
The causal of immunophenotypic traits to Alzheimer's disease (GCST90027158).

SUPPLEMENTARY TABLE S9
MR result of pleiotropy test from immune cells to AD (GCST90027158).

SUPPLEMENTARY TABLE S10
MR result of pleiotropy test from AD (GCST90027158) to immune cells.

References

Abualrous, E. T., Stolzenberg, S., Sticht, J., Wieczorek, M., Roske, Y., Gunther, M., et al. (2023). MHC-II dynamics are maintained in HLA-DR allotypes to ensure catalyzed peptide exchange. *Nat. Chem. Biol.* 19, 1196–1204. doi: 10.1038/s41589-023-01316-3

Alzheimer's disease facts and figures (2024). *Alzheimers Dement.* 20, 3708–3821. doi: 10.1002/alz.13809

Anderson, K. M., Olson, K. E., Estes, K. A., Flanagan, K., Gendelman, H. E., and Mosley, R. L. (2014). Dual destructive and protective roles of adaptive immunity in neurodegenerative disorders. *Transl. Neurodegener.* 3:25. doi: 10.1186/2047-9158-3-25

Bellenguez, C., Kucukali, F., Jansen, I. E., Kleineidam, L., Moreno-Grau, S., Amin, N., et al. (2022). New insights into the genetic etiology of Alzheimer's disease and related dementias. *Nat. Genet.* 54:412—436. doi: 10.1038/s41588-022-01024-z

Burgess, S., Thompson, S. G., and Collaboration, C. C. G. (2011). Avoiding bias from weak instruments in Mendelian randomization studies. *Int. J. Epidemiol.* 40, 755–764. doi: 10.1093/ije/dyr036

Cao, W., and Zheng, H. (2018). Peripheral immune system in aging and Alzheimer's disease. *Mol. Neurodegener.* 13:51. doi: 10.1186/s13024-018-0284-2

Celis-Giraldo, C., Ordonez, D., Diaz-Arevalo, D., Bohorquez, M. D., Ibarrola, N., Suarez, C. F., et al. (2024). Identifying major histocompatibility complex class II-DR molecules in bovine and swine peripheral blood monocyte-derived macrophages using mAb-L243. *Vaccine.* 42, 3445–3454. doi: 10.1016/j.vaccine.2024.04.042

Chen, C., Wang, P., Zhang, R. D., Fang, Y., Jiang, L. Q., Fang, X., et al. (2022). Mendelian randomization as a tool to gain insights into the mosaic causes of autoimmune diseases. *Autoimmun. Rev.* 21:103210. doi: 10.1016/j.autrev.2022.103210

Chen, X., Firulyova, M., Manis, M., Herz, J., Smirnov, I., Aladyeva, E., et al. (2023). Microglia-mediated T cell infiltration drives neurodegeneration in tauopathy. *Nature* 615, 668–677. doi: 10.1038/s41586-023-05788-0

Chen, X., and Holtzman, D. M. (2022). Emerging roles of innate and adaptive immunity in Alzheimer's disease. *Immunity* 55, 2236–2254. doi: 10.1016/j.immuni.2022.10.016

DeMaio, A., Mehrotra, S., Sambamurti, K., and Husain, S. (2022). The role of the adaptive immune system and T cell dysfunction in neurodegenerative diseases. *J. Neuroinflammation* 19:251. doi: 10.1186/s12974-022-02605-9

Draude, G., von Hundelshausen, P., Frankenberger, M., Ziegler-Heitbrock, H. W., and Weber, C. (1999). Distinct scavenger receptor expression and function in the human CD14(+)/CD16(+) monocyte subset. *Am. J. Physiol.* 276, H1144–1149. doi: 10.1152/ajpheart.1999.276.4.H1144

Emdin, C. A., Khera, A. V., and Kathiresan, S. (2017). Mendelian Randomization. *JAMA* 318, 1925–1926. doi: 10.1001/jama.2017.17219

Feng, G., Wines, B. D., Kurtovic, L., Chan, J. A., Boeuf, P., Mollard, V., et al. (2021). Mechanisms and targets of Fcgamma-receptor mediated immunity to malaria sporozoites. *Nat. Commun.* 12:1742. doi: 10.1038/s41467-021-21998-4

Frost, G. R., Jonas, L. A., and Li, Y. M. (2019). Friend, foe or both? Immune activity in Alzheimer's disease. *Front. Aging Neurosci.* 11:337. doi: 10.3389/fnagi.2019.00337

Gate, D., Saligrama, N., Leventhal, O., Yang, A. C., Unger, M. S., Middeldorp, J., et al. (2020). Clonally expanded CD8 T cells patrol the cerebrospinal fluid in Alzheimer's disease. *Nature* 577, 399–404. doi: 10.1038/s41586-019-1895-7

Glass, C. K., Saijo, K., Winner, B., Marchetto, M. C., and Gage, F. H. (2010). Mechanisms underlying inflammation in neurodegeneration. *Cell* 140, 918–934. doi: 10.1016/j.cell.2010.02.016

Griffith, B. D., Turcotte, S., Lazarus, J., Lima, F., Bell, S., Delrosario, L., et al. (2022). MHC class II expression influences the composition and distribution of immune cells in the metastatic colorectal cancer microenvironment. *Cancers* 14:4092. doi: 10.3390/cancers14174092

Habib, N., McCabe, C., Medina, S., Varshavsky, M., Kitsberg, D., Dvir-Szternfeld, R., et al. (2020). Disease-associated astrocytes in Alzheimer's disease and aging. *Nat. Neurosci.* 23, 701–706. doi: 10.1038/s41593-020-0624-8

Jorfi, M., Maaser-Hecker, A., and Tanzi, R. E. (2023a). The neuroimmune axis of Alzheimer's disease. *Genome Med.* 15:6. doi: 10.1186/s13073-023-01155-w

Jorfi, M., Park, J., Hall, C. K., Lin, C. J., Chen, M., von Maydell, D., et al. (2023b). Infiltrating CD8(+) T cells exacerbate Alzheimer's disease pathology in a 3D human neuroimmune axis model. *Nat. Neurosci.* 26, 1489–1504. doi: 10.1038/s41593-023-01415-3

Keren-Shaul, H., Spinrad, A., Weiner, A., Matcovitch-Natan, O., Dvir-Szternfeld, R., Ulland, T. K., et al. (2017). A unique microglia type associated with restricting development of Alzheimer's disease. *Cell* 169, 1276–1290 e1217. doi: 10.1016/j.cell.2017.05.018

Kim, K., Wang, X., Ragonnaud, E., Bodogai, M., Illouz, T., DeLuca, M., et al. (2021). Therapeutic B-cell depletion reverses progression of Alzheimer's disease. *Nat. Commun.* 12:2185. doi: 10.1038/s41467-021-22479-4

Kunkle, B. W., Grenier-Boley, B., Sims, R., Bis, J. C., Damotte, V., Naj, A. C., et al. (2019). Genetic meta-analysis of diagnosed Alzheimer's disease identifies new risk loci and implicates Abeta, tau, immunity and lipid processing. *Nat. Genet.* 51, 414–430. doi: 10.1038/s41588-019-0358-2

Kurki, M. I., Karjalainen, J., Palta, P., Sipila, T. P., Kristiansson, K., Donner, K. M., et al. (2023). FinnGen provides genetic insights from a well-phenotyped isolated population. *Nature* 613, 508–518. doi: 10.1038/s41586-022-05473-8

Larsson, S. C., Butterworth, A. S., and Burgess, S. (2023). Mendelian randomization for cardiovascular diseases: principles and applications. *Eur. Heart J.* 44, 4913–4924. doi: 10.1093/eurheartj/ehad736

Leng, F., and Edison, P. (2021). Neuroinflammation and microglial activation in Alzheimer disease: where do we go from here? *Nat. Rev. Neurol.* 17, 157–172. doi: 10.1038/s41582-020-00435-y

Liddelow, S. A., Guttenplan, K. A., Clarke, L. E., Bennett, F. C., Bohlen, C. J., Schirmer, L., et al. (2017). Neurotoxic reactive astrocytes are induced by activated microglia. *Nature* 541, 481–487. doi: 10.1038/nature21029

Livingston, G., Huntley, J., Sommerlad, A., Ames, D., Ballard, C., Banerjee, S., et al. (2020). Dementia prevention, intervention, and care: 2020 report of the Lancet Commission. *Lancet* 396, 413–446. doi: 10.1016/S0140-6736(20)30367-6

Machhi, J., Yeapuri, P., Lu, Y., Foster, E., Chikhale, R., Herskovitz, J., et al. (2021). CD4+ effector T cells accelerate Alzheimer's disease in mice. *J. Neuroinflammation* 18, 272. doi: 10.1186/s12974-021-02308-7

Nebel, R. A., Aggarwal, N. T., Barnes, L. L., Gallagher, A., Goldstein, J. M., Kantarci, K., et al. (2018). Understanding the impact of sex and gender in Alzheimer's disease: a call to action. *Alzheimers. Dement.* 14, 1171–1183. doi: 10.1016/j.jalz.2018.04.008

Paterson, R. L., La Manna, M. P., Arena De Souza, V., Walker, A., Gibbs-Howe, D., Kulkarni, R., et al. (2024). An HLA-E-targeted TCR bispecific molecule redirects T cell immunity against Mycobacterium tuberculosis. *Proc. Natl. Acad. Sci. USA.* 121, e2318003121. doi: 10.1073/pnas.2318003121

Rajesh, Y., and Kanneganti, T. D. (2022). Innate immune cell death in neuroinflammation and Alzheimer's disease. *Cells* 11:1885. doi: 10.3390/cells11121885

Rajmohan, R., and Reddy, P. H. (2017). Amyloid-beta and phosphorylated tau accumulations cause abnormalities at synapses of Alzheimer's disease neurons. *J. Alzheimers. Dis.* 57, 975–999. doi: 10.3233/JAD-160612

Sala, P., Tonutti, E., Feruglio, C., Florian, F., and Colombatti, A. (1993). Persistent expansions of CD4+ CD8+ peripheral blood T cells. *Blood* 82, 1546–1552. doi: 10.1182/blood.V82.5.1546.1546

Serbina, N. V., Jia, T., Hohl, T. M., and Pamer, E. G. (2008). Monocyte-mediated defense against microbial pathogens. *Annu. Rev. Immunol.* 26, 421–452. doi: 10.1146/annurev.immunol.26.021607.090326

Simren, J., Leuzy, A., Karikari, T. K., Hye, A., Benedet, A. L., Lantero-Rodriguez, J., et al. (2021). The diagnostic and prognostic capabilities of plasma biomarkers in Alzheimer's disease. *Alzheimers. Dement.* 17, 1145–1156. doi: 10.1002/alz.12283

Sun, L., Su, Y., Jiao, A., Wang, X., and Zhang, B. (2023a). T cells in health and disease. *Signal Transduct Target Ther* 8, 235. doi: 10.1038/s41392-023-01471-y

Sun, N., Victor, M. B., Park, Y. P., Xiong, X., Scannail, A. N., Leary, N., et al. (2023b). Human microglial state dynamics in Alzheimer's disease progression. *Cell* 186, 4386–4403 e4329. doi: 10.1016/j.cell.2023.08.037

Suni, M. A., Ghanekar, S. A., Houck, D. W., Maecker, H. T., Wormsley, S. B., Picker, L. J., et al. (2001). CD4(+)CD8(dim) T lymphocytes exhibit enhanced cytokine expression, proliferation and cytotoxic activity in response to HCMV and HIV-1 antigens. *Eur. J. Immunol.* 31, 2512–2520. doi: 10.1002/1521-4141(200108)31:8<2512::aid-immu2512>3.0.co;2-m

Vierstra, J., Lazar, J., Sandstrom, R., Halow, J., Lee, K., Bates, D., et al. (2020). Global reference mapping of human transcription factor footprints. *Nature* 583, 729–736. doi: 10.1038/s41586-020-2528-x

Villemagne, V. L., Burnham, S., Bourgeat, P., Brown, B., Ellis, K. A., Salvado, O., et al. (2013). Amyloid beta deposition, neurodegeneration, and cognitive decline in sporadic Alzheimer's disease: a prospective cohort study. *Lancet Neurol.* 12, 357–367. doi: 10.1016/S1474-4422(13)70044-9

Wu, K. M., Zhang, Y. R., Huang, Y. Y., Dong, Q., Tan, L., and Yu, J. T. (2021). The role of the immune system in Alzheimer's disease. *Ageing Res. Rev.* 70, 101409. doi: 10.1016/j.arr.2021.101409

Wu, Z., Zhang, Z., Lei, Z., and Lei, P. (2019). CD14: Biology and role in the pathogenesis of disease. *Cytokine Growth Factor Rev.* 48, 24–31. doi: 10.1016/j.cytogfr.2019.06.003

Xia, X., Jiang, Q., McDermott, J., and Han, J. J. (2018). Aging and Alzheimer's disease: comparison and associations from molecular to system level. *Aging Cell* 17, e12802. doi: 10.1111/acel.12802

Xiong, L. L., Xue, L. L., Du, R. L., Niu, R. Z., Chen, L., Chen, J., et al. (2021). Single-cell RNA sequencing reveals B cell-related molecular biomarkers for Alzheimer's disease. *Exp. Mol. Med.* 53, 1888–1901. doi: 10.1038/s12276-021-00714-8

Xu, H., and Jia, J. (2021). Single-cell RNA sequencing of peripheral blood reveals immune cell signatures in Alzheimer's disease. *Front. Immunol.* 12:645666. doi: 10.3389/fimmu.2021.645666

Yu, J. T., Xu, W., Tan, C. C., Andrieu, S., Suckling, J., Evangelou, E., et al. (2020). Evidence-based prevention of Alzheimer's disease: systematic review and meta-analysis of 243 observational prospective studies and 153 randomised controlled trials. *J. Neurol. Neurosurg. Psychiatr.* 91, 1201–1209. doi: 10.1136/jnnp-2019-321913

Zhang, W., Xiao, D., Mao, Q., and Xia, H. (2023). Role of neuroinflammation in neurodegeneration development. *Signal Transduct Target Ther* 8:267. doi: 10.1038/s41392-023-01486-5

Zhang, X. X., Tian, Y., Wang, Z. T., Ma, Y. H., Tan, L., and Yu, J. T. (2021). The epidemiology of Alzheimer's disease modifiable risk factors and prevention. *J. Prev. Alzheimers Dis.* 8, 313–321. doi: 10.14283/jpad.2021.15

Zhao, P., Xu, Y., Jiang, L., Fan, X., Li, L., Li, X., et al. (2022). A tetravalent TREM2 agonistic antibody reduced amyloid pathology in a mouse model of Alzheimer's disease. *Sci. Transl. Med.* 14:eabq0095. doi: 10.1126/scitranslmed.abq0095

Ziegler-Heitbrock, L., Ancuta, P., Crowe, S., Dalod, M., Grau, V., Hart, D. N., et al. (2010). Nomenclature of monocytes and dendritic cells in blood. *Blood* 116, e74–80. doi: 10.1182/blood-2010-02-258558

frontiers | Frontiers in Aging Neuroscience

TYPE Review
PUBLISHED 17 July 2024
DOI 10.3389/fnagi.2024.1402774

OPEN ACCESS

EDITED BY
Rodrigo Morales,
University of Texas Health Science Center at Houston, United States

REVIEWED BY
Arun Kumar Yadawa,
University of Connecticut Health Center, United States
Salvatore Saieva,
University of Texas Health Science Center at Houston, United States

*CORRESPONDENCE
Ming Chen
✉ chenming@ahmu.edu.cn
Jinyu Mei
✉ meijinyu@ahmu.edu.cn

†These authors have contributed equally to this work

RECEIVED 18 March 2024
ACCEPTED 04 July 2024
PUBLISHED 17 July 2024

CITATION
Tao B, Gong W, Xu C, Ma Z, Mei J and Chen M (2024) The relationship between hypoxia and Alzheimer's disease: an updated review.
Front. Aging Neurosci. 16:1402774.
doi: 10.3389/fnagi.2024.1402774

The relationship between hypoxia and Alzheimer's disease: an updated review

Borui Tao[1,2†], Wei Gong[3†], Chengyuan Xu[1], Zhihui Ma[1], Jinyu Mei[3*] and Ming Chen[1*]

[1]Department of Pharmacology, School of Basic Medical Sciences, Anhui Medical University, Hefei, China, [2]The First Clinical Medical College, Anhui Medical University, Hefei, China, [3]Department of Otorhinolaryngology Head and Neck Surgery, The Second Affiliated Hospital of Anhui Medical University, Hefei, China

Alzheimer's disease (AD) is one of the most common neurodegenerative diseases, and the most prevalent form of dementia. The main hallmarks for the diagnosis of AD are extracellular amyloid-beta (Aβ) plaque deposition and intracellular accumulation of highly hyperphosphorylated Tau protein as neurofibrillary tangles. The brain consumes more oxygen than any other organs, so it is more easily to be affected by hypoxia. Hypoxia has long been recognized as one of the possible causes of AD and other neurodegenerative diseases, but the exact mechanism has not been clarified. In this review, we will elucidate the connection between hypoxia-inducible factors-1α and AD, including its contribution to AD and its possible protective effects. Additionally, we will discuss the relationship between oxidative stress and AD as evidence show that oxidative stress acts on AD-related pathogenic factors such as mitochondrial dysfunction, Aβ deposition, inflammation, etc. Currently, there is no cure for AD. Given the close association between hypoxia, oxidative stress, and AD, along with current research on the protective effects of antioxidants against AD, we speculate that antioxidants could be a potential therapeutic approach for AD and worth further study.

KEYWORDS

Alzheimer's disease, hypoxia, HIF-1α, oxidative stress, Aβ, mitochondrial dysfunction, inflammation, tau

1 Introduction

Alzheimer's disease (AD) is one of the most common neurodegenerative diseases, and the most prevalent form of dementia. It usually manifests as a gradual decline in episodic memory and cognitive abilities, leading to impairments in language, visuospatial skills, and often behavioral disturbances like apathy, aggression, and depression (Høgh, 2017; Porsteinsson et al., 2021). The main neuropathological criteria for the diagnosis of AD are extracellular amyloid-beta (Aβ) plaque deposition and intracellular accumulation of highly hyperphosphorylated Tau protein as neurofibrillary tangles (Long and Holtzman, 2019). As the population ages, the incidence of AD continues to rise (Weller and Budson, 2018). According to Alzheimer's Disease International the prevalence of dementia is about 50 million people worldwide, and is predicted to more than triple by 2050 as the population ages (Lane et al., 2018; Scheltens et al., 2021). Over the next few years, there's an anticipated

spike in dementia prevalence, particularly in low and middle income countries, aligning with the rising incidence of cardiovascular disease, hypertension, and diabetes, while on the contrary, emerging evidence indicates a decline in dementia incidence in high-income countries, although the evidence supporting a decrease in prevalence is less convincing (Lane et al., 2018; Scheltens et al., 2021). In the United States, unpaid dementia caregiving was valued at US$346.6 billion in 2023 and may exceed US$600 billion in 2050 which results in great societal burden (Lane et al., 2018; Alzheimer's Association, 2024). AD is a heterogeneous disease with a complicated pathophysiology. Mounting evidence show that AD is 60%∼80% dependent on heritable factors and there are several hypothesizes such as the amyloid and neuro-inflammation hypothesis (Liu et al., 2019). Hypoxia is also believed to have a tight connection with AD. Our brain consumes 20% of the oxygen and maintains a continually active state relying on the oxygen (Bailey, 2019). As a result of the high energy-consumption of the brain, it is more likely to be influenced by hypoxia than any other organ. Neurons, as the basic functional unit of the brain, are also likely to be influenced by hypoxia as they contain low levels of glutathione which plays crucial roles in the antioxidant defense system and the maintenance of redox homeostasis in neurons (Aoyama, 2021). Since the 19th century, people realized that hypoxia can lead to neurological consequences (Burtscher et al., 2021). There are evidences showing that hypoxia has a tight connection with AD. Studies show that the risk of AD increases a lot after persistent systemic hypoxia or stroke (Vijayan and Reddy, 2016; Sriram et al., 2022) and reduced oxygen supply has also been observed in both AD pathology and the aging process (Adeyemi et al., 2021). As the underlying molecular mechanisms connecting hypoxia with AD is still unclear, the involvement of kynurenine pathway has gained interest. Tryptophan (Trp) is an essential amino acid as it cannot be produced in human body and it is a precursor to a number of metabolites like serotonin, melatonin, and niacin as well as neurotransmitters (Mohapatra et al., 2021). The kynurenine pathway is one of the three major pathways of Trp metabolism which metabolizes 90% of Trp into kynurenic acid, xanthurenic acid, picolinic acid, quinolinic acid, and nicotinamide adenine dinucleotide (Cervenka et al., 2017; Doifode et al., 2021). Studies have found that the several metabolites of kynurenine pathway including quinolinic acid, kynurenine and 3-hydroxykynurenine are associated with AD, due to their involvement in excitotoxic neurotransmission, oxidative stress, uptake of neurotransmitter, amyloid aggregation, and inflammation (Wang et al., 2015; Venkatesan et al., 2020; Sharma et al., 2022). Studies also found that hypoxia can induce the increase of Trp production thus leading to more metabolites of kynurenine pathway, thus suggesting a connection between hypoxia and AD (Mohapatra et al., 2021). However, there are researches showing that the increase of Trp in hypoxia is due to the decrease of kynurenine pathway function suggesting that Trp catabolites are not key of factors in the pathophysiology of AD (Mohapatra et al., 2021; Almulla et al., 2022). There is also evidence showing that hypoxia is related with AD. Chronic intermittent hypoxia (CIH) is a feature of obstructive sleep apnea (OSA). Recent studies on OSA compared the serum levels of Aβ proteins and tau proteins in 46 cognitively normal OSA patients and 30 healthy controls: the results showed that patients with OSA had significantly higher median serum levels of $A\beta_{40}$, $A\beta_{42}$ and total tau than controls. One study also found that Aβ level are associated with the changes in sleep architecture, specifically, rapid eye movement sleep was negatively correlated with Aβ proteins. Another study on APP/PS1 mice (an animal model of AD) examined the effects of CIH on cognition and hippocampal function and found that CIH induced long-term potentiation dysfunction of the hippocampus in APP/PS1 mice as they found the decrease of N-methyl-D-aspartic acid receptor (NMDAR) NR1 subunit and postsynaptic density 95 (PSD95) in the hippocampus of APP/PS1 mice after CIH treatment (Li and Ye, 2024). NMDAR is a type of ionotropic glutamate receptor found in nerve cells while PSD95 is a scaffolding protein found in the post-synaptic density of neurons. They are both crucial for synaptic plasticity, learning, and memory processes in the brain. These results suggest that CIH is related to the AD (Bhuniya et al., 2022).

As the accurate pathogenesis of AD is still unknown, a good understanding of the relationship between hypoxia and AD can help us know more about this disease and help discover potential therapeutic approaches for it. In this review, we focus on the relationship between hypoxia-inducible factors-1α (HIF-1α) with AD as well as the link between oxidative stress and AD.

2 HIF-1α is an essential factor in AD onset

2.1 Structure and function of HIF-1α

Hypoxia-inducible factors (HIFs) are transcription factors consisting of α and β subunits that regulate cellular reactions to low oxygen levels. The latter is a constructive subunit which forms a heterodimeric complex with the former, while the former is an oxygen-sensitive subunit, thus, the transcriptional activity of HIF-1 is primarily regulated by the levels of HIF-1α protein (Forsythe et al., 1996; Zagórska and Dulak, 2004; Figure 1).

Three isoforms of HIF-α (HIF-1α, HIF-2α, HIF-3α) have been identified. Among the three types of HIF-α isoforms, HIF-1α is involved in the acute hypoxic response associated with erythropoietin, whereas HIF-2α is associated with the response to chronic hypoxia (Xie et al., 2019). Under normal oxygen conditions, HIF-1α undergoes degradation through a process involving the von Hippel-Lindau (VHL) protein. Prolyl hydroxylase enzymes (PHDs) are a group of enzymes which can be found in various tissues and cells throughout the body, including the liver, kidneys, and heart. They are involved in the modification of proteins, specifically in the hydroxylation of proline residues. In normoxia, PHDs are active and hydroxylate specific proline residues on HIF-1α at P402 and P564. This hydroxylation marks HIF-1α for recognition by the VHL protein, which is part of an E3 ubiquitin ligase complex. Upon binding to hydroxylated HIF-1α, the VHL complex ubiquitinates HIF-1α. This ubiquitination signals for the proteasomal degradation of HIF-1α, preventing its accumulation and subsequent activation of HIF-1. This process is a key regulatory mechanism that ensures HIF-1α is degraded under normoxic conditions, maintaining cellular homeostasis in the presence of sufficient oxygen (Yu et al., 2001; Semenza, 2007; Figure 1). Conversely, under hypoxic conditions, HIF-1 levels can quickly increase in order to adapt from anoxic condition

(Wang et al., 1995). In low oxygen condition, PHDs are less active: as a result, HIF-1α is not hydroxylated as extensively. With reduced hydroxylation and degradation, HIF-1α accumulates in the cytoplasm, where it stabilizes and can translocate into the cell nucleus. In the nucleus, HIF-1α forms a complex with HIF-1β. This heterodimeric complex is the active form of HIF-1. The HIF-1 complex binds to specific DNA sequences called Hypoxia-Response Elements (HREs) in the promoter regions of target genes (Yang C. et al., 2021). CREB-binding protein (CBP) and p300 are related transcriptional coactivators that play important roles in regulating gene expression by interacting with a variety of transcription factors. They possess histone acetyltransferase activity, which allows them to modify chromatin structure and promote transcription (Wu et al., 2013). When HIF-1α is stabilized under hypoxic conditions, the C-terminal transactivation domain forms a complex with CBP/p300. The latter then acetylates specific lysine residues on HIF-1α, enhancing its transcriptional activity. This acetylation event facilitates the recruitment of additional transcriptional machinery, leading to the transcription of genes involved in cellular adaptation to low oxygen levels (Figure 1; Dames et al., 2002; Wu et al., 2013). Finally, under hypoxic conditions, HIF-1α together with other molecular mediators like peroxisome proliferator-activated receptor γ coactivator α (PGC-1α), c-MYC (a protein plays a crucial role in regulating cell growth, proliferation and apoptosis), SIRT1 (a protein involved in regulating various cellular processes such as aging, DNA repair, metabolism, and stress response), and AMPK (an enzyme that plays a crucial role in cellular energy homeostasis which is activated in response to low cellular energy levels) become activated and function as transcription factors, regulating the expression of genes involved in various adaptive responses (Ham and Raju, 2017). HIF-1 promotes the cellular adaptation to hypoxia by activating genes that enhance oxygen delivery. For example, VEGF, acting as the downstream target gene of HIF-1α, is crucial in controlling angiogenesis (formation of new blood vessels). Research indicates that the HIF-1α/VEGF pathway participates in various pathophysiological processes, including inflammation, ischemia-reperfusion injury, oxidative stress, and other conditions associated with angiogenesis or vascular remodeling as well as tumor immunity (Palazon et al., 2017; Liu et al., 2018; Lin et al., 2019; Chen et al., 2022). HIF-1α is also involved in the acute hypoxic response associated with erythropoiesis (Sala et al., 2018; Xie et al., 2019; Hirota, 2021). Additionally, it stimulates glycolysis, a process that does not rely on oxygen, providing an alternative energy source when oxygen availability is limited (Cheng et al., 2014; Wang et al., 2021).

2.2 HIF-1α in Alzheimer's disease: friend or foe?

Amyloid-beta is formed by the sequential cleavage of amyloid precursor protein (APP) by β-secretases (BACE1) as well as γ-secretases (Sun et al., 2017) and its accumulation in brain tissue is now acknowledged as the major pathogenic event in AD (Zou et al., 2020). BACE1 serves as a pivotal enzyme in APP processing, linked to the generation of the membrane-bound C-terminal fragment C99 (APP-C99) and its production. Numerous studies have highlighted the involvement of BACE1 regulation in AD pathogenesis, including Aβ accumulation and memory impairment associated with Aβ (Ohno et al., 2004; Laird et al., 2005). γ-Secretase is a macromolecular complex that contains four essential subunits: anterior pharynx-defective 1 (Aph1), nicastrin (NCT), presenilin enhancer 2 (Pen-2), and its catalytic core presenilin (PS) (Yang G. et al., 2021). Aβ exists in a variety of species, including monomers, soluble oligomers, protofibrils, and insoluble fibrils, which are eventually deposited as senile plaques (Huynh et al., 2017; Chai et al., 2021). Specifically, Aβ peptides can transform structurally from monomers into β-stranded fibrils via multiple oligomeric states. Structured oligomers among different Aβ species are suggested to be more toxic than fibrils and the identification of Aβ oligomers has proven challenging due to their diversity and instability (Lee et al., 2017). Research on the relationship between hypoxia and Aβ generation has been conducted for a long time, however, the specific mechanisms remain unclear. We suggest that HIF-1α may connect them. A number of studies highlight that hypoxia, through the mediation of HIF-1α, leads to an increase in BACE1 expression and contributes to elevated Aβ production which is considered the driving force of AD according to the amyloid hypothesis, the most accepted theory for AD pathogenesis (Zhang et al., 2007; Guglielmotto et al., 2009). *In vitro* and *in vivo* studies indicate that hypoxia up-regulates BACE1 expression through a biphasic mechanism both *in vitro* and *in vivo*. The early post-hypoxic upregulation of BACE1 depends on the production of reactive oxygen species (ROS) caused by the sudden interruption of the mitochondrial electron transport chain, which will be discussed in the next part, while the late expression of BACE1 is attributed to the activation of HIF-1α (Guglielmotto et al., 2009). A study by Zhang et al. (2007) further elucidated that overexpression of HIF-1α leads to elevated levels of both BACE1 mRNA and protein, while when HIF-1α is downregulated, BACE1 levels decrease. Meanwhile, this study also shows that hypoxia treatment after HIF-1α activation does not further increase the expression of BACE1, suggesting that hypoxia-induced BACE1 expression is predominantly mediated by HIF-1α (Zhang et al., 2007). In addition, HIF-1α is able to bind and activate γ-secretase, thus promoting the production of Aβ under hypoxic conditions and reduced blood flow in the brain (Alexander et al., 2022). Another study also showed that HIF-1α activated BACE1 and γ-secretase through different ways: HIF-1α transcriptionally upregulates BACE1 and non-transcriptionally activates γ-secretase for Aβ production (Alexander et al., 2022). Moreover, HIF-1α also plays a crucial role in regulating Aβ generation under the influence of other environmental factors like high-glucose. Specifically, studies have indicated that BACE1 localizes within the lipid raft, and alterations in cholesterol levels within these rafts could impact BACE1 function, consequently affecting Aβ generation. This implies that modifications to lipid rafts induced by hyperglycemia might serve as a potential initiator of AD pathogenesis. Under high glucose conditions, increased levels of ROS trigger the activation of HIF-1α and liver X receptor α (LXRα) which is a key factor regulating intracellular cholesterol. This stimulation leads to the reorganization of lipid rafts, thereby enhancing the production of Aβ mediated by BACE1 (Lee et al., 2016).

Tau protein, encoded by MAPT on chromosome 17Q21, is a microtubule-associated protein (Lou et al., 2023).

Hyperphosphorylation of Tau leads to its pathological aggregation, thus eventually promoting the formation of intracellular neurofibrillary tangles (NFTs). These NFTs, along with Aβ plaques, are characteristic features of AD (Scheltens et al., 2021; Figure 2). There is evidence showing that under intermittent hypoxia conditions, the levels of Tau protein in the serum increase, indicating a close relationship between hypoxia and Tau protein (Bhuniya et al., 2022). However, the specific mechanism of how hypoxia affects tau metabolism remains unclear. A recent study suggested HIF-1α may play a vital role in tau pathology. Under conditions of chronic hypoxia, HIF-1α leads to a deficiency in leucine carboxyl methyltransferase 1 (LCMT1) and protein phosphatase 2A (PP2A), thereby mediating the abnormal hyperphosphorylation of Tau protein (Lei et al., 2022). LCMT1 is an enzyme that plays a role in the methylation of the carboxyl group on leucine residues in proteins. The specific function of LCMT1 includes regulating the activity of PP2A, a critical enzyme involved in the regulation of various cellular processes such as cell division, signal transduction, and metabolism. LCMT1-mediated methylation of PP2A catalytic subunits enhances the activity of PP2A, thereby affecting its ability to dephosphorylate target proteins and modulating cellular signaling pathways (Lei et al., 2022). The methylation activity of LCMT1 can influence the phosphorylation levels of Tau protein, thereby regulating the biological functions of Tau. Specifically, the methylation activity of LCMT1 may contribute to maintaining the normal physiological state of Tau protein, preventing its excessive phosphorylation. However, if LCMT1 function is impaired or disrupted, it may lead to the abnormal phosphorylation of Tau protein, thus contributing to the pathogenesis of neurological disorders, such as AD (Sontag et al., 2013, 2014). Another study conducted on Sprague-Dawley rats shows that there is a significant increase in the phosphorylated PP2A and a significant decrease in the methylated PP2A levels in the rats' hippocampus after hypoxia treatment. Combined with the elevated tau protein levels in rats, it can be concluded that hypoxia can lead to inactivation of PP2A, resulting in hyperphosphorylation of tau protein and memory deficits (Zhang et al., 2014). However, there are also studies showing that HIF-1α plays a protective role in tau pathology in AD. Glucose transporters (GLUTs) are proteins that facilitate the transport of glucose across cell membranes. They play a crucial role in glucose uptake, particularly in cells that rely heavily on glucose for energy, such as neurons. According to Liu et al. (2008), decreased brain levels of HIF-1α in AD patients were linked to the downregulation of GLUT-1 and GLUT-3 compared to age-matched controls. This impedes glucose uptake and metabolism, ultimately resulting in reduced O-GlcNAcylation and subsequent hyperphosphorylation of tau (Liu et al., 2008). T-2 toxin is a type A trichothecene mycotoxin produced by certain *Fusarium* species. It has been regarded as a neurotoxin as it can enter the brain through the blood-brain barrier. After entering the brain, T-2 toxin can cause further damage by triggering oxidative stress, neuroinflammation, and even apoptosis and it can also induce the rise of phosphorylated tau protein. A study has found that T-2 toxin can induce the expression of hyperphosphorylated tau (Zhao et al., 2024). In Zhao et al.'s (2024) study, they found the level of hyperphosphorylated tau induced by T-2 toxin increased when HIF-α signaling was inhibited. This suggested that HIF-1α played a protective role in the T-2 toxin-induced expression of hyperphosphorylated tau (Zhao et al., 2024). Taken together, we have sufficient reasons to believe that HIF-1α is associated with tau pathology in AD, however, the specific mechanism remains unclear and requires further research.

Inflammation is a pathological process characterized by injury or destruction of tissues. There is a substantial amount of evidence indicating that both neuro-inflammation and the inflammation in periphery are also a significant factor in the development of AD (Heneka et al., 2015; Ozben and Ozben, 2019; Xie et al., 2021; Lou et al., 2023). Zhao et al. (2021) found that HIF-1α is implicated in the inflammatory response and oxidative stress in the condition of elevated glucose levels and hypoxia. This study observed that high glucose and hypoxia upregulated HIF-1α expression, while downregulated HIF-1α decreased the level of inflammation (Zhao et al., 2021). Astrocytes have been shown to participate in both innate and subsequent adaptive immune responses (Han et al., 2021). HIF-1α was identified as a mediator in the transcriptional regulation of chemokines, specifically monocyte chemoattractant proteins 1 (MCP-1/CCL2) and 5 (Ccl12), in hypoxic astrocytes (Mojsilovic-Petrovic et al., 2007). Interleukin-1 (IL-1β) beta is a mediator that triggers inflammation. Another comparative study shows that HIF-1α mediates transcriptional activation of IL-1β in astrocyte cultures which also demonstrates the association between HIF-1α and inflammation in astrocyte (Zhang et al., 2006). On the other hand, HIF-1α also plays an important role in the pathology of neuroinflammation in microglia. A study shows Aβ exposure initiates immediate microglial inflammation and this process is proved to rely on the mTOR-HIF-1α pathway (Baik et al., 2019). These pieces of evidence suggest that HIF-1α is related to inflammation. Interestingly, the interaction between HIF-1α and inflammation seems influenced by the degree of inflammation. A study by de Lemos et al. (2013) revealed that HIF-1α assumes a significant role in an acute inflammation model induced by pro-inflammatory TNF-α, IL-1β, and IFN-γ while in a chronic model of inflammation using an APP/PS1 transgenic mouse model of AD HIF-1α seems to have no effect. This phenomenon could possibly be explained by the deactivation of relevant cells following acute inflammatory responses. In fact, studies indicate that once activated by acute inflammation, microglial cells enter a state of chronic tolerance due to extensive defects in energy metabolism and subsequent attenuation of immune responses, including cytokine secretion and phagocytosis (Baik et al., 2019).

Despite numerous evidence confirming HIF-1α as a risk factor in AD, intricately linked to key mechanisms such as Aβ aggregation, tau phosphorylation, neuroinflammation, some studies suggest that HIF-1α may exhibit a protective role in the onset of AD. Desferoxamine (DFO) is a medication used to treat iron overload in conditions such as thalassemia and hemochromatosis. Research indicates that DFO has a protective effect against neurological damage caused by ischemia and hypoxia (Li et al., 2008). A comparative study suggests that inhibiting HIF-1α diminishes the protective effect of DFO, indicating that DFO's neuroprotection involves the induction of HIF-1α (Hamrick et al., 2005). Methylene blue (MB) is another drug with neuroprotective effects. Investigations have shown that, the nuclear translocation of HIF-1α increased nearly threefold after MB treatment compared to the control group. This suggests that its protective effect may be linked to HIF-1α (Ryou et al., 2015). Due to hypoxia and ischemia being significant risk factors for various neurological diseases, the protective role of HIF-1α in

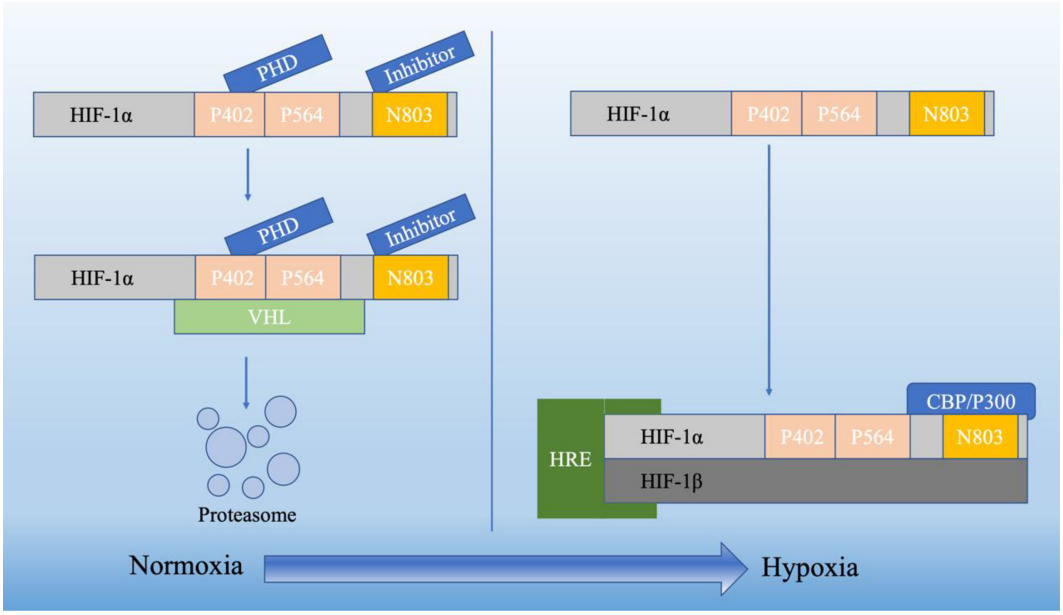

FIGURE 1
The HIF-1α undergoes distinct cleavage processes in normoxia and hypoxia. In normoxia, hydroxylation of two proline residues and acetylation of a lysine residue within the oxygen-dependent degradation domain prompt its binding to the VHL E3 ligase complex, initiating degradation through the ubiquitin-proteasome pathway. Conversely, in hypoxia, the HIF-1α subunit attains stability and engages with coactivators like CBP/P300, orchestrating the regulation of gene expression.

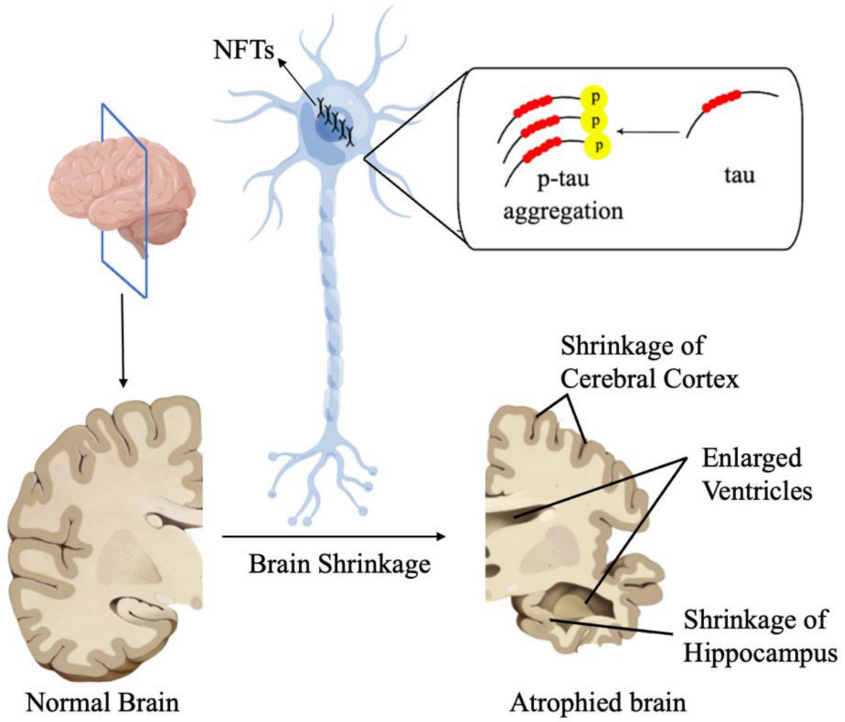

FIGURE 2
In AD, Tau proteins undergo pathological aggregation, leading to the formation of NFTs. These NFT plaques are one of the characteristic features of AD.

hypoxia and ischemia indirectly suggests its protective effects in AD and other neurodegenerative disorders. Other studies also indicate that HIF-1α is a crucial component in several other neuroprotective pathways. Cardamonin is a chalcone with neuroprotective activity. Compelling evidence showed that in middle cerebral artery occlusion-treated mice, cardamonin reduced

brain injury and stimulated the activation of the HIF-1α/VEGFA signaling and blocking the HIF-1α/VEGFA signaling with an inhibitor can reverse such protective effects. This indicates that HIF-1α is involved in neuroprotective activity (Ni et al., 2022). Due to the fact that ischemia-reperfusion injury concurrently triggers neuropathology and gene expression associated with AD, including the development of amyloid plaques, neurofibrillary tangles, and hippocampal atrophy, which are crucial for the progression of AD (Pluta and Ulamek-Koziol, 2021), the protective role of HIF-1α against ischemia-reperfusion injury indirectly suggests its protective effects against AD.

3 Oxidative stress and AD

Oxidative stress refers to an imbalance between the production of ROS and the body's ability to detoxify them or repair the resulting damage. ROS are highly reactive molecules containing oxygen that can damage cells and tissues in the body. Oxidative stress can result from various factors such as environmental pollutants, toxins, poor diet, radiation, smoking, and even normal metabolic processes in the body (Lim and Thurston, 2019). Hypoxia can also lead to different pathological processes that can eventually develop into oxidative stress. Hypoxia undoubtedly has a close relationship with mitochondrial dysfunction as hypoxic condition can promote the production of ROS, cause damage to mitochondrial membrane potential (MMP) and mitochondrial DNA (mtDNA) and further lead to the insufficient energy production. Recent studies on cold inducible RNA binding protein (Cirbp) suggested that it can rescue cognitive retardation and dendritic spine injury as Cirbp can reduce the abnormal expression of PSD95, a vital synaptic scaffolding molecule, and attenuate hypoxia induced deficiency of energy and oxidative stress (Zhou et al., 2021; Liu et al., 2022). Cirbp can also control mitochondrial homeostasis and ATP biogenesis at hypoxic condition by sustaining the protein levels of respiratory chain complexes II (SDHB) and IV (MT-CO1) and directly binding 3′UTR of Atp5g3 (Liu et al., 2022). In conclusion, hypoxia is one of the most important factors leading to oxidative stress as it can induce unfavorable factors like mitochondrial dysfunction, Aβ accumulation as well as inflammation. At the same time, hypoxia can also directly lead to oxidative stress. It is reported that hypoxic conditions could upregulate HIF-1α expression and HIF-1α can regulate oxidative stress through HIF-1α/JMHD1A pathway (Zhao et al., 2021). However, there are also researches showing that HIF-1α plays a protective role against oxidative stress. Research showed the expression of mito-HIF-1α, a mitochondrial-targeted form of HIF-1α, can decrease apoptosis induced by hypoxia or H_2O_2 treatment (Li H. et al., 2019). Mito-HIF-1α can also reduce the production of ROS and the collapse of mitochondrial membrane potential (Li H. et al., 2019) which means it can protect mitochondria from oxidative stress and hypoxia.

When oxidative stress overwhelms the body's antioxidant defenses, it can lead to damage to proteins, lipids, and DNA, contributing to various diseases such as cancer, neurodegenerative disorders, cardiovascular diseases, and aging. As the accurate pathogenesis of AD is still unknown, oxidative stress is supposed to play an important role in the pathogenesis of AD and is supposed to be a potential treatment target for AD. Oxidative stress is one of the major events involved in AD (Tönnies and Trushina, 2017; Dumitrescu et al., 2018; Ionescu-Tucker and Cotman, 2021). Currently, many studies on AD focus on the degeneration of neuronal cells, which can be caused by several risk factors, including oxidative stress. The damaged DNA bases, protein oxidation and lipid peroxidation products in brain after oxidative stress are sings of AD (Nunomura and Perry, 2020). Recent studies have found significant differences in 8-OHdG and 8-OHdG/2-dG between patients with mild cognitive impairment due to AD and normal elderly subjects. Both of 8-OHdG and 8-OHdG/2-dG are markers of DNA oxidative damage and can be used to assess the oxidative damage to the DNA (Peña-Bautista et al., 2019). In addition, oxidative stress also leads to the differences in protein between AD patients and normal people. Hydroxyl free radicals are known to convert phenylalanine to the non-physiological isomers of tyrosine o-tyrosine and m-tyrosine (o-Tyr and m-Tyr) (Mohás-Cseh et al., 2022). Previous research found protein oxidation (m-Tyr and o-Tyr) in AD plasma and CSF samples (Ryberg et al., 2004; Ahmed et al., 2005). Meanwhile, since 3-nitrotyrosine (3-NT) is a marker of protein oxidation, there are also studies suggesting using 3-NT as a marker for early diagnosis of AD (Ryberg et al., 2004). Herpes simplex virus type-1 (HSV-1), a DNA neurotropic virus, has been considered a potential etiological agent of AD through inducing incomplete autophagic response according to previous research (Santana et al., 2012; De Chiara et al., 2019). Oxidative stress induced by HSV-1 infection may promote the development of AD. Oxidative stress could significantly enhance HSV-1 infection-mediated intracellular Aβ accumulation and further inhibit its secretion into extracellular media (Santana et al., 2013). Additionally, studies found that at the prodromal stage of AD, there are oxidized RNAs including mRNA, rRNA, and tRNA have been identified in patients' brains. Oxidative stress interferes with both translational machineries and regulatory mechanisms of noncoding RNAs, especially microRNAs and leads to retarded or aberrant protein synthesis (Nunomura and Perry, 2020). As one of the AD central pathological lesions in brain, NFTs are composed mainly of hyperphosphorylated tau (Naseri et al., 2019) and oxidative stress has a close relationship with tau pathology. Early studies found that specific fatty acid oxidative products could provide a direct link between oxidative stress mechanisms and the formation of NFTs in AD (Gamblin et al., 2000). All these evidence show that oxidative stress indeed takes part in the pathology of AD and oxidative damage of DNA can be an early marker of AD. Besides the direct connections, oxidative stress is also linked with AD due to some key events like Aβ accumulation, inflammation, mitochondrial dysfunction, metal dysregulation, and protein misfolding. In the next section, we will explore how the oxidative stress due to factors like mitochondrial dysfunction, DNA damage, Aβ pathology, and inflammation can be prodromal to AD.

3.1 Mitochondrial dysfunction and oxidative stress

Mitochondria play an important role in cells, including ATP production, intracellular Ca^{2+} regulation, ROS production, and cell damage and death (Bhatti et al., 2017; Marín et al., 2020).

Research has shown that mitochondrial dysfunction is associated with AD. For example, due to the special open circular structure of mtDNA, it is highly vulnerable to oxidative damage. ROS leads to the oxidation of guanosine to form 8-OHdG and results in mtDNA mutations including base mispairing, random point mutation as well as deletions (Soltys et al., 2019; Antonyová et al., 2020) and the mutations in mtDNA are linked with misfolding and aggregation of Aβ, α-syn and tau, and neuronal apoptosis (Sengupta et al., 2015; Antonyová et al., 2020). Moreover, the connection between the impact of mtDNA haplogroups B5a on the onset of AD and mitochondrial abnormalities under oxidative stress has also been demonstrated (Bi et al., 2015). Mitochondrial dysfunction has connection with ROS accumulation. Early-onset Alzheimer's disease (EOAD) refers to AD that develops in individuals under the age of 65. Clinical studies have implied that changes in mtDNA methylation and transitions (position 5633: T → C; position 7476T: C → T; and position 15812A: G → A) can play a significant role in the development of EOAD (Chagnon et al., 1999). Thus, considering the relationship between AD and mitochondrial dysfucntion, if there is evidence showing that mitochondrial dysfunction is related to oxidative stress, we can infer that AD is also related to oxidative stress.

Mitochondria are the primary site of ROS which are closely associated with oxidative stress. Therefore, it can be inferred that mitochondrial dysfunction is related to oxidative stress. ROS species are the product of one-electron reduction of oxygen and include singlet oxygen ($1O_2$), superoxides ($O_2\cdot^-$), peroxides (H_2O_2), hydroxyl radical (·OH), and hypochlorous acid (HClO) (Taysi et al., 2019; Sahoo et al., 2022; Figure 3). Complexes I and III of the mitochondrial respiratory chain are the major sited of superoxide production (Mailloux and Harper, 2011). As a by-product of cellular metabolism, ROS has both beneficial and deleterious effects on our health. On one hand ROS contribute to the healthy cell function as they play an essential role in the regulation of growth, apoptosis, autophagy, memory, blood pressure, cognitive function as well as immune function (Scherz-Shouval et al., 2007; Oswald et al., 2018; Luo et al., 2019; Lloberas et al., 2020). Also, recent research showed that ROS has antimicrobial activity against Gram-positive and Gram-negative viruses as well as fungi (Dryden, 2018) and play a role in modulating endoplasmic reticulum and Golgi homeostasis (Mennerich et al., 2019). However, at high concentrations, ROS are harmful for living organisms as ROS are included in processes of many diseases like metabolic disorders, genetic diseases, diabetes, cancer as well as neurodegenerative diseases. The accumulation of ROS is related to lipid peroxidation, protein oxidation and DNA damage which are all features of oxidative stress (Su et al., 2019; Juan et al., 2021).

Furthermore, oxidative stress can induce damage to mitochondria through ROS which is characterized by the cytochrome c (cyt C) release and the increase in mtDNA fragmentation (Rizwan et al., 2020).

Cytochrome c is a small heme protein associated with the inner membrane of the mitochondria. It plays a crucial role in the electron transport chain, transferring electrons between Complex III and Complex IV. cyt C is closely linked to the production of ROS in the mitochondria. During the electron transport chain, electrons are transferred through various complexes, including cyt C. If the electron transfer process is inefficient, electrons can prematurely reduce oxygen, leading to the formation of $O_2\cdot^-$, a type of ROS. Additionally, when cyt C is released into the cytosol during apoptosis, it can enhance ROS production, which further contributes to cellular damage and the progression of cell death (Radi et al., 2014; Cadenas, 2018). Thus, considering cyt C is one of the important part of mitochondria, we can infer that mitochondria dysfunction has a connection with oxidative stress. On the other hand, mtDNA is highly susceptible to ROS influence due to its attachment with inner membrane and the lack of protective histones or nonhistone proteins. Evidence shows that when exposed directly to ROS, the levels of oxidative mtDNA damage are higher and more extensive compared to nuclear DNA (Richter et al., 1988). There is also a vicious cycle theory of mitochondrial ROS production which proposes a self-perpetuating cycle where mitochondrial dysfunction leads to increased ROS production. This elevated ROS generation, in turn, causes further damage to mitochondrial components, exacerbating dysfunction and ROS production (Bandy and Davison, 1990).

3.2 Aβ and oxidative stress

Alzheimer's disease is a progressive neurodegenerative condition characterized by the accumulation of extracellular Aβ plaques and intracellular neurofibrillary tangles composed of hyperphosphorylated tau-protein in specific regions of the human brain, notably cortical and limbic areas. Clinical signs include memory impairment and deteriorating neurocognitive function. Dysregulated processing of APP by β-secretases and γ-secretases results in the generation of Aβ40 and $Aβ_{42}$ monomers, which subsequently aggregate to form senile plaques (Soria Lopez et al., 2019; Tiwari et al., 2019). Given the relationship between Aβ and AD, and considering the compelling evidence indicating the involvement of Aβ in oxidative stress, it can be inferred that oxidative stress is associated with AD.

Amyloid-beta has indeed been proven to be associated with oxidative stress in AD pathogenesis and progression (Tamagno et al., 2012; Hilt et al., 2018; Mcdonald et al., 2021), both *in vivo* and *in vitro* investigation.

Electron paramagnetic resonance (EPR), also known as electron spin resonance (ESR), is a technique which is particularly useful in studying paramagnetic species, like free radicals (Dikalov et al., 2018; Sahu and Lorigan, 2020). $Aβ_{1-40}$ and $Aβ_{25-35}$ fragments refer to specific shorter protein of the full Aβ peptide sequence. Studies have found that they participated in the pathology of AD and related with other neurodegenerative disorders (Kaminsky et al., 2010; Yang et al., 2020). Spin trapping experiments conducted by Butterfield et al. (1994) employing highly purified N-tert-butyl-phenylnitrone (PBN) revealed that both $Aβ_{1-40}$ and $Aβ_{25-35}$ autonomously prompted the transformation of PBN from its non-paramagnetic nitrone form to the stable, paramagnetic nitroxide form in phosphate buffered saline (PBS), and the reaction only achievable through interaction with a free radical (Butterfield et al., 1994; Hensley et al., 1995). Comparable to $Aβ_{1-40}$, $Aβ_{1-42}$ was likewise demonstrated to produce an EPR signal within this framework. Protein carbonyl and 3-NT are indicators of protein oxidation (Campolo et al., 2020; Akagawa, 2021). Studies *in vitro* also find $Aβ_{25-35}$, $Aβ_{1-40}$,

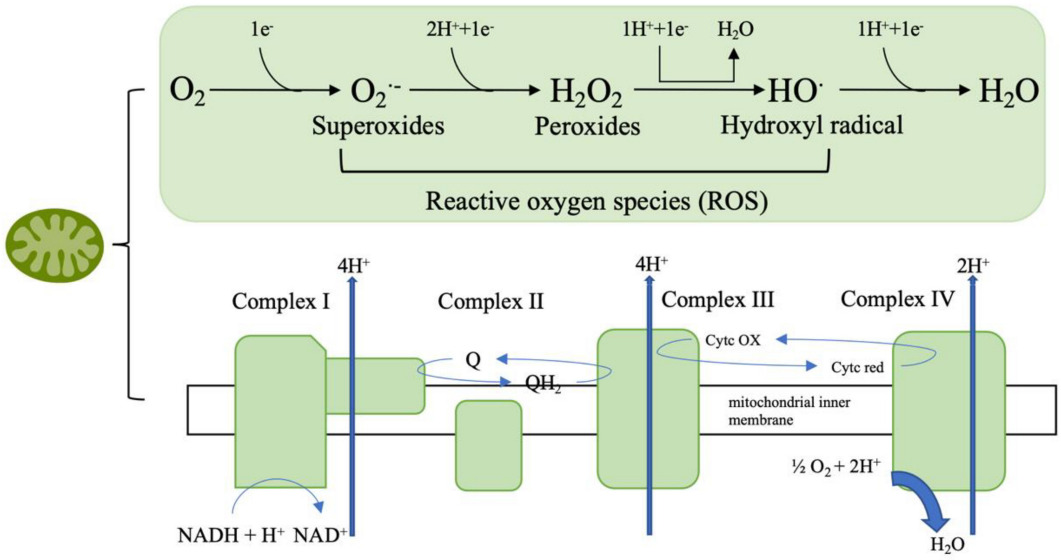

FIGURE 3
The mitochondrial respiratory chain involves a series of protein complexes (I–IV) that transfer electrons from NADH and $FADH_2$ to oxygen, thus creating an electrochemical gradient that pumps protons across the inner mitochondrial membrane. This gradient drives ATP synthesis through ATP synthase. During this process, molecular oxygen can be partially reduced to form reactive oxygen species (ROS) such as superoxide ($O_2 \cdot^-$), hydrogen peroxide (H_2O_2), and hydroxyl radicals (HO·), which are eventually converted to water (H_2O).

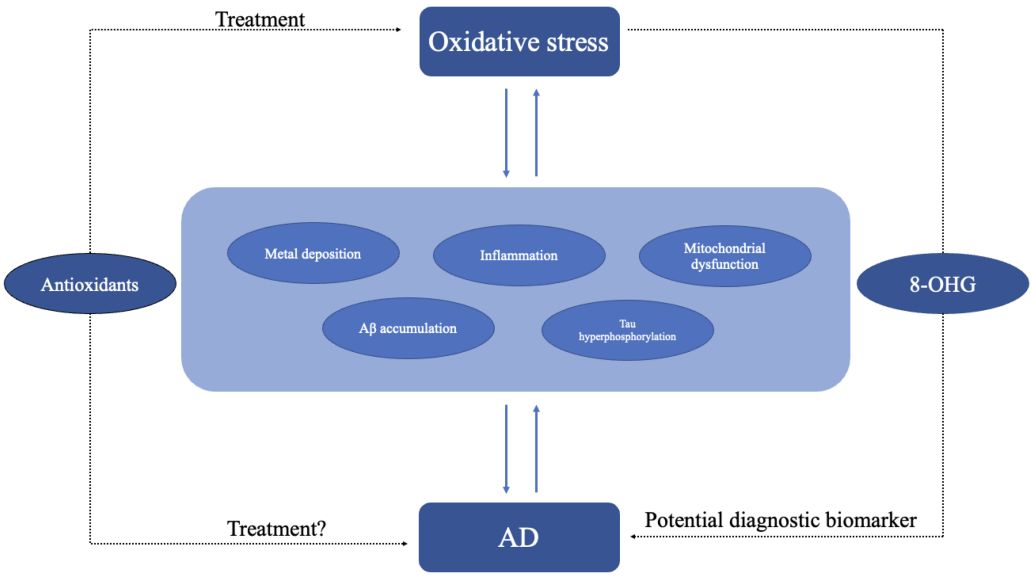

FIGURE 4
Oxidative stress may lead to AD through different pathogenesis including inflammation, metal deposition, mitochondrial dysfunction, and Aβ accumulation. In turn AD itself may exacerbate oxidative stress. Antioxidant might be an effective treatment for oxidative stress. As oxidative stress plays an important role in AD, the use of antioxidant molecules is also a potential treatment for AD. Oxidative stress products like 8-OHG could be diagnostic biomarkers of AD.

and $A\beta_{1-42}$ were demonstrated to cause notable rises in protein carbonyls as well as 3-NT in cortical synaptosomes, cultured hippocampal neurons, primary neuronal cultures, and cultured astrocytes (Harris et al., 1995a,b; Yatin et al., 1998). When it comes to *in vivo* researches, studies suggest that Aβ increases the generation of ROS in neurons through activation of the NADPH oxidase. Moreover, Aβ induces mitochondrial depolarization through calcium overload and free radical production, which can ultimately lead to oxidative damage and trigger cell death via the opening of the mitochondrial permeability (Angelova and Abramov, 2017; Chauhan and Chauhan, 2020). AD patients show an abnormal level of brain metals including copper, zinc, iron, calcium, and aluminum (Tong et al., 2018; Huat et al., 2019; Mcdonald et al., 2021; Peng et al., 2021; Plascencia-Villa and Perry, 2021), the incorrect accumulation of the metal in different brain regions induces oxidative stress (Wang et al., 2020). Evidence

indicate that Aβ plays a significant role in metal-induced oxidative stress in AD patients. The binding of iron to Aβ can induce misfolded Aβ aggregating, leading to the formation of neurotic plaques and can also increase neurotoxicity of Aβ (Rogers et al., 2019). At the same time Aβ can be a pro-oxidant, and when it is complexed with copper or iron, it can produce ROS (H_2O_2) by redox activity and causes oxidative damage to protein and lipid (Greenough et al., 2013; Wang et al., 2020). Different mentals may have distinct roles in AD pathology. The role of copper as a risk factor for AD has been confirmed to promote the aggregation of Aβ *in vitro*. Additionally, copper enhances APP translation via the 5′ untranslated region (5′ UTR) of mRNA in SH-SY5Y cells, and increases amyloidogenic processing and the expression of related pro-inflammatory cytokines (such as MCP-5) in Alzheimer's APP/PS1 double transgenic mice (Yang et al., 2019). Zinc, on the other hand, performs a protective effect as zinc can exchange with copper in the Aβ-copper complex and protect cells from oxidation (Vašák and Meloni, 2017). Studies have found that antioxidants can improve AD symptoms by alleviating oxidative stress, and Aβ is involved in this process. Nobiletin is a bioflavonoid isolated from citrus fruits peels with anti-oxidative function. In a study, rats were treated with nobiletin after bilateral intrahippocampal (CA1 subfield) injection of $A\beta_{1-40}$. Research found that mice treated with nobiletin performed better in behavioral observations and memory performance compared to the control group. Nobiletin treatment was also associated with lower hippocampal levels of ROS and partial reversal of superoxide dismutase (SOD) activity (Ghasemi-Tarie et al., 2022). These findings indicated that nobiletin prevents $A\beta_{1-40}$-induced AD via the inhibition of oxidative stress. N-adamantyl-4-methylthiazol-2-amine (KHG26693) is a new thiazole derivative and was reported that it effectively inhibits Aβ-induced oxidative damage in primary cortical neuron cultures (Cho et al., 2016). In a recent study, malondialdehyde (sign of lipid oxidation) and protein carbonyl (sign of protein oxidation) levels increased in the Aβ-treated group and were significantly downregulated by KHG26693 treatment. Meanwhile KHG26693 significantly decreased Aβ-induced ROS generation by 47% compared to the control group (Kim et al., 2017). These results illustrate that KHG26693's protection against Aβ-induced oxidative stress stems from its ability to restrain the excessive generation of ROS triggered by Aβ. Other antioxidants like benzothiazole, azelnidipine, engeletin, adenosine, and epigallocatechin gallate have the similar effect of ameliorating Aβ-related oxidative stress by different pathways including Keap1/Nrf2 pathway, NFκB pathway, and ERα pathway, etc and have a potential therapeutic efficacy in AD (Cifelli et al., 2016; Zhang et al., 2017; Teng et al., 2019; Huang et al., 2020; Zeng et al., 2022).

The studies here discussed demonstrated that Aβ is associated with oxidative stress. Therefore, we can infer that oxidative stress is related to AD due to its role on Aβ production and deposition.

3.3 Inflammation and oxidative stress

Inflammation is a physiological response to harmful stimuli, such as pathogens, damaged cells, or irritants. It is a protective mechanism that aims to remove the harmful stimuli and initiate the healing process. There are two stages of inflammation, acute and chronic inflammation. While acute inflammation is typically a short-term and beneficial response, chronic inflammation can contribute to various diseases, including arthritis, cardiovascular diseases, and cancer (Hussain and Harris, 2007; Lin and Karin, 2007). Numerous research and studies highlight that both systemic inflammation and neuroinflammation are tightly connect with the pathology of AD (Doifode et al., 2021; Twarowski and Herbet, 2023). Specifically, neuroinflammation denotes an inflammatory reaction occurring within the central nervous system (CNS), triggered by diverse pathological insults such as infection, trauma, ischemia, and toxins. This cascade entails the release of pro-inflammatory cytokines like IL-1β, IL-6, IL-18, and tumor necrosis factor (TNF), chemokines including C-C motif chemokine ligand 1 (CCL1), CCL5, and C-X-C motif chemokine ligand 1 (CXCL1), as well as small-molecule mediators like prostaglandins and nitric oxide (NO) by innate immune cells in the CNS. Microglia and astrocytes orchestrate this response principally (DiSabato et al., 2016; Leng and Edison, 2021). Research on neuroinflammation suggests that microglia, astrocytes, and neurons collaborate to drive neurodegeneration in a coordinated manner. Studies have demonstrated that Aβ activates the NF-κB pathway in astrocytes, leading to heightened complement C3 release. Subsequently, C3 acts on C3a receptors present on neurons and microglia, culminating in neuronal dysfunction and microglial activation (Lian et al., 2015). Conversely, activated microglia have been found to induce neurotoxic astrocytes by secreting IL-1α, C1q, and TNF. This interplay between microglia and astrocytes may establish a positive feedback loop in AD, perpetuating an uncontrolled and self-amplifying inflammatory response (Leng and Edison, 2021). Additionally, aberrant neuronal-glial communication has been observed in AD. Under normal circumstances, neuronal-microglial communication via CD200-CD200R and CX3CL1-CX3CR1 (microglial receptor) signaling pathways help maintaining microglial homeostasis. However, reduced expression of CD200, CD200R, and CX3CR1 in the brains of individuals with AD suggests a loss of regulatory control over microglial behavior (Bolós et al., 2017). When it comes to systemic inflammation, cross-sectional investigations reveal that individuals with cognitive impairment showed heightened systemic inflammation and elevated microglial activation compered to cognitively healthy subjects (Surendranathan et al., 2018). There are also evidences showing that gut inflammation can affect AD pathology through gut-brain axis (Abdel-Haq et al., 2019; Doifode et al., 2021). As discussed earlier, both neuroinflammation and systemic inflammation are linked to AD. Therefore, demonstrating the association between inflammation and oxidative stress indirectly implies a connection between oxidative stress and the occurrence of AD. Inflammation and oxidative stress seem like two indivisible parts in a large number of diseases including cardiovascular diseases, cancer, and AD (Chamorro et al., 2016; Marchev et al., 2017; Papaconstantinou, 2019; Li et al., 2020; Figure 4). Hypoxia is a common feature in inflammation and can lead to chronic inflammation through the activation of NF-κB and multiple isoforms of HIFs and PHDs (Watts and Walmsley, 2019; Korbecki et al., 2021). A treatment that may regulate both inflammation and oxidative stress at the same time is the inhibition of TREM1 (Li Z. et al., 2019). Moreover, mounting evidence suggest that continued oxidative stress can lead to chronic inflammation by activating a variety of transcription factors like NF-κB, AP-1, p53,

HIF-1α, PPAR-γ, β-catenin/Wnt, and Nrf2 (Reuter et al., 2010; Fan et al., 2013; Korbecki et al., 2021). These transcription factors link inflammation to diseases through different signaling pathways. For example, NF-κB and STAT3 are rapidly activated in response to diverse stimuli, including oxidative stress. Upon activation, they govern the expression of genes involved in anti-apoptotic functions, proliferation, and immune responses. Some of these genes overlap, requiring transcriptional cooperation between the two factors. The activation and interplay of STAT3 and NF-κB are pivotal in regulating the interaction between malignant cells and their microenvironment, particularly with inflammatory and immune cells infiltrating tumors (Grivennikov and Karin, 2010; Fan et al., 2013). Metals also play an important role in inflammation. Zinc, as an essential micronutrient, is involved in both inflammation and oxidative stress. The lack of Zinc can elevate inflammatory response as it is involved in the NF-κB pathway (Gammoh and Rink, 2017). Chronic inflammation manifests through heightened production of inflammatory cytokines. In Certain conditions like obesity which correlates with chronic inflammation, individuals with inadequate zinc intake exhibit reduced plasma and intracellular zinc levels, coupled with elevated gene expression of IL-1α, IL-1β, and IL-6, in contrast to those with sufficient zinc intake (Gammoh and Rink, 2017). As critical participants in inflammation, microglia and astrocytes can be regulated by ROS as well as by pro-inflammatory molecules such as MAPK and NF-κB pathway and other pathways (Park et al., 2015). On the other hand, microglia and astrocytes can release pro-inflammatory molecules like cytokines and ROS (Chen and Zhong, 2014). In addition, microglia and astrocytes interact with Aβ. The accumulation of neurotoxic Aβ itself can be regulated by microglia and their receptors as microglia can phagocyte Aβ (Ennerfelt et al., 2022), while Aβ can activate both microglia and astrocytes and be deposited in brain thus leading to ROS production: this in turn may result in oxidative stress and potentially lead to AD and other neurodegenerative disease (Chen and Zhong, 2014). A recent study revealed a critical function of SYK signaling in microglia as it can impede the development of disease-associated microglia, alter AKT/GSK3β-signaling and restrict Aβ phagocytosis by microglia (Ennerfelt et al., 2022). The strong correlation between inflammation and oxidative stress is further evidenced by studies demonstrating aggravated inflammatory phenotype in the absence of antioxidant defense proteins, such as superoxide dismutases, heme oxygenase-1, and glutathione peroxidases or overexpression of ROS producing enzymes, for example, NADPH oxidases (Steven et al., 2019).

4 Antioxidants are potential treatments for AD

As AD has caused great social burden, there is an urgent need for new therapeutic targets and approaches. Efforts concentrating on lowering amyloid beta or hyperphosphorylated Tau protein have mostly proven unsuccessful in clinical trials. As emerging evidence shows oxidative stress may be one of the key mechanisms of AD, the antioxidants have become a potential treatment for AD (Ionescu-Tucker and Cotman, 2021; Figure 4). Walnuts, one of the most common antioxidative foods in our daily life, can reduce oxidative stress by decreasing the generation of free radicals and has a beneficial effect on memory, learning, anxiety (Chauhan and Chauhan, 2020). Researches on the APP-transgenic AD mouse model have shown that mice with a walnut-based diet had an improvement in antioxidant defense and significant reductions in free radicals' levels, lipid peroxidation and protein oxidation compared with a control diet (Chauhan and Chauhan, 2020). Recent studies on PTEN-induced putative kinase 1 (PINK1) show that PINK1 overexpression can reverse the abnormal changes in mitochondria dynamics, defective mitophagy and decreased ATP levels in the hippocampus (Du et al., 2017). PINK1 overexpression activates Nrf2 signaling increases the expression of antioxidant proteins and reduces oxidative damage. PINK1 can also alleviate tau hyperphosphorylation through PI3K/Akt/GSK3β signaling (Wang et al., 2022). As an electron and proton carrier, Coenzyme Q10 (CoQ10) or ubiquinone plays an important part in mitochondrial bioenergetics and has long been used as antioxidant and mitochondrial energizer (Garrido-Maraver et al., 2014; Li X. et al., 2019; Alimohammadi et al., 2021). Recent studies showed CoQ10 can protect cells from lipid peroxidation-mediated cell death thus potentially reducing oxidative stress and conferring neuroprotective properties (Arslanbaeva et al., 2022). UBIA prenyltransferase domain-containing protein 1 (UBIAD1) which is responsible for the biosynthesis of non-mitochondrial CoQ10 has a similar effect like CoQ10 (Arslanbaeva et al., 2022).

5 Conclusion

This review primarily summarizes the impact of hypoxia on AD focusing on two aspects: HIF-1α and oxidative stress. Hypoxia is the direct and the most important consequence of both HIF-1α release and oxidative stress. These two phenomena are linked to pathological hallmarks of AD like the aggregation of Aβ, mitochondrial dysfunction and tau accumulation, thus suggesting that hypoxia is linked to AD. Current research indicates that HIF-1α has a relationship with Aβ pathology of AD. HIF-1α can increase Aβ production by regulating the expression of BACE-1. Moreover, recent studies have found an interaction between HIF-1α and γ-secretase. HIF-1α not only binds to γ-secretase but also activates it, promoting the production of Aβ under hypoxic conditions and reducing cerebral blood flow. Additionally, HIF-1α plays a crucial role as a key regulator of Aβ generation under the influence of high glucose and other environmental factors. Specifically, under high glucose conditions, increased ROS levels trigger the activation of HIF-1α and LXRα/ABCA1. This stimulation leads to lipid raft rearrangement, enhancing the production of Aβ mediated by BACE1. HIF-1α is also associated with tau phosphorylation and neuroinflammation as it can lead to a deficiency in LCMT1 as well as PP2A. Also, HIF-1α mediates neuroinflammatory responses in microglial cells through mTOR-HIF-1α pathways also involving Aβ. Moreover, compelling studies have provided evidence of a protective role for HIF-1α in neurodegenerative diseases like AD. For example, inhibiting HIF-1α diminishes the protective effect of DFO, which plays a crucial role in managing iron metabolism disorders and has a protective effect against neurological damage caused by ischemia and hypoxia (Li et al., 2008). This indicates that HIF-1α might not only serve as a potential target for AD drugs but also potentially plays a direct protective role to AD and other

neurodegenerative disease. However, further investigations are needed to confirm our hypothesis. Oxidative stress interacts with various AD risk factors, including mitochondrial dysfunction, Aβ aggregation, and neuroinflammation. Studies found that protein oxidation (m-Tyr/Phe and o-Tyr/Phe) in AD plasma and CSD samples which confirms oxidative stress is associated with the development of AD. Also, we explored the possibility of using antioxidants as potential therapeutic agents for AD. Efforts aimed at lowering amyloid beta or hyperphosphorylated Tau protein have mostly proven unsuccessful in clinical trials. Emerging evidence suggests that oxidative stress may be one of the key mechanisms of AD, therefore, the antioxidants emerge as potential treatments for AD, thus prompting further investigations.

Author contributions

MC: Writing – review & editing. BT: Writing – original draft. WG: Writing – original draft. CX: Writing – original draft. ZM: Writing – original draft. JM: Writing – review & editing.

Funding

The author(s) declare financial support was received for the research, authorship, and/or publication of this article. This study was supported by grants from the National Natural Science Foundation of China (No. 82371541), the project for the improvement of research skill in Anhui Medical University (No. 2021xkjT003), Talent Training Program from the School of Basic Medical Sciences of Anhui Medical University (No. 2022YPJH201), Research Fund of Anhui Institute of Translational Medicine (No. 2022zhyx-C11), and Provincial Training Project of Innovation and Entrepreneurship for Undergraduates (S202310366031).

Conflict of interest

The authors declare that the research was conducted in the absence of any commercial or financial relationships that could be construed as a potential conflict of interest.

Publisher's note

All claims expressed in this article are solely those of the authors and do not necessarily represent those of their affiliated organizations, or those of the publisher, the editors and the reviewers. Any product that may be evaluated in this article, or claim that may be made by its manufacturer, is not guaranteed or endorsed by the publisher.

References

Abdel-Haq, R., Schlachetzki, J., Glass, C., and Mazmanian, S. (2019). Microbiome-microglia connections via the gut-brain axis. *J. Exp. Med.* 216, 41–59. doi: 10.1084/jem.20180794

Adeyemi, O., Awakan, O., Afolabi, L., Rotimi, D., Oluwayemi, E., Otuechere, C., et al. (2021). Hypoxia and the kynurenine pathway: Implications and therapeutic prospects in Alzheimer's disease. *Oxid. Med. Cell Longev.* 2021:5522981. doi: 10.1155/2021/5522981

Ahmed, N., Ahmed, U., Thornalley, P., Hager, K., Fleischer, G., and Münch, G. (2005). Protein glycation, oxidation and nitration adduct residues and free adducts of cerebrospinal fluid in Alzheimer's disease and link to cognitive impairment. *J. Neurochem.* 92, 255–263. doi: 10.1111/j.1471-4159.2004.02864.x

Akagawa, M. (2021). Protein carbonylation: Molecular mechanisms, biological implications, and analytical approaches. *Free Radic. Res.* 55, 307–320. doi: 10.1080/10715762.2020.1851027

Alexander, C., Li, T., Hattori, Y., Chiu, D., Frost, G., Jonas, L., et al. (2022). Hypoxia Inducible Factor-1α binds and activates γ-secretase for Aβ production under hypoxia and cerebral hypoperfusion. *Mol. Psychiatry* 27, 4264–4273. doi: 10.1038/s41380-022-01676-7

Alimohammadi, M., Rahimi, A., Faramarzi, F., Golpour, M., Jafari-Shakib, R., Alizadeh-Navaei, R., et al. (2021). Effects of coenzyme Q10 supplementation on inflammation, angiogenesis, and oxidative stress in breast cancer patients: A systematic review and meta-analysis of randomized controlled- trials. *Inflammopharmacology* 29, 579–593. doi: 10.1007/s10787-021-00817-8

Almulla, A., Supasitthumrong, T., Amrapala, A., Tunvirachaisakul, C., Jaleel, A., Oxenkrug, G., et al. (2022). The tryptophan catabolite or kynurenine pathway in Alzheimer's disease: A systematic review and meta-analysis. *J. Alzheimers Dis.* 88, 1325–1339. doi: 10.3233/JAD-220295

Alzheimer's Association. (2024). Alzheimer's disease facts and figures. *Alzheimers Dement.* 20, 3708–3821.

Angelova, P., and Abramov, A. (2017). Alpha-synuclein and beta-amyloid - different targets, same players: Calcium, free radicals and mitochondria in the mechanism of neurodegeneration. *Biochem. Biophys. Res. Commun.* 483, 1110–1115. doi: 10.1016/j.bbrc.2016.07.103

Antonyová, V., Kejík, Z., Brogyányi, T., Kaplánek, R., Pajková, M., Talianová, V., et al. (2020). Role of mtDNA disturbances in the pathogenesis of Alzheimer's and Parkinson's disease. *DNA Repair* 91-92:102871. doi: 10.1016/j.dnarep.2020.102871

Aoyama, K. (2021). Glutathione in the Brain. *Int. J. Mol. Sci.* 22:5010. doi: 10.3390/ijms22095010

Arslanbaeva, L., Tosi, G., Ravazzolo, M., Simonato, M., Tucci, F. A., Pece, S., et al. (2022). UBIAD1 and CoQ10 protect melanoma cells from lipid peroxidation-mediated cell death. *Redox. Biol.* 51:102272. doi: 10.1016/j.redox.2022.102272

Baik, S., Kang, S., Lee, W., Choi, H., Chung, S., Kim, J., et al. (2019). A breakdown in metabolic reprogramming causes microglia dysfunction in Alzheimer's disease. *Cell Metab.* 30:493–507.e6. doi: 10.1016/j.cmet.2019.06.005

Bailey, D. (2019). Oxygen, evolution and redox signalling in the human brain; quantum in the quotidian. *J. Physiol.* 597, 15–28. doi: 10.1113/JP276814

Bandy, B., and Davison, A. (1990). Mitochondrial mutations may increase oxidative stress: Implications for carcinogenesis and aging? *Free Radic. Biol. Med.* 8, 523–539. doi: 10.1016/0891-5849(90)90152-9

Bhatti, J., Bhatti, G., and Reddy, P. (2017). Mitochondrial dysfunction and oxidative stress in metabolic disorders – A step towards mitochondria based therapeutic strategies. *Biochim. Biophys. Acta Mol. Basis Dis.* 1863, 1066–1077. doi: 10.1016/j.bbadis.2016.11.010

Bhuniya, S., Goyal, M., Chowdhury, N., and Mishra, P. (2022). Intermittent hypoxia and sleep disruption in obstructive sleep apnea increase serum tau and amyloid-beta levels. *J. Sleep Res.* 31:e13566. doi: 10.1111/jsr.13566

Bi, R., Zhang, W., Yu, D., Li, X., Wang, H., Hu, Q., et al. (2015). Mitochondrial DNA haplogroup B5 confers genetic susceptibility to Alzheimer's disease in Han Chinese. *Neurobiol Aging* 36:1604.e7–16. doi: 10.1016/j.neurobiolaging.2014.10.009

Bolós, M., Llorens-Martín, M., Perea, J., Jurado-Arjona, J., Rábano, A., Hernández, F., et al. (2017). Absence of CX3CR1 impairs the internalization of Tau by microglia. *Mol. Neurodegener.* 12:59. doi: 10.1186/s13024-017-0200-1

Burtscher, J., Mallet, R., Burtscher, M., and Millet, G. (2021). Hypoxia and brain aging: Neurodegeneration or neuroprotection? *Ageing Res. Rev.* 68:101343. doi: 10.1016/j.arr.2021.101343

Butterfield, D., Hensley, K., Harris, M., Mattson, M., and Carney, J. (1994). beta-Amyloid peptide free radical fragments initiate synaptosomal lipoperoxidation in a sequence-specific fashion: Implications to Alzheimer's disease. *Biochem. Biophys. Res. Commun.* 200, 710–715. doi: 10.1006/bbrc.1994.1508

Cadenas, S. (2018). Mitochondrial uncoupling, ROS generation and cardioprotection. *Biochim. Biophys. Acta Bioenerg.* 1859, 940–950. doi: 10.1016/j.bbabio.2018.05.019

Campolo, N., Issoglio, F., Estrin, D., Bartesaghi, S., and Radi, R. (2020). 3-Nitrotyrosine and related derivatives in proteins: Precursors, radical intermediates and impact in function. *Essays Biochem.* 64, 111–133. doi: 10.1042/EBC20190052

Cervenka, I., Agudelo, L., and Ruas, J. (2017). Kynurenines: Tryptophan's metabolites in exercise, inflammation, and mental health. *Science* 357:eaaf9794. doi: 10.1126/science.aaf9794

Chagnon, P., Gee, M., Filion, M., Robitaille, Y., Belouchi, M., and Gauvreau, D. (1999). Phylogenetic analysis of the mitochondrial genome indicates significant differences between patients with Alzheimer disease and controls in a French-Canadian founder population. *Am. J. Med. Genet.* 85, 20–30.

Chai, A., Lam, H., Kockx, M., and Gelissen, I. (2021). Apolipoprotein E isoform-dependent effects on the processing of Alzheimer's amyloid-β. *Biochim. Biophys. Acta Mol. Cell Biol. Lipids* 1866:158980. doi: 10.1016/j.bbalip.2021.158980

Chamorro, A., Dirnagl, U., Urra, X., and Planas, A. M. (2016). Neuroprotection in acute stroke: Targeting excitotoxicity, oxidative and nitrosative stress, and inflammation. *Lancet Neurol.* 15, 869–881. doi: 10.1016/S1474-4422(16)00114-9

Chauhan, A., and Chauhan, V. (2020). Beneficial Effects of walnuts on cognition and brain health. *Nutrients* 12:550. doi: 10.3390/nu12020550

Chen, W., Wu, P., Yu, F., Luo, G., Qing, L., and Tang, J. (2022). HIF-1α regulates bone homeostasis and angiogenesis, participating in the occurrence of bone metabolic diseases. *Cells* 11:3552. doi: 10.3390/cells11223552

Chen, Z., and Zhong, C. (2014). Oxidative stress in Alzheimer's disease. *Neurosci. Bull.* 30, 271–281. doi: 10.1007/s12264-013-1423-y

Cheng, S., Quintin, J., Cramer, R., Shepardson, K., Saeed, S., Kumar, V., et al. (2014). mTOR- and HIF-1α-mediated aerobic glycolysis as metabolic basis for trained immunity. *Science* 345:1250684. doi: 10.1126/science.1250684

Cho, C., Kim, E., Kim, J., Choi, S., Yang, S., and Cho, S. W. (2016). N-Adamantyl-4-methylthiazol-2-amine suppresses amyloid β-induced neuronal oxidative damage in cortical neurons. *Free Radic. Res.* 50, 678–690. doi: 10.3109/10715762.2016.1167277

Cifelli, J., Chung, T., Liu, H., Prangkio, P., Mayer, M., and Yang, J. (2016). Benzothiazole amphiphiles ameliorate amyloid β-related cell toxicity and oxidative stress. *ACS Chem. Neurosci.* 7, 682–688. doi: 10.1021/acschemneuro.6b00085

Dames, S., Martinez-Yamout, M., De Guzman, R., Dyson, H., and Wright, P. (2002). Structural basis for Hif-1 alpha /CBP recognition in the cellular hypoxic response. *Proc. Natl. Acad. Sci. U.S.A.* 99, 5271–5276. doi: 10.1073/pnas.082121399

De Chiara, G., Piacentini, R., Fabiani, M., Mastrodonato, A., Marcocci, M., Limongi, D., et al. (2019). Recurrent herpes simplex virus-1 infection induces hallmarks of neurodegeneration and cognitive deficits in mice. *PLoS Pathog.* 15:e1007617. doi: 10.1371/journal.ppat.1007617

de Lemos, M., de la Torre , A. V., Petrov, D., Brox, S., Folch, J., Pallàs, M., et al. (2013). Evaluation of hypoxia inducible factor expression in inflammatory and neurodegenerative brain models. *Int. J. Biochem. Cell Biol.* 45, 1377–1388. doi: 10.1016/j.biocel.2013.04.011

Dikalov, S., Polienko, Y., and Kirilyuk, I. (2018). Electron paramagnetic resonance measurements of reactive oxygen species by cyclic hydroxylamine spin probes. *Antioxid. Redox Signal.* 28, 1433–1443. doi: 10.1089/ars.2017.7396

DiSabato, D., Quan, N., and Godbout, J. (2016). Neuroinflammation: The devil is in the details. *J. Neurochem.* 139, 136–153. doi: 10.1111/jnc.13607

Doifode, T., Giridharan, V., Generoso, J., Bhatti, G., Collodel, A., Schulz, P., et al. (2021). The impact of the microbiota-gut-brain axis on Alzheimer's disease pathophysiology. *Pharmacol. Res.* 164:105314. doi: 10.1016/j.phrs.2020.105314

Dryden, M. (2018). Reactive oxygen species: A novel antimicrobial. *Int. J. Antimicrob. Agents* 51, 299–303. doi: 10.1016/j.ijantimicag.2017.08.029

Du, F., Yu, Q., Yan, S., Hu, G., Lue, L., Walker, D., et al. (2017). PINK1 signalling rescues amyloid pathology and mitochondrial dysfunction in Alzheimer's disease. *Brain* 140, 3233–3251. doi: 10.1093/brain/awx258

Dumitrescu, L., Popescu-Olaru, I., Cozma, L., Tulbă, D., Hinescu, M., Ceafalan, L., et al. (2018). Oxidative Stress and the Microbiota-Gut-Brain Axis. *Oxid Med Cell Longev.* 2018:2406594. doi: 10.1155/2018/2406594

Ennerfelt, H., Frost, E., Shapiro, D., Holliday, C., Zengeler, K., Voithofer, G., et al. (2022). SYK coordinates neuroprotective microglial responses in neurodegenerative disease. *Cell* 185:4135–4152.e22. doi: 10.1016/j.cell.2022.09.030

Fan, Y., Mao, R., and Yang, J. (2013). NF-κB and STAT3 signaling pathways collaboratively link inflammation to cancer. *Protein Cell* 4, 176–185. doi: 10.1007/s13238-013-2084-3

Forsythe, J., Jiang, B., Iyer, N., Agani, F., Leung, S., Koos, R., et al. (1996). Activation of vascular endothelial growth factor gene transcription by hypoxia-inducible factor 1. *Mol. Cell Biol.* 16, 4604–4613. doi: 10.1128/MCB.16.9.4604

Gamblin, T., King, M., Kuret, J., Berry, R., and Binder, L. (2000). Oxidative regulation of fatty acid-induced tau polymerization. *Biochemistry* 39, 14203–14210. doi: 10.1021/bi001876l

Gammoh, N., and Rink, L. (2017). Zinc in infection and inflammation. *Nutrients* 9:624. doi: 10.3390/nu9060624

Garrido-Maraver, J., Cordero, M., Oropesa-Avila, M., Vega, A., de la Mata, M., Pavon, A. D., et al. (2014). Clinical applications of coenzyme Q10. *Front. Biosci.* 19:619–633. doi: 10.2741/4231

Ghasemi-Tarie, R., Kiasalari, Z., Fakour, M., Khorasani, M., Keshtkar, S., Baluchnejadmojarad, T., et al. (2022). Nobiletin prevents amyloid β1-40-induced cognitive impairment via inhibition of neuroinflammation and oxidative/nitrosative stress. *Metab. Brain Dis.* 37, 1337–1349. doi: 10.1007/s11011-022-00949-y

Greenough, M., Camakaris, J., and Bush, A. (2013). Metal dyshomeostasis and oxidative stress in Alzheimer's disease. *Neurochem. Int.* 62, 540–555. doi: 10.1016/j.neuint.2012.08.014

Grivennikov, S., and Karin, M. (2010). Dangerous liaisons: STAT3 and NF-kappaB collaboration and crosstalk in cancer. *Cytokine Growth Factor Rev.* 21, 11–19. doi: 10.1016/j.cytogfr.2009.11.005

Guglielmotto, M., Aragno, M., Autelli, R., Giliberto, L., Novo, E., Colombatto, S., et al. (2009). The up-regulation of BACE1 mediated by hypoxia and ischemic injury: Role of oxidative stress and HIF1alpha. *J. Neurochem.* 108, 1045–1056. doi: 10.1111/j.1471-4159.2008.05858.x

Ham, P., and Raju, R. (2017). Mitochondrial function in hypoxic ischemic injury and influence of aging. *Prog. Neurobiol.* 157, 92–16. doi: 10.1016/j.pneurobio.2016.06.006

Hamrick, S., McQuillen, P., Jiang, X., Mu, D., Madan, A., and Ferriero, D. M. (2005). A role for hypoxia-inducible factor-1alpha in desferoxamine neuroprotection. *Neurosci. Lett.* 379, 96–100. doi: 10.1016/j.neulet.2004.12.080

Han, R., Kim, R., Molofsky, A., and Liddelow, S. (2021). Astrocyte-immune cell interactions in physiology and pathology. *Immunity* 54, 211–224. doi: 10.1016/j.immuni.2021.01.013

Harris, M., Carney, J., Cole, P., Hensley, K., Howard, B., Martin, L., et al. (1995a). beta-Amyloid peptide-derived, oxygen-dependent free radicals inhibit glutamate uptake in cultured astrocytes: Implications for Alzheimer's disease. *Neuroreport* 6, 1875–1879. doi: 10.1097/00001756-199510020-00013

Harris, M., Hensley, K., Butterfield, D., Leedle, R., and Carney, J. (1995b). Direct evidence of oxidative injury produced by the Alzheimer's beta-amyloid peptide (1-40) in cultured hippocampal neurons. *Exp. Neurol.* 131, 193–202. doi: 10.1016/0014-4886(95)90041-1

Heneka, M., Carson, M., El Khoury, J., Landreth, G., Brosseron, F., Feinstein, D., et al. (2015). neuroinflammation in Alzheimer's disease. *Lancet Neurol.* 14, 388–405. doi: 10.1016/S1474-4422(15)70016-5

Hensley, K., Butterfield, D., Mattson, M., Aksenova, M., Harris, M., Wu, J., et al. (1995). A model for beta-amyloid aggregation and neurotoxicity based on the free radical generating capacity of the peptide: Implications of "molecular shrapnel" for Alzheimer's disease. *Proc. West Pharmacol. Soc.* 38, 113–120.

Hilt, S., Altman, R., Kálai, T., Maezawa, I., Gong, Q., Wachsmann-Hogiu, S., et al. (2018). A bifunctional anti-amyloid blocks oxidative stress and the accumulation of intraneuronal amyloid-beta. *Molecules* 23:2010. doi: 10.3390/molecules23082010

Hirota, K. (2021). HIF-α prolyl hydroxylase inhibitors and their implications for biomedicine: A comprehensive review. *Biomedicines* 9:468. doi: 10.3390/biomedicines9050468

Høgh, P. (2017). [Alzheimer's disease]. *Ugeskr. Laeger* 179:296.

Huang, Z., Ji, H., Shi, J., Zhu, X., and Zhi, Z. (2020). Engeletin attenuates Aβ1-42-induced oxidative stress and neuroinflammation by Keap1/Nrf2 pathway. *Inflammation* 43, 1759–1771. doi: 10.1007/s10753-020-01250-9

Huat, T., Camats-Perna, J., Newcombe, E., Valmas, N., Kitazawa, M., and Medeiros, R. (2019). Metal toxicity links to Alzheimer's disease and neuroinflammation. *J. Mol. Biol.* 431, 1843–1868. doi: 10.1016/j.jmb.2019.01.018

Hussain, S., and Harris, C. (2007). Inflammation and cancer: An ancient link with novel potentials. *Int. J. Cancer* 121, 2373–2380. doi: 10.1002/ijc.23173

Huynh, T., Davis, A., Ulrich, J., and Holtzman, D. (2017). Apolipoprotein E and Alzheimer's disease: The influence of apolipoprotein E on amyloid-β and other amyloidogenic proteins. *J. Lipid Res.* 58, 824–836. doi: 10.1194/jlr.R075481

Ionescu-Tucker, A., and Cotman, C. (2021). Emerging roles of oxidative stress in brain aging and Alzheimer's disease. *Neurobiol. Aging* 107, 86–95. doi: 10.1016/j.neurobiolaging.2021.07.014

Juan, C., Pérez de la Lastra, J. M., Plou, F. J., and Pérez-Lebeña, E. (2021). The chemistry of reactive oxygen species (ROS) revisited: Outlining their role in biological macromolecules (DNA, lipids and proteins) and induced pathologies. *Int. J. Mol. Sci.* 22:4642. doi: 10.3390/ijms22094642

Kaminsky, Y., Marlatt, M., Smith, M., and Kosenko, E. (2010). Subcellular and metabolic examination of amyloid-beta peptides in Alzheimer disease pathogenesis: Evidence for Abeta(25-35). *Exp. Neurol.* 221, 26–37. doi: 10.1016/j.expneurol.2009.09.005

Kim, J., Cho, C., Hahn, H., Choi, S., and Cho, S. (2017). Neuroprotective effects of N-adamantyl-4-methylthiazol-2-amine against amyloid β-induced oxidative stress in mouse hippocampus. *Brain Res. Bull.* 128, 22–28. doi: 10.1016/j.brainresbull.2016.10.010

Korbecki, J., Simińska, D., Gąssowska-Dobrowolska, M., Listos, J., Gutowska, I., Chlubek, D., et al. (2021). Chronic and cycling hypoxia: Drivers of cancer chronic inflammation through HIF-1 and NF-κB activation: A review of the molecular mechanisms. *Int. J. Mol. Sci.* 22:10701. doi: 10.3390/ijms221910701

Laird, F., Cai, H., Savonenko, A., Farah, M., He, K., Melnikova, T., et al. (2005). BACE1, a major determinant of selective vulnerability of the brain to amyloid-beta amyloidogenesis, is essential for cognitive, emotional, and synaptic functions. *J. Neurosci.* 25, 11693–11709. doi: 10.1523/JNEUROSCI.2766-05.2005

Lane, C., Hardy, J., and Schott, J. (2018). Alzheimer's disease. *Eur. J. Neurol.* 25, 59–70. doi: 10.1111/ene.13439

Lee, H., Ryu, J., Jung, Y., Lee, S., Kim, J., Lee, S., et al. (2016). High glucose upregulates BACE1-mediated Aβ production through ROS-dependent HIF-1α and LXRα/ABCA1-regulated lipid raft reorganization in SK-N-MC cells. *Sci. Rep.* 6:36746. doi: 10.1038/srep36746

Lee, S., Nam, E., Lee, H., Savelieff, M., and Lim, M. (2017). Towards an understanding of amyloid-β oligomers: Characterization, toxicity mechanisms, and inhibitors. *Chem. Soc. Rev.* 46, 310–323. doi: 10.1039/c6cs00731g

Lei, L., Feng, J., Wu, G., Wei, Z., Wang, J., Zhang, B., et al. (2022). HIF-1α causes LCMT1/PP2A deficiency and mediates tau hyperphosphorylation and cognitive dysfunction during chronic hypoxia. *Int. J. Mol. Sci.* 23:16140. doi: 10.3390/ijms232416140

Leng, F., and Edison, P. (2021). Neuroinflammation and microglial activation in Alzheimer disease: Where do we go from here? *Nat. Rev. Neurol.* 17, 157–172. doi: 10.1038/s41582-020-00435-y

Li, G., Ding, K., Qiao, Y., Zhang, L., Zheng, L., Pan, T., et al. (2020). Flavonoids regulate inflammation and oxidative stress in cancer. *Molecules* 25:5628. doi: 10.3390/molecules25235628

Li, H., Zhou, Y., Li, L., Li, S., Long, D., Chen, X., et al. (2019). HIF-1α protects against oxidative stress by directly targeting mitochondria. *Redox Biol.* 25:101109. doi: 10.1016/j.redox.2019.101109

Li, Z., Wu, F., Xu, D., Zhi, Z., and Xu, G. (2019). Inhibition of TREM1 reduces inflammation and oxidative stress after spinal cord injury (SCI) associated with HO-1 expressions. *Biomed. Pharmacother.* 109, 2014–2021. doi: 10.1016/j.biopha.2018.08.159

Li, X., Zhan, J., Hou, Y., Hou, Y., Chen, S., Luo, D., et al. (2019). Coenzyme Q10 regulation of apoptosis and oxidative stress in H2O2 induced BMSC death by modulating the Nrf-2/NQO-1 signaling pathway and its application in a model of spinal cord injury. *Oxid. Med. Cell Longev.* 2019:6493081. doi: 10.1155/2019/6493081

Li, J., and Ye, J. (2024). Chronic intermittent hypoxia induces cognitive impairment in Alzheimer's disease mouse model via postsynaptic mechanisms. *Sleep Breath.* 28, 1197–1205. doi: 10.1007/s11325-023-02970-6

Li, Y., Ding, S., Xiao, L., Guo, W., and Zhan, Q. (2008). Desferoxamine preconditioning protects against cerebral ischemia in rats by inducing expressions of hypoxia inducible factor 1 alpha and erythropoietin. *Neurosci. Bull.* 24, 89–95. doi: 10.1007/s12264-008-0089-3

Lian, H., Yang, L., Cole, A., Sun, L., Chiang, A., Fowler, S., et al. (2015). NFκB-activated astroglial release of complement C3 compromises neuronal morphology and function associated with Alzheimer's disease. *Neuron* 85, 101–115. doi: 10.1016/j.neuron.2014.11.018

Lim, C., and Thurston, G. (2019). Air pollution, oxidative stress, and diabetes: A life course epidemiologic perspective. *Curr. Diab. Rep.* 19:58. doi: 10.1007/s11892-019-1181-y

Lin, C., Lan, Y., Ou, M., Ji, L., and Lin, S. (2019). Expression of miR-217 and HIF-1α/VEGF pathway in patients with diabetic foot ulcer and its effect on angiogenesis of diabetic foot ulcer rats. *J. Endocrinol. Invest.* 42, 1307–1317. doi: 10.1007/s40618-019-01053-2

Lin, W., and Karin, M. (2007). A cytokine-mediated link between innate immunity, inflammation, and cancer. *J. Clin. Invest.* 117, 1175–1183. doi: 10.1172/JCI31537

Liu, J., Wang, W., Wang, L., Chen, S., Tian, B., Huang, K., et al. (2018). IL-33 initiates vascular remodelling in hypoxic pulmonary hypertension by up-regulating HIF-1α and VEGF expression in vascular endothelial cells. *EBioMedicine* 33, 196–210. doi: 10.1016/j.ebiom.2018.06.003

Liu, P., Xie, Y., Meng, X., and Kang, J. (2019). History and progress of hypotheses and clinical trials for Alzheimer's disease. *Signal. Transduct. Target Ther.* 4:29. doi: 10.1038/s41392-019-0063-8

Liu, Y., Liu, F., Iqbal, K., Grundke-Iqbal, I., and Gong, C. (2008). Decreased glucose transporters correlate to abnormal hyperphosphorylation of tau in Alzheimer disease. *FEBS Lett.* 582, 359–364. doi: 10.1016/j.febslet.2007.12.035

Liu, Y., Xue, C., Lu, H., Zhou, Y., Guan, R., Wang, J., et al. (2022). Hypoxia causes mitochondrial dysfunction and brain memory disorder in a manner mediated by the reduction of Cirbp. *Sci. Total Environ.* 806:151228. doi: 10.1016/j.scitotenv.2021.151228

Lloberas, J., Muñoz, J., Hernández-Álvarez, M., Cardona, P., Zorzano, A., and Celada, A. (2020). Macrophage mitochondrial MFN2 (mitofusin 2) links immune stress and immune response through reactive oxygen species (ROS) production. *Autophagy* 16, 2307–2309. doi: 10.1080/15548627.2020.1839191

Long, J., and Holtzman, D. (2019). Alzheimer disease: An update on pathobiology and treatment strategies. *Cell* 179, 312–339. doi: 10.1016/j.cell.2019.09.001

Lou, T., Tao, B., and Chen, M. (2023). Relationship of apolipoprotein E with Alzheimer's disease and other neurological disorders: An updated review. *Neuroscience* 514, 123–140. doi: 10.1016/j.neuroscience.2023.01.032

Luo, Z., Xu, X., Sho, T., Zhang, J., Xu, W., Yao, J., et al. (2019). ROS-induced autophagy regulates porcine trophectoderm cell apoptosis, proliferation, and differentiation. *Am. J. Physiol. Cell Physiol.* 316, C198–C209. doi: 10.1152/ajpcell.00256.2018

Mailloux, R., and Harper, M. (2011). Uncoupling proteins and the control of mitochondrial reactive oxygen species production. *Free Radic. Biol. Med.* 51, 1106–1115. doi: 10.1016/j.freeradbiomed.2011.06.022

Marchev, A., Dimitrova, P., Burns, A., Kostov, R., Dinkova-Kostova, A., and Georgiev, M. (2017). Oxidative stress and chronic inflammation in osteoarthritis: Can NRF2 counteract these partners in crime? *Ann. N. Y. Acad. Sci.* 1401, 114–135. doi: 10.1111/nyas.13407

Marín, R., Chiarello, D., Abad, C., Rojas, D., Toledo, F., and Sobrevia, L. (2020). Oxidative stress and mitochondrial dysfunction in early-onset and late-onset preeclampsia. *Biochim. Biophys. Acta Mol. Basis Dis.* 1866:165961. doi: 10.1016/j.bbadis.2020.165961

Mcdonald, J., Dhakal, S., and Macreadie, I. (2021). A toxic synergy between aluminium and amyloid beta in yeast. *Int. J. Mol. Sci.* 22:1835. doi: 10.3390/ijms22041835

Mennerich, D., Kellokumpu, S., and Kietzmann, T. (2019). Hypoxia and reactive oxygen species as modulators of endoplasmic reticulum and Golgi homeostasis. *Antioxid. Redox Signal.* 30, 113–137. doi: 10.1089/ars.2018.7523

Mohapatra, S., Sadik, A., Sharma, S., Poschet, G., Gegner, H., Lanz, T., et al. (2021). Hypoxia routes tryptophan homeostasis towards increased tryptamine production. *Front. Immunol.* 12:590532. doi: 10.3389/fimmu.2021.590532

Mohás-Cseh, J., Molnár, G., Pap, M., Laczy, B., Vas, T., Kertész, M., et al. (2022). Incorporation of oxidized phenylalanine derivatives into insulin signaling relevant proteins may link oxidative stress to signaling conditions underlying chronic insulin resistance. *Biomedicines* 10:975. doi: 10.3390/biomedicines10050975

Mojsilovic-Petrovic, J., Callaghan, D., Cui, H., Dean, C., Stanimirovic, D., and Zhang, W. (2007). Hypoxia-inducible factor-1 (HIF-1) is involved in the regulation of hypoxia-stimulated expression of monocyte chemoattractant protein-1 (MCP-1/CCL2) and MCP-5 (Ccl12) in astrocytes. *J. Neuroinflamm.* 4:12. doi: 10.1186/1742-2094-4-12

Naseri, N., Wang, H., Guo, J., Sharma, M., and Luo, W. (2019). The complexity of tau in Alzheimer's disease. *Neurosci Lett.* 705, 183–194. doi: 10.1016/j.neulet.2019.04.022

Ni, H., Li, J., Zheng, J., and Zhou, B. (2022). Cardamonin attenuates cerebral ischemia/reperfusion injury by activating the HIF-1α/VEGFA pathway. *Phytother. Res.* 36, 1736–1747. doi: 10.1002/ptr.7409

Nunomura, A., and Perry, G. (2020). RNA and oxidative stress in Alzheimer's disease: Focus on microRNAs. *Oxid. Med. Cell Longev.* 2020:2638130. doi: 10.1155/2020/2638130

Ohno, M., Sametsky, E., Younkin, L., Oakley, H., Younkin, S., Citron, M., et al. (2004). BACE1 deficiency rescues memory deficits and cholinergic dysfunction in a mouse model of Alzheimer's disease. *Neuron* 41, 27–33. doi: 10.1016/s0896-6273(03)00810-9

Oswald, M., Garnham, N., Sweeney, S., and Landgraf, M. (2018). Regulation of neuronal development and function by ROS. *FEBS Lett.* 592, 679–691. doi: 10.1002/1873-3468.12972

Ozben, T., and Ozben, S. (2019). Neuro-inflammation and anti-inflammatory treatment options for Alzheimer's disease. *Clin. Biochem.* 72, 87–89. doi: 10.1016/j.clinbiochem.2019.04.001

Palazon, A., Tyrakis, P., Macias, D., Veliça, P., Rundqvist, H., Fitzpatrick, S., et al. (2017). An HIF-1α/VEGF-A axis in cytotoxic T cells regulates tumor progression. *Cancer Cell* 32:669–683.e5. doi: 10.1016/j.ccell.2017.10.003

Papaconstantinou, J. (2019). The role of signaling pathways of inflammation and oxidative stress in development of senescence and aging phenotypes in cardiovascular disease. *Cells* 8:1383. doi: 10.3390/cells8111383

Park, J., Min, J., Kim, B., Chae, U., Yun, J., Choi, M., et al. (2015). Mitochondrial ROS govern the LPS-induced pro-inflammatory response in microglia cells by regulating MAPK and NF-κB pathways. *Neurosci. Lett.* 584, 191–196. doi: 10.1016/j.neulet.2014.10.016

Peña-Bautista, C., Tirle, T., López-Nogueroles, M., Vento, M., Baquero, M., and Cháfer-Pericás, C. (2019). Oxidative damage of DNA as early marker of Alzheimer's disease. *Int. J. Mol. Sci.* 20:6136. doi: 10.3390/ijms20246136

Peng, Y., Chang, X., and Lang, M. (2021). Iron homeostasis disorder and Alzheimer's disease. *Int. J. Mol. Sci.* 22:2442. doi: 10.3390/ijms222212442

Plascencia-Villa, G., and Perry, G. (2021). Preventive and therapeutic strategies in Alzheimer's disease: Focus on oxidative stress, redox metals, and ferroptosis. *Antioxid. Redox Signal.* 34, 591–610. doi: 10.1089/ars.2020.8134

Pluta, R., and Ulamek-Koziol, M. (2021). Genes associated with Alzheimer's disease affecting ischemic neurodegeneration of the hippocampal CA3 region. *Neural Regen. Res.* 16, 1392–1393. doi: 10.4103/1673-5374.300982

Porsteinsson, A., Isaacson, R., Knox, S., Sabbagh, M., and Rubino, I. (2021). Diagnosis of early Alzheimer's disease: Clinical practice in 2021. *J. Prev. Alzheimers. Dis.* 8, 371–386. doi: 10.14283/jpad.2021.23

Radi, E., Formichi, P., Battisti, C., and Federico, A. (2014). Apoptosis and oxidative stress in neurodegenerative diseases. *J. Alzheimers Dis.* 42, S125–S152. doi: 10.3233/JAD-132738

Reuter, S., Gupta, S., Chaturvedi, M., and Aggarwal, B. (2010). Oxidative stress, inflammation, and cancer: How are they linked? *Free Radic. Biol. Med.* 49, 1603–1616. doi: 10.1016/j.freeradbiomed.2010.09.006

Richter, C., Park, J., and Ames, B. (1988). Normal oxidative damage to mitochondrial and nuclear DNA is extensive. *Proc. Natl. Acad. Sci. U.S.A.* 85, 6465–6467. doi: 10.1073/pnas.85.17.6465

Rizwan, H., Pal, S., Sabnam, S., and Pal, A. (2020). High glucose augments ROS generation regulates mitochondrial dysfunction and apoptosis via stress signalling cascades in keratinocytes. *Life Sci.* 241:117148. doi: 10.1016/j.lfs.2019.117148

Rogers, J., Xia, N., Wong, A., Bakshi, R., and Cahill, C. (2019). Targeting the iron-response elements of the mRNAs for the Alzheimer's amyloid precursor protein and ferritin to treat acute lead and manganese neurotoxicity. *Int. J. Mol. Sci.* 20:994. doi: 10.3390/ijms20040994

Ryberg, H., Söderling, A., Davidsson, P., Blennow, K., Caidahl, K., and Persson, L. (2004). Cerebrospinal fluid levels of free 3-nitrotyrosine are not elevated in the majority of patients with amyotrophic lateral sclerosis or Alzheimer's disease. *Neurochem. Int.* 45, 57–62. doi: 10.1016/j.neuint.2003.12.012

Ryou, M., Choudhury, G., Li, W., Winters, A., Yuan, F., Liu, R., et al. (2015). Methylene blue-induced neuronal protective mechanism against hypoxia-reoxygenation stress. *Neuroscience* 301, 193–203. doi: 10.1016/j.neuroscience.2015.05.064

Sahoo, B., Banik, B., Borah, P., and Jain, A. (2022). Reactive oxygen species (ROS): Key components in cancer therapies. *Anticancer Agents Med. Chem.* 22, 215–222. doi: 10.2174/1871520621666210608095512

Sahu, I., and Lorigan, G. (2020). Electron paramagnetic resonance as a tool for studying membrane proteins. *Biomolecules* 10:763. doi: 10.3390/biom10050763

Sala, M., Chen, C., Zhang, Q., Do-Umehara, H., Wu, W., Misharin, A., et al. (2018). JNK2 up-regulates hypoxia-inducible factors and contributes to hypoxia-induced erythropoiesis and pulmonary hypertension. *J. Biol. Chem.* 293, 271–284. doi: 10.1074/jbc.RA117.000440

Santana, S., Bullido, M., Recuero, M., Valdivieso, F., and Aldudo, J. (2012). Herpes simplex virus type I induces an incomplete autophagic response in human neuroblastoma cells. *J. Alzheimers Dis.* 30, 815–831. doi: 10.3233/JAD-2012-112000

Santana, S., Sastre, I., Recuero, M., Bullido, M., and Aldudo, J. (2013). Oxidative stress enhances neurodegeneration markers induced by herpes simplex virus type 1 infection in human neuroblastoma cells. *PLoS One* 8:e75842. doi: 10.1371/journal.pone.0075842

Scheltens, P., De Strooper, B., Kivipelto, M., Holstege, H., Chételat, G., Teunissen, C., et al. (2021). Alzheimer's disease. *Lancet* 397, 1577–1590. doi: 10.1016/S0140-6736(20)32205-4

Scherz-Shouval, R., Shvets, E., Fass, E., Shorer, H., Gil, L., and Elazar, Z. (2007). Reactive oxygen species are essential for autophagy and specifically regulate the activity of Atg4. *EMBO J.* 26, 1749–1760. doi: 10.1038/sj.emboj.7601623

Semenza, G. (2007). Hypoxia-inducible factor 1 (HIF-1) pathway. *Sci. STKE* 2007:cm8. doi: 10.1126/stke.4072007cm8

Sengupta, U., Guerrero-Muñoz, M., Castillo-Carranza, D., Lasagna-Reeves, C., Gerson, J., Paulucci-Holthauzen, A., et al. (2015). Pathological interface between oligomeric alpha-synuclein and tau in synucleinopathies. *Biol. Psychiatry* 78, 672–683. doi: 10.1016/j.biopsych.2014.12.019

Sharma, V., Singh, T., Prabhakar, N., and Mannan, A. (2022). Kynurenine Metabolism and Alzheimer's disease: the potential targets and approaches. *Neurochem. Res.* 47, 1459–1476. doi: 10.1007/s11064-022-03546-8

Soltys, D., Pereira, C., Rowies, F., Farfel, J., Grinberg, L., Suemoto, C., et al. (2019). Lower mitochondrial DNA content but not increased mutagenesis associates with decreased base excision repair activity in brains of AD subjects. *Neurobiol. Aging* 73, 161–170. doi: 10.1016/j.neurobiolaging.2018.09.015

Sontag, J., Nunbhakdi-Craig, V., and Sontag, E. (2013). Leucine carboxyl methyltransferase 1 (LCMT1)-dependent methylation regulates the association of protein phosphatase 2A and Tau protein with plasma membrane microdomains in neuroblastoma cells. *J. Biol. Chem.* 288, 27396–27405. doi: 10.1074/jbc.M113.490102

Sontag, J., Wasek, B., Taleski, G., Smith, J., Arning, E., Sontag, E., et al. (2014). Altered protein phosphatase 2A methylation and Tau phosphorylation in the young and aged brain of methylenetetrahydrofolate reductase (MTHFR) deficient mice. *Front. Aging Neurosci.* 6:214. doi: 10.3389/fnagi.2014.00214

Soria Lopez, J., González, H., and Léger, G. (2019). Alzheimer's disease. *Handb. Clin. Neurol.* 167, 231–255. doi: 10.1016/B978-0-12-804766-8.00013-3

Sriram, S., Mehkri, Y., Quintin, S., and Lucke-Wold, B. (2022). Shared pathophysiology: Understanding stroke and Alzheimer's disease. *Clin. Neurol. Neurosurg.* 218:107306. doi: 10.1016/j.clineuro.2022.107306

Steven, S., Frenis, K., Oelze, M., Kalinovic, S., Kuntic, M., Bayo Jimenez, M., et al. (2019). Vascular inflammation and oxidative stress: Major triggers for cardiovascular disease. *Oxid. Med. Cell Longev.* 2019:7092151. doi: 10.1155/2019/7092151

Su, L., Zhang, J., Gomez, H., Murugan, R., Hong, X., Xu, D., et al. (2019). Reactive oxygen species-induced lipid peroxidation in apoptosis, autophagy, and ferroptosis. *Oxid. Med. Cell Longev.* 2019:5080843. doi: 10.1155/2019/5080843

Sun, L., Zhou, R., Yang, G., and Shi, Y. (2017). Analysis of 138 pathogenic mutations in presenilin-1 on the in vitro production of Aβ42 and Aβ40 peptides by γ-secretase. *Proc. Natl. Acad. Sci. U.S.A.* 114, E476–E485. doi: 10.1073/pnas.1618657114

Surendranathan, A., Su, L., Mak, E., Passamonti, L., Hong, Y., Arnold, R., et al. (2018). Early microglial activation and peripheral inflammation in dementia with Lewy bodies. *Brain* 141, 3415–3427. doi: 10.1093/brain/awy265

Tamagno, E., Guglielmotto, M., Monteleone, D., and Tabaton, M. (2012). Amyloid-β production: Major link between oxidative stress and BACE1. *Neurotox. Res.* 22, 208–219. doi: 10.1007/s12640-011-9283-6

Taysi, S., Tascan, A., Ugur, M., and Demir, M. (2019). Radicals, oxidative/nitrosative stress and preeclampsia. *Mini Rev. Med. Chem.* 19, 178–193. doi: 10.2174/1389557518666181015151350

Teng, T., Ridgley, D., Tsoy, A., Sun, G., Askarova, S., and Lee, J. (2019). Azelnidipine attenuates the oxidative and NFκB pathways in amyloid-β-stimulated cerebral endothelial cells. *ACS Chem. Neurosci.* 10, 209–215. doi: 10.1021/acschemneuro.8b00368

Tiwari, S., Atluri, V., Kaushik, A., Yndart, A., and Nair, M. (2019). Alzheimer's disease: Pathogenesis, diagnostics, and therapeutics. *Int. J. Nanomed.* 14, 5541–5554. doi: 10.2147/IJN.S200490

Tong, B. C., Wu, A., Li, M., and Cheung, K. (2018). Calcium signaling in Alzheimer's disease & therapies. *Biochim. Biophys. Acta Mol. Cell Res.* 1865, 1745–1760.

Tönnies, E., and Trushina, E. (2017). Oxidative stress, synaptic dysfunction, and Alzheimer's disease. *J. Alzheimers Dis.* 57, 1105–1121. doi: 10.3233/JAD-161088

Twarowski, B., and Herbet, M. (2023). Inflammatory processes in Alzheimer's disease-pathomechanism, diagnosis and treatment: A review. *Int. J. Mol. Sci.* 24:6518. doi: 10.3390/ijms24076518

Vašák, M., and Meloni, G. (2017). Mammalian metallothionein-3: New functional and structural insights. *Int. J. Mol. Sci.* 18:1117. doi: 10.3390/ijms18061117

Venkatesan, D., Iyer, M., Narayanasamy, A., Siva, K., and Vellingiri, B. (2020). Kynurenine pathway in Parkinson's disease-An update. *eNeurologicalSci* 21:100270. doi: 10.1016/j.ensci.2020.100270

Vijayan, M., and Reddy, P. (2016). Stroke, vascular dementia, and Alzheimer's disease: Molecular links. *J. Alzheimers Dis.* 54, 427–443. doi: 10.3233/JAD-160527

Wang, G., Jiang, B., Rue, E., and Semenza, G. (1995). Hypoxia-inducible factor 1 is a basic-helix-loop-helix-PAS heterodimer regulated by cellular O2 tension. *Proc. Natl. Acad. Sci. U.S.A.* 92, 5510–5514. doi: 10.1073/pnas.92.12.5510

Wang, J., Zhu, W., Han, J., Yang, X., Zhou, R., Lu, H., et al. (2021). The role of the HIF-1α/ALYREF/PKM2 axis in glycolysis and tumorigenesis of bladder cancer. *Cancer Commun.* 41, 560–575. doi: 10.1002/cac2.12158

Wang, L., Yin, Y., Liu, X., Shen, P., Zheng, Y., Lan, X., et al. (2020). Current understanding of metal ions in the pathogenesis of Alzheimer's disease. *Transl. Neurodegener.* 9:10. doi: 10.1186/s40035-020-00189-z

Wang, Q., Liu, D., Song, P., and Zou, M. (2015). Tryptophan-kynurenine pathway is dysregulated in inflammation, and immune activation. *Front. Biosci.* 20:1116–1143. doi: 10.2741/4363

Wang, X., Qi, L., Cheng, Y., Ji, X., Chi, T., Liu, P., et al. (2022). PINK1 overexpression prevents forskolin-induced tau hyperphosphorylation and oxidative stress in a rat model of Alzheimer's disease. *Acta Pharmacol. Sin.* 43, 1916–1927. doi: 10.1038/s41401-021-00810-5

Watts, E., and Walmsley, S. (2019). Inflammation and hypoxia: HIF and PHD isoform selectivity. *Trends Mol. Med.* 25, 33–46. doi: 10.1016/j.molmed.2018.10.006

Weller, J., and Budson, A. (2018). Current understanding of Alzheimer's disease diagnosis and treatment. *F1000Res* 7, 1000–1161. doi: 10.12688/f1000research.14506.1

Wu, D., Zhang, R., Zhao, R., Chen, G., Cai, Y., and Jin, J. (2013). A novel function of novobiocin: Disrupting the interaction of HIF 1α and p300/CBP through direct binding to the HIF1α C-terminal activation domain. *PLoS One* 8:e62014. doi: 10.1371/journal.pone.0062014

Xie, J., Van Hoecke, L., and Vandenbroucke, R. (2021). The impact of systemic inflammation on Alzheimer's disease pathology. *Front. Immunol.* 12:796867. doi: 10.3389/fimmu.2021.796867

Xie, Y., Shi, X., Sheng, K., Han, G., Li, W., Zhao, Q., et al. (2019). PI3K/Akt signaling transduction pathway, erythropoiesis and glycolysis in hypoxia (Review). *Mol. Med. Rep.* 19, 783–791. doi: 10.3892/mmr.2018.9713

Yang, C., Zhong, Z., Wang, S., Vong, C., Yu, B., and Wang, Y. T. (2021). HIF-1: Structure, biology and natural modulators. *Chin. J. Nat. Med.* 19, 521–527. doi: 10.1016/S1875-5364(21)60051-1

Yang, G., Zhou, R., Guo, X., Yan, C., Lei, J., and Shi, Y. (2021). Structural basis of γ-secretase inhibition and modulation by small molecule drugs. *Cell* 184:521–533.e14. doi: 10.1016/j.cell.2020.11.049

Yang, F., Pei, R., Zhang, Z., Liao, J., Yu, W., Qiao, N., et al. (2019). Copper induces oxidative stress and apoptosis through mitochondria-mediated pathway in chicken hepatocytes. *Toxicol. Vitro* 54, 310–316. doi: 10.1016/j.tiv.2018.10.017

Yang, Y., Huang, L., Hsieh, S., and Huang, L. (2020). Dynamic blood concentrations of Aβ1-40 and Aβ1-42 in Alzheimer's disease. *Front. Cell Dev. Biol.* 8:768. doi: 10.3389/fcell.2020.00768

Yatin, S., Aksenova, M., Aksenov, M., Markesbery, W., Aulick, T., and Butterfield, D. (1998). Temporal relations among amyloid beta-peptide-induced free-radical oxidative stress, neuronal toxicity, and neuronal defensive responses. *J. Mol. Neurosci.* 11, 183–197. doi: 10.1385/JMN:11:3:183

Yu, F., White, S., Zhao, Q., and Lee, F. S. (2001). HIF-1alpha binding to VHL is regulated by stimulus-sensitive proline hydroxylation. *Proc. Natl. Acad. Sci. U.S.A.* 98, 9630–9635. doi: 10.1073/pnas.181341498

Zagórska, A., and Dulak, J. (2004). HIF-1: The knowns and unknowns of hypoxia sensing. *Acta Biochim. Pol.* 51, 563–585.

Zeng, M., Feng, A., Zhao, C., Zhang, B., Guo, P., Liu, M., et al. (2022). Adenosine ameliorated Aβ25-35-induced brain injury through the inhibition of apoptosis and oxidative stress via an ERα pathway. *Brain Res.* 1788:147944. doi: 10.1016/j.brainres.2022.147944

Zhang, C., Yang, X., Li, L., Sui, X., Tian, Q., Wei, W., et al. (2014). Hypoxia-induced tau phosphorylation and memory deficit in rats. *Neurodegener. Dis.* 14, 107–116. doi: 10.1159/000362239

Zhang, W., Petrovic, J., Callaghan, D., Jones, A., Cui, H., Howlett, C., et al. (2006). Evidence that hypoxia-inducible factor-1 (HIF-1) mediates transcriptional activation of interleukin-1beta (IL-1beta) in astrocyte cultures. *J. Neuroimmunol.* 174, 63–73. doi: 10.1016/j.jneuroim.2006.01.014

Zhang, X., Zhou, K., Wang, R., Cui, J., Lipton, S., Liao, F., et al. (2007). Hypoxia-inducible factor 1alpha (HIF-1alpha)-mediated hypoxia increases BACE1 expression and beta-amyloid generation. *J. Biol. Chem.* 282, 10873–10880. doi: 10.1074/jbc.M608856200

Zhang, Z., Li, Y., and Zhao, R. (2017). Epigallocatechin gallate attenuates β-amyloid generation and oxidative stress involvement of PPARγ in N2a/APP695 cells. *Neurochem. Res.* 42, 468–480. doi: 10.1007/s11064-016-2093-8

Zhao, M., Wang, S., Zuo, A., Zhang, J., Wen, W., Jiang, W., et al. (2021). HIF-1α/JMJD1A signaling regulates inflammation and oxidative stress following hyperglycemia and hypoxia-induced vascular cell injury. *Cell Mol. Biol. Lett.* 26:40. doi: 10.1186/s11658-021-00283-8

Zhao, Y., Valis, M., Wang, X., Nepovimova, E., Wu, Q., and Kuca, K. (2024). HIF-1α is a "brake"; in JNK-mediated activation of amyloid protein precursor and hyperphosphorylation of tau induced by T-2 toxin in BV2 cells. *Mycotoxin. Res.* 40, 223–234. doi: 10.1007/s12550-024-00525-6

Zhou, Y., Lu, H., Liu, Y., Zhao, Z., Zhang, Q., Xue, C., et al. (2021). Cirbp-PSD95 axis protects against hypobaric hypoxia-induced aberrant morphology of hippocampal dendritic spines and cognitive deficits. *Mol. Brain* 14:129. doi: 10.1186/s13041-021-00827-1

Zou, K., Abdullah, M., and Michikawa, M. (2020). Current Biomarkers for Alzheimer's disease: From CSF to blood. *J. Pers. Med.* 10:85. doi: 10.3390/jpm10030085

Frontiers in
Aging Neuroscience

Explores the mechanisms of central nervous system aging and age-related neural disease

The third most-cited journal in the field of geriatrics and gerontology, with a focus on understanding the mechanistic processes associated with central nervous system aging.

Discover the latest Research Topics

See more →

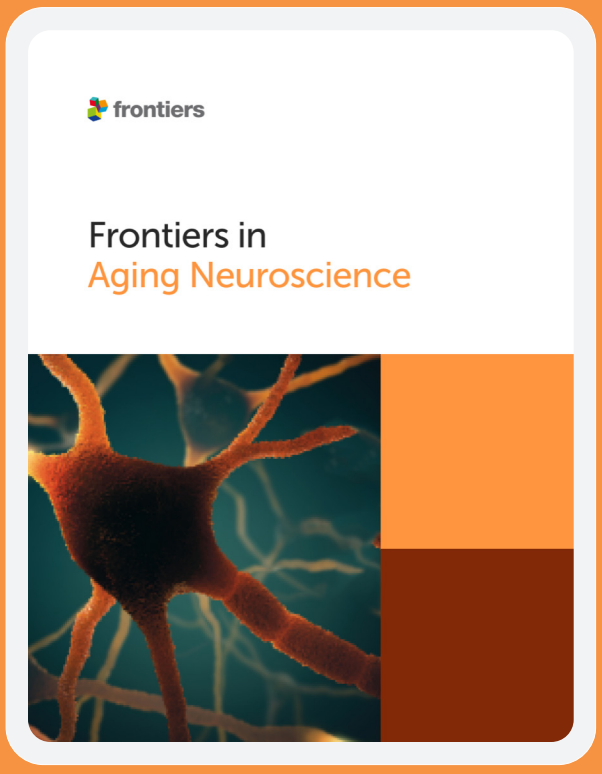

Frontiers

Avenue du Tribunal-Fédéral 34
1005 Lausanne, Switzerland
frontiersin.org

Contact us

+41 (0)21 510 17 00
frontiersin.org/about/contact